VELOCITY INVESTIGATION OVER A SEISMIC REFLECTION ANOMALY IN THE ZELTEN FIELD, LIBYA

by

NAJIM MOHAMMED BEN-AYAD

B.Sc. (1980) - Faculty of Petroleum and Mining Engineering - Tripoli

Thesis submitted for the degree of Master of Science (by research) at the Department of Geology and Applied Geology, University of Glasgow.

June 1991

DECLARATION

The material presented in this thesis is the results of independent research by the author undertaken between November 1988 and June 1991 at the Department of Geology and Applied Geology, University of Glasgow. Any published or unpublished papers have been given full acknowledgment in the text.

Ben-Ayad N. M.

Professor Dave K. Smythe

Department of Geology and Applied Geology,
University of Glasgow.

Dedicated to my parents and my family

Acknowledgements

The research leading to this thesis was carried out at the Department of Geology & Applied Geology, University of Glasgow. I am indebted to Professor B. E. Leake, the head of the department, for allowing me the use of the facilities of the department during this research.

I would like to extend my sincere thanks to the management of Sirte Oil Company and in particular the management of the Exploration Department for giving me this opportunity, for the scholarship, for their permission to release the data, and for their support.

I would like to thank my supervisor Professor Dave K. Smythe for his guidance and support. Also for his considerable help, constructive advice, and assistance throughout this project.

I am grateful to Dr. Doyle R. Watts for reading the thesis, for his corrections, comments, and suggestions. I also thank Dr. J. J. Doody for his corrections.

I thank the management of Weybridge office, especially Dr. Reza Sedghat for providing the data, . My appreciation goes to the technical staff at the Department of Geology & Applied Geology; in particular to Mr. Robert T. Cumberland, and Mr. Jim Kavanagh for their computer help, and Mr. Douglas Mclean for his great photographic production.

I also extend my thanks to my postgraduate student friends and colleagues in the department for their support; in particular to Yahya Salem and Fathi Ghrouda for their discussions during this study.

I would like to take this opportunity to thank my parents, my wife, my son Ahmed, and my daughter Ibtehal for their patience, moral, understanding, and support.

Page

Page

Page

Page

List of Figures

Chapter 1

Chapter 2

Page

Page

Page

Page

Page

Page

Page

Page

Page

Chapter 5

Page

Page

Page

Page

Page

List of Tables

Page

Appendix 2.1

Appendix 4.4

Appendix 5.1

Summary

The Zelten field was discovered in 1959. The first well was drilled by ESSO Standard Libya. More than 178 wells have since been drilled, most of them into the reservoir (the Zelten member). The last few wells have been drilled by Sirte Oil Company who are now the owners of the field.

Part of the aim of the study was to look at a 'reef' or velocity anomaly which had been drilled, and to see whether it is purely a geophysical artefact, or whether it is a real geological feature..

A velocity study was made for the nine wells in the area which have velocity surveys. More than 150 velocity analysis tabulations available from 17 seismic lines were studied. Time and velocity - depth curves, rms velocity plots, Dix average velocity plots, and rms iso-velocity contour maps have been produced. Statistical work has been carried out on the velocity study, to demonstrate relationships between some of the parameters.

Seventeen seismic lines (Vibroseis data), covering an area of 350 km^2, have been chosen from 1984/85 seismic survey for the re-interpretation. Three horizons that are of interest have been chosen and correlated, namely the Sheghega, Domran, and Ruaga horizons. Two-way time, velocity, and depth contour maps have been produced. Most of them have been produced using automated contouring, but three of two-way time maps have been produced using hand contouring.

A static correction study has been carried out on a part of the seismic line where some uphole data has been provided. New seismic processing software (SierraSEIS) available in the department was used, making the reprocessing more easier and more convenient. Nine kilometres of the seismic reflection data across a seismic reflection anomaly from line 6V256-85 were reprocessed. Some Fortran77 programs were written to handle the data to make the study more convenient and faster.

It was concluded that the discontinuity of the reflectors underneath the anomaly is due to the distortion of the raypaths of the near traces by shallow features.

CHAPTER (1)

INTRODUCTION

1.1 *Exploration history*

The search for oil in Libya began in 1953, and by 1958 a few promising discoveries had been made. The Sirte Basin, with an onshore area of approximately 375,000 km^2, contains 14 giant oil and gas fields. The first such giant is the Zelten field (Fig.1.1).

The spectacular Zelten field in the Sirte Basin, discovered in 1959, is found in reefal occurrences in the Fogha Group. The first well, C1-6, was drilled in March 1959 by ESSO Standard Libya Company, and showed a potential reservoir in the highly porous Zelten Member. This well was followed by a succession of others.

More than 178 exploration and outpost wells have been drilled in Zelten field area. Over 150 oil production wells have been drilled into the reservoir (Zelten Member). Some of the other wells are dry, and some injection wells were drilled. A few wells have been drilled into the Gargaf formation (Cambro-Ordovician age), the others to the Zelten Member ("the main pay") of the Ruaga Formation.

The last few wells have been drilled by Sirte Oil Company, now the owners of the Zelten field. The last two wells, GGGG1-6 and KKKK1-6, were drilled on a seismic anomaly interpreted as a Palaeocene pinnacle reef. However, data from the two wells do not show the presence of a reef. It is this problem that forms the subject of study.

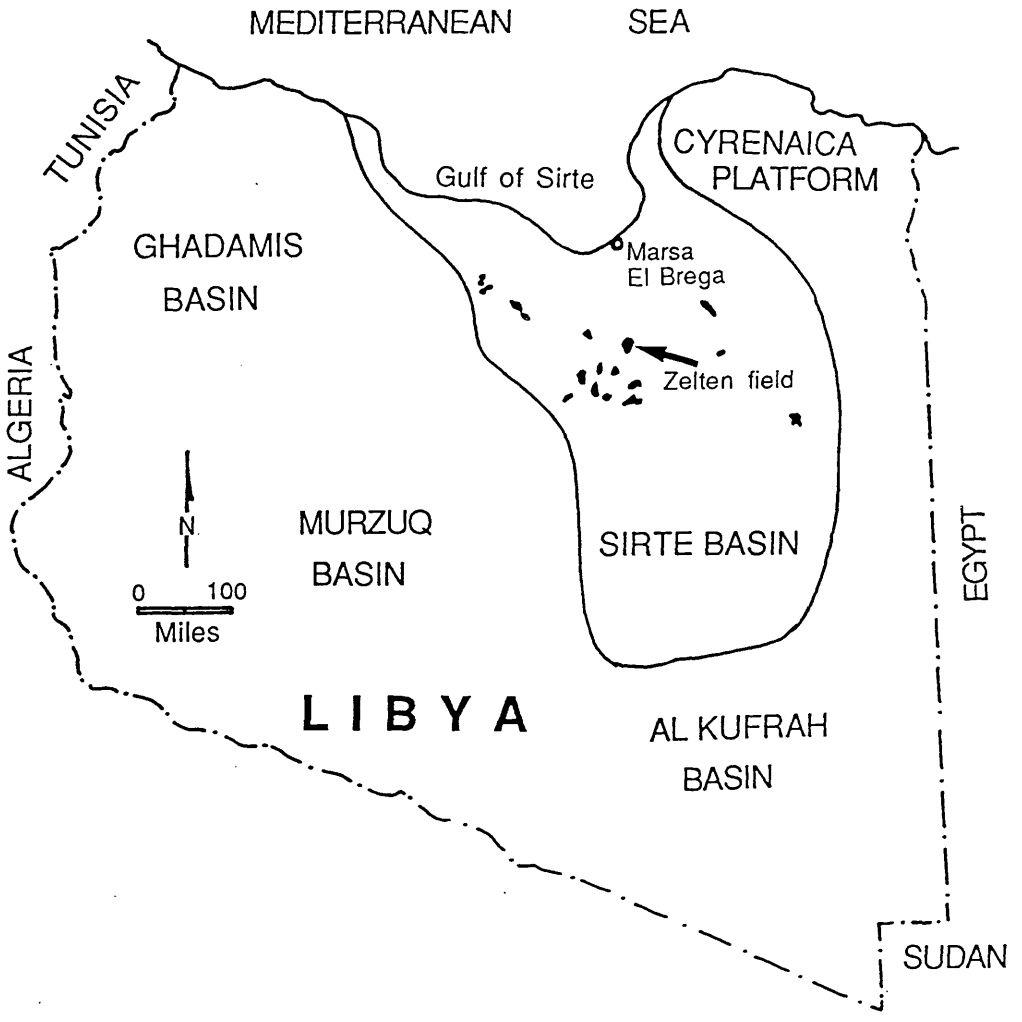

Fig. 1.1 Location of Sirte Basin, and other main basins in Libya, showing Zelten and other giants fields in Sirte Basin, (after Bebout and Pendexter, 1975).

1.2 *Field location*

The Zelten field is located approximately 160 km south of the Mediterranean coast in the centre of the Cretaceous-Tertiary Sirte Basin of Libya, in Concession 6 between 28° - 29° N and 19° - 20° E. It lies south of the coastal town of Marsa El Brega, (Fig.1.2) owned by Sirte Oil Company.

1.3 *Geological history*

All basins contain some source rocks, some reservoir and cap rocks. Sedimentary basin development begins with a major transgressive phase and ends with a major regressive phase. Trangressions and regressions thus represent important events in basin evolution (Ala 1985).

Over 50% of Libya's oil reserves occur in strata of Cretaceous age. The producing sediments are associated with Sirte Basin shore lines of the initial Cretaceous transgression.

An excess of 8 km of predominantly marine late Mesozoic and Tertiary sediments have accumulated in the deeper segments of the basin. Although Palaeozoic deposition was generally widespread across the Northern portion of the African continent, within the Sirte Basin only a meagre record of that era remains after the erosion, following the Hercynian orogeny.

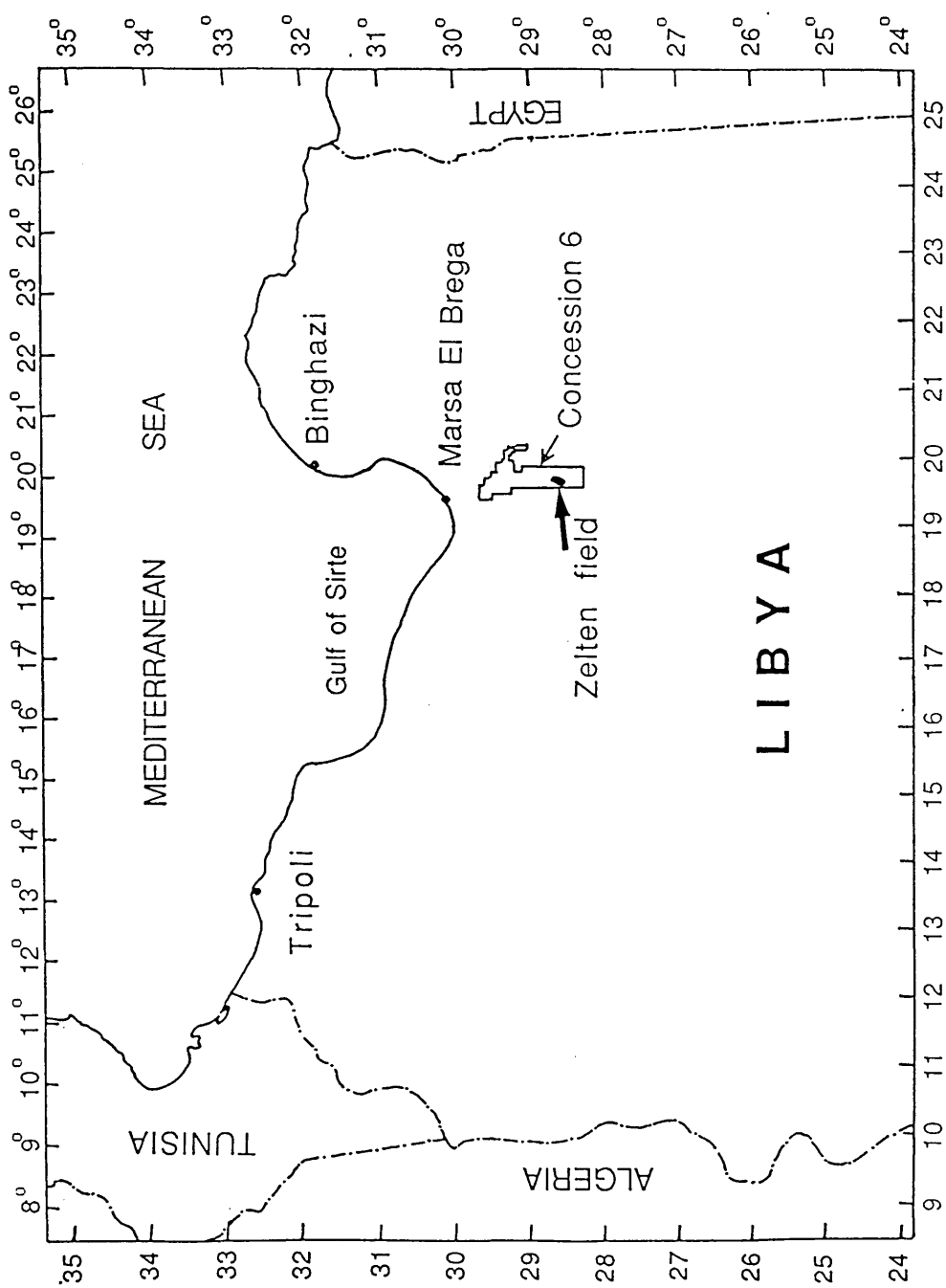

Fig. 1.2 Location of Concession 6 and Zelten field.

Five major crustal upwarps, the Nafusah and Al-Gargaf in Western Libya, the Tibisti in Southern Libya, and the Sirte and Kalanshiyu arches of Central and Eastern Libya became strong positive features by end of this orogeny. During the early Cenomanian the Sirte Basin developed structurally. At this time there occurred a collapse of the Sirte and Tibisti arches. The major faults and other structural elements of the basin were either initiated or strongly rejuvenated during this collapse, and a series of tilted horsts and grabens developed. They generally trend northwest to southeast, or east to west. The largest of these grabens is the Sirte Basin trough (Fig.1.3) (Gumati and Kanes 1985).

Deposits accumulated in six large basins between Algeria and Arabian-Nubian shield during a major regression in Latest Jurassic and Early Cretaceous time (Van Houten 1980) (Fig. 1.4).

The locations of the Ghadames (Northwestern Libya and adjacent Tunisia and Algeria) basins, Sirte (North - Central Libya) basins, Northern (Egypt) basins, Murzuk (Southwestern Libya Northern Chad) basins, Kufrah (Southeastern Libya and nearby Sudan) basins, and Southern (Egypt) basins (Van Houten 1980) are also shown in Figure (1.4).

The Late Cretaceous and Early Tertiary rocks contain large accumulations of hydrocarbons, which have been the target for the numerous exploration oil wells drilled in the region.

Marine rocks of Late Cretaceous age, chiefly carbonates, are present in most of Northern Libya. In the Sirte embayment, rocks of Late Cretaceous

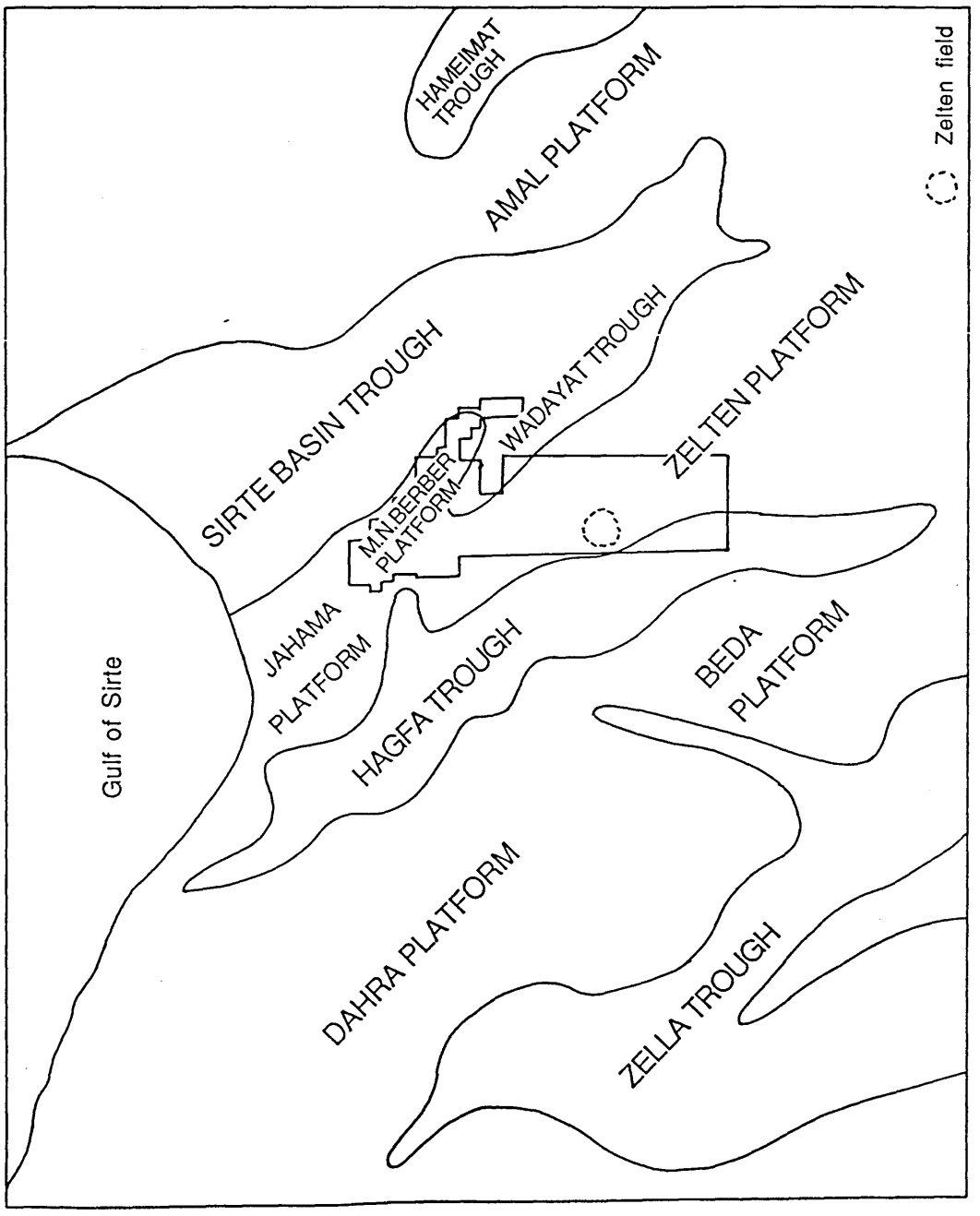

Fig. 1.3 Upper Cretaceous structural setting of central Sirte Basin, (after Calbick and Smith, 1967).

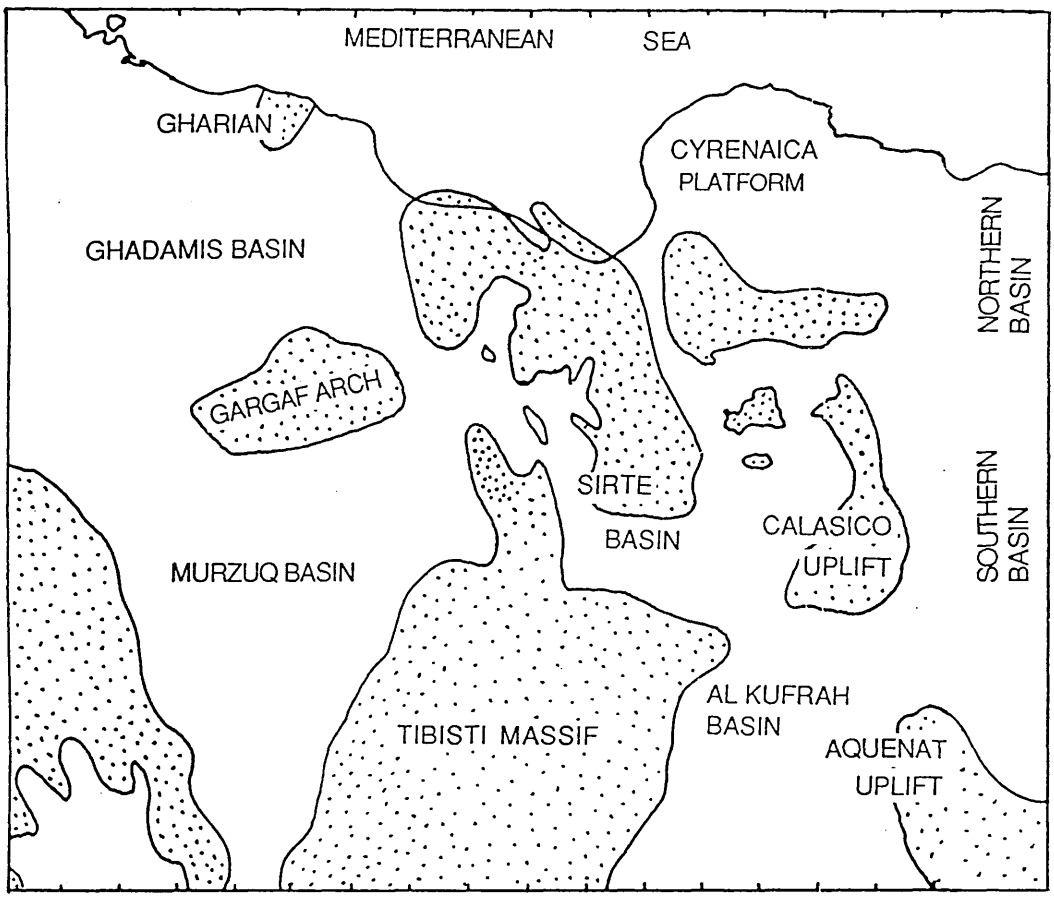

Fig. 1.4 Regressive deposits in Latest Jurassic-Early Cretaceous, (after Franklyn B. Van Houten, 1980).

age are much more varied, as a result of the block faulting (Conant and Goudarzi 1967).

Rocks of Tertiary age, chiefly carbonates, are widespread in northern Libya and in the northeast, from long high escarpments. In the Sirte embayment the strata are much more varied, especially in the subsurface. In the deepest part of the embayment, extending south - southeast from the head of the Gulf of Sirte. (Conant and Goudarzi 1967).

1.4 *Geological setting*

The complex structural pattern of horsts and grabens in the Sirte Basin began forming in the Late Jurassic-Early Cretaceous, and continued to develop until at least the Miocene and probably to the Holocene (Selley 1968, Gumati and Kanes 1985). During this time, widespread subsidence and continental sedimentation of the Nubian Sandstone occurred in the southeastern and southwestern Sirte Basin (Gumati and Kanes 1985).

Cretaceous block faulting divided the Sirte Basin into a series of northwest-southeast trending ridges and troughs (Bebout and Pendexter 1975). A major marine transgression in Palaeocene and Eocene times extended southward from the main basin into a deep embayment (Benfield and Wright 1978), and seemingly ended in the Early Palaeocene. The following regressive sequence culminated with the Zelten Member, and the overlying Meghil Member was deposited at the beginning of the next major transgression (Bebout and Pendexter 1975).

The pre-existing Cretaceous structures are still evident in the Tertiary, however, because shallow water carbonate materials were deposited on the buried highs, and deeper water carbonate materials in the troughs (Bebout and Pendexter 1975).

1.5 *Structure*

The Sirte embayment, commonly termed the Sirte Basin, is a complex block-faulted and downwarped structure and it is the youngest of the basins mentioned above. Block faulting started in Late Cretaceous time and continued until the present (Conant and Goudarzi 1967).

Structurally, the Sirte Basin is mainly affected by rift-type faults (according to the Klemme (1980) classification of the basins), which decrease in throw to the south (Benfield and Wright 1978). It is a cratonic rift, resulting from a Suez-type crustal extension of an old eroded basement and Palaeozoic uplift, extending to the south to the Al-Kufrah basin and, via a major marine embayment in Eocene time, to the Tibisti massif.

Concentrations of oil and gas in commercially significant quantities (fields) occur in sedimentary basins. Sedimentation within the basin has continued at varying rates from its initiation in the Late Cretaceous until the Quarternary (Benfield and Wright 1978) which has given a thick sedimentary section. This thick sedimentary section makes the basin a favourable environment for the formation, migration and entrapment of oil and gas (Ala 1985).

Early sedimentation was highly differentiated, with deposition of large quantities of organic-rich shales in the grabens, and with carbonates on the horsts , but as transgression continued, Cretaceous sedimentation became more uniformly argillaceous (El-Hawat 1978).

Shallow water carbonate sediments within the Heira Shale (Mabruk, Ora, and Meem Members) accumulated on some of the ridges, such as the Zelten ridge, until Late Palaeocene and Early Eocene (Zelten and Meghil Members of the Ruaga), when Carbonate sedimentation spread over the entire basin (Bebout and Pendexter 1975). The thick rich coloured shale which is present in the grabens is believed to be an important source of oil and gas, and the carbonates (limestone, dolomite, and calcarenite) on the horsts serve as oil and gas reservoirs (Conant and Goudarzi 1967).

1.6 *Field Geology*

A general description of geology of the Zelten field from the local columnar section (Fig.1.5) is as follows:

1.6.1 The Gehenna Group sediments are Oligocene in age, divided into two rock units, the Muailah and Etel Formations. The upper unit, the Muailah Formation, is a sandstone, limestone and siltstone in lithology. The lower unit, the Etel Formation, is a calcareous shale formation some times describe as a dolomitic shale.

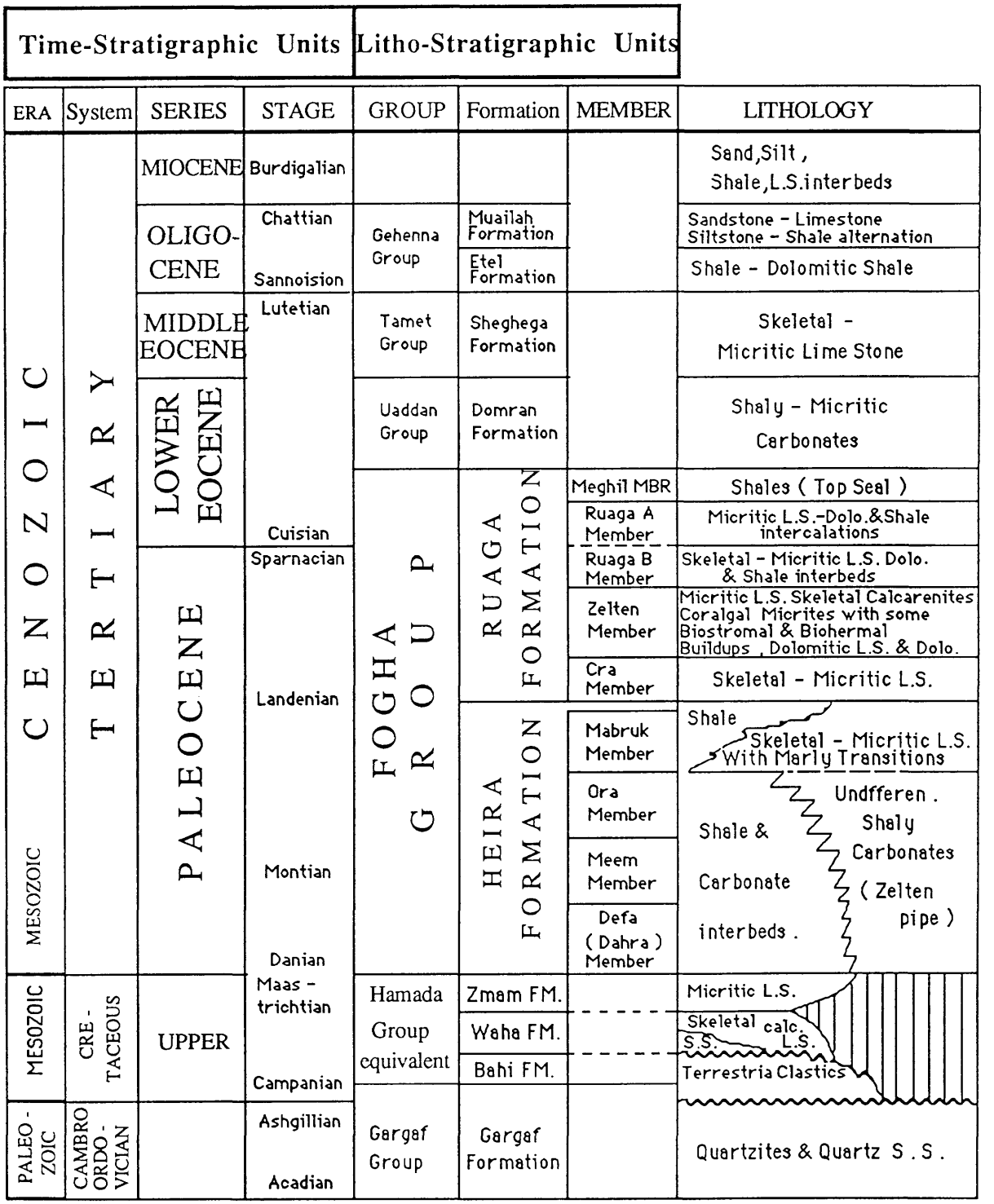

Fig.1.5. Local columnar section for Zelten field (LIBYA) (modified after Sirte Oil Company internal report).

1.6.2 The Tamet Group sediments are Middle Eocene in age. It has one rock unit, the Sheghega Formation, described as a skeletal micritic limestone.

1.6.3 The Uaddan Group sediments are Lower Eocene in age. It has one rock unit, the Domran Formation, a shaly-micritic carbonate.

1.6.4 The Fogaha Group sediments are Lower Eocene and Palaeocene in age. However, all the potential plays are in the Palaeocene.

The Fogaha Group is divided into two rock units, the Ruaga and Heira Formations.

The uppermost unit, the Ruaga Formation, consists of three Members:

(1) The Meghil Shale Member which forms the cap rock for the Zelten reservoir. Within this Member two porous limestone horizons, known as the Ruaga"A" and the Ruaga"B", are developed over the Zelten field.

(2) The Zelten Member, a porous reefal complex which is the main pay in the Zelten field area. Dolomite in the lower part of Zelten Member ranges in thickness from zero in the northern part of the field to more then 80 m, 8 km south of the field.

(3) The Cra Member, a tight Limestone.

The lower unit is the Heira Formation, a shaly formation. Over much of the Sirte Basin it contains the following carbonate members:

(1) The Mabruk member.

(2) The Ora member.

(3) The Meem member.

These members of the Heira Formation contain small oil accumulation within structural traps over a broad area in the Sirte Basin.

The Zelten Member ("main pay") of Ruaga Formation and underlying Heira Shale are considered by Esso Libya geologists to be Palaeocene, the overlying Member, the Meghil, is dated as Early Eocene (Bebout and Pendexter 1975).

1.6.6 The sediments equivalent to the Hamada Group in Western Libya, are of Upper Cretaceous age. This Group is divided into three rock units, the Zmam, Waha and Bahi Formations.

The upper unit, the Zmam Formation, is a micritic limestone in lithology. The middle unit, the Waha Formation in the south and southeast of the Zelten field, is a sandstone and skeletal calcareous limestone in the southeast and calcareous limestone in the south. The lower unit, The Bahi Formation, is a terrestrial clastic sediment in the south and in the southeast.

1.6.7 The underlying Gargaf Group sediments are partly Cambro-Ordovician in age, containing the Gargaf Formation which is quartzite and quartzitic sandstone. Until recently, the whole formation was considered to be of Cambro-Ordovician age. However, the study of core samples from

wells in the Sirte Basin revealed that this formation is of Cretaceous age in its upper part and of Cambro-Ordovician in age in its lower part (Bonnefous 1972).

The absence of Upper Palaeozoic and Mesozoic sediments suggests that the area was domed, faulted, and eroded during the Late Mesozoic (Gumati and Kanes 1985).

Below the Gargaf Group is the basement. Most of the exposed basement rocks are certainly of Pre-Cambrian age, but recent K-Ar dating indicates that some of the buried granites in the floor of Sirte embayment may be of Early Palaeozoic age, coeval with the pan-African orogeny.

1.7 *Aims of the study*

1.7.1 *Data available*

In the area of study the following data are available for this project:

(1) Seventeen reflection seismic sections from lines, totalling 314 km of 48-fold Vibroseis data acquired in the same seismic survey in 1984/85 (Figure 1.6).

(2) Geological and geophysical reports for wells C114, C59, C85, VV1, and YYY1, containing the formation tops and corresponding times.

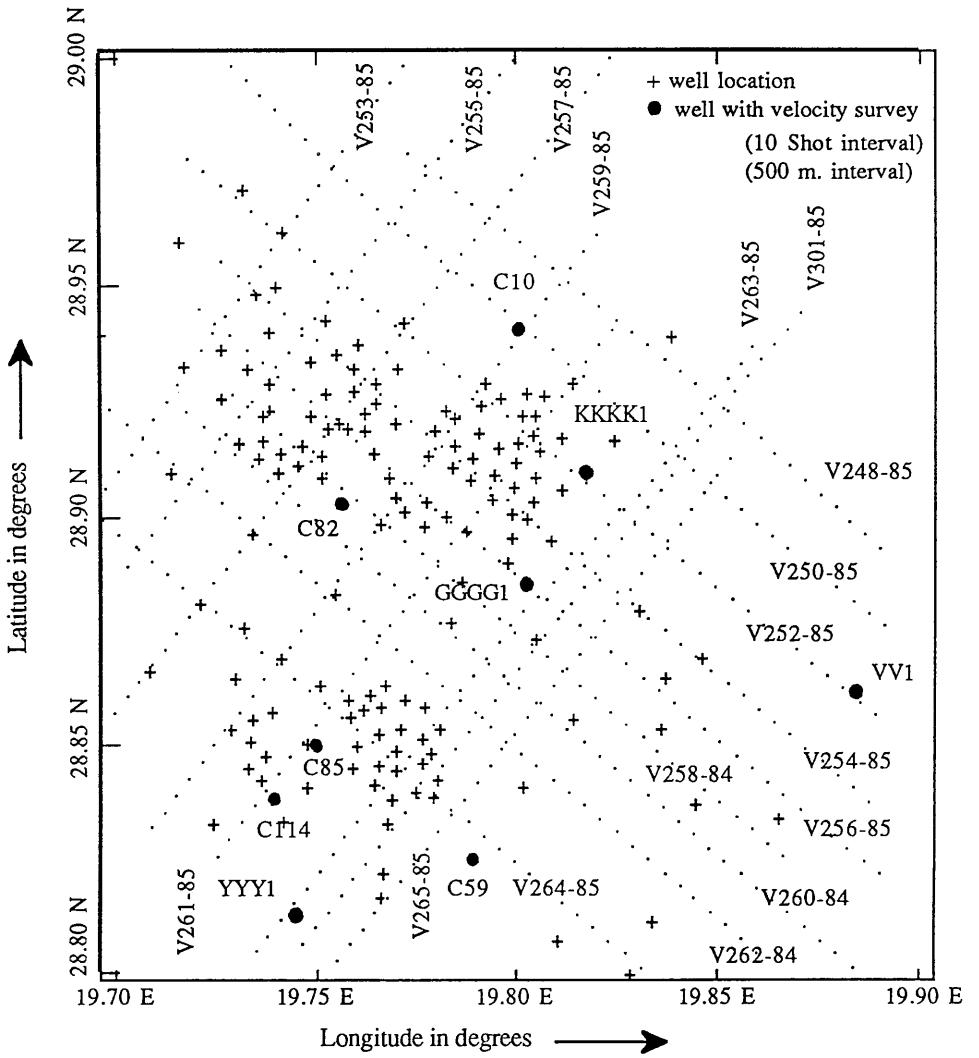

Fig. 1.6 Shot point location map showing well locations.

(3) Velocity survey logs for wells C114, C85, C59, C10, and YYY1.

(4) Checkshot survey records for old wells C59, C82, C85, and YYY1, and for recent wells GGGG1 and KKKK1.

(5) Completion logs for wells C82, C45, C1, C10, C85, C114, and C8.

(6) Company data base of formation tops in the Zelten field area for 170 wells shown in Figure 1.6.

(7) Demultiplexed data on magnetic tapes for seismic line 6V265-85, covering shot points 200 to 379.

(8) Copy of the field documents for seismic line 6V265-85.

(9) Uphole data available for stations 147, 234, 298, 317, 379, and 505 on seismic line 6V265-85.

(10) Some geological internal reports.

1.7.2 *The seismic anomaly*

The presence of the seismic anomaly appears in seismic line 6V256-58 at shot point 310 in the Heira formation (see Chapter 4, Fig.4.5f). It was interpreted as a Palaeocence pinnacle reef, before the drilling of well GGGG1-6 on the location of the seismic anomaly. The well does not prove the presence of a reef, but produces oil from the Mabruk limestone, which

has not been tested before. Suringa (1988) described the picking of the Mabruk as somewhat questionable, as it is parallel to the Ruaga formation. He also mentioned that the Mabruk map should be very similar to the map for the Ruaga formation.

1.7.3 *Aims*

The aim of the study is to investigate the reef anomaly, to see whether it is purely a geophysical artefact, or whether it is a real geological feature. The approach taken has been as follows, in approximate chronological order:

(1) Re-interpretation of the seismic lines, choosing three stratigraphic markers that are of interest, and producing maps of two-way times, velocity, and depth.

(2) Velocity study in the area, compiling average and interval velocities contour maps.

(3) Static correction comparison between the different kinds of statics on line 6V265-85 (s.p. 147 - 505).

(4) Reprocessing part of the seismic line 6V265-85 where the seismic anomaly appears, using different kinds of statics to see the effect of the static problem.

CHAPTER (2)

VELOCITY MEASUREMENTS

2.1 *Introduction*

The variation of velocity as a function of depth is an important parameter in the interpretation of seismic data. A knowledge of velocities is necessary to the geophysicist and interpreter for several purposes:

(1) For normal-move out corrections and migration.
(2) To convert reflection times to depth.
(3) To help to identify lithology and zones of over-pressured shale.

Shooting a well for velocity gives good estimates of the gross velocity layering. Most of the contractors now provide a tool to get fine velocity detail by producing a continuous velocity log.

Nine of the wells in the area of study have data for velocity study, as shown in Figure 1.6 (Chapter 1) marked by star spots. Velocity surveys in these wells were obtained with different kinds of shooting techniques; some were shot in early and mid sixties using explosives (dynamite), the others in 1989 using air guns or vibrators as a source.

As will be shown below, the well velocity information is essential to tie and correlate horizons to the seismic reflection data.

2.2 *Well shooting*

It is useful for the interpreter to have well surveys available in the area, to give a good correlation between the seismic reflections and lithology

and the boundaries of the formation. Shooting a well involves measurements of travel time of seismic wave from sources at or near the surface to a receiver located at various depths in the well. To obtain vertical travel times, the measurements must be corrected for angularity, as shown for an old dynamite survey in Figure 2.1. Because the source must necessarily be offset from the well bore, well shooting gives good estimates of the gross velocity layering (Al-Chalabi, 1974).

2.3 *Continuous velocity logs*

The invention of the continuous velocity log (CVL) by Summers and Broding (1952) provided, for the first time, the fine detail of velocity layering. This type of log is also a very good correlation tool.

Figure 2.2 is a schematic of the logging tool, which consists of an acoustic transmitter as a source S. This is usually an electro-mechanical device that produces pressure pulses transmitted through the borehole fluid to the wall of the hole.

The energy is transmitted by a refraction path to two pressure detectors R1 and R2, with acoustic insulators separating the two elements by a known fixed distance. The difference in travel time is measured electronically.

Fig.2.1. Schematic cross-section of well velocity survey.

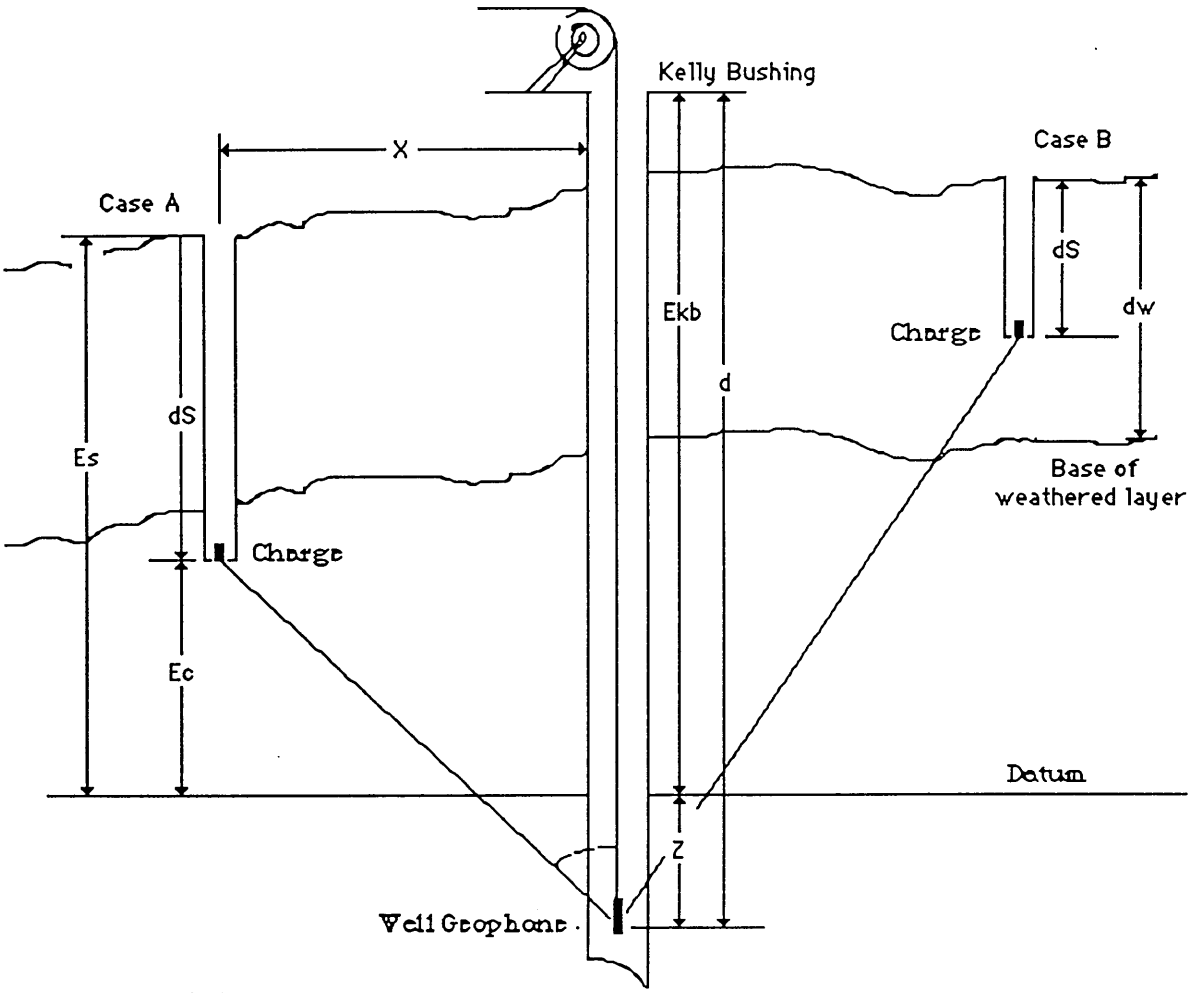

Abbreviations:

K.B.	=Kelly bushing.	VT	=Uphole time.
d	=Depth of well geophone below K.B.	ds	=Depth of shot.
Ekb	=Elevation of K.B. above datum.	Ve	=Elevation velocity.
Z	=Depth of geophone below datum.	Δt	=Interval distance.
Es	=Elevation of shot point above datum.	Δtc	=Interval travel time.
Ec	=Elevation of charge above datum.	dw	=Depth of weathering layer.
β	=Incident angle at well geophone levels.		
x	=Horizontal distance from well to shot point.		
t	=Observed travel time for charge to well geophone.		
tc	$= (t \cos \beta) - te$ (Corrected travel time).		

Va $= \left(\frac{Z}{tc}\right)$ (Average velocity). Vi $= \left(\frac{\Delta t}{\Delta tc}\right)$ (Interval velocity).

$$te = \begin{cases} \left(\frac{Ec}{Ve}\right) & \text{for case A} \\ \left[\left(\frac{dw - ds}{Vw}\right) + \left(\frac{Es - dw}{Ve}\right)\right] & \text{for case B} \end{cases}$$

Fig. 2.2. Schematic diagram of sonic logging tool.

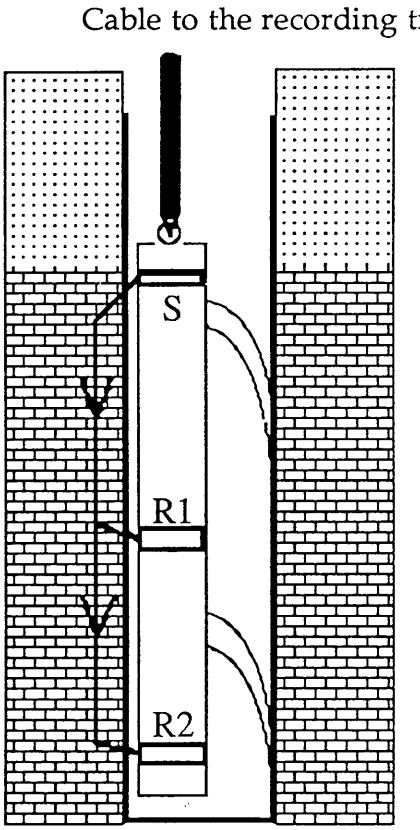

From the high pulse repetition rate relative to the tool being slowly pulled up the hole, the set of measurements produces essentially a continuous measure of transit time (Al-Chalabi 1974, Waters 1978). These velocities appear to be reasonably representative of the velocities of seismic waves through the corresponding formation except when (Waters, 1978):

(1) There is invasion of a porous formation by drilling fluid.

(2) The hole diameter is very large or irregular.

(3) The formation velocity is lower than the P-wave velocity through the drilling fluid.

2.4 *Velocity surveys*

In the area of study, where different kinds of survey have been used, an explosive technique of shooting (dynamite) was used in the early and mid-sixties. Figures 2.3, 2.4, 2.5, and 2.6 show the geophone plans and the seismic velocity survey for wells C85, C82, C59, and YYY1 respectively. These shot-holes were drilled, loaded, and surveyed by Esso Standard Libya Inc. In a recent survey, as shown in Figures 2.7, and 2.8 for wells GGGG1, and KKKK1, air guns and vibrators were used as a source, respectively.

In the old survey as shown in Figures 2.3, 2.4, 2.5, and 2.6 for wells C85, C82, C59, and YYY1 respectively. A number of shot-holes were drilled at different locations to different depths, depending on the amount of charge and depth of the test level. The amount of charge was increased as the depth in the shot-hole increased to give enough penetration for the wave to reach to the recording depth. They recorded 12, 11, 12, and 10 different levels in the wells, respectively. The deepest level tested was at 2438, 2423, 2217, and 3831 m. respectively. There were a number of reference geophones on the surface, at the well head, and at different distances away from the well.

In a recent survey for well GGGG1-6 (Figure 2.7), an air gun was used as a source, by making a hole beside the well filled with water, into which the source gun is lowered. The tool is moved down to the deepest level and recording is started. Then the tool is moved up to the next level for recording, and so on.

Fig.2.3. Shothole and geophone plan for well C85-6.

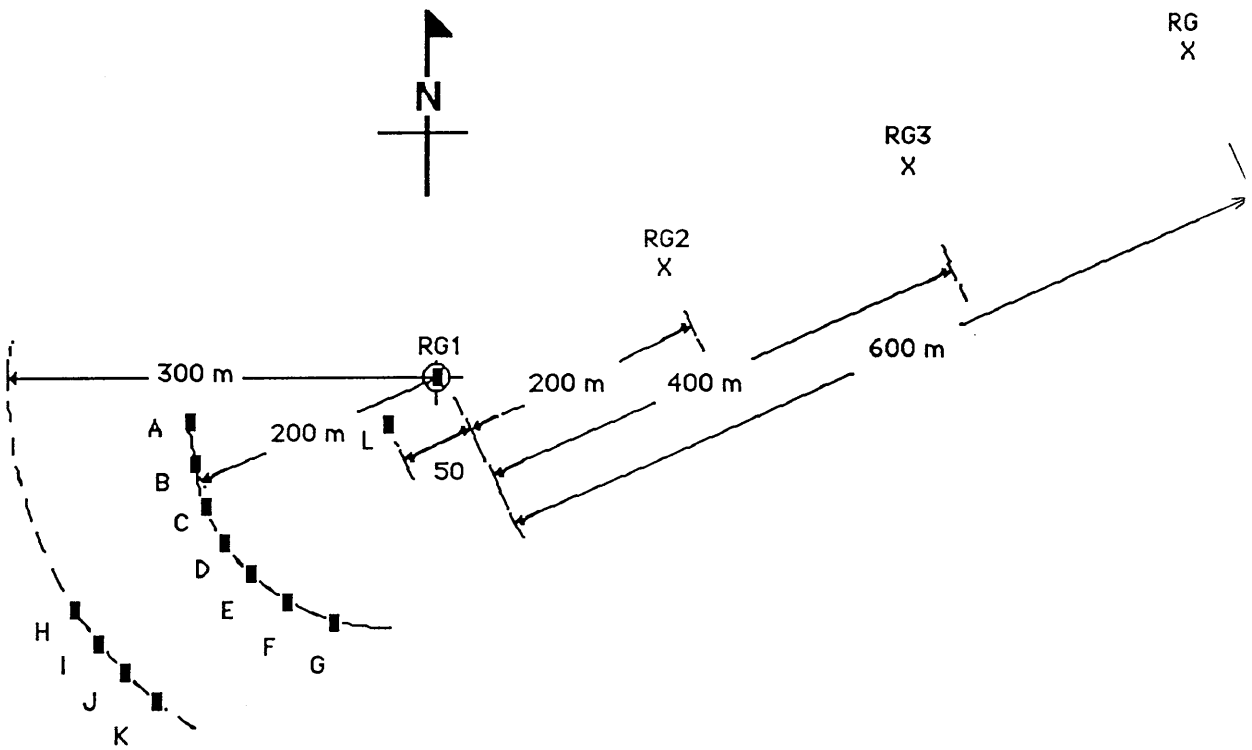

Reference geophones at well head, 200 m, 400 m, and 600 m ENE of well.

Seismic velocity survey for well C85-6:

		First run (15/5/66)	Second run (2/6/66)
(1)	Recording equipment	= ABV/ABD/BER 62	
(2)	Well geophone type	= GCE 101	
(3)	Elevation datum	= sea level.	
(4)	Levels tested	= 3	9
(5)	Deepest level tested	= 668 m.	2438 m.
(6)	Well geophone records	= 3	9
(7)	Normal shothole depth	= 9-18 m.	18-30 m.
(8)	Range of charges	= 10-40 lbs	40-100 lbs.
(9)	Total explosive used	= 70 lbs	760 lbs.
(10)	Total detonators used	= 6	18
(11)	Number of shotholes drilled	= 12	

(12) Shotholes drilled, loaded, and surveying by ESSO Standard Libya Inc.

Remark:

Surface velocity = 1646 m /s.

Fig.2.4. Shothole and geophone plane for well C82-6.

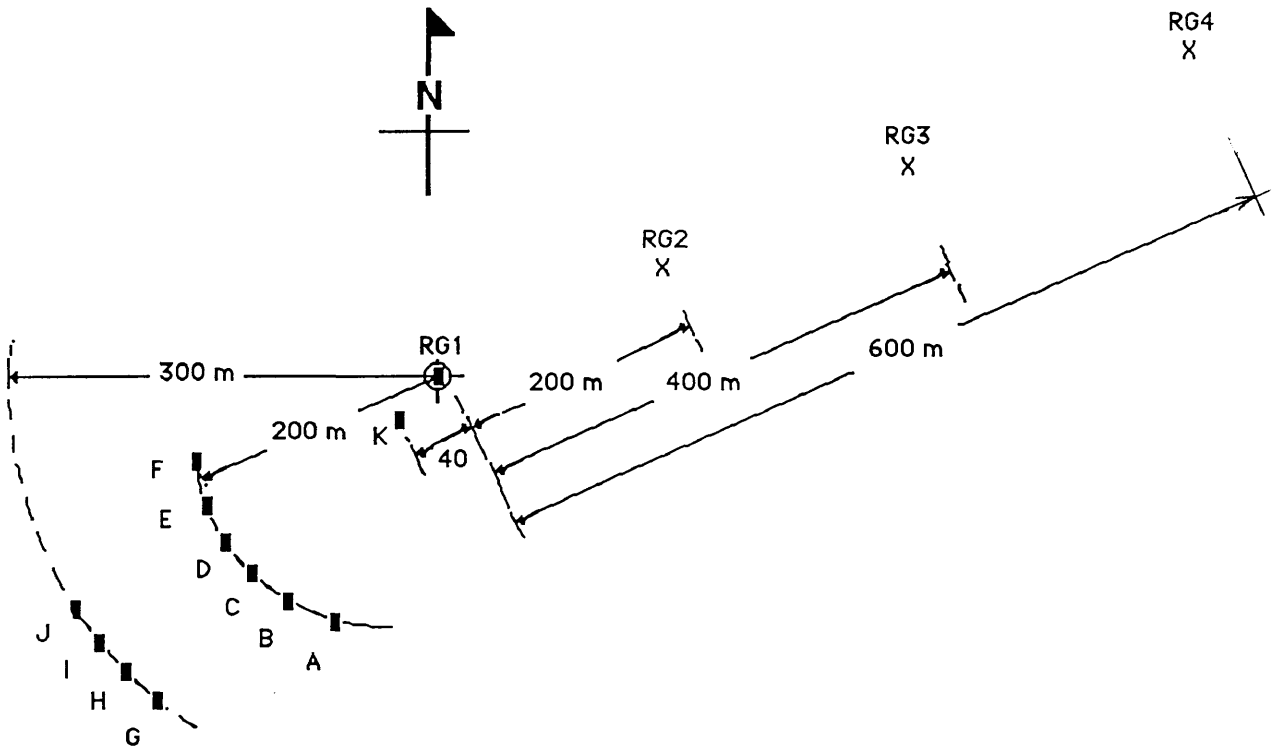

Reference geophones at well head, 200 m, 400 m, and 600 m ENE of well.

Seismic velocity survey for well C82-6:

		First run (15/5/66) Second run (2/6/66)			
(1)	Recording equipment	=ABV/ABD/BER 62			
(2)	Well geophone type	=GCE 101 for run 1 =GCH for runs 2 and 3.			
(3)	Elevation datum	=sea level.			
(4)	Levels tested	= 11			
(5)	Deepest level tested	= 2423 m.			
(6)	Well geophone records	= 11			
(7)	Normal shothole depth	= 30 m.	24 m.	18 m.	12 m.
(8)	Range of charges	= 100 lbs.	to	10 lbs.	
(9)	Total explosive used	= 730 lbs.			
(10)	Total detonators used	= 11			
(11)	Number of shotholes drilled	= 12			

(12) Shotholes drilled, loaded, and surveying by ESSO Standard Libya Inc.

Remark:

Surface velocity = 1475 m /s.

Fig.2.5. Shothole and geophone plan for well C59-6.

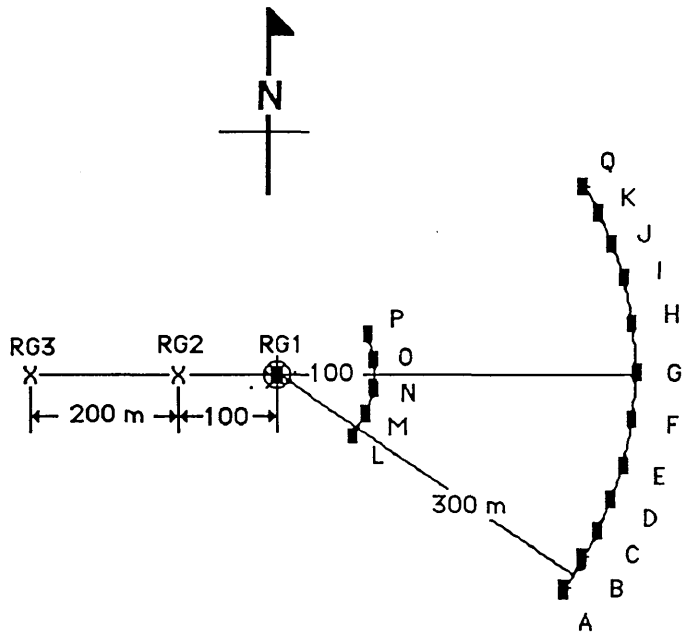

Reference geophones at well head, 100 m and 300 m west of well.

Seismic velocity survey for well C59-6:

		First run (22/12/63)	Second run (15/1/64)
(1)	Recording equipment	=ABV/ABD/BER 62	
(2)	Well geophone type	=GCE 101	
(3)	Elevation datum	=sea level.	
(4)	Levels tested	= 9	4
(5)	Deepest level tested	= 1788 m.	2217 m.
(6)	Well geophone records	= 9	5
(7)	Normal shothole depth	= 12 m.	24 m.
(8)	Range of charges	= 20-60 lbs.	60-80 lbs.
(9)	Total explosive used	= 320 lbs	440 lbs.
(10)	Total detonators used	= 9	6
(11)	Number of shotholes drilled	= 17	

(12) Shotholes drilled, loaded, and surveying by ESSO Standard Libya Inc.

Fig.2.6. Well shot holes reflection spread for well YYY1-6.

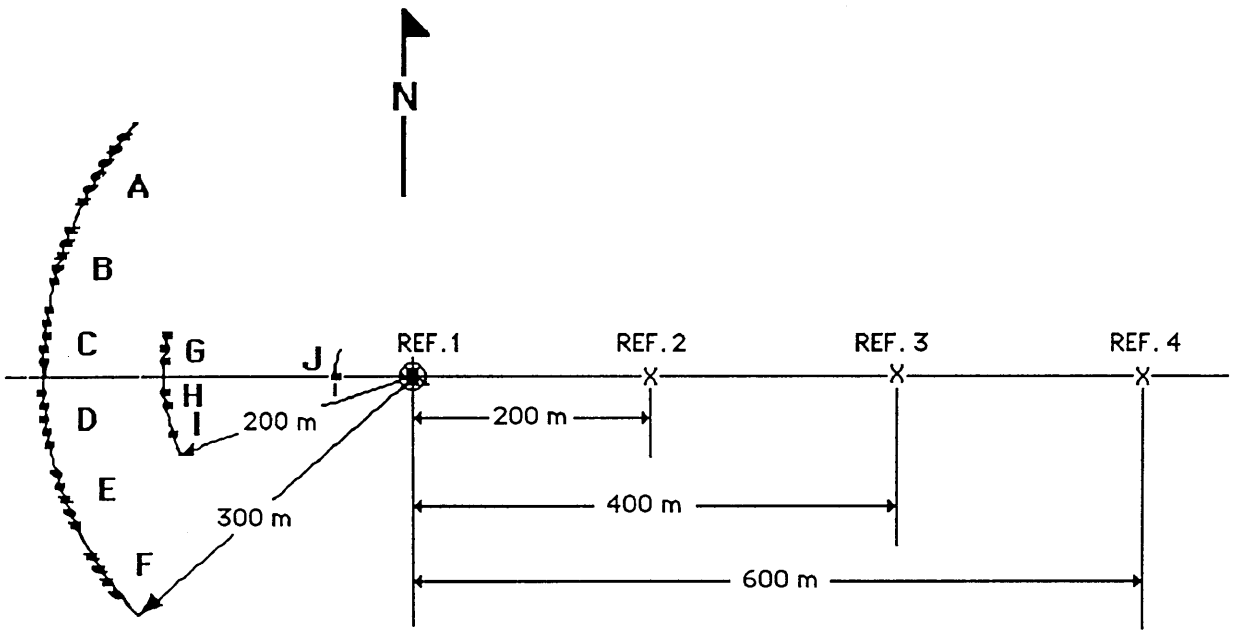

Reference geophones at well head, 200 m, 400 m, and 600 m east of well.

Seismic velocity survey for well YYY1-6:

		First run	Second run
(1)	Recording equipment	=	
(2)	Well geophone type	=	
(3)	Elevation datum	=sea level.	
(4)	Levels tested	= 4	6
(5)	Deepest level tested	= 3831 m.	
(6)	Well geophone records	= 4	6
(7)	Normal shothole depth	= 6 m.	
(8)	Range of charges	= 15 lbs.	
(9)	Total explosive used	= 555 lbs.	
(10)	Total detonators used	=	
(11)	Number of shotholes drilled	= 37	

Remarks:

1	Surface velocity	= 1440 m /s.
2	Shot holes spacing	= 2 m.
3	Shot groups spacing	= 7 m.

Fig.2.7. Surface setup for check-shot survey for well GGGG1-6.

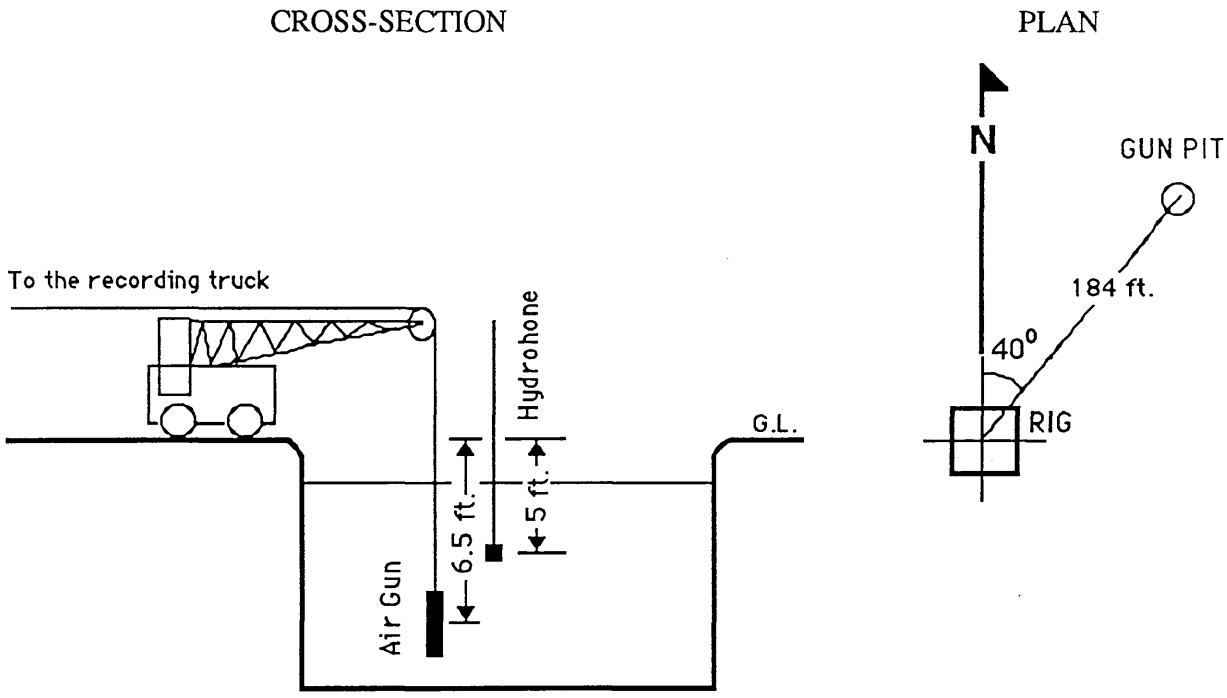

Seismic data:

1	SRD to ground level (G.L.)	= 156 m.
2	SRD to rotary table	= 163 m.
3	Gun depth below ground level	= 2 m.
4	Hydrophone depth below ground level	= 1.5 m.
5	Source offset distance	= 56 m.
6	Source offset azimuth	= 40 Deg.
7	Down-hole geophone type	= 4 HSI
8	Surface sensor type	= Geospace MP-8C.
9	Gun volume	= 200.
10	Source type	= Air gun.

Remarks:

1. Check-shot levels were selected by the client.
2. Check-shot at SRD was repeated at end of the survey for data quality control.
3. Client supplied surface velocity (2600 m/s).
4. Check-shot at some specified levels were not presented due to degraded data quality.
5. Lowest descent of tool was 2292 m. as a result, the deepest check-shot was at this depth.

As shown in Figure 2.8 for well KKKK1-6, a vibrator truck, was used as a source producing a sweep.

2.5 *Fortran programs*

There are three groups of data available from the wells. The first group of data comprises geological and geophysical reports by Sirte geologists for wells C114, C59, C85, VV1, and YYY1. The second group of data are velocity survey logs for wells C114, C85, C59, C10, and YYY1, and the third group of data are check-shot survey records for wells C59, C82, C85, YYY1, GGGG1 and KKKK1. These data contain information such as corrected time, with corresponding depth and formation depth. Fortran77 programs have been written by the author to handle the three groups separately, to calculate some parameters such as average velocity, interval velocity, and rms velocity at different formations or different levels of shooting. These two programs are CVL and CVL3. One or other of them is used according to what type of data is available as an input for the program to run. Listings of the source code for the two programs are given in Appendix 2.1.

2.5.1 *Program steps*

The CVL program handles the first group of data. The first step in this program is to read the names of the two input files and one output file, which is necessary for the program to run. The first input file contains some information such as company computer code, depth, and sub-surface time (recorded time), for 12 formations. The second input file contains some other information such as well name, latitude, longitude, kelly Bushing

Fig.2.8. Surface setup for check-shot survey for well KKKK1-6

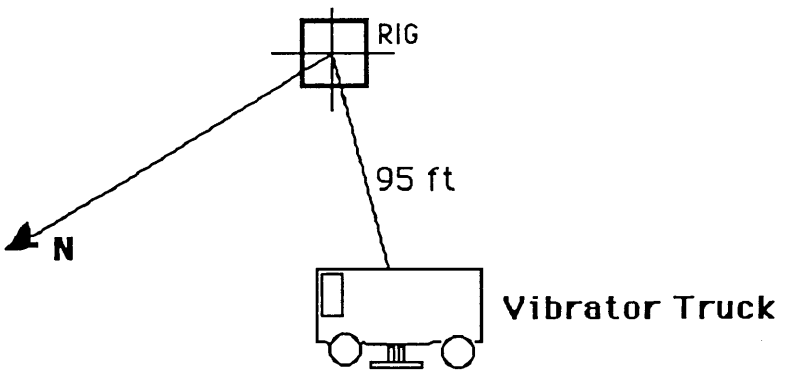

Remarks:

1	SRD	= 164 m.
2	Vibrator offset	= 29 m.
3	Vibrator azimuth	= 300 Deg.
4	Start/stop frequency	= 10-50 Hz.
5	Duration	= 12 s.
6	Taper	= 0.2 s.

elevation, one way static correction, and ground level, for the five wells available. A detailed flowchart corresponding to the above outline is shown in Figure 2.9.

The CVL3 program handles the second group of data. The first step in this program is to read the names of the one input file and one output file, which is necessary for the program to run. The first input file contains some information such as number of shots, and depth time pairs for the six wells available. A detailed flowchart corresponding to the above outline is shown in Figure 2.10.

2.5.2 *Program calculations and results*

The output file from the CVL program contains some information and calculated results such as company computer code, drilling depth, sub-surface depth, sub-surface time, sub-sea depth, sub-sea time, thickness, difference in time, interval velocity, average velocity, and rms velocity, as shown in Appendix 2.2.

The output file from the CVL3 program contains results such as depth, time, average velocity, and interval for each level of shooting.

Figures 2.11-2.15 show the average velocity, interval velocity, rms velocity, and two way time curves versus depth below datum plane (sea level), for wells C114, C59, C85, VV1, and YYY1 respectively, using the computer program CVL. Two-way travel time is used to facilitate comparison with seismic sections. The results are listed in Tables 2.1, 2.2, 2.3,

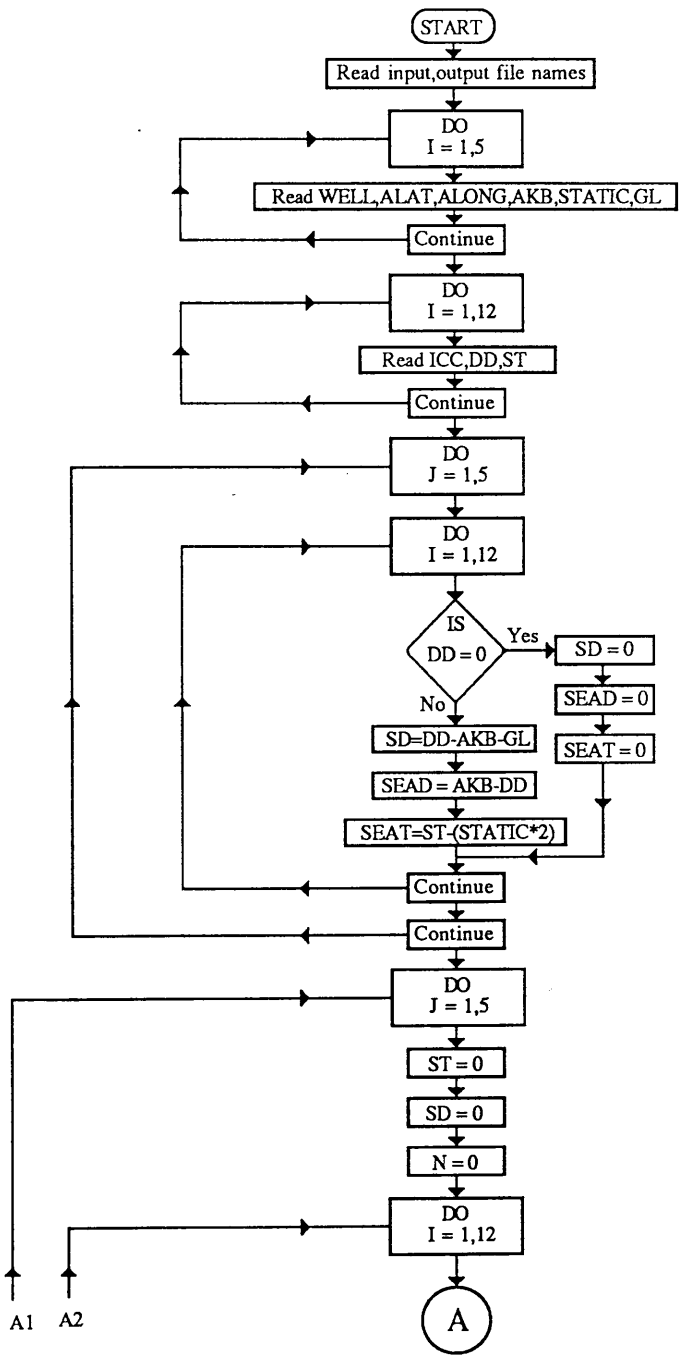

I - Counter for well data.
WELL - Well name.
ALAT - Latitude of the well.
ALONG - Longitude of the well.
AKB - Elevation of the kelly bushing.
STATIC - Static correction.
GL - Ground level elevation.

I - Counter for the formations.

ICC - Company computer code.
DD - Drilling depth.
ST - Time corresponding to the DD.

J - Counter for well data.

I - Counter for formation.

SD - Subsurface depth.

SEAD - Subsea depth.

SEAT - Subsea time.

J - Counter for the well data.

I - Counter for the formation.

Fig.2.9. Detailed flowchart for the CVL program.

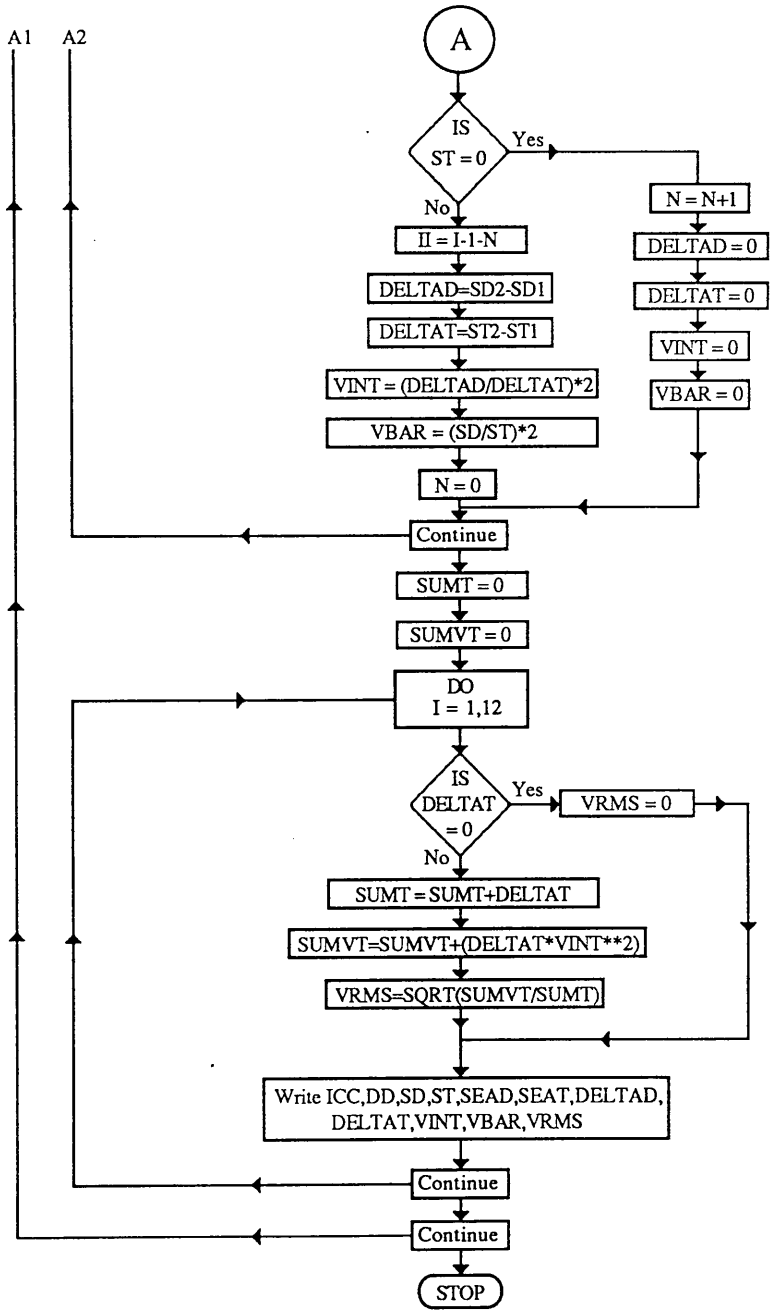

DELTAD - Difference in depth.

DELTAT - Difference in time.

VINT - Interval velocity.

VBAR - Average velocity.

SUMT - Summation of the interval time.

SUMVT - Summation of the product of the velocity and time.

I - Counter for formation.

VRMS - Root mean square velocity.
SQRT - Square root function.

Fig.2.9. (Continued) Detailed flowchart for the CVL program.

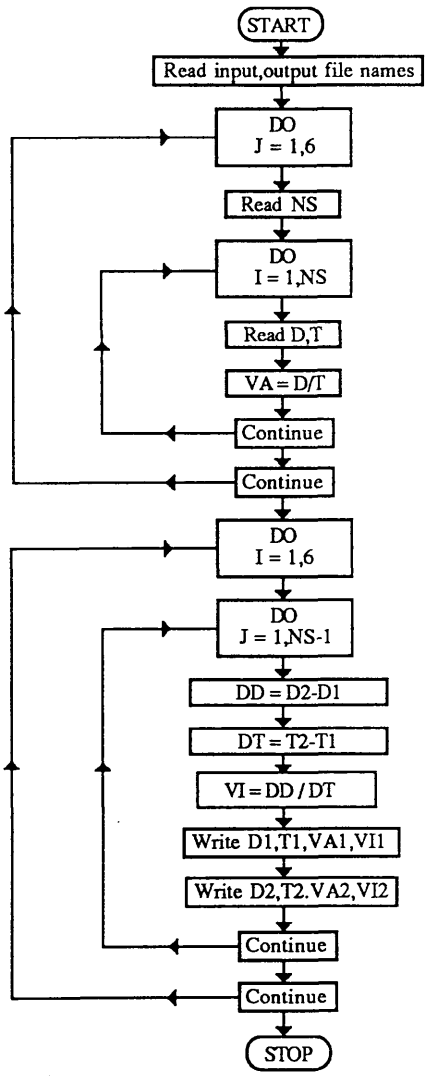

J - Counter for the well data.

NS - Number of picked levels.

I - Counter for the levels.

D - Depth of the corresponding level.
T - Time of the corresponding depth.
VA - Average velocity.

I - Counter for the well data.

J - Counter for the picked levels.

DD - Difference in depth.
DT - Difference in time.

VI - Interval velocity.

Fig.2.10. Detailed flowchart for the CVL 3 program.

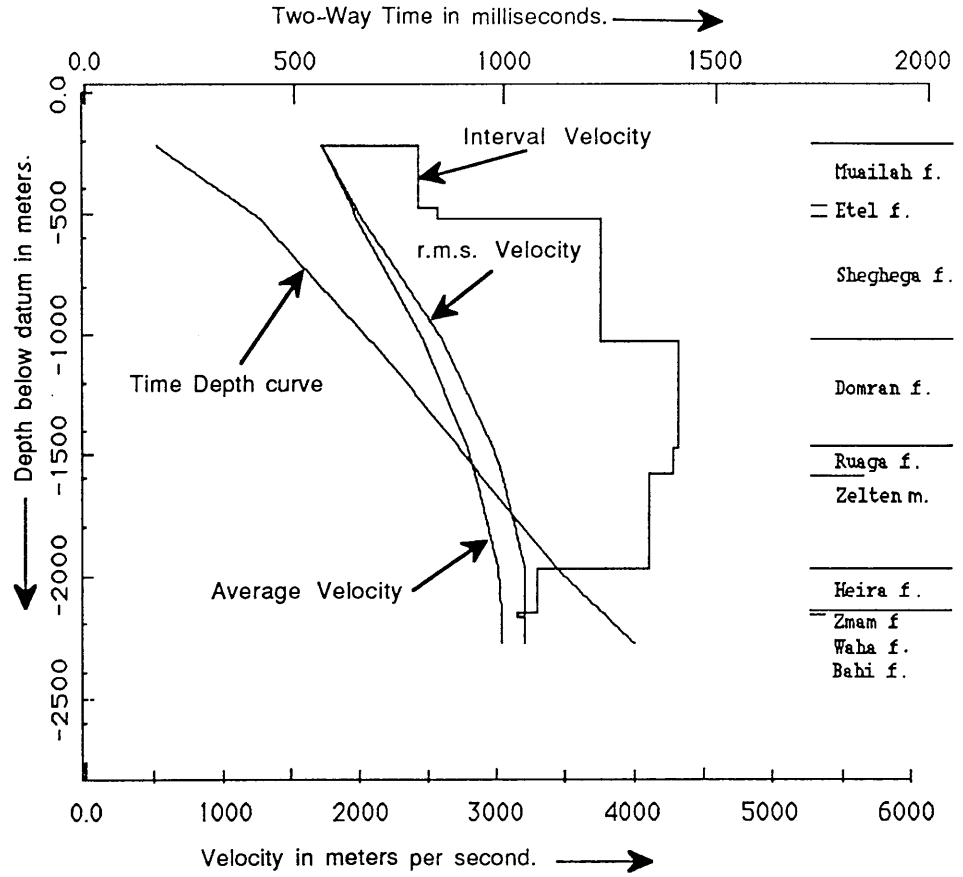

Fig.2.11. Velocity and time depth curves for well C114-6.

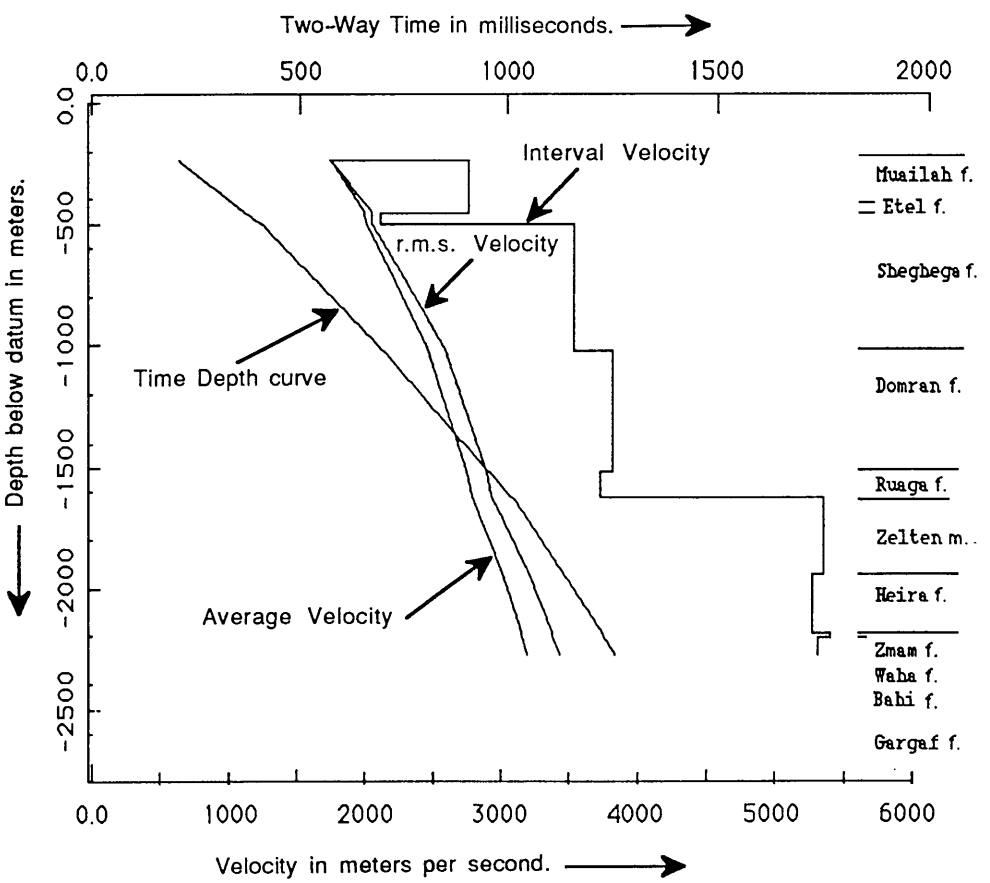

Fig.2.12. Velocity and time depth curves for well C59-6.

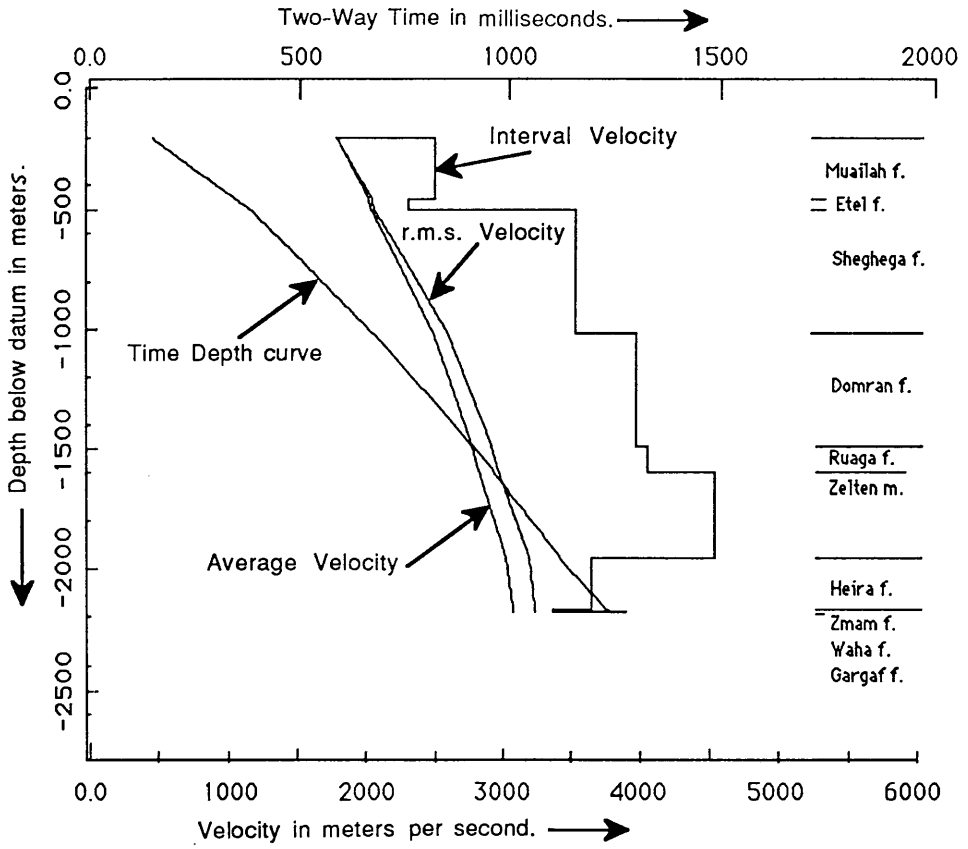

Fig.2.13. Velocity and time depth curves for well C85-6.

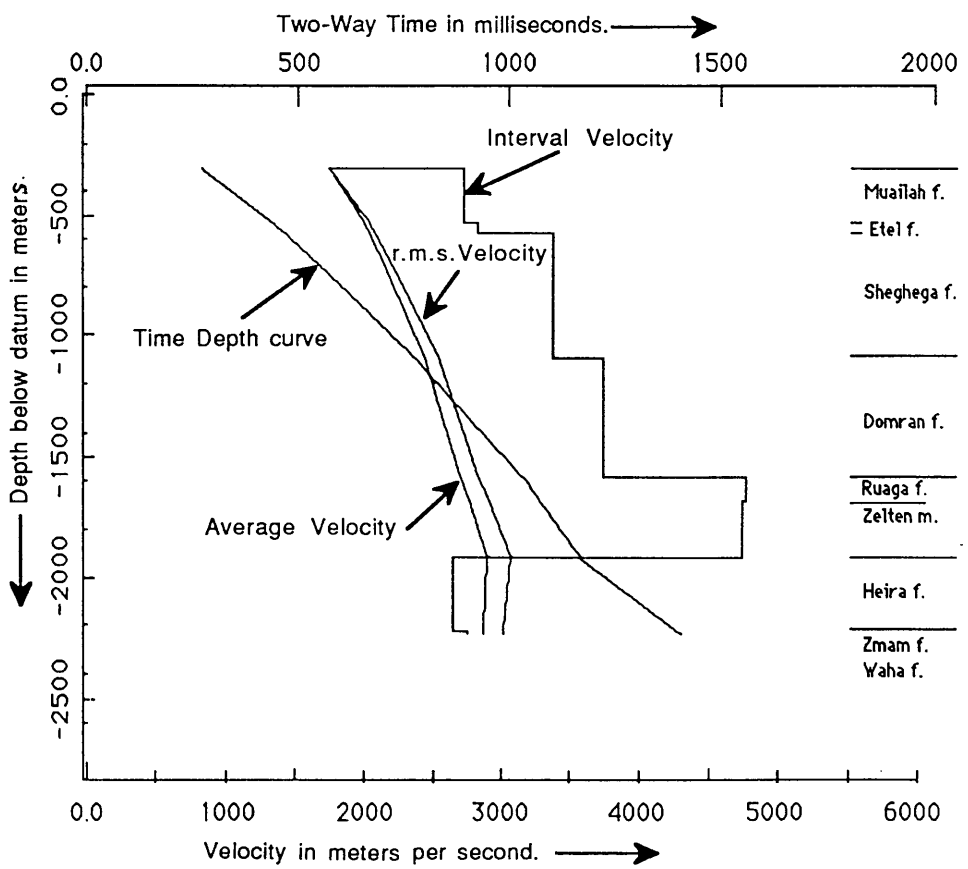

Fig.2.14. Velocity and time depth curves for well VV1-6.

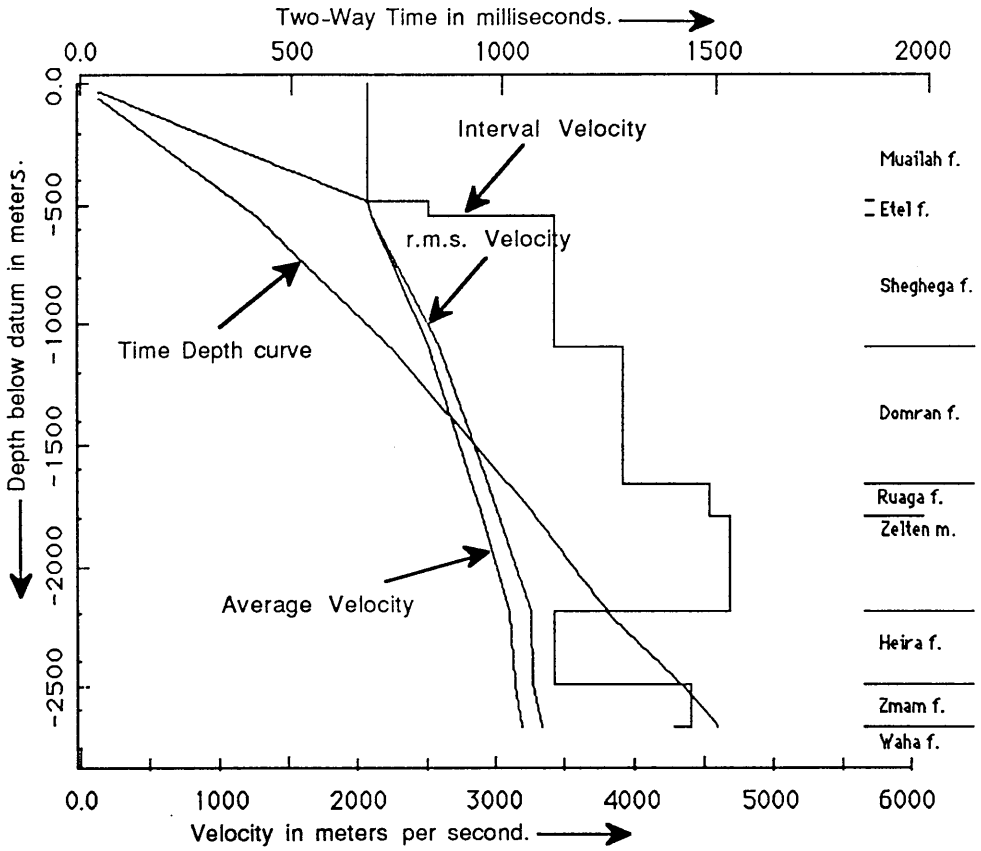

Fig.2.15. Velocity and time depth curves for well YYY1-6.

2.4, and 2.5 respectively at the formation boundaries (Appendix 2.2), based on data from the geological and geophysical reports available.

Figures 2.16-2.20 show the average velocity, interval velocity, rms velocity, and two way time curves versus depth below datum plane (sea level), for wells C114, C85, C59, C10, and YYY1 respectively, using the computer program CVL. The results are listed in Tables 2.6, 2.7, 2.8, 2.9, and 2.10 respectively at the formation boundaries (Appendix 2.2), based on data from the velocity survey logs available.

Figures 2.21-2.26 show the average velocity, interval velocity, rms velocity, and one way time curves versus depth below datum plane (sea level), for wells C59, C82, C85, YYY1, GGGG1, and KKKK1 respectively, using the computer program CVL3, output data results at different levels of recording, based on check-shot survey record logs available.

Looking at the results from different sources for the same well, such as Figures 2.11 and 2.16 for well C114 (results listed in tables 2.1 and 2.6 respectively of Appendix 2.2), shows that the velocities derived from the first group of data are higher than the ones derived from the second group of data. The differences are due to the different two-way times applied in each group at the same formation depth. The same result is found in well C85 (Figures 2.13 and 2.17; results listed in Tables 2.3 and 2.7 respectively of Appendix 2.2), and in well YYY1 (Figures 2.15 and 2.20; results listed in Tables 2.5 and 2.10 respectively of Appendix 2.2). A slight difference in velocities is seen in Figures 2.12 and 2.18 for the well C59, the results of which are listed in Tables 2.2 and 2.8 respectively (Appendix 2.2).

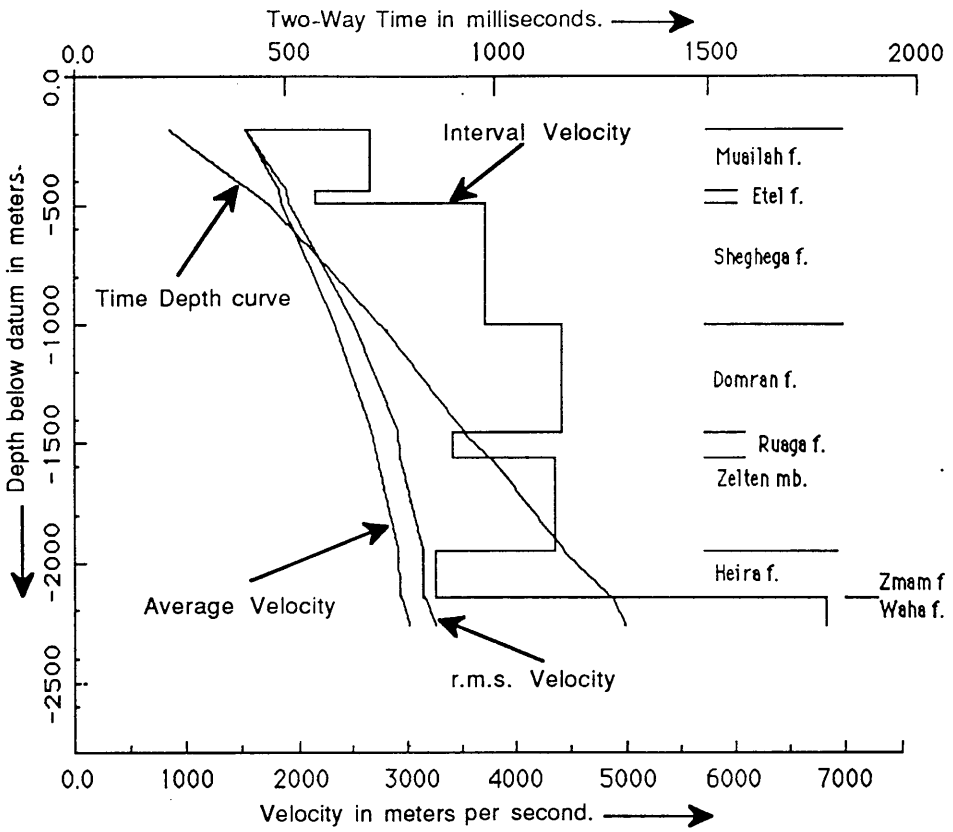

Fig.2.16. Velocity and time depth curves for well C114-6.

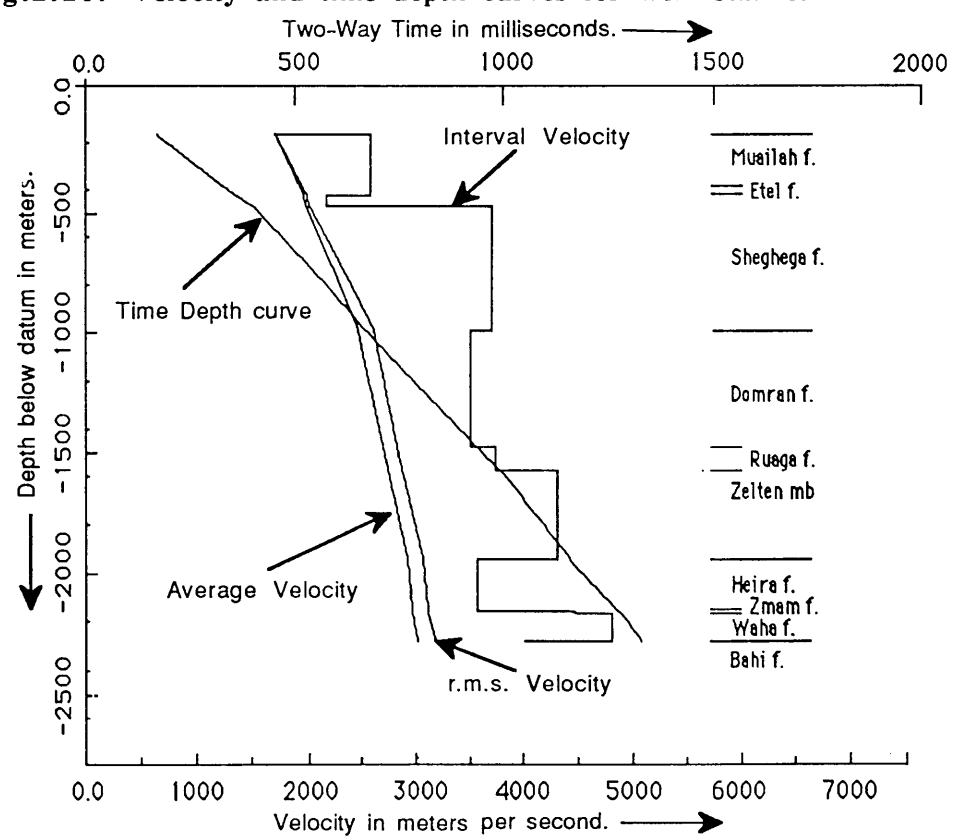

Fig.2.17. Velocity and time depth curves for well C85-6.

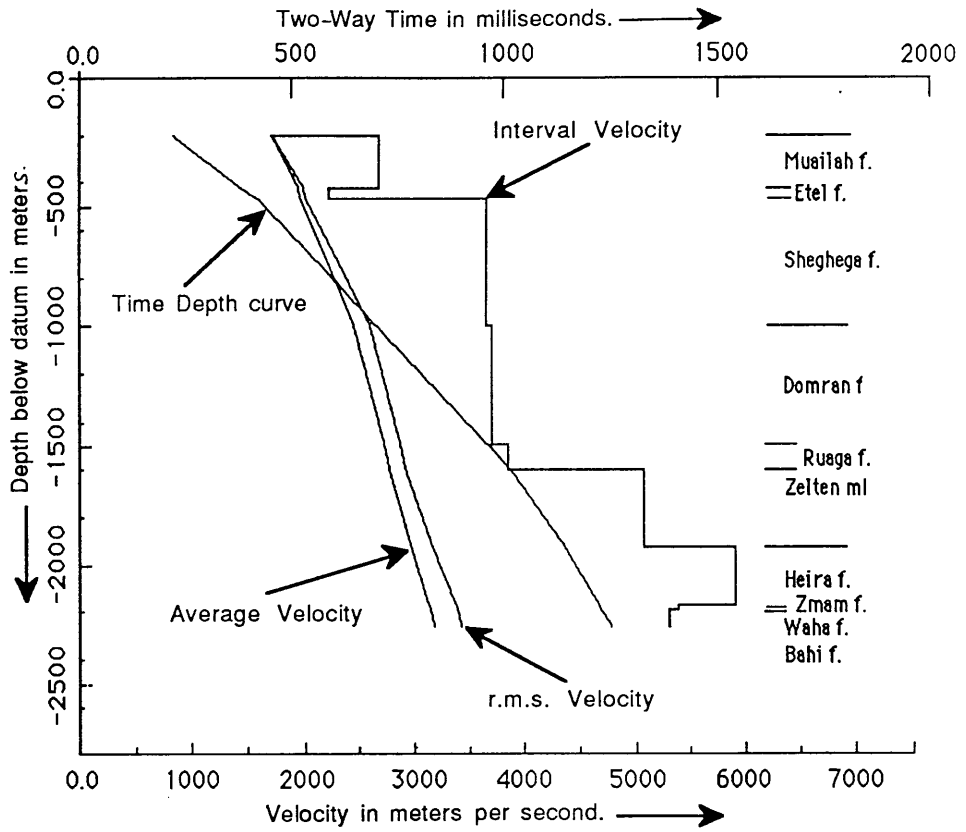

Fig.2.18. Velocity and time depth curves for well C59-6.

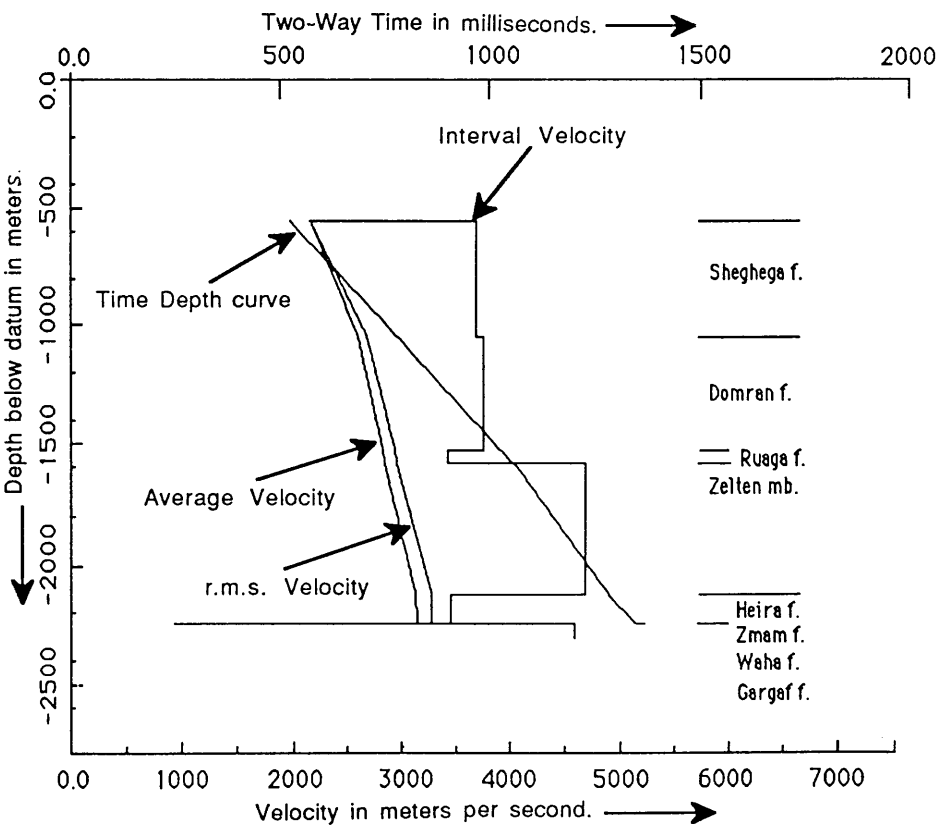

Fig.2.19. Velocity and time depth curves for well C10-6.

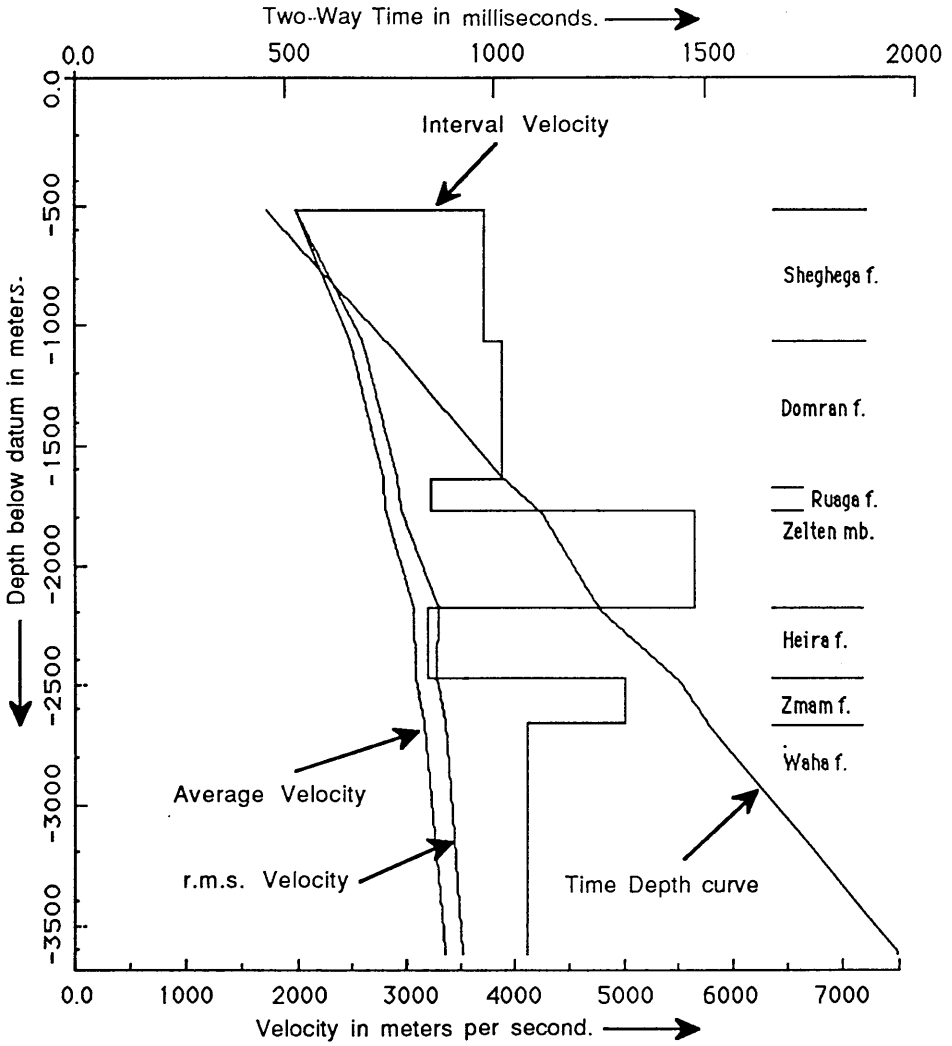

Fig.2.20. Velocity and time depth curves for well YYY1-6.

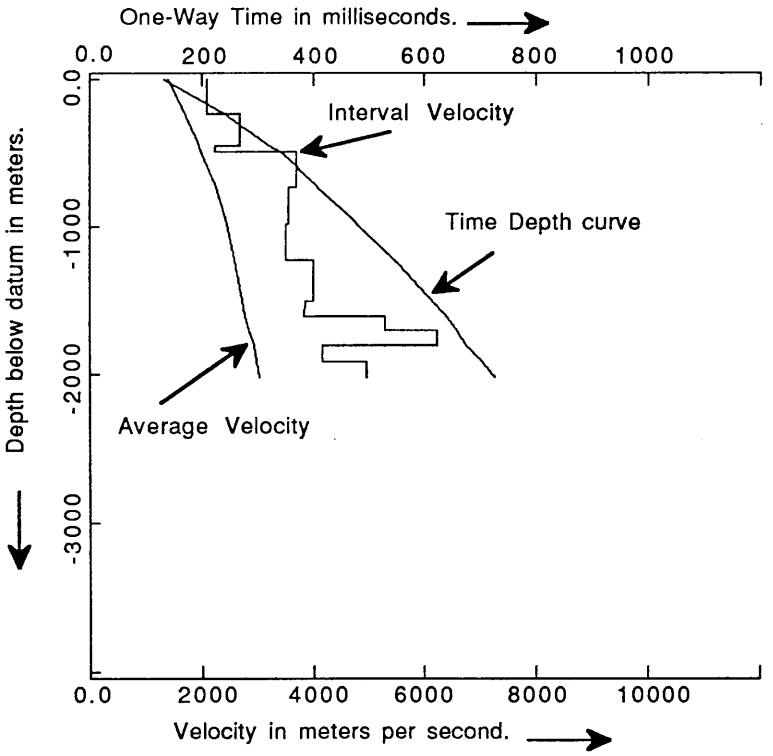

Fig.2.21. Velocity and time depth curves for well C59-6.

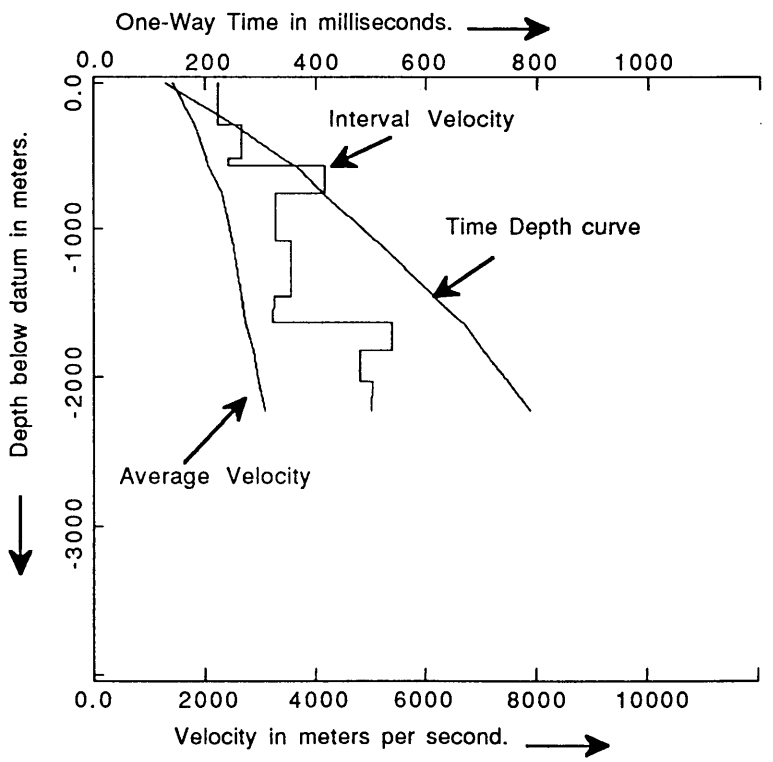

Fig.2.22. Velocity and time depth curves for well C82-6.

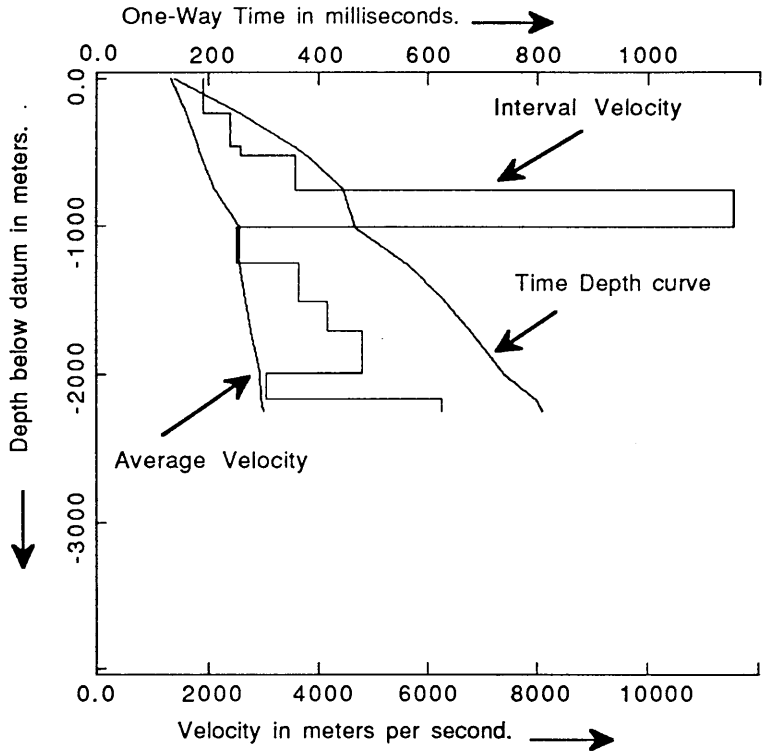

Fig.2.23. Velocity and time depth curves for well C85-6.

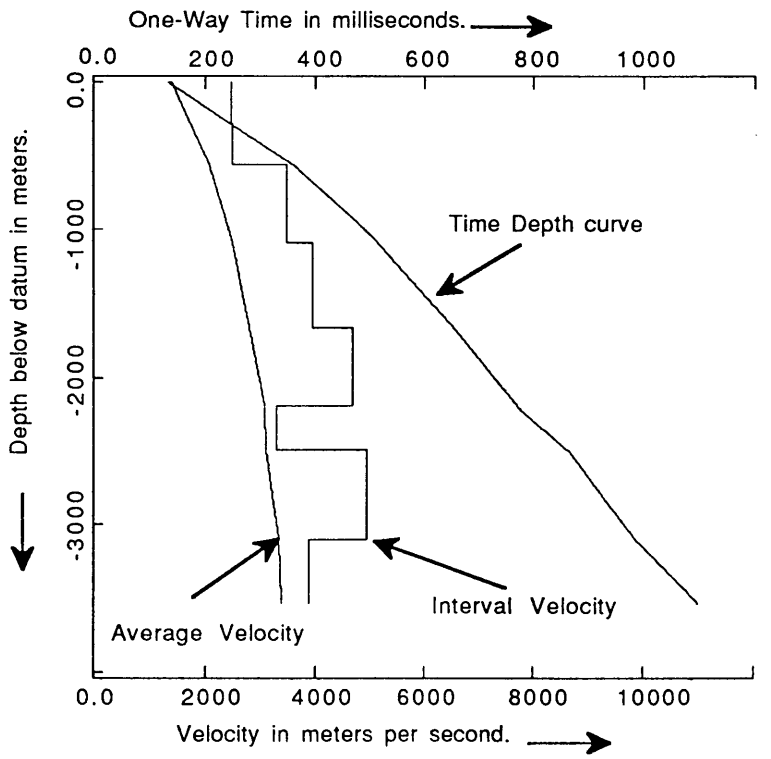

Fig.2.24. Velocity and time depth curves for well YYY1-6.

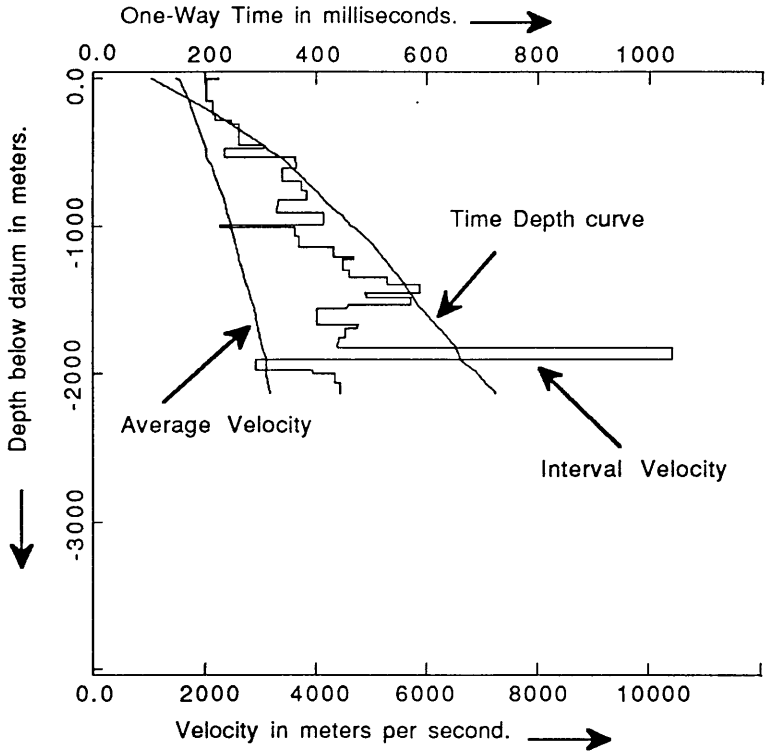

Fig.2.25. Velocity and time depth curves for well GGGG1-6.

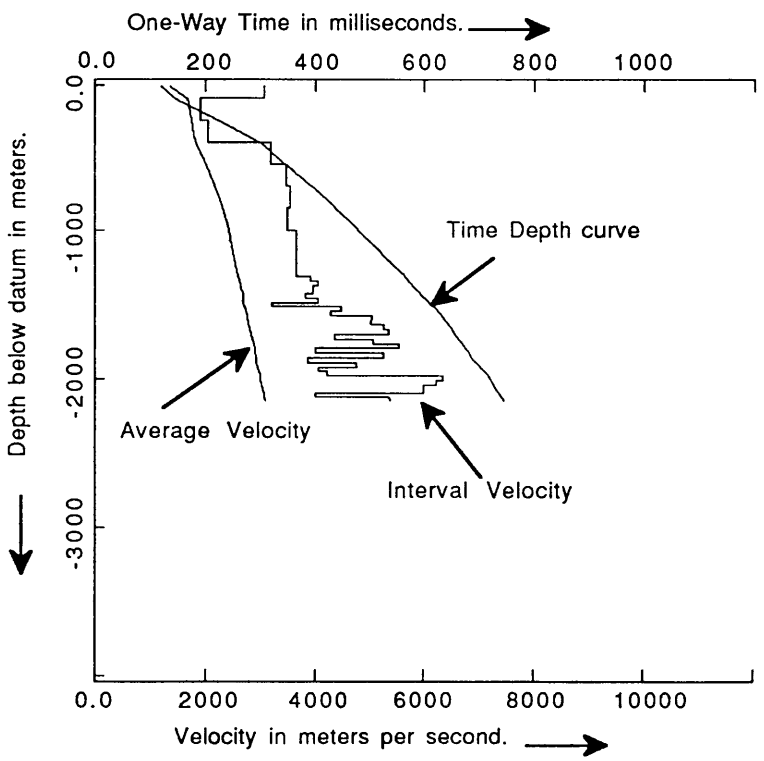

Fig.2.26. Velocity and time depth curves for well KKKK1-6.

All the figures above show a clear picture of the velocity relationship, that rms velocity is always greater than or equal to the average velocity, and that difference increases with depth. In Chapter 3 other relationships are discussed in more detail.

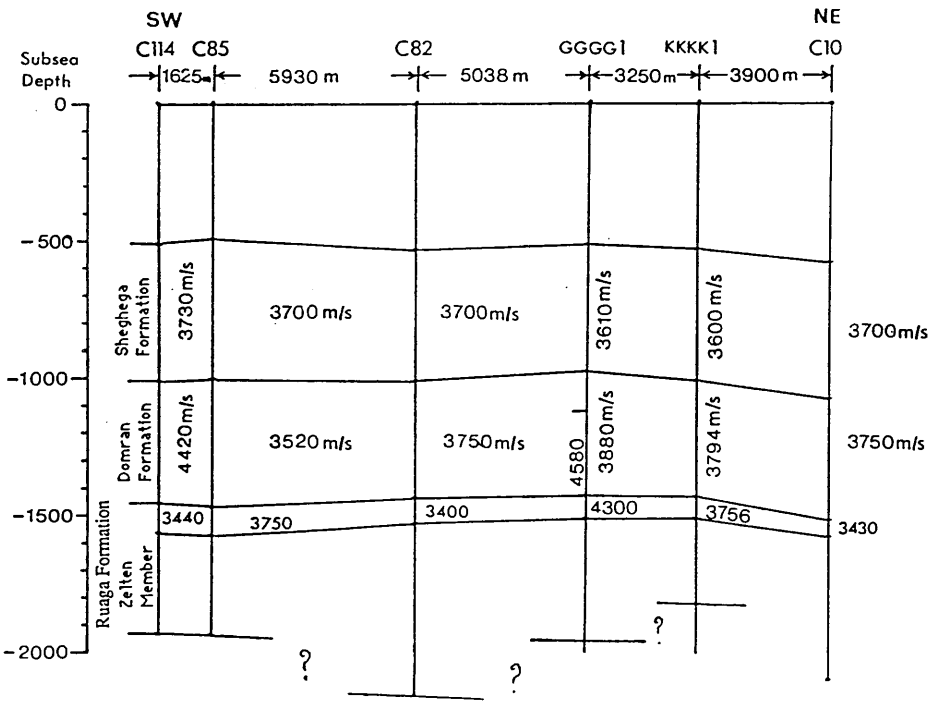

Fig. 2.27 Well correlation showing the interval velocity of the Sheghega formation, Domran formation, and the top of Ruaga formation from sonic logs generated in C114, C85, C82, GGGG1, KKKK1, and C10.

Figure 2.27 shows the lateral variations of the interval velocity by sonic logs over the field in southwest-northeast direction. The interval velocity does not change much for the Sheghega formation, but for the Domran formation there are two high interval velocity under the well C114-6 and well GGGG1-6 locations. Other clear high interval velocity found for the top of the Ruaga formation under the well GGGG1-6 location.

CHAPTER (3)

VELOCITY ANALYSIS

3.1 *Introduction*

Velocities of seismic waves depend mainly on the elastic properties of the minerals making up the rock material itself. Most rocks have complex micro-structure, with pore spaces between grains, which may contain fluids or other soft material such as clay. For such rocks, velocity is very much dependent on the porosity and on the material filling the pores (Dobrin & Savit, 1988).

In most sedimentary rocks, the velocity is dependent on the actual velocity of the minerals constituting the solid rock matrix, the porosity, the pressure, and the velocity of the fluid filling the pore spaces (Dobrin & Savit, 1988).

3.2 *Factors affecting velocity*

A simple linear relationship equation has been found by Wyllie et al. (1958) between the reciprocal of velocity and porosity, where the rock is composed of two materials, the matrix and the fluid filling the pore spaces between the grains.

$$\frac{1}{V} = \frac{\varnothing}{V_f} + \frac{1-\varnothing}{V_m} \qquad \text{.....(3.1)}$$

where

V = Velocity of the saturated rock.

V_m = Velocity of the matrix material.

V_f = Velocity of the fluid in the pore space.

$\varnothing$ = Fractional porosity.

From the above equation, it is clear that as the porosity increases the velocity decreases. In general, as the density of the rock or the material increases the velocity also increases, so that dense rocks have high velocity. Normally porosity decreases with depth of burial. As the rock is buried deeper, the overburden pressure increases and porosity decreases (Sheriff, 1978). We can say in general that the velocity increases with loss of porosity, so that velocity therefore increases with depth.

Pickett (1969) developed an equation like equation 3.1, which, as mentioned above, from theoretical considerations, is:-

$$\frac{1}{V} = A + B\,\varnothing \qquad \text{.....(3.2)}$$

Where A and B depend on the lithological parameters and depth of burial.

Faust (1951) made a statistical study of the effect of the age of rock on seismic velocity. He showed that for sandstones and shales the velocity can be expressed empirically as

$$V = K\,Z^{\frac{1}{6}}\,A^{\frac{1}{6}} \qquad \text{.....(3.3)}$$

where

K = Constant equal to 38.2 when Z is in metres, T in years, and V in m/s

Z = Depth of burial

A = Age of formation

He found that velocity increases with the age of rocks according to the 1/6 power of the age. Through time, much may happen to the rock, including cementation, deformation, re-crystallization, etc.

Figure 3.1 summarises the factors that influence seismic velocity in sandstone. These factors are ranked in order of importance.

Factors Decreasing Velocity	Porosity Clay content Sand
Factors Increasing Velocity	Lime content Dolomitization
Factors Decreasing Porosity	Depth Max. Depth of burial Age Cementation

Fig. 3.1. Factors affecting velocity.

Porosity is the most important factor in lowering velocity. Shale has a tendency to lower velocity, more than sand. Dolomite tends to raise velocity. A limey shale will have a higher velocity than a sandy shale and a sandy limestone will have a lower velocity than pure limestone but higher than pure sand (Sheriff, 1978).

3.3 *Seismic velocity terminology*

In geophysical work there are many types of velocity, but these velocities are related to each other.

3.3.1 *Interval velocity* (V_I)

Interval velocity is defined by the formula.

$$V_I = \frac{\Delta z}{\Delta t} \qquad \text{.....(3.4)}$$

where

Δz = Difference in depth

Δt = Difference in time

V_I = Interval velocity

through a layer in which the velocity is assumed to be constant.

Interval velocity is a very useful parameter as a lithological indicator. It can be obtained both from well velocity surveys and from CDP reflection data.

3.3.2 *Instantaneous velocity* (V_{INS})

Instantaneous velocity is the interval velocity measured by a continuous velocity logging tool when the distance between the receivers is very small, it is represented by a differential equation

$$V_{INS} = \lim_{\Delta t \to 0} \frac{\Delta z}{\Delta t} = \frac{dz}{dt} \qquad \text{.....(3.5)}$$

where

dt = Difference in time as Δt tends to zero

dz = Difference in depth as ΔZ tends to zero

V_{INS} = Instantaneous velocity (Interval velocity), at that particular depth.

3.3.3 *Average velocity* (V_{ave})

Average velocity is the interval velocity measured through a number of layers, as shown in Figure 3.2.

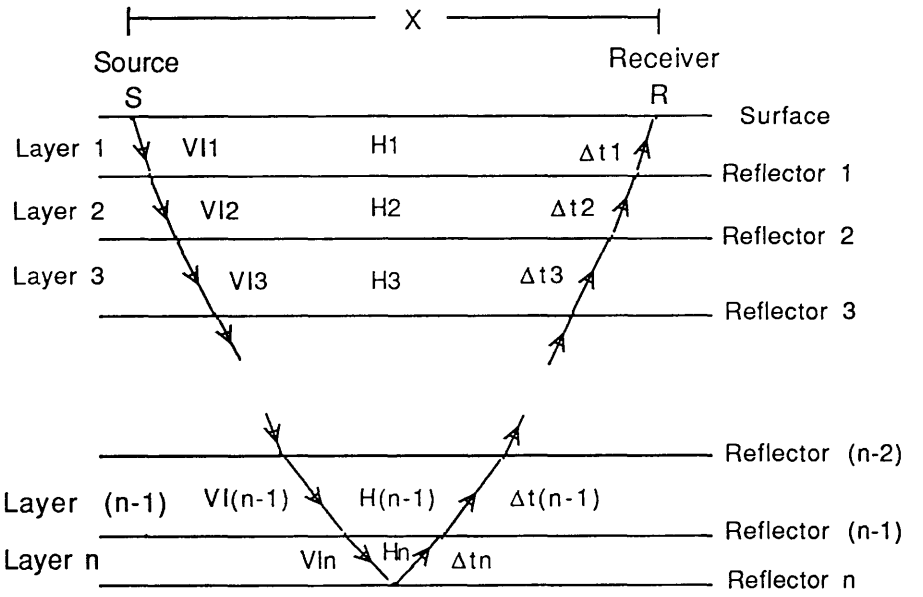

Fig.3.2. General model for the reflection path for the horizontal layers.

and is defined by the formula.

$$V_{ave} = \left[\frac{H_1 + H_2 + \cdots\cdots + H_n}{\Delta t_1 + \Delta t_2 + \cdots\cdots + \Delta t_n} \right] \qquad \text{for n layers, ...(3.6)}$$

where

Δt_n = Time through the n^{th} layer

V_{ave} = Average velocity

Equation 3.6 may be expressed in the form

$$V_{ave} = \left[\frac{V_{I1}\Delta t_1 + V_{I2}\Delta t_2 + \cdots\cdots + V_{In}\Delta t_n}{\Delta t_1 + \Delta t_2 + \cdots\cdots + \Delta t_n} \right] \quad \text{.....(3.7)}$$

$$V_{ave} = \left[\frac{\sum_{i=1}^{n} V_{Ii}\Delta t_i}{\sum_{i=1}^{n} \Delta t_i} \right] \quad \text{.....(3.8)}$$

V_{In} = Interval velocity for the n^{th} layer

This average velocity is a time-weighted average of the component interval velocities. It is a good means of converting reflection time to depth.

3.3.4 RMS velocity (V_{rms})

RMS velocity is the weighted root mean square of the component interval velocities (Hatton, et al. 1986). Its formula is

$$V_{rms} = \left[\frac{V_{I1}^{2}\Delta t_1 + V_{I2}^{2}\Delta t_2 + \cdots\cdots + V_{In}^{2}\Delta t_n}{\Delta t_1 + \Delta t_2 + \cdots\cdots + \Delta t_n} \right]^{\frac{1}{2}} \text{ for n layers, ...(3.9)}$$

$$V_{rms} = \left[\frac{\sum_{i=1}^{n} V_{Ii}^{2}\Delta t_i}{\sum_{i=1}^{n} \Delta t_i} \right]^{\frac{1}{2}} \quad \text{.....(3.10)}$$

3.3.5 *Normal moveout velocity* (V_{nmo})

Normal moveout is the difference in TWT between a receiver at an offset X as compared to a zero-offset receiver. Normal moveout velocity is the velocity derived from plotting a curve for the square of the reflection time versus the square of the distance between the source and the receiver, as shown in Figure 3.3. Figure 3.4 is a schematic diagram of the simple case of a flat horizon. This type of velocity is used in computing the dynamic (NMO) correction for shot-receiver offset as shown in Figures 3.5, and 3.6.

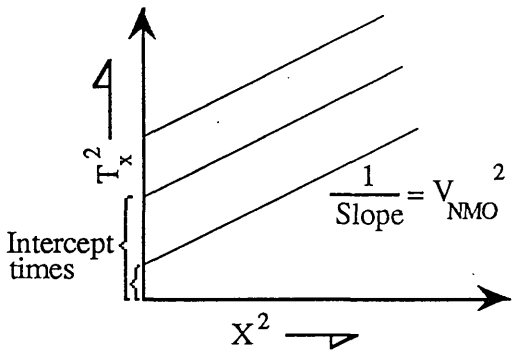

Fig.3.3. X^2-T^2 Plot.

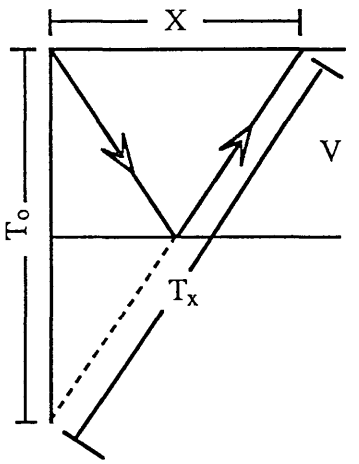

Fig.3.4. Simple horizontal plane reflector model.

The equation used for the NMO correction is

$$T_x^2 = T_0^2 + \frac{X^2}{V_{NMO}^2} \quad \text{.....(3.11)}$$

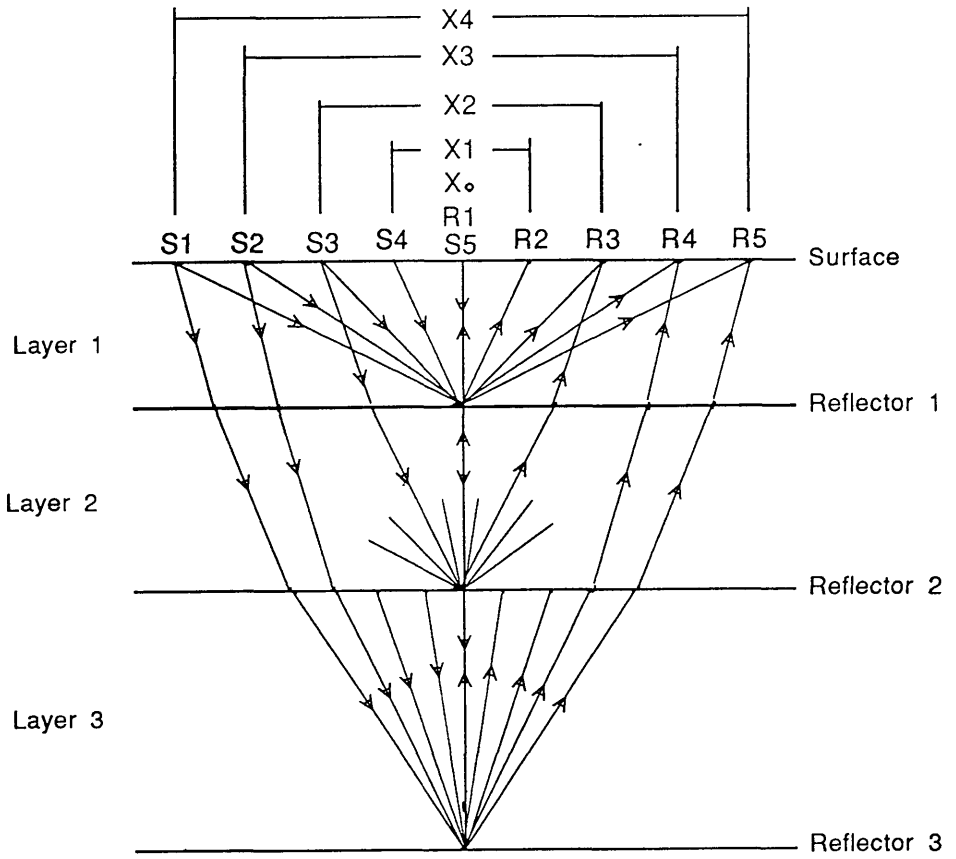

Fig.3.5. Common depth point model for horizontal layering.

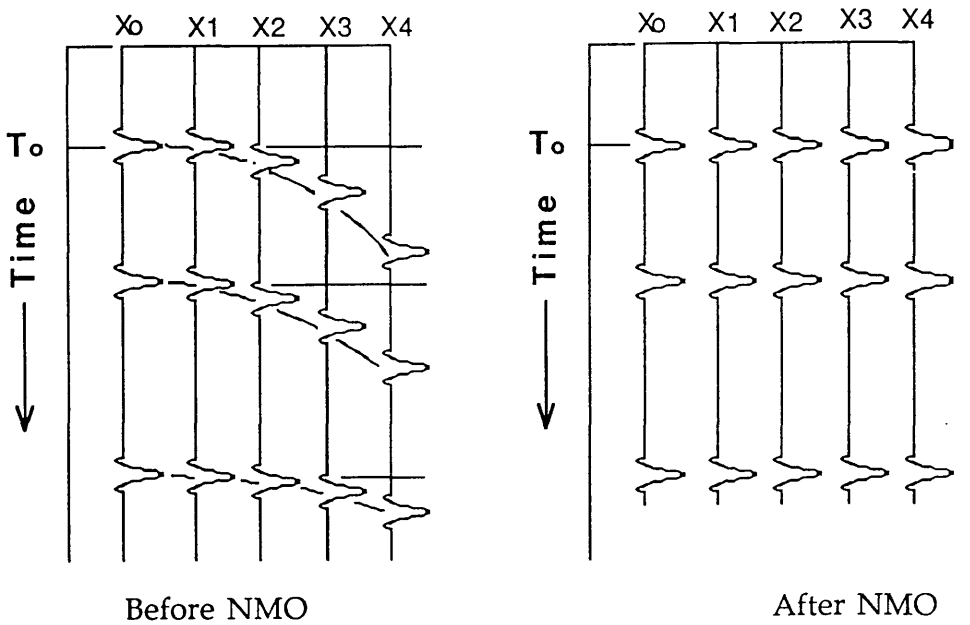

Fig.3.6. Five trace gather for 3 layers before and after NMO correction.

or in terms of V_{nmo}

$$V_{NMO} = \frac{X}{\sqrt{\left(T_x^{\,2} - T_0^{\,2}\right)}} \qquad \text{.....(3.12)}$$

where

T_0 = Zero offset time

X = Source-receiver offset

T_x = Reflection time for any offset X

It is possible to determine normal moveout velocity (V_{nmo}) using the X^2-T^2 method by plotting the square of the reflection time versus the square of the distance between source and receivers (Fig. 3.3). The arrival time of the reflected energy in equation 3.11 depends not only on the reflection depth and the velocity above the reflector but also on the offset distance. From the plot in Figure 3.3, we get a straight line whose slope $1/(V_{nmo})^2$ and whose intercept is $T_o^{\,2}$.

3.3.6 *Dix interval velocity* (V_{ID})

Dix (1955) showed how to calculate interval velocities from normal moveout velocity, with his equation

$$V_{ID_{n-1,n}} = \left[\frac{V_{NMO_n}^{\,2} T_{0_n} - V_{NMO_{n-1}}^{\,2} T_{0_{n-1}}}{T_{0_n} - T_{0_{n-1}}} \right]^{\frac{1}{2}} \quad \text{for the last layer ...(3.13)}$$

where

$V_{NMO_{n-1}}$ = Normal moveout velocity for the $(n-1)^{th}$ layer.

V_{NMO_n} = Normal moveout velocity for the n^{th} layer.

$T_{0_{n-1}}$ = Time through the (n-1) layer.

T_{0_n} = Time through the n^{th} layer.

$V_{ID_{n-1,n}}$ = Dix interval velocity of the n^{th} layer.

3.3.7 *Dix average velocity* (V_{AD})

Dix average velocity V_{AD} is a time-weighted average velocity of the component Dix interval velocities, calculated by the equation:

$$V_{AD} = \left[\frac{V_{ID_1} \Delta t_1 + V_{ID_2} \Delta t_2 + \cdots\cdots + V_{ID_n} \Delta t_n}{\Delta t_1 + \Delta t_2 + \cdots\cdots + \Delta t_n} \right] \text{ for n layers, (3.14)}$$

where

V_{ID_1} = Dix interval velocity for the 1^{st} layer.

V_{ID_2} = Dix interval velocity for the 2^{nd} layer.

V_{ID_n} = Dix interval velocity for the n^{th} layer.

Δt_1 = Time through the 1^{st} layer.

Δt_2 = Time through the 2^{nd} layer.

Δt_n = Time through the n^{th} layer.

3.4 *Velocity calculation*

Velocities can be calculated from seismic data using normal moveout. This velocity is used in common depth point stacking to bring the arrival time of the particular reflection to the same travel time for different offsets, and hence is called normal moveout velocity (V_{nmo}) as shown in Figure 3.6.

In the case where the layers are planar and horizontal, and the offsets are small, Dix (1955) showed that the normal moveout velocity (V_{nmo}) is equivalent to the root mean square velocity (V_{rms}). The effect is that the normal moveout velocity (V_{nmo}) is always greater than average velocity (V_{ave}).

This velocity is commonly used for calculating depths in areas where there is no borehole data available, but if this is not the case (as in the present study), it is clear that the root mean square velocity is greater than average velocity by a small amount.

The relationship between root mean square velocity and average velocity was shown by Al-Chalabi (1974), who relates the two velocities through a quantity which he called the heterogeneity factor (H):-

$$V_{rms} = (1 + H)^{\frac{1}{2}} V_{ave} \qquad \text{.....(3.15)}$$

H is a positive quantity, being equal to zero only when all the layers have the same velocity (a homogeneous ground). Equations 3.15 illustrates quantitatively the observation that the rms velocity equals the average velocity when the ground is homogeneous, and progressively exceeds it as the ground becomes more heterogeneous.

Interval velocities can be calculated by using root mean square velocities directly in the Dix formula in equation (3.13).

The Dix velocities are correct only for the cases where the layers are horizontal, and are larger than the true interval velocities for dipping reflectors, and can be corrected by dividing by cosine of the dip.

Shah (1973) extended the concept of root mean square velocity to dipping beds. He derives what he calls the normal moveout velocity, defined by

$$V_{nmo,n}^{2} = \frac{1}{(T_o \cos^2 \beta_o)} \sum_{i=1}^{n} V_i^2 T_i \prod_{j=1}^{i-1} \left(\frac{\cos^2 \alpha_j}{\cos^2 \beta_j} \right) \text{ for the } n^{th} \text{ layer} \quad ...(3.16)$$

where α_j is the angle of the incidence at the j^{th} interface

β_j is the angle of the transmittance at the j^{th} interface

β_o is the emergence angle of the raypath that is normal to the n^{th} interface

For flat (non-dipping) beds, the normal moveout velocity reduces to Dix's root mean square velocity. In the case of a single dipping layer, root mean square velocity reduces to a result given by Levin (1971), who derived the travel time equation for the dipping layer case, given by:-

$$t_{(x)}^2 = t_{(0)}^2 + \frac{x^2 \cos \beta_o}{v^2} \quad .....(3.17)$$

This is again the equation for a hyperbola, where the NMO velocity is given by the medium velocity, divided by cosine of the dip angle (Levin 1971, Montalbetti 1971).

$$V_{nmo} = \frac{V_1}{\cos \beta_o} \qquad \text{.....(3.18)}$$

Levin extended his work to the case of dipping layers with all layers having the same dip.

$$V_{nmo}^2 = \frac{1}{(T_o \cos^2 \beta_o)} \sum_{i=1}^{n} V_i^2 T_i \qquad \text{.....(3.19)}$$

$$V_{nmo} = \frac{V_{rms}}{\cos \beta_o} \qquad \text{.....(3.20)}$$

The implication is that stacking of a dipping event requires a velocity that is normally greater than the rms velocity of the medium above the reflector.

3.5 *Fortran programs*

They are more then 150 velocity analysis tabulations available from 17 seismic lines with which to start work. These data, comprising two-way time, stacking velocity, and Dix interval velocity, are tabulated at different levels of picking. New two-way time values were picked from the re-interpretation of the seismic sections at three chosen horizons (Chapter 4), programs were designed to handle these kind of data.

In the area of study most of the seismic lines which have been used in the re-interpretation were shot in straight lines, except for lines V248, V250, and V263. Rather than picking the coordinates of each shot point

location, and feeding this information (plus others) into the programs, only the first and the last shot point coordinates were picked. For the others, coordinates were picked where the line changed its direction. The program which handles this particular case is called COORDINATE. It calculates the coordinates for every shot point required, where the two-way time been picked on the seismic sections. The program source listing is shown in Appendix 3.1.

The second program (ALL2) was designed for the velocity analysis data that appears in the boxes on the top of the seismic sections. Each line is handled separately. It then writes the results and calculations in an easy format for contouring. The program source listing is shown in Appendix 3.2.

The third program (BOXMATCH) was also designed to handle the data for each seismic line separately. Using the output file from the COORDINAT program, and the results from the first output from the ALL2 program, it calculates the velocities at all shot points for the three chosen horizons on the particular seismic line, and calculates the depths, differences in depths, and differences in two-way times between the chosen horizons. The program source listing is shown in Appendix 3.3.

3.5.1 *Program calculations and results*

The simplest case of the polynomial equation as shown in Appendix 3.7 was used in the above program calculation.

Flowcharts corresponding to COORDINATE, ALL2, and BOXMATCH are shown in Figures 3.7, 3.8, and 3.9.

The output file from the COORDINATE program contains information and the results, such as shot point number, corresponding latitude, longitude, and two-way time value for the horizon 1, 2, and 3.

For graphical and output data length reasons, seven output files are produced from an ALL2 program run. These contain results such as average velocity, interval velocity, depth, difference in time, and difference in velocity, designed for average and interval velocity plots.

For the same reasons mentioned above, three output files result from a run of the BOXMATCH program. These contain results such as average velocity for the three horizons, and depth, for all required shot points in one output file, and for shot points which have velocity analysis in another output file. The last output file contains all differences in time and depth for the three horizons.

3.6 *Data analysis*

In order to see the relationships between the velocities and two-way times at the velocity analysis locations of a particular seismic line, using the output files from the ALL2 program, two S macros were designed to handle these data to generate graphical plots. The S graphic system is a high level language and software for data analysis and graphics routines, and runs under the Unix operating system.

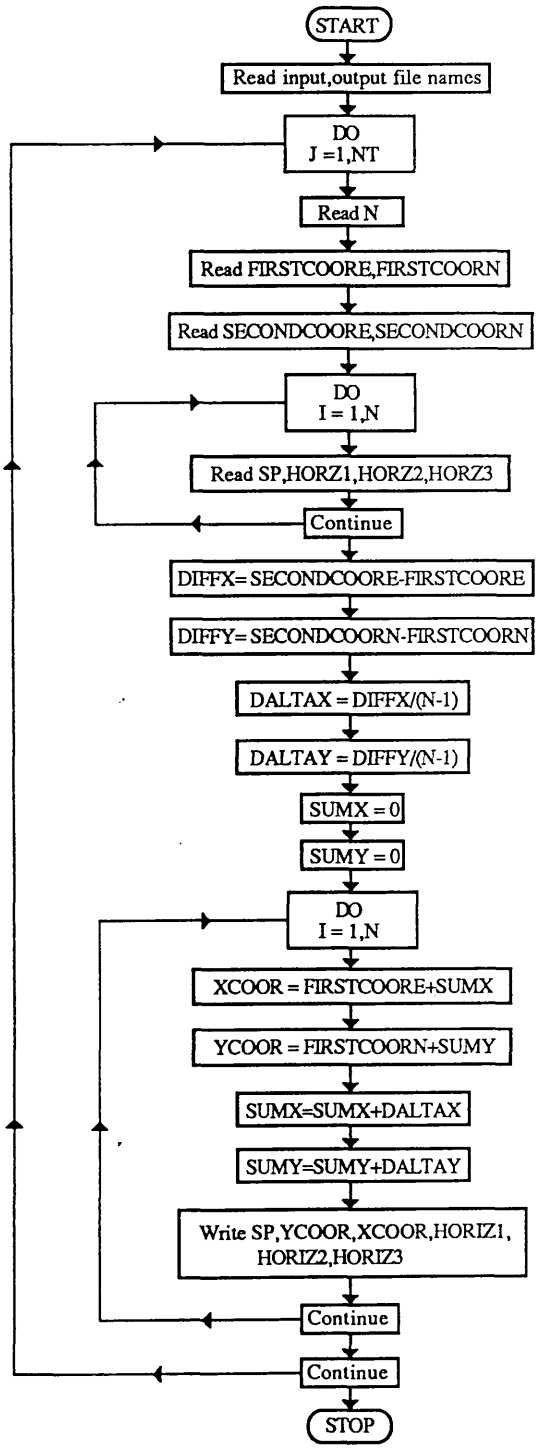

J - Counter for straight lines.

N - Number of the picked shot points.

FIRSTCOORE - Latitude of the first shot point in the line.
FIRSTCOORN - Longitude of the first shot point in the line.
SECONDCOORE - Latitude of the last shot point in the line.
SECONDCOORN - Longitude of the last shot point in the line.
I - Counter for picked shot points.

SP - Shot point number.
HORIZ1 - Time for horizon (1).
HORIZ2 - Time for horizon (2).
HORIZ3 - Time for horizon (3).
DIFFX - Difference in latitude.

DIFFY - Difference in longitude.

DALTAX - Latitude increment.

DALTAY - Longitude increment.

SUMX - Summation of latitude.

SUMY - Summation of longitude.

I - Counter for picked shot points.

XCOOR - Required latitude of the shot point.

YCOOR - Required longitude of the shot point.

Fig.3.7. Detailed flowchart for the COORDINATE program.

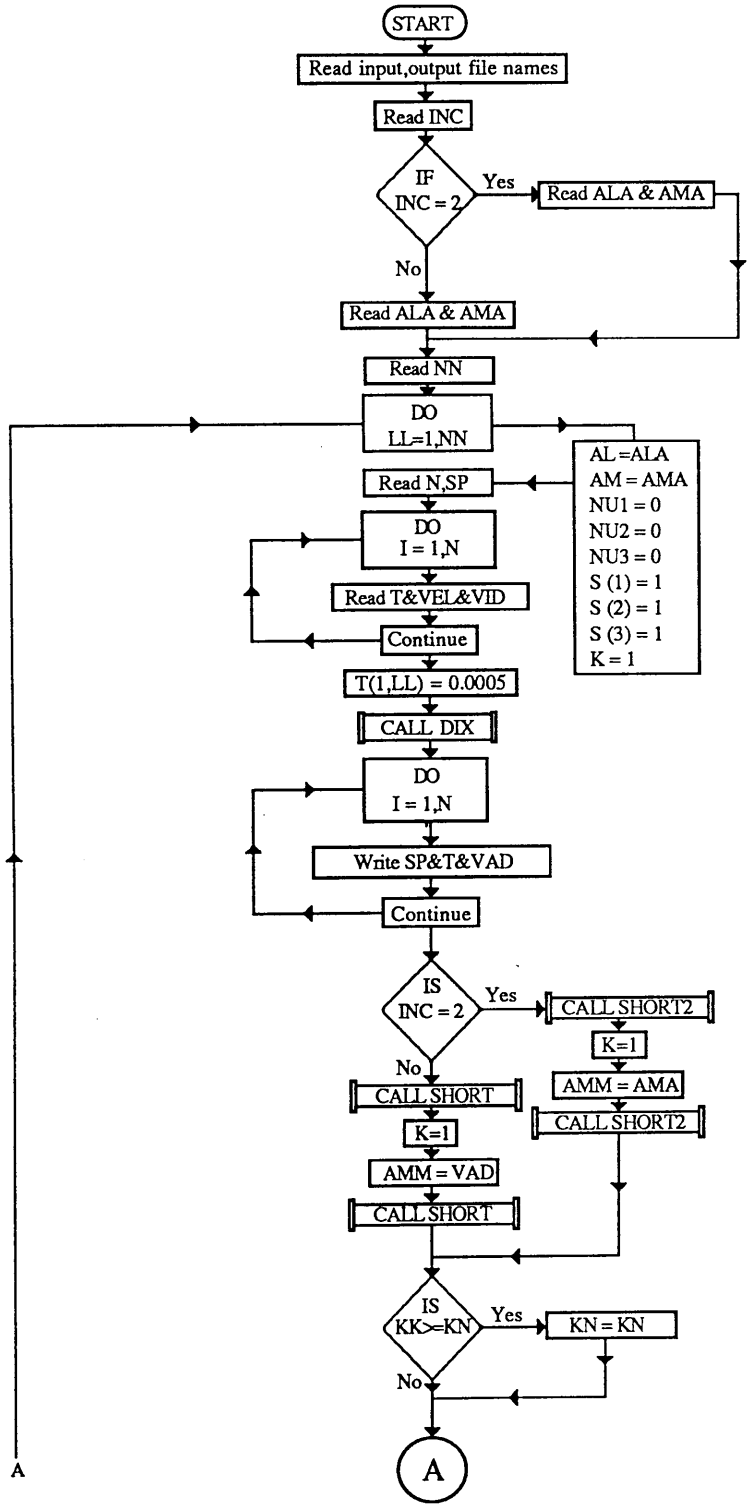

INC - Number equal 1 if velocity increment.
2 if time increment.

ALA - Increment value (time or velocity).
AMA- Starting value (time or velocity).

NN - Number of velocity analysis boxes.

LL - Counter for the boxes.

NU1 - Counter for time values less than 4 s.
NU2 - Counter for time values less than 4 s.
NU3 - Counter for time values less than 2 s.
S - Starting counting number.
K - Counter of data.
N - Number of picked levels.
SP - Shot point number.
N - Counter for levels.
T - Two way time.
VEL - Root mean square velocity.
VID - Dix interval velocit.
CALL DIX - Call subroutine DIX.

I - Counter for levels.

VAD - Dix average velocity.

CALL SHORT2 - Call subroutine SHORT2.

CALL SHORT - Call subroutine SHORT.

Fig.3.8. Detailed flowchart for the ALL2 program.

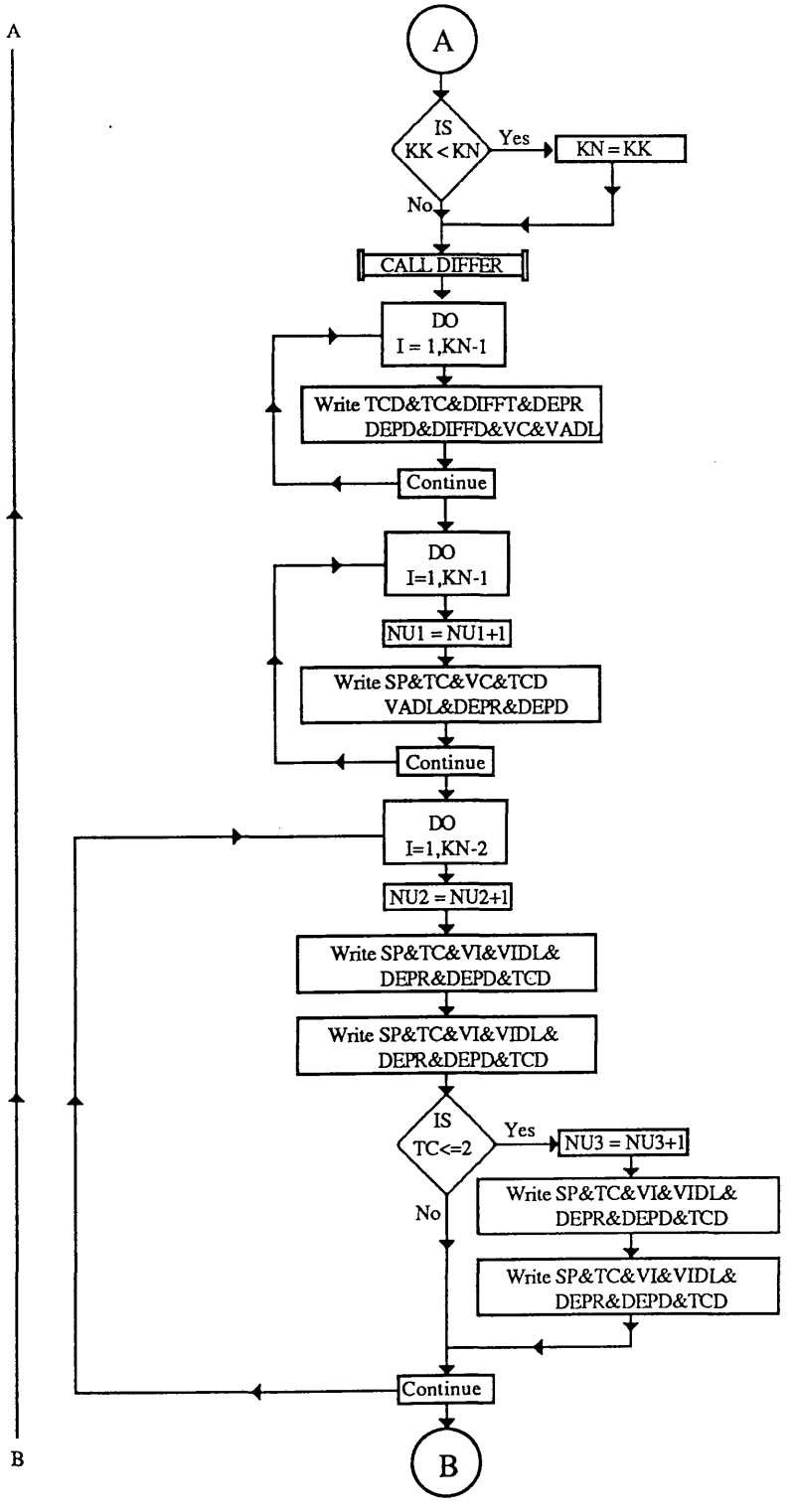

CALL DIFFER - Call subroutine DIFFER.

I - Counter for shot point number.

TC - Interpolated time corresponding to the m velocity.
TCD - Interpolated time corresponding to the Di velocity.
DEPR - Depth using rms velocity.
DEPD - Depth using Dix average velocity.
DIFFD - Difference in depth (DEPR-DEPD).
DIFFT - Difference in time (TC-TCD).
VC - Interpolated rms velocity.
VADL - Interpolated Dix average velocity .

I - Counter for shot point number.

I - Counter shot point number.

VIDL - Interpolated Dix interval velocity.
VI - Interval velocity.

Fig.3.8. (Continued) Detailed flowchart for the ALL2 program.

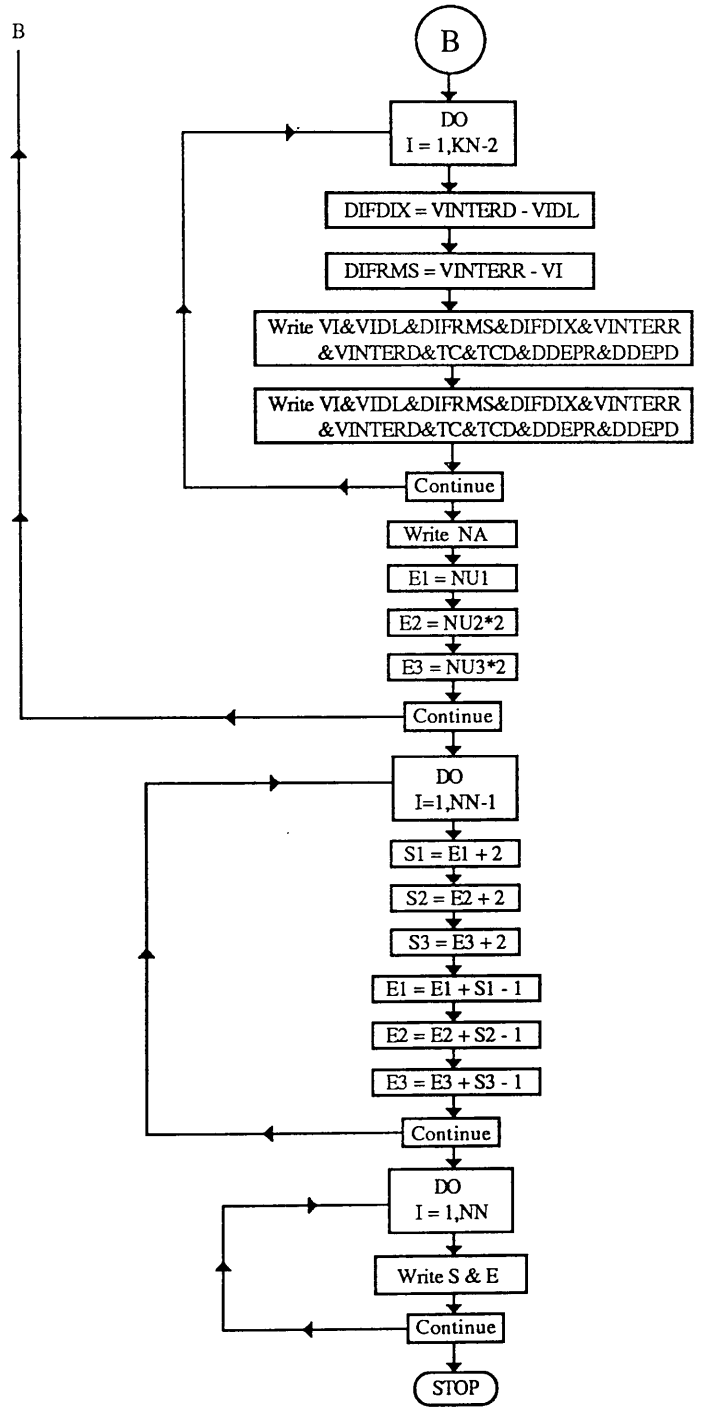

I - Counter for shot point number.

VIDL - Interpolated Dix interval velocity.
VINTERD - Dix interval velocity calculated from DIFFER subroutine.
DIFDIX - Difference in Dix interval velocity.

VI - Interval velocity.
VINTERR - Interval velocity (rms) calculated from DIFFER subroutine.
DIFRMS -Difference in interval velocity (rms).
DDEPR - Difference in depth calculated from DIFFER subroutine.
DDEPD - Difference in depth calculated from DIFFER subroutine.

E1 - Ending counter number for average velocity values.
E2 - Ending counter number for all interval velocity values haveing time.
E3 - Ending counter number for interval velocity values haveing time less than 2 s.

I - Counter for number of boxes.

S1 - Starting counter number for average velocity values.
S2 - Starting counter number for all interval velocity values haveing time.
S3 - Starting counter number for interval velocity values haveing time less than 2 s.

I - Counter for number of boxes.

Fig.3.8. (Continued) Detailed flowchart for the ALL2 program.

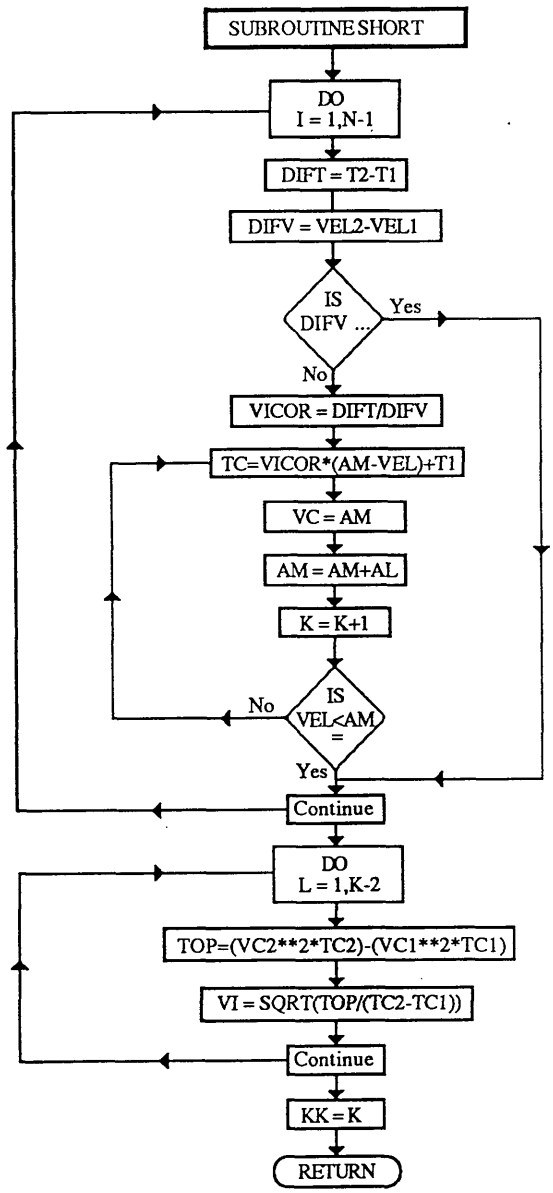

I - Counter for calculated loops.

T - Time.
DIFT - Difference in time.
VEL - Velocity.
DIFV - Difference in velocity.

TC - Interpolated time.

VC - Corresponding velocity.
AM - Starting velocity.
AL - Velocity increment.

L - Counter for shot point number.

SQRT - Square root function.
VI - Interval velocity.

Fig.3.8. (Continued) Detailed flowchart for SHORT subroutine.

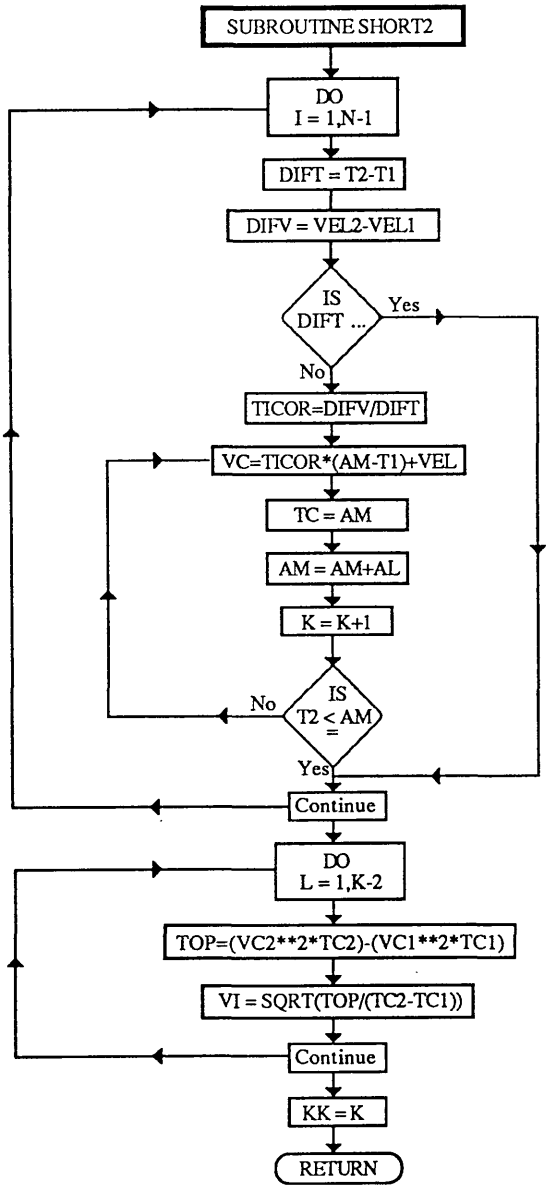

I - Counter for calculated loops.

T - Time.
DIFT - Difference in time.
VEL - Velocity.
DIFV - Difference in velocity.

VC - Interpolated velocity.

TC - Corresponding time.
AM - Starting time.
AL - Time increment.

L - Counter for shot point number.

SQRT - Square root function.
VI - Interval velocity.

Fig.3.8. (Continued) Detailed flowchart for SHORT2 subroutine.

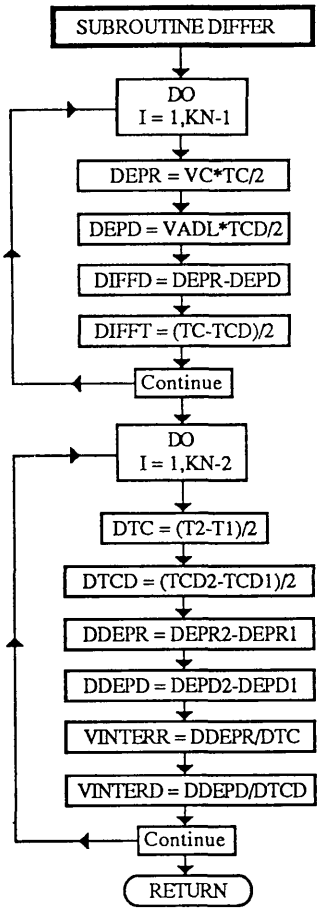

I - Counter for shot point number.

VC - RMS velocity.
TC - Time corresponding to VC.
DEPR - Depth calculated using rms velocity.
VADL - Interpolated Dix average velocity.
TCD - Time corresponding to VADL.
DEPD - Depth calculated using Dix average velocity.
DIFFD - Difference in depth (DEPR-DEPD).
DIFFT - Difference in time (TC-TCD).

I - Counter for shot point number.

DTC - Difference in time corresponding to rms velocity.
DTCD - Difference in time corresponding to Dix average velocity.
DDEPR - Difference in depth corresponding to rms velocity.
DDEPD - Difference in depth corresponding to Dix average velocity.
VINTERR - Interval velocity (rms).

VINTERD - Dix interval velocity.

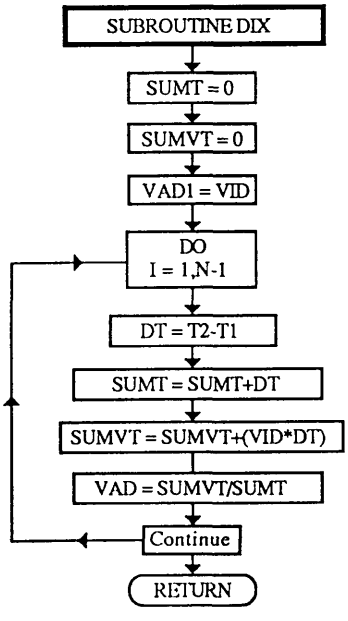

SUMT - Summation of the time.

SUMVT - Summation of the product velocity and time.
VID - Dix interval velocity.
VAD1 - First Dix average velocity.

I - Counter for calculated loops.

T - Time.
DT - Difference in time.

VAD - Dix average velocity.

Fig.3.8. (Continued) Detailed flowchart for DIFFER and DIX subroutines

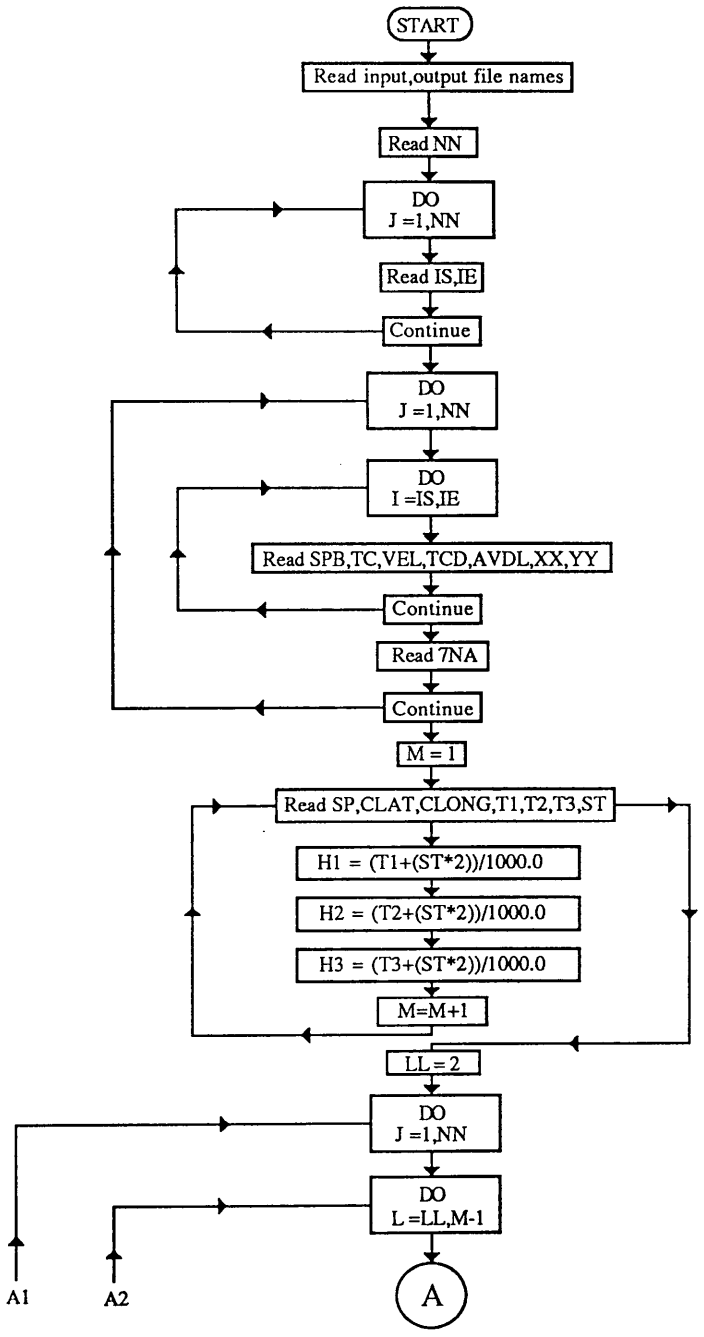

NN - Number of velocity analysis boxes.

J - Counter for number of boxes.

IS - Started counter of data.
IE - Ended counter of data.

J - Counter for number of boxes.

I - Counter for data number.

SPB - Shot point number at the location of the velocity analysis.
VEL - RMS velocity.
AVDL - Dix interval velocity.
TC - Time corresponding to the rms velocity.
TCD - Time corresponding to the Dix average velocity.
XX - Depth corresponding to the rms velocity.
YY - Depth corresponding to the Dix average velocity.
M - Counter for picked shot point.

SP - Shot point number.
CLAT - Latitude for SP.
CLONG - Longitude for SP.
T1 - Picked two-way time for the horizons1.
T2 - Picked two-way time for the horizons2.
T3 - Picked two-way time for the horizons3.
ST - One-way static correction at SP.
H1 - Subsurface two-way time for the horizons1.
H2 - Subsurface two-way time for the horizons2.
H3 - Subsurface two-way time for the horizons3.

J - Counter for number of boxes.

L - Counter for picked shot point.

Fig.3.9. Detailed flowchart for the BOXMATCH program.

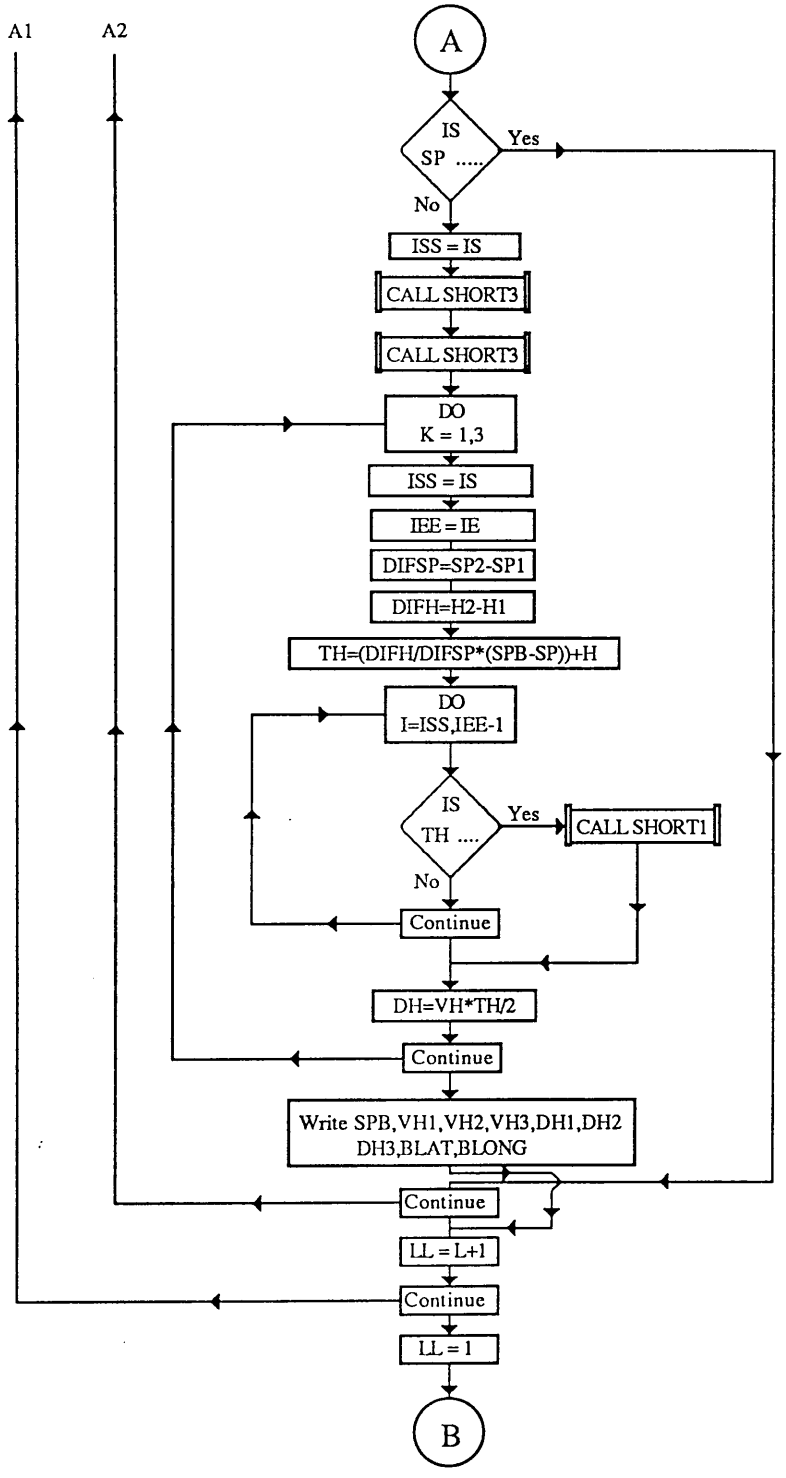

ISS - Starting counter of data.

CALL SHORT3 - Call subroutine SHORT3.

K - Counter for the horizons.

ISS - Starting counter of data.
IEE - Ended counter of data.
H2 - Time at SP2 (Second shot point).
H1 - Time at SP1 (First shot point).
DIFSP - Difference in shot point.
DIFH - Difference in time.
H - Time.
TH - Two way time to the horizons at SPB location.

I - Counter for data number.

CALL SHORT1 - Call subroutine SHORT1.

VH - Velocity corresponding to TH for SPB calculated from SHORT1 subroutine.
DH - Depth corresponding to TH and VH at SPB location.

VH1 - Velocity for horizon (1).
VH2 - Velocity for horizon (2).
VH3 - Velocity for horizon (3).
DH1 - Depth for horizon (1).
DH2 - Depth for horizon (2).
DH3 - Depth for horizon (3).

BLAT - Latitude for SPB calculated from SHO subroutine.
BLONG - Longitude for SPB calculated from SHORT3 subroutine.

Fig.3.9. (Continued) Detailed flowchart for the BOXMATCH program.

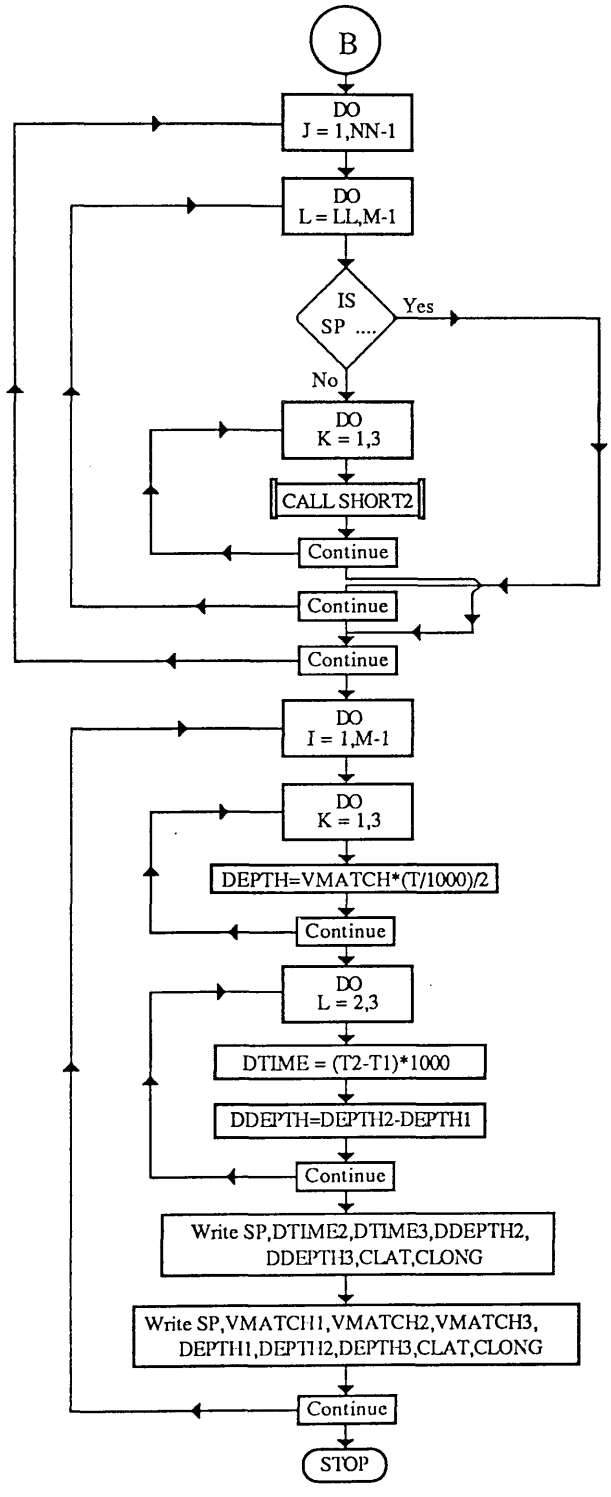

J - Counter for loops.

L - Counter for picked shot point.

K - Counter for horizons.

CALL SHORT2 - Call subroutine SHORT2.

I - Counter for picked shot point.

K - Counter for horizons.

VMATCH - Required velocity corresponding to SP calculated from SHORT2 subroutine.

DEPTH - Required depth to the horizon at SP location.

L - Counter for layers.

DTIME - Difference in time.

DDEPTH - Difference in depth.

Fig.3.9. (Continued) Detailed flowchart for the BOXMATCH program.

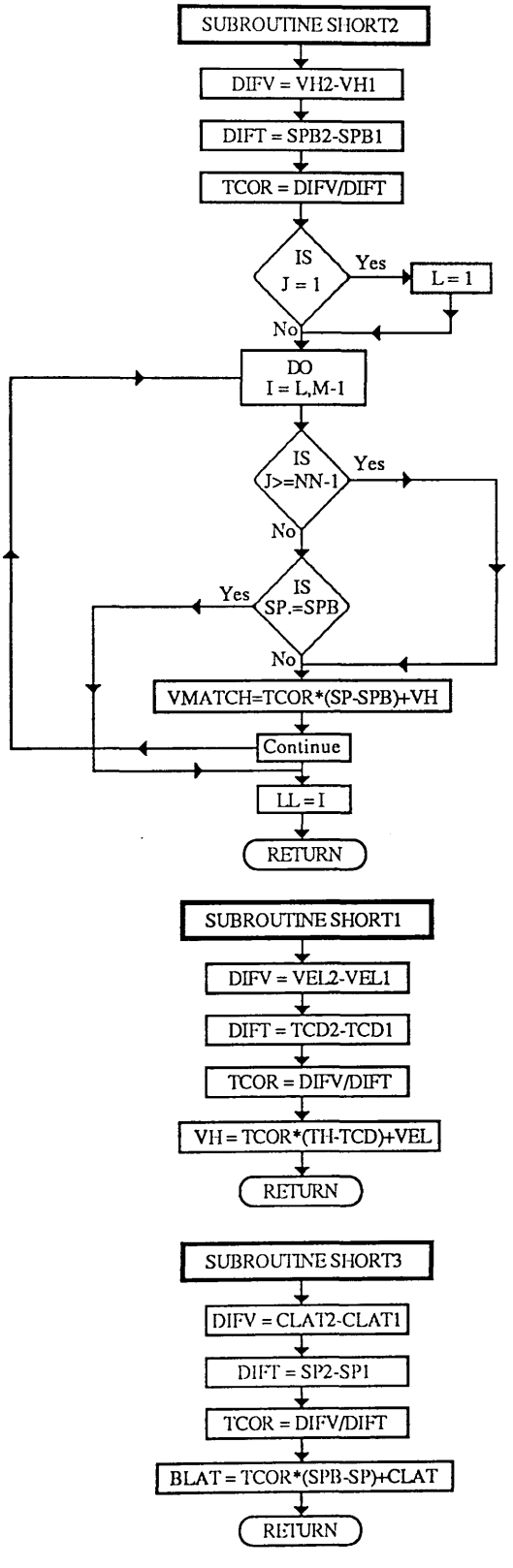

DIFV - Difference in velocity.

DIFT - Difference in shot point.

I - Counter for picked shot point.

SP - Shot point number.
SPB - Shot point number at velocity analysis.

VMATCH - Velocity.

DIFV - Difference in velocity.

DIFT - Difference in depth.

VH - Interpolated velocity.

DIFV - Difference in latitude or longitude.

DIFT - Difference in shot point.

BLAT - Interpolated Latitude or longitude.

Fig.3.9. (Continued) Detailed flowchart for SHORT1, SHORT2 and SHORT3 subroutines.

The first macro called GATEST, produces two plots, the first of stacking velocity (V_{stk}) versus two-way time, and the second of Dix average velocity versus two-way time, for each line separately.

The second macro (GATEST2) was designed to produced four different plots of interval velocity versus two-way time. The first plot uses the interval velocity derived from the depth (D1, derived from the application of the stacking velocity) of equation 3.4, the second plot uses the interval velocity derived from the depth (D2, derived from the application of the Dix average velocity) of equation 3.4, the third plot uses the interval velocity derived from stacking velocity of equation 3.13, and the fourth plot uses the interval velocity derived from equation 3.13 (assuming that the stacking velocity equal to the Dix average velocity).

The commands of the two macros are shown in Appendix 3.4. The results from these two macros are discussed in Section 3.6. below.

The results from the two macros GATEST and GATEST2 are shown in Figure 3.10 and in Appendix 3.5 (Figures 3.11 - 3.27), each Figure has six plots a, b, c, d, e, and f. It is difficult to recognize the difference between the stacking velocity plot (Fig. 3.10a) and the Dix average velocity plot (Fig. 3.10b) because of the small velocity scale, and because they have the same shape.

The velocity curves for each shot point have been shifted by a constant amount corresponding to its location (see Appendix 3.4) for ease of comparison.

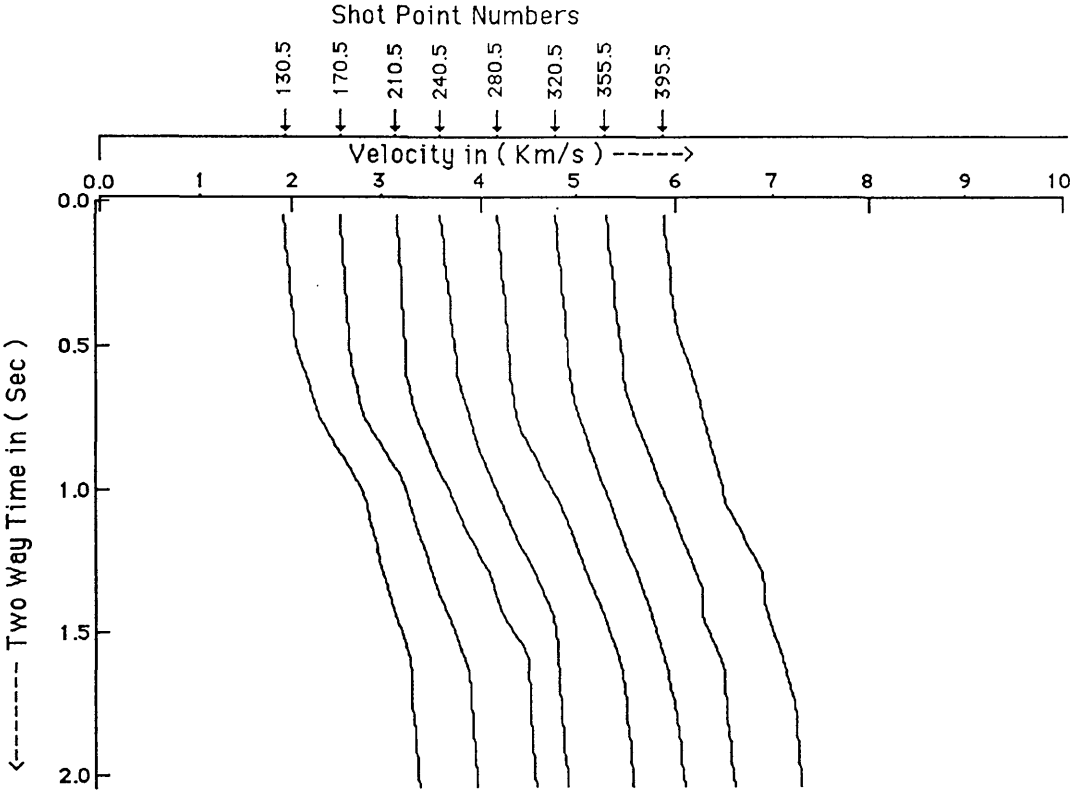

Fig.3.10a Stacking velocity - two-way time relationships along seismic line 6V248.

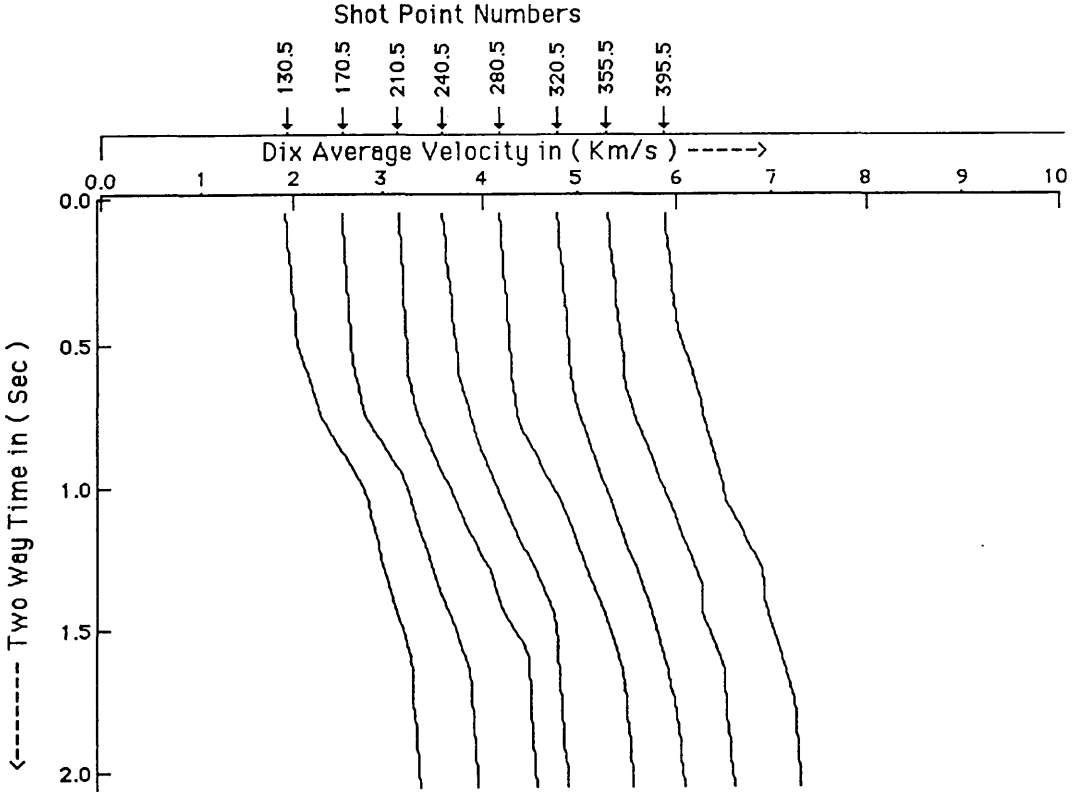

Fig.3.10b Dix average velocity - two-way time relationships along seismic line 6V248.

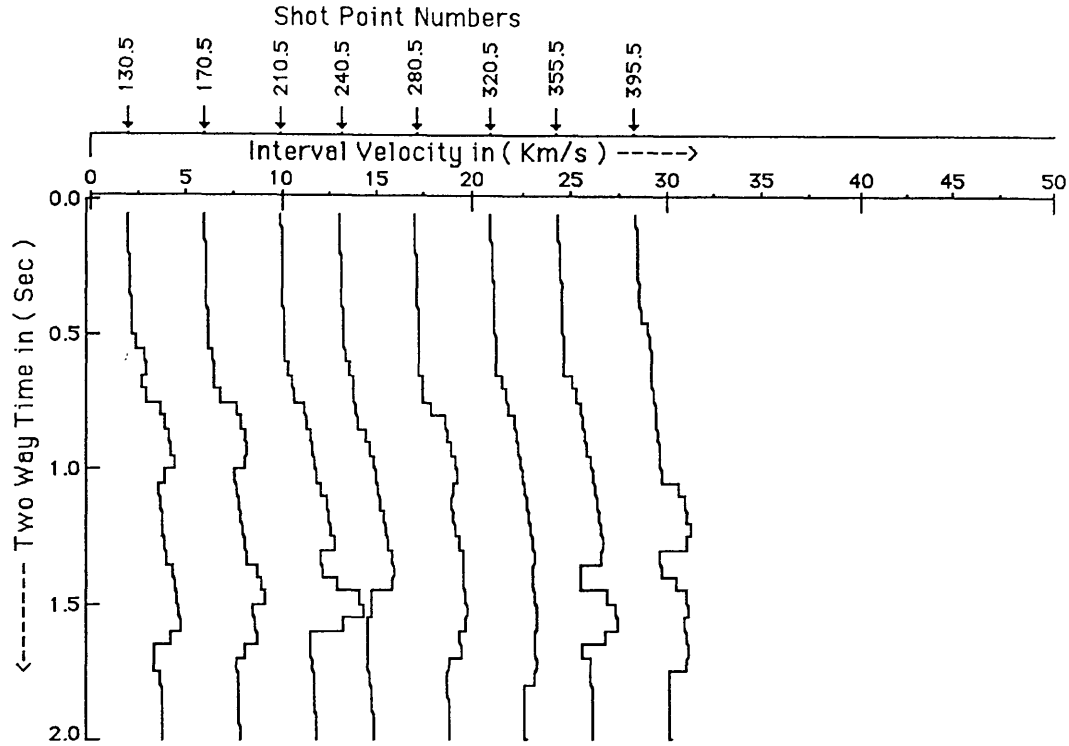

Fig.3.10c Interval velocity - two-way time relationships along seismic line 6V248, using the depth (D1) applied on equation (3.4).

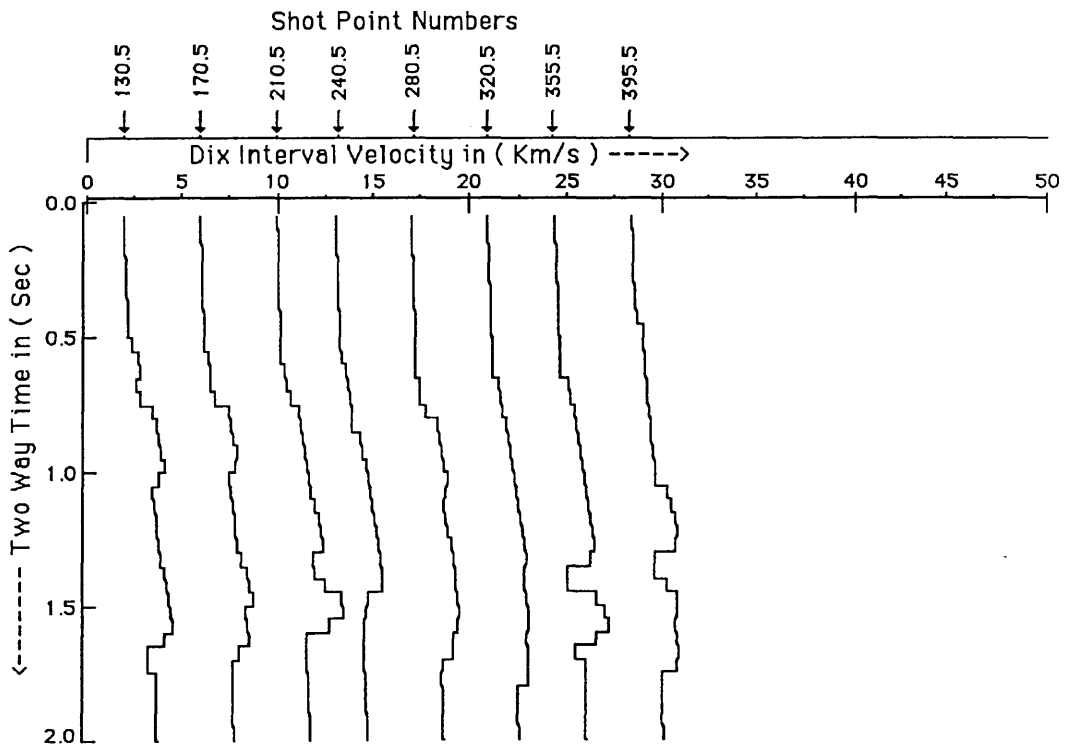

Fig.3.10d Interval velocity - two-way time relationships along seismic line 6V248, using the depth (D2) applied on equation (3.4).

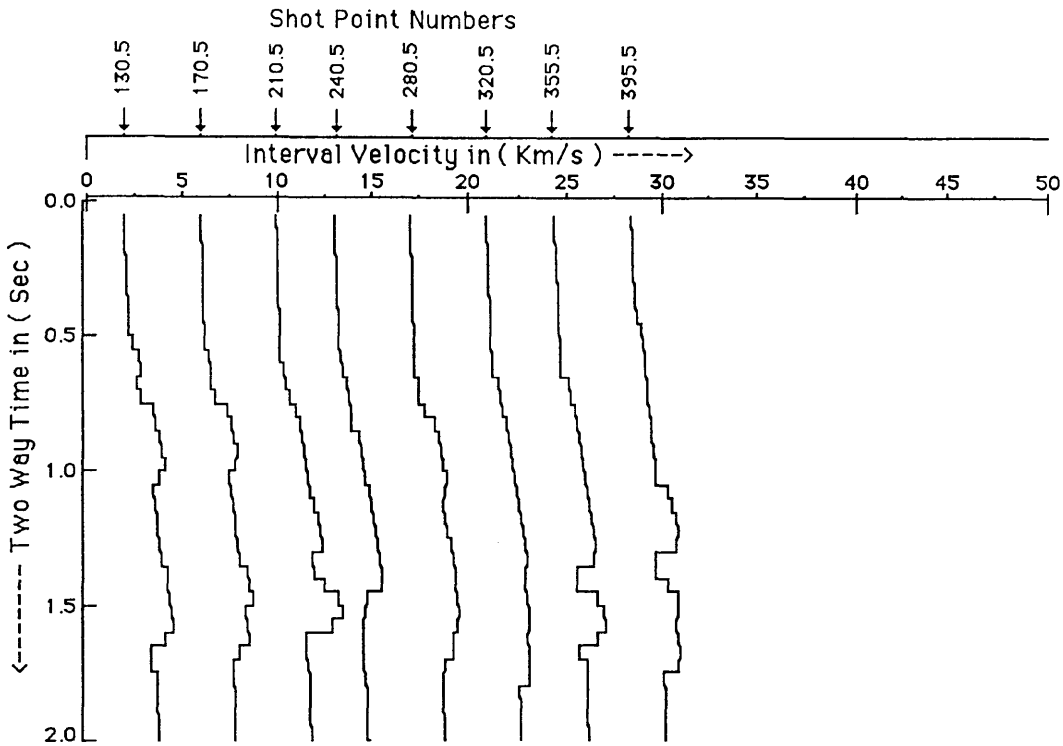

Fig.3.10e Interval velocity - two-way time relationships along seismic line 6V248, using stacking velocity applied on equation (3.13).

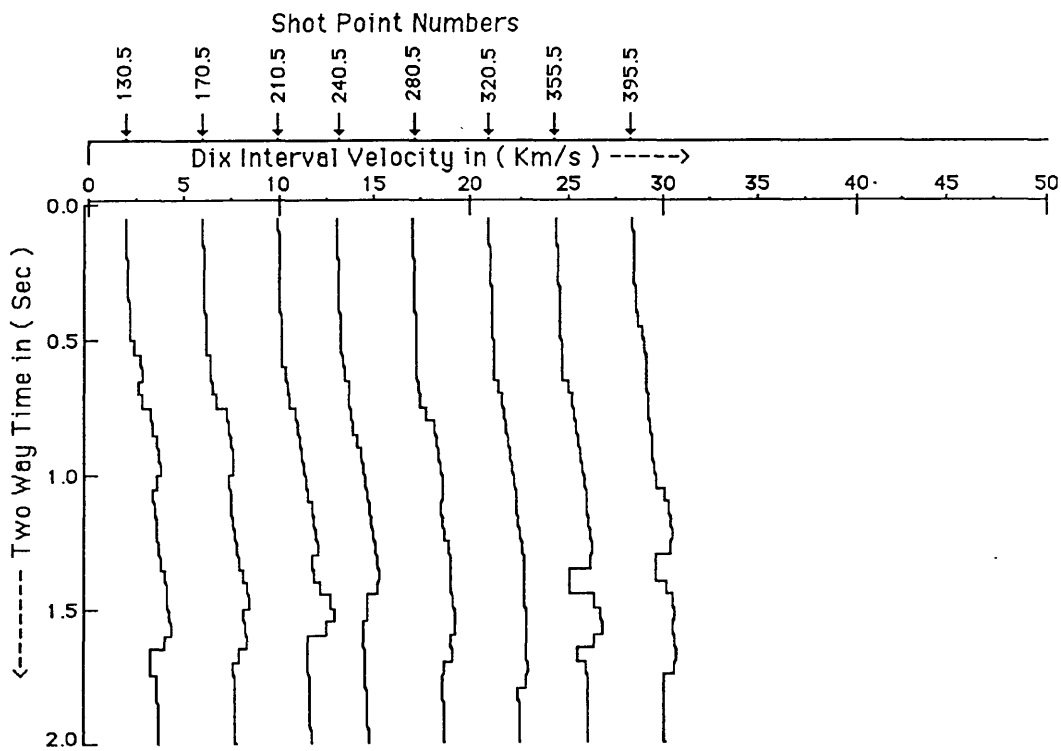

Fig.3.10f Interval velocity - two-way time relationships along seismic line 6V248, using Dix average velocity applied on equation (3.13).

As mentioned above, the stacking velocity is always higher than the Dix average velocity. The difference is demonstrated in the statistical section below.

One assumption has been made in equation 3.13, to generate the plot f (Fig. 3.10). It was assumed that Dix average velocity is equal to the stacking velocity.

Figure 3.27 shows an interpolated subsurface stacking velocity contour plot for one seismic line. Plots for the other lines are in Appendix 3.6 (Figures 3.28 - 3.43).

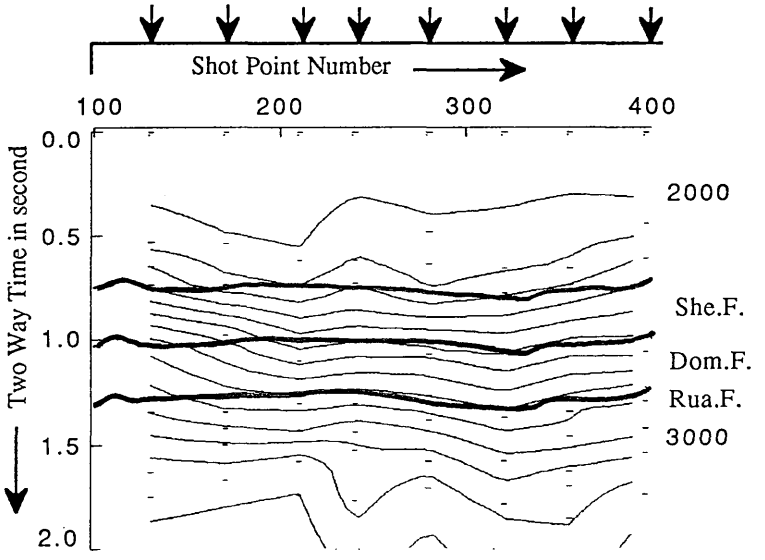

Fig. 3.27 Interpolated stacking velocities on line 6V248-85. Velocity analyses are made at locations indicated by ↓ at top. Times individual picks are shown by small dashes. Computer interpolates in time and then in space to get complete stacking velocity field indicated by the 100 m/s contours. Time picks from seismic section for different horizons are shown in red.

The computer interpolates in time and then in space to generate a complete stacking velocity field contoured at 100 m/s. The velocity analyses were made at locations indicated by an arrow at the top of the Figure. The times picked from the seismic section every 10 shot-points for the three chosen horizons are connected up, as shown by solid lines.

Figure 3.28 and the others in the Appendix 3.6 give a good indication of the stacking velocity. It shows how accurate or otherwise the velocity picks are in relation to the geology.

In general, the figures show that most of the time, values at the velocity analysis locations were picked close to the chosen horizons, which are strong reflections.

3.6.1 *Statistical work*

Some of the S language statistical functions are now used to provide a clear picture of the relationships between parameters such as velocity, depth, two-way time, etc.

One of the functions fits linear models, such as reg(x,y), where x is a matrix for fitting $y = a + b\,x$ whose columns are the predictor variables and y is a vector to be fitted to the linear model. This function is written as

```
regxy <- reg(x,y)
```

After plotting the data, another useful graphical technique for linear regression and other model fitting situations is to plot a fitted line on the data from which it was derived. This is done by the function abline(a,b), which plots the line whose equation is y = a + b x . This function also recognizes the structure returned by the model fitting functions like reg and draws the line defined by the coefficients of a simple regression. This is done by abline(regxy).

3.6.1.1 *Correlation*

There are three patterns one can observe on a scatterplot:

(1) The variables are positively correlated if the larger values of one variable tend to be associated with larger values of other variable, and similarly with smaller values of each variable.

(2) The variables are negatively correlated if the larger values of one variable tend to be associated with smaller values of the other.

(3) The variables are uncorrelated if the two variables are not related to each other.

3.6.1.2 *Linear regression*

A strong relationship between two variables can help us predict one variable if the other is known. The simplest way to deal with this type is linear regression, which assumes that the dependence of one variable on the other can be described by the equation of a straight line (Isaaks 1989).

$$y = ax + b$$

where a is the slope, and b is the constant (intercept).

In the present study a number of data pairs were used to calculate a linear regression equation for the velocity in m/s and the two-way travel time in s. For the data corresponding to two-way times less than or equal 2 s for predicting the stacking velocity (V_{stk}) from the two-way time (T), we get:

$$V_{stk} = (891 \pm 2)\,T + (1685 \pm 3) \quad \ldots\ldots\ldots\ldots\ldots\ldots\ldots\ldots\ldots\ldots (3.21)$$

In the top of the column a in Figure 3.44 this line is superimposed on the scatterplot. Equation 3.21 therefore gives us a prediction for the stacking velocity (V_{stk}) from the two-way time (T). Time is shown increasing downwards on the vertical axis.

For the data corresponding to two-way times less than or equal 2 s. for predicting the stacking velocity (V_{stk}) from the depth (D_{stk}), we get:

$$V_{stk} = (0.50 \pm 0.001)\,D_{stk} + (1852 \pm 2) \quad \ldots\ldots\ldots\ldots\ldots\ldots\ldots\ldots (3.22)$$

In the top of the column b in Figure 3.44 this line is superimposed on the scatterplot. Equation 3.22 therefore gives us a prediction for the stacking velocity (V_{stk}) from the depth (D_{stk}). Depth is shown increasing downwards on the vertical axis.

The straight-line fits in the top row in Figure 3.44 are clearly a poor fit to the S-shape of the data. We can subdivide the data into vertical zones A, B, and C as shown, and fit separate straight lines to each sub-zone. These are shown in the graphs beneath, and summarised in Table 3.1.

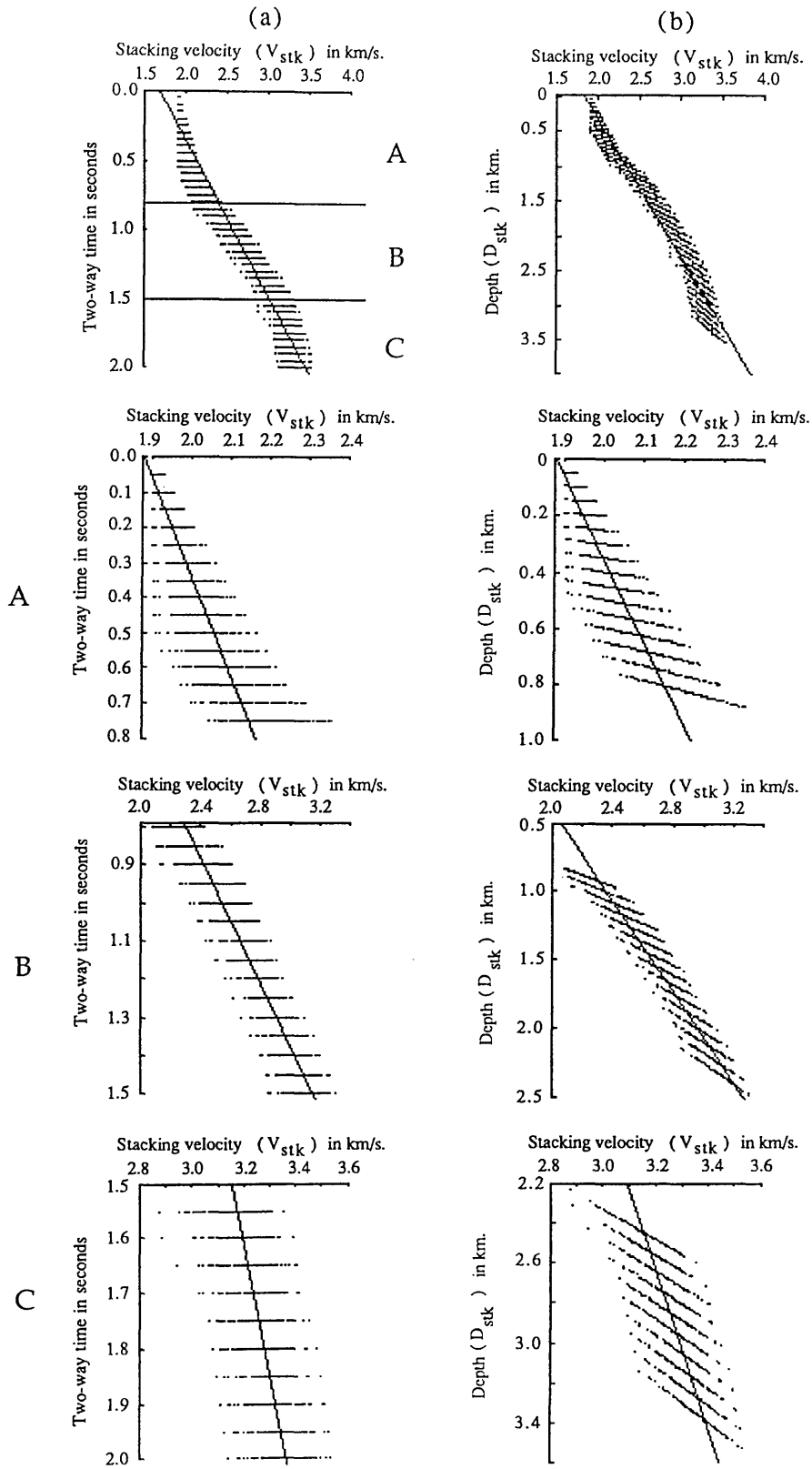

Fig. 3.44 Linear regression lines superimposed on stacking velocity (V_{stk}) and two-way time scatterplot are shown in column a and on stacking velocity (V_{stk}) and depth (D_{stk}) scatterplot are shown in column b. The data set is shown in the top row. It is also subdivided into vertical zones A, B, and C as shown separately in the 3 rows below.

Table 3.1. Summary of the coefficients derived from the straight-line fit.

Time versus stacking velocity (V_{stk})				Depth (D_{stk}) versus stacking velocity (V_{stk})		
		Coefficients			Coefficients	
		a*	b*		a	b
Whole T	0 - 2.0	891 ± 2	1685 ± 3		0.50 ± .001	1852 ± 2
A:	0 - 0.8	358 ± 4	1877 ± 2		0.34 ± .003	1881 ± 2
B:	0.8 - 1.5	1214 ± 8	1332 ± 9		0.60 ± .003	1768 ± 5
C:	1.5 - 2.0	412 ± 12	2536 ± 22		0.25 ± .005	2545 ± 14

* a is the slope, and b is the intercept.

The same analysis can be carried out for the Dix average velocity as has been done for the stacking velocity.

For the data corresponding to two-way times less than or equal 2 s. for predicting the Dix average velocity (V_{da}) from the two-way time (T), we get:

$$V_{da} = (796 \pm 2)\, T + (1714 \pm 2) \quad \ldots\ldots\ldots\ldots\ldots\ldots\ldots\ldots\ldots\ldots (3.23)$$

In the top of the column a in Figure 3.45 this line is superimposed on the scatterplot.

As before, we can plot V_{da} against depth (Fig. 3.45b), and also subdivide the time/depth scale into three zones A, B, and C. These are shown in the graphs of Figure 3.45, and the data for the linear fitting process are summarised in Table 3.2.

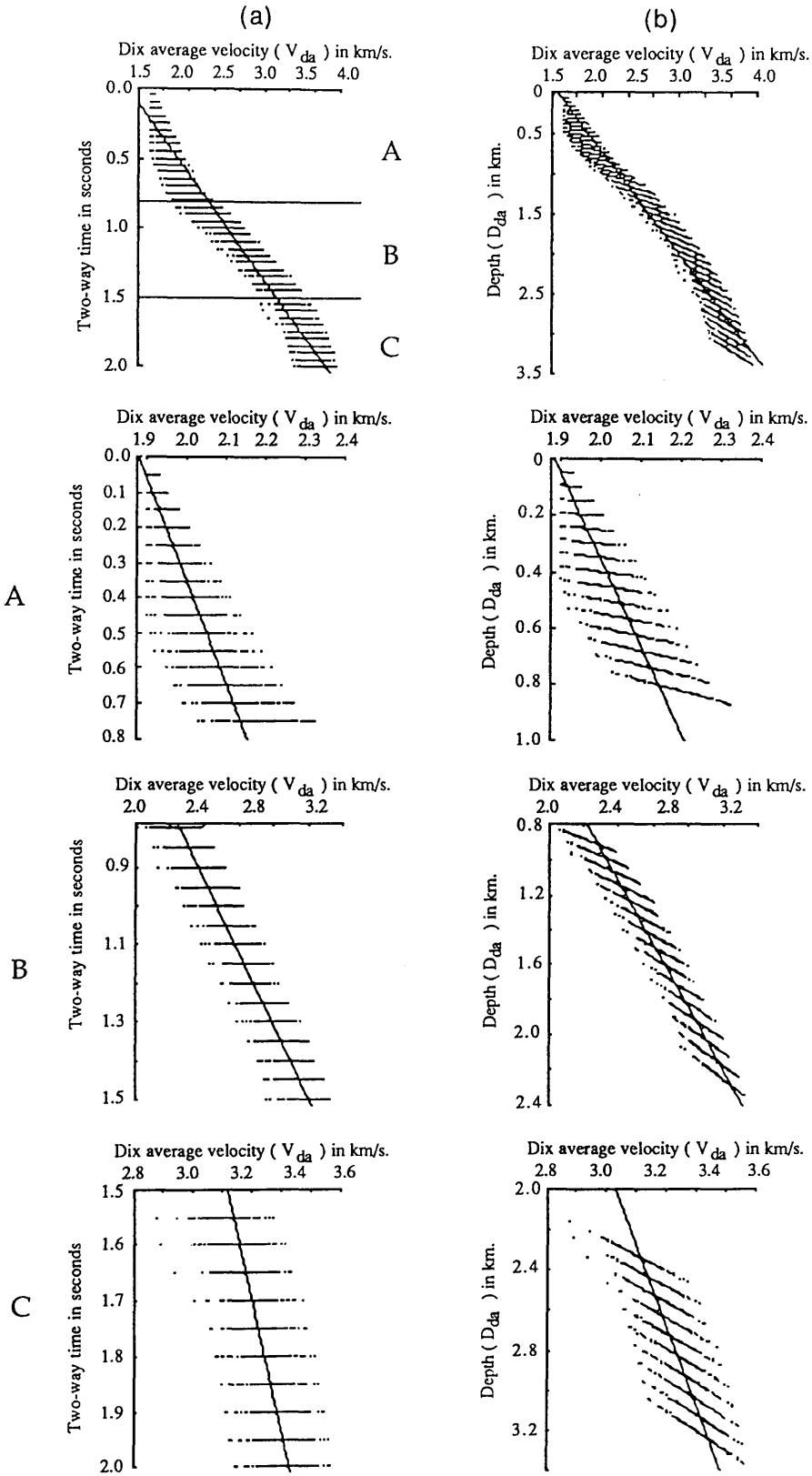

Fig. 3.45 Linear regression lines superimposed on Dix average velocity (V_{da}) and two-way time scatterplot are shown in column a and on Dix average velocity (V_{da}) and depth (D_{da}) scatterplot are shown in column b. The data set is shown in the top row. It is also subdivided into vertical zones A, B, and C as shown separately in the 3 rows below.

Table 3.2. Summary of the coefficients derived from the straight-line fit.

Time versus Dix average velocity (V_{da})				Depth (D_{da}) versus Dix average velocity (V_{da})		
		Coefficients			Coefficients	
		a*	b*		a	b
Whole T	0 - 2.0	796 ± 2	1714 ± 2		0.47 ± .001	1855 ± 2
A:	0 - 0.8	344 ± 4	1881 ± 2		0.33 ± .003	1884 ± 2
B:	0.8 - 1.5	1066 ± 7	1413 ± 8		0.56 ± .003	1772 ± 4
C:	1.5 - 2.0	427 ± 11	2376 ± 19		0.25 ± .004	2426 ± 12

* a is the slope, and b is the intercept.

Alternatively, we can represent our data in the form of the Faust equation (Section 3.2). Equation 3.3 may be expressed in the form

$$V = K Z^{n} \quad \text{.....(3.24)}$$

$$\log_{10} V = \log_{10} K + n \log_{10} Z$$

$$y = b + a x$$

It is a straight line equation on log-log scale, where a is the slope equal to the n, and b is the constant (intercept) equal to the $\log_{10} K$.

For the data corresponding to two-way times less than or equal 2 s. for predicting the logarithm of the stacking velocity ($\log_{10}(V_{stk})$) from the logarithm of the depth ($\log_{10}(Depth_{stk})$), we get:

$$\log_{10}(V_{stk}) = 0.18 \log_{10}(Depth_{stk}) + 2.87 \quad \text{.....} \quad (3.25)$$

In the top of the column a in Figure 3.46 this line is superimposed on the scatterplot. Equation 3.25 therefore gives us a prediction for the logarithm of the stacking velocity ($\log_{10}(V_{stk})$) from the logarithm of the depth ($\log_{10}(Depth_{stk})$). Logarithm of the depth is shown increasing downwards on the vertical axis.

For the data corresponding to two-way times less than or equal 2 s for predicting the logarithm of the Dix average velocity ($\log_{10}(V_{da})$) from the logarithm of the depth ($\log_{10}(Depth_{da})$), we get:

$$\log_{10}(V_{da}) = 0.17 \log_{10}(Depth_{da}) + 2.90 \quad \text{..... (3.26)}$$

In the top of the column b in Figure 3.46 this line is superimposed on the scatterplot. Equation 3.26 therefore gives us a prediction for the logarithm of the Dix average velocity ($\log_{10}(V_{da})$) from the logarithm of the depth ($\log_{10}(Depth_{da})$). Logarithm of the depth is shown increasing downwards on the vertical axis. The straight-line fits in the top row in Figure 3.46 are clearly a poor fit to the S-shape of the data. We can subdivide the data into vertical zones A, B, and C as shown, and fit separate straight lines to each sub-zone. These are shown in the graphs of Figure 3.46, and summarised in Tables 3.3 and 3.4.

The coefficients of the Faust equation for the data in Table 3.3 are summarised in Table 3.4.

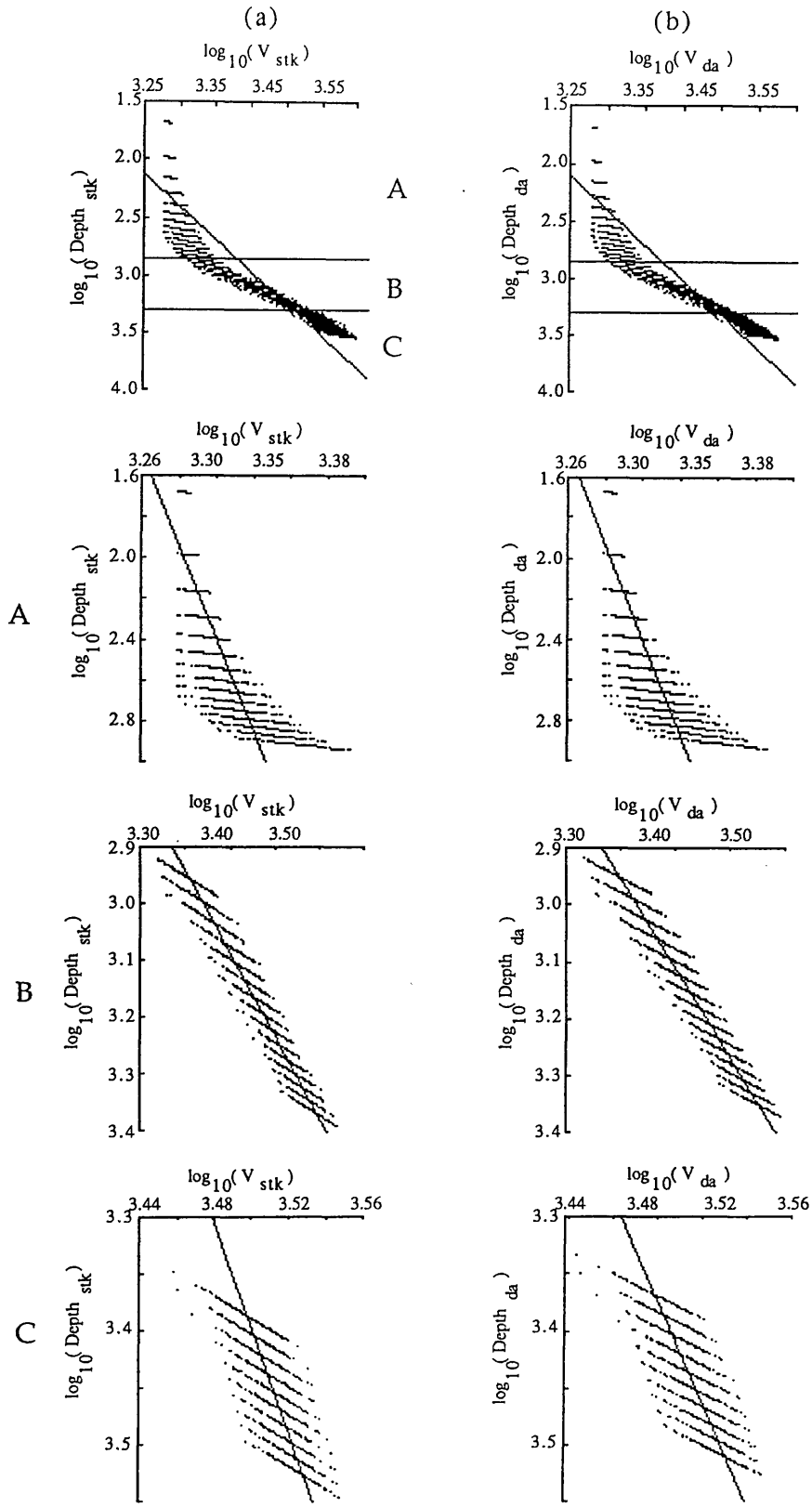

Fig. 3.46 Linear regression lines superimposed on $\log_{10}(V_{stk})$ and $\log_{10}(Depth_{stk})$ scatterplot are shown in column a and on $\log_{10}(V_{da})$ and $\log_{10}(Depth_{da})$ scatterplot are shown in column b. The data set is shown in the top row. It is also subdivided into vertical zones A, B, and C as shown separately in the 3 rows below.

Table 3.3. Summary of the coefficients derived from the straight-line fit.

$\log_{10}(Depth_{stk})$ versus $\log_{10}(V_{stk})$				$\log_{10}(Depth_{da})$ versus $\log_{10}(V_{da})$			
		Coefficients				Coefficients	
		a*	b*			a	b
Whole T	0 - 2.0	0.18	2.87			0.17	2.90
A:	0 - 0.8	0.04	3.19			0.04	3.20
B:	0.8 - 1.5	0.34	2.34			0.32	2.40
C:	1.5 - 2.0	0.22	2.75			0.23	2.72

* a is the slope, and b is the intercept.

Table 3.4. Summary of the coefficients of the Faust equation from Figure 3.46.

Stacking velocity				Dix average velocity			
		Coefficients				Coefficients	
		n	k			n	k
Whole T	0 - 2.0	0.18	736			0.17	794
A:	0 - 0.8	0.04	1566			0.04	1576
B:	0.8 - 1.5	0.34	217			0.32	252
C:	1.5 - 2.0	0.22	558			0.23	523

For the data corresponding to two-way times less than or equal 2 s. for predicting the difference in depth (stk - Dix av.) (ΔD) from the two-way time (T), we get:

$$\Delta D = (82.1 \pm 0.4)\, T - (33.6 \pm 0.4) \quad \ldots\ldots\ldots\ldots\ldots\ldots \quad (3.27)$$

In the top of the column a in Figure 3.47 this line is superimposed on the scatterplot. Equation 3.27 therefore gives us a prediction for the difference in depth (ΔD) from the two-way time (T). Time is shown increasing downwards on the vertical axis.

We can define the percentage values for the fractional difference in velocity (V_{stk}-V_{da}) (PER) in term of V_{da} as:

$$\% \text{ PER} = \left(\frac{V_{stk} - V_{da}}{V_{da}} \right) \times 100 \quad \text{.....(3.28)}$$

By plotting in the form of a histogram (column b in Figure 3.47), it can be seen that there are two strong groupings around 0% and 4%.

The straight-line fits in the top of the column a in Figure 3.47 are clearly a poor fit to the S-shape of the data. We can subdivide the data into vertical zones A, B, and C as shown, and fit separate straight lines to each sub-zone. These are shown in the graphs of Figure 3.47a, and summarised in Table 3.5.

The histogram for zone A shows a clear grouping around 0%, which indicates that there is no difference between the stacking velocity and the Dix average velocity in the shallow horizons ($V_{stk} \cong V_{da}$). For zone B the data group around 2-5%, which indicates that there is a slight difference between the stacking velocity and the Dix average velocity ($V_{stk} > V_{da}$ by 2-3%), and for zone C the data are group around 3-6%, which indicates that there is a big difference between the stacking velocity and the Dix average velocity ($V_{stk} > V_{da}$ by 3-6%).

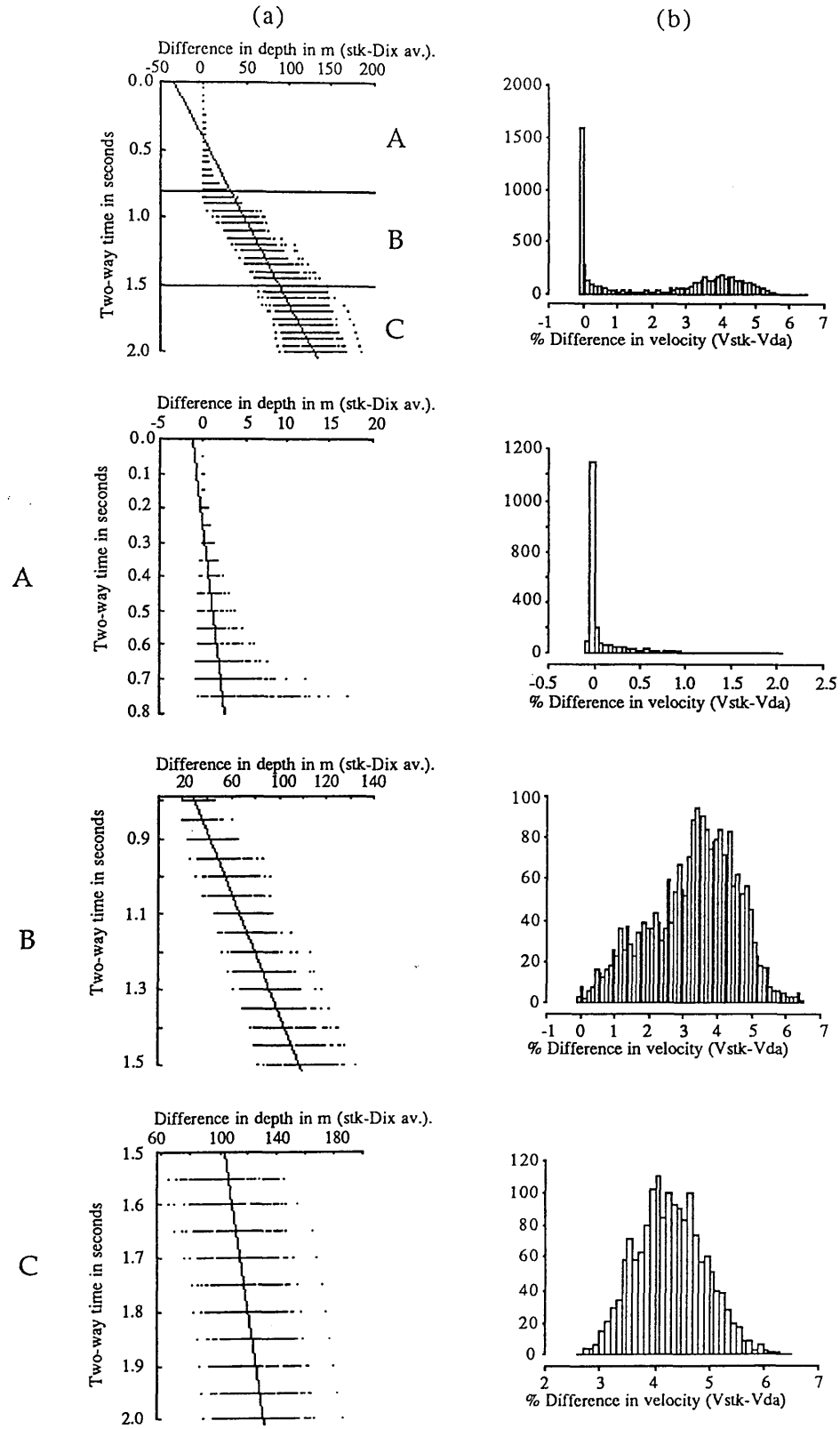

Fig. 3.47 Linear regression lines superimposed on difference in depth and two-way time scatterplot are shown in column a and histograms of the percentage are shown in column b. The data set is shown in the top row. It is also subdivided into vertical zones A, B, and C as shown separately in the 3 rows below.

Table 3.5. Summary of the coefficients derived from the straight-line fit.

Time versus Difference in depth		
	Coefficients	
	a*	b*
Whole T 0 - 2.0	82.1 ± 0.4	-33.6 ± 0.4
A: 0 - 0.8	4.8 ± 0.2	-1.2 ± 0.1
B: 0.8 - 1.5	127.1 ± 1.1	-91.5 ± 1.3
C: 1.5 - 2.0	54.2 ± 3.0	23.0 ± 5.3

* a is the slope, and b is the intercept.

For the data corresponding to two-way times less than or equal 2 s. for predicting the percentage of the difference in velocity (PER) from the two-way time (T), we get:

$$PER = (3.06 \pm 0.02)\, T - (0.80 \pm 0.02) \quad \ldots\ldots\ldots\ldots (3.29)$$

In the top of the column a in Figure 3.48 this line is superimposed on the scatterplot. Equation 3.29 therefore gives us a prediction for the percentage of the difference in velocity (PER) from the two-way time (T). Time is shown increasing downwards on the vertical axis.

For the data corresponding to two-way times greater than or equal 2 s. for predicting the percentage of the difference in velocity (PER) from the difference in depth (ΔD), we get:

$$PER = 0.04\, \Delta D + (0.50 \pm 0.01) \quad \ldots\ldots\ldots\ldots (3.30)$$

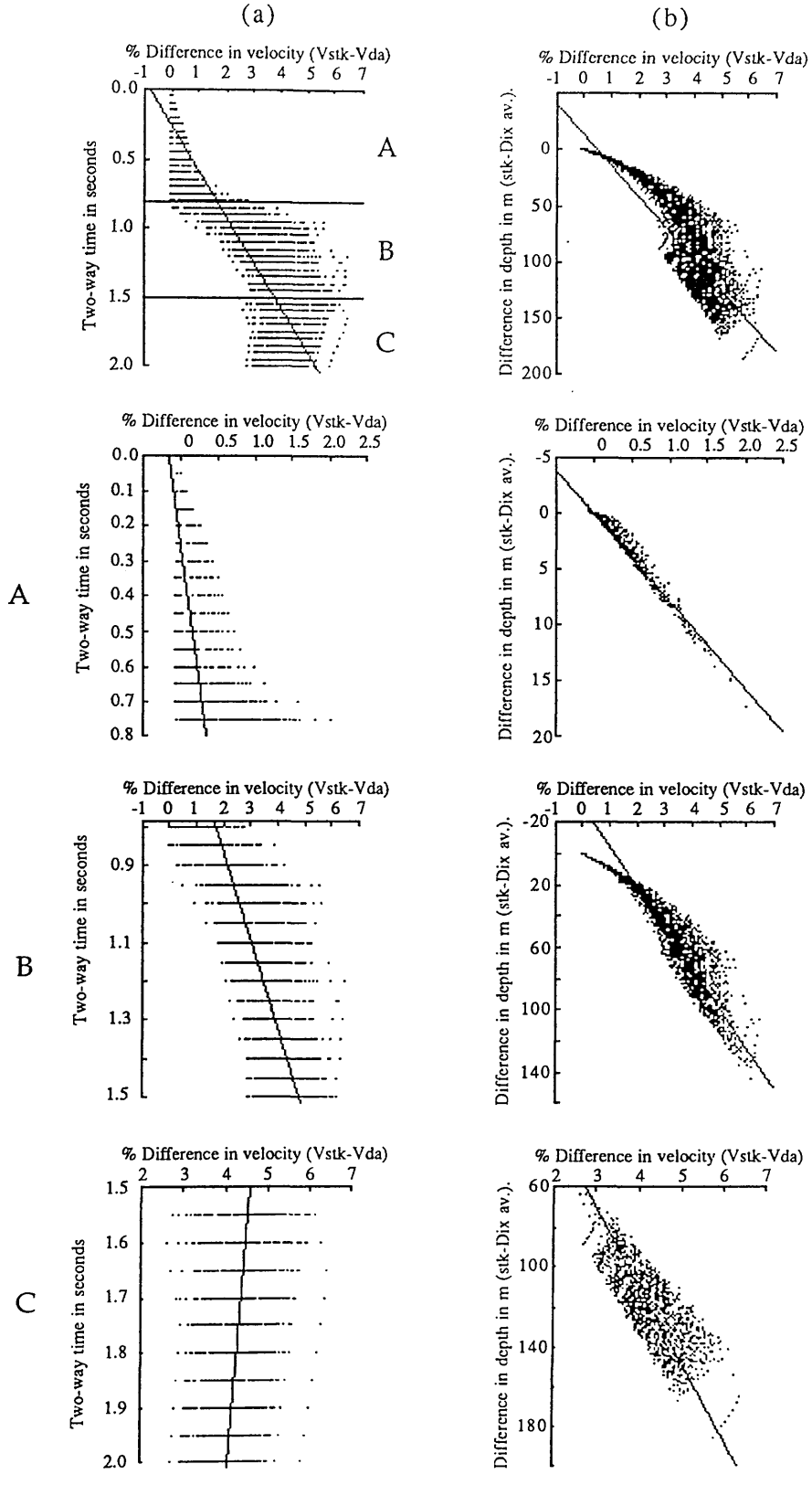

Fig. 3.48 Linear regression lines superimposed on percentage and two-way time scatterplot are shown in column a and on percentage and difference in depth scatterplot are shown in column b. The data set is shown in the top row. It is also subdivided into vertical zones A, B, and C as shown separately in the 3 rows below.

In the top of the column b in Figure 3.48 this line is superimposed on the scatterplot. Equation 3.30 therefore gives us a prediction for the percentage of the difference in velocity (PER) from the difference in depth (ΔD). Difference in depth is shown increasing downwards on the vertical axis.

The straight-line fits in the top row in Figure 3.48 are clearly a poor fit to the data. We can subdivide the data into vertical zones A, B, and C as shown, and fit separate straight lines to each sub-zone. These are shown in the graphs of Figure 3.48, and summarised in Table 3.6.

Table 3.6. Summary of the coefficients derived from the straight-line fit.

	Time versus Difference in velocity		Difference in depth versus Difference in velocity	
	Coefficients			Coefficients
	a*	b*		a b
Whole T 0 - 2.0	3.06 ± .02	-0.80 ± .02		0.04 ± 0.0 0.50 ± .01
A: 0 - 0.8	0.63 ± .02	-0.16 ± .01		0.13 ± 0.0 0.0
B: 0.8 - 1.5	4.42 ± .08	-1.80 ± .09		0.04 ± 0.0 1.16 ± .02
C: 1.5 - 2.0	-1.04 ± .11	6.13 ± .19		0.03 ± 0.0 1.22 ± .06

* a is the slope, and b is the intercept.

For the data corresponding to two-way times less than or equal 2 s. for predicting the heterogeneity factor (H) (Section 3.4) from the two-way time (T), assuming that the stk velocity is equal to the rms velocity, we get:

$$H = 0.06\,T - 0.02 \quad \text{..... (3.31)}$$

In the top of Figure 3.49 this line is superimposed on the scatterplot. Equation 3.31 therefore gives us a prediction for the heterogeneity factor (H)

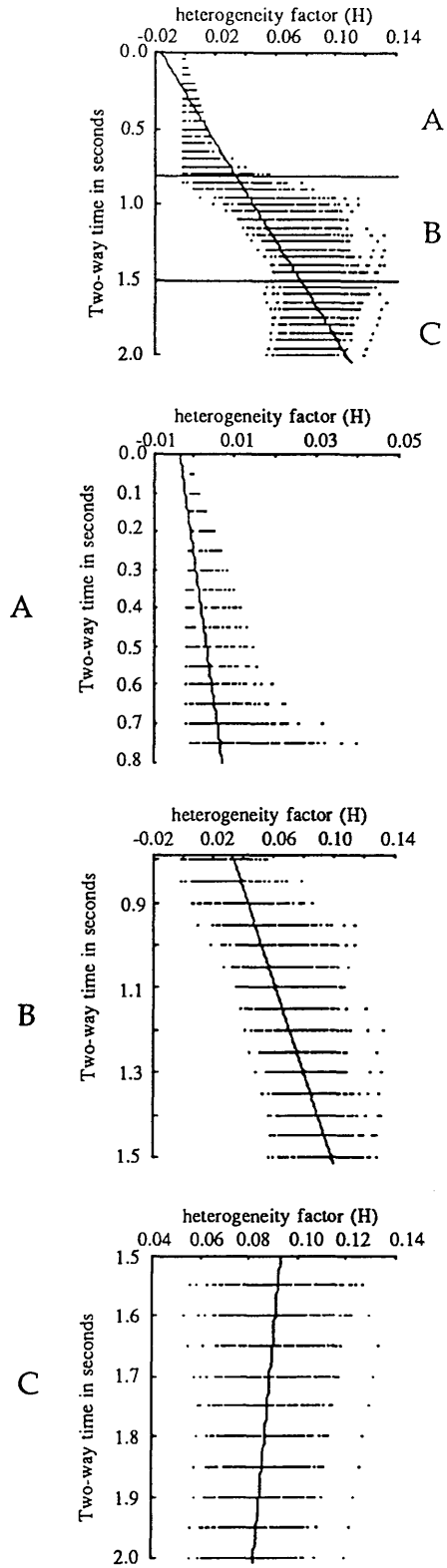

Fig. 3.49 Linear regression lines superimposed on heterogeneity factor and two-way time scatterplot are shown in the figure. The data set is shown in the top row. It is also subdivided into vertical zones A, B, and C as shown separately in the 3 rows below.

from the two-way time (T). Time is shown increasing downwards on the vertical axis.

The straight-line fits in the top of Figure 3.49 are clearly a poor fit to the S-shape of the data. We can subdivide the data into vertical zones A, B, and C as shown, and fit separate straight lines to each sub-zone. These are shown in the graphs of Figure 3.49, and summarised in Table 3.7.

From the subdivided zones A, B, and C in Figure 3.49, it is clear that the heterogeneity factor varies between 0-1%, 2-10%, and 8-10% respectively. It is fairly constant in zones A and C, but increases with depth in zone B.

Table 3.7. Summary of the coefficients derived from the straight-line fit.

Time versus heterogeneity factor (H)		
	Coefficients	
	a*	b*
Whole T 0 - 2.0	0.06	-0.02
A: 0 - 0.8	0.01	0.0
B: 0.8 - 1.5	0.09	-0.04
C: 1.5 - 2.0	-0.02	0.13

* a is the slope, and b is the intercept.

CHAPTER (4)

CONTOURING, MAPPING AND INTERPRETATION

4.1 *Introduction*

The object of seismic interpretation is usually to prepare contour maps showing the depth to different reflectors which have been picked on the seismic section (McQuillin, Bacon, and Barclay, 1979). The key to contouring is the shape characteristic of typical geological surfaces (Badley, 1985). Some other maps rather than depth maps can be made for each sequence unit showing the geographical distribution of parameters such as thickness and shape of the unit (Sheriff, 1980).

Three stratigraphic markers that are of interest to oil and gas prospectors in the area of study and the surrounding region have been chosen for contouring. They are as follows: Top of the Sheghega Formation, top of the Domran Formation, and the top of the Ruaga Formation.

The top of Ruaga formation was chosen because it contains the Zelten member, which is a producing zone. The other two horizons were chosen because they are important zones in the neighbouring fields. These markers can be correlated easily from well to well, being good reflectors.

Reflection seismic data acquired by the Vibroseis method, covering an area of 350 km^2, have been chosen from the 1984/85 seismic survey, for the re-interpretation.

4.2 *Seismic data*

The seismic database consists of 17 lines totalling 314 km. of 48 fold Vibroseis data acquired in 1984/85 (Figure 4.1). Reflections from all formations of interest in the area of study have two-way travel times of less than 2 s. Reflection data quality is moderate to good in general, being very good at the top of the Palaeocene Zelten member and in Ruaga formation and shallow formations. Quality is moderate, at the same time difficult to interpret, at the Upper Cretaceous Zmam formation and deeper levels.

These seismic data provide a good coverage for preliminary mapping of the interesting formations. Reflection seismic lines are orientated in a NW-SE and SW-NE direction with approximately 3 km average spacing (Figure 4.1). In 1988 more seismic lines were shot in between, according to the seismic anomalies recognised by interpretation 1984/85 data. The final re-interpretation, presented in this project, used only the 1984/85 seismic data.

4.2.1 *Data acquisition*

The data were recorded by the Bulgarian oil company (BOCO) crew 9. Four truck-mounted vibrators sweep simultaneously in source arrays appropriately designed to attenuate surface noise and to improve the weak signal to noise ratio. Another two vibrators were on standby in case of one of the four vibrators broke down. Each vibrator is coupled to the land surface and a long train of waves of progressively increasing or decreasing frequency is generated over a period of time (10 s.).

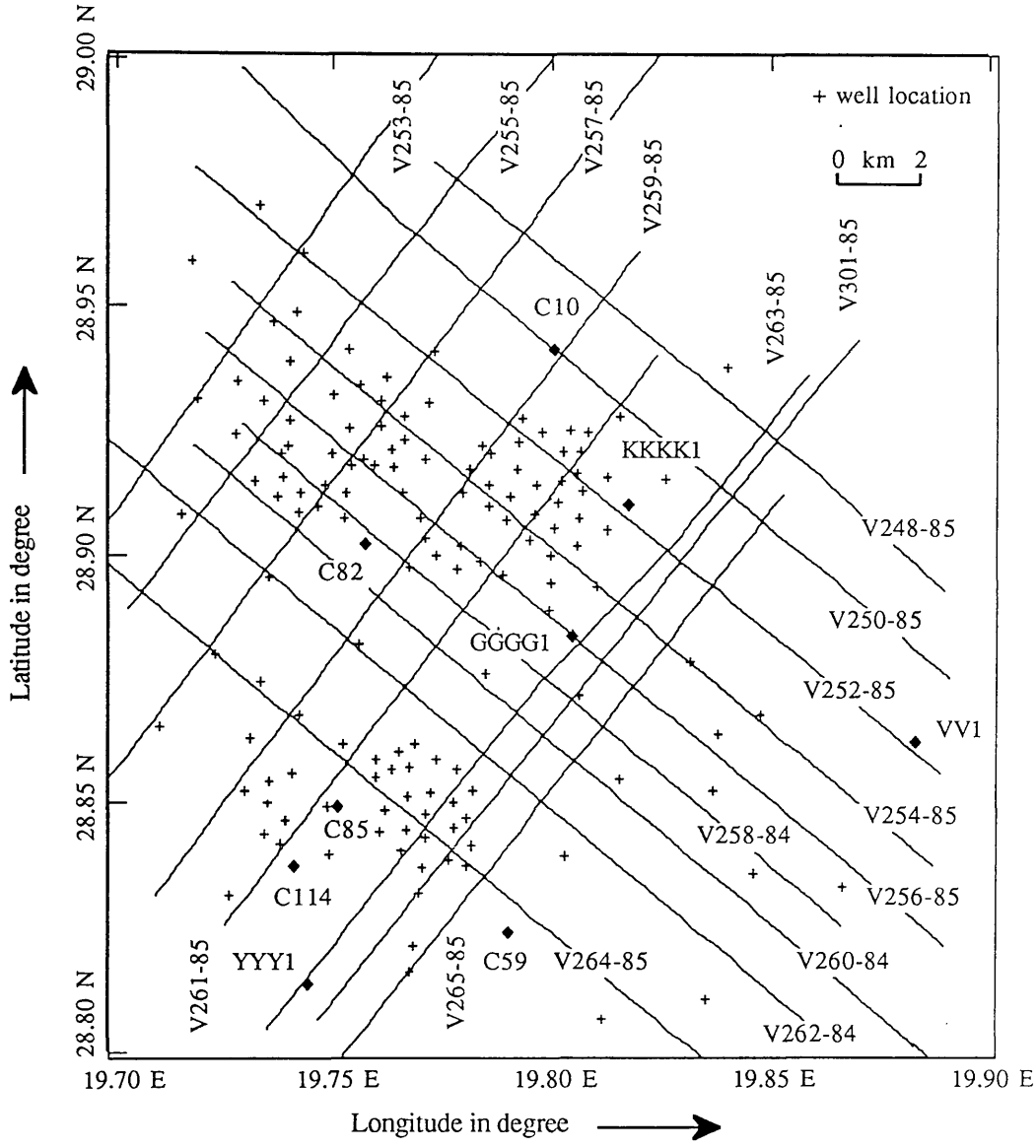

Fig. 4.1 Seismic line location map, showing well locations.

The two kinds of sweeps the vibrator could generate are an upsweep (increasing frequency input) from 8-48 Hz, as in our case, or a downsweep (decreasing frequency input). The outputs from either kind of sweep are summed and correlated with the input sweeps to provide a conventional field record.

Receiver arrays were designed to attenuate surface noise and to improve the weak signal to noise ratio.

The field acquisition conditions were fair, with rough terrain over the most of the program area, but shooting of some of the seismic lines across the field itself caused some problems. The field acquisition parameters were based on the results of a noise study carried out in the area. Figures 4.2 a, b, and c show the source array, receiver array, and spread diagram respectively, which were chosen for this particular survey from the noise study results. Four seconds two-way time were recorded. The most significant parameters are:

Sweep frequency ..... 8-48 Hz
Sweep length ..... 10 s.
Recording length ..... 14 s.
Sample rate ..... 4 ms.
Geophone group interval ..... 50 m.
V.P. interval ..... 50 m.
Number of vibrators 4
Number of sweeps 8

(a) Source array.

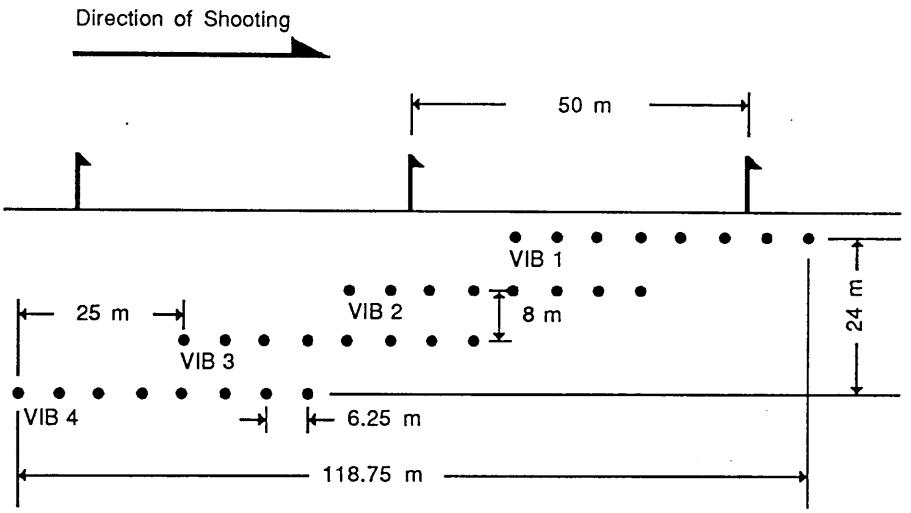

(b) Receiver array.

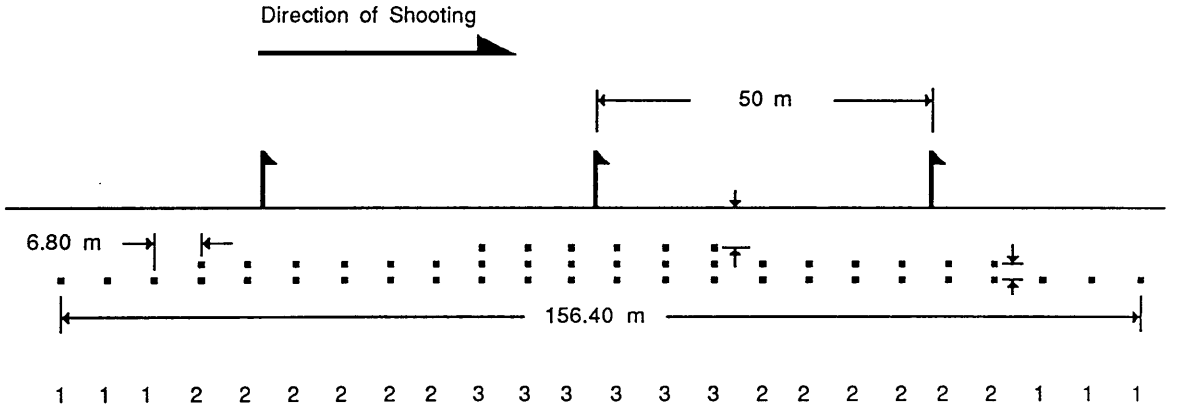

(c) Spread diagram.

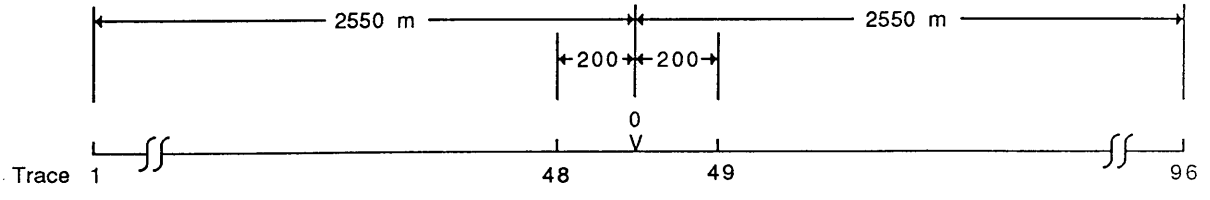

Fig. 4.2 Source array, receiver array, and spread diagram.

Full details of the recording parameters are shown on the left side of the labels of the seismic sections (Figure 4.3). We expect good quality data over a flat area when the weather is good, and worse data near the fault zones and/or in bad weather. Rough terrain, where the acquisition parameters such as receiver and source arrays do not work well, is probably the cause of a lot of the noise on the records.

A drilling and uphole shooting program was carried out, normally at the intersection of seismic lines, and provided accurate information about the weathering layers for static calculations.

Table 4.1 shows all the seismic lines which have been used in the re-interpretation.

Table 4.1 Seismic line summary.

(a) Strike lines

SL	FSP	LSP	LC	DIR
V248	100	400	15	SE
V250	120	540	21	SE
V252	130	560	21.5	SE
V254	100	510	20.5	SE
V256	100	530	21.5	SE
V258	260	610	17.5	SE
V260	260	690	21.5	SE
V262	160	550	19.5	SE
V264	150	490	17	SE

(b) Dip lines

SL	FSP	LSP	LC	DIR
V253	110	410	15	SW
V255	110	420	15.5	SW
V257	130	530	20	SW
V259	110	470	18	SW
V261	110	430	16	SW
V263	110	490	19	SW
V301	100	490	19.5	SW
V265	100	420	16	SW

Abbreviations: SL = Seismic line number; LC = Length of coverage in km; FSP = First shot point; LSP = Last shot point; DIR = Direction of shooting (towards)

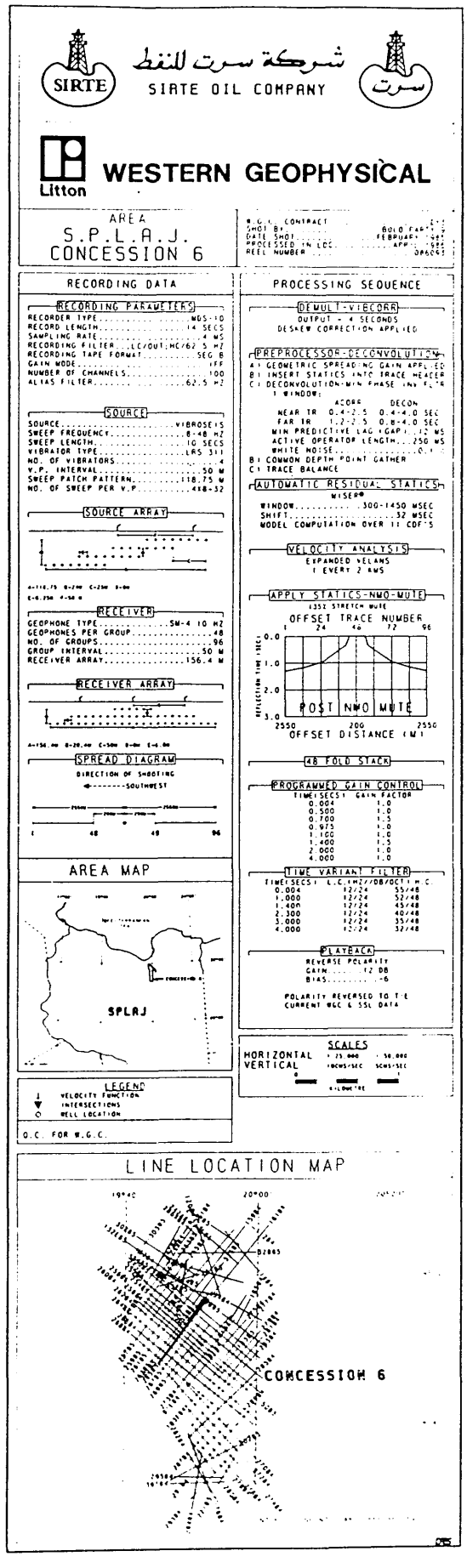

Figure 4.3. label of the seismic section.

Part (a) from Table 4.1 shows the seismic lines parallel to the main fault in the area. Part (b) shows the seismic lines crossing the main fault.

4.2.2 *Data processing*

The data were processed by Western Geophysical Company (WGC), which has the best reputation for processing such data. The selection of processing parameters was based on the results of a standard series of processing tests. Full details processing parameters are shown on the right side of the labels of the seismic sections (Figure 4.3).

The client (Sirte Oil Company) provided two formulae -"Sabkha and Lehib"- for the static calculation to be used in the processing the seismic lines rather than the uphole data calculation.

4.3 *Reflection identification*

Starting with geological knowledge of the area and well log analysis in the area of study will not only give us a useful geological picture, but also show where strong reflections might be expected, where there is a change in an acoustic impedance. So the first step is to use the sonic log or CVL (Continuous Velocity Log), which was recorded for wells C10, C59, C82, C85, C114, VV1, YYY1, GGGG1, and KKKK1 and tied to the seismic times for horizon identification. Three seismic events were marked and correlated, namely, Sheghega, Domran, and Ruaga.

It is necessary to use a time-depth curve or log incorporating the results of well check shots, to relate the seismic events to the geological horizons. Seismic events or reflectors on the seismic section are usually continuous over a limited region such as the study area, except for faults which introduce discontinuities in the reflectors (Stulken, 1941; McQuillin, Bacon, and Barclay, 1979). The edge of the faults causes diffraction patterns on un-migrated section. These are often useful in locating the fault plane, which should pass through the apex of the hyperbola (McQuillin, Bacon, and Barclay, 1979).

In the case of major faults it is usual (in the absence of any well information) to use the reflection character as a guide to the correlation across the fault. It can be done by folding the section so as to bring the two sides of the fault together, and moving one up or down to match the reflection character.

The character of the reflection is highly dependent on processing parameters which may change over a major fault. In this stage it is useful to make a rough map of the main structural features, which can be very helpful in contouring.

4.4 *Closing loops*

After the picks have been settled the loop tying can begin. The best place to start interpretation is the area where the seismic data are good and the selected horizons are well developed. The dip lines are usually easier to interpret. Laying them out in sequence it is possible to follow the major

structures across the area, and mark in the main faults (McQuillin, Bacon, and Barclay, 1979).

Off-structure areas of interpretation can give good results, because in the structural highs, where the wells have usually been drilled, the sequences are thinner and seismic resolution is poor (McQuillin, Bacon, and Barclay, 1979). The main objective of line tying and interpretation is to trace the lateral continuity of all selected events in the area (Badley, 1985).

Alignment, or phase correlation from trace to trace, is the most important feature of an event, tracing the event laterally until there is a break in continuity, such as fault, pinch-out, or poor data area. However, rather than going too far in tracing the event it is better to follow loops around the seismic grid, by folding the line at intersections with the strike lines then transferring the picks on to the strike lines and along to the next dip line (Badley, 1985). The pick transfers to the new dip line are traced to the next strike line intersection and then back again to the original dip line, so closing a loop.

If the picks fit, that means the grid is tied and there is no correction to be made, but if not we should back-track, and locate the mis-tie and try again to close the loop. It is quite clear that there is no way to close the loops around a fault if there is no well data, but if we have wells, as in the present area, the correlation can be made (Badley, 1985).

4.4.1 *Mis-ties*

Sometimes it is necessary to introduce faults unsupported by other evidence in order to make sure that a picked reflector ties around a loop of the grid survey (McQuillin, Bacon, and Barclay, 1979). These should be in the area between the intersection of lines during tracing the events, but at the intersections these mis-ties cause a lot of problems. The cause of these mis-ties are:

(1) Difficulty with polarity reversals between sections.

(2) Differences in processing parameters, causing a strong change in reflector characteristics, such as stacking velocities, deconvolution and filter settings.

(3) Other causes of mis-ties are differences in stacking velocities not due to the mis-picking of the velocities, but due to the interpolation between the two velocity analyses. This may cause a mis-tie at an intersection. The other is the effect of dip, which may cause the actual reflection points at the intersection of two un-migrated sections to be slightly different on the two lines.

After examination of all the intersection mis-ties, we can apply a smooth shift to the shot point values between the intersections to eliminate the mis-ties values at the intersection. If the mis-tie shift is small it may neglected in the regional mapping (McQuillin, Bacon, and Barclay, 1979).

4.4.2 *Seismic sections*

Seventeen seismic sections were selected for re-interpretation, and three horizons for mapping. Figures 4.4 a - n show some of the interpreted seismic sections. All the seismic sections are of reverse polarity to match the old seismic sections. A new map was prepared showing only those lines used in the re-interpretaion (Figure 4.1).

4.5 *Digitisation*

The first step in making a contour map from the picked seismic section is the measurement of two-way time to the picked horizons along seismic section. These data values will then be transferred to the shot point location map in order to produce a contour map of structure in two-way time.

4.5.1 *Methods of reading*

There are two methods of reading the times from the seismic section:

(1) The first method is manually reading directly by hand, in which the horizontal intervals between reading depend on the complexity of the structure visible on the seismic section and the scale of final map. In the present case, where the mapping is at a scale of 1:25,000 and the horizons are almost flat, the horizontal interval between readings is 500 m, equivalent to 10 shot points. Figure 1.6 (Chapter 1) shows on the shot point location map where the values of the two-way time have been picked.

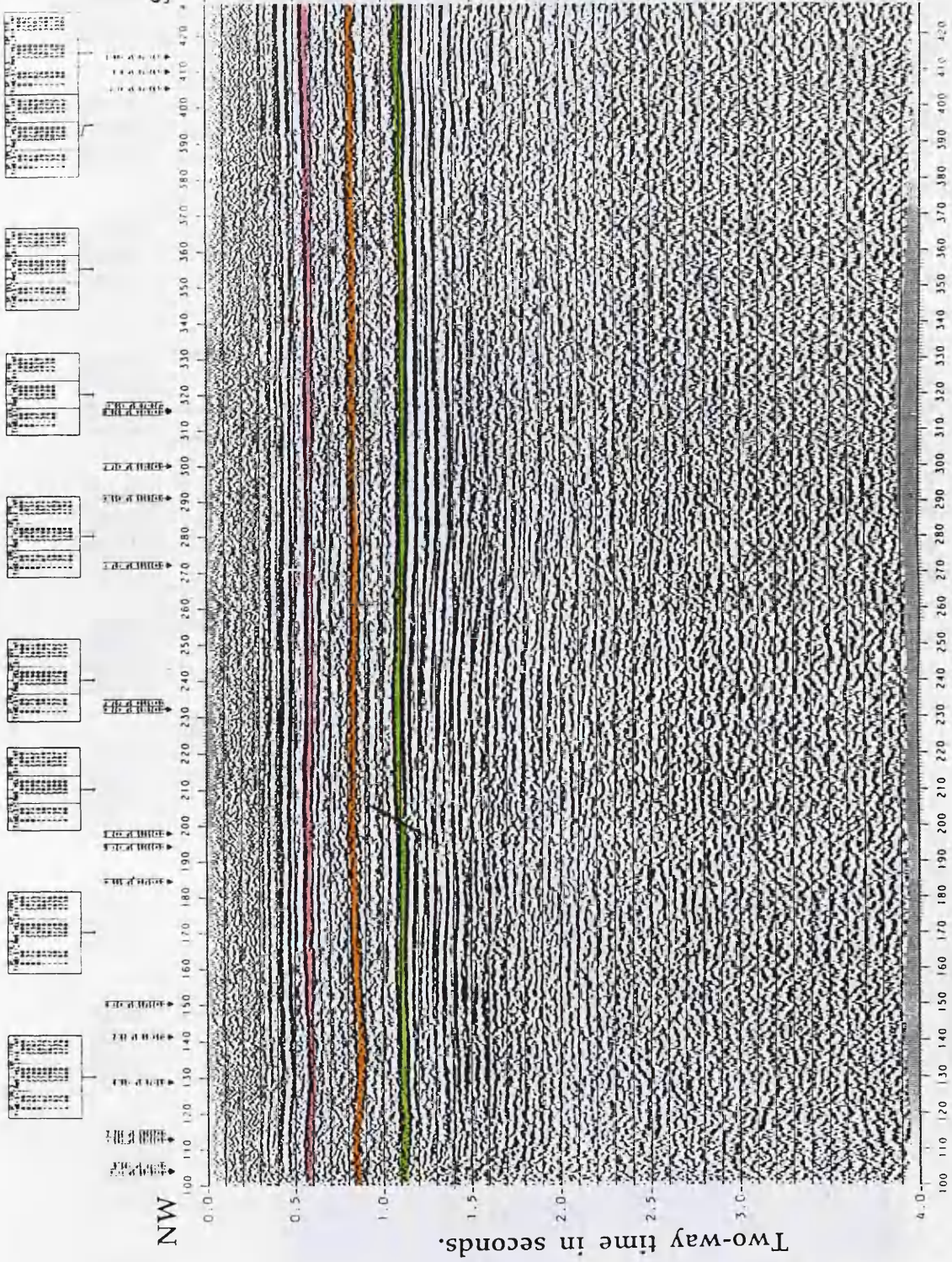

Fig.4.4a Seismic line 6V248-85.

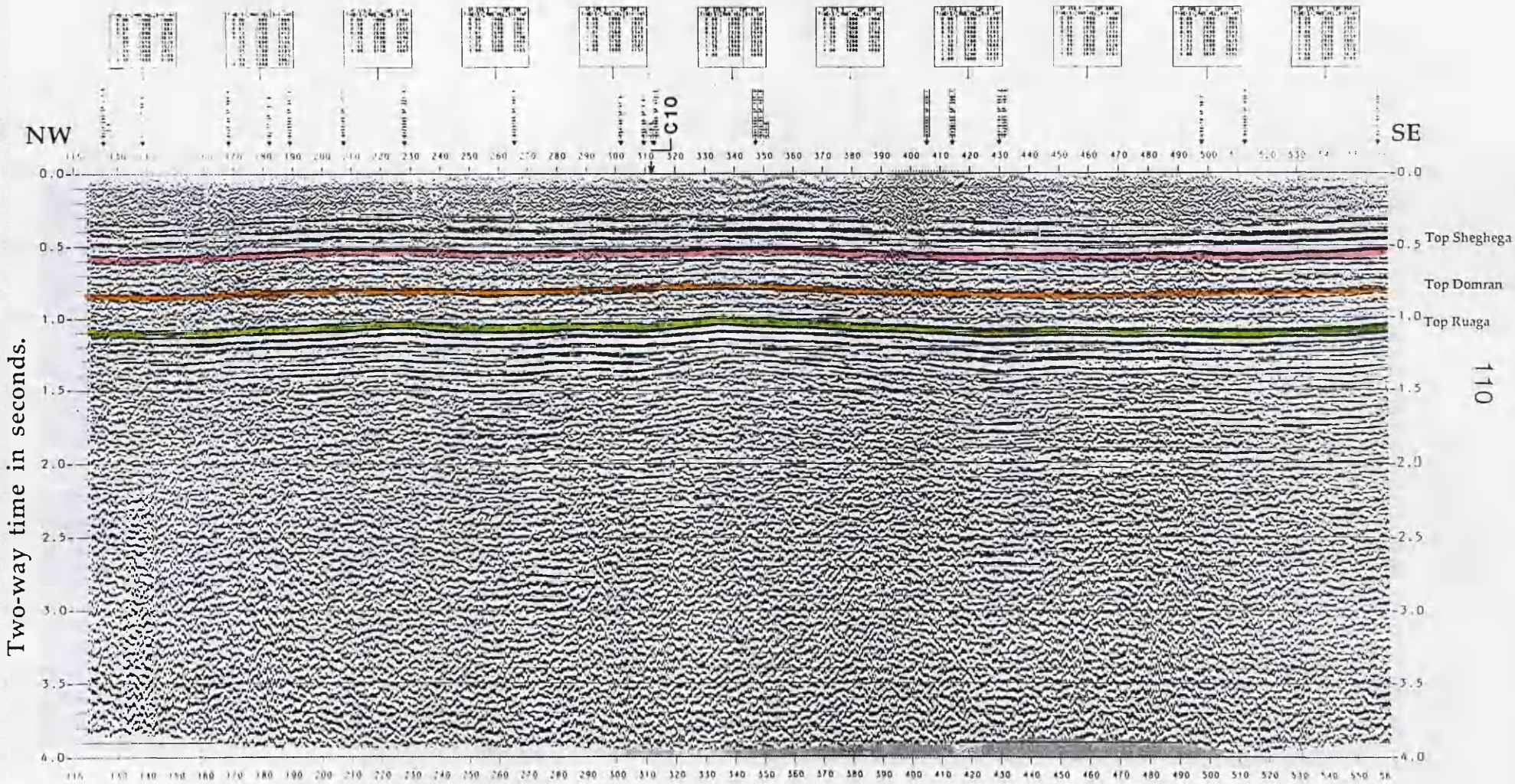

Fig.4.4b Seismic line 6V250-85.

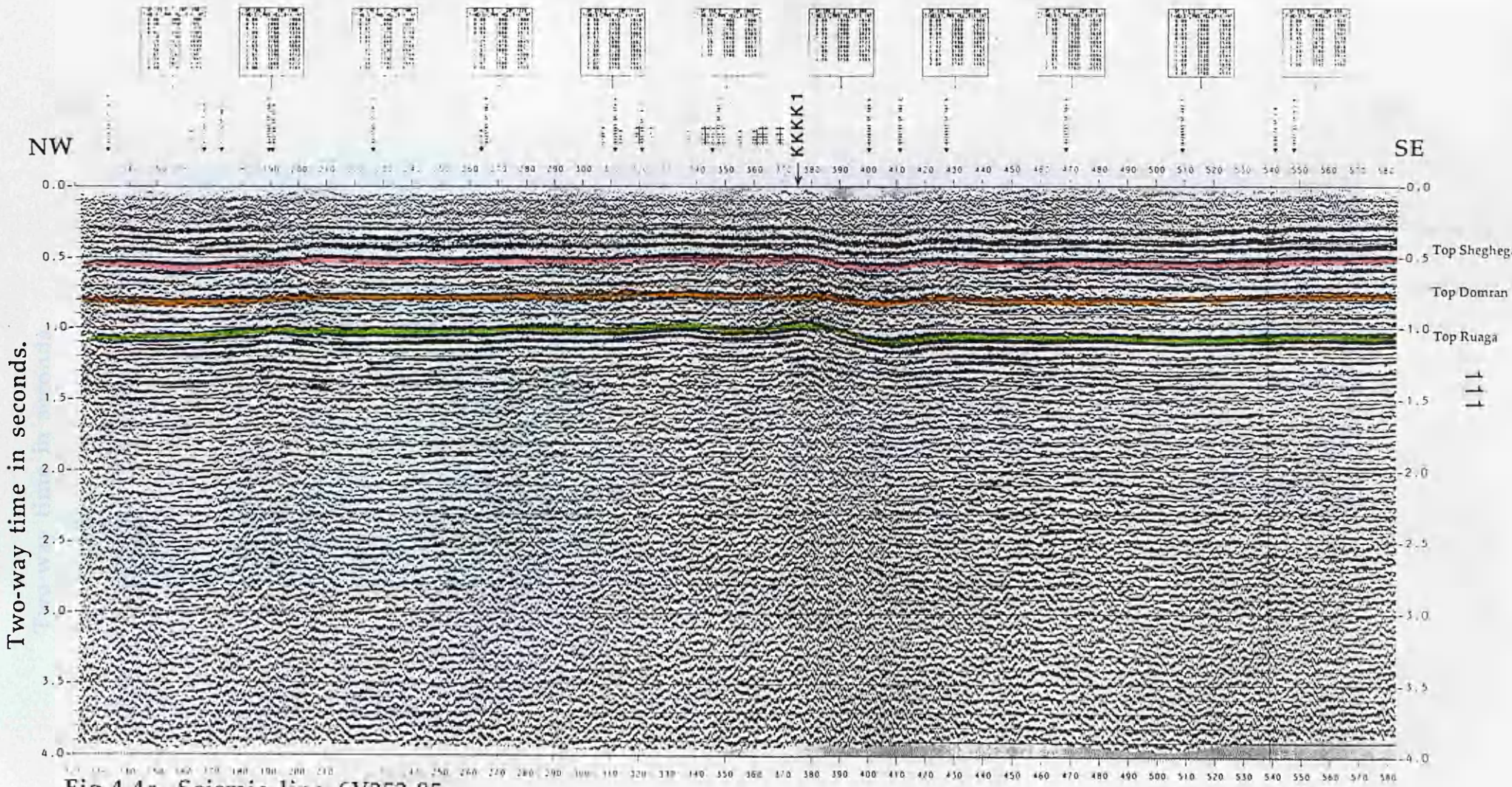

Fig.4.4c Seismic line 6V252-85.

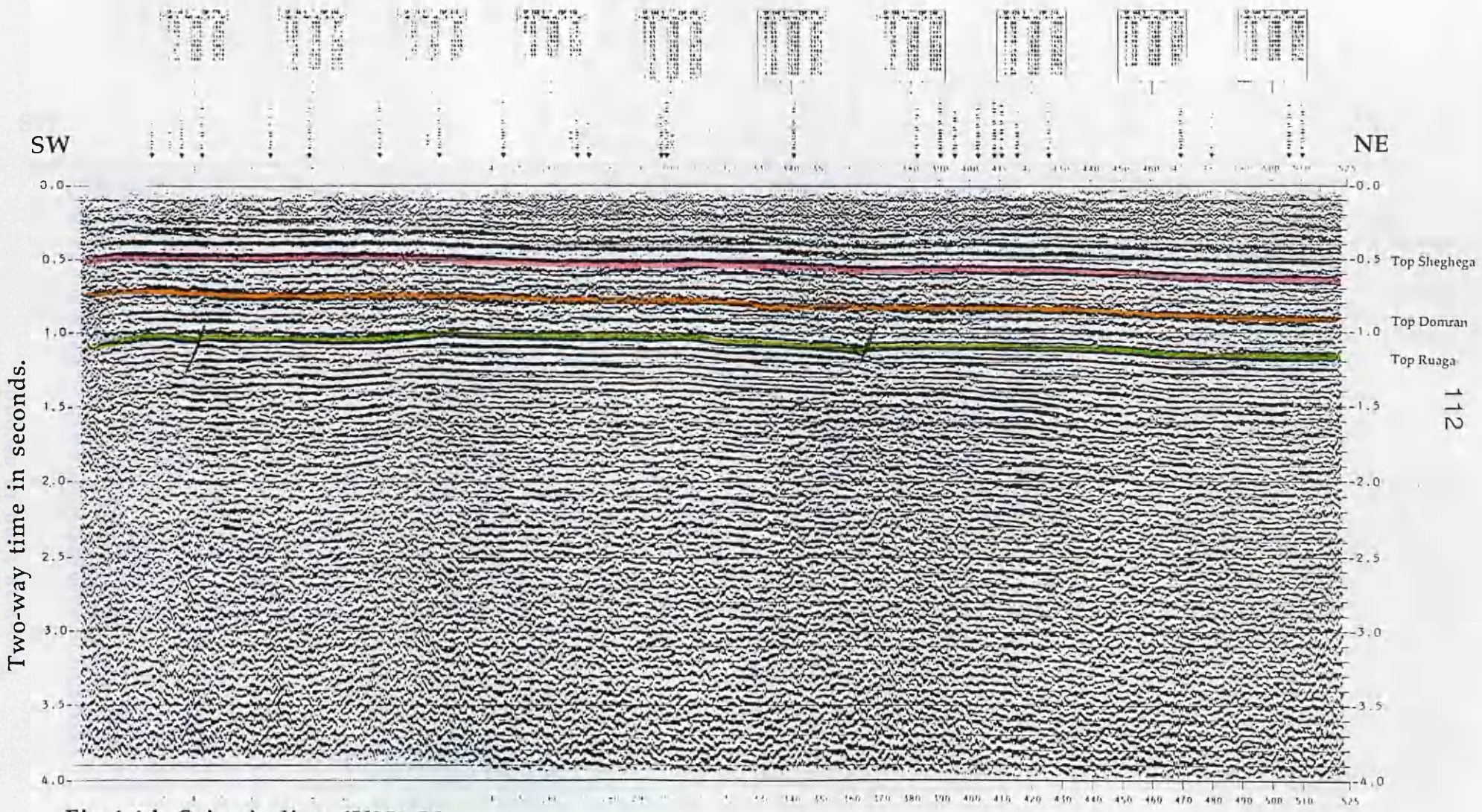

Fig.4.4d Seismic line 6V253-85.

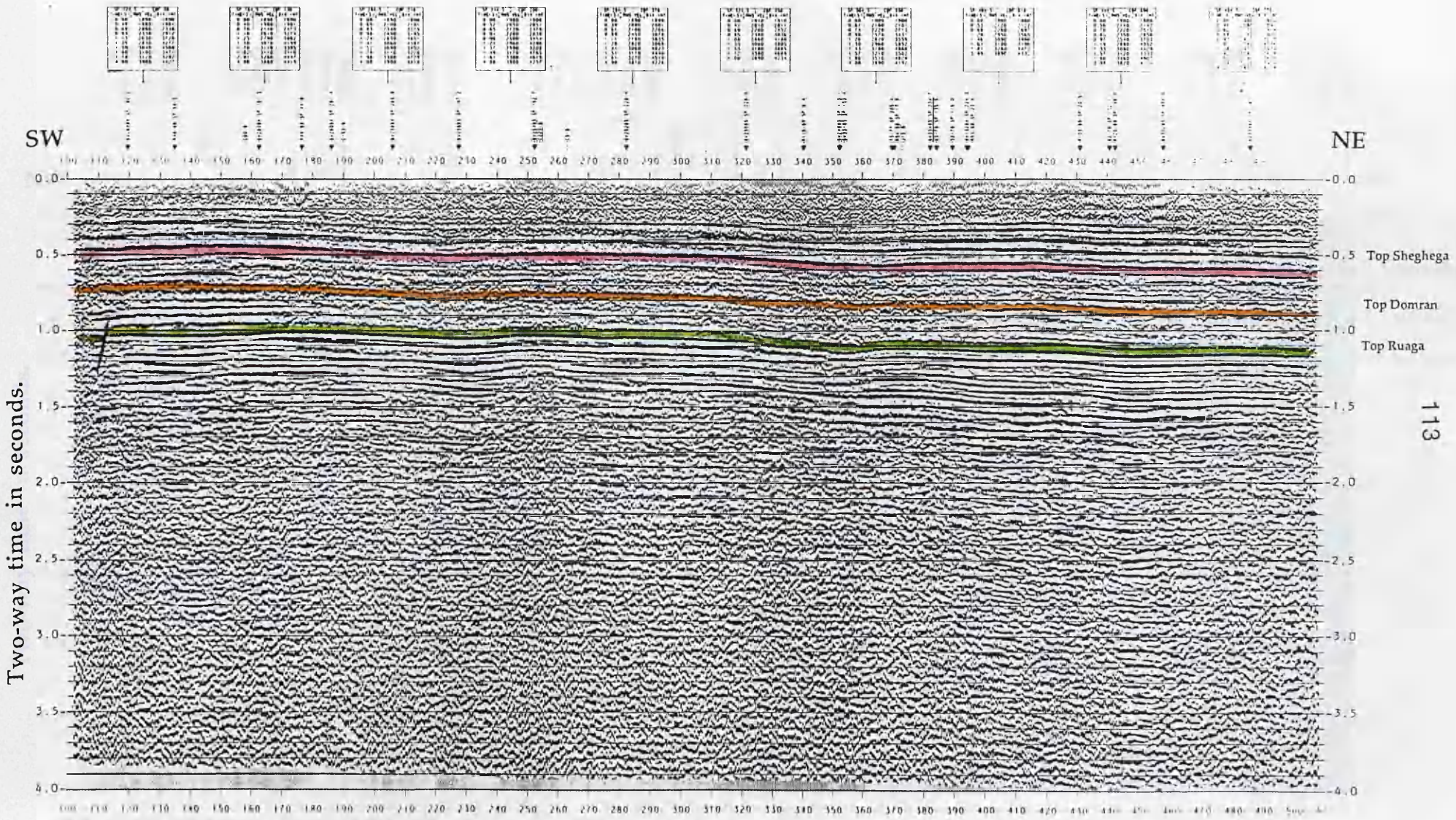

Fig.4.4e Seismic line 6V255-85.

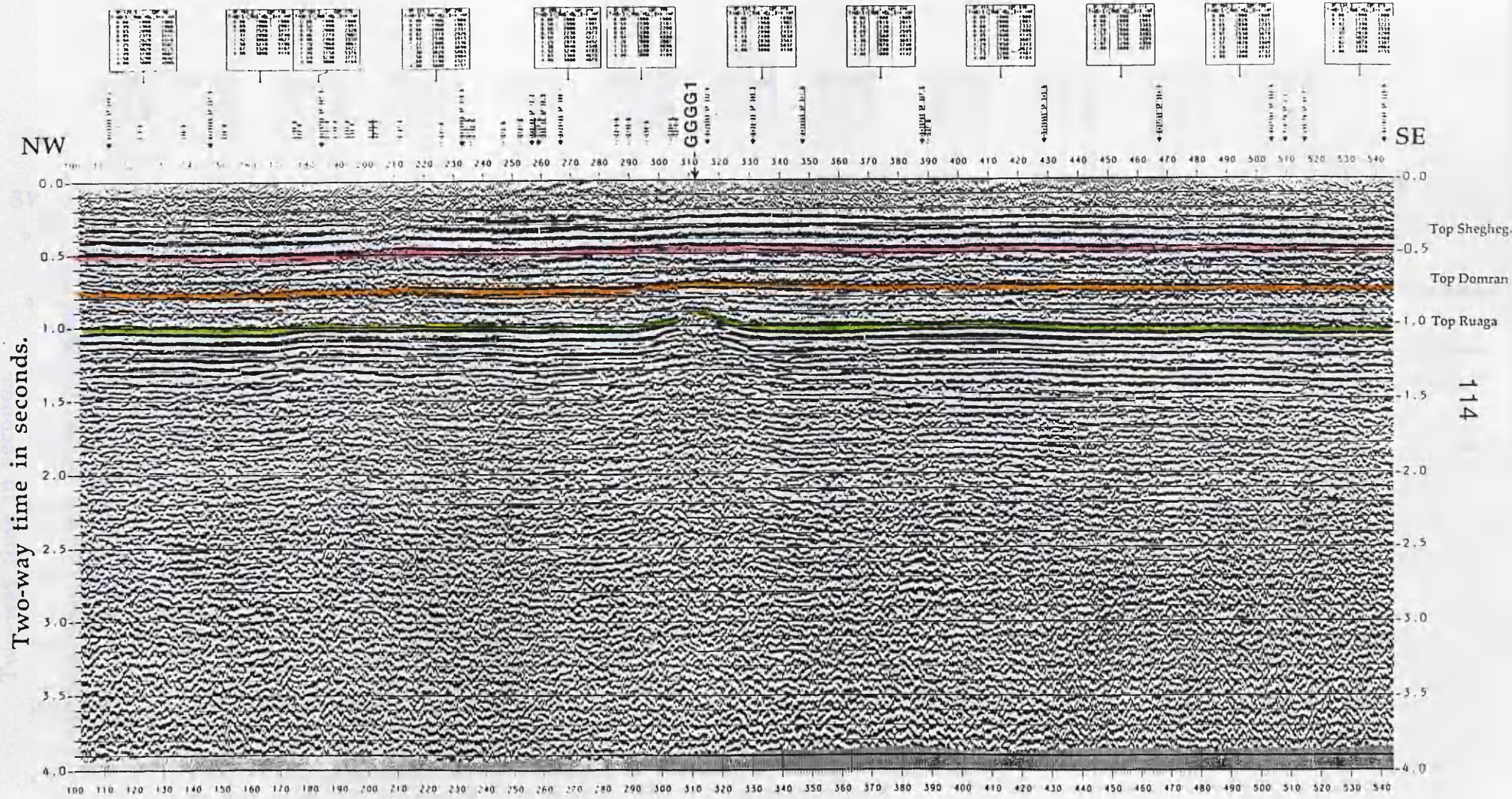

Fig.4.4f Seismic line 6V256-85.

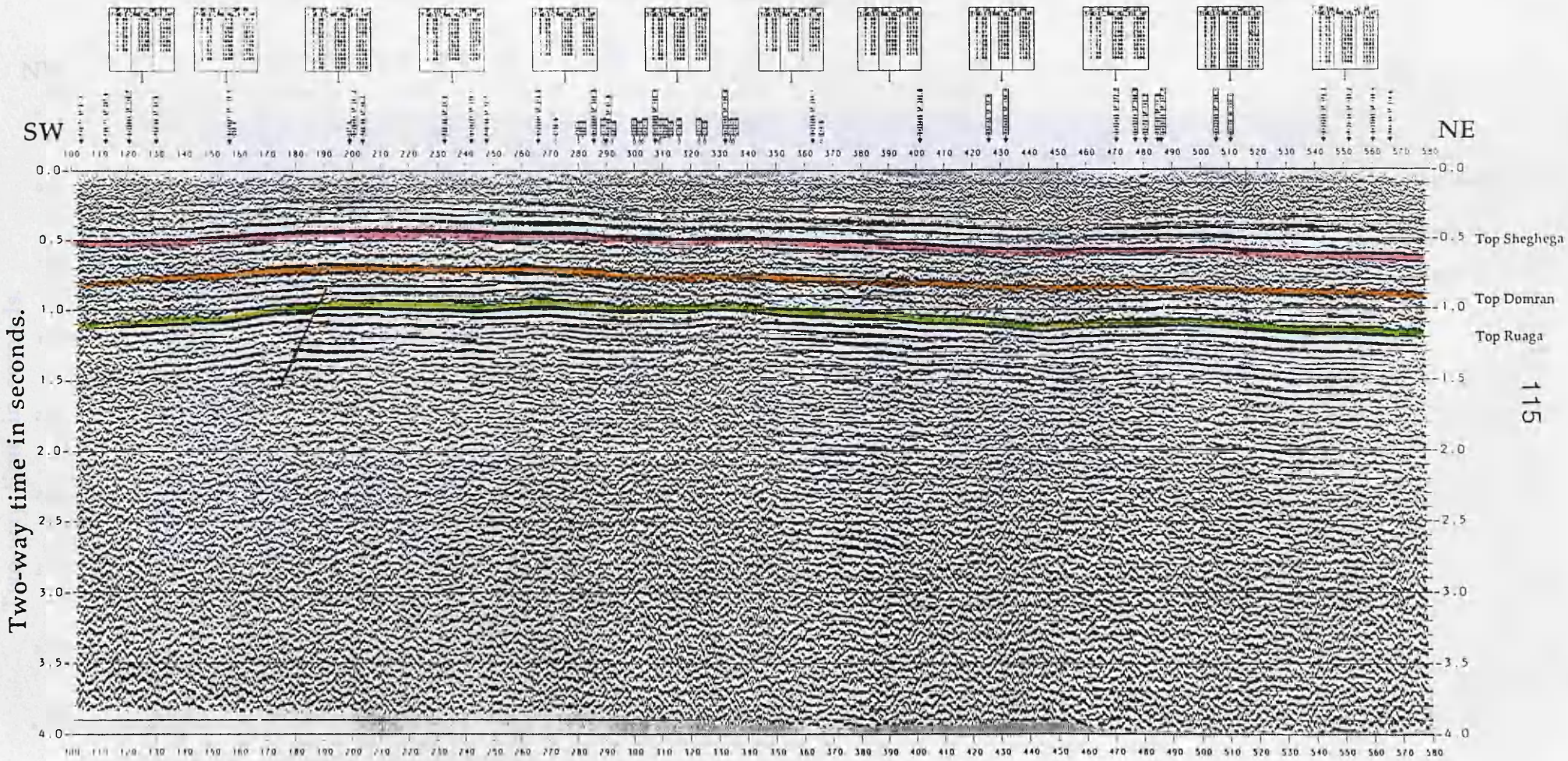

Fig.4.4g Seismic line 6V257-85.

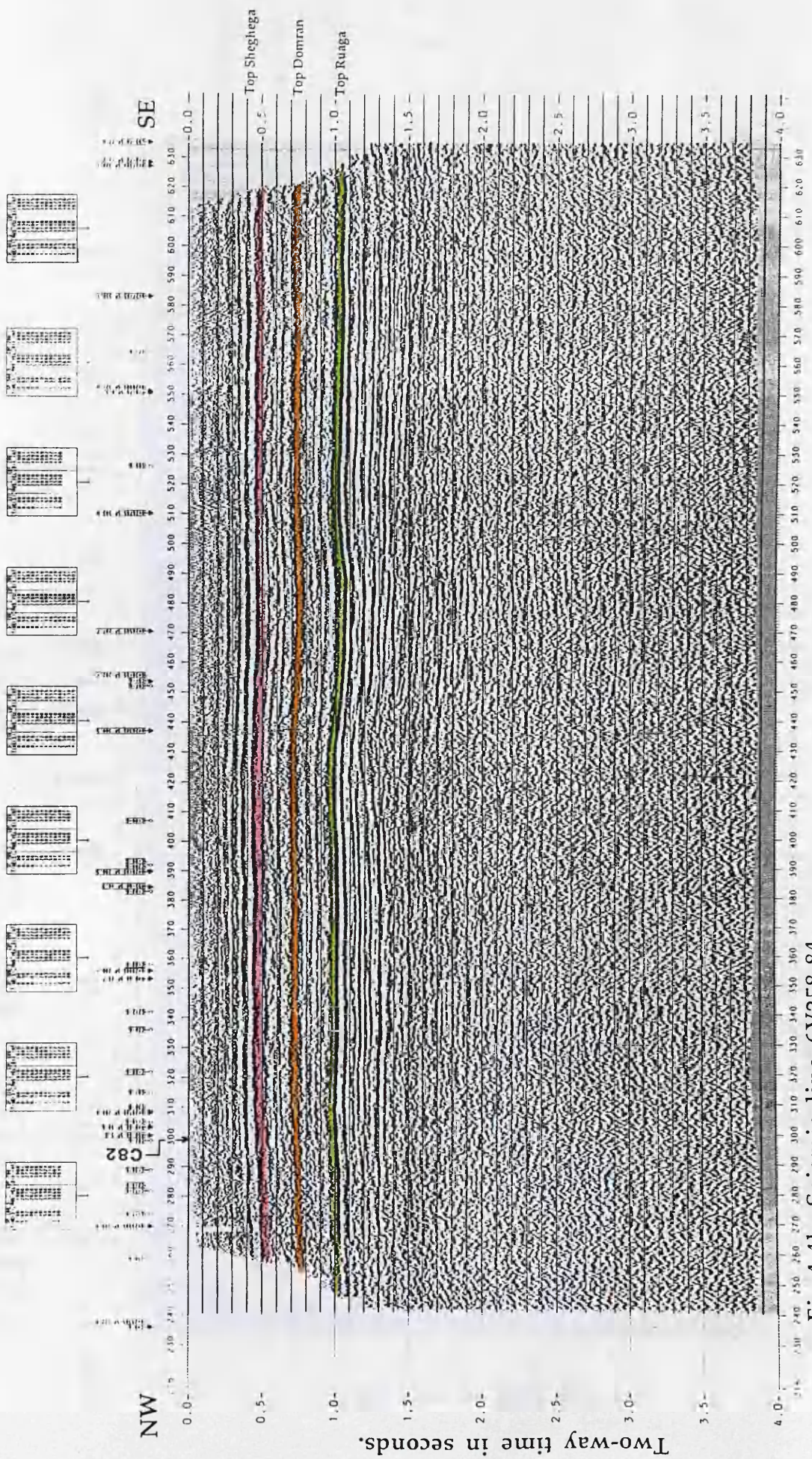

Fig.4.4h Seismic line 6V258-84.

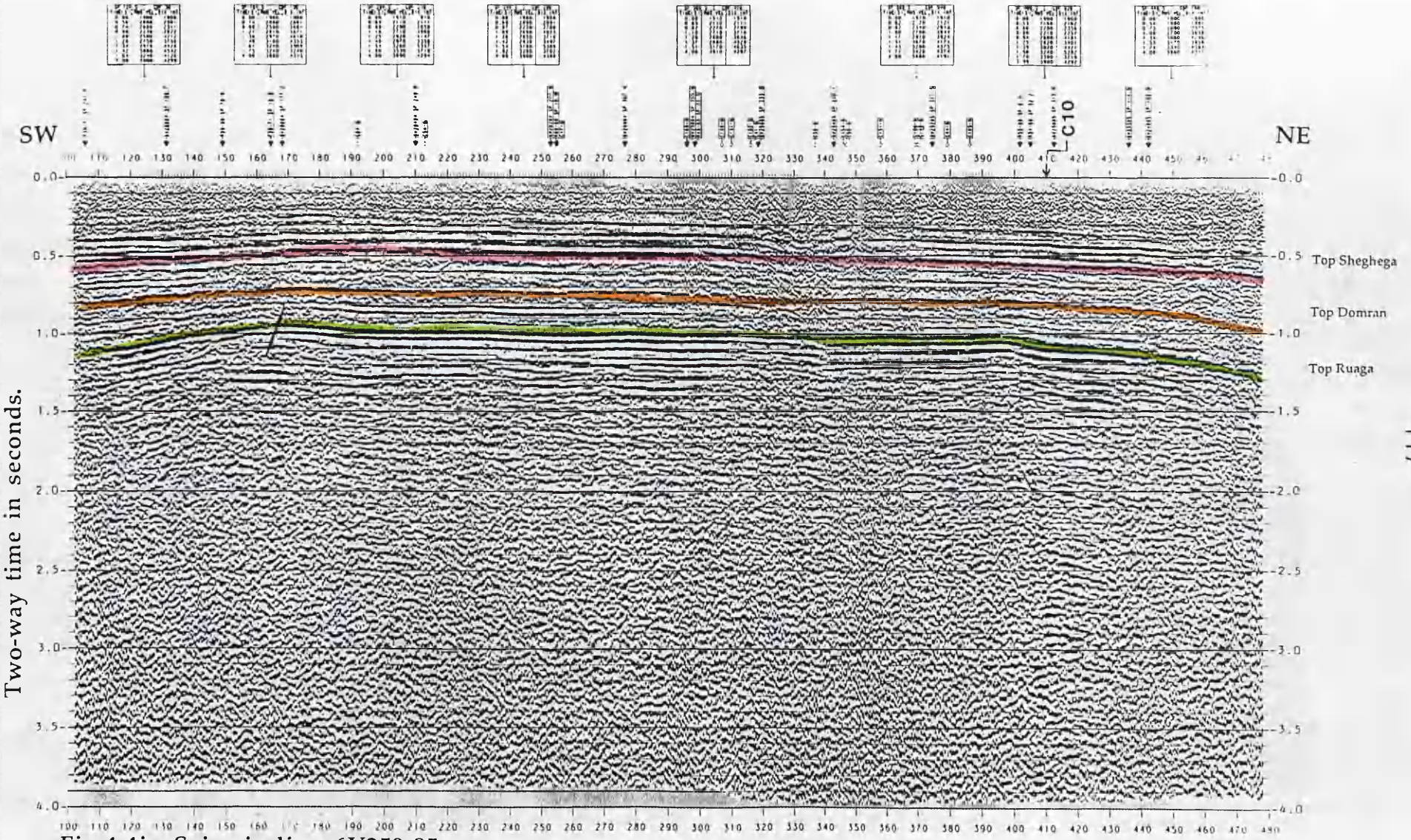

Fig.4.4i Seismic line 6V259-85.

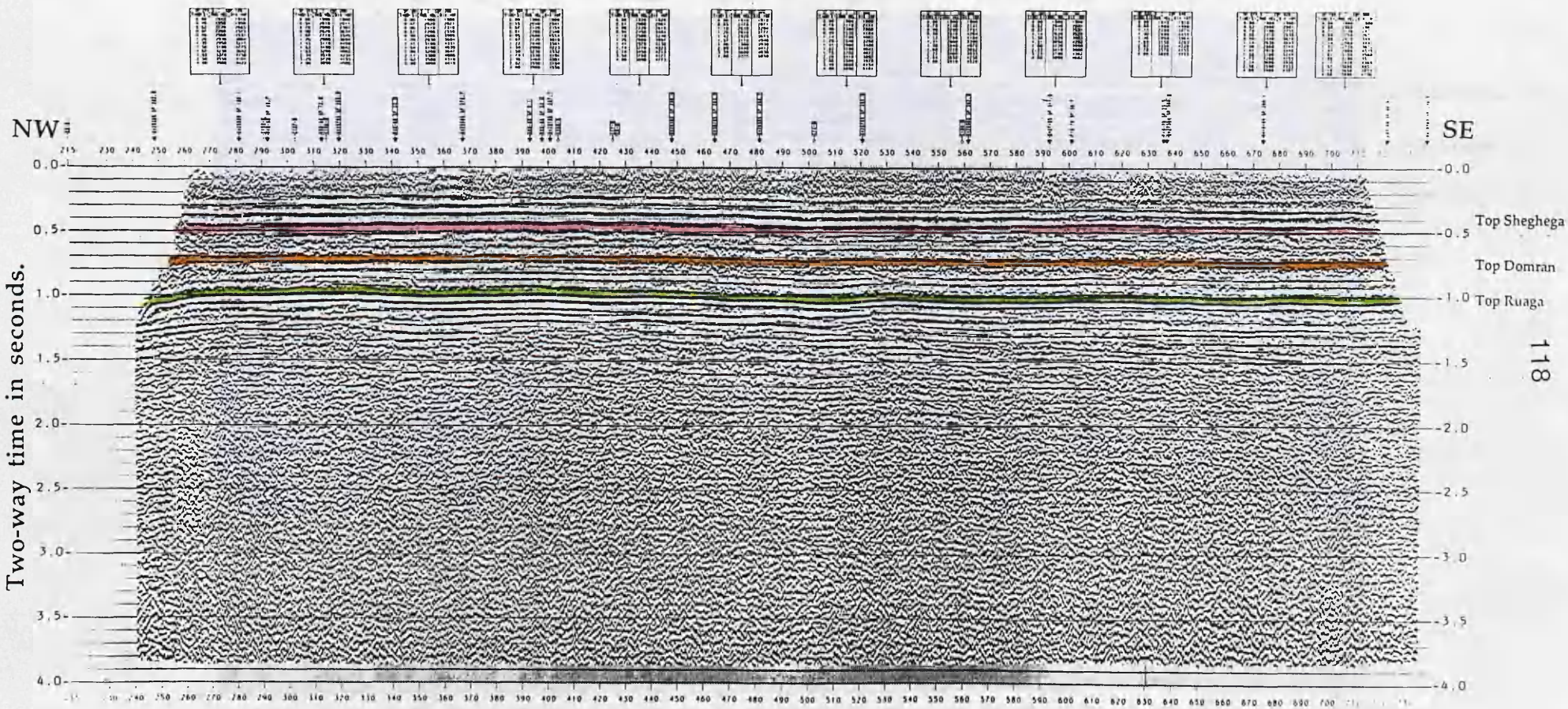

Fig.4.4j Seismic line 6V260-84.

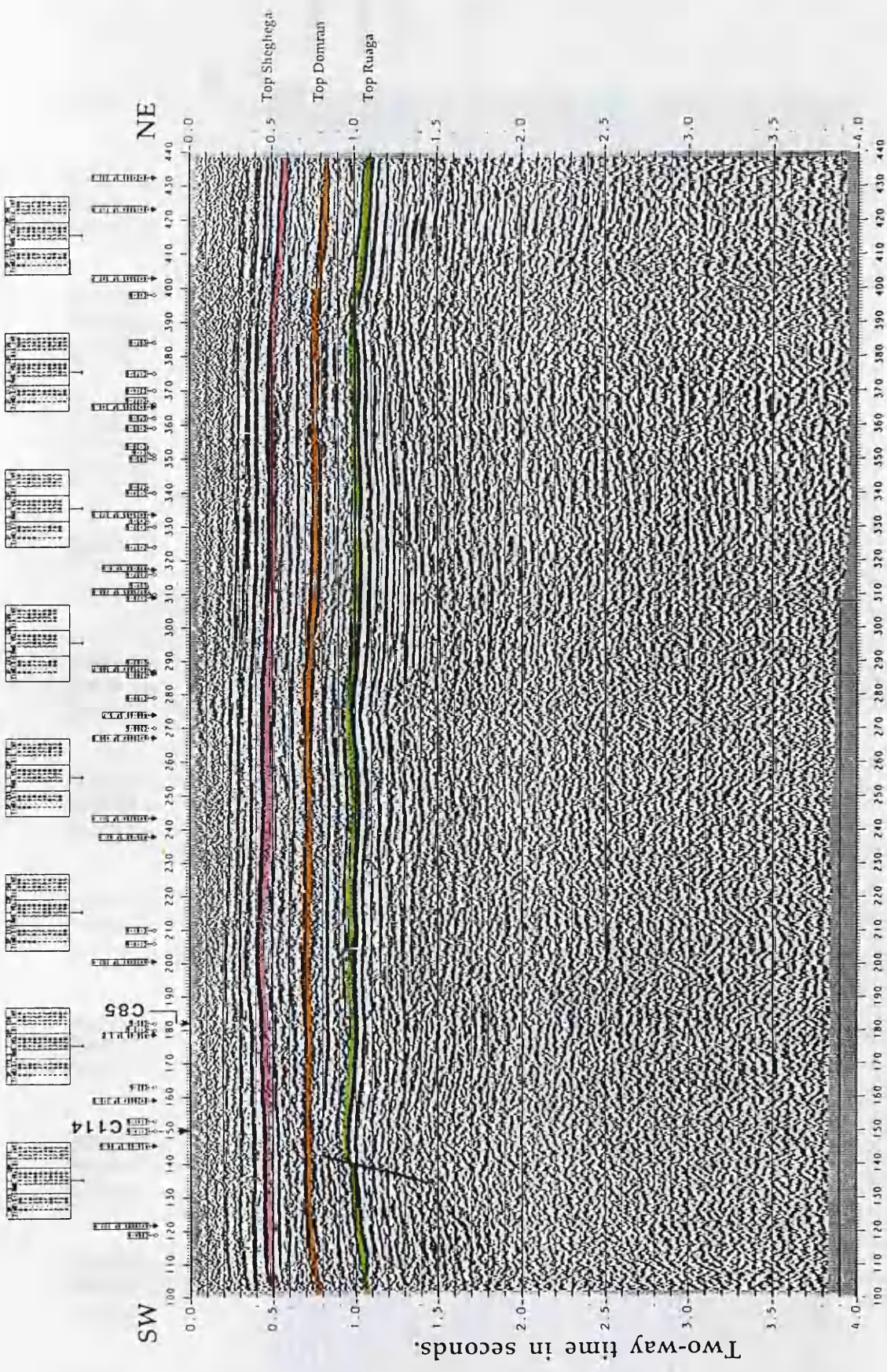

Fig.4.4k Seismic line 6V261-85.

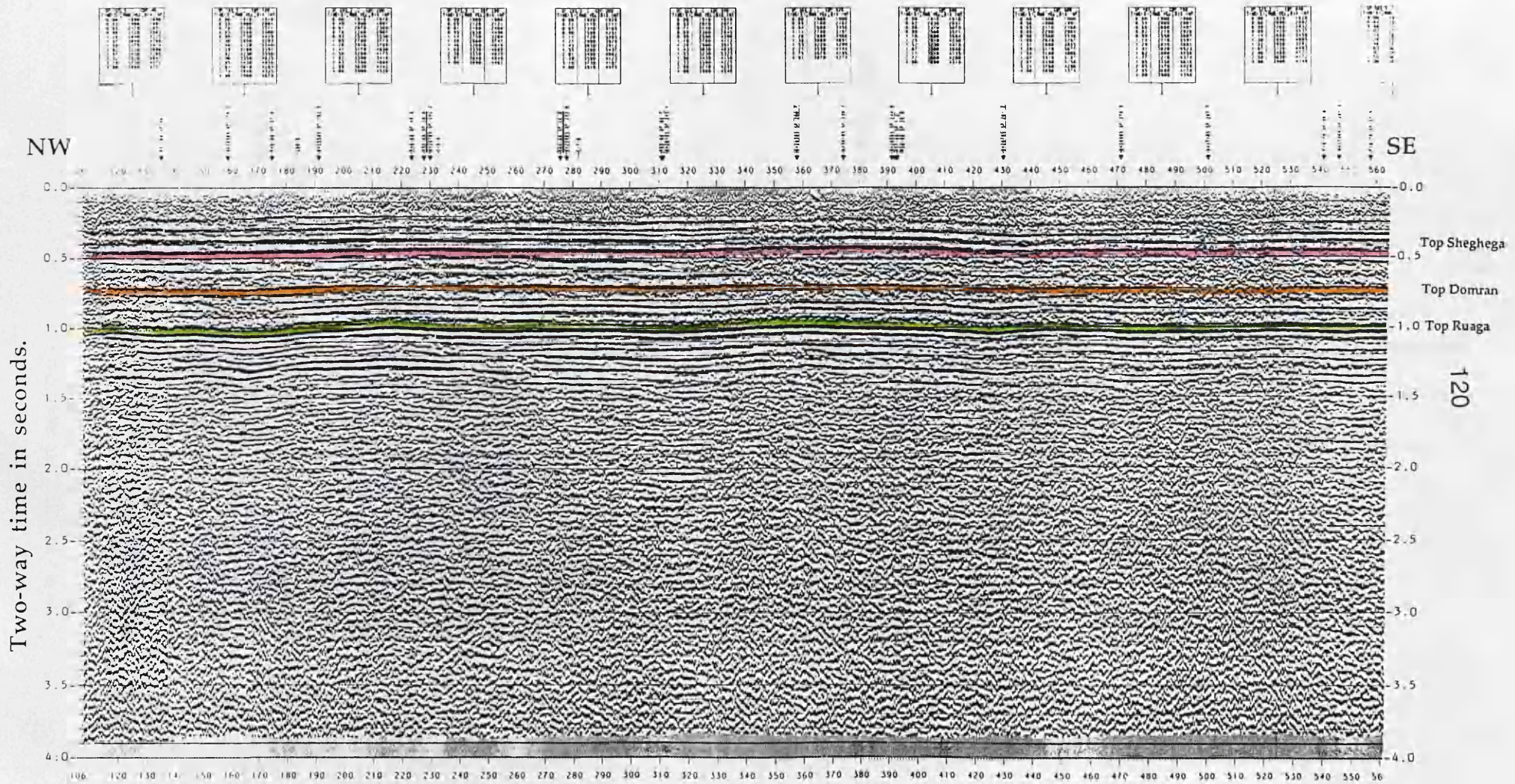

Fig.4.4l Seismic line 6V262-84.

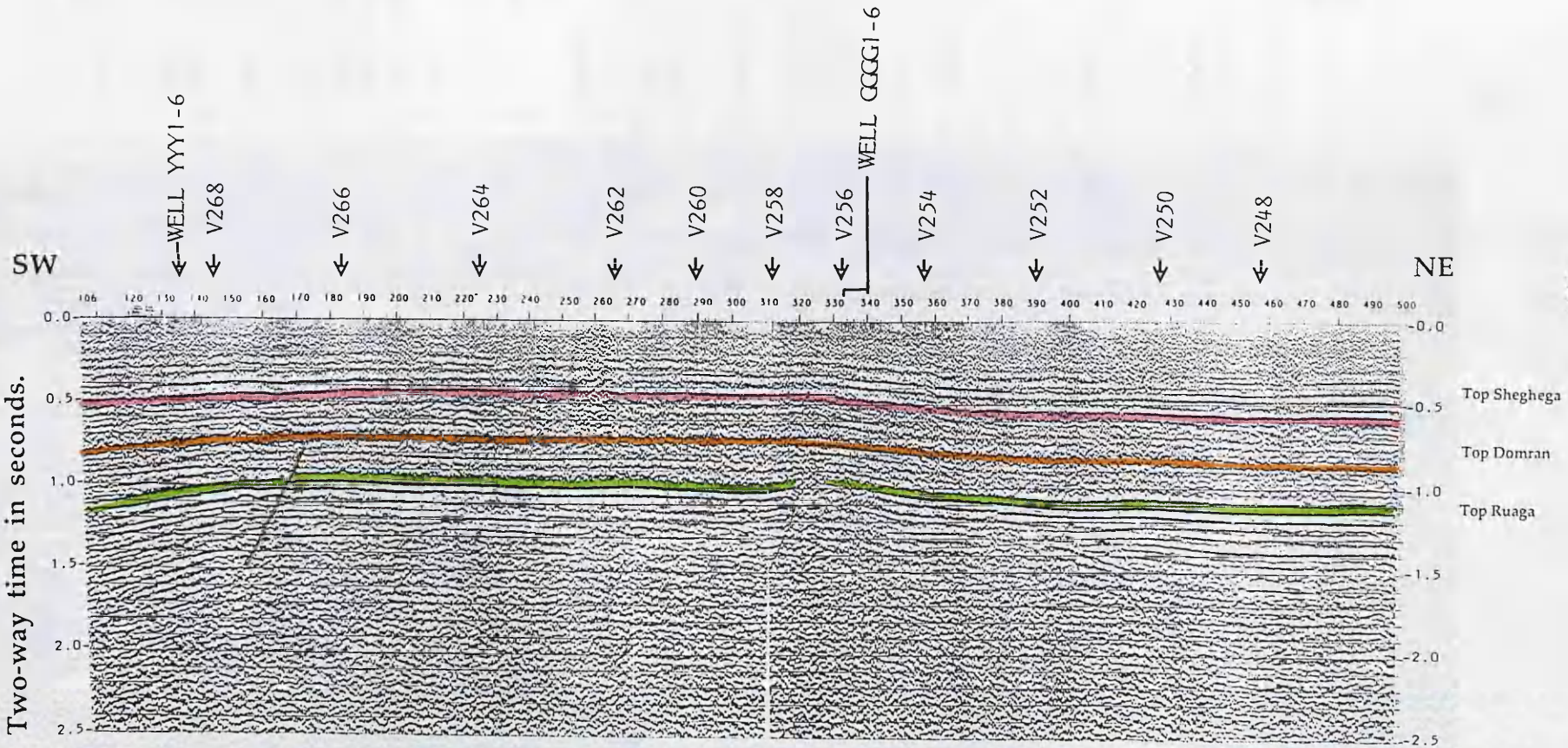

Fig.4.4m Seismic line 6V263-85.

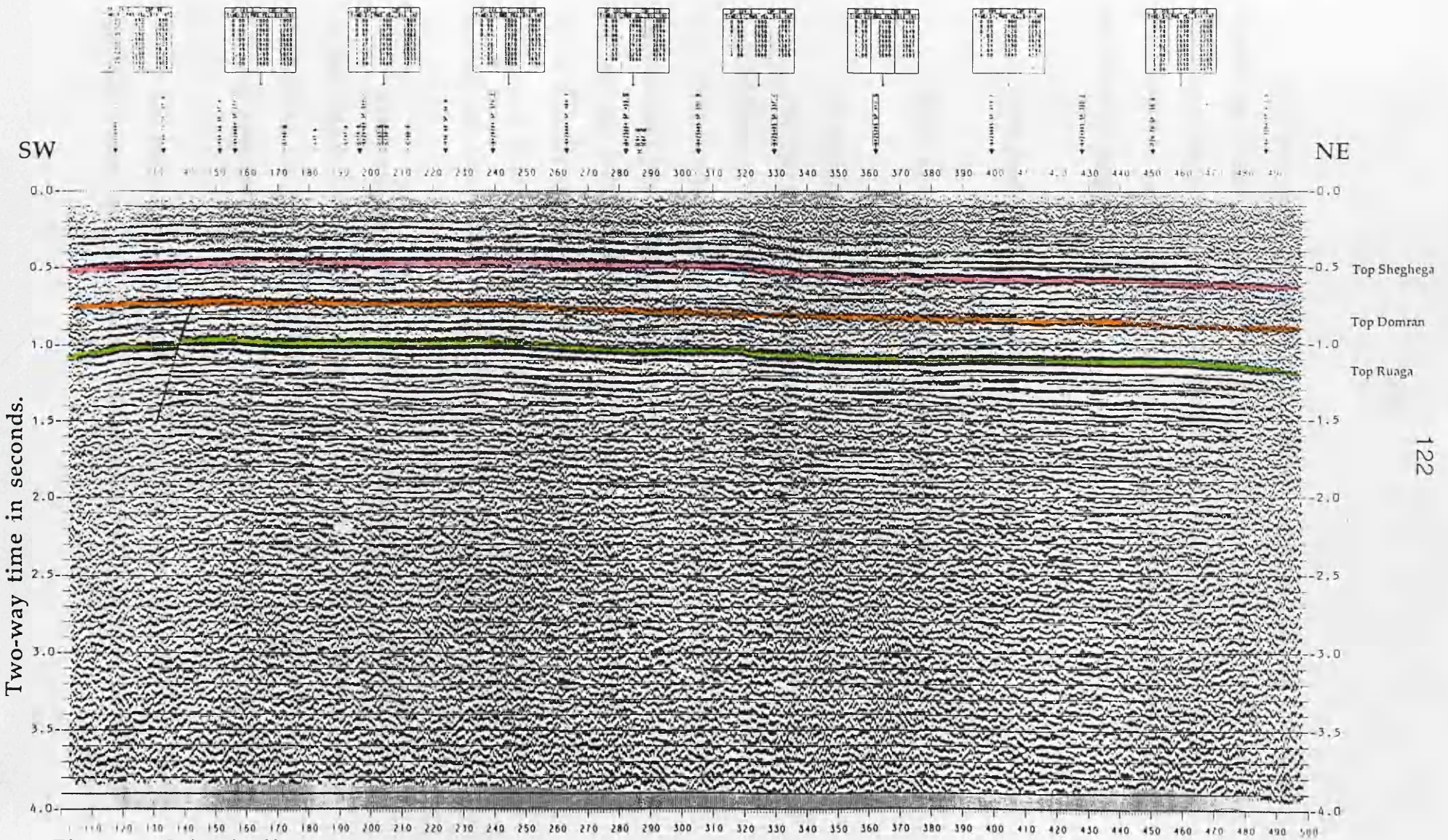

Fig.4.4n Seismic line 6V301-85.

(2) The second method is automated reading, using a computer digitising table, in which the horizontal intervals are very small (continuous reading). A computer program should be used to decrease the digitising to a suitable interval to have a clear set of posted values of the horizons for mapping.

4.6 *Map contouring techniques*

There are two techniques of map contouring:

(1) Manual contouring techniques

The first thing to do is to produce a contour map of two-way time to each horizon. It is necessary first to post the two-way time values onto a shot point location map. Before contouring you should mark all the faults on the map using suitable symbols showing the down-thrown side and up-thrown side with values for both sides and try to join them together; also try to identify the main trends by contouring the data roughly. Another useful task is to draw synclinal and anticlinal axes on the map, to ensure that all contours intersecting them turn along the same structural axis.

There are other details to mark on the map before contouring, such as the highs, lows, valleys, noses, no data areas,etc. Contour interval depends on the depth resolution required of the map or map surface and the map scale used.

On manual contouring most of the problems can solved by using common sense, such as mis-ties, or incorrect values where the trend is

disturbed. The final unmigrated stacked data was used for timing and mapping in this area.

As an example of this technique, three time contour maps for the Sheghega, Domran, and Ruaga formations have been made on the shot point location maps of 1:25,000 scale, and then been reduced to A4 paper size. These maps are demonstrated in section 4.9.

(2) Automated contouring techniques

The next step after digitising the two-way time from the seismic sections is to digitise the shot point location map so that a map of two-way times posted in their correct positions can be produced automatically. It is possible after this stage to produce a computerised contour map.

Automated contouring of seismic data faces two main problems. Firstly the seismic data forms a far from ideal grid for automated contouring, except for 3-D surveys where the data are close enough. Secondly, mis-ties, which can vary from small to significant, will occur at practically every line intersection.

In the present study a slightly different procedure from the above was used in contouring the data. Instead of using a digitising table two-way times from the seismic section were manually picked every 10 shot points, handling the mis-ties at the intersections by adding to or subtracting from the values of the picked shots near the intersections, before storing the data in the computer. For the map location, the output results from the COORDINATE program provided a digitised shot point location or

coordinate file in the computer together with the previous file, for contouring the data.

Using the above computer contouring can cause another kind of mis-tie at the intersection, depending on how close the posted values are. If they are close enough together the mis-ties become smaller. Here the 500 m posted value spacing looks very reasonable, so it was expected that this kind of mis-tie at the intersections might occur. The cause of these mis-ties is the interpolation between the velocity analysis points and between the picked shot point values. These mis-tie values from the two-way time, Dix average velocity, and the corresponding depth at the intersections of the seismic lines for the three chosen horizons, were listed in Table 4.2 given in Appendix 4.1. These mis-tie values vary from small to significant, causing an artificial dense contouring at the intersection. The problem can be cured if the posted value spacing is made sufficiently small.

These mis-tie values were contoured, to make the interpretation much easier. Figure 4.5 shows mis-ties in the two-way time computer contour map at the top of the Sheghega formation marker (Horizon 1), based on the the intersection data. This contour map shows that most of the intersections have very small values, while some have big values, where the contour were dense. There the values vary between -10 and +10 ms.

Figure 4.6 shows the mis-ties in Dix average velocity at the top of the Sheghega formation marker, based on the the intersection data. This computer-contoured map shows that most of the intersections have very

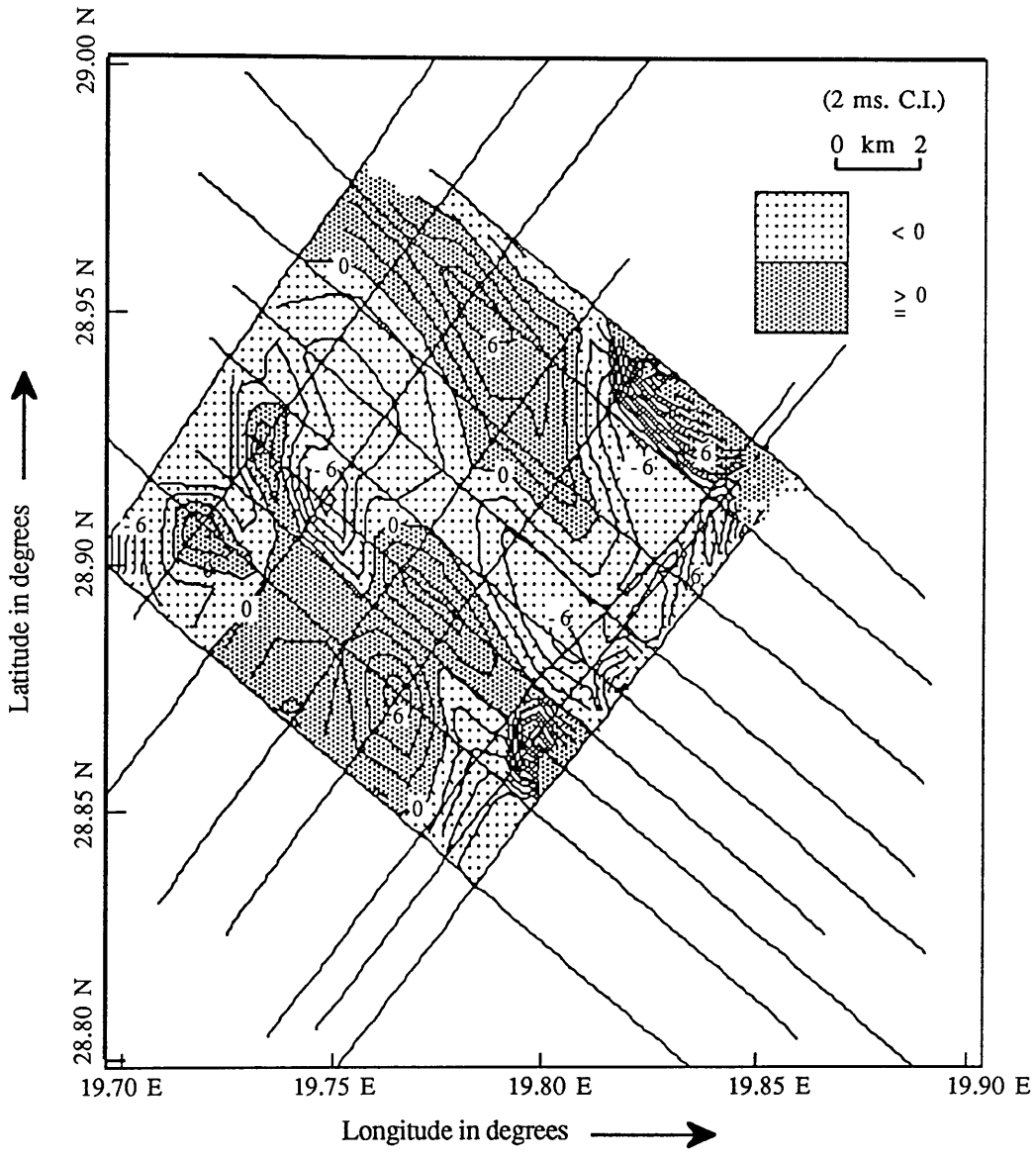

Fig.4.5 Two-way time mis-tie contour map in milliseconds at the top of the Sheghega formation, based on the seismic line intersection data.

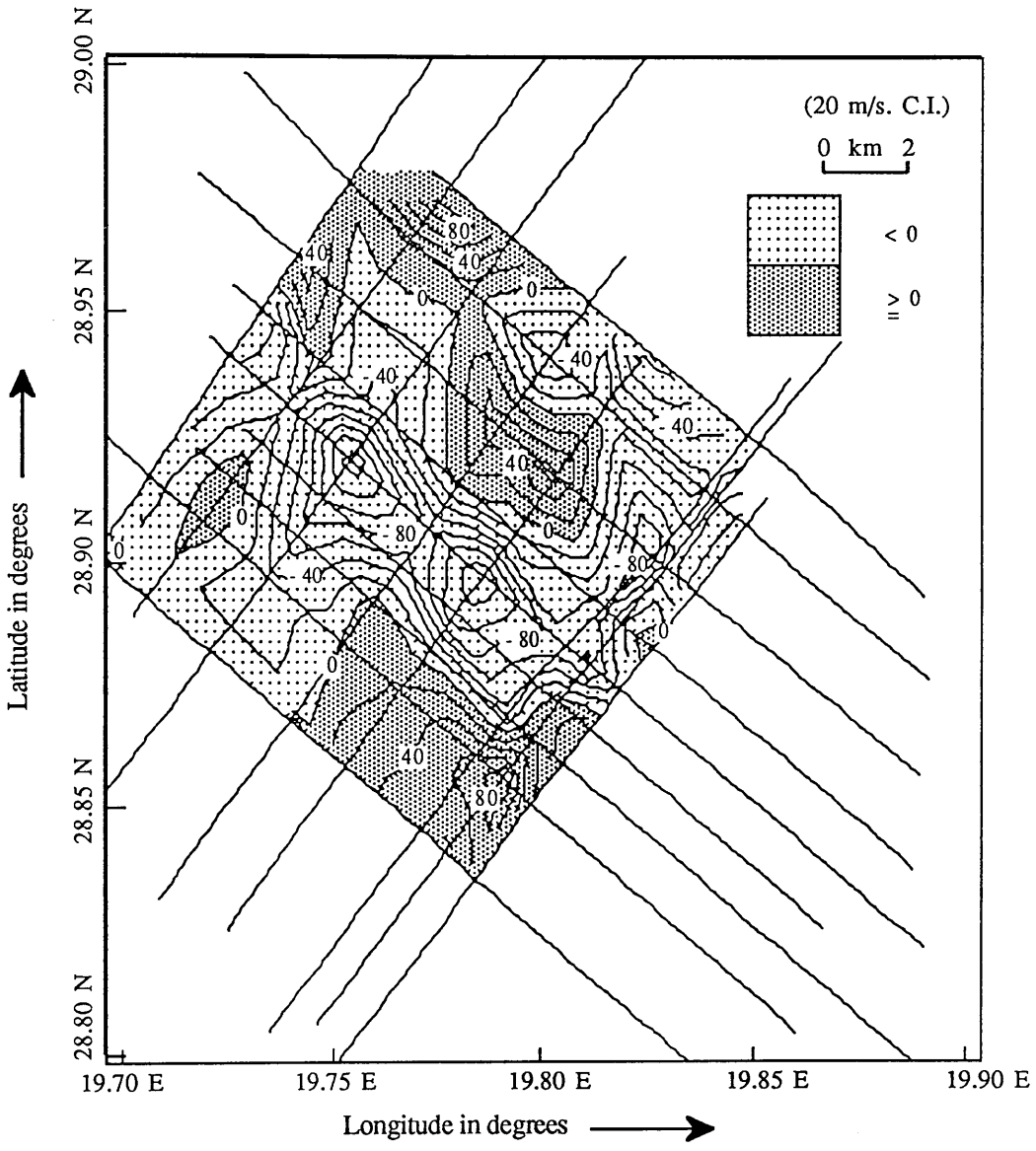

Fig.4.6 Velocity mis-tie contour map in meters per second at the top of the Sheghega formation, based on the seismic line intersection data.

small values, but there are some large values where the contour were dense. These values vary between -100 and +100 m/s.

Figure 4.7 shows the mis-ties in the depth as a computer-contoured map for the top of the Sheghega formation marker, based on the the seismic line intersection data. This contour map shows that most of the intersections have very small values. Large values, where the contours were dense, vary between -40 and +30 m.

The velocity and depth mis-tie contour maps for the Sheghega formation show similar zones of high, medium, and low values, and they have the same trend of contours.

Mis-tie contour maps for the top of the Domran formation marker are shown in Figures 4.8-4.10, and for the top of the Ruaga formation in Figures 4.11-4.13. Each trio of maps comprises the mis-ties in two-way time, Dix average velocity, and depth, as discused above for the Sheghega formation. The maps have generally similar characteristics, except that the peak-to-peak values of the contoured variable are somewhat larger for the deeper horizons.

There is little similarity between the two-way time maps for the three horizons, but the velocity and depth maps, respectively, do show some similarities between the three horizons. This suggests that the major mis-tie is caused by the velocity interpolation, discussed above. This error feeds through into the depth maps.

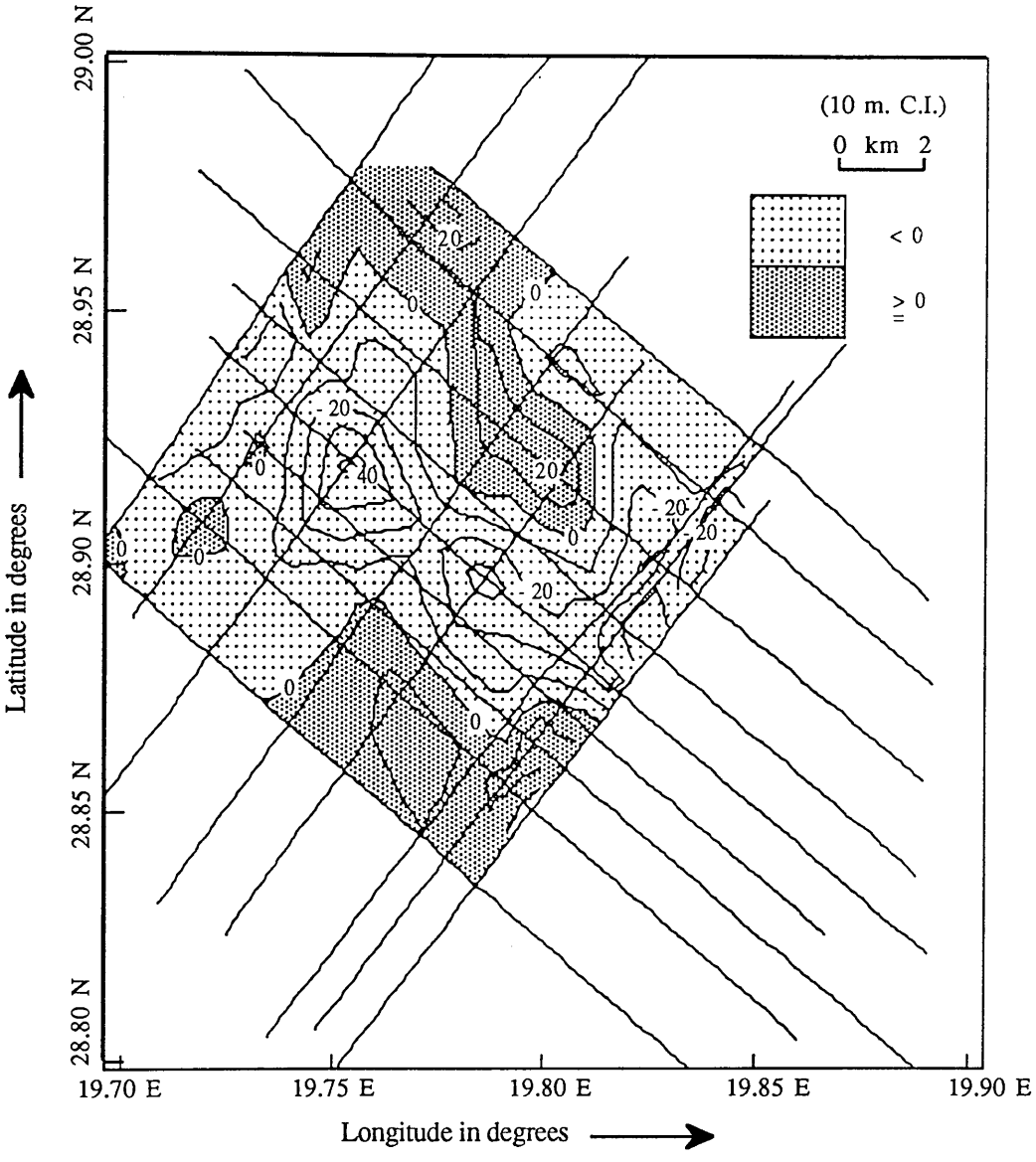

Fig.4.7 Depth mis-tie contour map in meters at the top of the Sheghega formation, based on the seismic line intersection data.

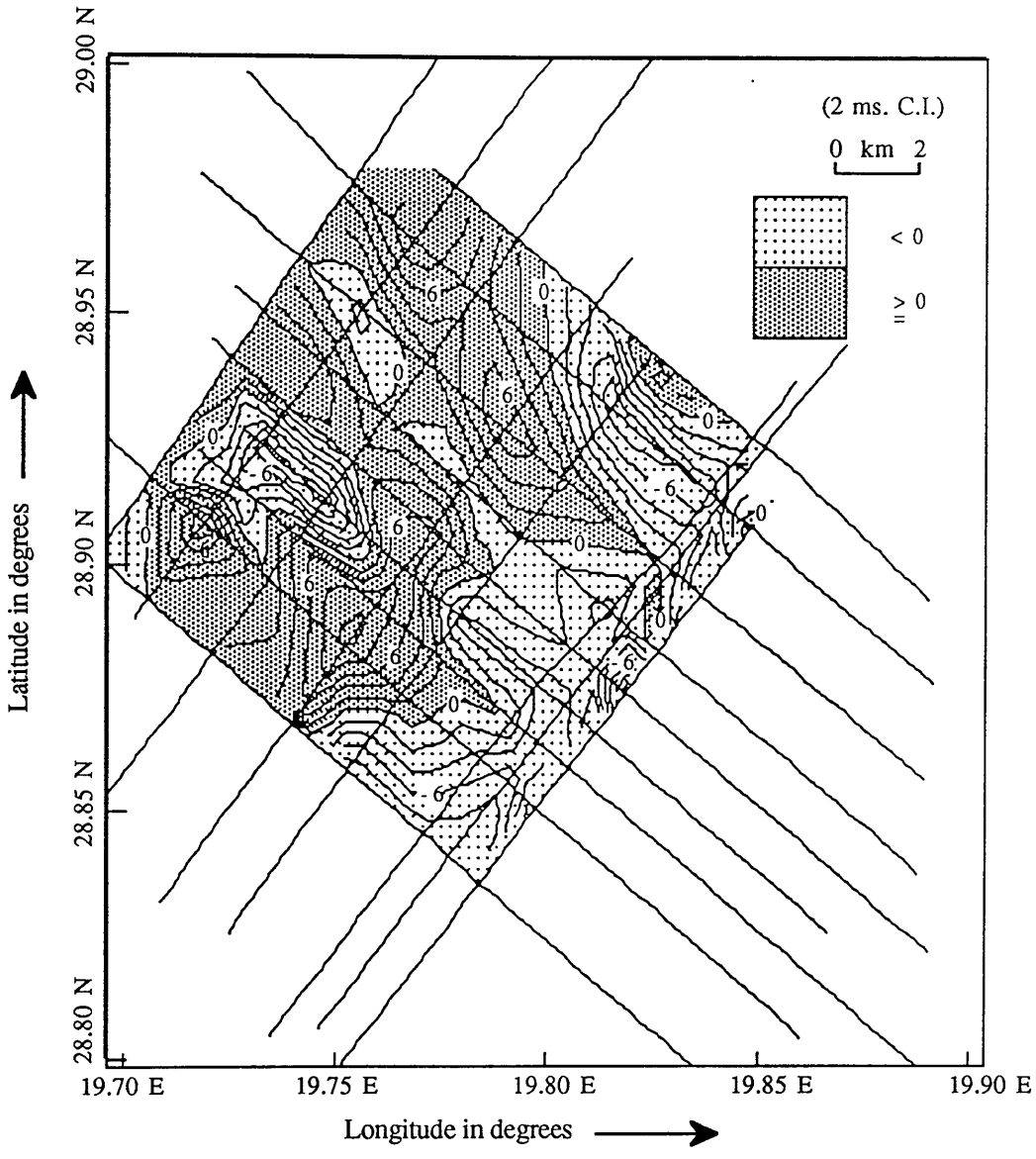

Fig.4.8 Two-way time mis-tie contour map in milliseconds at the top of the Domran formation, based on the seismic line intersection data.

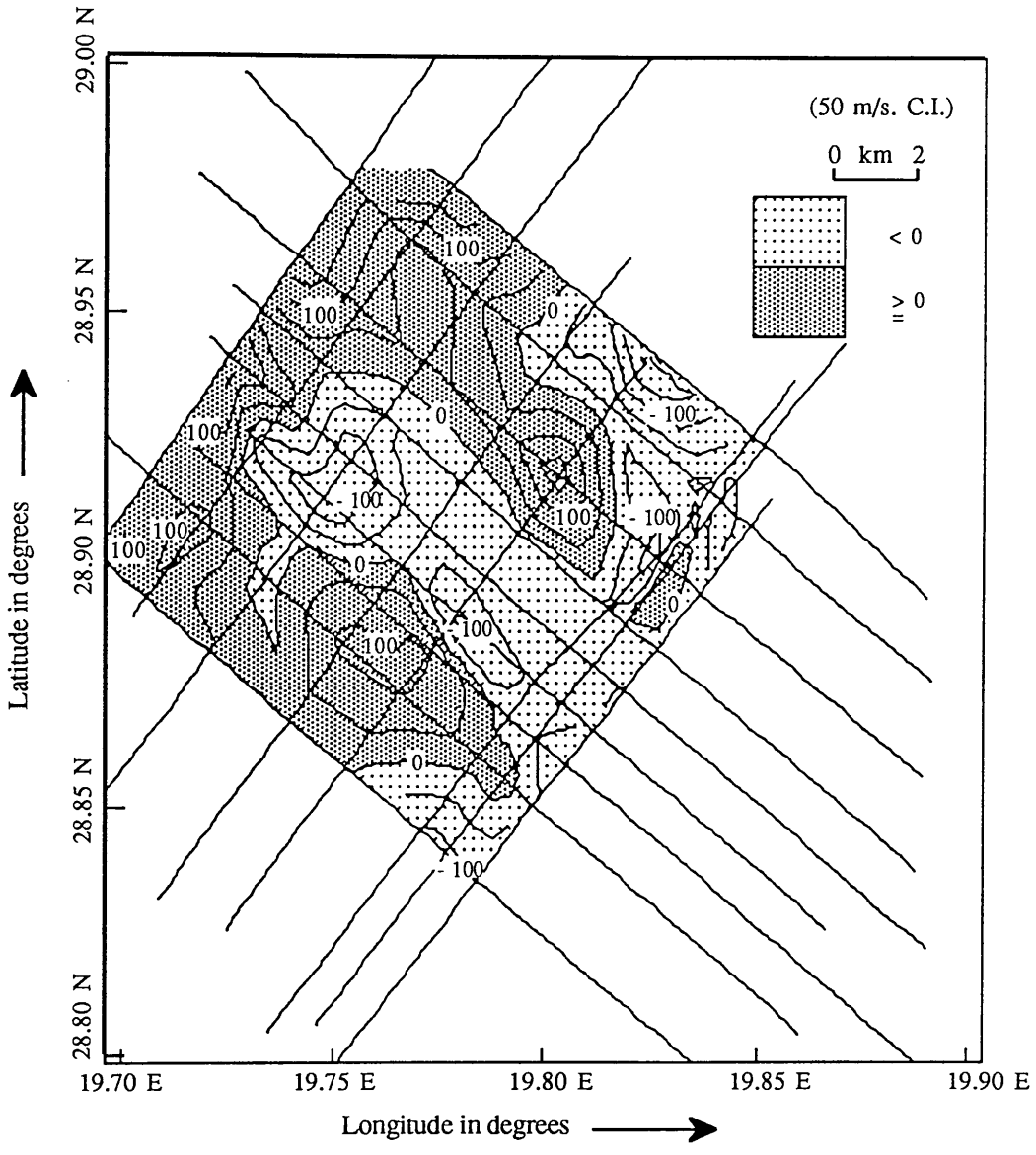

Fig.4.9 Velocity mis-tie contour map in meters per second at the top of the Domran formation, based on the seismic line intersection data.

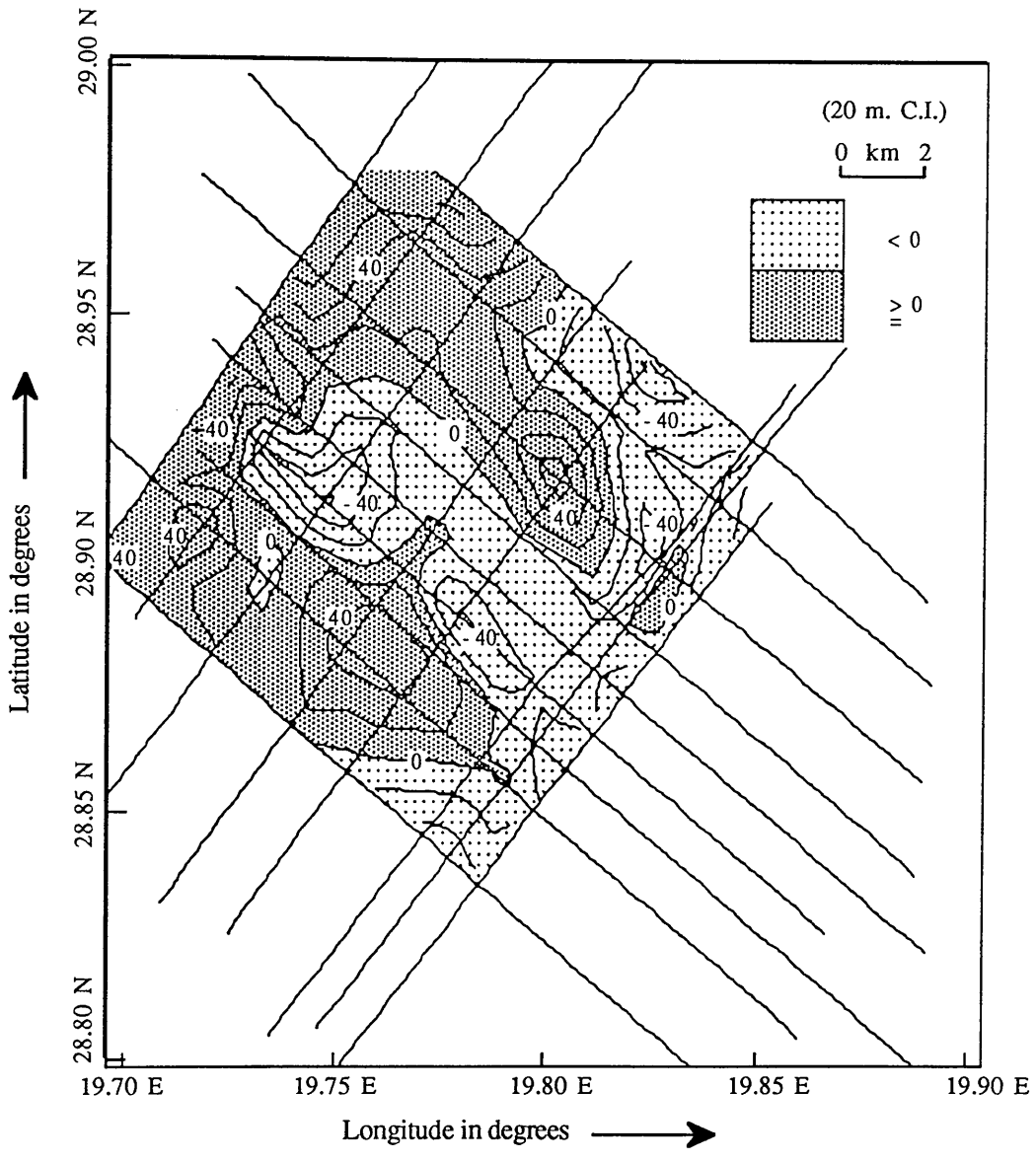

Fig.4.10 Depth mis-tie contour map in meters at the top of the Domran formation, based on the seismic line intersection data.

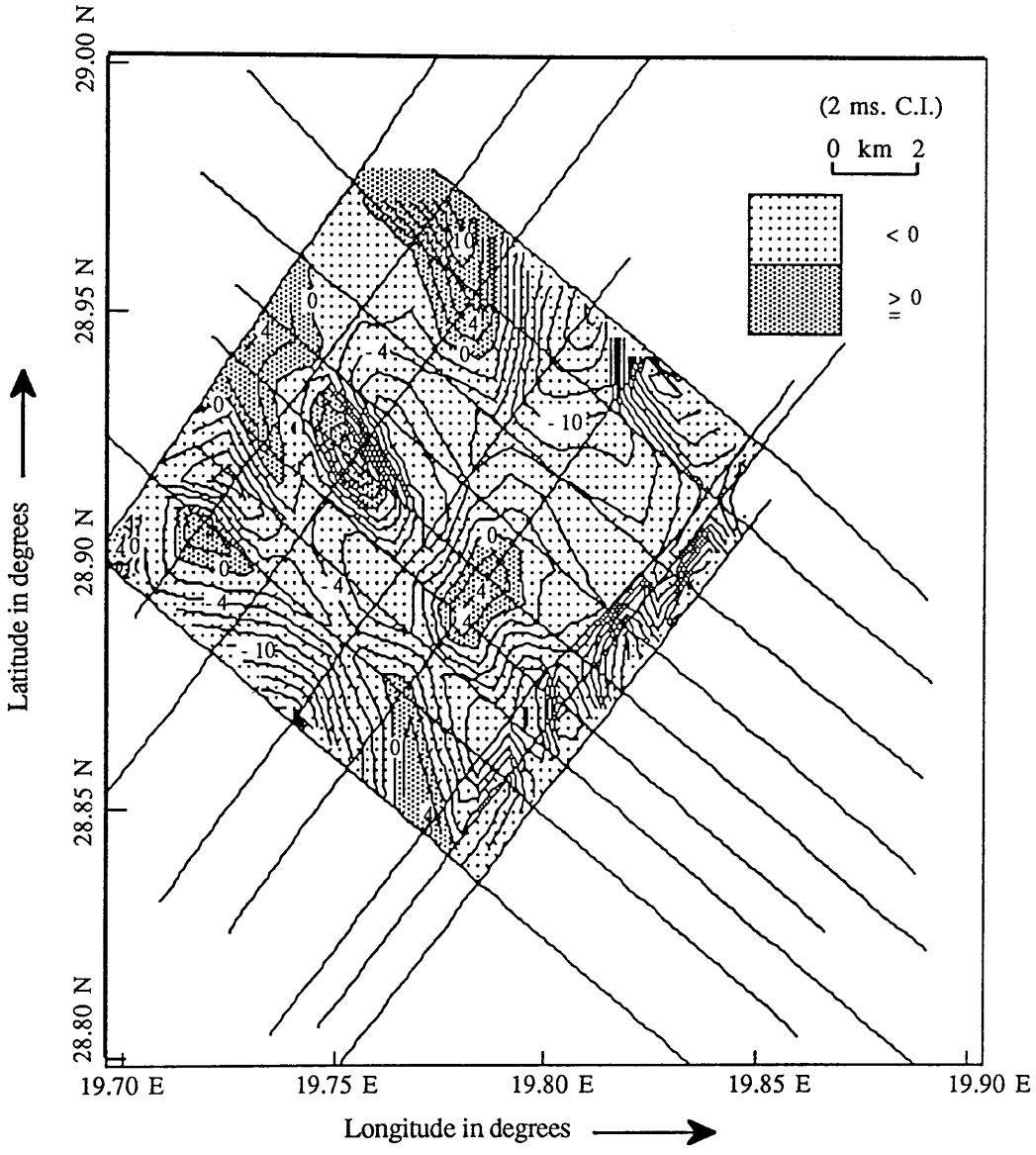

Fig.4.11 Two-way time mis-tie contour map in milliseconds at the top of the Ruaga formation, based on the seismic line intersection data.

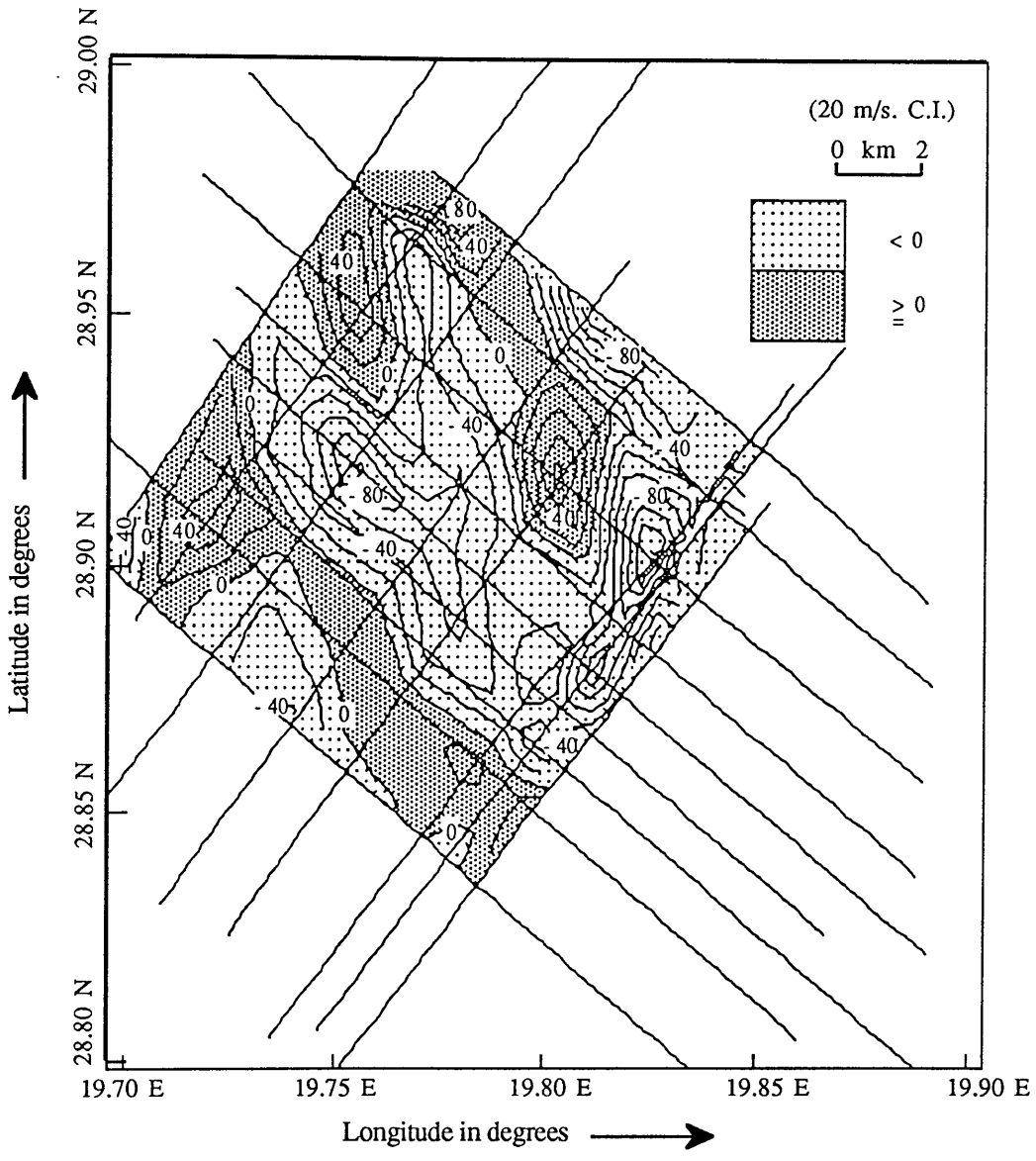

Fig.4.12 Velocity mis-tie contour map in meters per second at the top of the Ruaga formation, based on the seismic line intersection data.

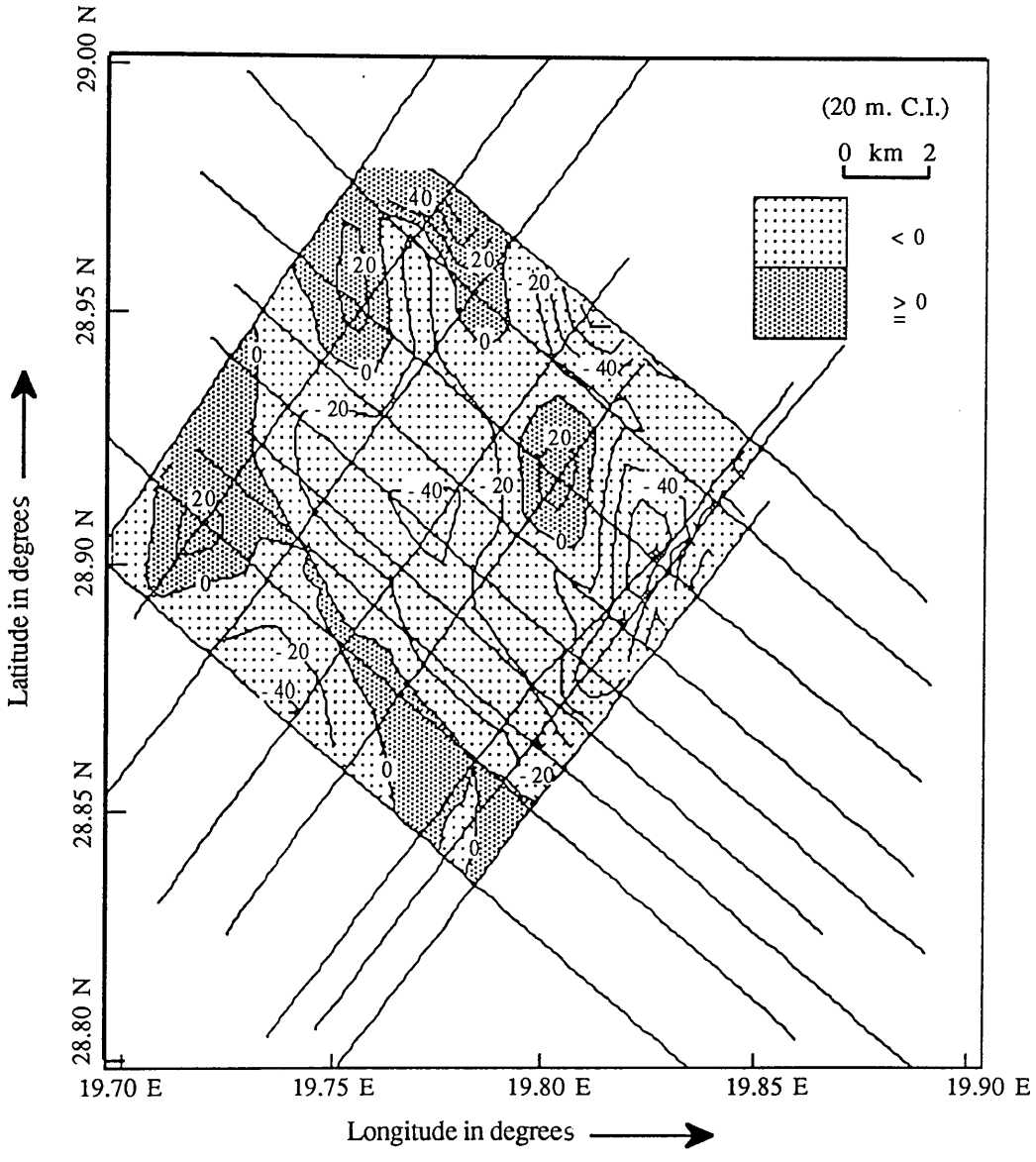

Fig.4.13 Depth mis-tie contour map in meters at the top of the Ruaga formation, based on the seismic line intersection data.

4.7 *Fortran programs*

Two Fortran77 programs were written to handle the data files transferred from S (Language and system for interactive data analysis) into the Sun Unix ('suilven') system. Listings of the source code of the steps to transfer the files is given in Appendix 4.2.

At the end of transfer steps we produce three output files, which are used in the programs. The first program, DIGITAL, was designed to calculate the corresponding depth from two-way time based on seismic data, after digitising the depth contour map based on the well data.

The second program, DIGITAL2, was designed to calculate the two-way time values for the well locations after digitising the two-way time contour map based on seismic data. Listings of the source code for the two programs is given in Appendix 4.3.

4.7.1 *Program steps*

The first step in the DIGITAL program is to read the names of the four input files and one output file, then print the number corresponding to the horizon you are working on. These are necessary steps for the program to run. There are two kinds of input data. The first kind contains three input files, which are transferred from S to 'suilven'. The first input file contains forty longitude values. These values should be in a 5 by 8 matrix form. The second input file contains forty latitude values corresponding to the data in the first input file; these values should also be in a 5 by 8 matrix form. The

third input file contains 1600 values of the depth based on well data, corresponding to the coordinate values in the first and second input files. These values should be in an one column matrix (vector) form. The second kind of input data contains one input file, which is the output file from the COORDINATE program (Chapter 3). A detailed flowchart corresponding to the above outline is shown in Figure 4.14.

The first step in the DIGITAL2 program is to read the names of the four input files and one output file, then print the number corresponding to the horizon you are working on. These are necessary steps for the program to run. There are two kinds of input data. The first kind contains three input files, which are transferred from S to 'suilven'. The three files are in the same format as described above for DIGITAL, only the third file contains values of the two-way time based on seismic data rather then the depth values. The second kind of input data contains one input file, which contains latitude, longitude, and depth to the top of horizon 1, depth to the top of horizon 2, depth to the top of horizon 3, thickness of horizon 1, and thickness of horizon 2. A detailed flowchart corresponding to the above outline is shown in Figure 4.15.

Both programs use the INT subroutine to calculate either depth or time for a given coordinate, using an interpolation between the values. A detailed flowchart corresponding to the INT subroutine outline is shown in Figure 4.16.

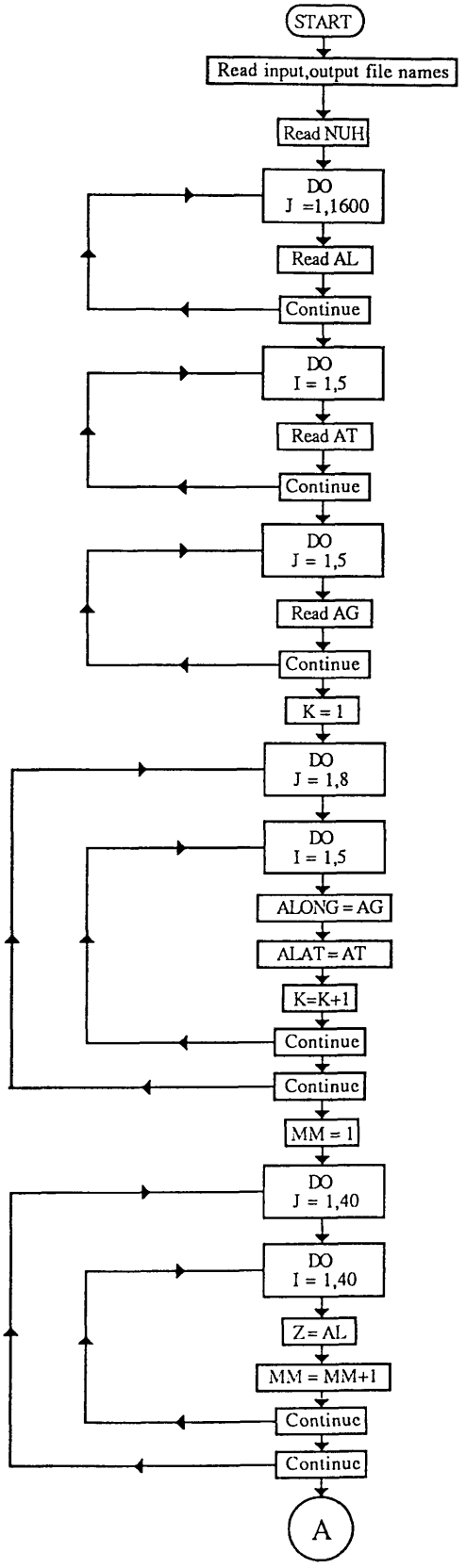

NUH - Horizon number.

J - Counter for depth values.

AL - Depth value.

I - Counter for matrix rows.

AT - Latitude value of the corresponding depth.

J - Counter for matrix rows.

AG - Longitude value of the corresponding depth.

J - Counter for matrix coloumns.

I - Counter for matrix rows.

ALONG - Longitude value.

ALAT - Latitude value.

J - Counter for matrix rows.

I - Counter for matrix rows.

Z - Depth value..

Fig.4.14. Detailed flowchart for the DIGITAL program.

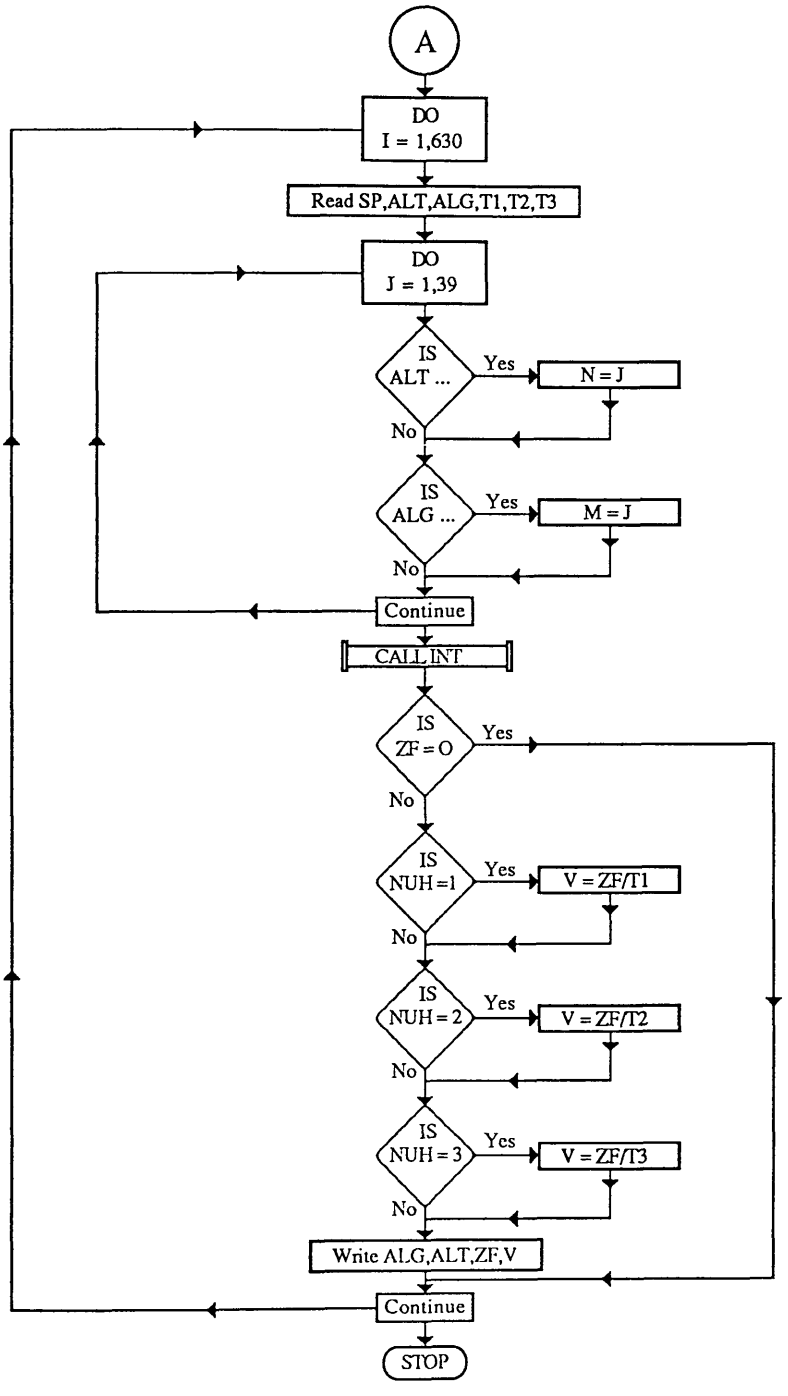

I - Counter for Shot point data.

SP - Shot point number.
ALT - Latitude value of the corresponding SP.
ALG - Longitude value of the corresponding SP.
T1 - Picked time for horizon (1).
T2 - Picked time for horizon (2).
T3 - Picked time for horizon (3).

I - Counter for loops of calculation.

ZF - Output depth value from subroutine INT calculation.

V - Average velocity.

Fig.4.14. (Continued) Detailed flowchart for the DIGITAL program.

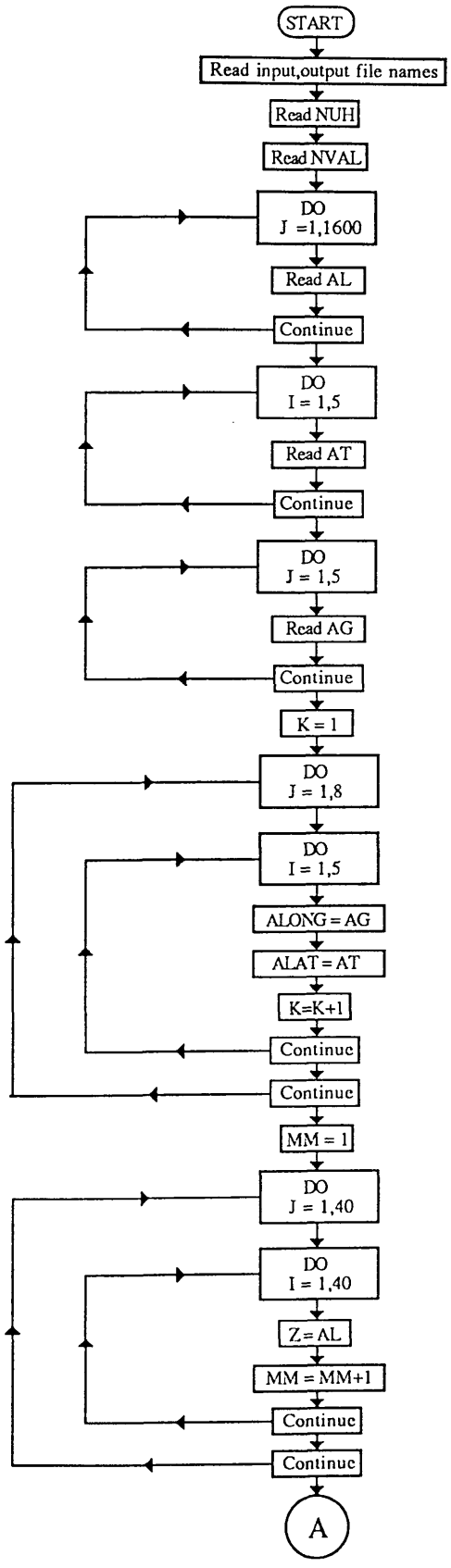

NUH - Horizon number.

NVAL - Number of input data.

J - Counter for two way time values.

AL - Two way time value.

I - Counter for matrix rows.

AT - Latitude value of the corresponding two way time.

I - Counter for matrix rows.

AG - Longitude value of the corresponding two way time.

J - Counter for matrix coloumns.

I - Counter for matrix rows.

ALONG - Longitude value.

ALAT - Latitude value.

J - Counter for matrix rows.

I - Counter for matrix coloumns.

Z - Two way time value.

Fig.4.15. Detailed flowchart for the DIGITAL 2 program.

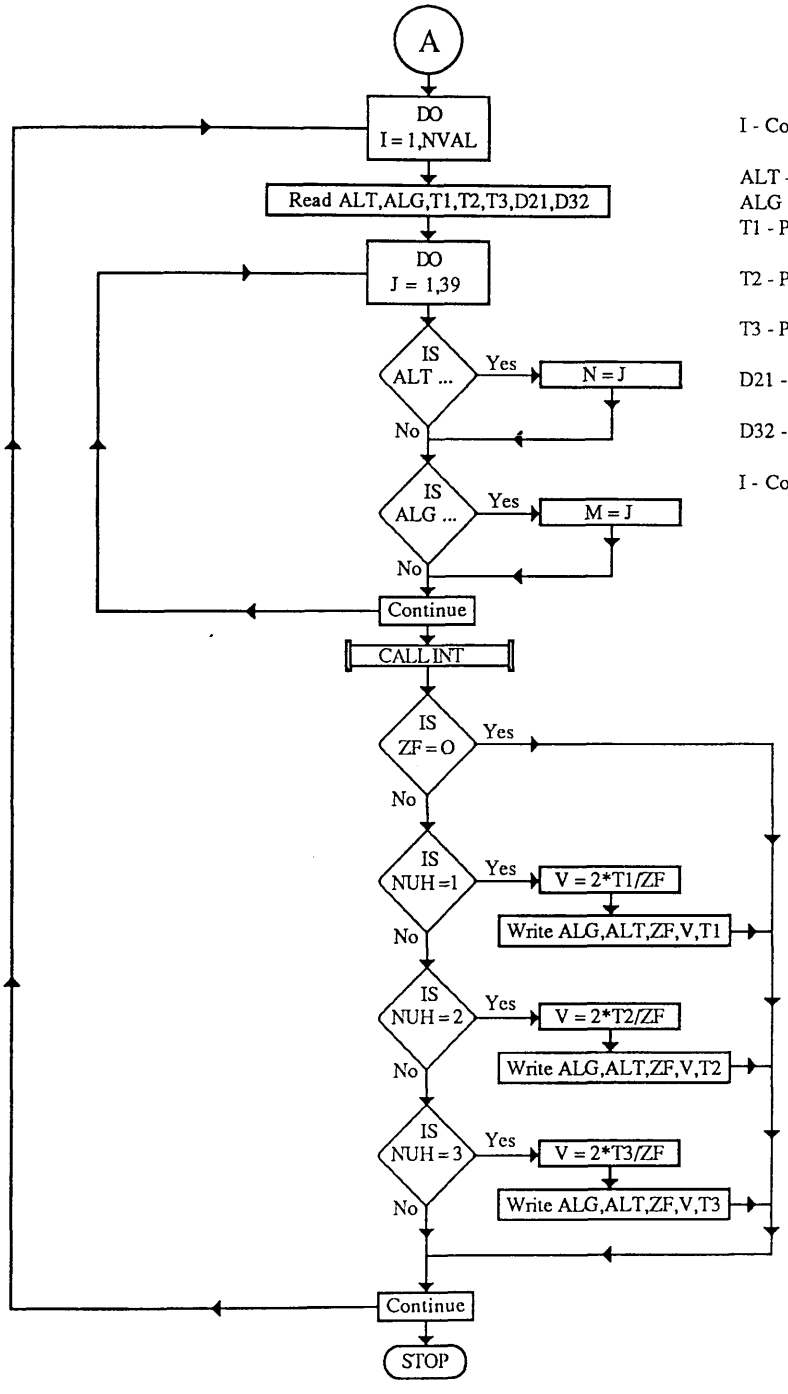

I - Counter for input data.

ALT - Latitude value.
ALG - Longitude value.
T1 - Picked time for horizon (1) corresponding to the coordinate.
T2 - Picked time for horizon (2) corresponding to the coordinate.
T3 - Picked time for horizon (3) corresponding to the coordinate.
D21 - Difference in depth between horizons 2 and 1.
D32 - Difference in depth between horizons 3 and 2.
I - Counter for loops of calculation.

ZF - Output two way time value from subroutine INT calculation.

V - Average velocity.

Fig.4.15. (Continued) Detailed flowchart for the DIGITAL 2 program.

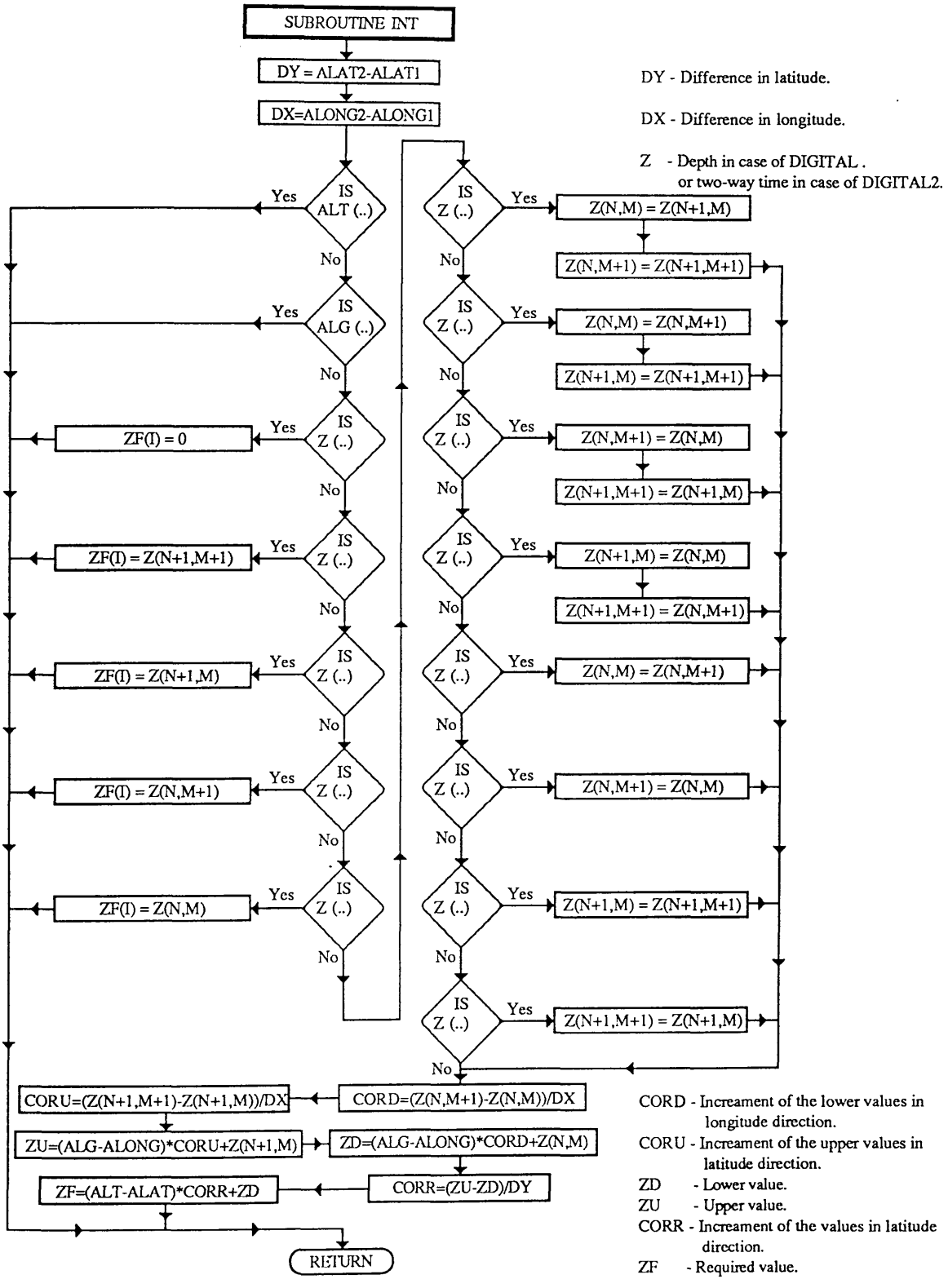

Fig.4.16. Detailed flowchart for the INT subroutine.

Some of the conditional statements (IF statement) in the three flowcharts have been shortened because they have long statements. For more details see the source code of the program.

4.7.2 *Program calculations and results*

One output file results from the DIGITAL program application. This contains shot point number, longitude and latitude corresponding to the shot point number, depth to the top of the chosen horizon, and velocity to the top of the chosen horizon.

One output file results from the DIGITAL2 program application. It contains shot point number, longitude and latitude corresponding to the shot point number, two-way time at that particular shot point, velocity to the top of the chosen horizon, and depth to the top of the chosen horizon.

4.8 *Data analysis*

Data gathered for the three horizons based on seismic sections data are shown in Appendix 4.4 (Table 4.3), and based on the well data are also shown in Appendix 4.4 (Table 4.4). Two S Macros were designed to handle these data to generate contour maps for the selection horizon. The first Macro is called VDCONT and the second is called PRE. The first macro depends on the second. These two macros were designed to produced contour map plots. The commands of the two macros are shown in Appendix 4.5.

4.9 *Map construction and data interpretation*

The main exploration objective in this area of the concession is the hydrocarbon trapped in structural closures in Ruaga formation. Therefore, efforts were directed at mapping this seismic horizon, plus two other seismic horizons above the Ruaga formation (the Sheghega and Domran formations). The final stacked data were used for timing and mapping in this area. Both techniques were used for mapping the two-way travel times as mentioned in Section 4.6, and only the automated ones were used for the other maps.

4.9.1 *Manual contouring technique*

The manual contouring technique (Section 4.6) was used to construct all maps discussed in this section.

(1) *Time structure contour maps*

Subsea two-way travel times for the three seismic horizons are read from the seismic sections, for every 10 shot points as mentioned in Section 4.5.1. Figure 1.6 (Chapter 1) shows the shot point location map where the values of the two-way time have been picked. For contouring, the two-way travel time values are first posted onto a shot point location map of 1:25,000 scale, contoured, and then reduced to A4 paper size.

(a) *Top of Sheghega formation time structure map*

The subsea two-way travel time structure contour map of the Sheghega event is shown in Figure 4.17. It shows a general dip towards the northeast. A possible large structural closure within the area can easily be identified on this map, at a time value of 450 ms.

(b) *Top of Domran formation time structure map*

The subsea two-way travel time structure contour map of the Domran event is shown in Figure 4.18. It shows the same general dip towards the northeast as mentioned above. Several structural closures within the area can be identified on this map, three at time values of 700 ms. and one at a value of 750 ms. In general the Sheghega and Domran maps have the same contour shape, and the horizons could therefore be approximately parallel to each other.

(c) *Top of Ruaga formation time structure map*

The subsea two-way travel time structure contour map of the Ruaga event is shown in Figure 4.19. It shows the same dip as is mentioned before. The map shows one possible large structure closure within the area, at a time value of 1000 ms. Within, there are four structural sub-closures at time values of 950 ms, which can easily be identified. One major SE-NW fault, crossing all SE-NW seismic lines and parallel to the others, divides the area into two major parts, the Zelten platform in the north and the Hagfa trough in the south.

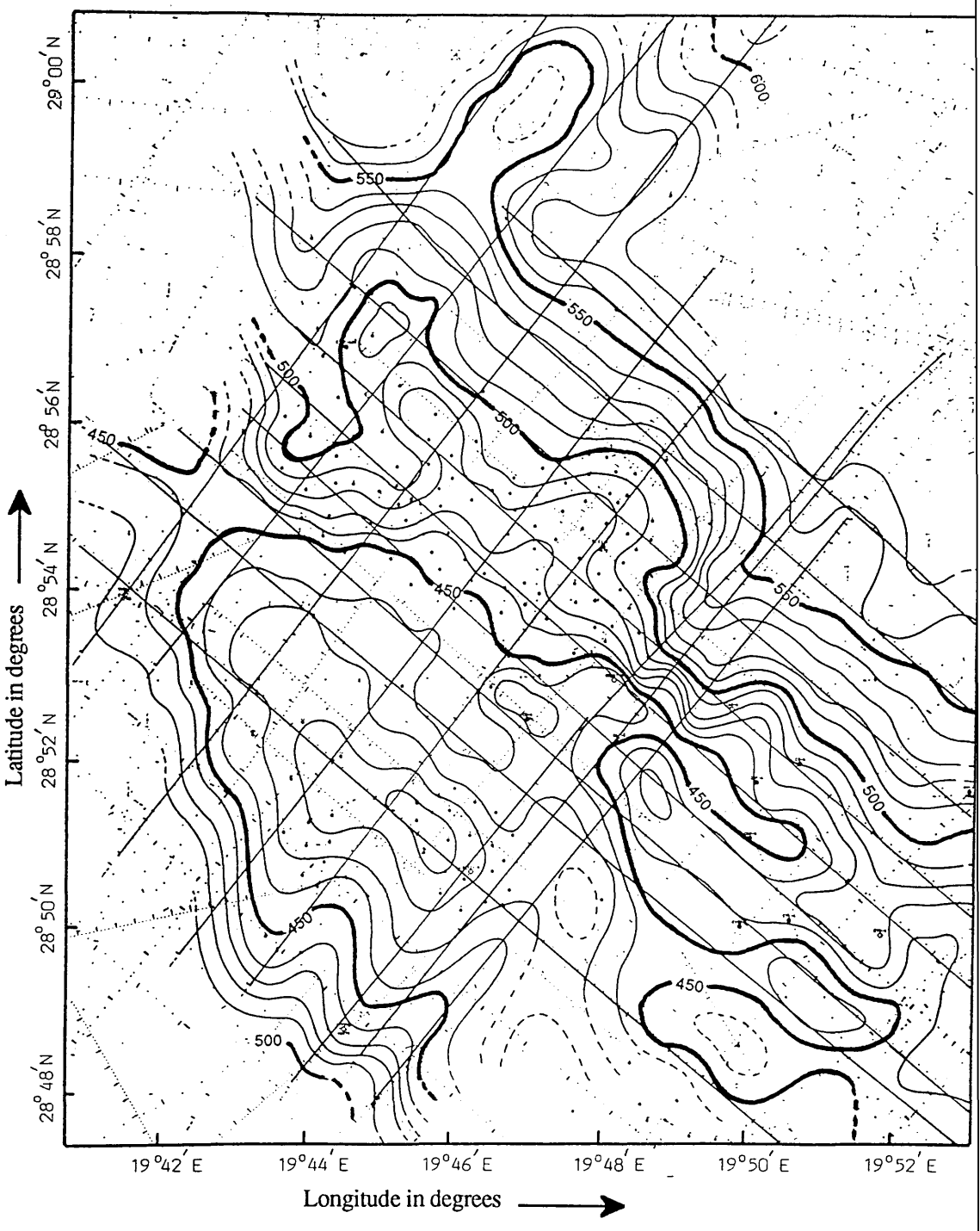

Fig. 4.17 Subsea T.W.Time contour map in milliseconds to the top of the Sheghega formation based on manual contouring of the seismic data.

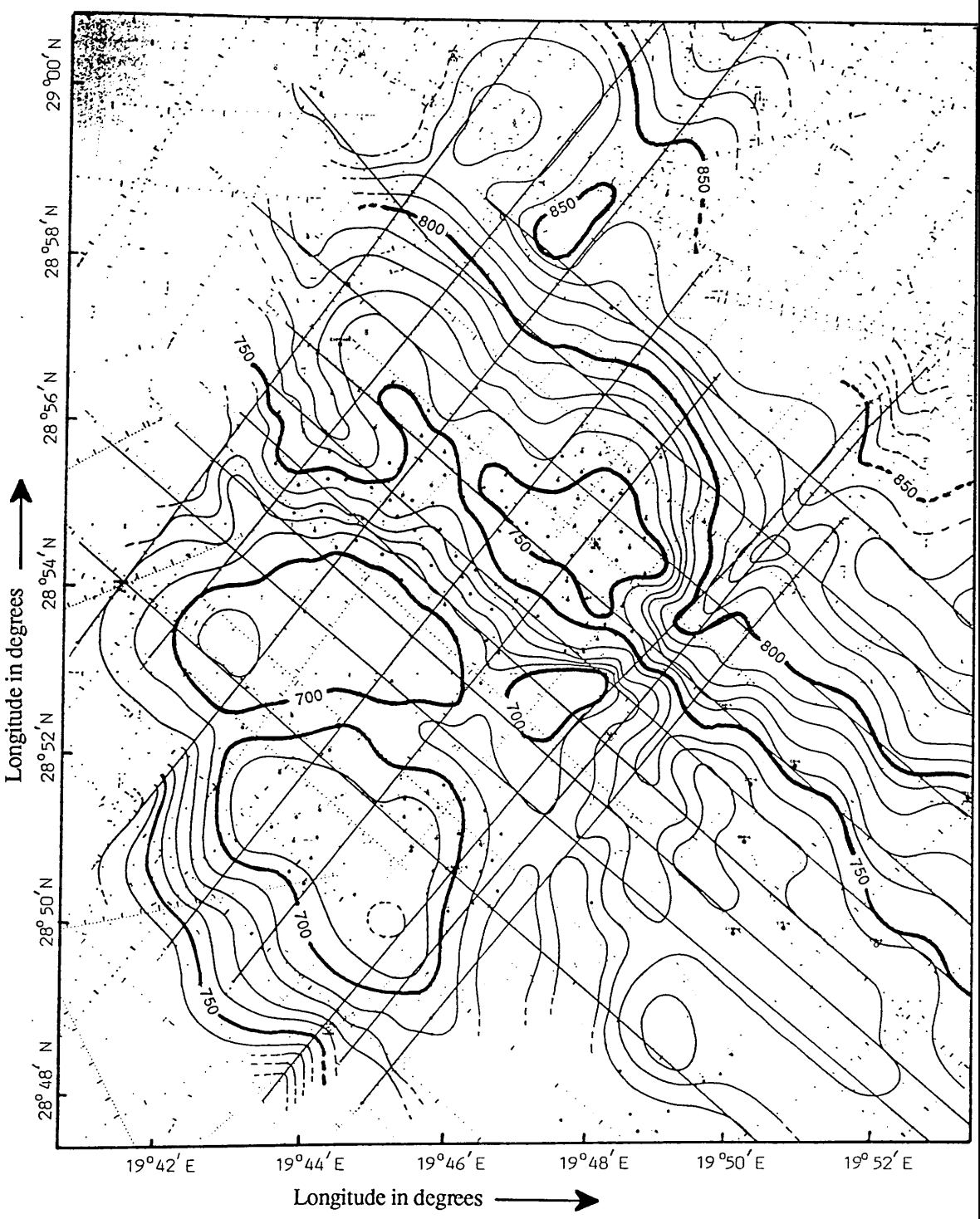

Fig. 4.18 Subsea T.W.Time contour map in milliseconds to the top of the Domran formation based on manual contouring of the seismic data.

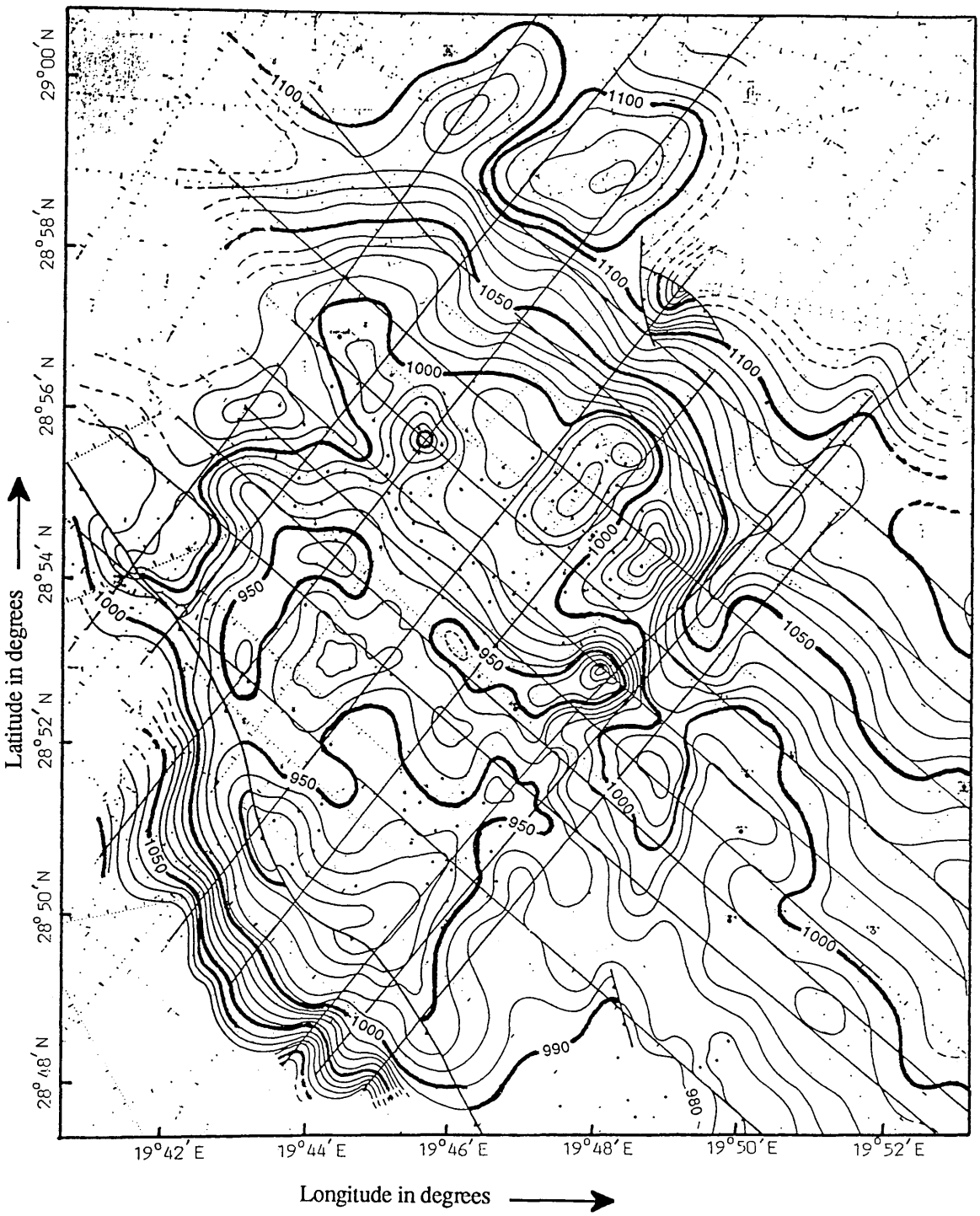

Fig. 4.19 Subsea T.W.Time contour map in milliseconds to the top of the Ruaga formation based on manual contouring of the seismic data.

4.9.2 *Automated contouring technique*

The automated contouring technique as mentioned in Section 4.6 was used to construct all maps discussed in this section. Figure 4.50 at the end of this chapter shows the maps flowchart for the the automated contouring maps. It also shows the way the maps were made and how they related to each other.

A *Maps based on seismic data*

(1) *Time structure contour maps*

Subsea two-way times for the three seismic horizons are read from the seismic sections, for every 10 shot points as mentioned in Section 4.5.1. Two-way travel time from the seismic sections was picked every 10 shot points. Mis-ties at the intersections were corrected before being stored in the computer. The time values for all timed shot points to the top of each horizon are shown in Appendix 4.4 (Table 4.3).

(a) *Top of Sheghega formation time structure map*

The subsea two-way seismic time structure map of the Sheghega event (Figure 4.20) shows a general dip towards the northeast. A clear large structural closure within the area can easily be identified on this map, at a time value of 450 ms. This map looks similar to that one produced by hand (Fig. 4.17).

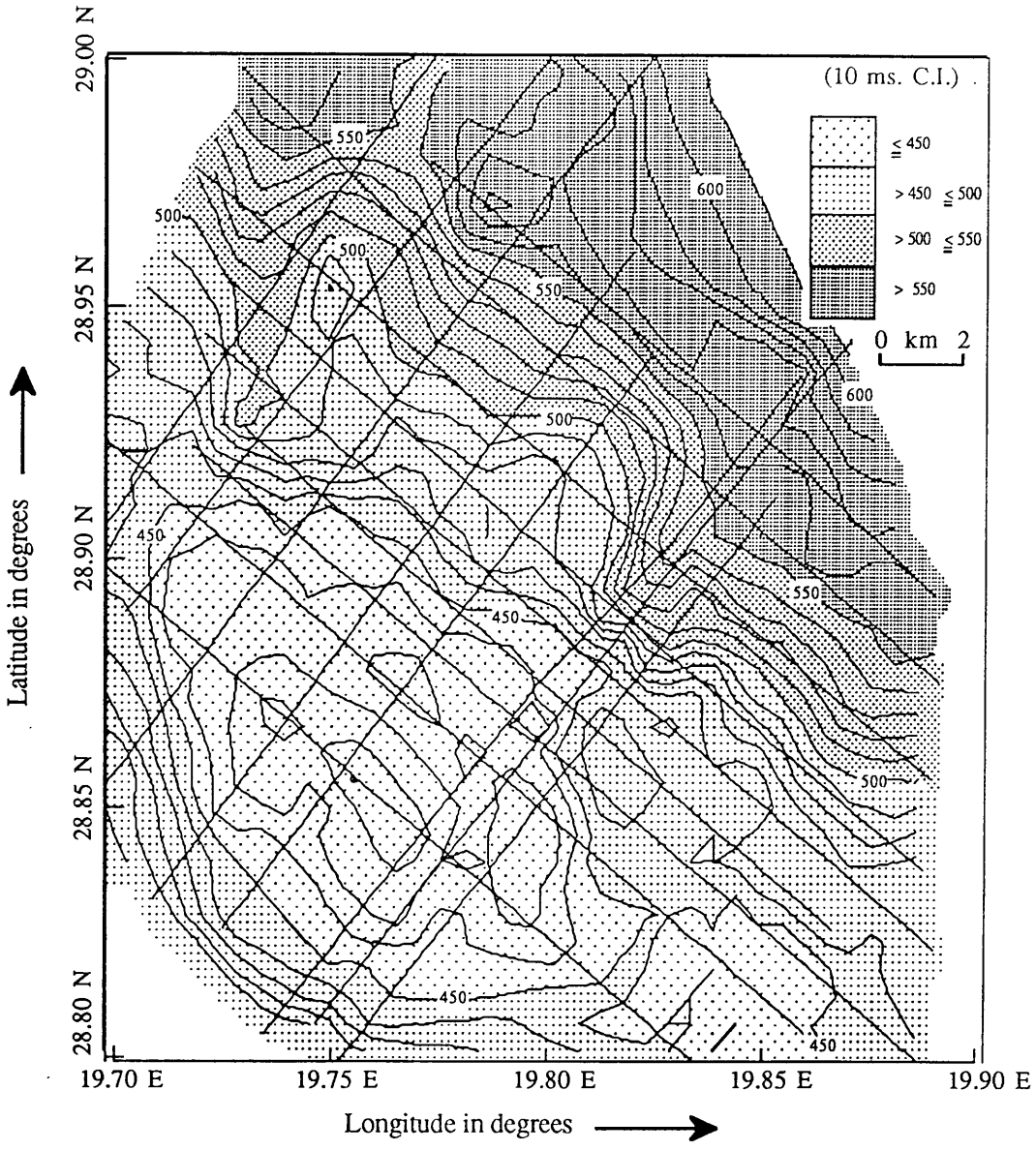

Fig. 4.20 Subsea T.W.time contour map in milliseconds to the top of the Sheghega formation based on automated contouring of the seismic data.

(b) *Top of Domran formation time structure map*

The subsea two-way seismic time structure map of the Domran event (Figure 4.21) shows the same general dip towards the northeast. One structural closure within the study area can be identified, at a time value of 720 ms. This map is quite similar to the one produced by hand, but with a few differences in the shape and size of the closure. In general the maps in Figures 4.18 and 4.21 have the same shape of contouring.

(c) *Top of Ruaga formation time structure map*

The subsea two-way seismic time structure map of the Ruaga event (Figure 4.22) shows the same dip towards the northeast as mentioned before. This map shows dense parallel contours crossing all SE-NW seismic lines and parallel to the others, in the southwest portion, and some other dense contouring is shown in the north portion. This is cause by the presence of the faults in the area, which the contouring software cannot handle. One large structure closure within the area at a time of 1000 ms. It contains one smaller closure at 960 ms. This map give a good quick picture of the contouring the horizon. Compared with the one produced by hand (Fig. 4.19), the manual contour map looks better and smoother than the automated one.

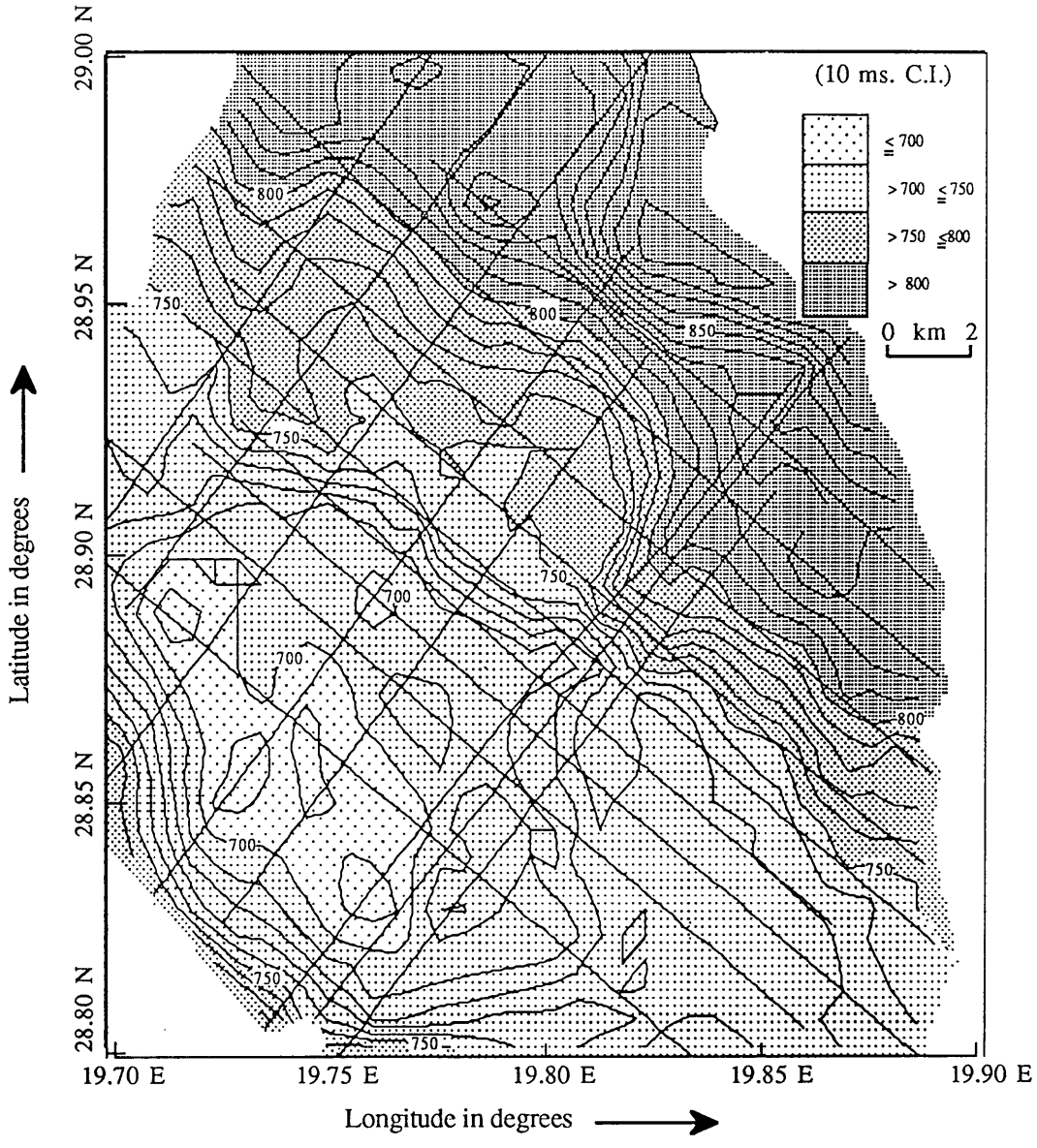

Fig. 4.21 Subsea T.W.time contour map in milliseconds to the top of the Domran formation based on automated contouring of the seismic data.

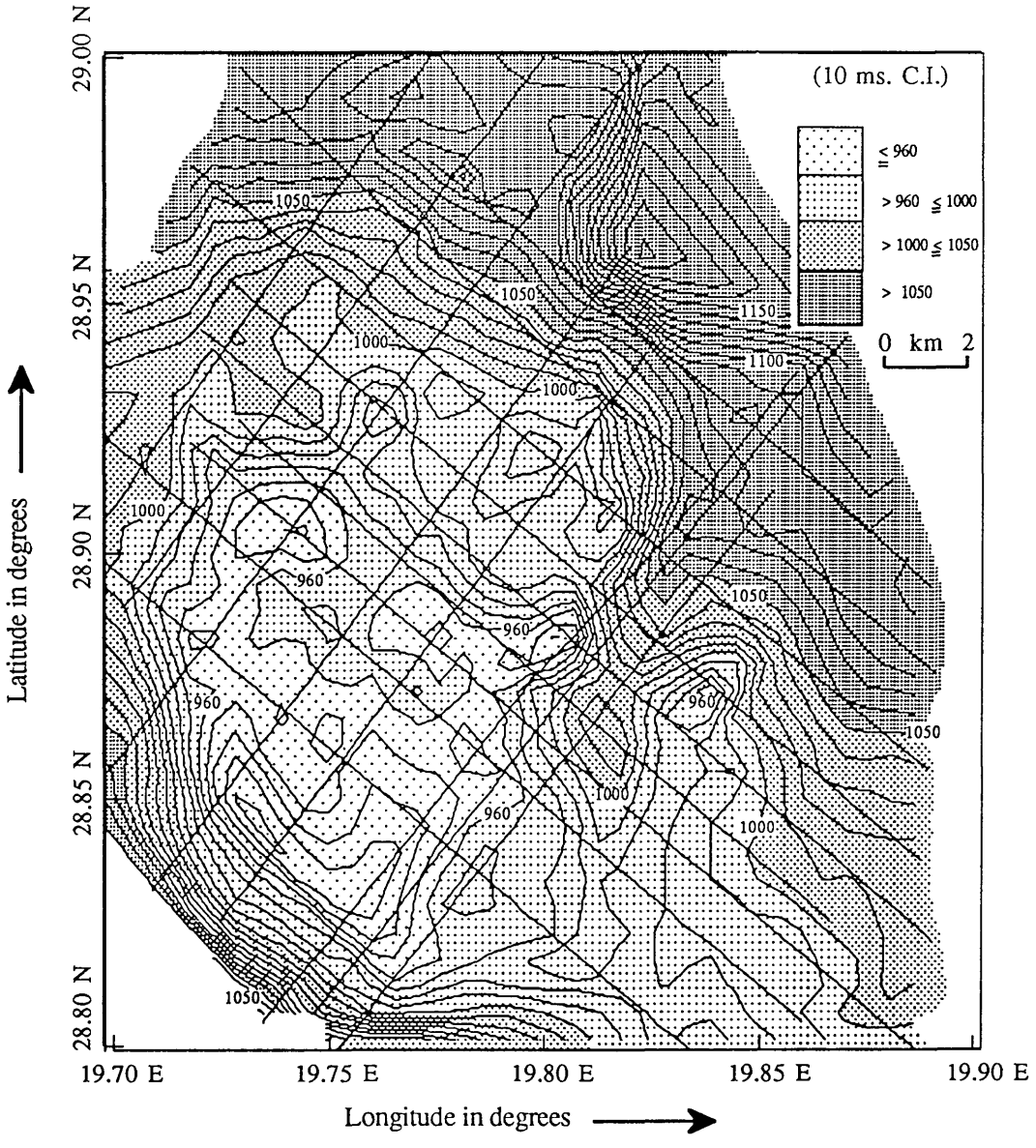

Fig. 4.22 Subsea T.W.time contour map in milliseconds to the top of the Ruaga formation based on automated contouring of the seismic data.

(2) *Average velocity contour maps*

In order to convert the subsea two-way time map to a depth map, we need to know the velocity distribution over the area. Because of the good quality seismic data in the area of study, the Dix average velocities, calculated by equation 3.13 (Chapter 3) from the velocity analysis, have been used as a source of the velocity information to build the velocity maps in this section. The velocity values for each posted shot point to the top of the each horizon are also given in Appendix 4.4 (Table 4.3).

(a) *Average velocity contour map to the Top of Sheghega formation*

Figure 4.23 shows the Dix average velocity, measured from the datum (sea level) to the top of the Sheghega formation. The velocity values range from 2080 to 2220 m/s in most of the study area, except for a small high closure in the north around the location of shot point 120 on seismic line V248-85, where the velocity is 2240 m/s. There is little overall difference in velocity, because of the shallow and flat horizon. There is dense contouring at the intersections because of the mis-ties mentioned in Section 4.6 (Fig. 4.6).

(b) *Average velocity contour map to the Top of Domran formation*

Figure 4.24 shows the Dix average velocity, measured from the datum (sea level) to the top of the Domran formation. The velocity values range from 2350 to 2550 m/s in most of the study area, except for a small high closure in the north around the location of shot point 120 on seismic

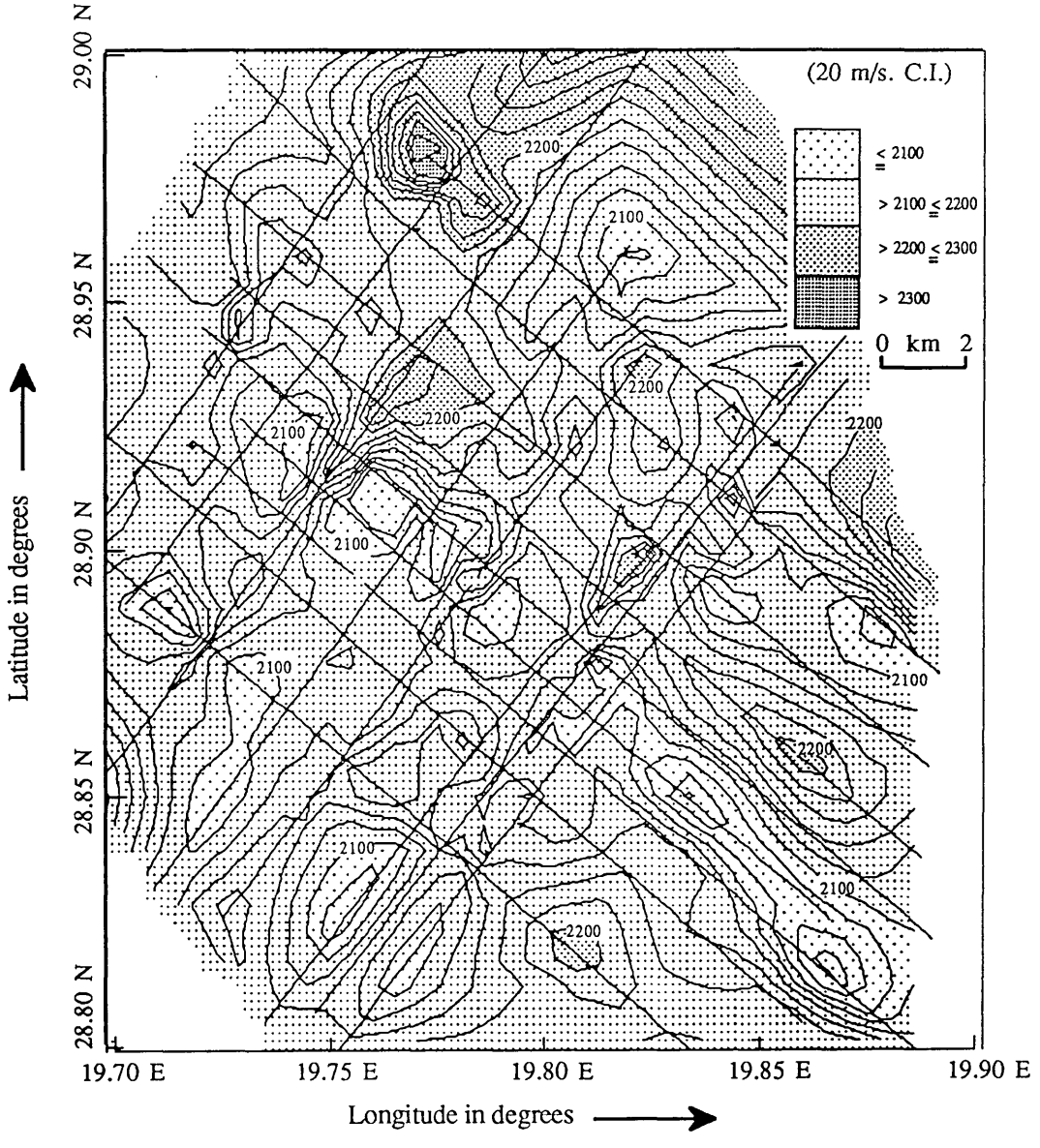

Fig. 4.23 Dix average velocity contour map in meters per second to the top of the Sheghega formation based on automated contouring of the seismic data.

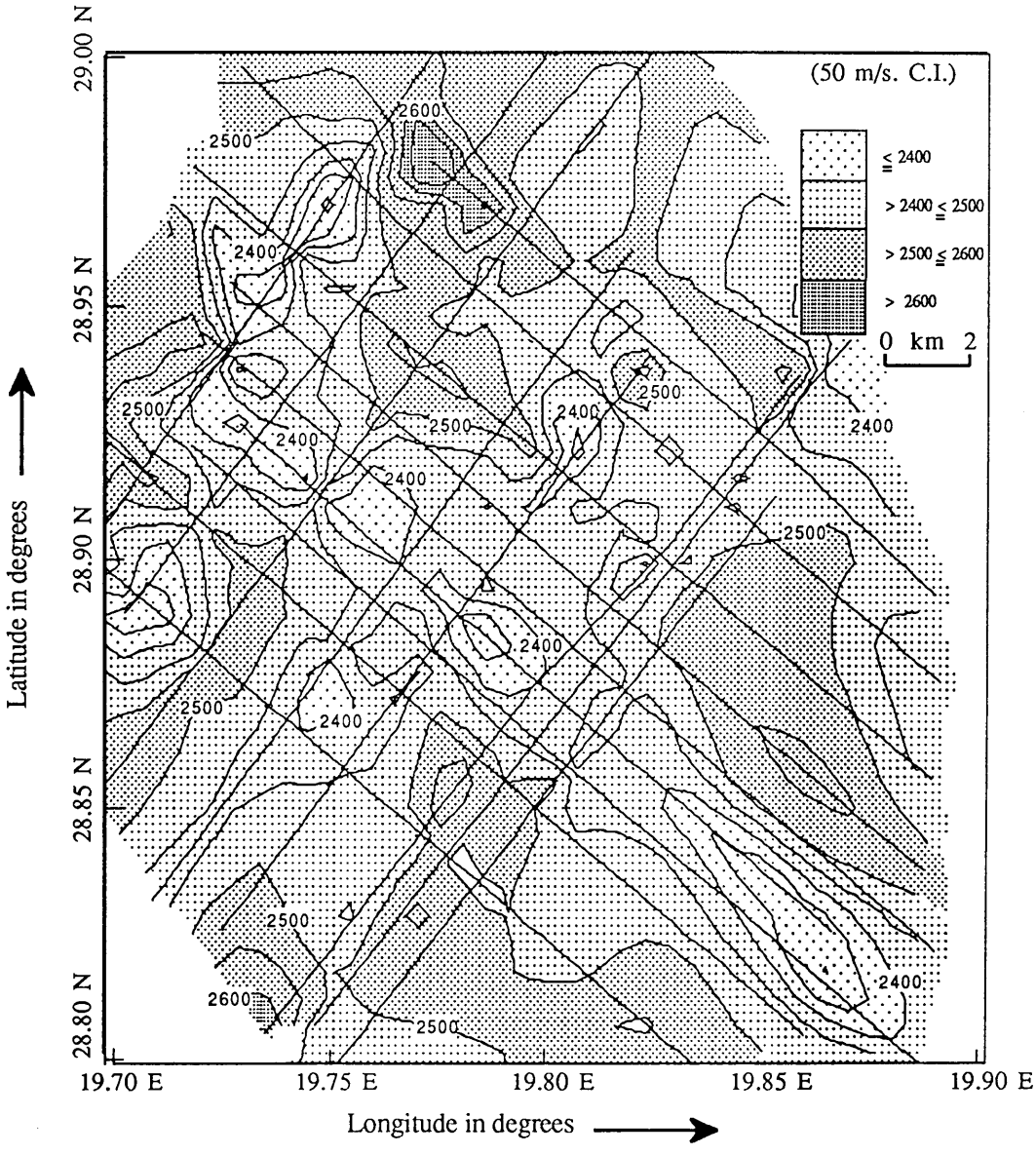

Fig. 4.24 Dix average velocity contour map in meters per second to the top of the Domran formation based on automated contouring of the seismic data.

line V248-85, where the velocity value of 2600 m/s. In general the map has the same shape as the map in Figure 4.23. There is dense contouring at the intersections especially in the northwest portion of the study area because of the mis-ties mentioned in Section 4.6 (Fig. 4.9).

(c) *Average velocity contour map to the Top of Ruaga formation*

Figure 4.25 shows the Dix average velocity, measured from the datum (sea level) to the top of the Ruaga formation. The velocity values range from 2650 to 22850 m/s in most of the study area. There is a small high closure in the north around shot point 450 on seismic line V259-85, with a velocity of 2900 m/s, and a high contour value in the south around the ends of the seismic lines V263-85 and V265-85, where the velocity value is 2900 m/s. There is irregular contouring at the intersections, especially in the middle portion of the study area, because of the mis-ties mentioned in Section 4.6 (Fig. 4.12).

(3) *Depth structure contour maps*

The Dix average velocity maps mentioned above were used to convert travel time to depth, by multiplying one-way times by velocities. The depth values for each required shot point to the top of the each horizon are also tabulated in Appendix 4.4 (Table 4.3).

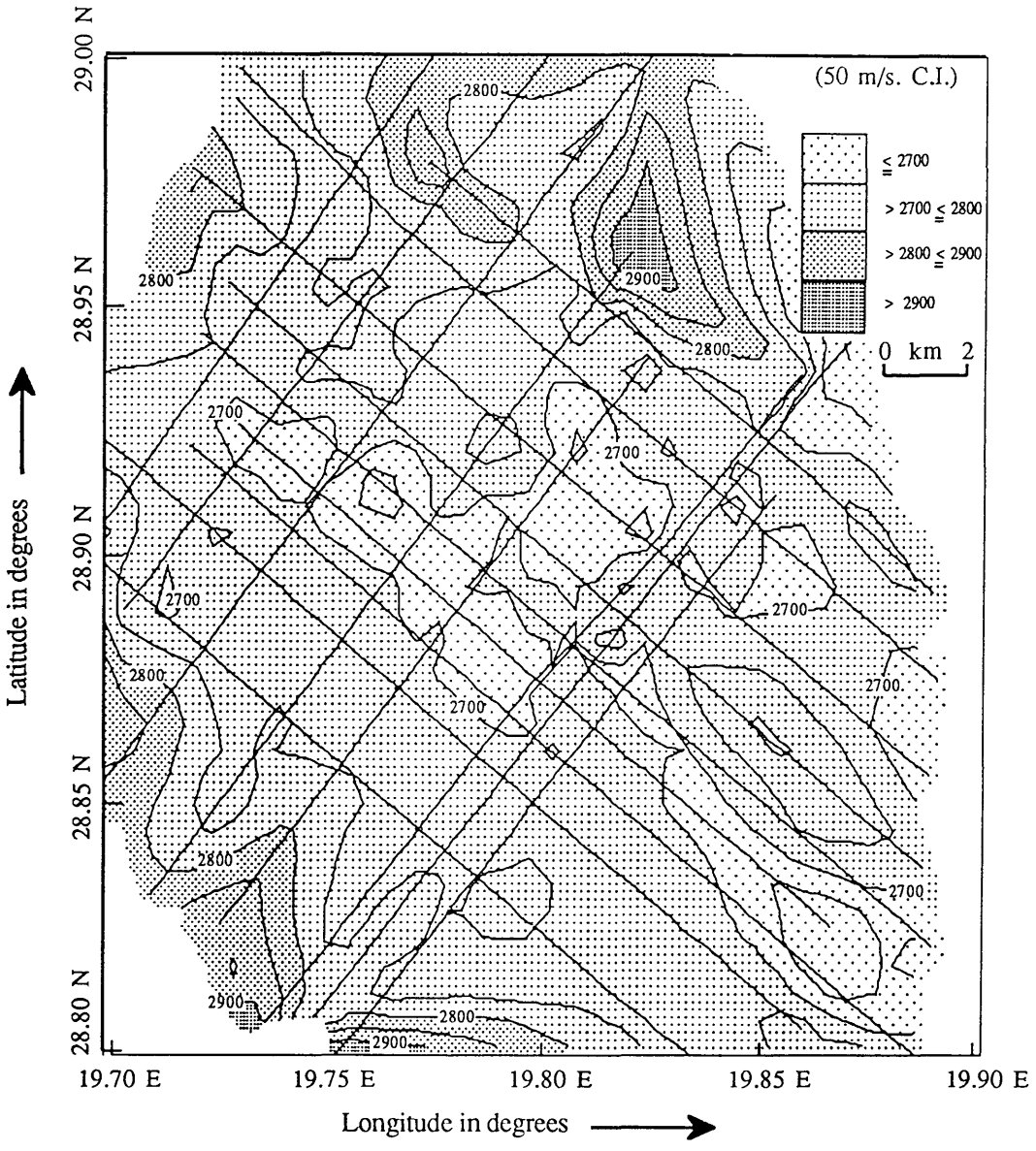

Fig. 4.25 Dix average velocity contour map in meters per second to the top of the Ruaga formation based on automated contouring of the seismic data.

(a) *Depth structure contour map of Sheghega formation*

Figure 4.26 shows the subsea depth contour map to the top of the Sheghega formation. A large structural closure, at a depth of 500 m. covers most of the study area. It also shows a general dip towards the northeast.

(b) *Depth structure contour map of Domran formation*

Figure 4.27 shows the subsea depth contour map to the top of the Domran formation. The map shows the same general dip towards the northeast. There are six small closures, at depths of 850 m. within the one large closure, at a depth of 900 m. There is the same dip towards the northeast, as has been seen as in the previous two depth maps.

(c) *Depth structure contour map of Ruaga formation*

Figure 4.28 shows the subsea depth contour map to the top of the Ruaga formation. This map also shows four closures, two large and two small, at depths of 1300 m. within the one large closure, at 1350 m. There are large gradients in the contours in the north and in the south of the area, at depths of more than 1500 m, because of the faulting.

(4) *Isochron contour maps*

Isochron values are calculated by subtracting the time values to the two different horizons at each required shot point. The isochron maps in this section are constructed by contouring the difference values for Sheghega

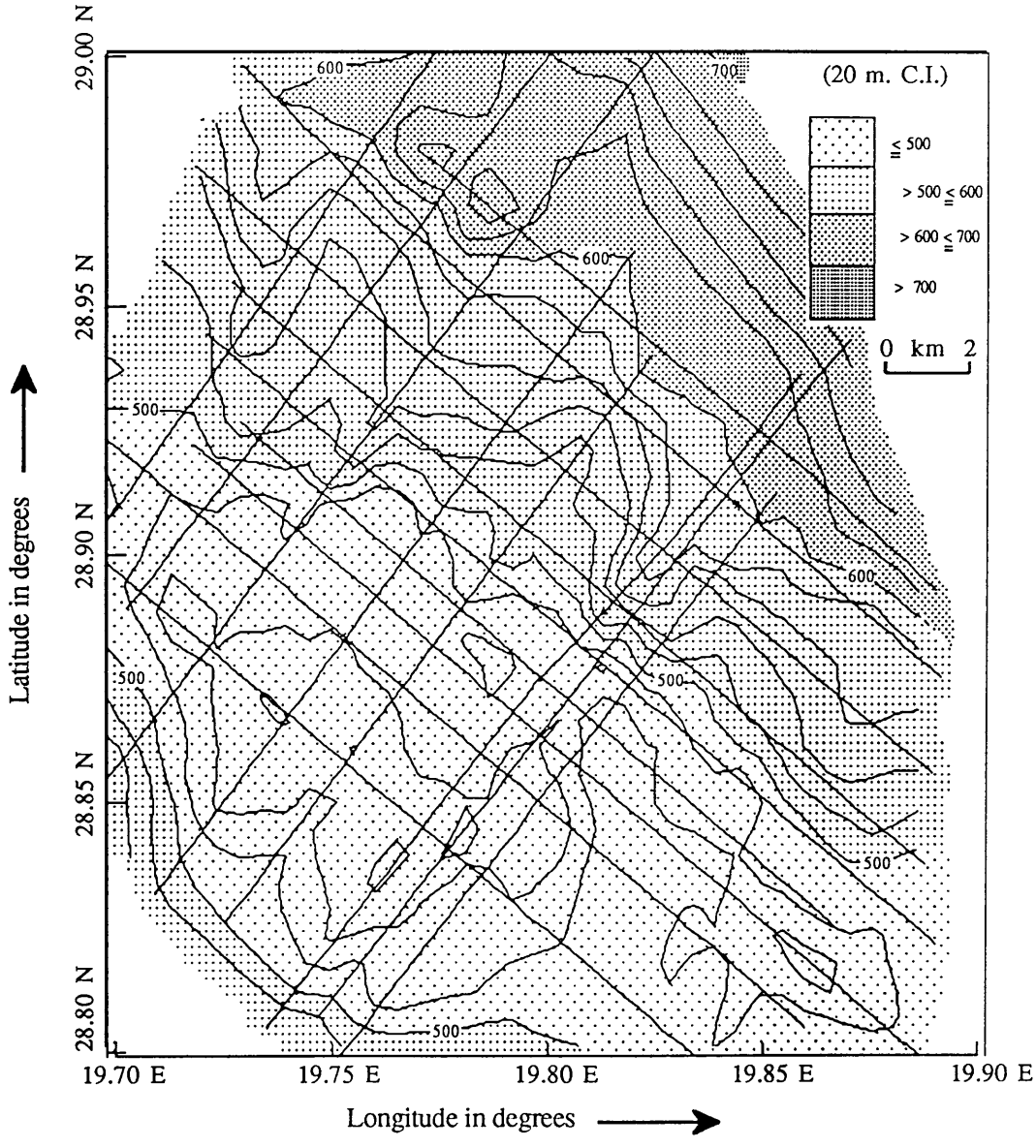

Fig. 4.26 Subsea depth contour map in meters to the top of the Sheghega formation based on automated contouring of the seismic data.

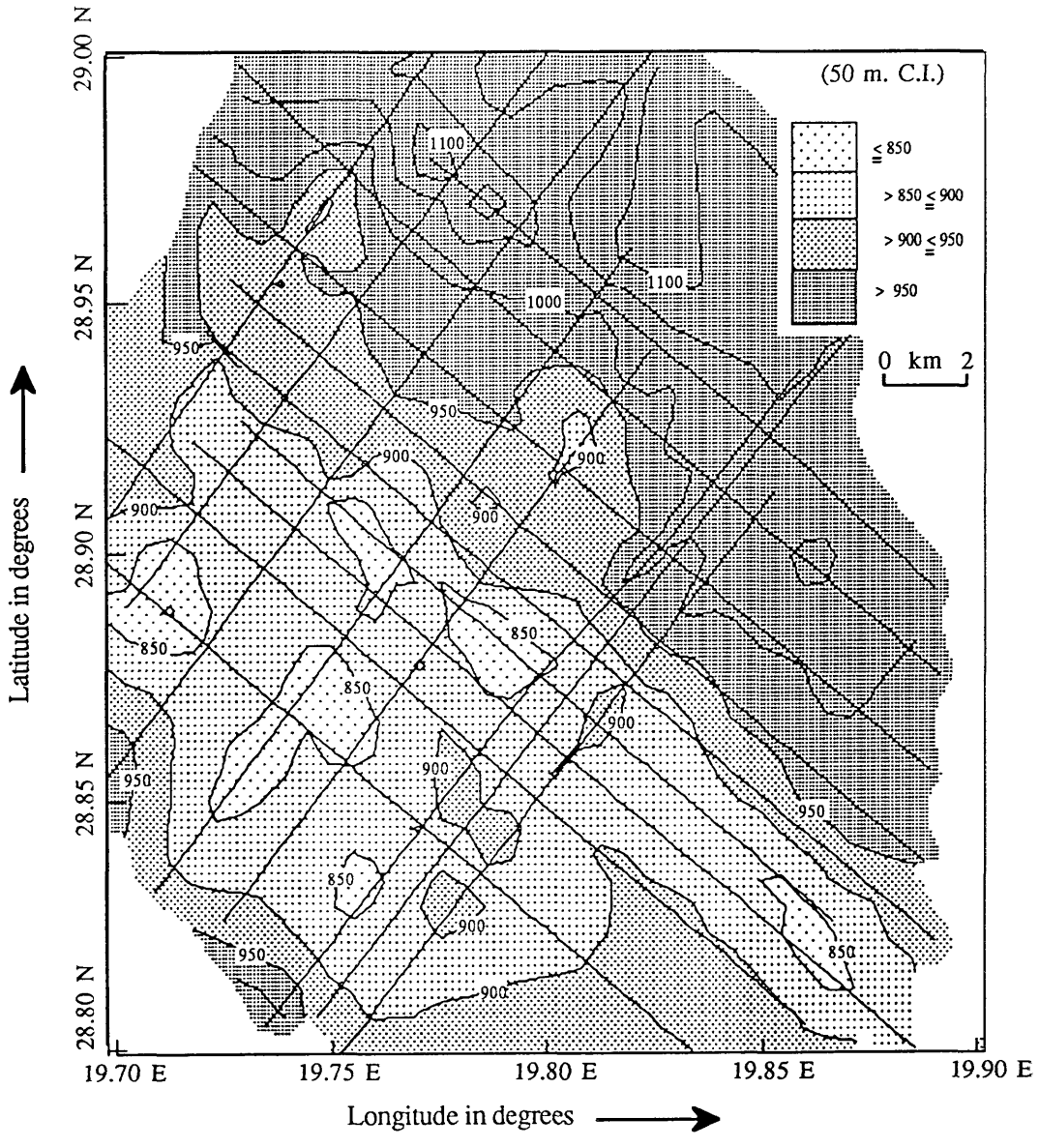

Fig. 4.27 Subsea depth contour map in meters to the top of the Domran formation based on automated contouring of the seismic data.

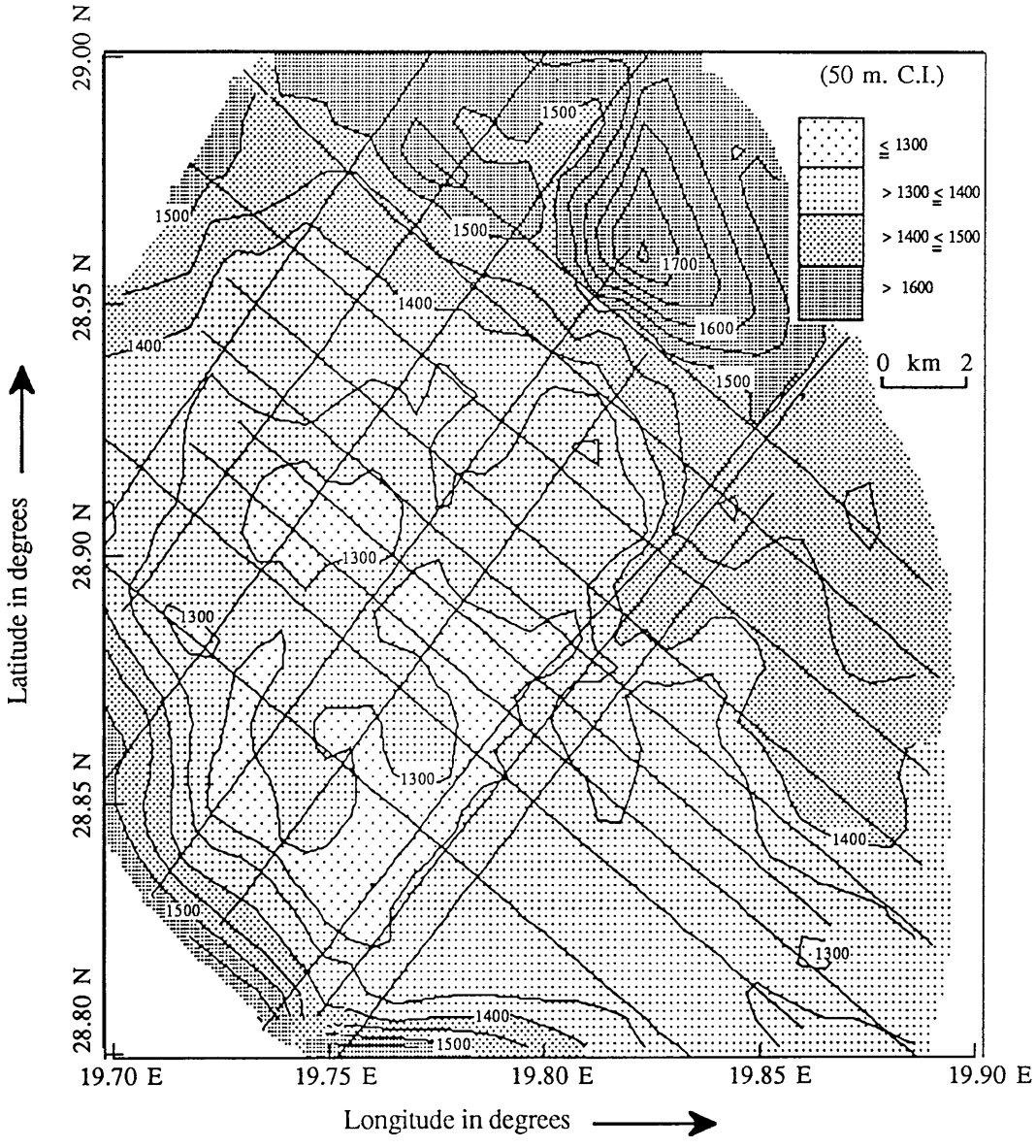

Fig. 4.28 Subsea depth contour map in meters to the top of the Ruaga formation based on automated contouring of the seismic data.

and Domran formations, to show thinning and thickening over the area in terms of time. The values for all required shot points for the Sheghega and Domran horizons are tabulated in Appendix 4.4 (Table 4.3) as difference in time.

(a) *Isochron contour map for Sheghega formation*

Figure 4.29 shows the isochron contour map for the Sheghega formation. The time difference values range from 255 to 280 ms. over most of the area. Also it shows one location where thickness is greater, in the northeast of the area.

(b) *Isochron contour map for Domran formation*

Figure 4.30 shows the isochron contour map for the Domran formation. The time difference values range from 230 to 270 ms. over most of the area. Also it shows two locations where thickness is greater, in the northeast and in the southwest of the area. This thickening is due to the presence of faults in the lower unit only. This map shows time thinning concentrated in the middle, surrounded by an area of thickening.

(5) *Isopach contour maps*

Isopach values are calculated by subtracting the depth values to the two different horizons at each required shot point. The isopach maps in this section are constructed by contouring the thickness values for the Sheghega and Domran formations. Thickness values for all required shot points for

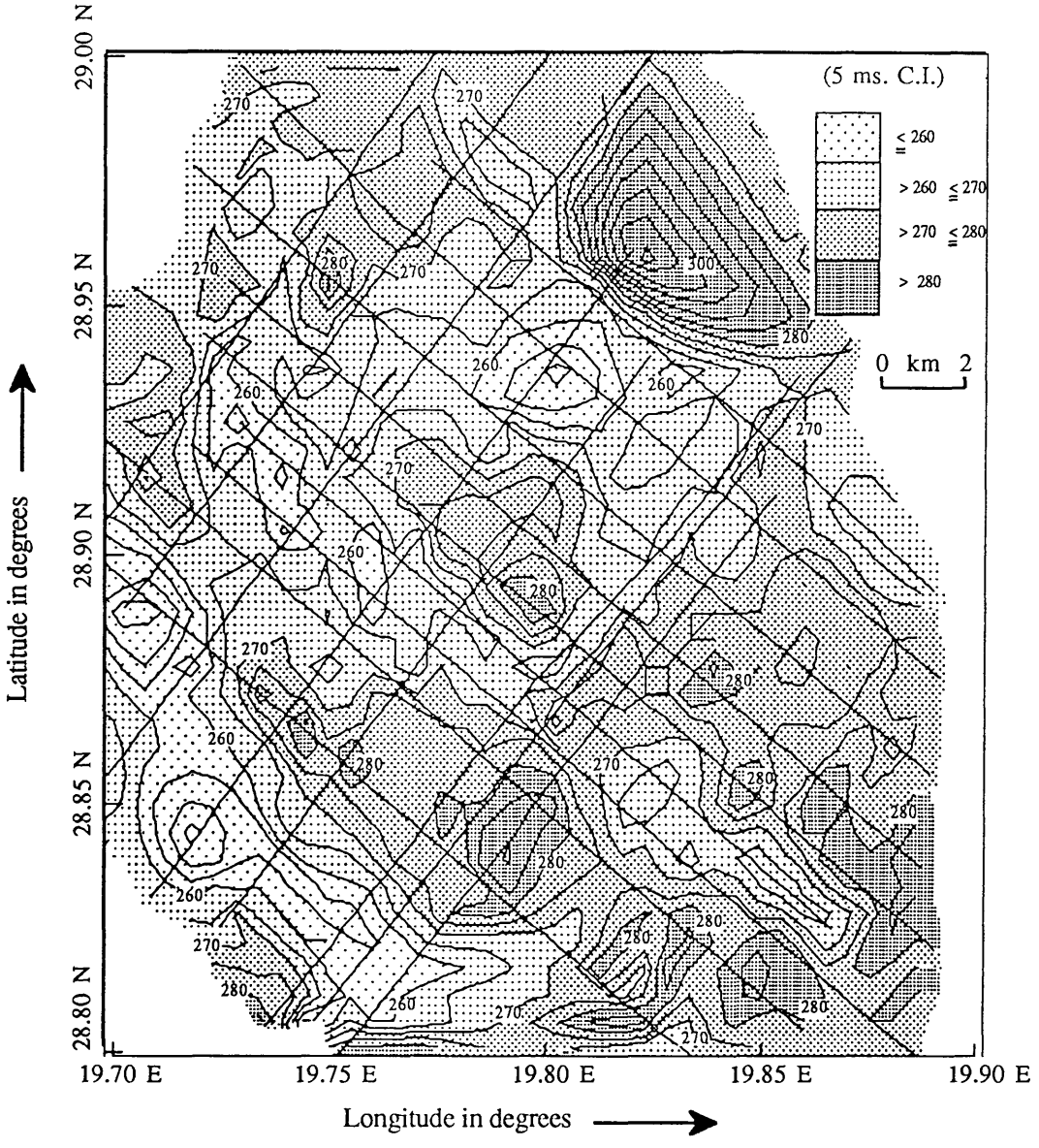

Fig. 4.29 Isochron contour map in milliseconds for the Sheghega formation based on automated contouring of the seismic data.

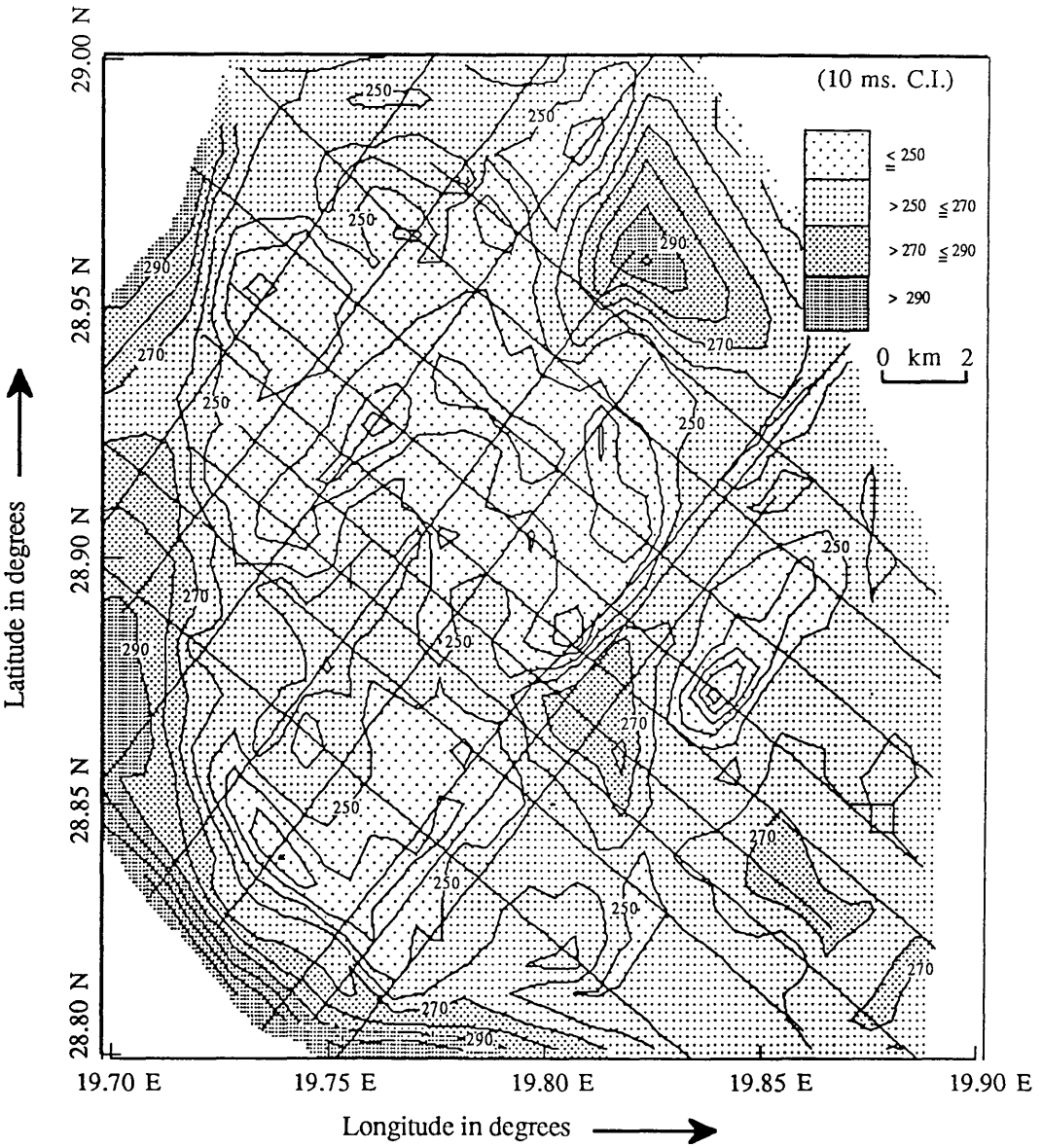

Fig. 4.30 Isochron contour map in milliseconds for the Domran formation based on automated contouring of the seismic data.

Sheghega and Domran horizons are tabulated in Appendix 4.4 (Table 4.3) as difference in depth.

(a) *Isopach contour map for Sheghega formation*

Figure 4.31 shows the isopach contour map for the Sheghega formation, in which thickness values range from 380 to 460 m. The map shows thickness thinning in most of the study area whereas thickness thickening in the northeast portion.

(b) *Isopach contour map for Domran formation*

Figure 4.32 shows the isopach contour map for the Domran formation, in which thickness values range from 380 to 460 m. over most of the area. Also it shows three thickness thickening area with large gradient in the northeast, northwest, and in the southwest portions of the area. This thickening is due to the presence of faults in the lower unit at the time of the depositional. This map shows thickness thinning concentrated in the middle, surrounded by thickness thickening area.

(6) *Interval velocity contour maps*

Equation 3.4 (Chapter 3; Section 3.3.1) been used for interval velocity calculations between the known horizons, by measuring the time and depth differences. The interval velocity maps show whether there are any lithological changes or lateral velocity variations. The interval velocity

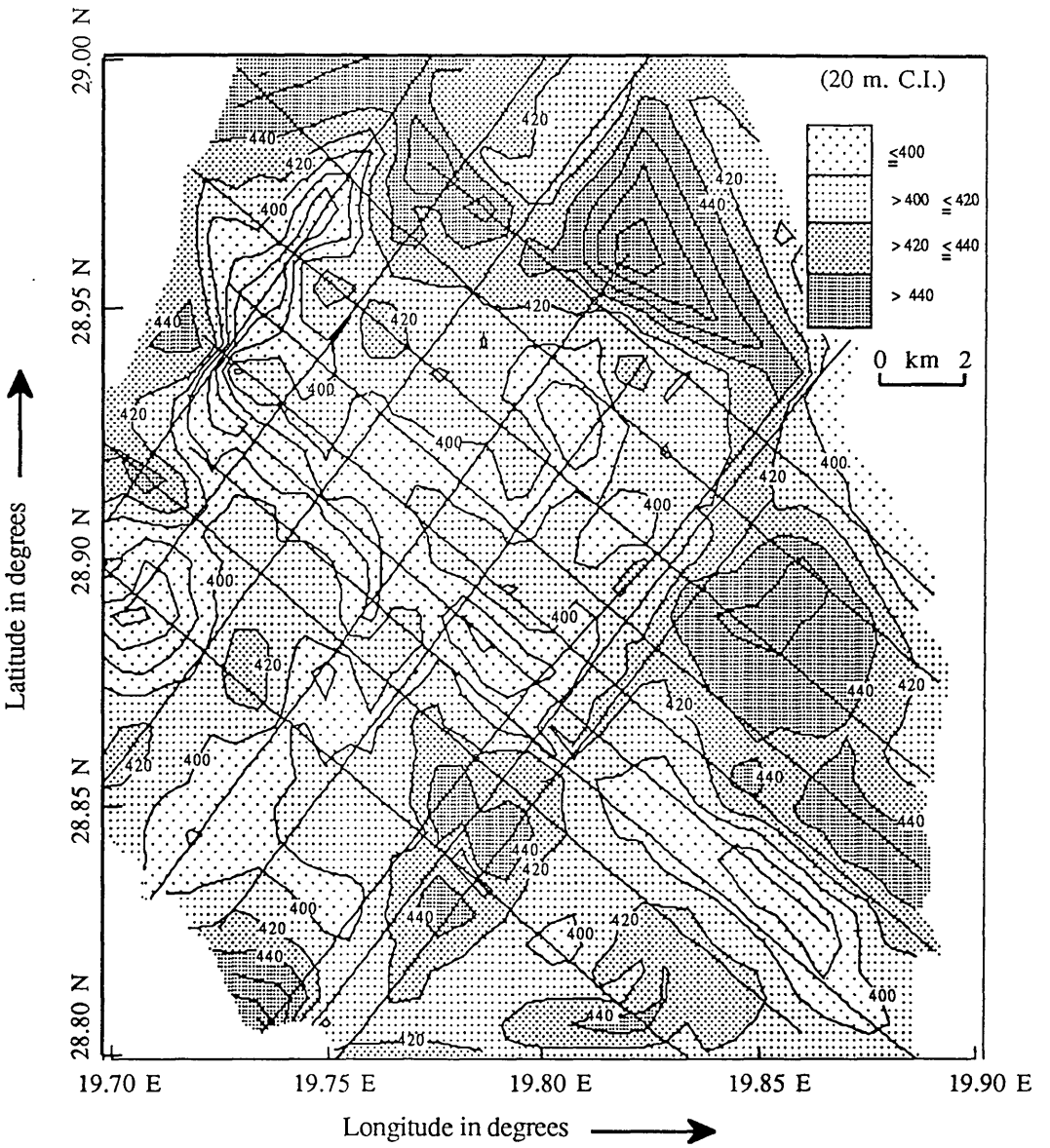

Fig. 4.31 Isopach contour map in milliseconds for the Sheghega formation based on automated contouring of the seismic data.

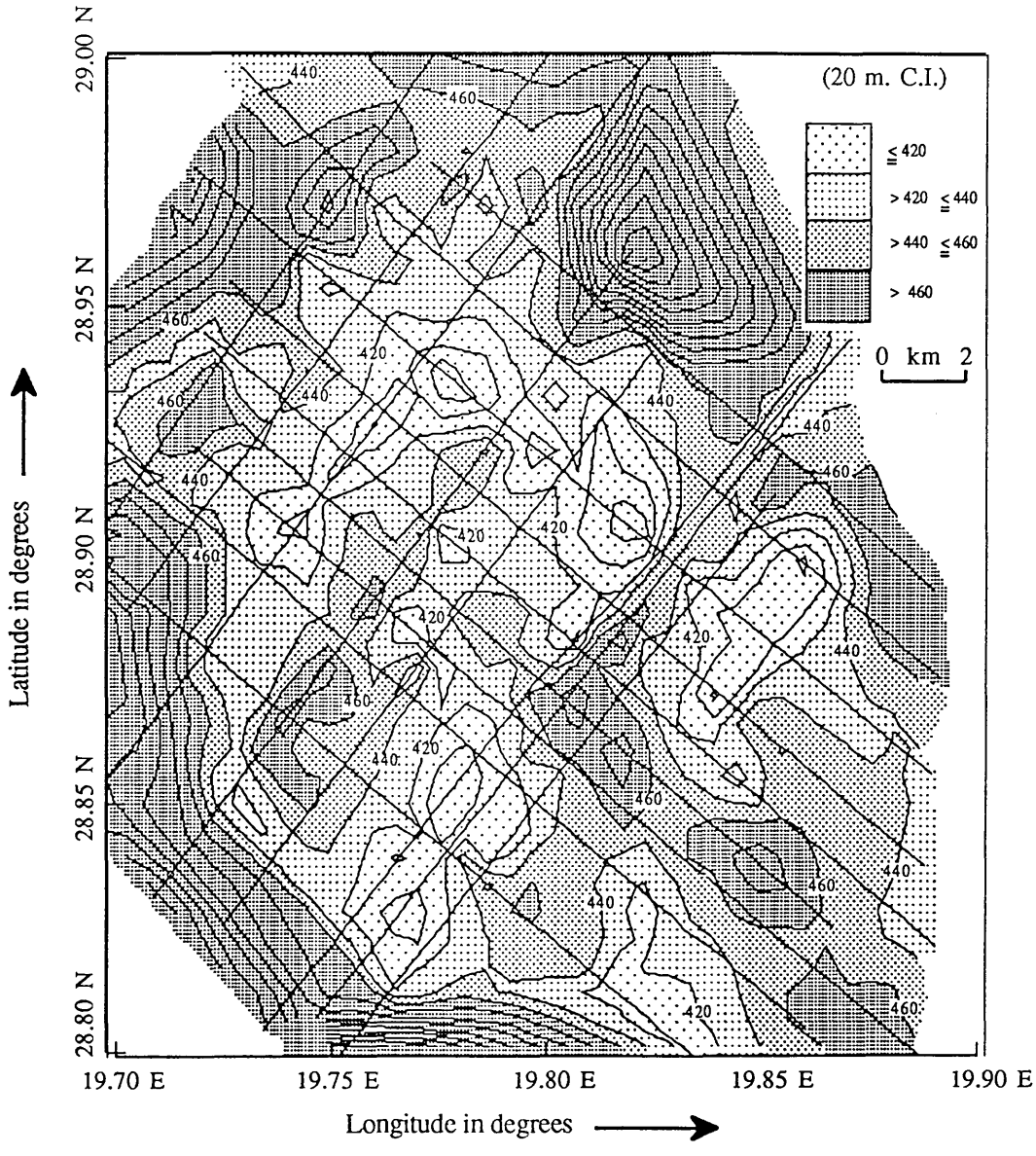

Fig. 4.32 Isopach contour map in milliseconds for the Domran formation based on automated contouring of the seismic data.

values for all required shot points for the Sheghega and Domran horizons are tabulated in Appendix 4.4 (Table 4.3).

(a) *Interval velocity contour map for Sheghega formation*

Figure 4.33 shows the interval velocity of the Sheghega formation, in which velocity values range from 2800 to 3300 m/s. The map shows a low velocity area, having values of below 3000 m/s, concentrated in the middle portion along the SE-NW axis of the study area, surrounded by high velocity contours. It also it shows dense low contouring values at the intersections in the northwest portion of the map, due to the high mis-tie values (Table 4.2 ; Appendix 4.1).

(b) *Interval velocity contour map for Domran formation*

Figure 4.34 shows the interval velocity of the Domran formation, in which velocity values range from 3300 to 4100 m/s. The high interval velocity in the northeast is probably due to the extrapolated values. Some small high velocity closures of 3600 m/s appear on the map. It also shows the same dense contouring at the intersections mentioned in the previous map, for the same reason.

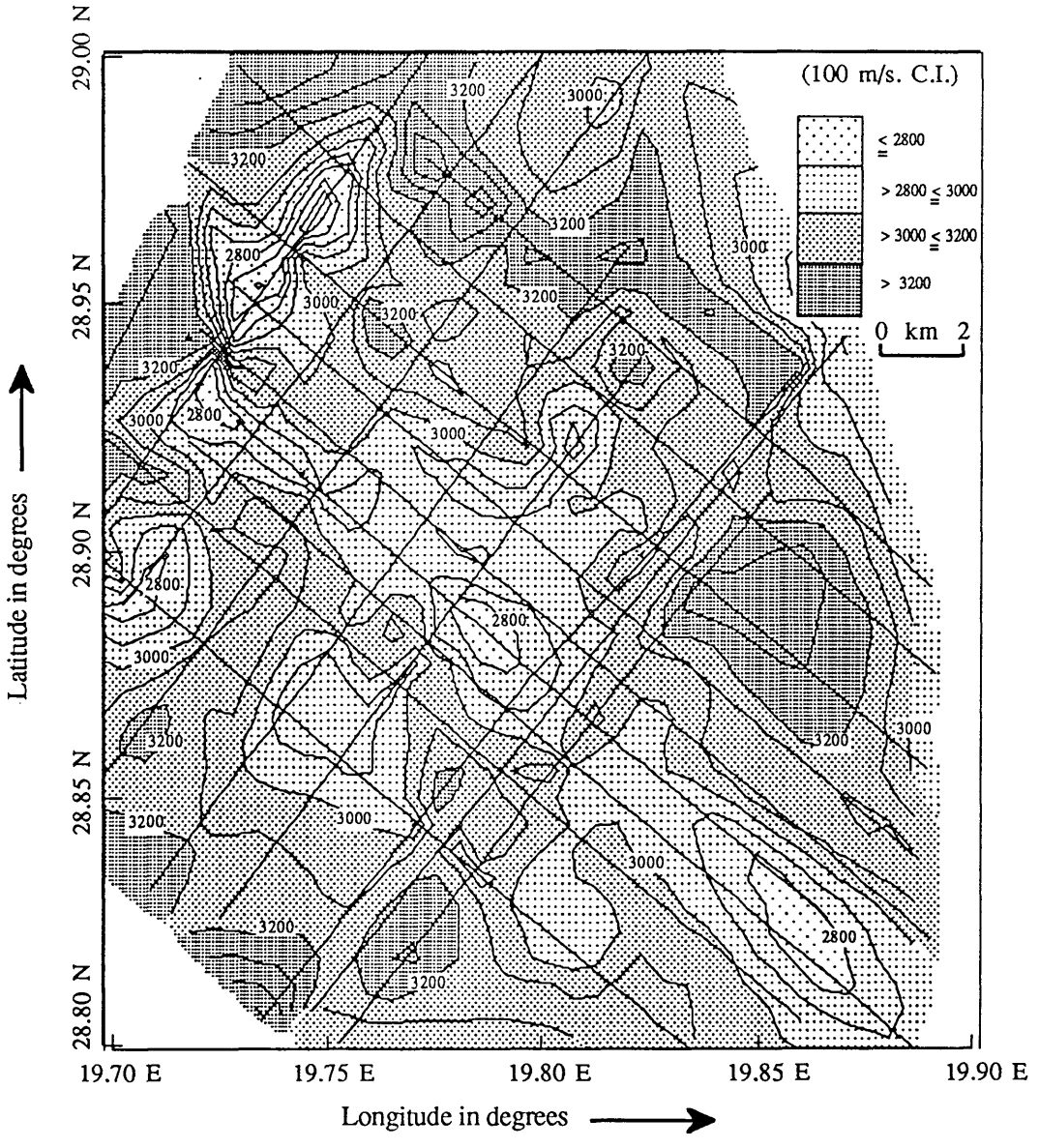

Fig. 4.33 Interval velocity contour map in meters per second for the Sheghega formation based on automated contouring of the seismic data.

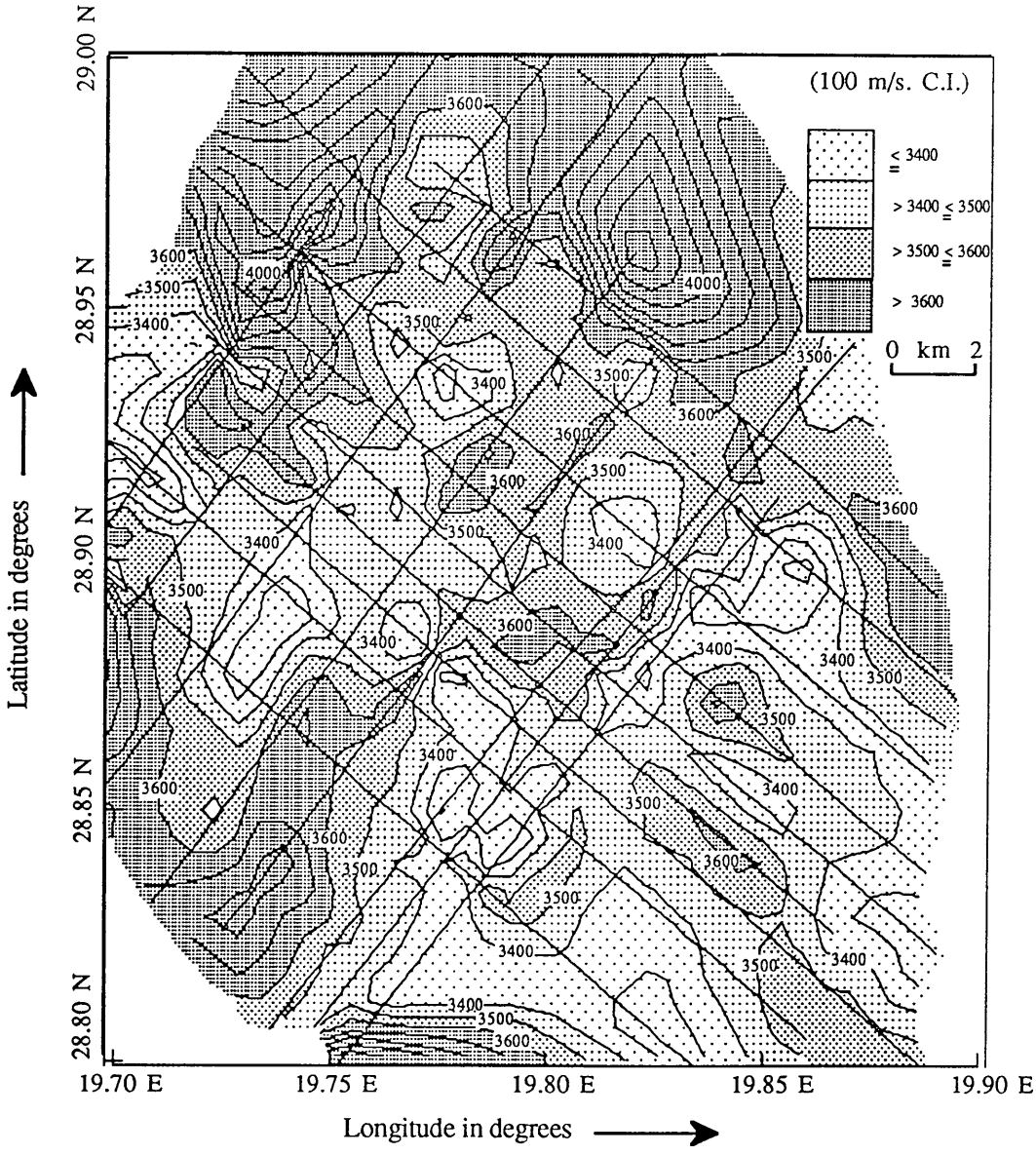

Fig. 4.34 Interval velocity contour map in meters per second for the Domran formation based on automated contouring of the seismic data.

B *Maps based on well data*

(1) *Depth structure contour maps*

The exact tops from the wells in the study area, from the company computer runs available, have been used to produce depth and thickness maps for the chosen horizons. The depth values from all the well information to the top of the each horizon are tabulated in Appendix 4.4 (Table 4.4). These are more reliable maps than the maps produced using the seismic data.

(a) *Depth structure contour map of Sheghega formation*

Figure 4.35 shows the subsea depth contour map to the top of the Sheghega formation. Comparing this map with the one produced using the seismic data (Fig. 4.26), this map shows smoother contours than the other, and also it shows greater depths, varying between 10 to 25 m in most of the area. Furthermore, the lack of well data in the southernmost part has left the contours open, whereas the seismic-based map (Fig. 4.26) clearly shows the closure round the field.

(b) *Depth structure contour map of Domran formation*

Figure 4.36 shows the subsea depth contour map to the top of the Domran formation. This map is quite similar in shape, having the same regional dip as in the previous map, but with a few differences in closure size. There is a small structural closure, at a depth of 1010 m, and another

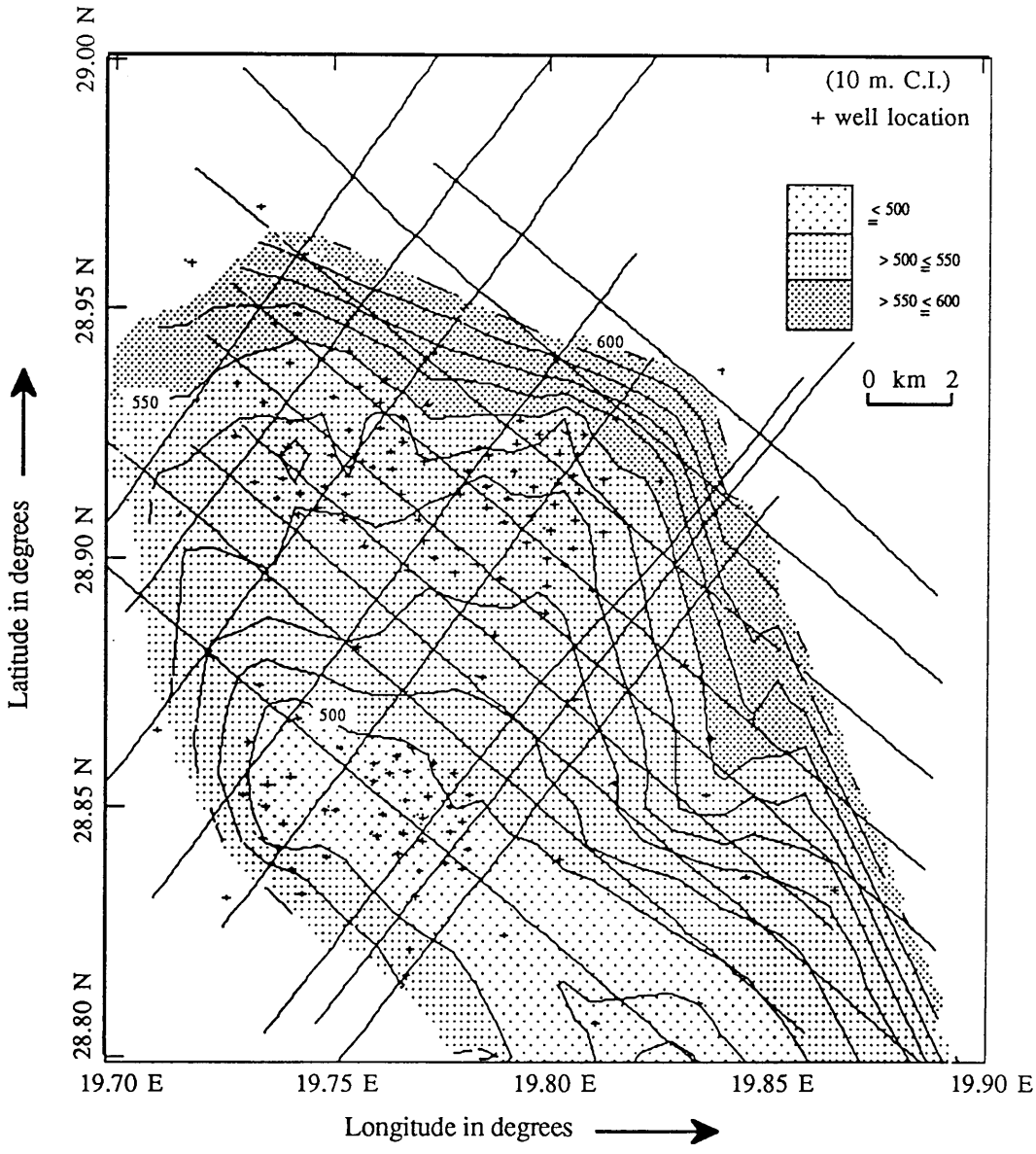

Fig. 4.35 Subsea depth contour map in meters to the top of the Sheghega formation based on well data.

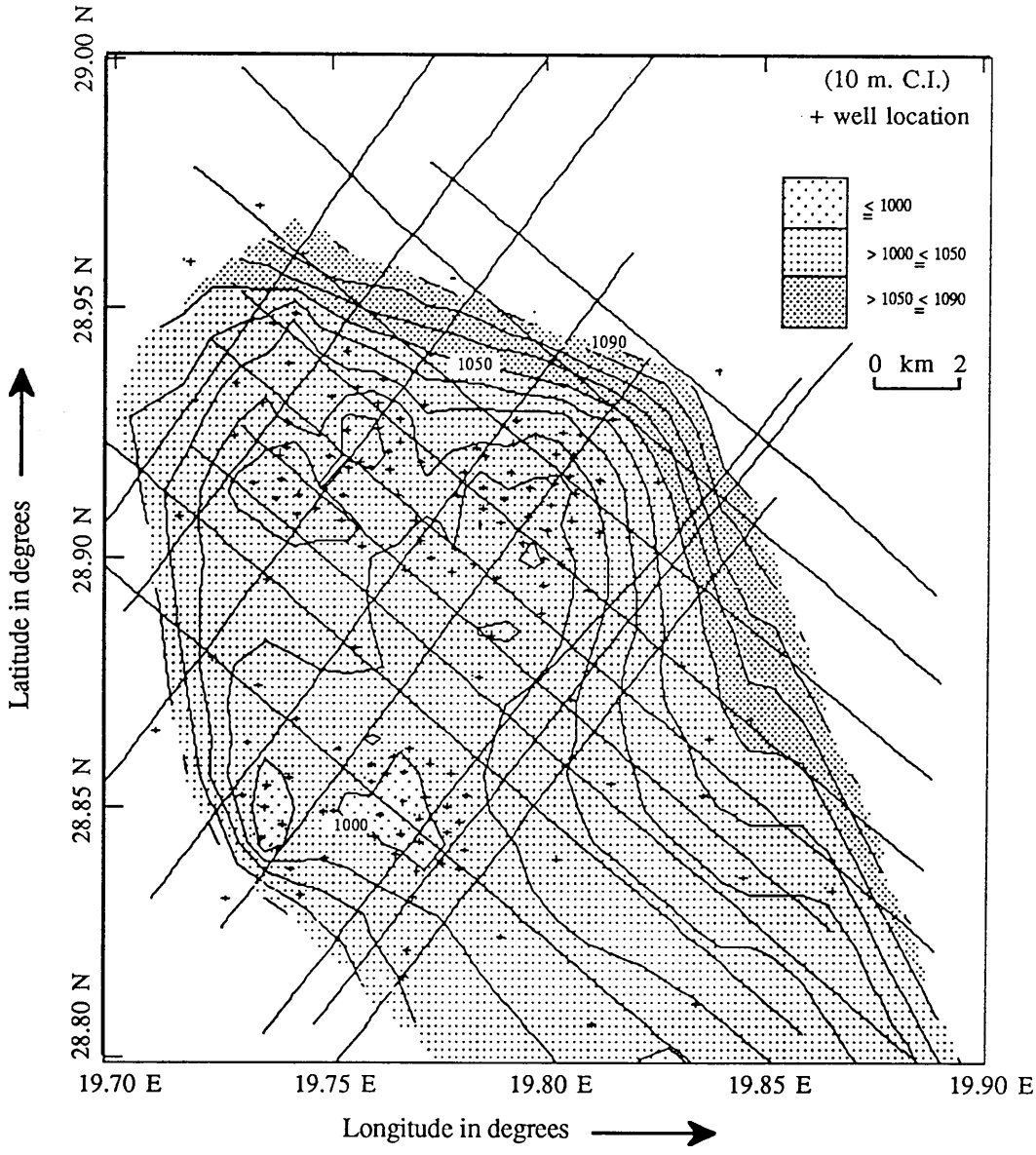

Fig. 4.36 Subsea depth contour map in meters to the top of the Domran formation based on well data.

possible large one, at the same depth, within which there are 4 other small closures at 1000 m. within the the large possible one. Comparing this map with the one produced using the seismic data (Fig. 4.27) this map also shows smoother contours than the other. It also shows greater depths, varying between 50 to 150 m. in most of the area. Again, the well-based map does not show contour closure in the south, due to the lack of wells.

(c) *Depth structure contour map of Ruaga formation*

Figure 4.37 shows the subsea depth contour map to the top of the Ruaga formation. The map also shows three closures, at depths of 1460, 1460, and 1470 m. within the possible large closure at 1500 m. There are large gradients in the northeast, west, and in the southwest portions of the area, having a SE-NW trend, because of the faulting which the contouring software program could not handle. Comparing this map with the one produced using the seismic data (Fig. 4.28), this map shows smoother contours than the other. It also shows greater depths, varying between 50 to 150 m in most of the area.

(2) *Isopach contour maps*

Thickness values are calculated by subtracting the depth values to the two different horizons at each well. The isopach maps in this section were constructed by contouring the thickness values for the Sheghega and Domran formations. Thickness values for all the required wells for the Sheghega and Domran horizons are tabulated in Appendix 4.4 (Table 4.4) as the difference in depth.

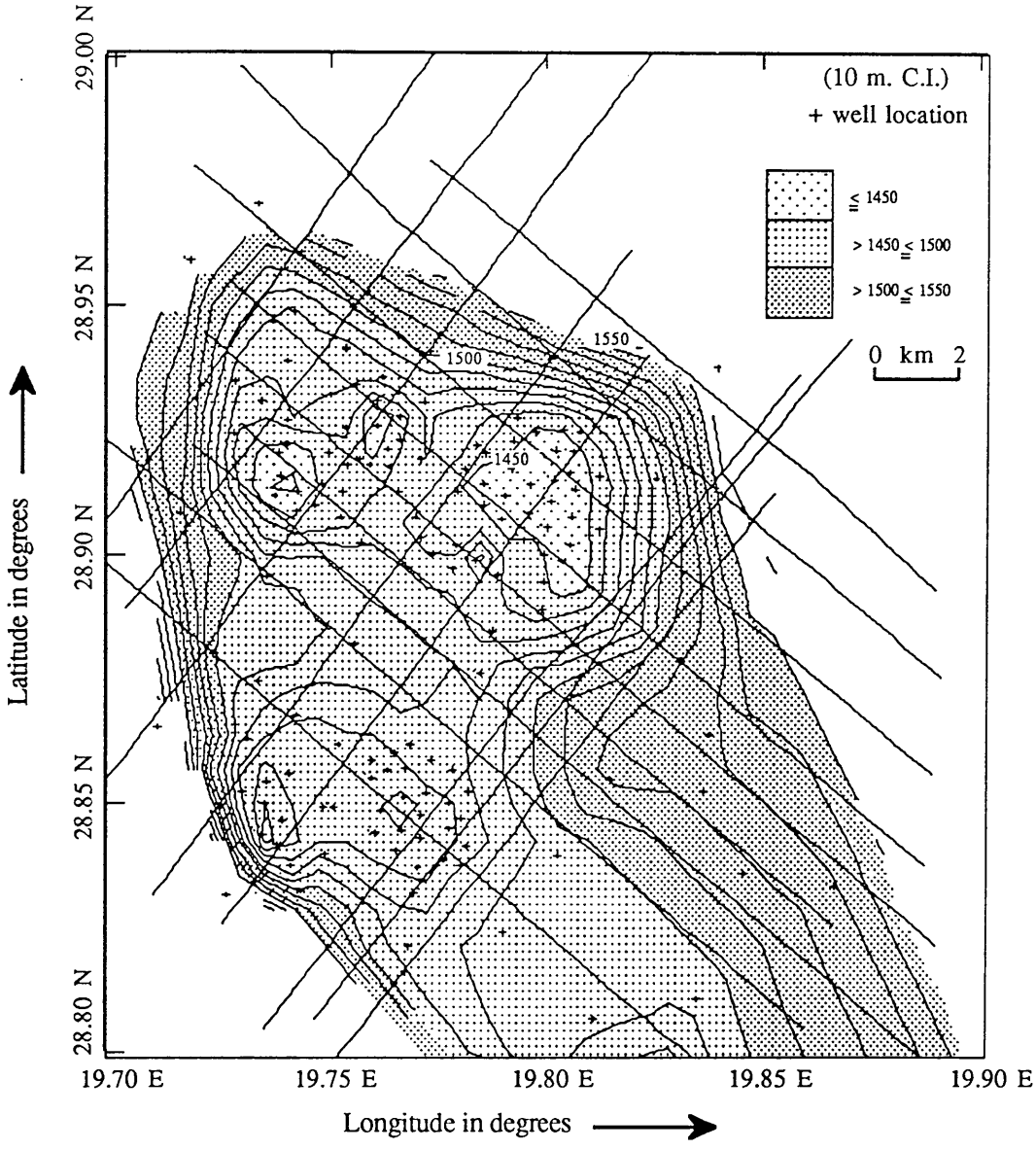

Fig. 4.37 Subsea depth contour map in meters to the top of the Ruaga formation based on well data.

(a) *Isopach contour map for Sheghega formation*

Figure 4.38 shows the isopach contour map for the Sheghega formation, in which the thickness values range from 470 to 520 m. The formation is thinner in the upper half of the map and thicker in the lower half of the area.

(b) *Isopach contour map for Domran formation*

Figure 4.39 shows the isopach contour map for the Domran formation, in which thickness values range from 430 to 490 m. The map shows thickening in the west and southwest portions of the study area. This thickening is due to the presence of faults in the lower unit at the time of deposition. Also it shows thinning concentrated in the middle portion of the study area, surrounded by a thicker area.

C *Maps produced after digitising time structure contour maps*

All maps in this section have been constructed after digitising the time maps which were produced from the seismic sections. The macro mentioned before (Appendix 4.2) and the DIGITAL (or DIGITAL2) program (Appendix 4.3) are used to produce files containing the values required to construct computerised contour maps.

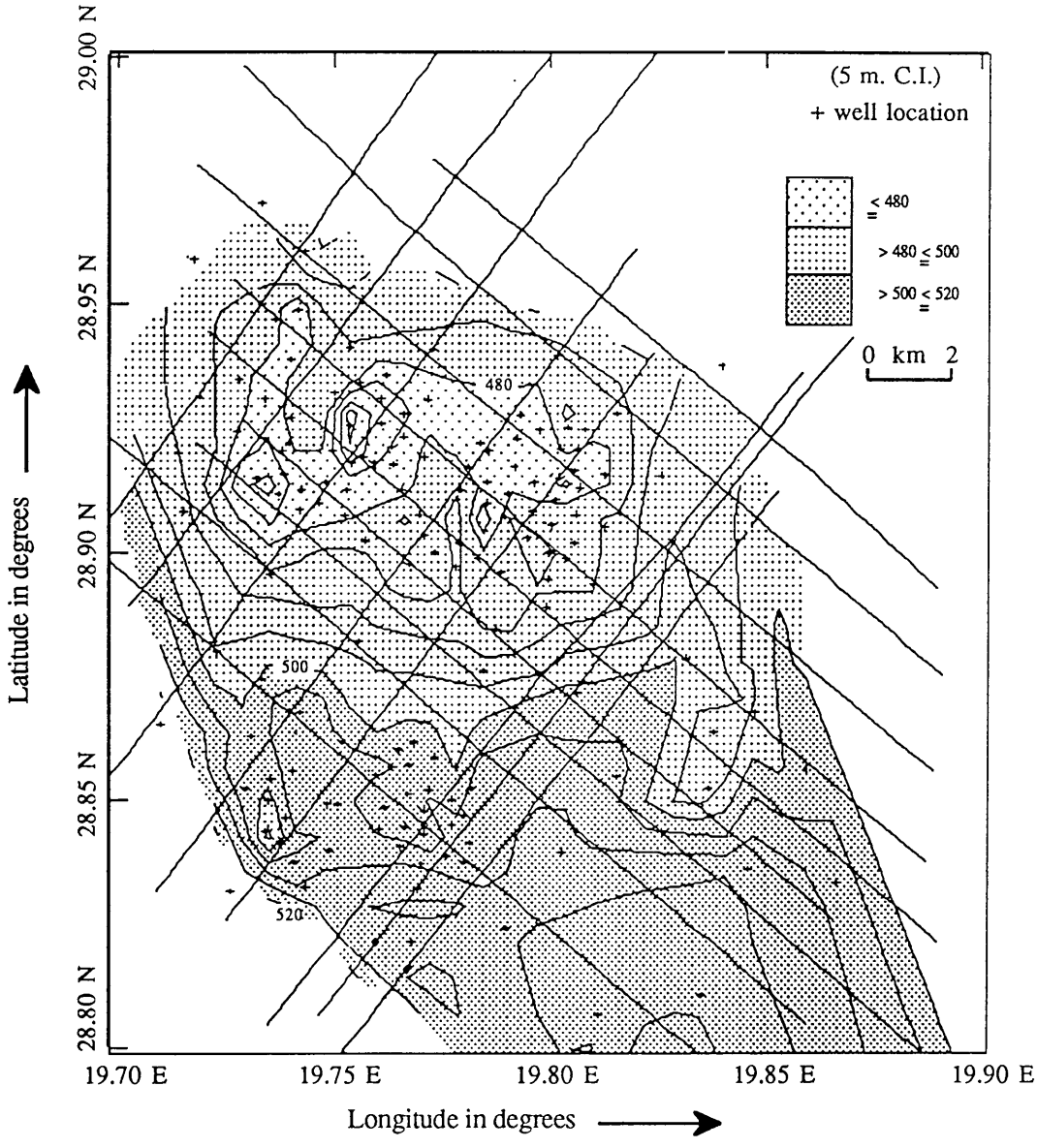

Fig. 4.38 Isopach contour map in meters of the Sheghega formation based on well data.

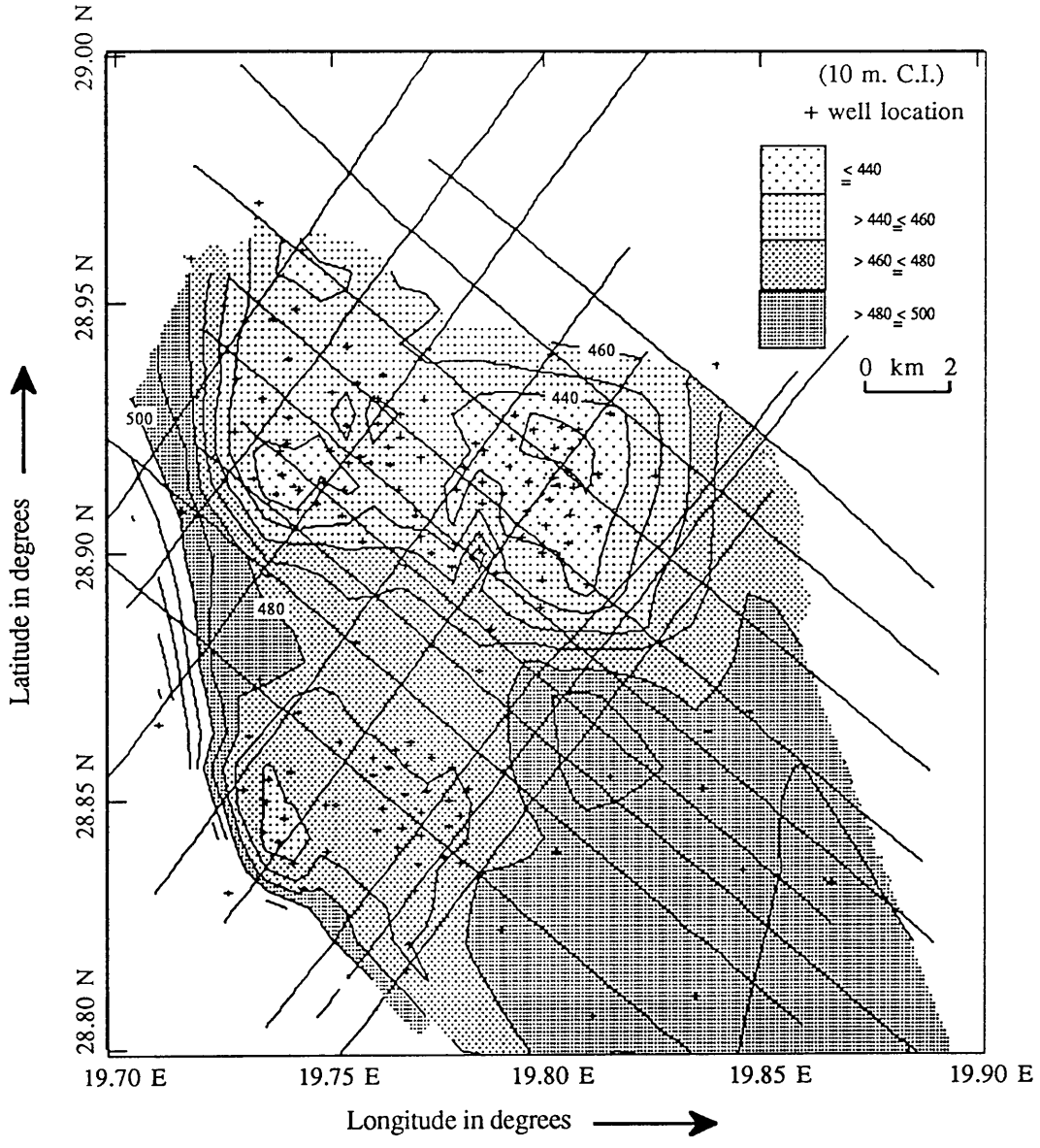

Fig. 4.39 Isopach contour map in meters of the Domran formation based on well data.

(1) *Time structure contour maps*

Subsea two-way travel times for the three seismic horizons for all the well locations are read from the digitised time maps, and stored in the computer to produced time structure maps. We expect the same shape and contour values of the time structure maps before and after the digitising in most of the area. Two-way travel time values for all wells to the top of each horizon are also tabulated in Appendix 4.4 (Table 4.4).

(a) *Top of Sheghega formation time structure map*

The subsea two-way travel time structure map of the Sheghega event is shown in Figure 4.40. It shows the same shape as the one in Figure 4.20; that is to be expected because they were produced from the same source of data. However, the digitised time contour map shows smoother and clearer closures than the other because fewer data have been used.

(b) *Top of Domran formation time structure map*

The subsea two-way travel time structure map of the Domran event is shown in Figure 4.41. The map is similar to the one mentioned before (Fig. 4.21), for the same reasons mentioned above. The map shows smoother contouring and the more clear closure.

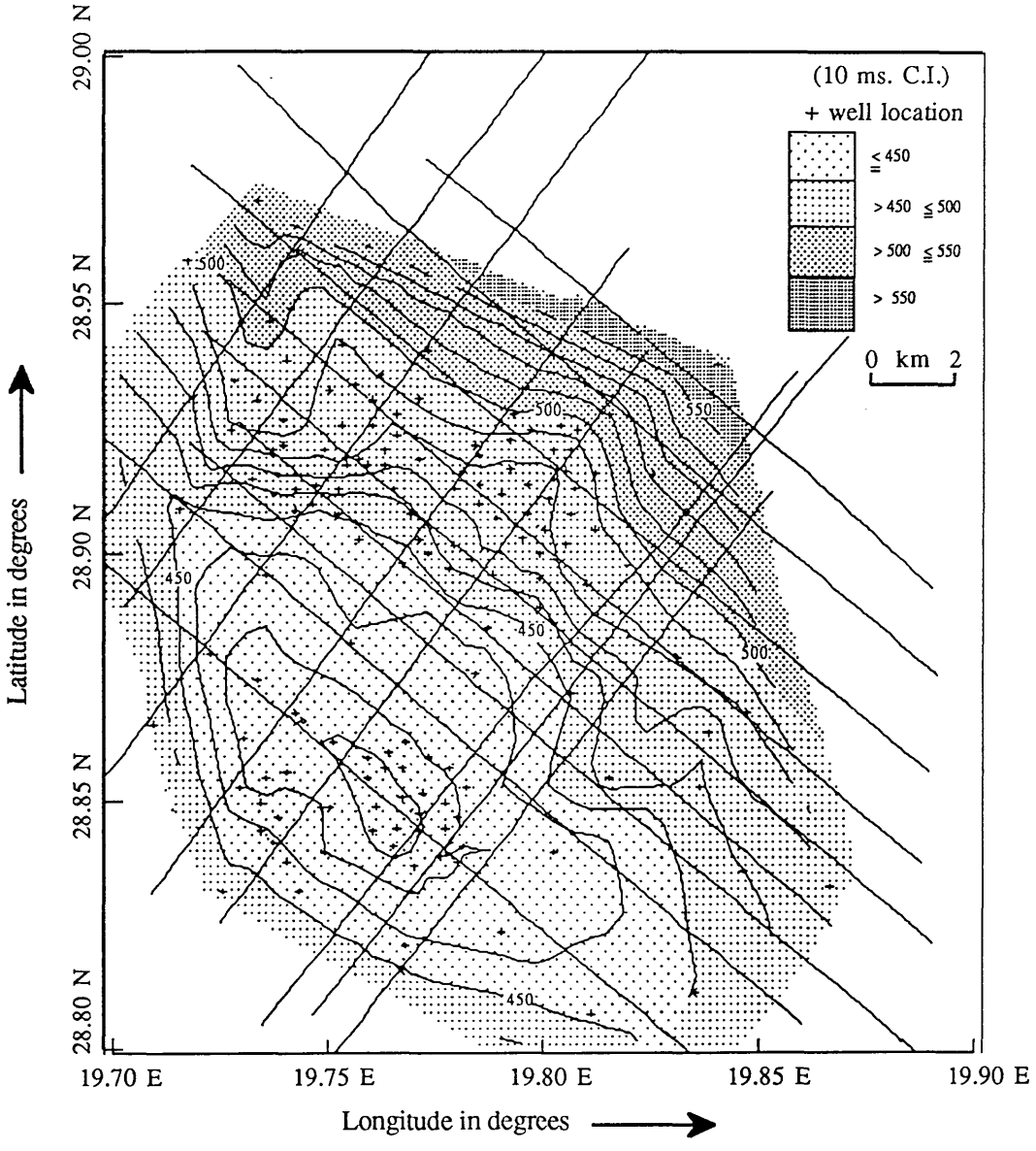

Fig. 4.40 Subsea T.W.time contour map in milliseconds to the top of the Sheghega formation based on well data (after digitising the time contour map based on seismic data interpretation).

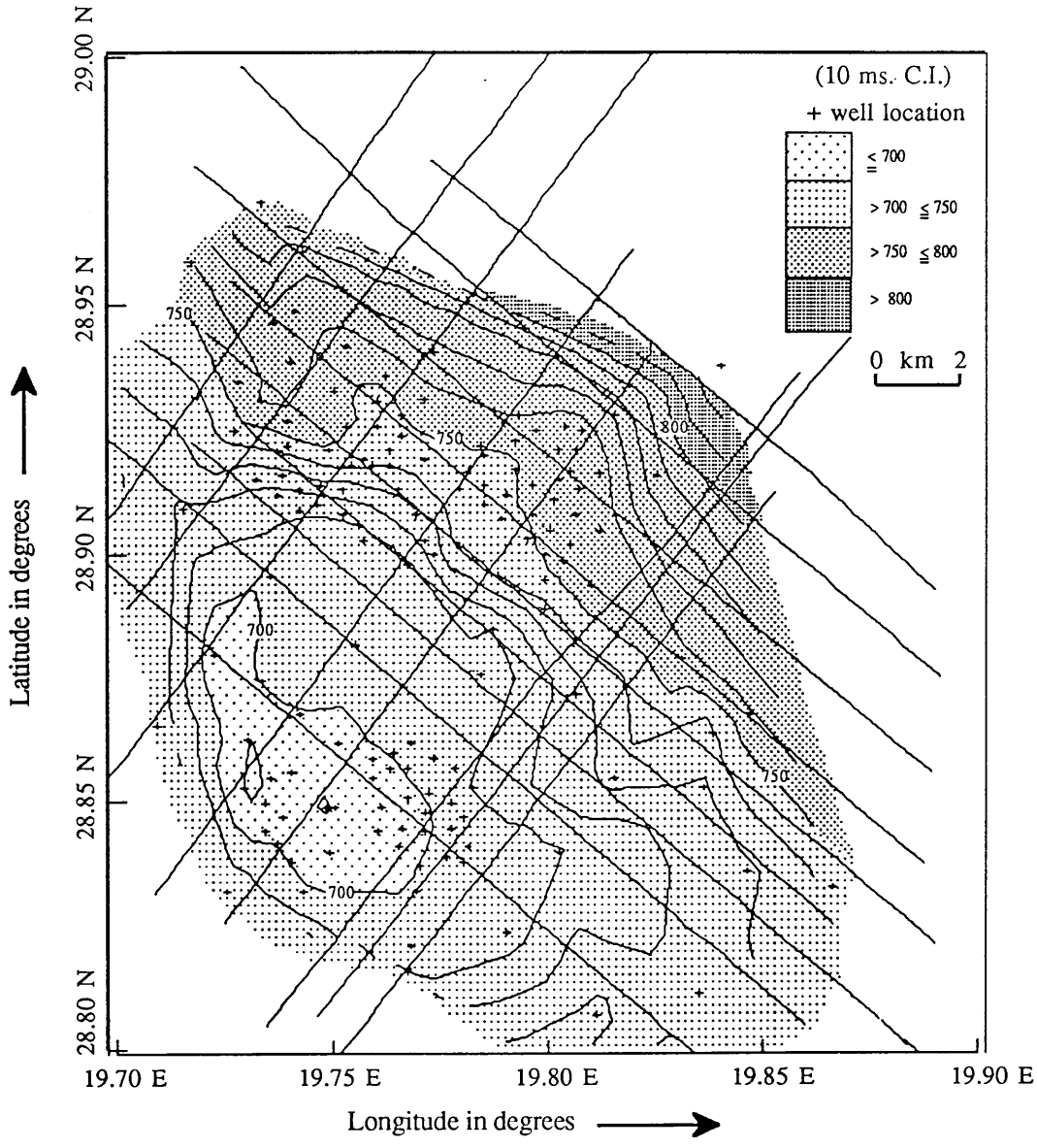

Fig. 4.41 Subsea T.W.time contour map in milliseconds to the top of the Domran formation based on well data (after digitising the time contour map based on seismic data interpretation).

(c) *Top of Ruaga formation time structure map*

The subsea two-way travel time structure map of the Ruaga event is shown in Figure 4.42. The map is also similar to the one mentioned before (Fig. 4.22), for the same reasons as mentioned in the previous two maps. The contouring is much smoother and the closure more clear.

(2) *Average velocity contour maps*

In order to determine the velocity distribution over the area where you have enough well top information and interpreted seismic sections, The average velocity for the three seismic horizons for all the well locations were calculated using equation 3.6 (Chapter 3). From the data stored in the computer after digitising the time maps (Figures 4.20, 4.21, and 4.22) and the tops of the formations from the wells, the most reliable average velocity maps can be produced. The velocity values for each required well to the top of the each horizons are also shown in Appendix 4.4 (Table 4.4).

(a) *Average velocity contour map to the Top of Sheghega formation*

Figure 4.43 shows the average velocity to the top of the Sheghega formation, calculated as mentioned above, in which the velocity values range from 2200 to 2400 m/s over most of the area. It also it shows two small high closures in the west and east portions around the intersection of the seismic lines V262-85 and V257-85 and around shot point 400 of the seismic lines V256-85 respectively, where the velocity value is 2420 m/s. The map in general shows little change in velocity values.

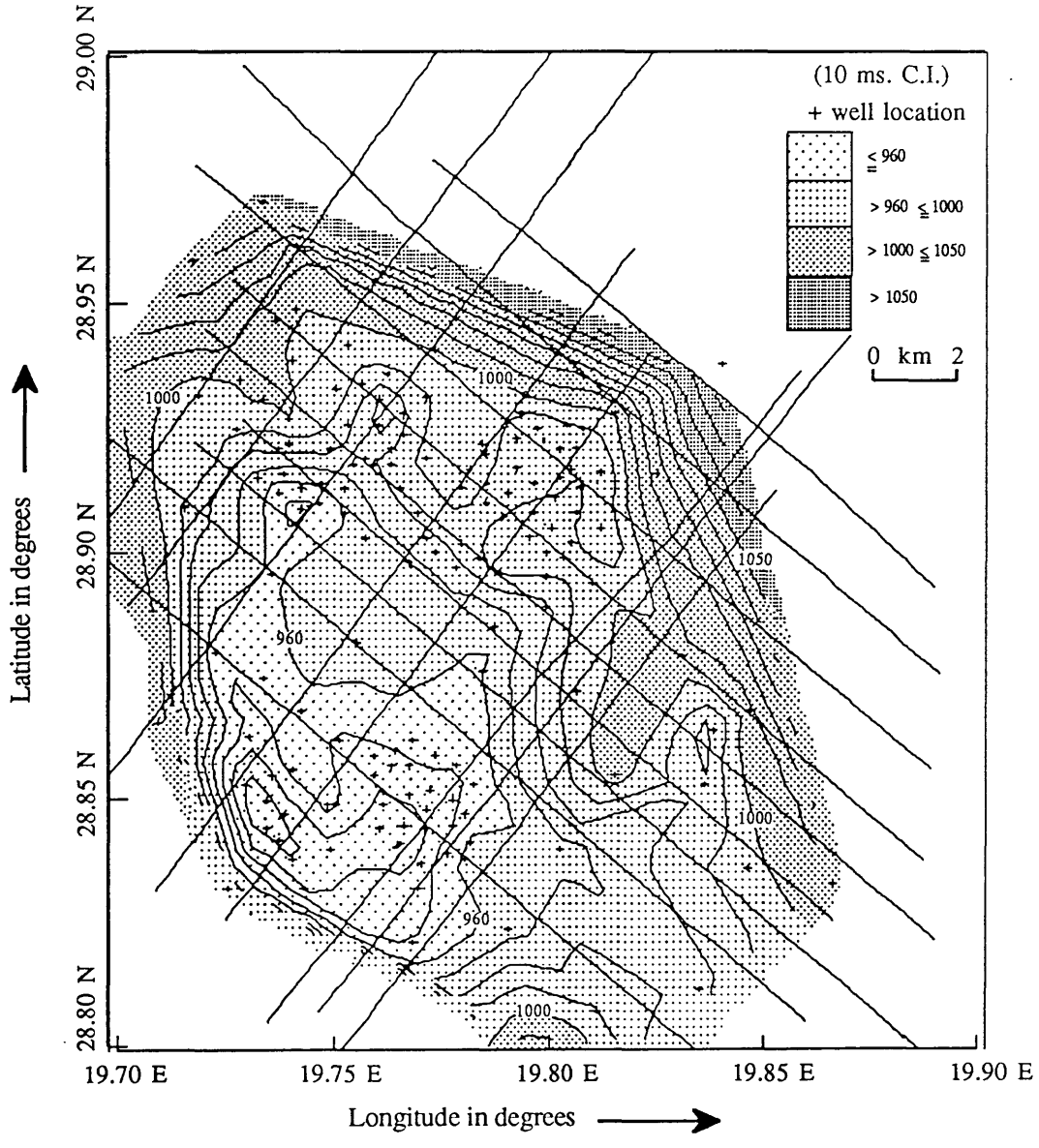

Fig. 4.42 Subsea T.W.time contour map in milliseconds to the top of the Ruaga formation based on well data (after digitising the time contour map based on seismic data interpretation).

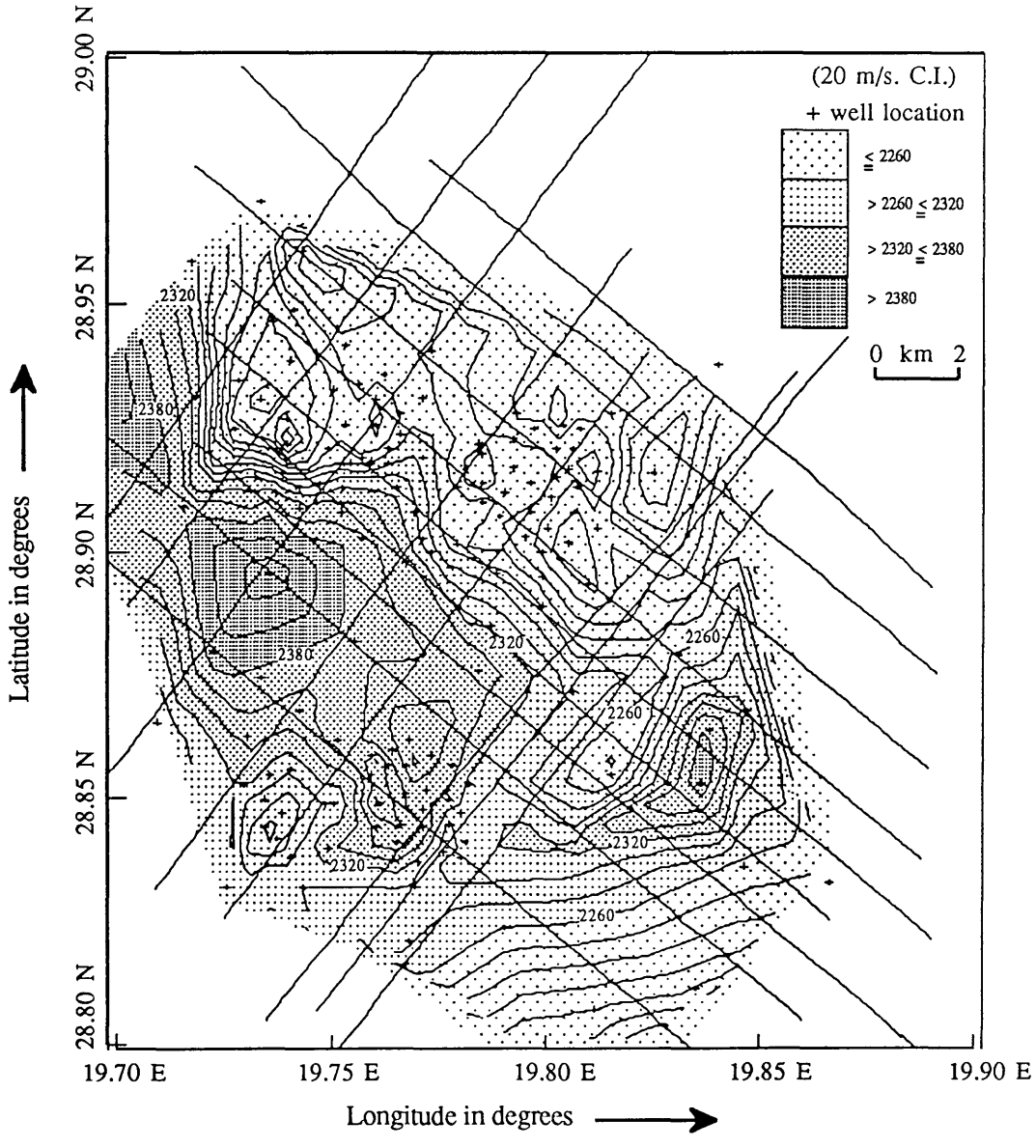

Fig. 4.43 Dix average velocity contour map in meters per second to the top of the Sheghega formation based on well data (after digitising the time contour map based on seismic data interpretation)

(b) *Average velocity contour map to the Top of Domran formation*

Figure 4.44 shows the average velocity to the top of the Domran formation, calculated as mentioned above. Velocity values range from 2700 to 2900 m/s. We can divide the area roughly into two zones by a SE-NW line. The northeast zone has an average velocity of 2750 m/s. and the other in the southwest, has an average velocity of 2850 m/s.

(c) *Average velocity contour map to the Top of Ruaga formation*

Figure 4.45 shows the average velocity to the top of the Ruaga formation, calculated as mentioned above. Velocity values range from 2920 to 3150 m/s. As with the previous map, we can divide the area roughly into two zones by a SE-NW line. The northeast zone has an average velocity of 2960 m/s. while the other has an average velocity of 3100 m/s.

(3) *Isochron contour maps*

Isochron values are calculated by subtracting the time values of the two different horizons at each well, after digitising the time contour maps. The isochron maps in this section are constructed by contouring the subtracted values for the Sheghega and Domran formations. These maps show time thinning and time thickening areas. The subtracted values for all the wells for the Sheghega and Domran horizons are shown in Appendix 4.4 (Table 4.4) as the difference in time.

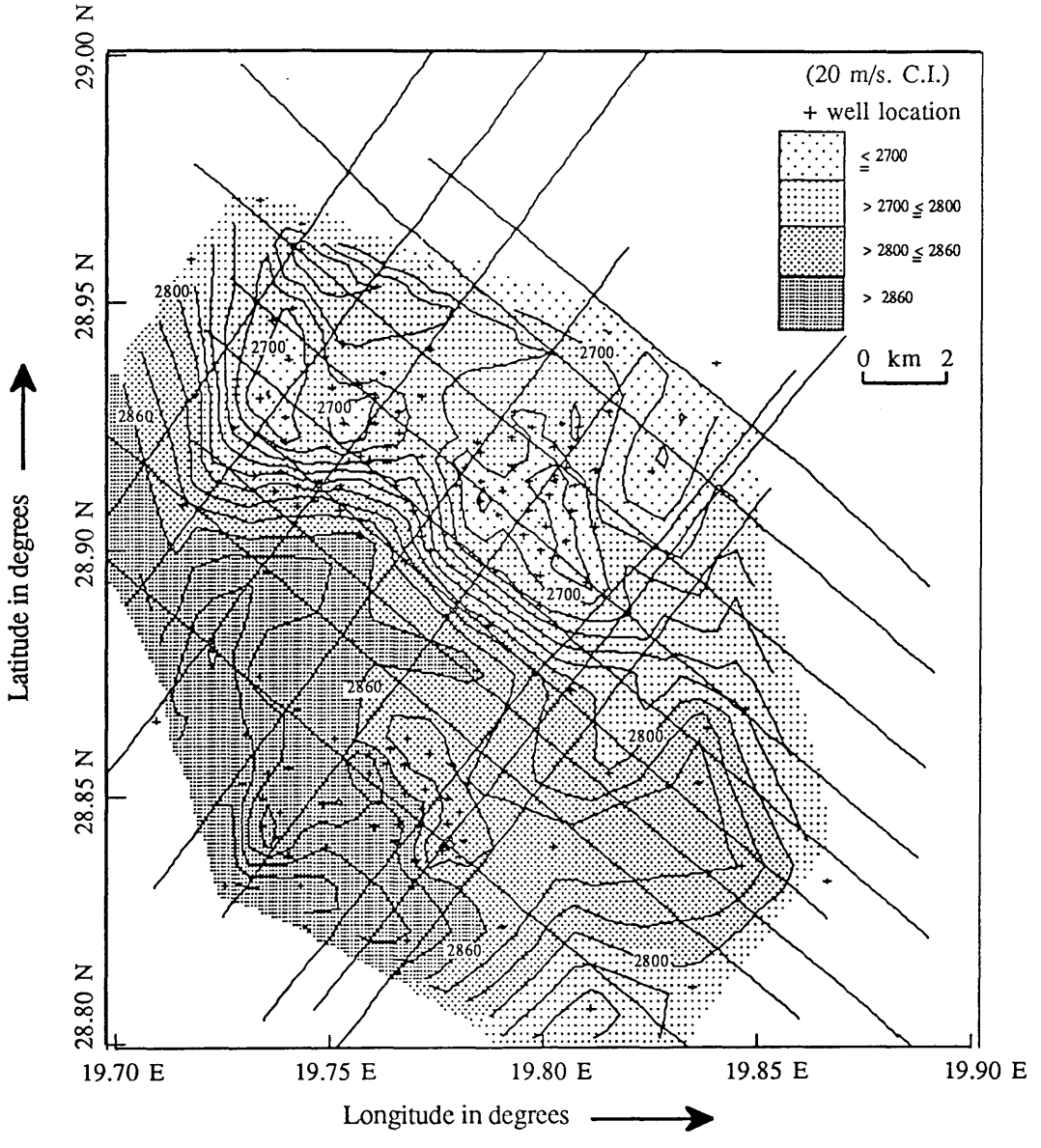

Fig. 4.44 Dix average velocity contour map in meters per second to the top of the Domran formation based on well data (after digitising the time contour map based on seismic data interpretation)

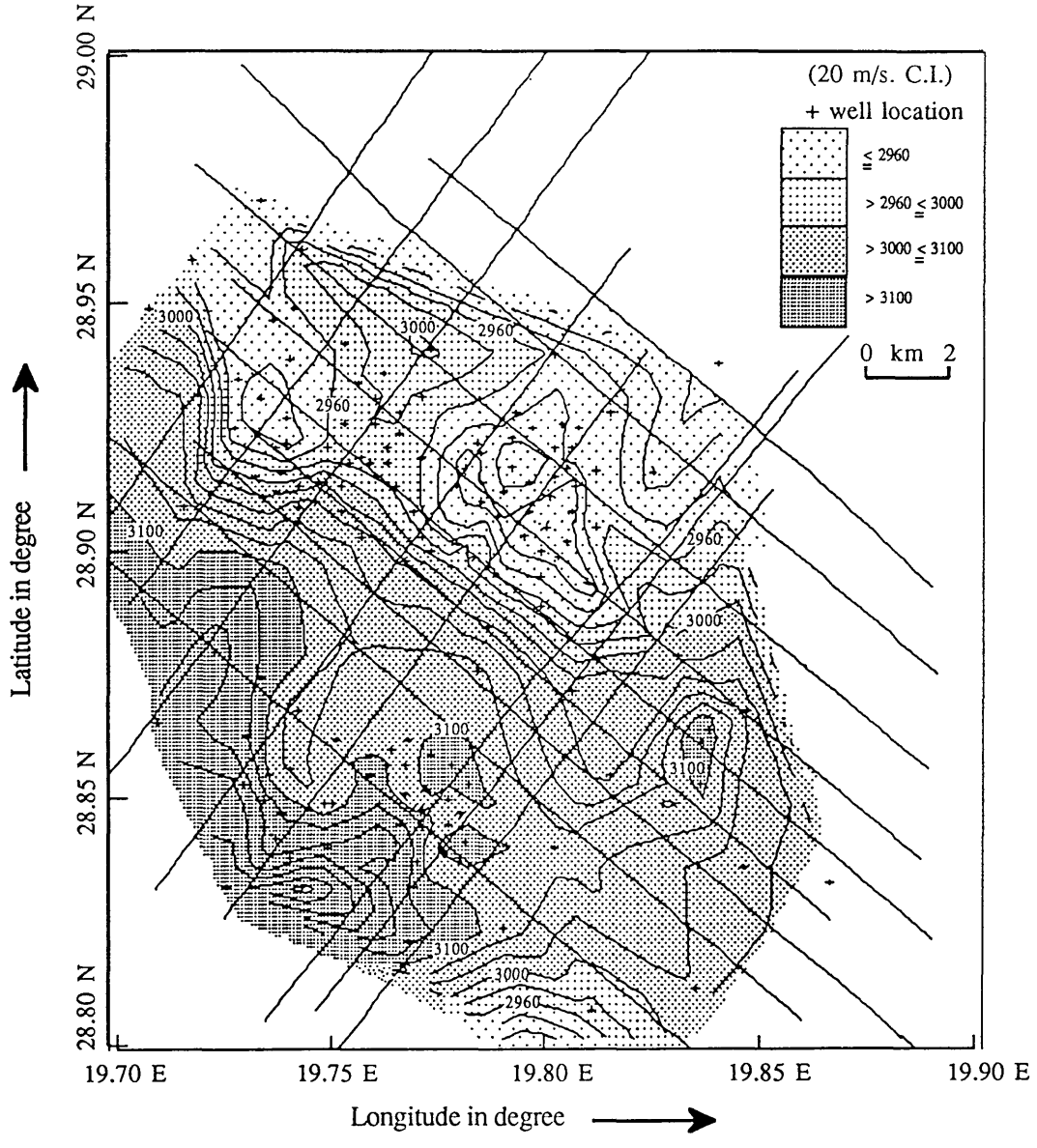

Fig. 4.45 Dix average velocity contour map in meters per second to the top of the Ruaga formation based on well data (after digitising the time contour map based on seismic data interpretation)

(a) *Isochron contour map for Sheghega formation*

Figure 4.46 shows the isochron contour map for the Sheghega formation, having the time difference values ranging from 255 to 280 ms, distributed over most of the area.

(b) *Isochron contour map for Domran formation*

Figure 4.47 shows the isochron contour map for the Domran formation. The time difference values range from 230 to 270 ms. Two thinner areas in the middle and in the south portions coincide with the areas where most of the wells have been drilled. They are surrounded by thicker areas. This thickening in the southwest is due to the presence of faults in the lower unit.

(4) *Interval velocity contour maps*

The same procedure as mentioned before was used to construct all the maps in this section. The interval velocity values for all required wells for the Sheghega and Domran horizons are shown in Appendix 4.4 (Table 4.4).

(a) *Interval velocity contour map for Sheghega formation*

Figure 4.48 shows the interval velocity of the Sheghega formation. Velocity values range from 3500 to 3900 m/s. The map shows that the velocity contours, having values various between 3500 and 3700 m/s in the

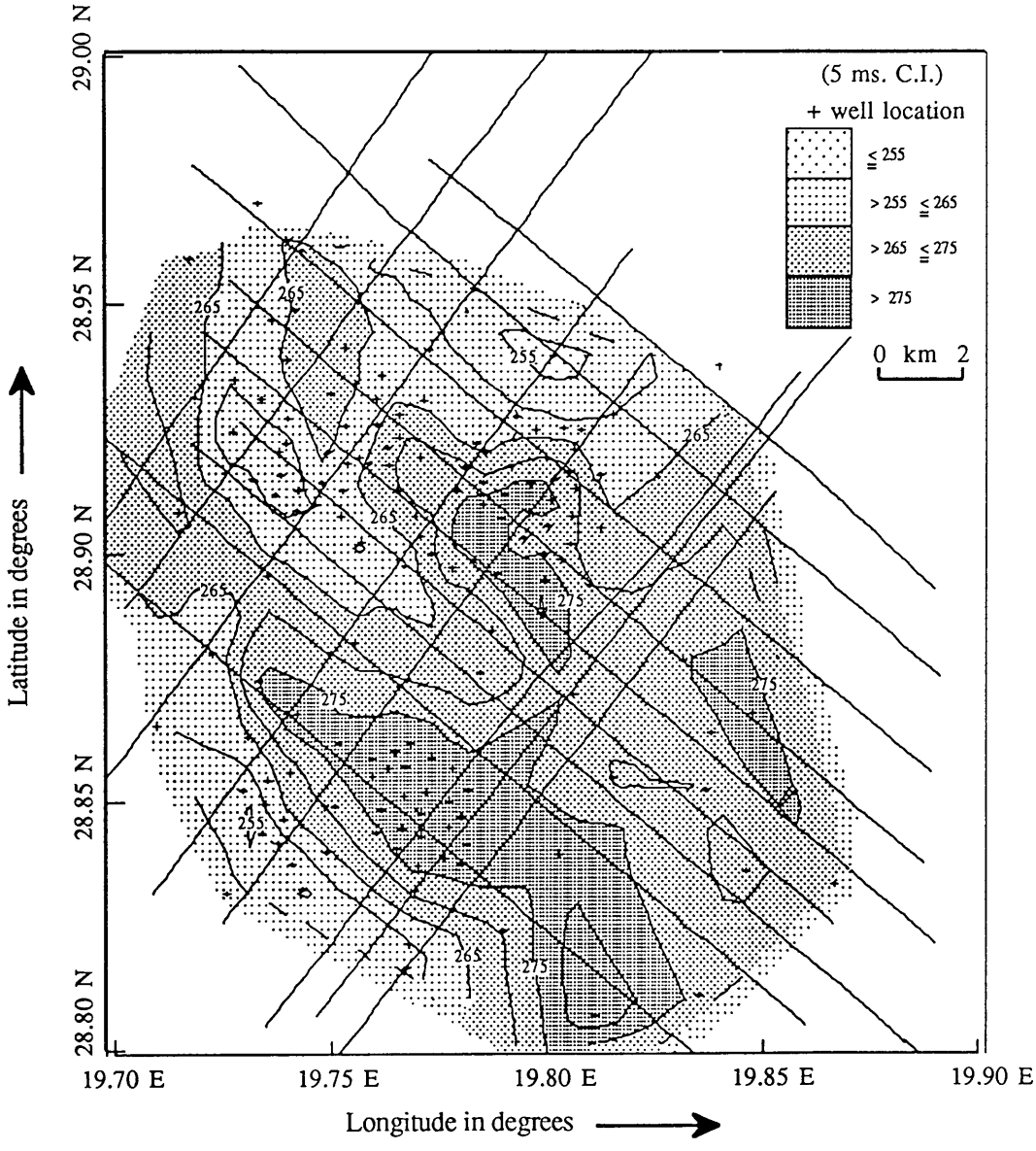

Fig. 4.46 Isochron contour map in milliseconds for the Sheghega formation based on well data (after digitising the time contour map based on seismic data interpretation)

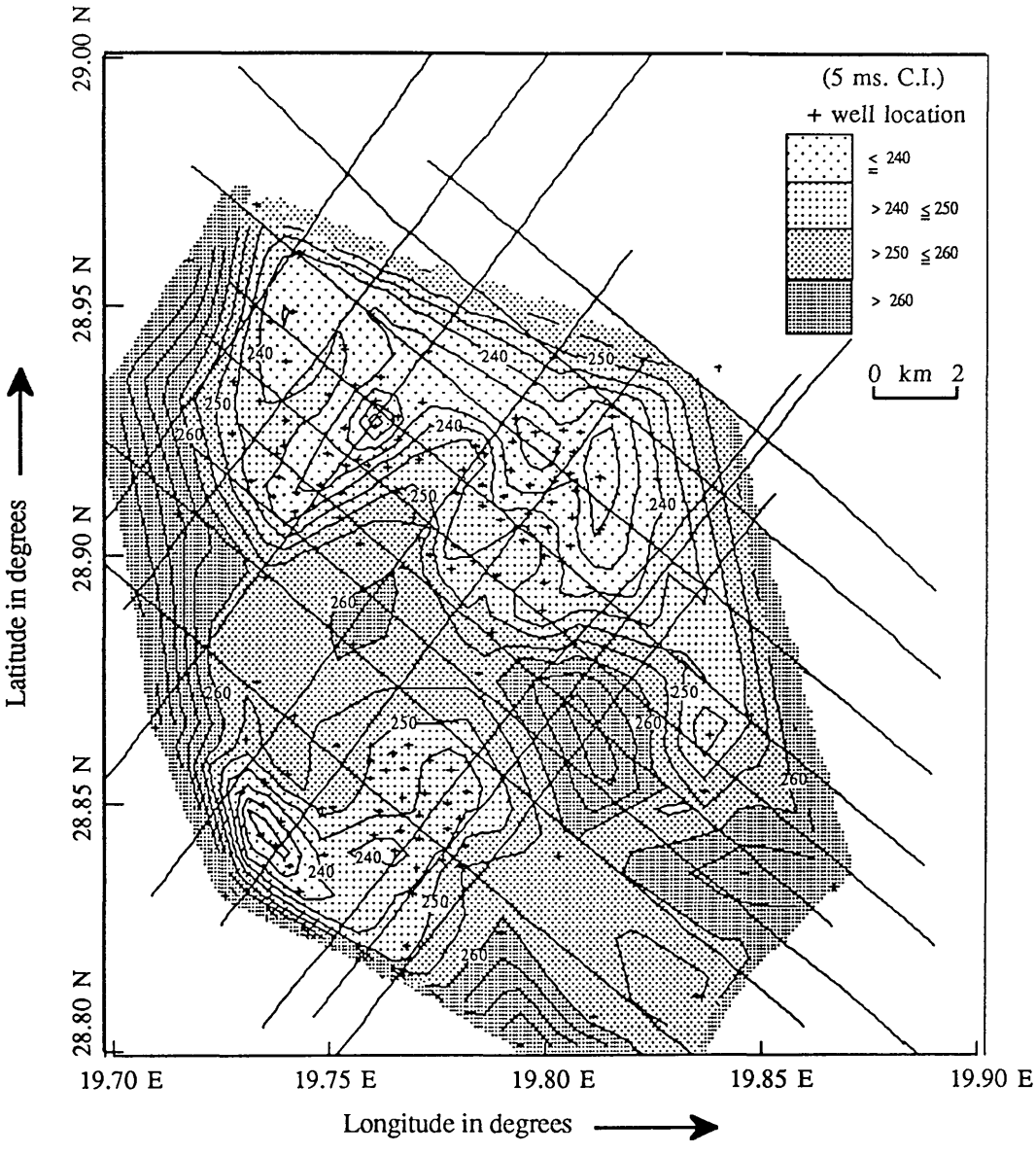

Fig. 4.47 Isochron contour map in milliseconds for the Domran formation based on well data (after digitising the time contour map based on seismic data interpretation)

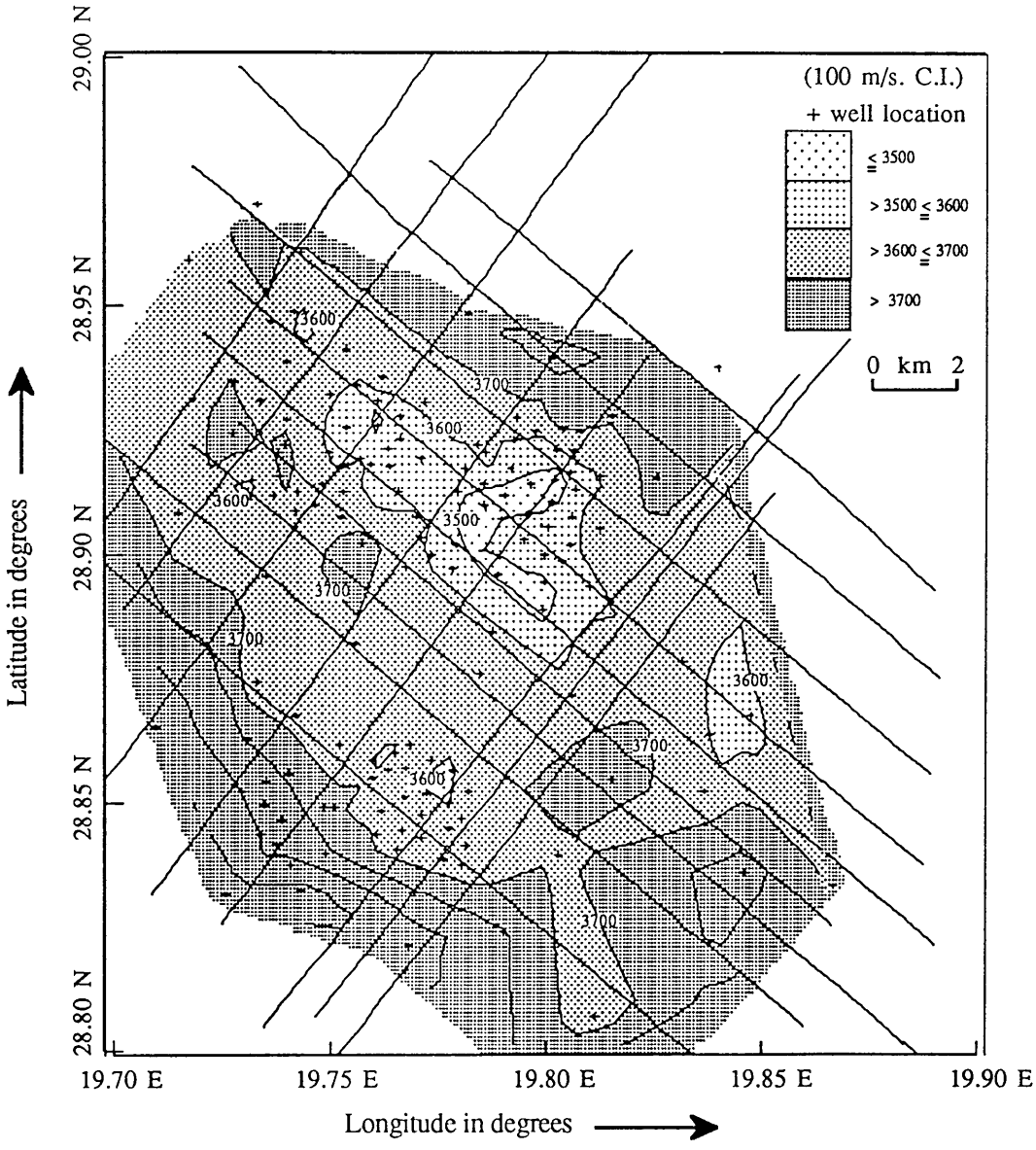

Fig. 4.48 Interval velocity contour map in meters per second for the Sheghega formation based on well data (after digitising the time contour map based on seismic data interpretation)

areas covered most of the wells, with small high closures contouring of 3700 m/s values in between. Higher velocity contour values surround the area of the wells.

(b) *Interval velocity contour map for Domran formation*

Figure 4.49 shows the interval velocity of the Domran formation, in which the velocity values range from 3600 to 3900 m/s. The map also shows low interval velocity contouring concentrated in the middle portion of the map, surrounded by high ones.

4.9.3 *Discussion*

The contour maps in Figures 4.40, 4.41, and 4.42 look good and smoother than the contour maps in Figures 4.20, 4.21, and 4.22, because they have less control points. The contour maps in Figures 4.46 and 4.47 also look good and smoother than the contour maps in Figures 4.29 and 4.30 for the same reasons mentioned before.

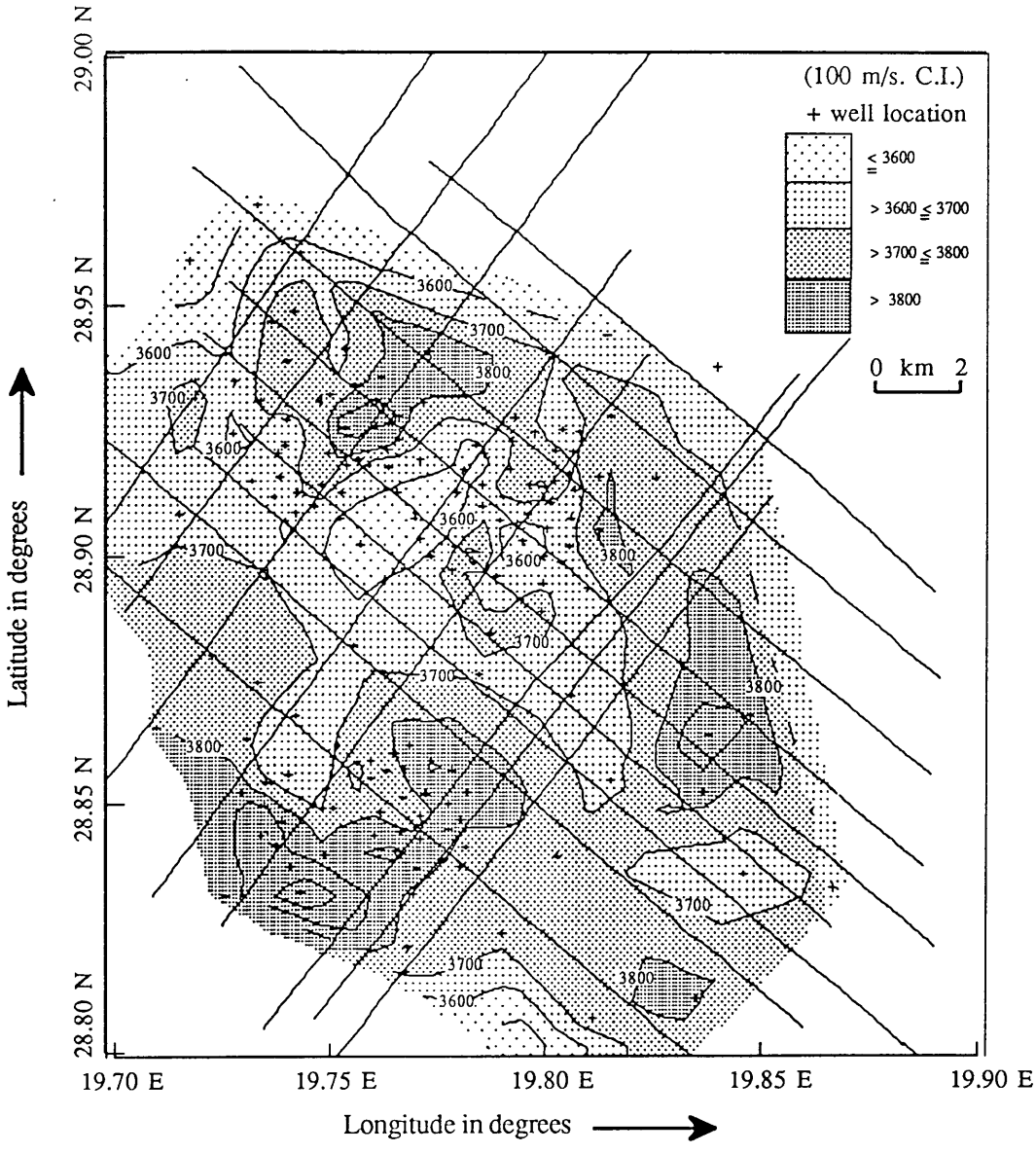

Fig. 4.49 Interval velocity contour map in meters per second for the Domran formation based on well data (after digitising the time contour map based on seismic data interpretation)

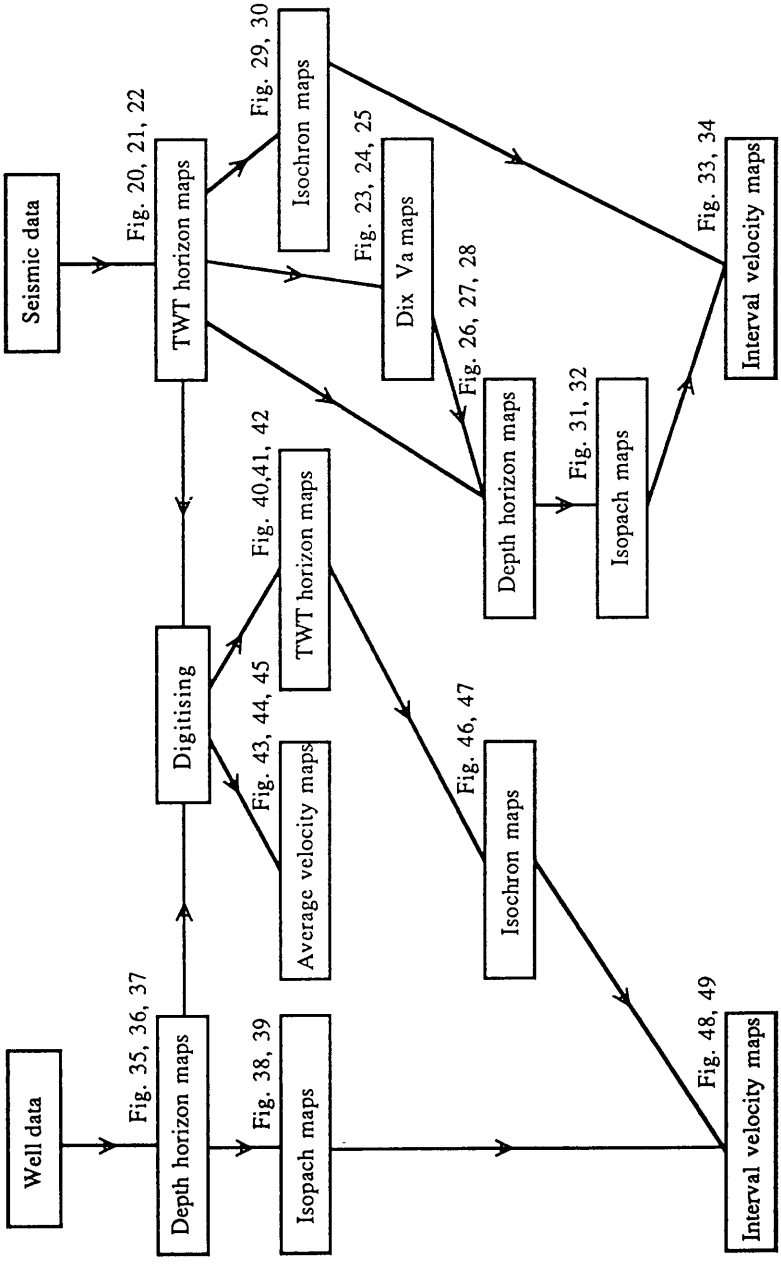

Fig. 4.50 Maps flowchart

CHAPTER (5)

STATIC CORRECTIONS

5.1 *Introduction*

One of the most important steps in land data processing is the static correction calculation, especially in areas of rough terrain, and in areas when near surface velocity is highly variable in either the vertical or horizontal direction.

If reflection waves from a flat subsurface interface are received by geophones spread over a hill, valley, or other topograhic feature, the reflection times would indicate a structure that could be associated with the elevations at the earth's surface rather than with those of the subsurface formations being mapped. From a knowledge of the elevations and near surface velocities, we can compute the variations in reflection time at points along the surface due to the topography. Removing this time variation is the elevation static correction.

The weathered layer lies just below the earth's surface, usually above the water table, and in Libya varies in thickness around 100 m. Its quite low seismic velocity, often between 400 and 1300 m/s in the area of study, causes variable time delay in the arrival of the deeper reflections. The velocity and thickness of this layer can change from one place to another. The weathered layer time variation must also be calculated and removed.

The basic elevation statics and residual static corrections are necessary to produce a good quality section. The purpose of the static correction is to remove the effects of the near surface. This is achieved by stripping away the upper surface above a datum plane. The static shift

should produce the same results as if the source and receivers were both placed at the datum.

5.2 *Static techniques*

There are two main types of technique to determine the thickness and velocity of the weathered layer at each receiver station:

(1) Directly measuring it through shot-hole information.

(2) Calculating it through refraction static routines.

Techniques are also available to determine the required corrections directly from reflection data by reconciling the time shifts needed to align different observation of the same reflection.

5.3 *Static correction effects*

Static corrections compensate for topographic irregularities and near-surface velocity variations. Static corrections affect:

(1) Reflection continuity.

(2) Structural geometry.

(3) Resolution.

(4) Velocity analysis accuracy.

The two types of static correction - datum correction and low velocity layer correction - are described below.

5.4 *Datum correction*

This is sometimes referred to as the elevation correction. In offshore seismic operations, with both source and hydrophone cables very close to a constant datum, sea level, it seems obvious to apply corrections. When applied the correction consists of adding the source and cable depths and dividing by the sea-water velocity.

On land, however, there is usually some topographic variation. In order to show the reflection times in their proper structural relation it is necessary to refer them to a datum. Any level can be chosen, but it is usual to use one that is below the lowest topographic point in the survey, and it is better if the chosen datum is below the low velocity layer (LVL).

The datum always corresponds to the zero time line on the seismic section. The travel paths though the weathering layer tend to be nearly vertical due to Snell's law, regardless of their direction of travel below the LVL (Dobrin and Savit 1988).

If we wish to relate all reflection times to the datum, we must in this case apply a correction for elevation difference. The correction for elevation difference can be made simply by subtracting (or adding) the time required for the wave to travel the vertical distance between a reference elevation (datum plane) and that of the earth's surface at the point in question. The correction is a time shift applied to the entire trace for (a) the receiver location and (b) the shot location. This requires a knowledge of the distance and the velocity involved. The distance is easily calculated from the

elevations of the shot, geophone and datum plane. The correct velocity is more of a problem. It is usually obtained from shallow refraction data, but borehole and shot-hole data as well as regional geological information can be helpful.

The use of an incorrect datum velocity will cause distortion of the seismic section. A common datum velocity is usually used for an entire area or survey. Since by their nature, seismic velocities are not constant, this means that we seldom have exactly the right datum velocity.

5.5 *Low velocity layer correction*

This is also known as the weathering correction. The low velocity layer correction compensates for differences introduced by changes in the thickness or character of the the low velocity layer, which usually consists of the unconsolidated material between the surface and bedrock.

Since the velocity of this material is very low, a small change in thickness can result in significant changes in reflection times. It is also necessary to remove the effects of the low velocity layer variations before traces can be stacked.

A number of methods have been devised for making the low velocity layer correction. They fall into two types:

(1) Methods based on the analysis of shallow refraction data.

(2) Residual Methods.

In the first method, we can pick and plot the times corresponding to the direct wave (first kicks), then we can calculate datum velocity, LVL velocity, and LVL thickness base on refraction principles as shown in Figure 5.1. We use a single point energy source and a single geophone per station.

The formula for refraction time from the first interface of a simple geological model with uniform lateral velocity is:

$$T_R = \frac{X}{V_2} + \frac{2H}{V_1 V_2}\sqrt{V_2^2 - V_1^2}$$

The basic formula assumes a shot depth of zero (surface energy) and non-dipping velocity interfaces (Espey 1983, Kearey and Brooks 1991). This formula will be recognized as the simple equation of a straight line for T as a function of X:

$$T = \frac{X}{V} + T_{in}$$

where T_{in} is the intercept on the time axis when X=0, and $\frac{1}{V}$ is the slope, where V is the velocity of the refracting layer.

It is possible to drive a fairly simple expression for the depth (H) of a refractor of the simple geological model mentioned above in terms of V_1, V_2, and the crossover distance (X_{cross}).

$$X_{cross} = 2H\left[\frac{V_2 + V_1}{V_2 - V_1}\right]^{\frac{1}{2}}$$

From this equation it may seen that the crossover distance is always greater than twice the depth to the refractor (Kearey and Brooks 1991).

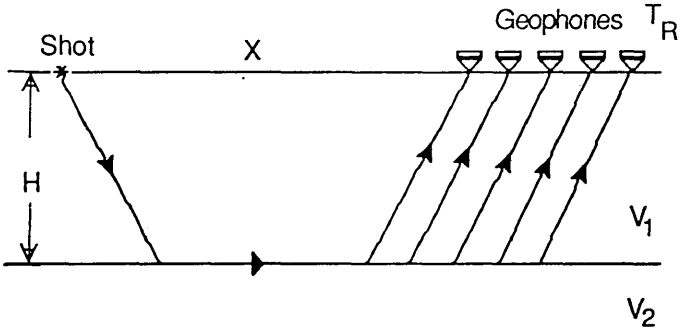

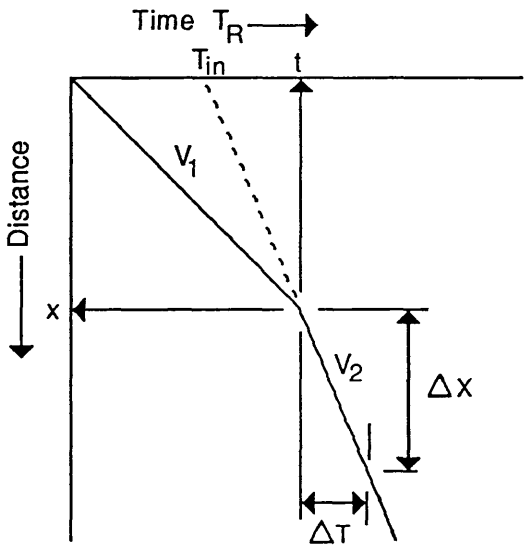

where X = Distance between the shot and the geophone
H = Depth of the weathering layer
T_R = Recorded time
T_{in} = Intercept time
V_1 = Weathering velocity (X/t)
V_2 = Subweathering velocity ($\Delta X/\Delta T$)

Fig.5.1. Refraction ray paths and time-distance curve.

If the subsurface interfaces are dipping a reversed profile is also recorded to obtain the apparent velocity and intercept times for the updip and downdip cases as shown in Figure 5.2.

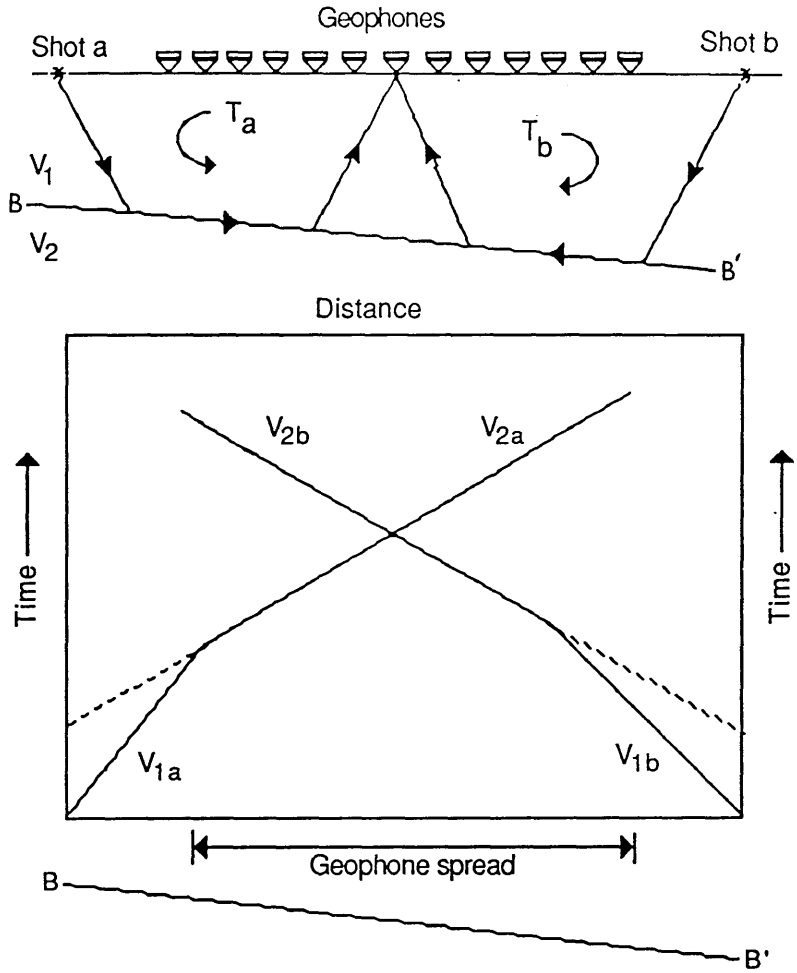

$$V_1 = (V_{1a} + V_{1b}) / 2$$

$$V_2 = (V_{2a} + V_{2b}) / 2$$

where T_a = Recorded time for shot a

T_b = Recorded time for shot b

V_1 = Average weathering velocity

V_2 = Average subweathering velocity

Fig.5.2. Reversed refraction profile

Suppose that the times corresponding to the direct wave for the reversed spread plot up as shown in the lower part of Figure 5.2. we can draw the 'best fit' lines for the velocities V_1 (LVL) and V_2 (datum velocity).

The base of the LVL lies in a general way along the straight line B-B'. If the weathering correction at the two ends of the spread is not the same, the correction can be interpolated evenly along the B-B' line.

In the second method, reflections are flattened by removing the appropriate normal moveout (NMO). They are then examined, trace by trace, and where necessary residual corrections are applied to each trace in order to make the reflection as smooth as possible. Smoothing one good reflection in this manner sometimes improves the quality of stacked weaker events, and it is always useful before stacking traces. It is especially popular in the processing of marine data, where shallow refraction methods cannot be used to correct for near surface velocity variations.

5.5.1 *Uphole surveys*

An uphole survey is one of the best methods of investigating the near-surface and finding the thickness and velocity of the low-velocity layer.

The most accurate of all weathering correction methods is made from dynamite data in which the source is below the base of weathering. The uphole times, the depth of source, and the elevation of the source are necessary to calculate the datum statics.

In the area of study, where surface sources (vibrators) have been used, information concerning the low velocity layer is acquired by the uphole surveys. An uphole survey requires a shothole deeper than the base

of the low velocity layer. Usually a complete spread of geophones plus an uphole geophone is used. Uphole times in a deep hole are measured by firing an explosive source at several different depths and recording the arrival times, as shown in Figure 5.3a, beginning at the bottom and continuing until the shot is just below the surface of the ground, to provide a plot of depth against time.

The vertical time correction must be done to the recorded uphole time as shown in Figure 5.3b and before plotting the time-depth curve. Average vertical times are plotted against shot depth. The slope of the curve associated with weathering shots gives the weathering velocity (V_w), and the break in slope usually defines the weathering depth (D_w) clearly. The slope of the curve associated with bedrock shots gives the required subweathering velocity (V_{sw}). A field example of six uphole survey data for different station locations on line 6V256-85 can be seen in Figure 5.4, showing the vertical velocity distribution near the surface above the datum plane (sea level).

Fig.5.3a. Plan view showing the positions of the geophone on the surface.

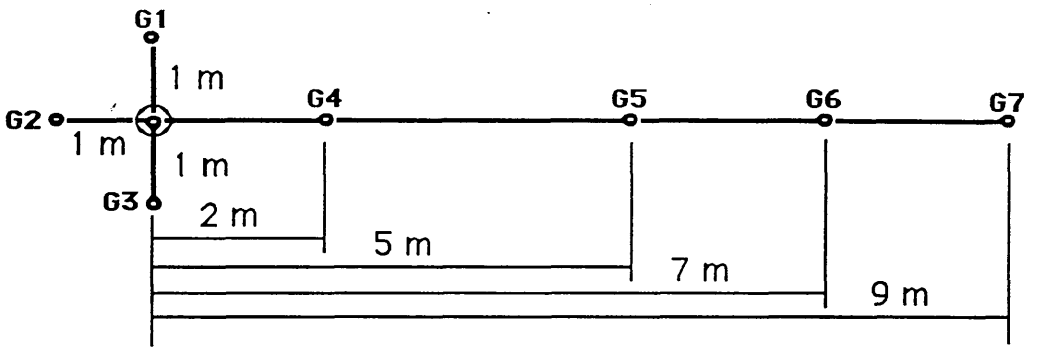

Fig.5.3b. Uphole calculation cross-section.

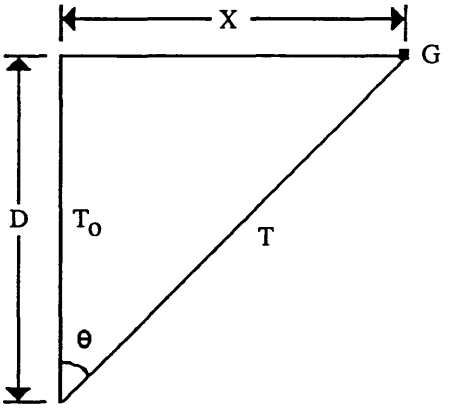

$$\tan\theta = \frac{X}{D}$$

$$\theta = \tan^{-1}\left(\frac{X}{D}\right)$$

$$T_o = T\cos\theta$$

where

X = Distance from the geophone (G) to the hole
D = Shot depth
T = Recorded time
T_0 = Vertical travel time (corrected time)

Figures 5.4 a-f show the velocity distribution in the weathering layer. A high velocity interbed appears clearly in two uphole locations; in fig.5.4b with a velocity of 2445 m/s., and fig.5.4d with a velocity of 2080 m/s.. A low velocity interbed appears clearly in three uphole locations; in Fig.5.4a with a velocity of 1280 m/s., fig.5.4e with a velocity of 1235 m/s., and fig.5.4f with a velocity of 1140 m/s. These figures are summarised in Table 5.1.

Uphole location		High velocity interbed			Low velocity interbed		
Station	Figure	Velocity	Depth	Thickness	Velocity	Depth	Thickness
147	5.4a				1280	83	23
234	5.4b	2445	11	20			
298	5.4c						
317	5.4d	2080	17	29			
379	5.4e				1235	74	26
505	5.4f				1140	64	24

Table 5.1. Velocity, thickness, and depth of the interbed within the weathering layer. These interbeds cause variable time delay in the arrival of the deeper reflections.

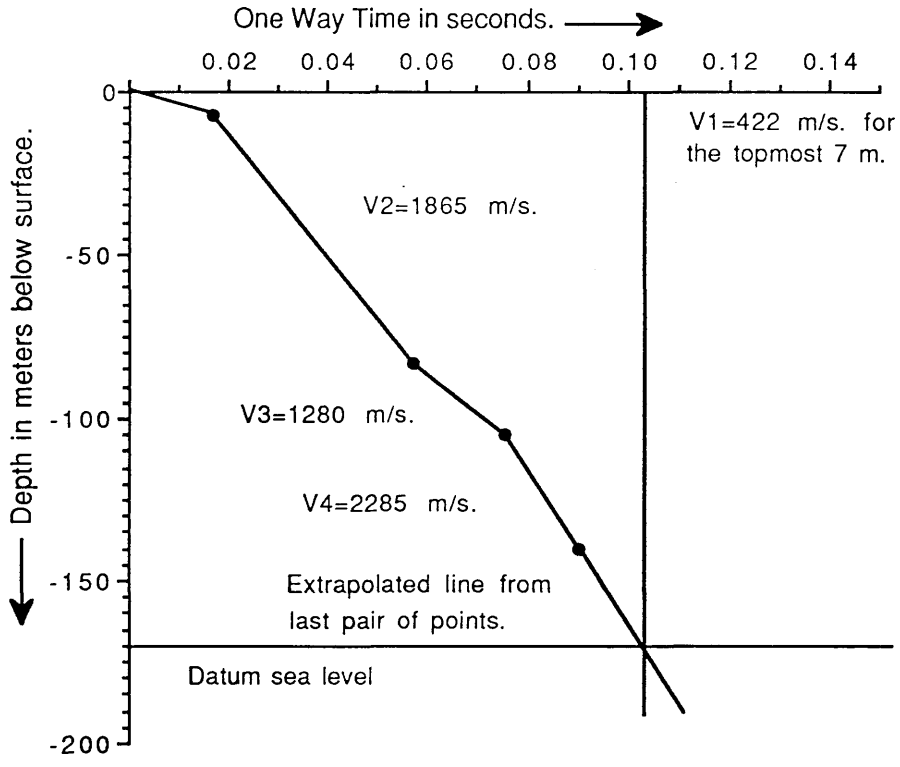

Fig.5.4a. Uphole Time Depth curve for station (147) on seismic line V256-85.

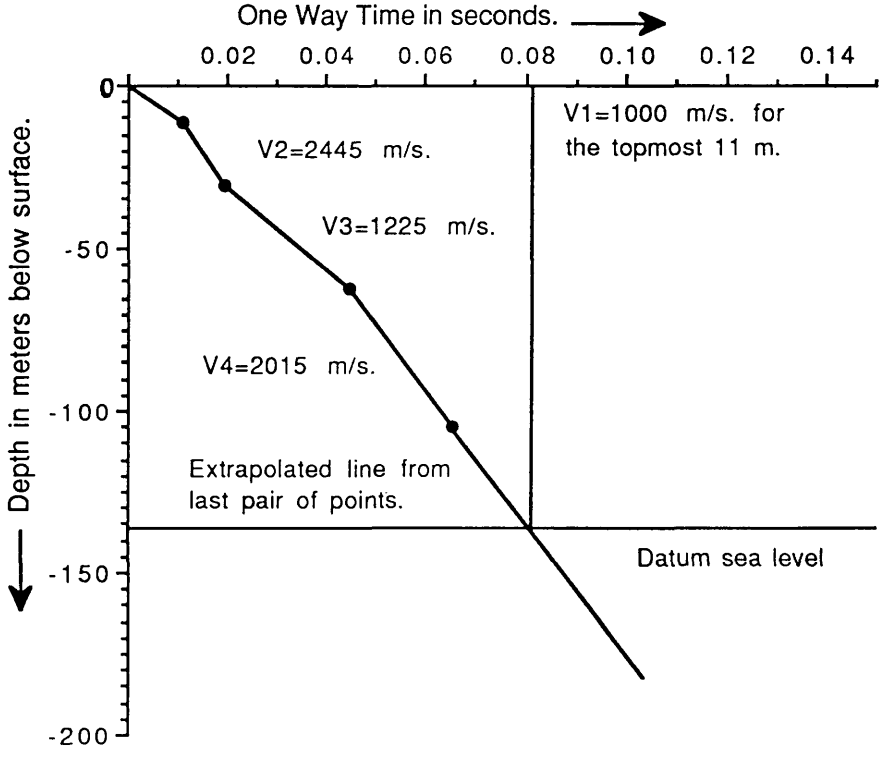

Fig.5.4b. Uphole Time Depth curve for station (234) on seismic line V256-85.

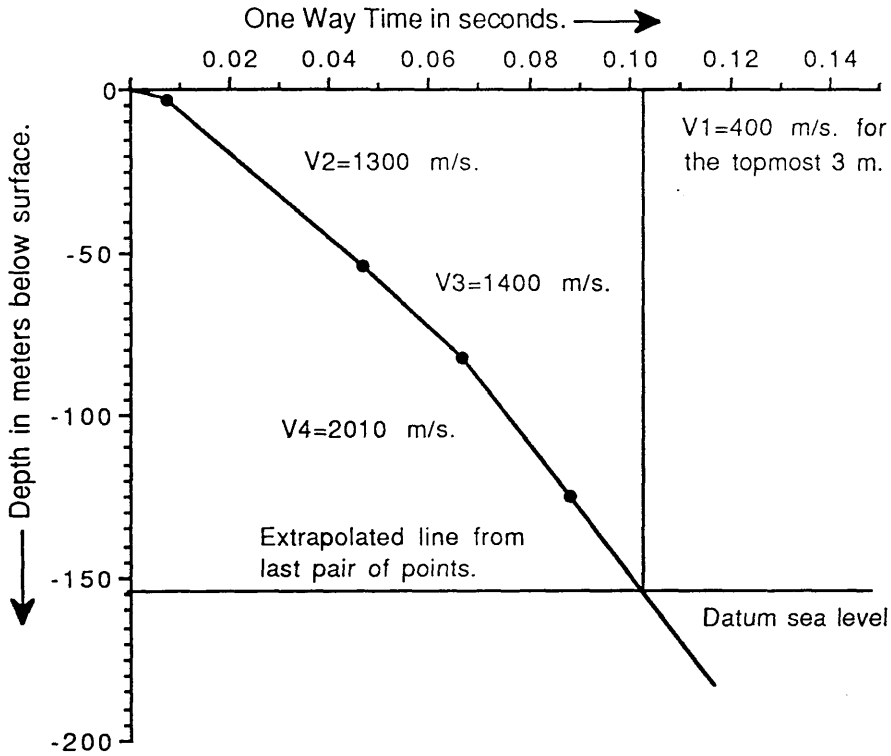

Fig.5.4c. Uphole Time Depth curve for station (298) on seismic line V256-85.

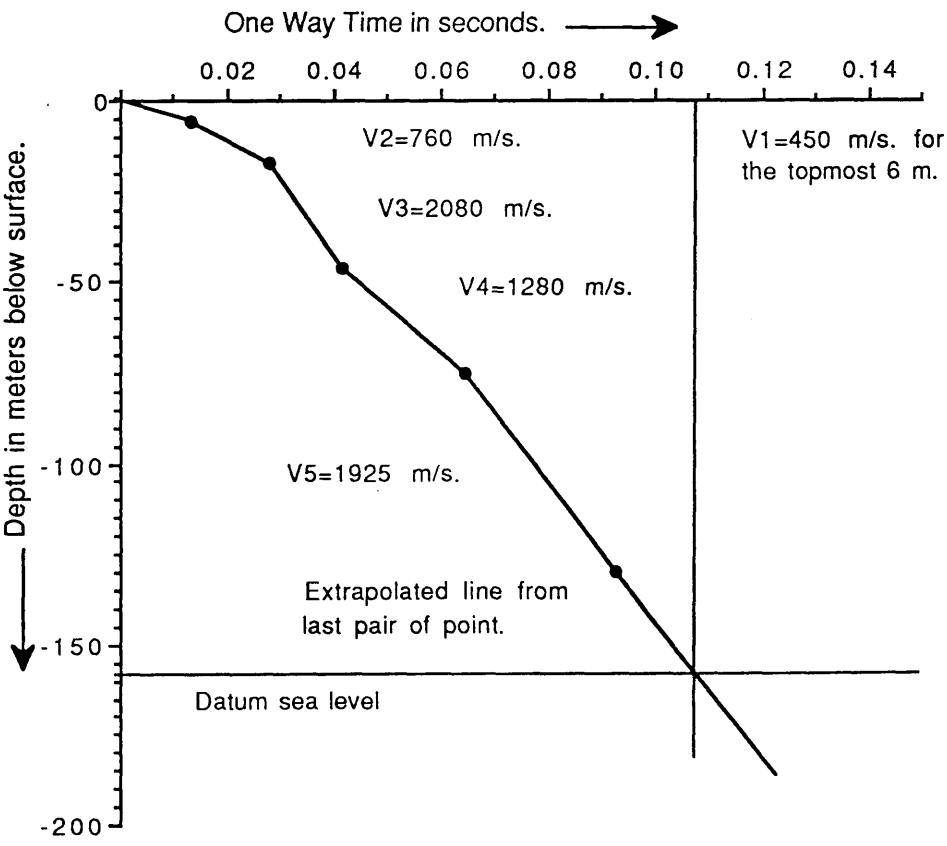

Fig.5.4d. Uphole Time Depth curve for station (317) on seismic line V256-85.

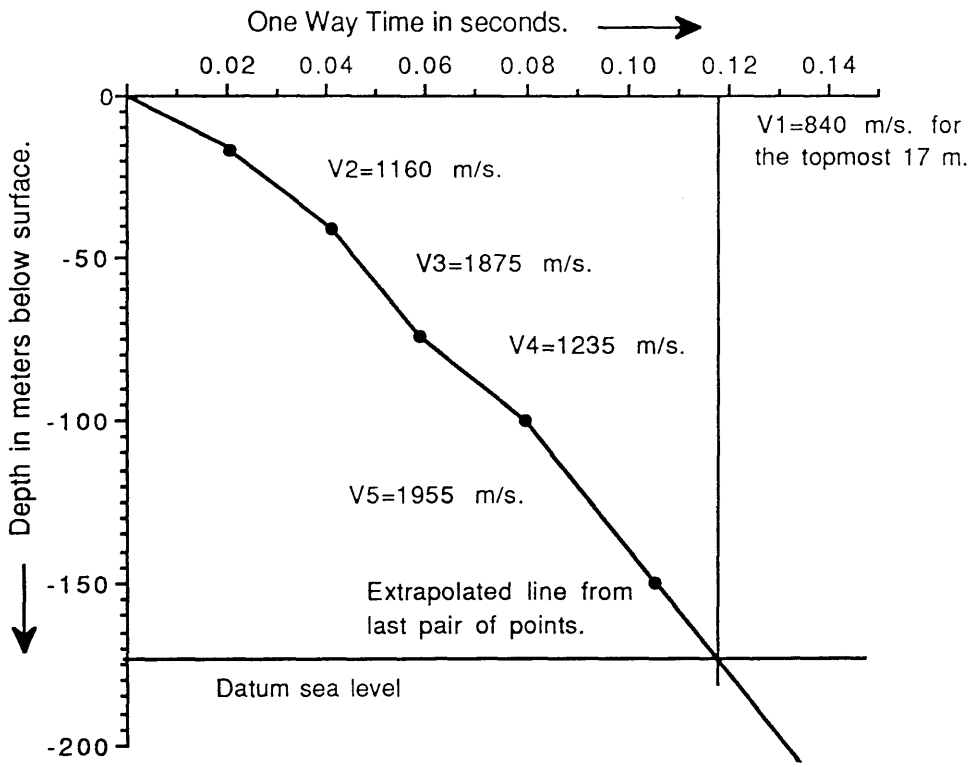

Fig.5.4e. Uphole Time Depth curve for station (379) on seismic line V256-85.

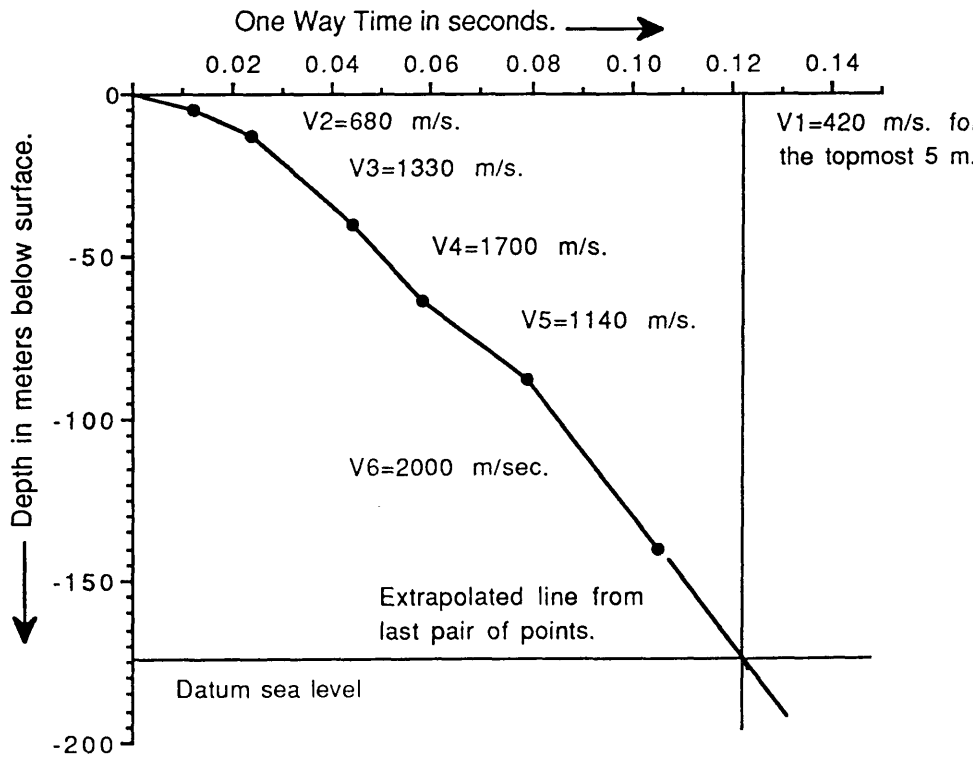

Fig.5.4f. Uphole Time Depth curve for station (505) on seismic line V256-85.

5.6 *Calculation of static corrections*

5.6.1 *Geometry of static corrections*

The purpose of the correction is to compensate for changes in elevation and for the near surface lateral changes in velocity. On the CDP data, static corrections are necessary for proper alignment of traces for stacking.

The basic static correction is composed of four parts:

(1) Low velocity layer (LVL) correction at the source.

(2) Datum correction at the source.

(3) Low velocity layer (LVL) correction at the receiver.

(4) Datum correction at the receiver.

The basic calculation is illustrated in Figure 5.5. When the shot hole is drilled to a depth below the LVL, the LVL correction at the source is not necessary. In this case the shot to datum time correction (T_{sd}) is calculated as shown in the figure. The calculation at the geophone station is more difficult since the exact thickness of the LVL is unknown. The interpolated thickness between the upholes was used. The correction at the geophone station (T_{gd}) formula is also shown.

In the seismic data used in the present study the seismic source array (vibrators) was on the surface. Holes were drilled to a depth below the LVL to calculate the static correction to the datum (sea level) at a particular shot. The source static correction and the receiver static correction are then calculated as shown in Figure 5.6.

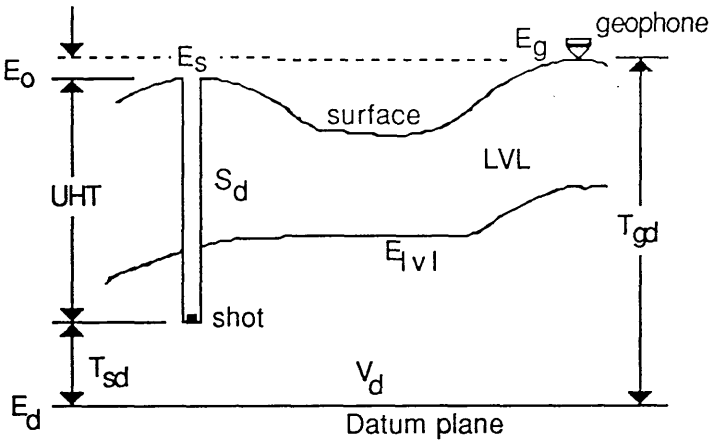

$$T_{dif} = \frac{(E_g - E_s)}{V_d} \qquad T_{sd} = \frac{(E_s - S_d - E_d)}{V_d}$$

$$T_{gd} = T_{sd} + UHT + T_{dif}$$

where

UHT = Uphole time
T_{sd} = Shot to datum time
T_{gd} = Geophone to datum time
LVL = Low velocity layer
E_s = Shot elevation
E_g = Geophone elevation
E_d = Datum elevation
E_{lvl} = Low velocity layer elevation
E_o = Difference in elevation (E_g - E_s)
T_{dif} = Difference in elevation time
S_d = Shot depth.
V_d = Datum velocity.

Fig.5.5. Shot and geophone corrections.

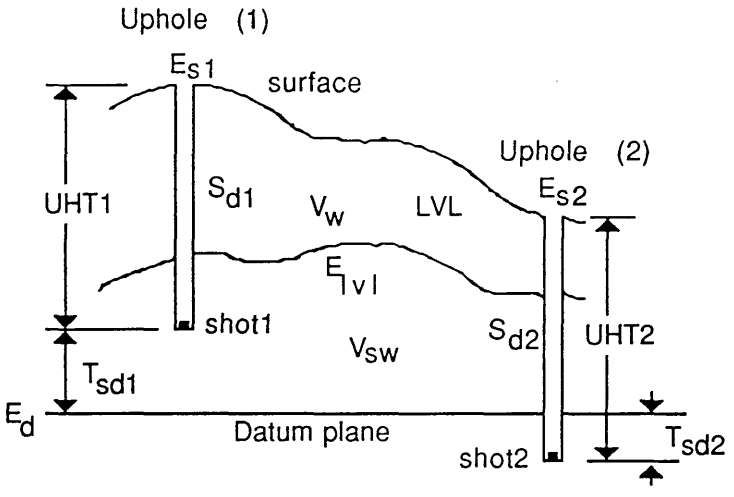

$$T_{sd1} = \frac{(E_{s1} - S_{d1} - E_d)}{V_{sw}}$$

$$T_{sd2} = \frac{(E_{s2} - S_{d2} - E_d)}{V_{sw}}$$

where

E_{s1} = Shot elevation for uphole 1
E_{s2} = Shot elevation for uphole 2
V_{sw} = Subweathering velocity
S_{d1} = Shot depth for uphole 1
S_{d2} = Shot depth for uphole 2
E_d = Datum elevation.
T_{sd1} = Shot to datum time.
T_{sd2} = Shot to datum time.

Fig.5.6. Static correction calculation for a surface energy source and a two layer model.

A new computer program (STATIC, described below) has been written for this particular case, and used to calculate the static correction for a part of line 6V256-85 from group station 147 to group station 505, which covers the reprocessed part of the line. The new static corrections for each source and receiver location are used in the reprocessing of this part of the line.

The accuracy of corrections calculated by the method used in the program is dependent on having valid information on shot hole depth, uphole times, shot/geophone elevation, some other parameters needed as an input before running the program, such as station number, and subweathering velocity. A knowledge of the thickness and velocity of the LVL increases the accuracy and the validity of the static time shifts applied. It is most important to do it correctly; if it is done incorrectly, small structures are missed and false prospects may be drilled.

5.6.2 *Fortran77 program STATIC*

This Fortran77 program has been written to calculate the static correction for the shots and receivers. A listing of the STATIC source code is given in Appendix 5.1. The program is designed to use three different kinds of static correction as shown in Figure 5.7, to compare between them. These are 'static', 'Lehib' and 'Sabkha'. Where the 'static' is the conventional static correction as shown in Figure 5.7, equations 5.6, depending on the interpolated between two upholes data, assuming constant weathering layer thickness, rather than assuming a constant weathering base. The other two -

Fig.5.7. Static equation used in static program.

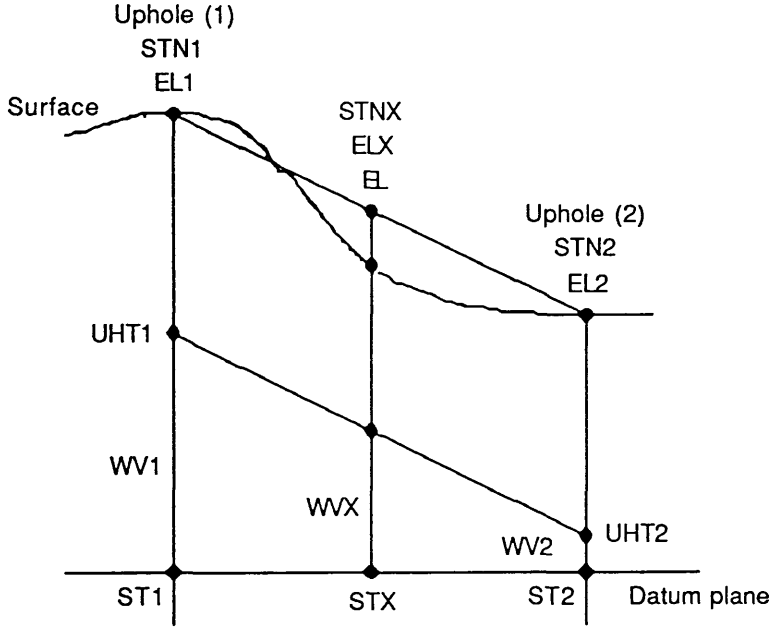

$$STX = \left[\left(\frac{ST\,2 - ST\,1}{STN\,2 - STN\,1}\right) \times (STNX - STN\,1)\right] + ST\,1 \quad \text{.....(5.1)}$$

$$WVX = \left[\left(\frac{WV\,2 - WV\,1}{STN\,2 - STN\,1}\right) \times (STNX - STN\,1)\right] + WV\,1 \quad \text{.....(5.2)}$$

$$ELX = \left[\left(\frac{EL\,2 - EL\,1}{STN\,2 - STN\,1}\right) \times (STNX - STN\,1)\right] + EL\,1 \quad \text{.....(5.3)}$$

$$DELX = EL - ELX \quad \text{.....(5.4)}$$

$$STXD = \left(\frac{DELX}{WVX}\right) \quad \text{.....(5.5)}$$

$$STATIC = STXD + STX \quad \text{.....(5.6)}$$

$$SABKHA = -\left[\left(\frac{ELEV.}{1500}\right) + 0.012\right] \quad s \quad \text{.....(5.7)}$$

$$LEHIB = -\left[\left(\frac{ELEV.}{1880}\right) + 0.007\right] \quad s \quad \text{.....(5.8)}$$

Fig.5.7. Continued.

Abbreviations:

STN1 = Station number 1
EL1 = Elevation for STN1 in meter
UHT1 = Uphole time for STN1 in second
WV1 = Subweathering velocity for STN1 in m/s
ST1 = Static correction calculated for STN1 in second

STN2 = Station number 2
EL2 = Elevation for STN2 in meter
UHT2 = Uphole time for STN2 in second
WV2 = Subweathering velocity for STN2 in m/s
ST2 = Static correction calculated for STN2 in second

STNX = Station number X
ELX = Interpolated elevation for STNX in meter
UHT1 = Uphole time for STNX in second
WVX = Subweathering velocity for STNX in m/s
STX = Static correction calculated for STNX in second

EL = Elevation for STNX in meter
DELX = Difference in elevation (EL-ELX) in meter
STXD = Time for the DELX in second

STATIC = Conventional static correction for STNX in second
SABKHA = Static formula in second
LEHIB = Lehib formula in second

'Sabkha' and 'Lehib'- were used by Sirte Oil Company for processing the data in the Zelten area.

Static corrections computed for the seismic lines consist of a simple elevation correction. However, two different replacement velocities have been used -'Sabkha' and 'Lehib'- as shown in Figure 5.7, equations 5.7 and 5.8 respectively, depending on the surface topography. Unfortunately the change from one formula to the other occurs right through the middle of the field.

The first step in this program is to read the names of the two input files and the two output files which are necessary for the program to run. The first input file contains some data and results from the uphole calculation, such as station number, elevation in meters, sub-weathering velocity in m/s, uphole depth in meters, and uphole time corresponding to the uphole depth in milliseconds. The second input file contains all the shot elevations if you are calculating shot static or all the receiver elevations if you are calculating receiver static. The first output file will contain all the shot or receiver statics, using the uphole information from the first input file.

The second output file will contain all the shot or receiver statics, using the formula which has been applied in previous processing of the seismic lines in the area of study, and the differences of the statics between the two methods of calculation. A detailed flowchart corresponding to the above outline is shown in Figure 5.8.

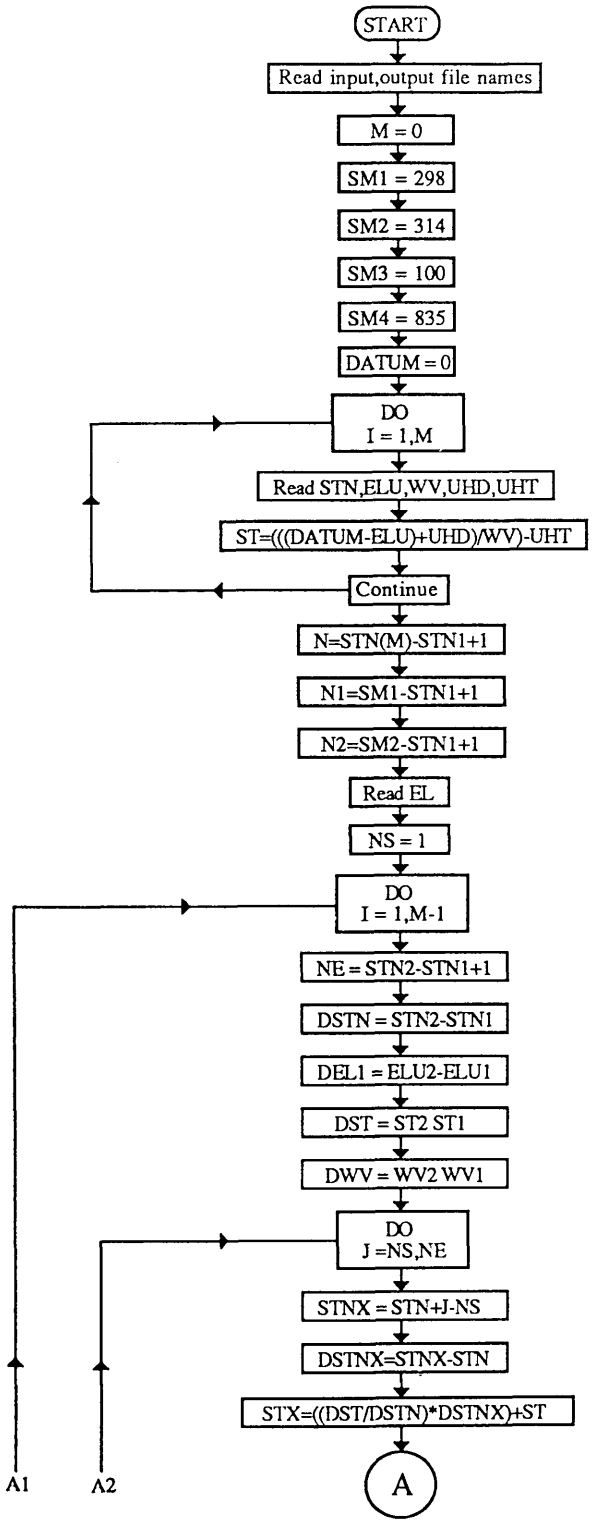

M - Number of upholes.
SM1 - Last station number in Lehib part.
SM2 - First station number in Sabkha part.
SM3 - First station number in Lehib part.
SM4 - Last station number in Sabkha part.
DATUM - Datum plane (sea level).

I - Counter for uphole data.
STN - Station number.
ELU - Uphole elevation.
WV - Weathering velocity.
UHD - Uphole depth.
UHT - Uphole time.
ST - Static correction at the uphole location.

N - Number of station.
N1 - Number of station in Lahib part.
N2 - Number of the first station in Sabkha.

EL - Elevation of the stations.

NS - Counter.

I - Counter of loops of the calculation.

NE - Number of stations to be calculated..
DSTN - Number of station intervals to be calculated.
DEL1 - Difference in elevation.
DST - Difference in static correction.
DWV - Difference in weathering velocity.

J - Counter for station number.

STNX - Station number to be calculated.
DSTNX - Difference in stations.
STX - Static correction at that particular - station.

Fig.5.8. Detailed flowchart for the STATIC program.

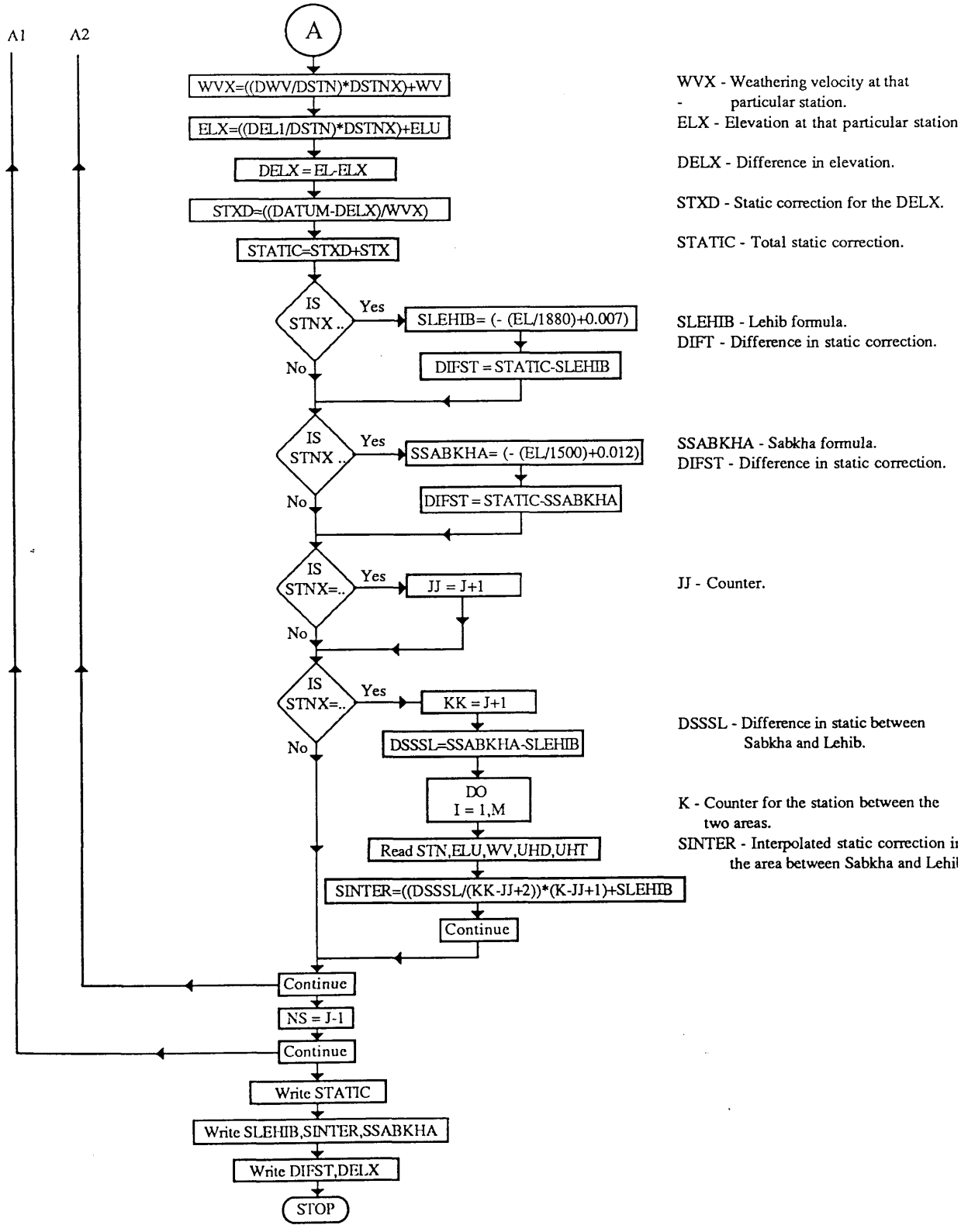

Fig.5.8. (Continued) Detailed flowchart for the STATIC program.

5.6.3 *Program results*

Table 5.2, showing selected static correction calculations for line 6V256-85 is given in Appendix 5.2. Figures 5.9a,b,c show the variation in elevation and one-way static calculation for shot locations, receiver locations, and both together, respectively.

From these figures we can divide the line into two parts. In the first part it is clear that the formula used gives a lower static correction than the uphole method. This is from the first shots up to shot point 314. The second part of the line shows that the formula used gives a higher static value than the uphole method for shot points 314-505.

These differences occur because different formulae - 'Lehib', and 'Sabkha' - have been applied. In the area where the Lehib formula was used, lower static values resulted, and in the area where the Sabkha formula was used, higher static values were used, than the static values should be.

These variations in the static correction cause reflectors to be shifted down in the Lehib area, and up in the Sabkha area. This variation is demonstrated in the Chapter 6.

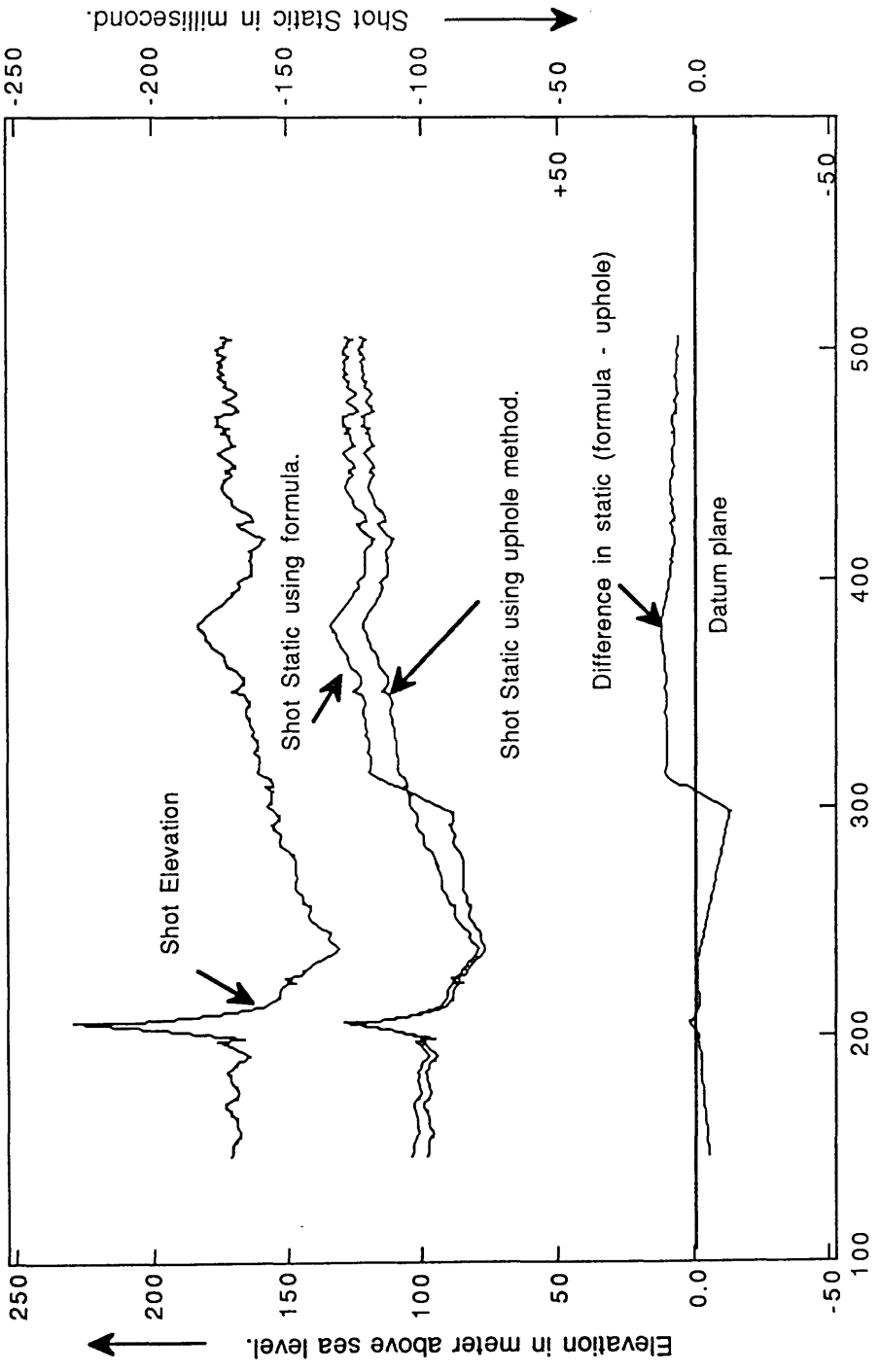

Fig.5.9a. Variation in elevation and static calculation for shot locations.

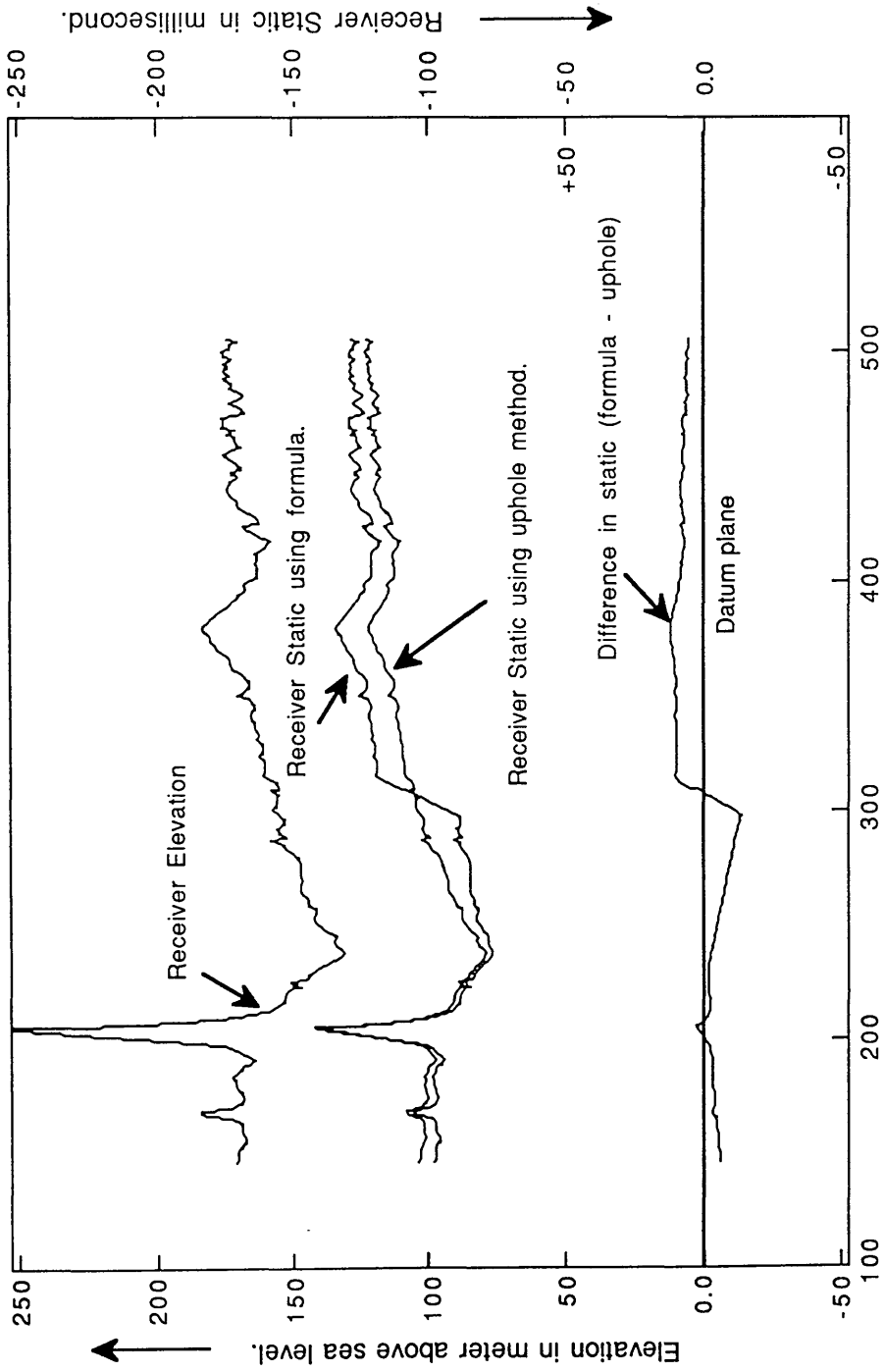

Fig.5.9b. Variation in elevation and static calculation for receiver locations.

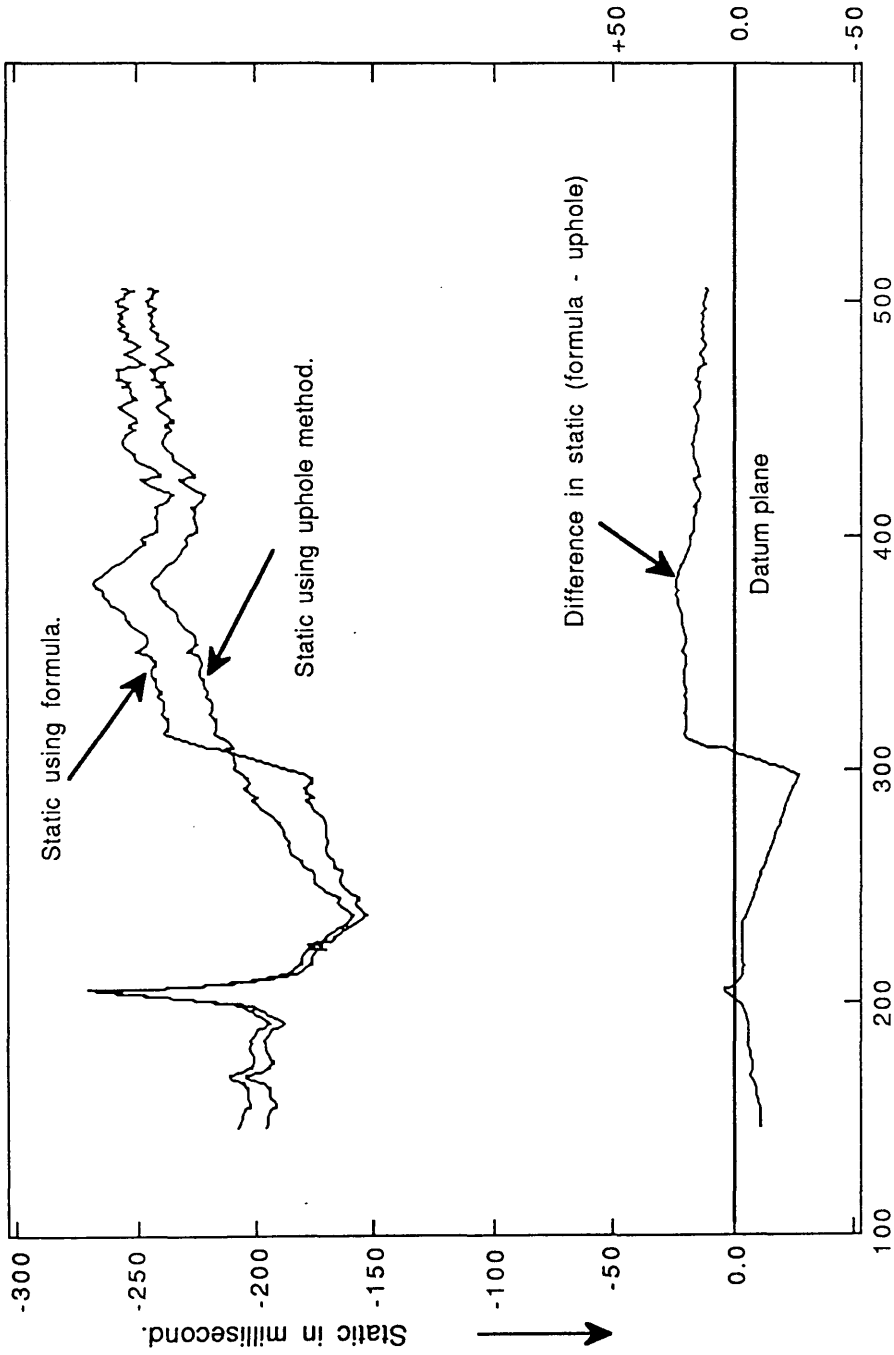

Fig.5.9c. Variation in the total static calculation for line 6V256-85.

CHAPTER (6)

REPROCESSING

6.1 Introduction.

The basic goal of seismic data processing is to transform the seismic signal recorded at the surface into a graphic display that will allow a reasonable interpretation of the subsurface geology.

Seismic data processing strategies and results are strongly affected by the field acquisition parameters. Surface conditions have a lot to do with the quality of data collected in the field. Other factors, such as weather conditions, care taken during recording, and condition of the recording equipment, also influence data quality. A main aim of processing is to suppress the noise and enhance the desired signal. This depends on the quality of the data acquisition.

In addition to field acquisition parameters, seismic data processing results also depend on the tools used for processing. High resolution data quality, for example, depends on careful handling in essentially every processing step.

One of the interpretation objectives is that the interpreter would like the data processing to produce a true and accurate geological model, but due to the highly complex nature of the subsurface and limitations on measuring techniques, we have to settle for a somewhat crude approximation of this ideal.

Part of line 6V256-85 from shot points 100 to 500 was selected for reprocessing, using the SierraSEIS package on the Sun computer network in the Geology and Applied Geology Department of Glasgow University.

Figure 6.1 shows a simplified flowchart for the processing.

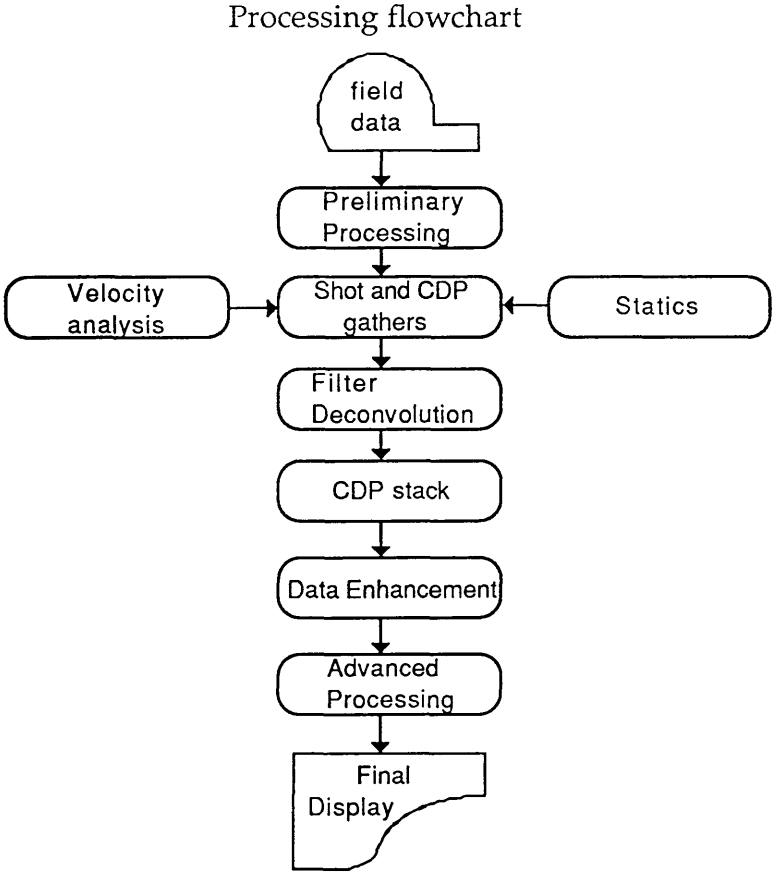

Figure 6.1 Simplified seismic data processing flowchart.

6.2 *Preliminary processing*

Preliminary processing, which includes formatting (demultiplex), editing, sorting, and bookkeeping steps, is shown in Figure 6.2. Once the data are summed together (the stacking process), previous errors in editing are probably undetectable and irrecoverable (Espey 1983).

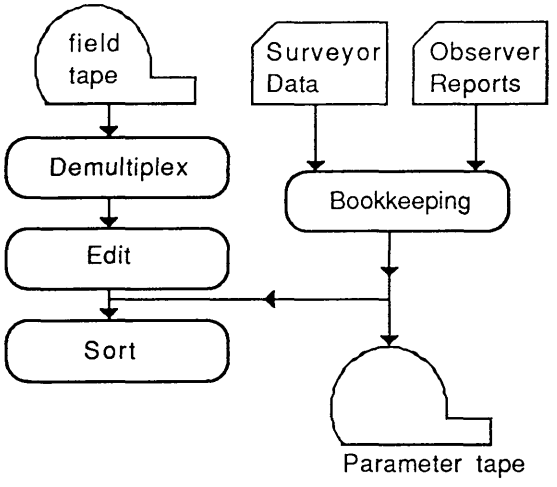

Figure 6.2 Preliminary processing flowchart.

The principal function of the first data processing step (demultiplexing) is to reformat the field data, from time scan sequence to trace sequence. In our case study, the tape supplied had already been demultiplexed. This had been done at CGG's (Compagnie Generale de Geophysique) processing centre.

The principal function of the second data processing step (editing), which is included in the GEOMETRY processor in SierraSEIS, is to remove undesirable noise. This function is an important one that should be performed by the processing analyst after every data processing run. There are some items that must be checked carefully during the editing of the field data, such as:

(1) Channel sequence and polarity

(2) Shot and cable geometry

(3) Cable noise

(4) Dead channels

(5) Man or track made noise

(6) Instrument noise

Editing out of most types of noise is usually accomplished by deletion of a trace or complete record (unwanted data) from the shot records. Processes such as zeroing have been applied to the bad traces to attenuate the noise.

6.3 *Automatic gain control* (AGC) *and muting*

The next step that is applied to the traces in the shot gathers is AGC, which applies balancing scalars that equalize amplitudes within a trace. Tests are carried out on the effect of different AGC windows before applying the AGC. Figures 6.3 a and b show the two shots before and after application of AGC (using a fixed window of 400 ms length) processor, respectively.

The next process is muting, which provides several options to remove unwanted data from the shot gather traces. This processor selectively zeros data samples at either ends of the input trace. Figure 6.3c shows muting applied to the two selected two shots at the front end of the traces.

6.4 *Deconvolution and filtering before stack*

Deconvolution (DECON) means removing, through data processing, undesirable effects which have occurred in the earth, by collapsing the seismic wavelet to approximately a spike (Yilmaz 1987). Wavelet compression is most obvious when compared with the gathers before

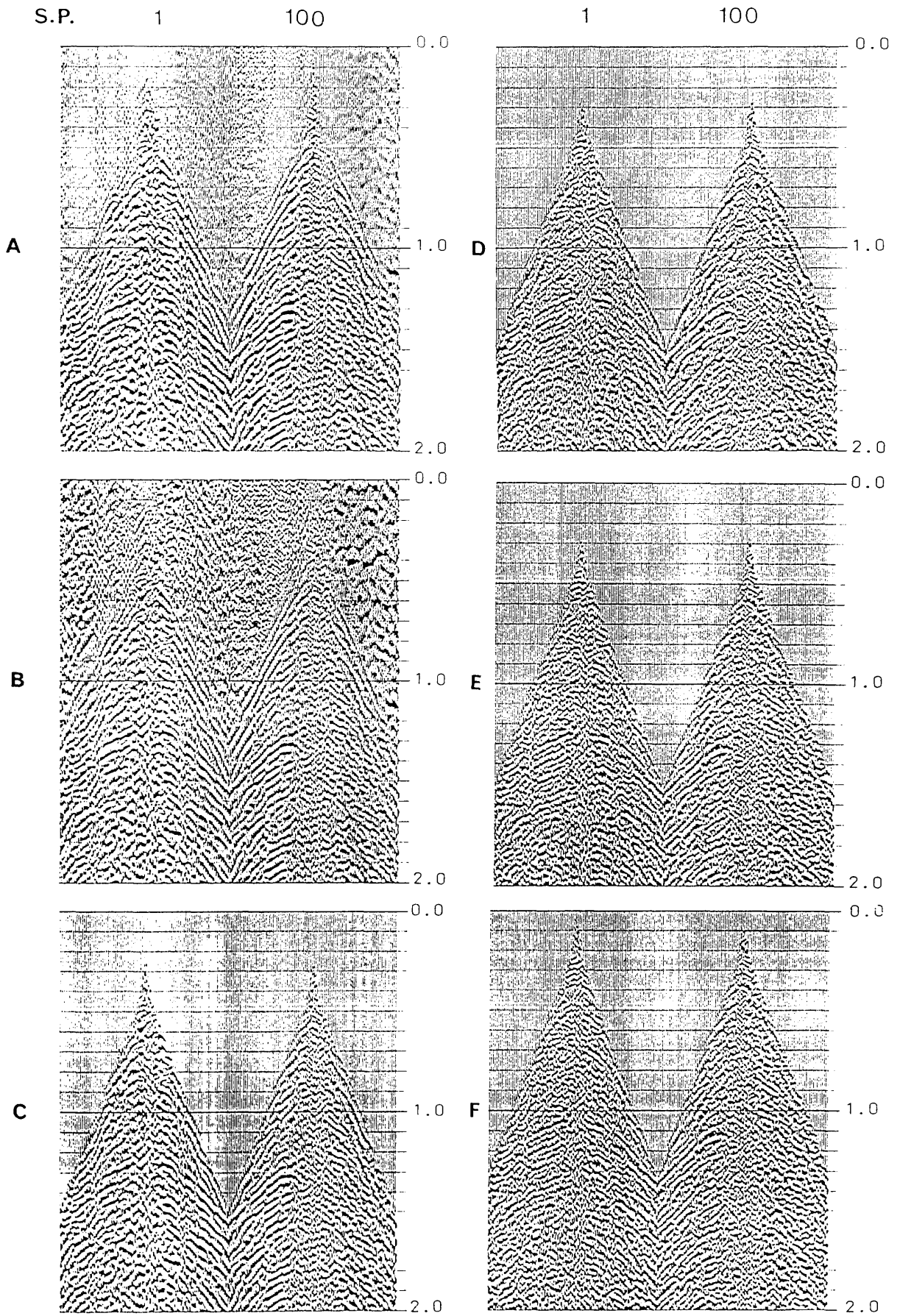

Fig.6.3 (a) Two selected shot gathers, (b) after applied AGC, (c) after applied mute, (d) after applied deconvolution, (e) after applied filter, (f) after applied "Equation" static correction.

DECON has been applied. After DECON the traces contain much more high-frequency energy, some of which, however, will be noise. Different kinds of tests of the DECON parameters have been carried out on the shots, such as:

(1) Length of the autocorrelation window
(2) Maximum lag
(3) Length of the predictive lag
(4) Starting time of autocorrelation window
(5) Pulse-shaping deconvolution
(6) Predictive deconvolution

Figure 6.3d shows the application of the chosen parameters of the pulse-shaping deconvolution on the same shots as in Figure 6.3c.

Because both high-frequency noise and signal are boosted after DECON, and the traces also contain some low-frequency noise, such as ground roll, and some high-frequency ambient noise, the data usually need filtering with a wide band-pass filter. Figure 6.4a shows frequency analysis of the shot point 1 for trace 1. It also shows that the dominant frequency is from 10 to 48 Hz. Figure 6.3e shows the application of the STVF processor with a band-pass filter of 12-50 Hz on the same shots as in Figure 6.3d.

6.5 *Static corrections*

The static correction processors compute and apply statics to seismic data traces. You can apply any type of static corrections to seismic data using SierraSEIS processors, such as:

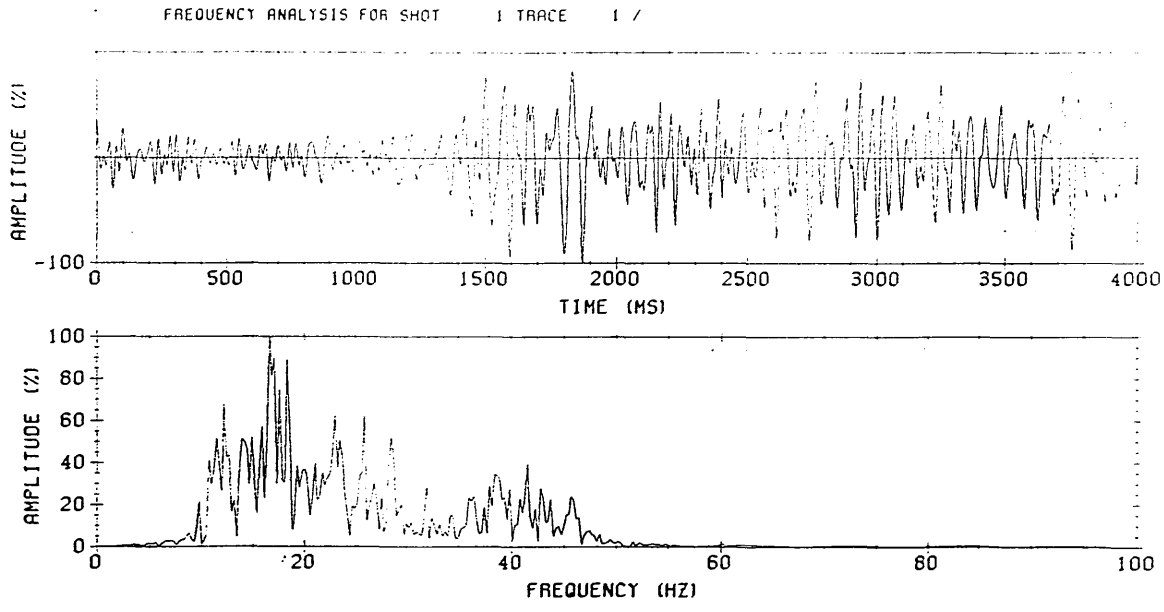

A

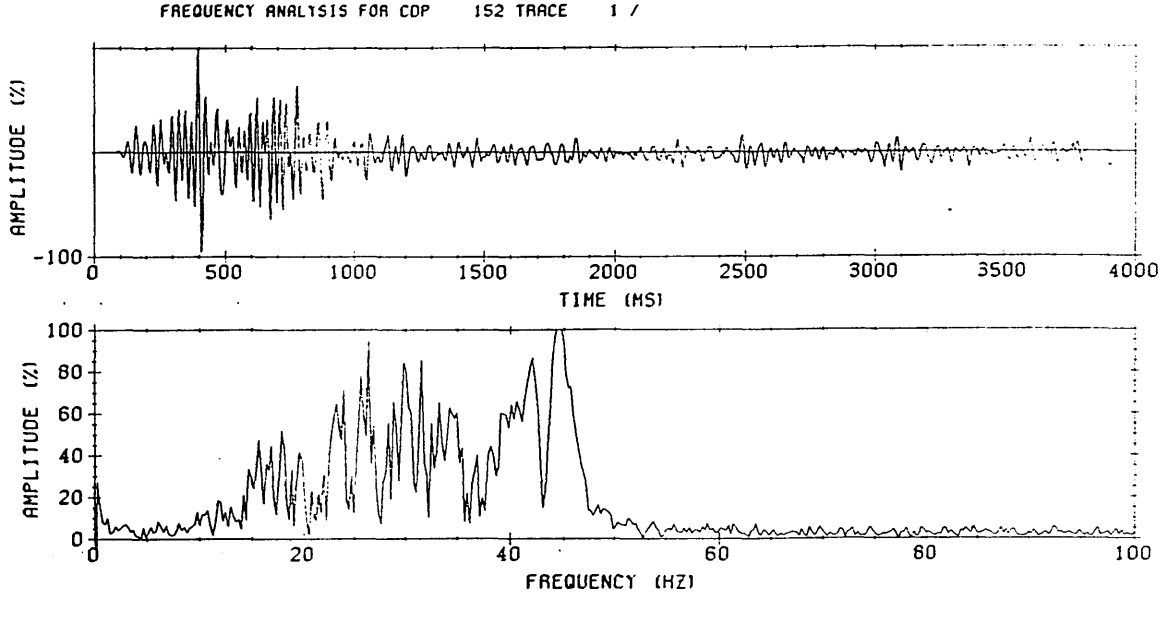

B

Fig.6.4 Frequency analysis on the (a) shot point 1 (trace 1).
(b) CDP 152 gather after stack.

(1) Geometry statics including shot statics and receiver statics (surface consistent)

(2) Residual statics (surface inconsistent)

Static calculations for the shot locations and receiver locations from the STATIC program application (Chapter 5), for the two different kinds of static correction, the conventional static ('Static'), and the formula static ('Lehib' and 'Sabhka') as shown in Figure 5.7 (Chapter 5) were applied to the data. First we start by applying the conventional static correction to the shot gathers. Figure 6.3f shows the application of the static correction on the same shots in Figure 6.3e.

6.6 *Common depth point* (CDP) *gathering*

Before velocity analysis, we sort the data into the desirable order (CDP gathers) for the velocity analysis and CDP processing. Figure 6.5a shows two selected CDP gathers.

6.7 *Velocity analysis and normal moveout* (NMO) *correction*

Velocity is defined as the propagation speed of the seismic wave, and is a property of the strata through which the wave moves. Seismic velocity is also important in data processing, to correct for the normal moveout due to the separation of the source and receiver, as mentioned in Section 3.3.5 (Chapter 3). The velocity needed in NMO correction (V_{nmo}) is different from sonic velocity, because the seismic wave propagates over an irregular

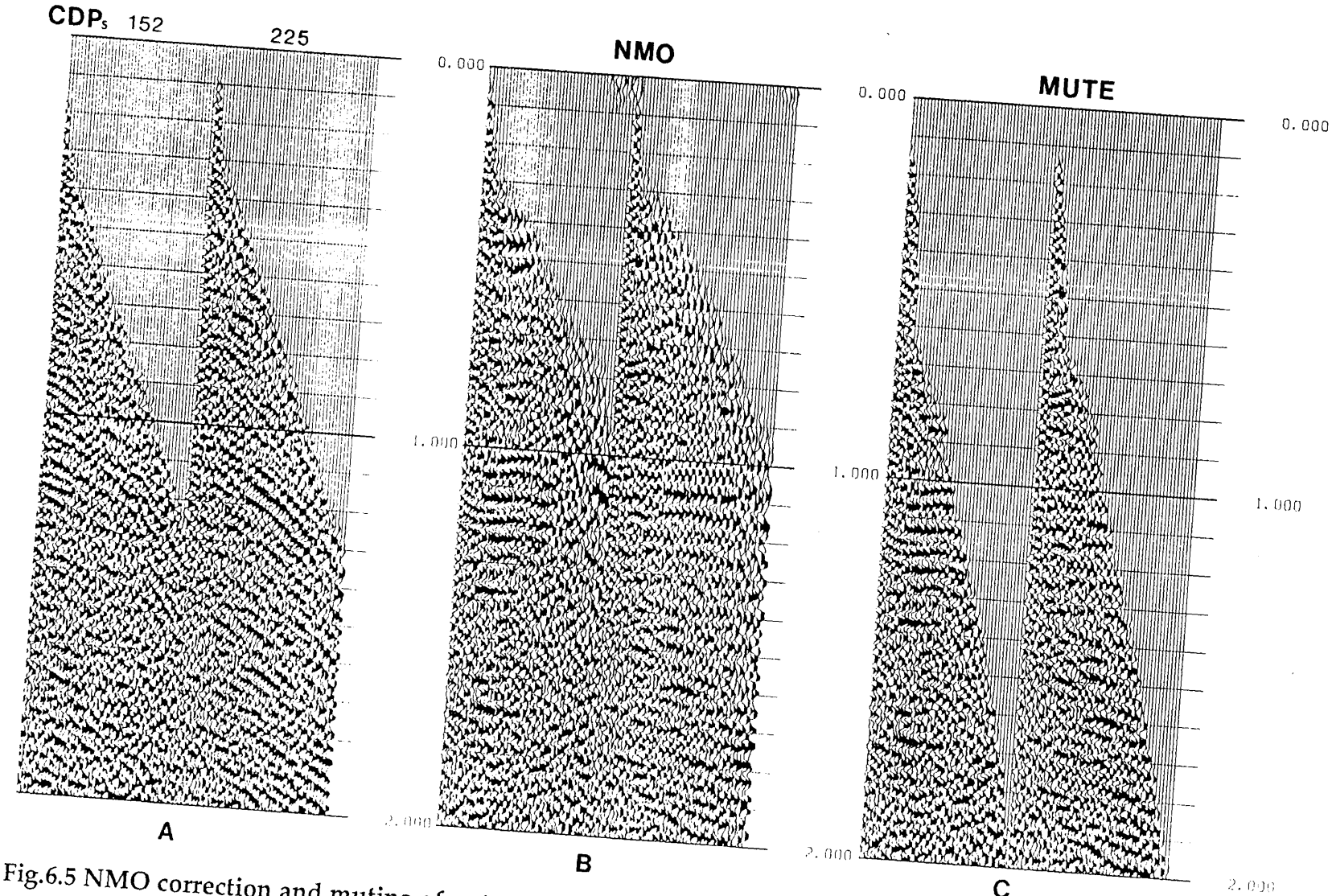

Fig.6.5 NMO correction and muting of a stretched zone on the field data;
(a) CDP gathers, (b) NMO correction, (c) mute.

path containing a wide range of interval velocities. If velocity did not change laterally, well sonic velocity might be used to compute the velocity function needed for NMO correction (Espey, 1983).

The purpose of the NMO correction in data processing is to remove the effect of the separation between the shot and receiver (Fig. 3.6, Chapter 3). The interpretation of the velocity analysis display is subject to the quality of the data and the velocity analyst's experience in identifying valid reflection events and isolating interferences such as multiples. The accuracy depends upon the time and velocity increments selected.

Fifteen locations have been chosen for the velocity analysis along the V256-85 seismic line. Two methods have been tested for such velocity accuracy: velocity spectra and velocity functions. The first one is available in the software package, but the second is not. For the second, eight different velocity functions for the velocity analysis have been designed and applied to the fifteen CDPs. Both gave us a good velocity analysis.

The top of Figure 6.6 shows the first two seconds of the velocity analysis for all the traces on CDP 157, as an example of the first method of the velocity analysis (velocity spectrum). Figure 6.7 shows an example of the second method of the velocity analysis (velocity function), applied on CDP 225, using eight different velocity functions. It also shows velocity increasing from left to right. The reflector at 1.1 s looks overcorrected on the first two left panels, horizontal (i.e. well corrected) on the third left panel, and undercorrected on the other panels. The CDP gathers display has a chequerboard effect, which could be due to the static problems. The gather is

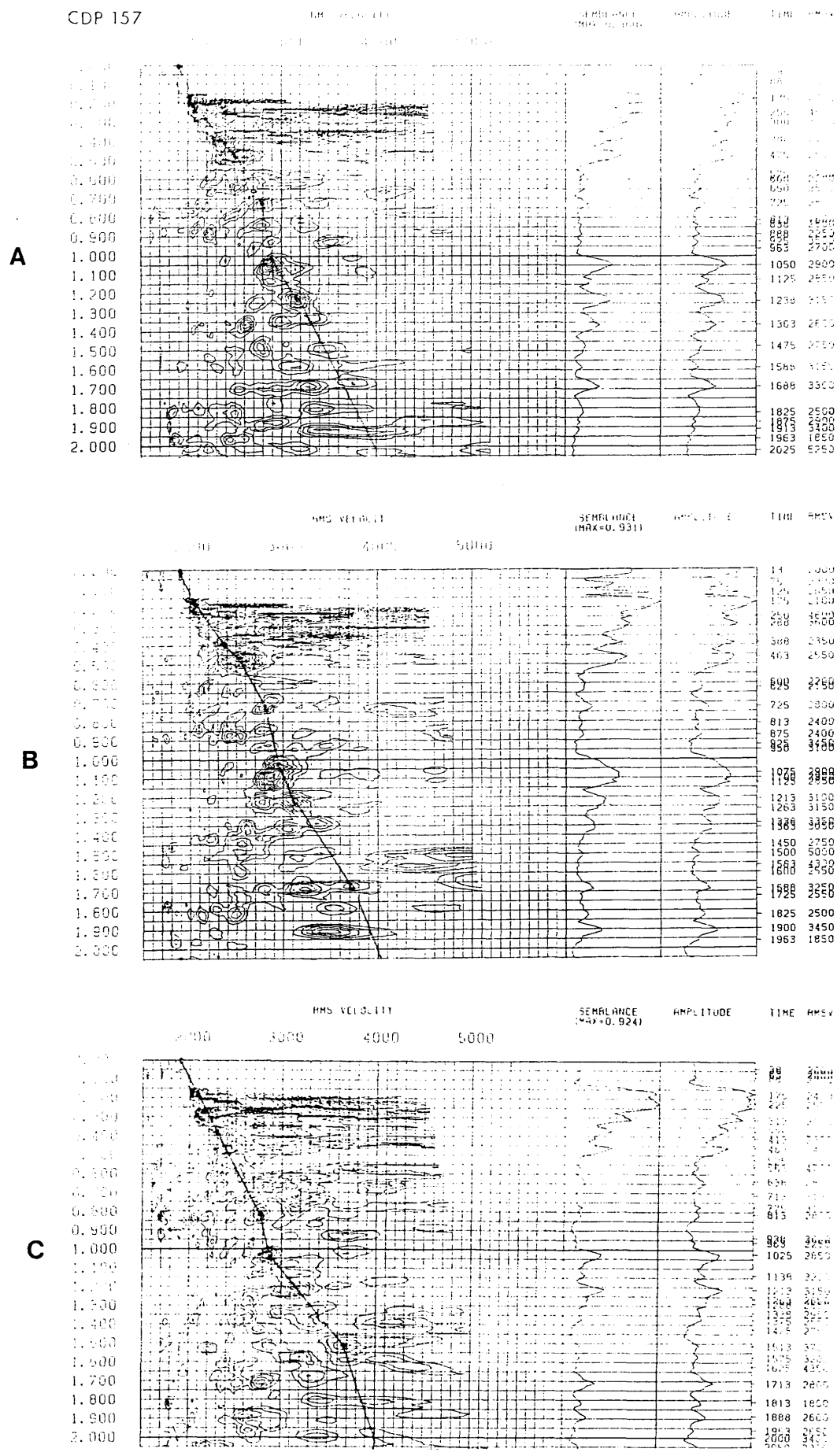

Fig.6.6 Velocity sepectra associated with (a) all traces in the CDP 157 gather;
(b) first half of the traces in the same CDP; (c) second half of the traces in the same CDP.

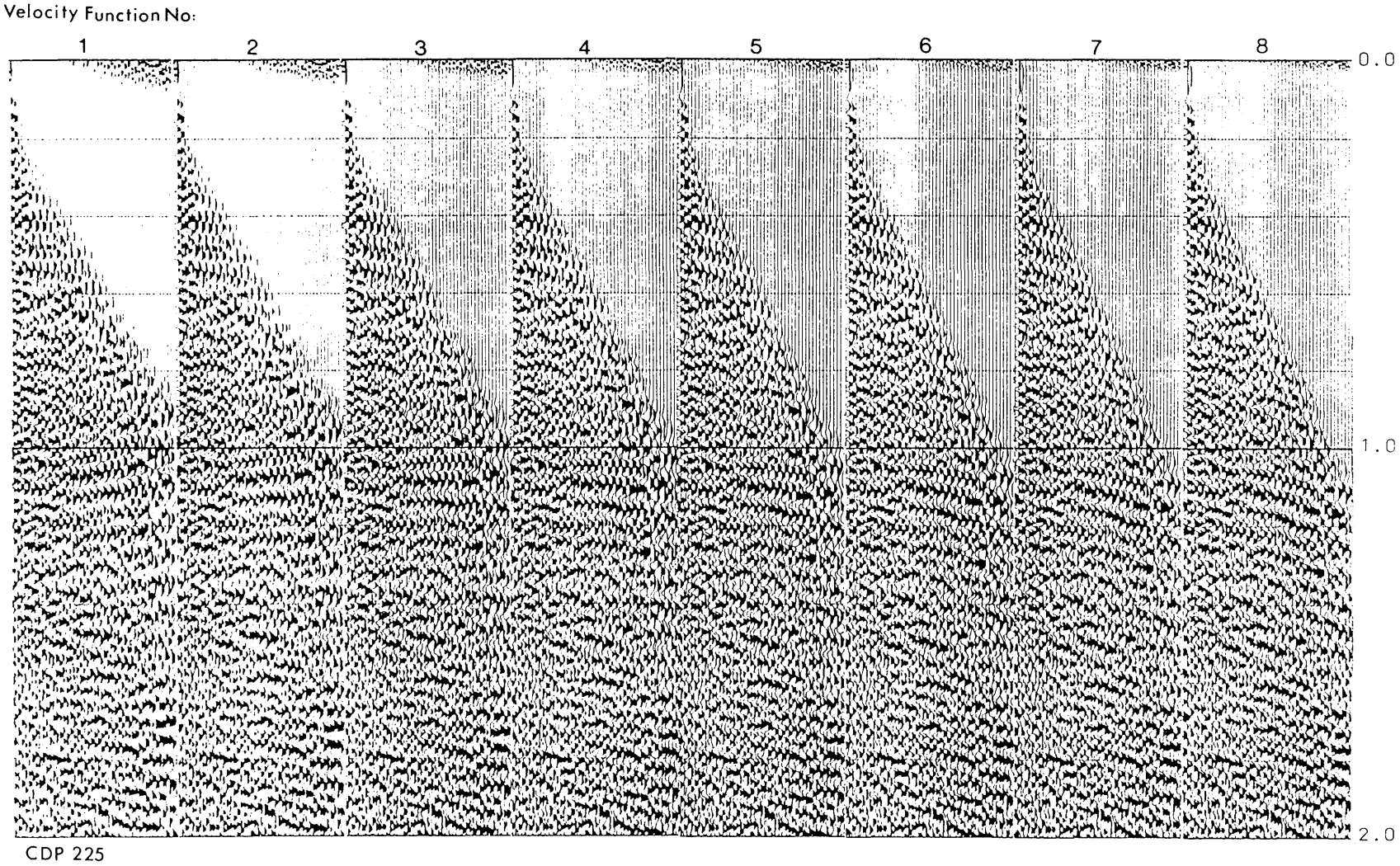

Fig.6.7 Velocity functions moveout corrections applied to the CDP 225 gather. Velocity functions values increases from left to right.

made up of alternate traces shot in one direction, then the other direction, laid out in order of increasing shot-receiver offset without regard to sign.

Because of the chequerboard effect mentioned above, we decided to separate the shot gathers traces into two halves; the first half contains traces 1-48, and the second half contains traces 49-96. Velocity analysis has been repeated for each half separately. These displays are shown in Figure 6.6 b and c. Figure 6.6 a, b, and c shows the same good reflector at 1.050, 1.075, and 1.025 s respectively, have the same stacking velocity. These differences in time varied from one place to another, which proves the bad data mentioned above.

6.8 *Common depth point* (CDP) *stacking*

Common depth point stacking is the most robust of the processes. By using redundancy in CDP recording, stacking can significantly suppress uncorrelated noise, thereby increasing the signal-to-noise (S/N) ratio (Yilmaz 1987, Anderson and McMechan 1990). It also can attenuate a large part of the coherent noise in the data, such as multiples. Because multiples have larger moveout than primaries, they are undercorrected and, hence, attenuated during stacking (Yilmaz 1987). Two different types of stacking have been tested on the data, the conventional stack and the median stack. The second looks more effective on the data, so the data have been stacked with the second type.

Before stacking the data, the mute process should be used on the CDPs after applying the NMO correction to remove the unwanted noise

(stretch zones) created by the NMO process. The selection of the mute pattern can be critical, since too much mute may reduce CDP fold and eliminate critical long offset traces at the target horizon. On the other hand, a mute that is too shallow will reduce data quality, due to the NMO stretch and refraction noise. Different mute patterns have been tested on the CDP gathers. Figure 6.5c shows one of the deep mute pattern applied to the same CDP gathers in Figure 6.5b. Figures 6.8 and 6.9 show two stacked sections with different static ("Equation" and "Formula") corrections applied, respectively, where the static "Equation" represents the conventional static and the static "Formula" represents the "Lehib' and Sabhka' together. In each Figure a different mute pattern has been applied.

The mute pattern applied to the data on Figures 6.8a and 6.9b, appears good, and is applied to all the sections. On the other hand, the deep mute pattern, which is applied to the data on Figures 6.8b and 6.9a, looks too deep. It reduces CDP fold and eliminates critical long offset traces as explained before. This deep mute causes discontinuities in the deep reflectors.

6.8.1 *Brute stack*

The quality of the stacked section is dependent on the quality of the data, the quality of the picked primary velocity function, and the chosen mute. Figures 6.8a, 6.10a, and 6.10b shows the brute-stack sections for all the traces group, the first half traces group, and the second half traces group in the CDPs respectively, using one velocity function. It is clear that the difference in time mentioned in Section 6.7 has affected the stacked sections.

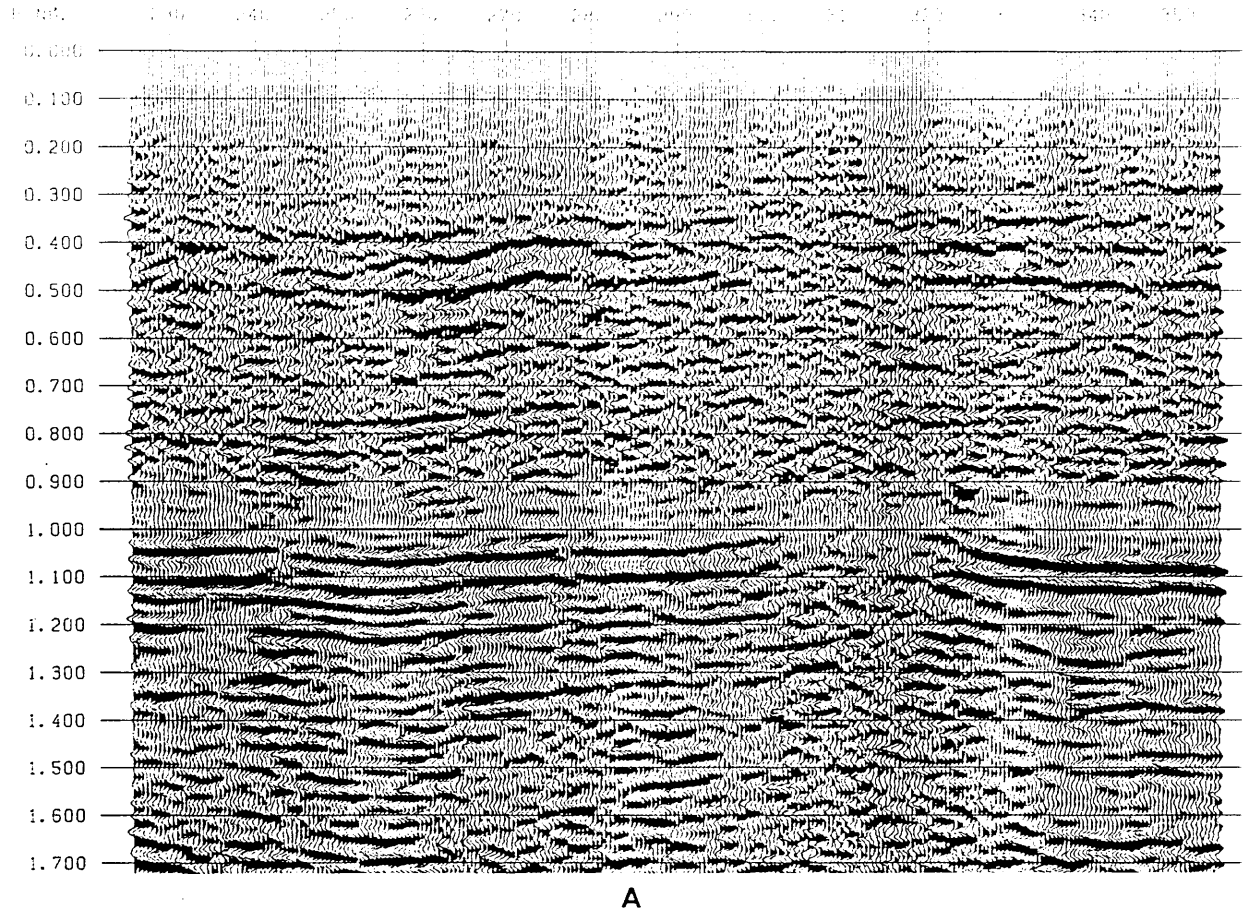

A

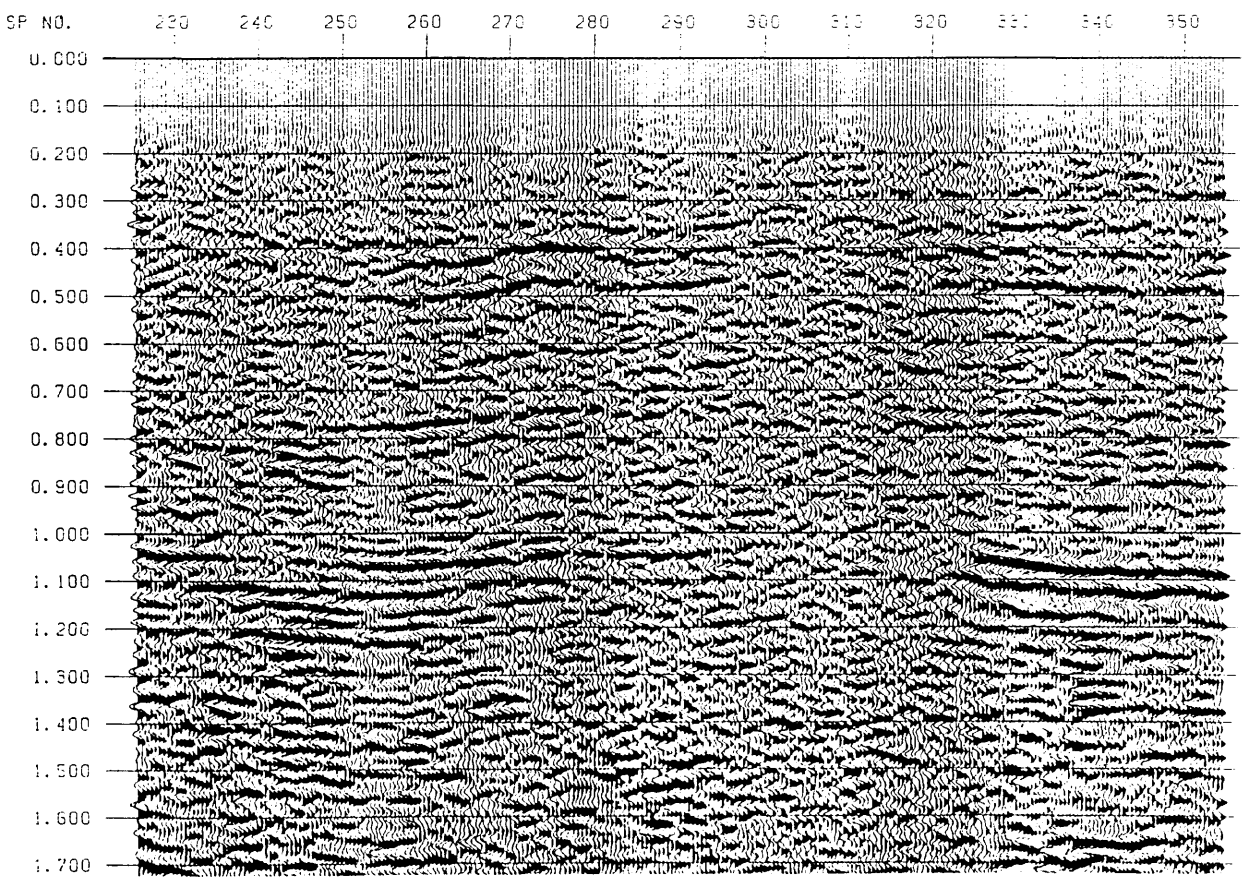

B

Fig.6.8 Brute stack sections, using "Equation" static correction;
(a) applied shallow mute pattern(b) applied deep mute pattern

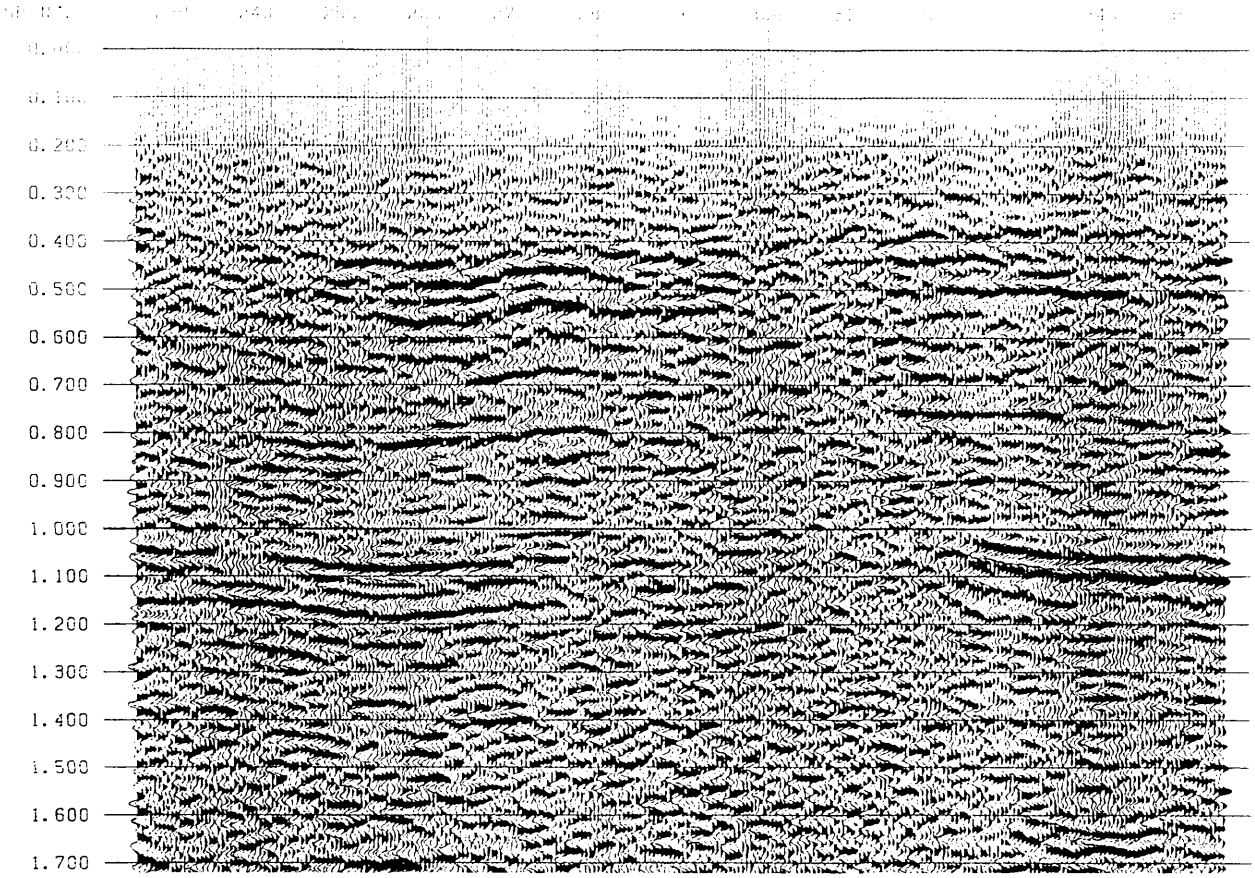

A

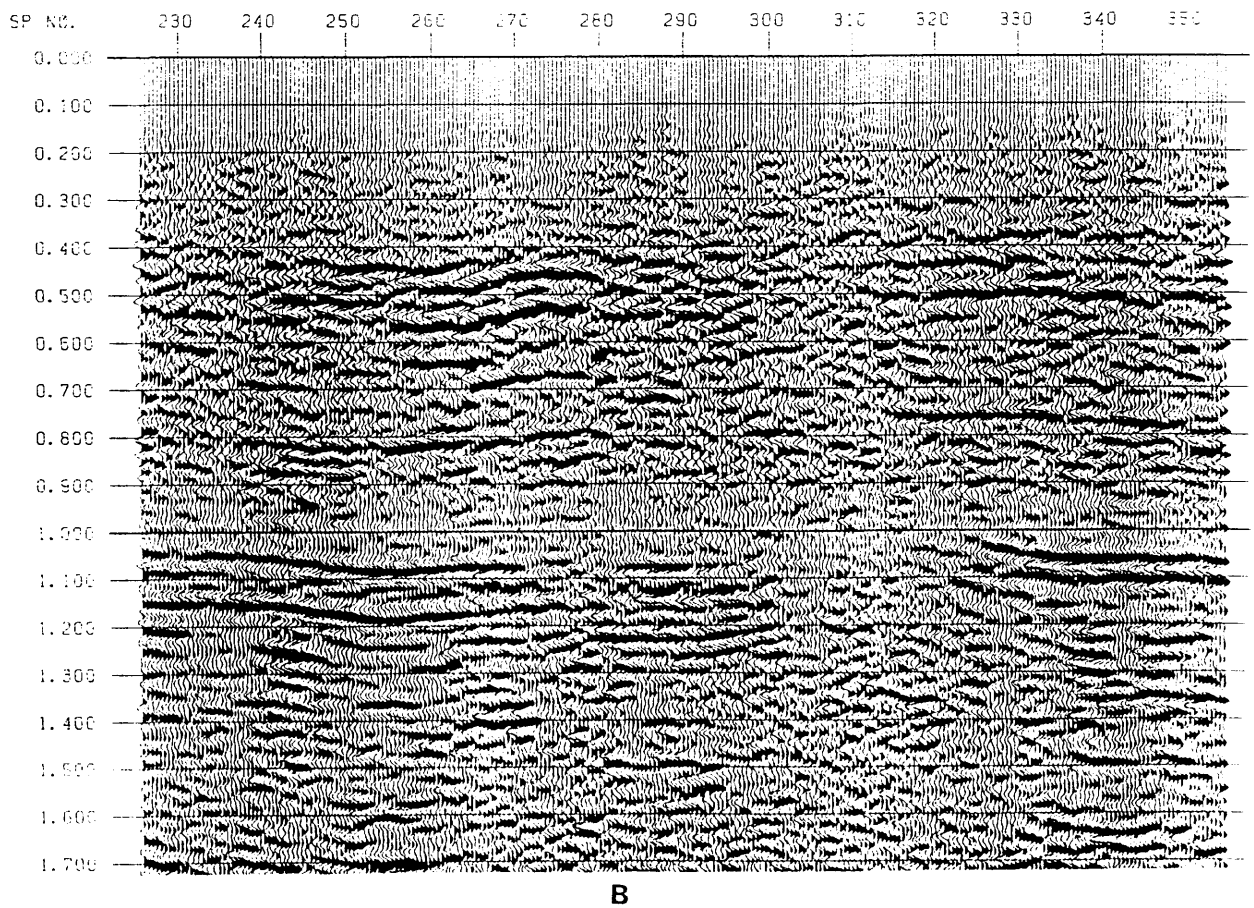

B

Fig.6.9 Brute stack sections, using "Formula" static correction;
(a) applied deep mute pattern; (b) applied shallow mute pattern.

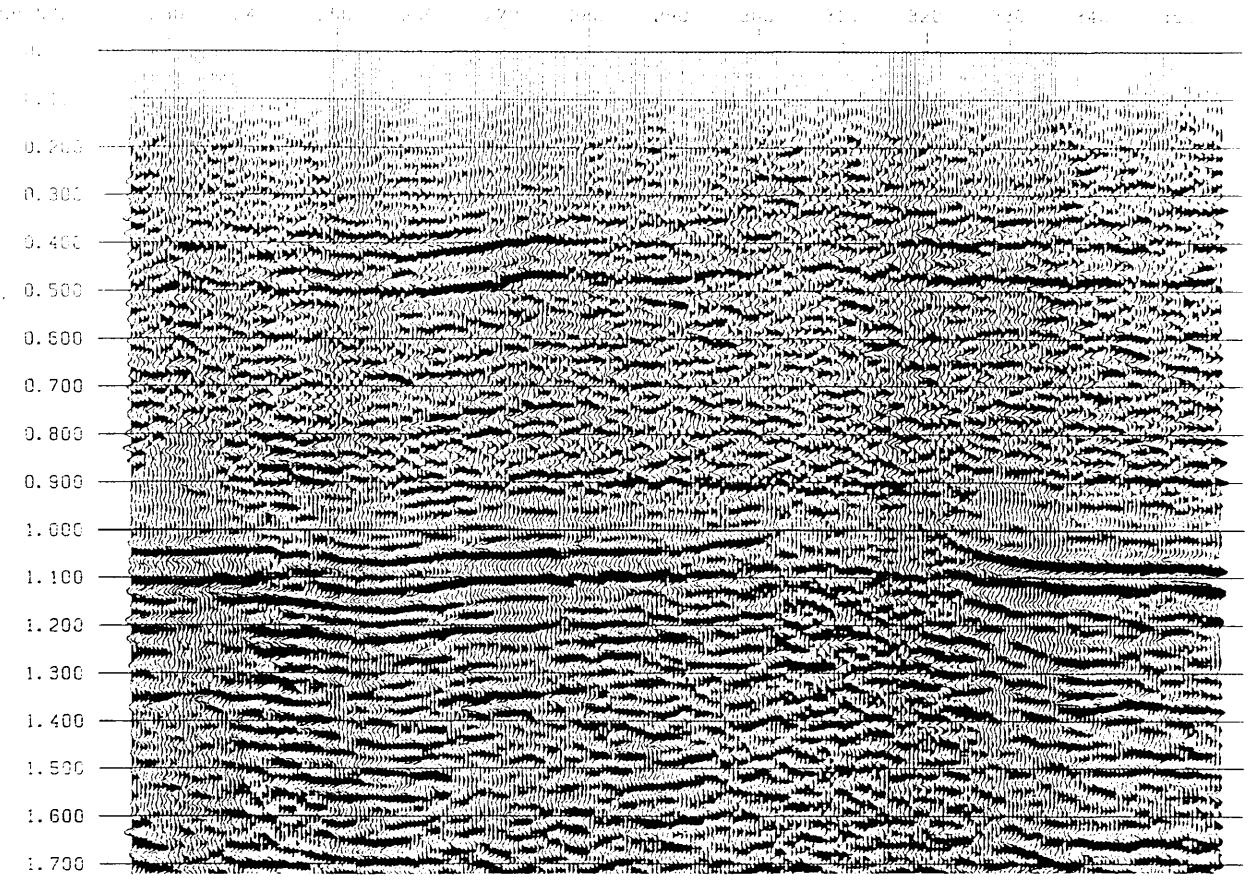

A

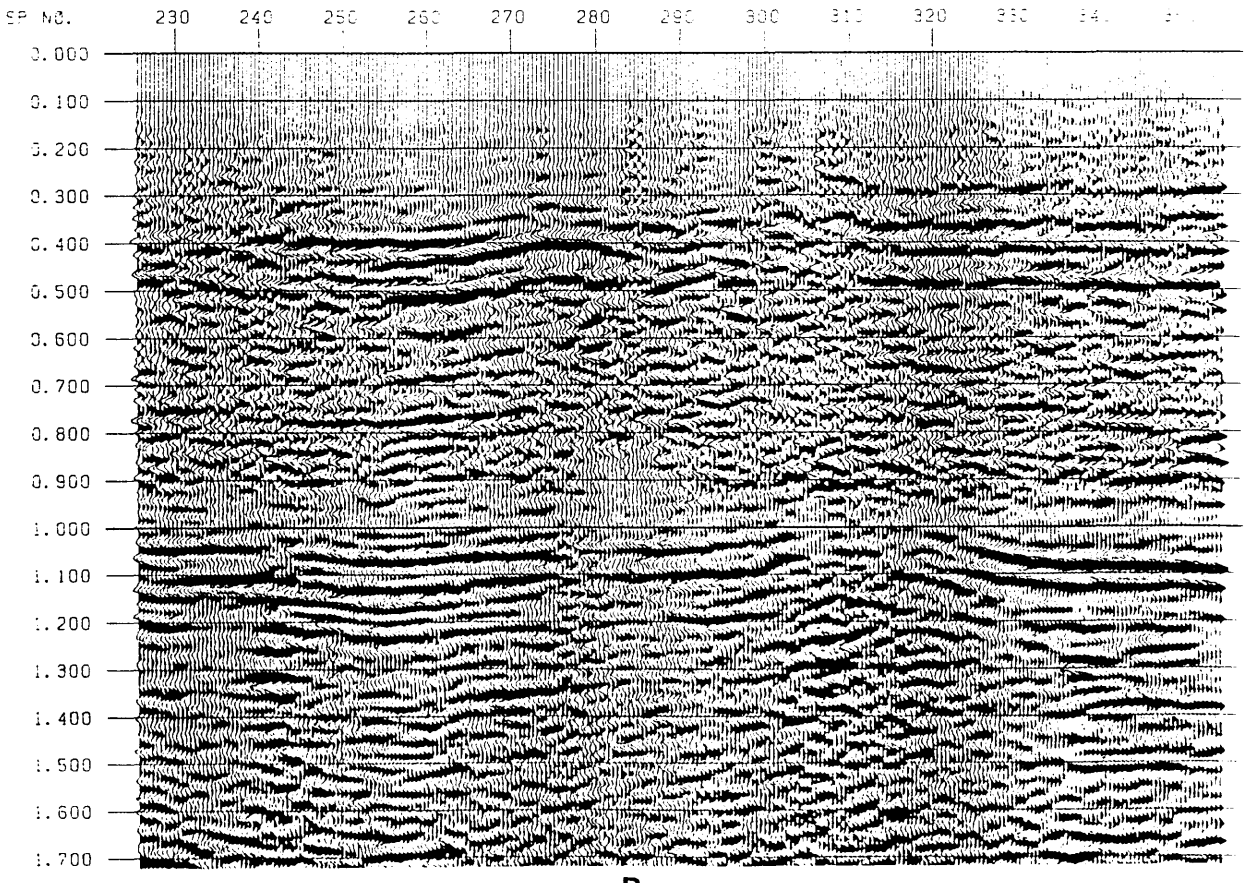

B

Fig.6.10 Brute stack sections, using "Equation" static correction of the; (a) first traces group; (b) second traces group.

6.9 *Residual static*

Residual statics are static corrections remaining after application of geometry statics. They are computed by the RSESTIM and RSCALCSC processors and are input to STATAPLY from a permanent disk file.

A reference section and the CDP gathered traces that were used to construct the reference section are input to the RSESTIM processor for residual statics. Individual CDP gathered traces are correlated with the reference trace that has the same CDP number. The cross-correlated output is then scanned for either the peak near to zero lag or the maximum peak value. The static picks that are output from the RSESTIM processor are stored in the SierraSEIS common ASTAT variable. The RSESTIM must be followed by the RSSAVE processor to save the information necessary for generating the surface-consistent solution.

6.10 *Deconvolution and filtering after stack*

The objective of deconvolution is to attenuate repetitive signals such as multiples and also to shape the propagating wavelet into a sharp high resolution pulse. The same kind of parameter tests mentioned in Section 6.4 have been repeated on the stacked section. New parameters have been chosen and applied to the data to produce the final section.

A frequency analysis made on the stacked traces shows the dominant frequencies of 12-45 Hz (Figure 6.4b). On the stacked sections, two different records from different places were filtered with a series of 10 Hz

wide band-pass filters. Figures 6.11 and 6.12 show a sequence of band-pass filter tests. The reflection signal on the 10 to 20 Hz panel exists down to about 2 s. On the 20 to 30 Hz panel, however, signal is still visible down to about 2 s. Moving to the higher frequencies panels, note that the signal level mainly is confined to increasingly shallower times. In general the data looks recognizable within the frequency band 12-45 Hz.

6.11 *Weighted stack*

Stacking using the arithmetic mean (straight stacking) does not maximize the S/N ratio of the stack if there are trace-to-trace variations in the S/N ratio. In this case, the S/N ratio of the stack is maximized by weighting each trace by its signal amplitude divided by its noise power, provided the noise is stationary (Anderson and McMechan 1990).

6.11.1 *Final section*

On the final stack, weighted traces have been used to improve the quality of the section. The data around the anomaly zone are still not good enough, and the discontinuity of the reflectors underneath the seismic anomaly is visible. Figures 6.13 and 6.14 show final unmigrated stacked sections for the data where "Equation" static correction have been applied (Figure 13a), the data where "Formula" static correction have been applied (Figure 13b), the first traces group of data where "Equation" static correction have been applied (Figure 14a), and the second traces group of data where "Equation" static correction has been applied (Figure 14b).

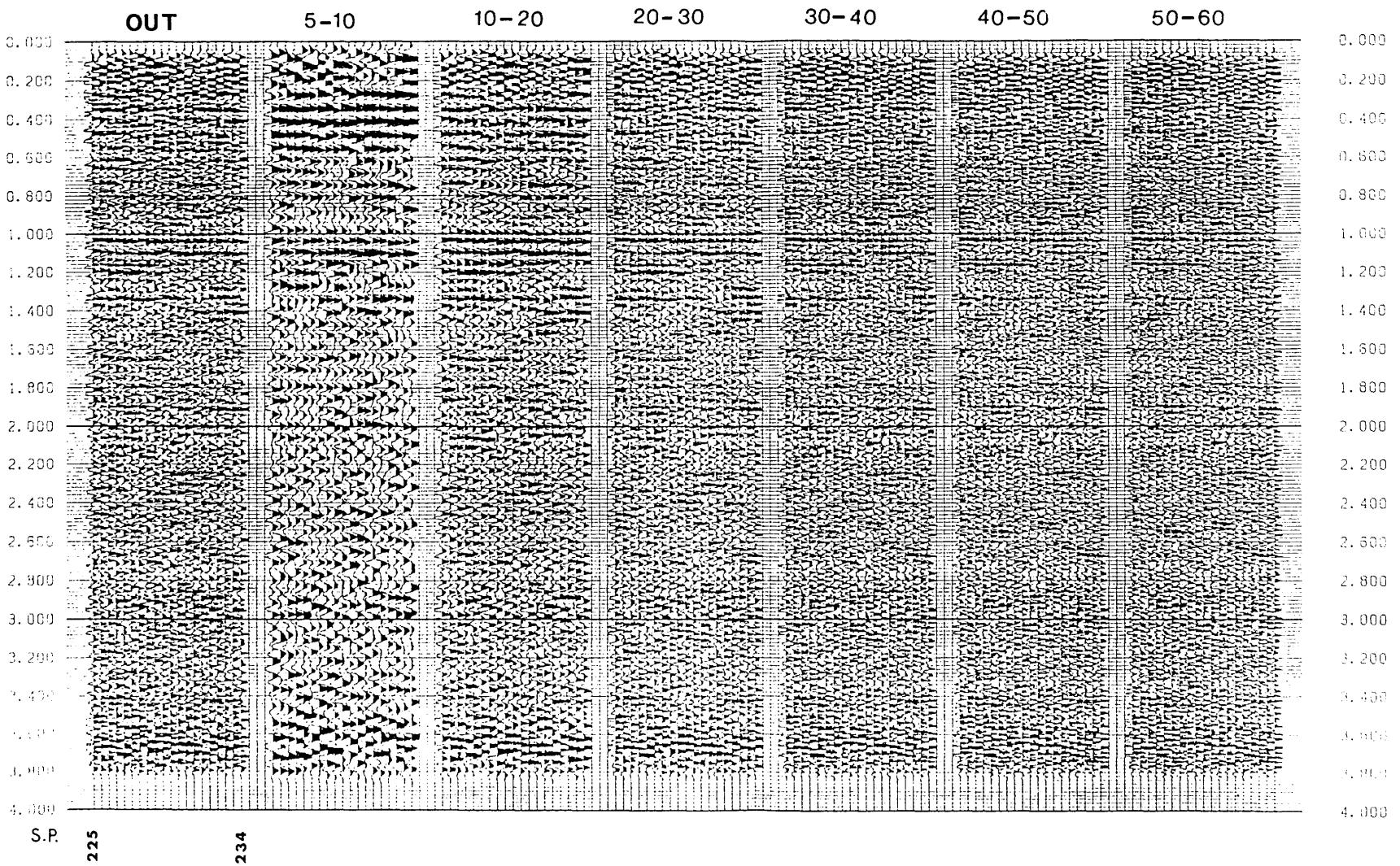

Fig.6.11 Stacked data (left panel) with its band-pass filtered versions.

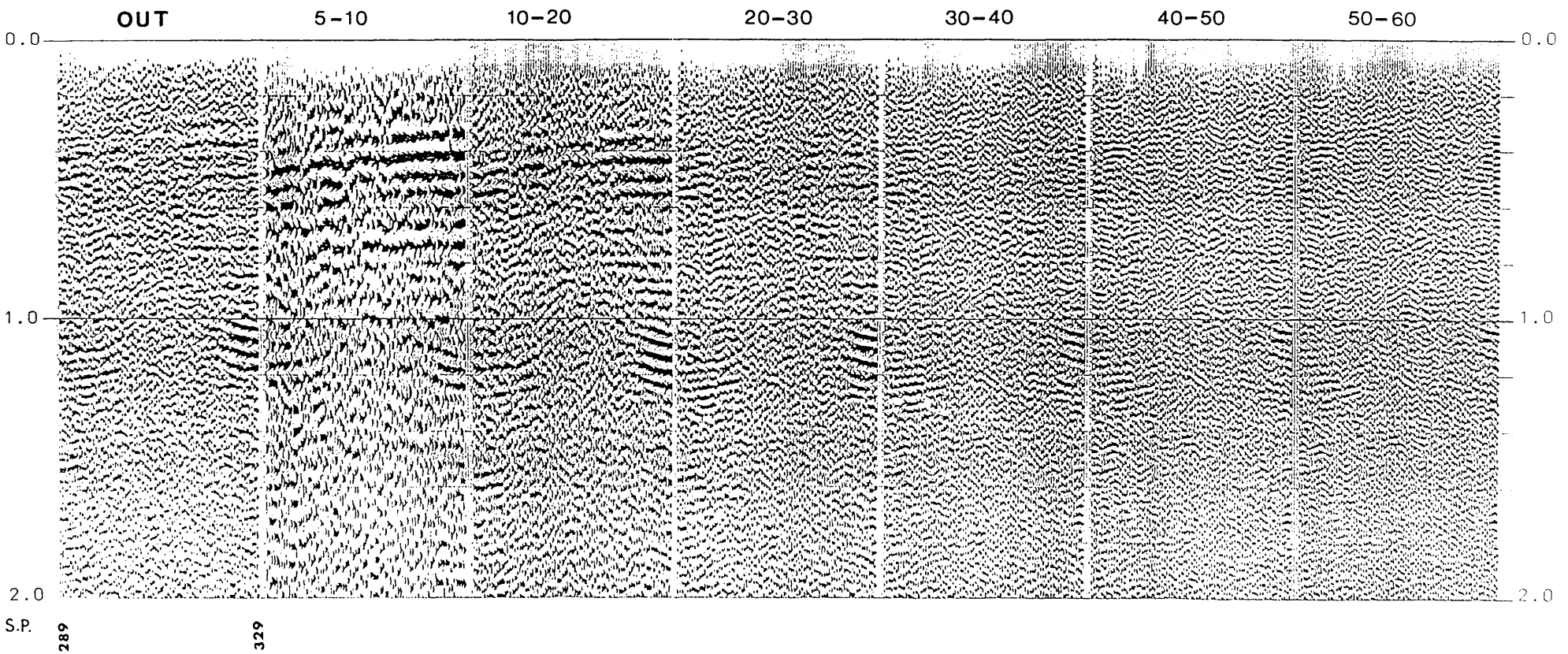

Fig.6.12 Stacked data (left panel) with its band-pass filtered versions.

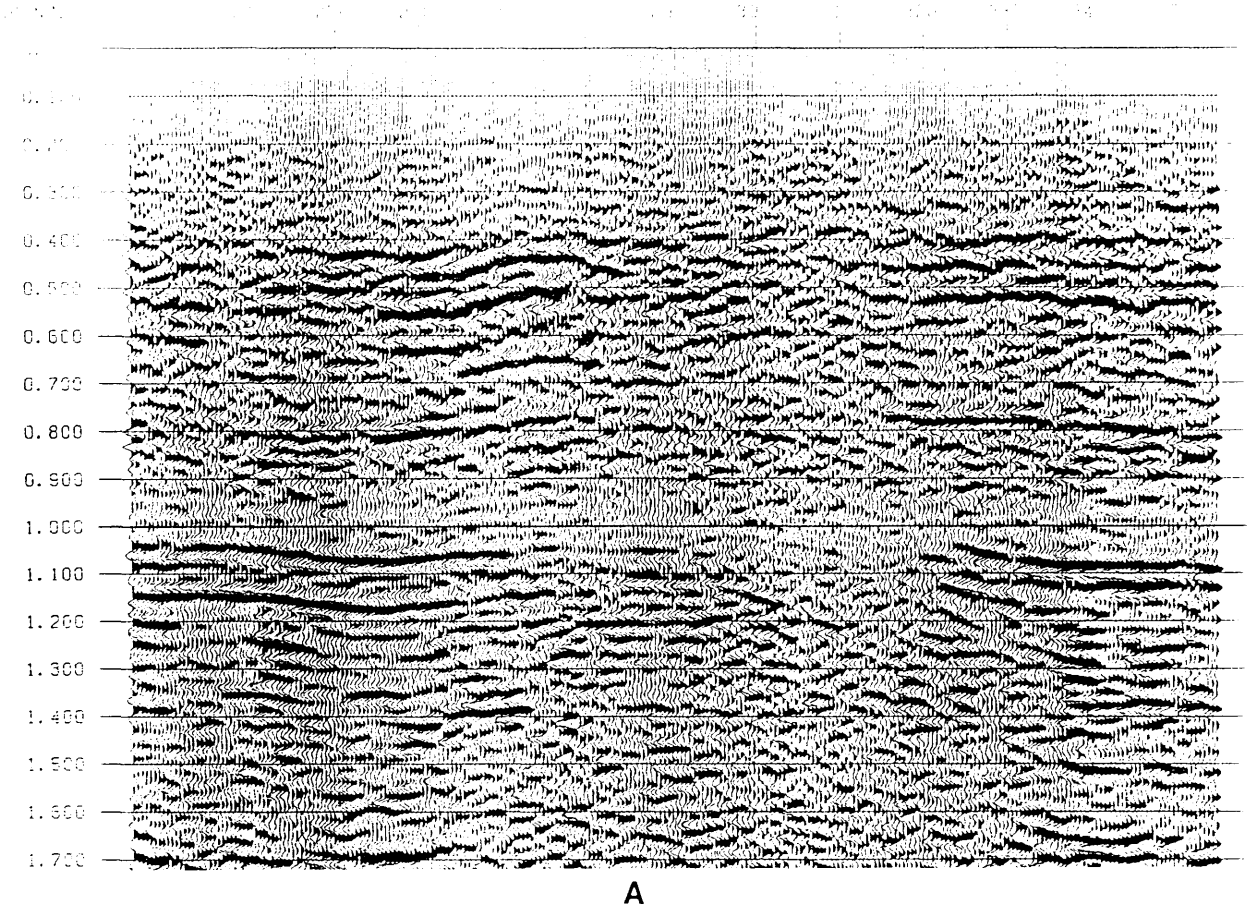

A

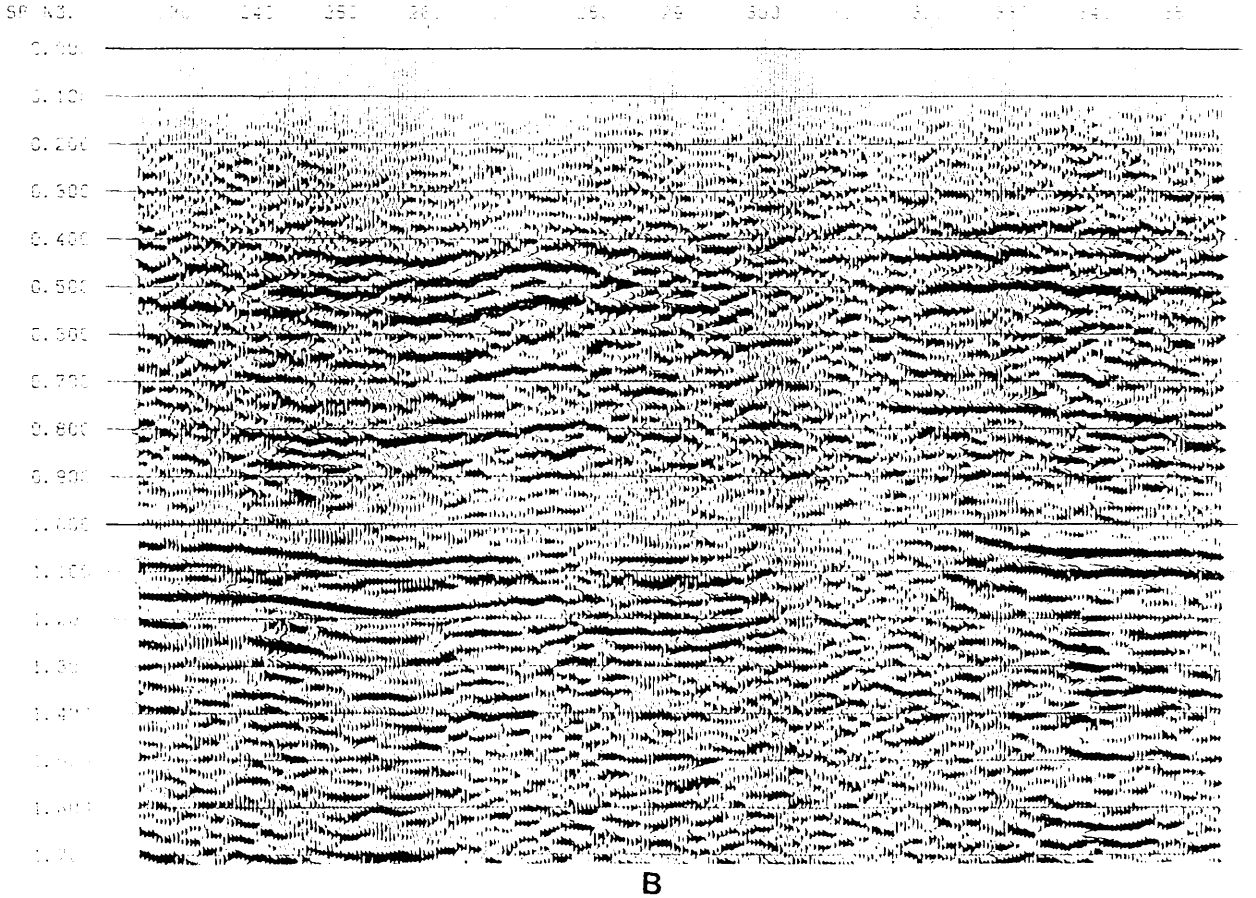

B

Fig.6.13 Final stack sections, using; (a) the "Equation" static correction
(b) the "Formula" static correction.

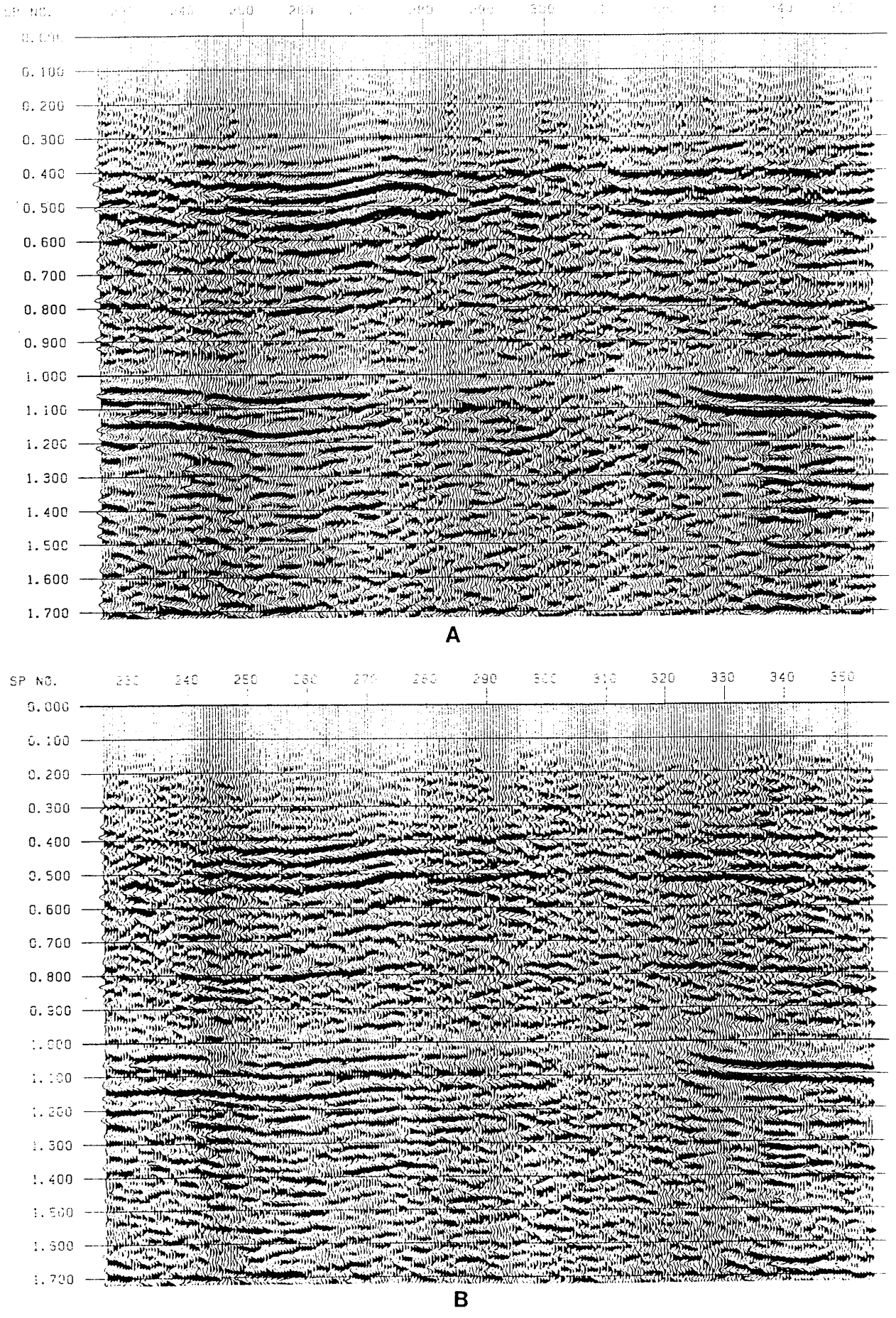

Fig.6.14 Final stack sections, using the "Equation" static correction of; (a) the second traces group; (b) the first traces group.

The time difference between the two applications of statics on the data on Figure 6.13 a and b, are apparent. Comparing the two sections of the two separated parts on Figure 6.14 a and b with the Figure 6.13a, the continuity of the reflectors looks good in the separate parts, especially in the shallow horizons.

6.11.2 *Undershooting technique*

Long in-line offsets are sometimes used where one cannot shoot and record over the desired region, perhaps because of structures, river levees, permit problems, etc.; this technique is called undershooting (Sheriff and Geldart, 1983). Such techniques are also useful where raypaths are so distorted by shallow features of limited extent that sense cannot be made of deeper events, as might be the situation in mapping underneath a salt-dome, reef or local region of very irregular topography or weathering (Sheriff and Geldart, 1983). This technique has been used on our data to see the effect of the seismic anomaly on the reflectors underneath. Different stacked sections have been produced of different offset groups to see the effect of the seismic anomaly on the continuity of the reflectors. Some of the middle offset groups stacked sections looks good and shows better continuity at 1.05 s. There are no shallow data on the sections produced, because of the far offsets used in stacking the data.

To produce a complete section, including the shallow data and the good data produced from the above technique, a sharp surgical mute at a combination of different offsets has been applied to the CDP gathers. It selects the shallow data from the near offset groups and deep data from the

good middle offset groups. Different surgical mutes have been tested. Figure 6.15 a and b shows two seismic sections for the first traces group of data and the second traces group of data, after the sharp surgical mute was applied. These seismic sections show better sections than the corresponding final stacked sections in Figure 6.14.

6.12 *Migration*

The goal of the migration process is to make the stacked section appear similar to the geological cross section along the seismic line. Ideally, we want to get a depth section from the stacked section. However, the migrated section commonly is displayed in time (Yilmaz 1987). The estimated velocity based on seismic and other data always is limited in accuracy. Therefore, depth conversion is not completely accurate. The effectiveness of migration is dependent on the use of accurate velocity control. Velocity that is too low will not migrate events far enough while too high a velocity will over-migrate the data.

Migration moves dipping reflectors into their true subsurface positions and collapses diffractions, thereby delineating detailed subsurface features such as fault planes (Yilmaz 1987). Figures 6.16a and 6.17a shows two stacked sections after migration of the same sections in Figure 6.13 a and b respectively, where the stacking velocity has been used in the migration. Figures 6.16b and 6.17b shows two migrated sections of the same sections in Figure 6.13 a and b respectively, where the stacking velocity increased by 10% has been used in the migration. The increase of the velocity by 10% of the stacking velocity does not affect the data. The finite-difference migration

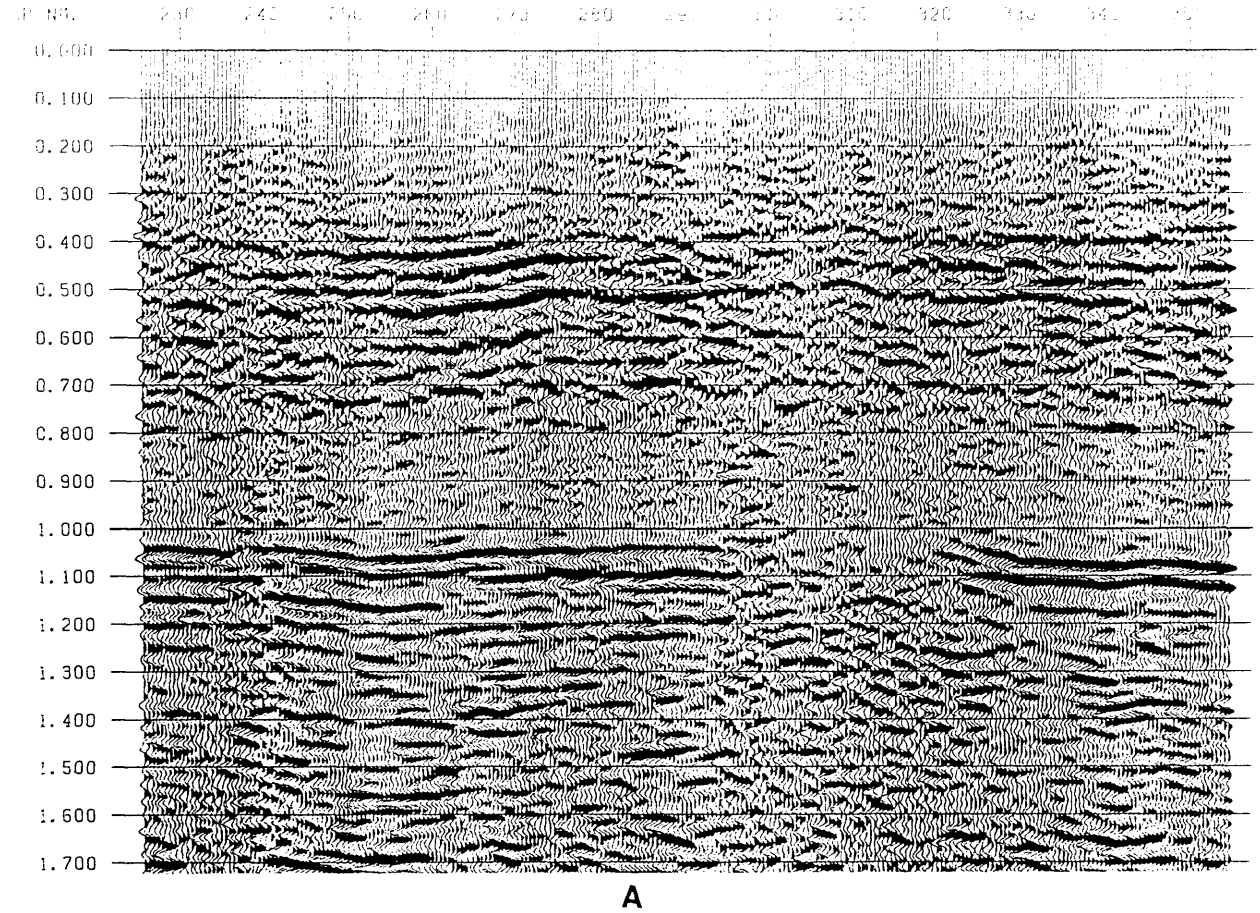

A

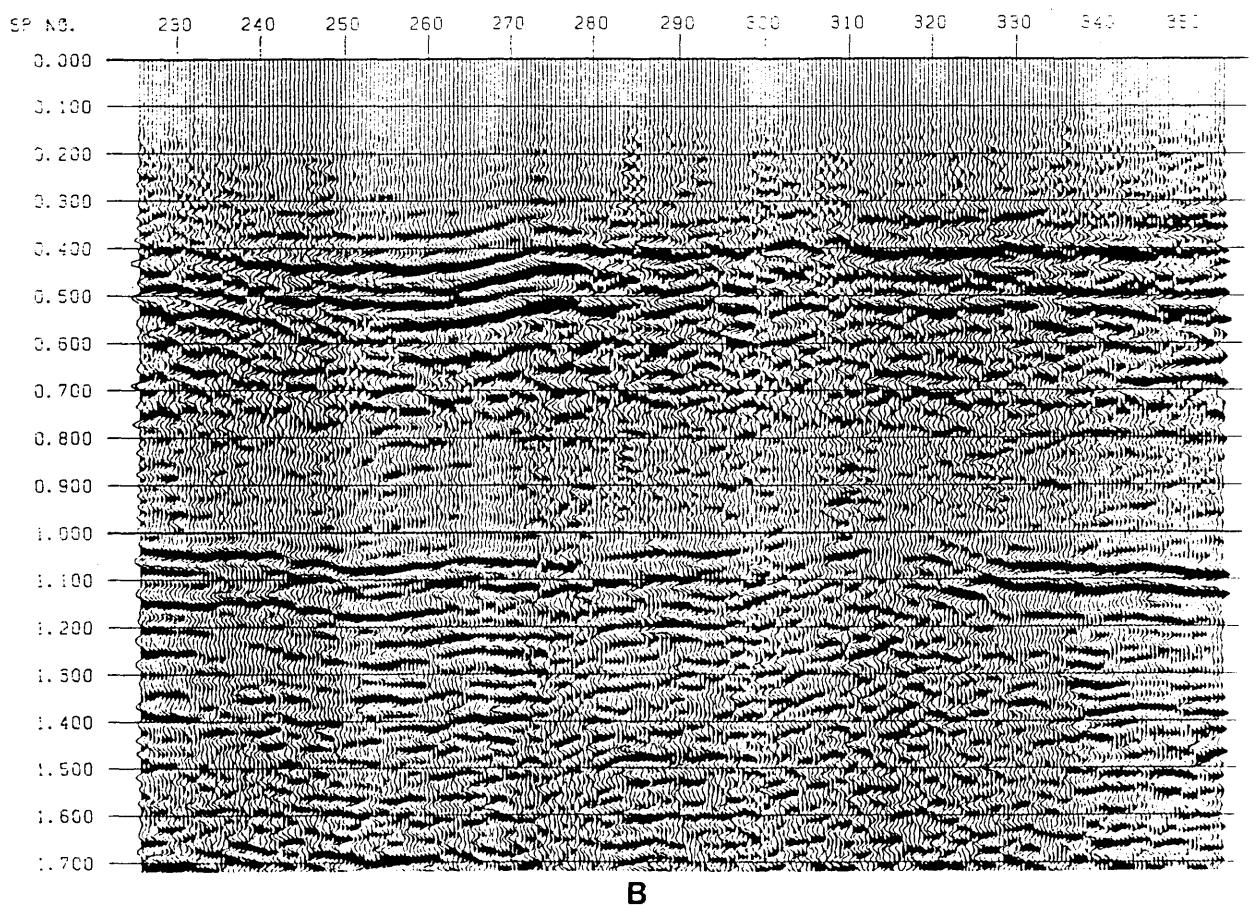

B

Fig.6.15 Final stack sections, using "Equation" static correction and sharp surgical mute of the ; (a) first traces group; (b) second traces group.

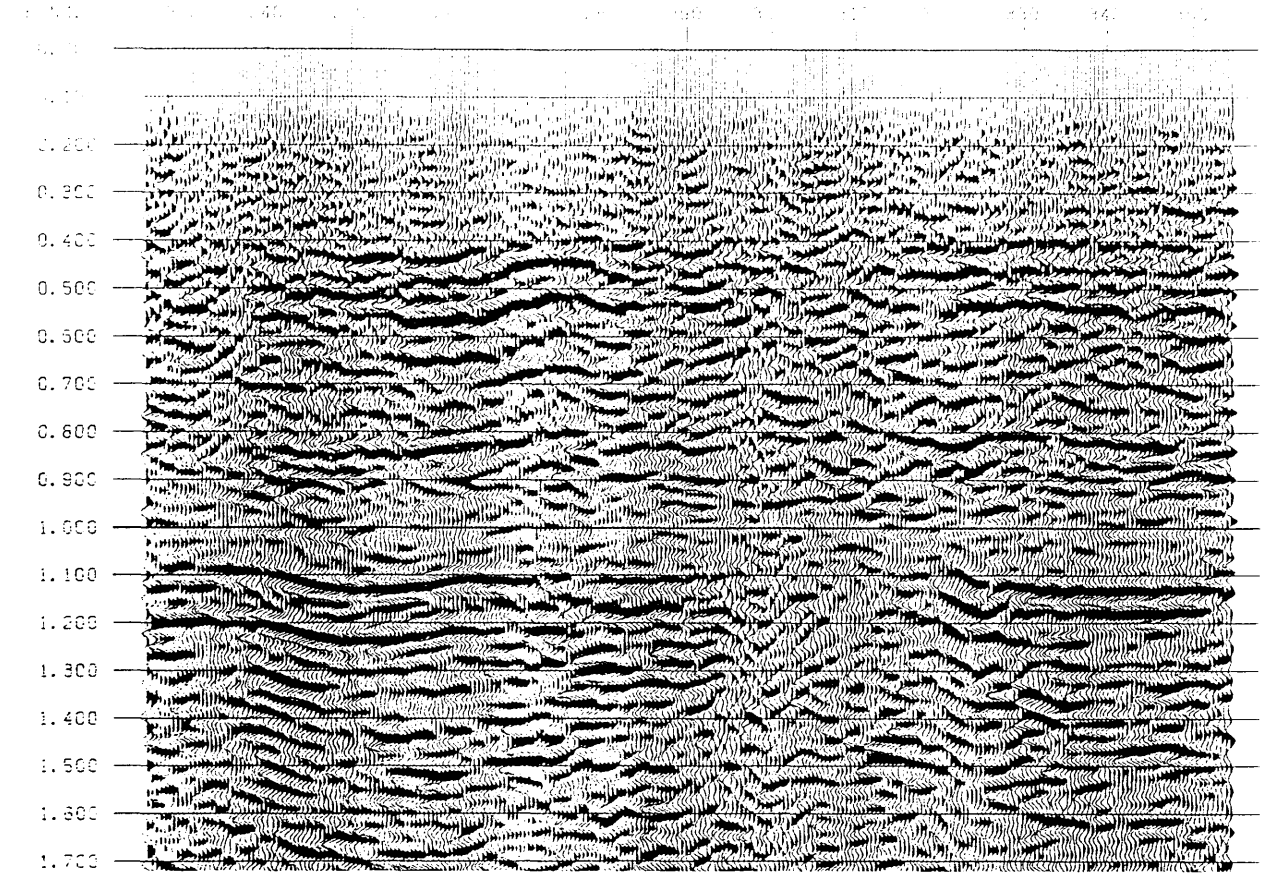

A

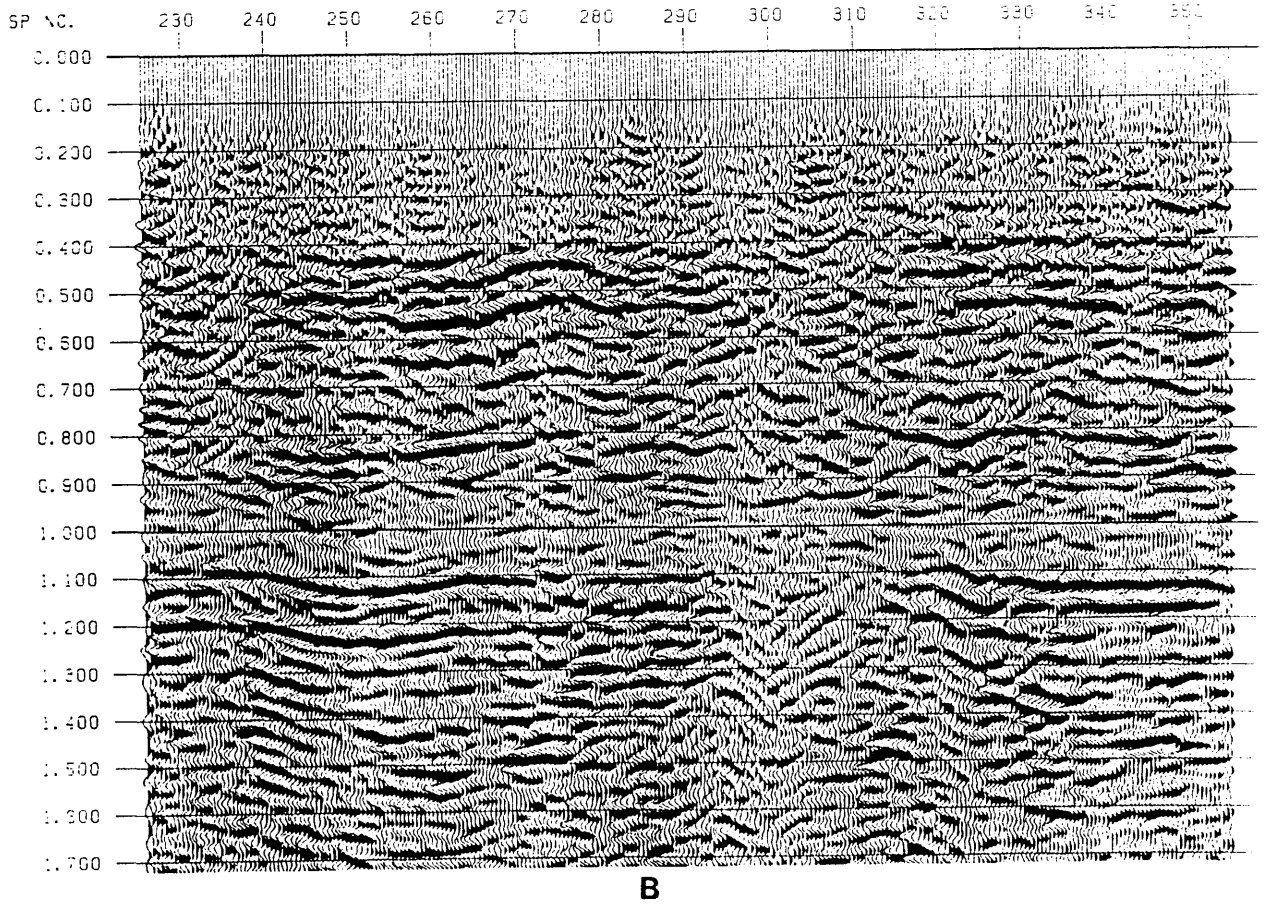

B

Fig.6.16 Time migration sections using "Equation" static correction and;
(a) using stacking velocity;
(b) using 10% higher than the stacking velocity.

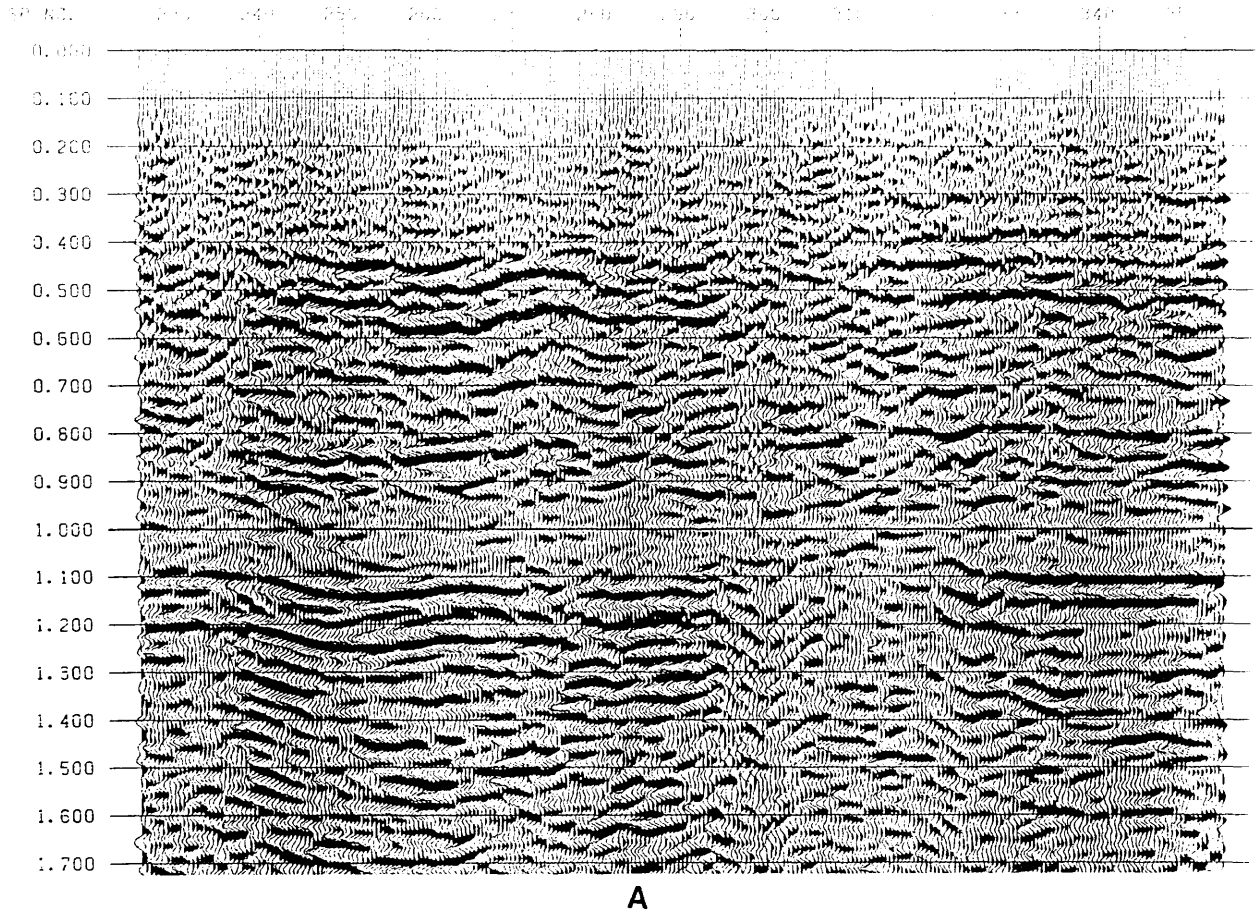

A

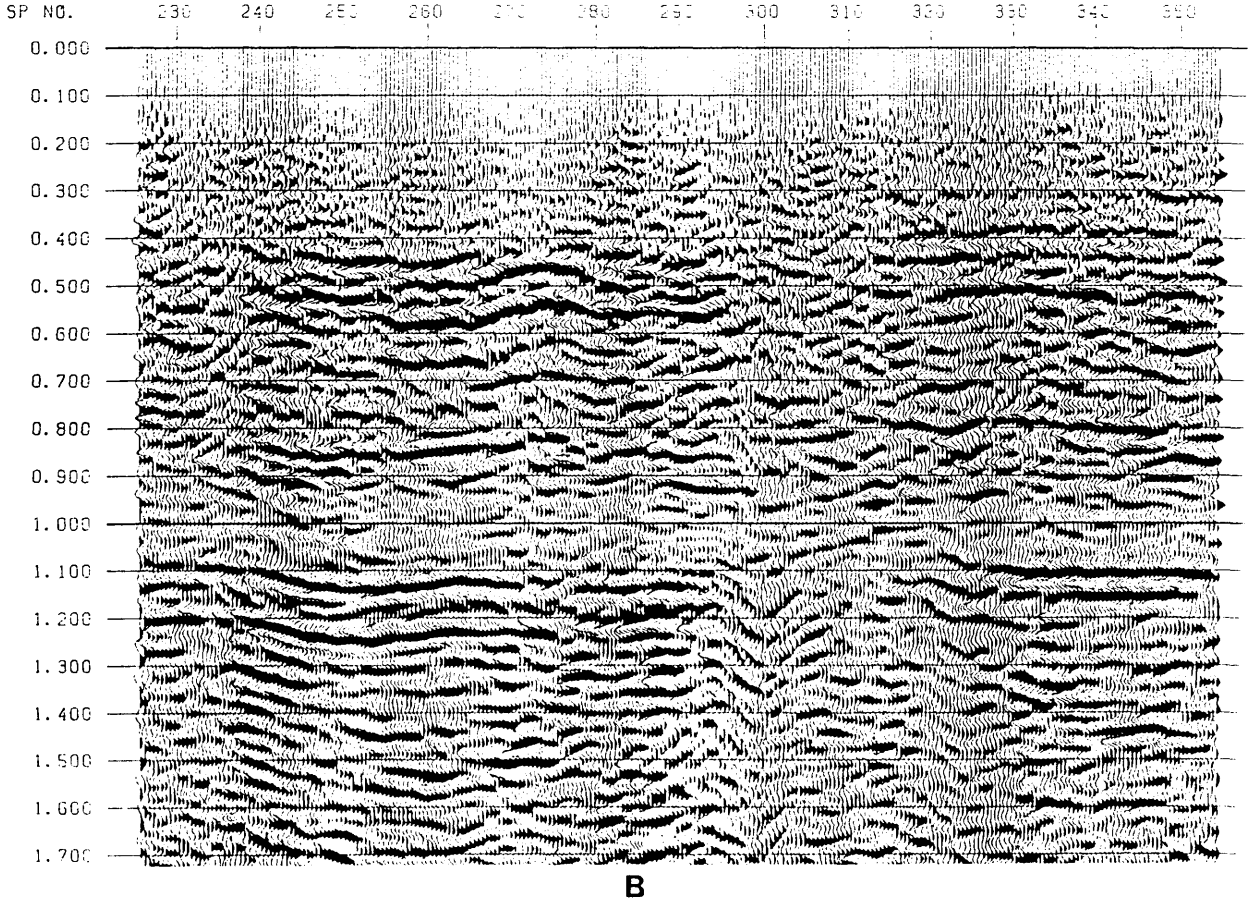

B

Fig.6.17 Time migration sections using "Formula" static correction and;
(a) using stacking velocity;
(b) using 10% higher than the stacking velocity.

method has been used to produce the migrated sections. Figure 6.18 shows the original stacked section processed by Western Geophysical Company in 1985. Figure 4.3 is an example of the Western processing. It also shows the location of the well GGGG1-6 at shot point 310. We can compare this section with the sections produced by the SierraSEIS software package. First, some structures appear in the new sections which have been flattened in the Western Geophysical section (Figure 6.18). Second, some continuity of the reflectors inside the anomaly zone were found in the new section (Figure 6.15b), but not in the Western Geophysical section (Figure 6.18). This difference may be due to the steps they used in the processing to align the horizons. This might allow us to re-interpret the seismic anomaly. The differenes between Western and our work are due to:-

(i) Western's automatic statics (Miser)

(ii) Differences in field statics

(iii) Differences in velocity analysis

Figure 6.19 shows a flowchart summarising the seismic reprocessing sequence. More details of the processing steps and the different parameters that have been used are given in Appendix 6.1.

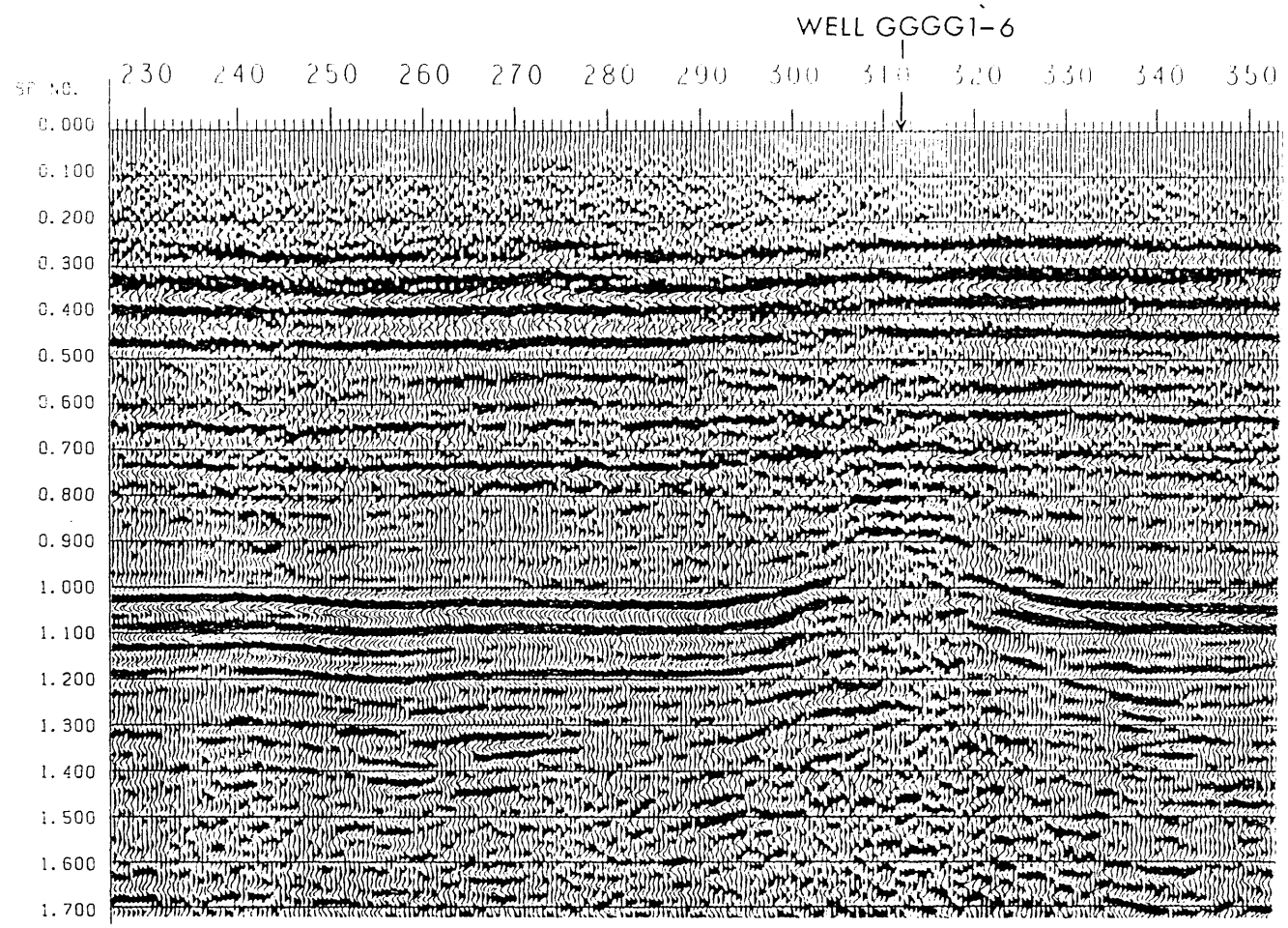

Fig.6.18 The original stacked seismic section, processed by Western Geophysical Company in 1985.

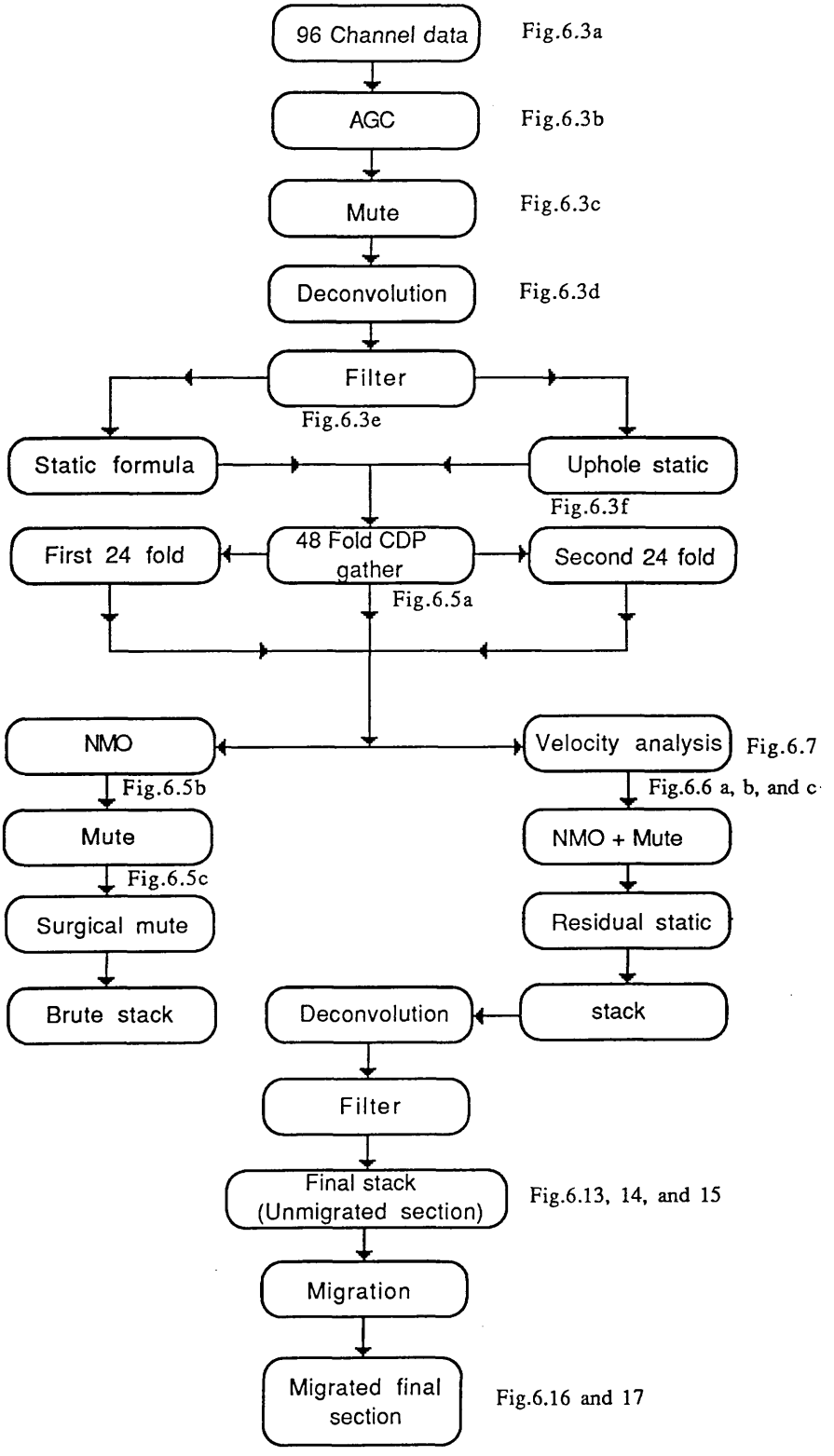

Figure 6.19 Flow-chart summarising the seismic reprocessing .

CHAPTER (7)

CONCLUSIONS

7.1 Conclusions

7.2 Suggestions and recommendations

7.1 *Conclusion*

The following points are the main conclusions which were derived from the work carried out in this project.

Some mistakes have been found in the data reports provided, compared with our program results (Chapter 1). A double check on the data reports provided should be carried out before any further use is made of them. Different sources of data in the same area have been interpreted by different persons, with different results, requiring a comparison and correlation of the results. Velocity surveys permitted identification of the horizons on the seismic sections for mapping and interpretation.

Analysis of the velocity tabulations on the seismic sections leads us to produce a number of velocity plots. Interpolated subsurface stacking velocity contour plots for the seismic lines are a good indication of the stacking velocity. It shows that the velocity picks used in the original processing are close to the geological boundaries.

From the statistical work which has been carried out on the velocity values (Chapter 3), relationships of velocity versus two-way time have been produced. In general, the line fitting equations resulting from subdivided zones look good and lead us to accept them.

Some relationships were represented in the Faust equation form, and the results may be used with the other new data in further work.

The percentage value for the difference in velocity (V_{stk}-V_{da}) relative to V_{da}, represented in the histogram form, shows strong groupings around 0% and 4% using all of the data. A change occurs in the subdivided zones, the data grouping around 0% in zone A, 2% and 5% in zone B, and 3% and 6% in zone C, zones A to C being from top to bottom, respectively. This indicates that there is a very small difference between the stacking velocity and the Dix average velocity in the shallow horizons, and then the stacking velocity is higher than the Dix average velocity by the percentage amount as we go deeper. These figures become clearer in the subdivided zones.

For shallow horizons the error in the converted depth using the stacking velocity is about 5 m, while for the deep horizons this error increases with depth and varies between 20-120 m.

The heterogeneity factor (H) calculated for our data in the subdivided zones A, B, and C varies between 0-1%, 2-10%, and 8-10%, respectively. It is fairly constant in zones A and C, but increases with depth in zone B.

With the geological knowledge of the area and well log analyses, we have a useful geological picture of the subsurface horizons. Manual contouring of the data produces a more realistic model than the one produced by automated contouring. This is because in manual contouring anomalous values can be neglected.

Computer contouring can cause a dense contouring at line intersections due to mis-ties. Any mis-ties should be corrected before storing the data in the computer for contouring. Mis-ties vary between -10 and +10 ms in two-way time, -100 and +100 m/s in velocity, and -40 and +30 m in depth.

The accuracy of the use of the DIGITAL program depends on the accuracy of the input data. These input data are dependent on the size of the grid used in the interpolating process before contouring. A grid size of 40 by 40 has been used in our data. As the grid size decreases more computer time is needed, but a more accurate dataset results. As the grid increases less computer time is needed, but a less accurate dataset is obtained. A minor change in the program code must be made to implement a grid.

The automated contouring created some false features at the ends of the seismic lines, because of unrealistic extrapolation of values by the computer. No interpretation was made in the areas where this happened. All the two-way time maps show a general dip towards the northeast. Each horizon velocity map shows little change. The isochron contour maps shows the thinning in the locations where the seismic anomaly is found. The same is found in the isopach contour maps in term of time.

High values found on the Domran interval velocity at the well GGGG1-6 location (Fig. 2.27), and on the Domran interval velocity contour map around the well GGGG1-6 (Fig. 4.34), might be the cause of the pull-up of deeper reflectors. The two-way time contour maps produced after digitising the time contour maps based on seismic data interpretation show

similarity to those produced by direct contouring, and are smoother. This proves that the processing and DIGITAL program work well.

The difference in static correction between the formula and the uphole static varied between 0 and -50 ms in the Lehib area and between 0 and 50 ms in the Sabkha area. Reflectors are shifted down in the first case and up in the second.

Small lateral velocity variation results from the velocity analysis in the Chapter 6, in the area of flatter subsurface horizons, increase in the area above the seismic anomaly.

Velocity function analysis applied to the CDPs and the velocity spectrum gave a good NMO velocity indicator. From the velocity analysis made and stacked sections produced, the static shift mentioned above has been recognized and detected.

Undershooting demonstrated that reflector continuity underneath the anomaly could be preserved.

Finally the investigations of the reef anomaly is proved that the anomaly it is purely a geophysical artefact (false time anomaly) and it is not a real geological feature. The presence of a false time anomaly above the GGGG1-6 well location is now believed to be due to the presence of the high interval velocity in the Domran formation (velocity pull-up) at the well location, while the other wells do not show any change in velocity at the same formation.

7.2 *Suggestions and recommendations*

The following is a summary of the suggestions and recommendations:

(1) Eight additional seismic lines were shot in between the seismic lines used in this study, and should be added to complete the study.

(2) It would be possible to extend the work into the area south of the Zelten field by including more seismic lines available in that area and so cover the Jabel field.

(3) More well data about the formation tops are available in the area and should be included in any further study, to improve the results of the present study and to find any link between the parameters.

(4) The reprocessing was not fully completed due to lack of time. So more work is needed to improve the quality of the seismic section produced in this study.

(5) Further investigations should consider the anomaly using the same reprocessing steps.

References

Al-Chalabi, M. 1974. An analysis of stacking, rms, average, and interval velocities of a horizontally layered ground. *Geophysical Prospecting* **22**, 458-475.

Ala, M. A. 1985. Applied structural geology and subsurface mapping. Unpublished seminar, Grand hotel, Tripoli.

Badley, M.E. 1985. Practical seismic interpretation. International Human Resources Development Corporation.

Bebout, D. G. and Pendexter, C. 1975. Secondary carbonate porosity as related to Early Tertiary depositional facias, Zelten field, Libya. *American Association of Petroleum Geologists Bulletin* **59**, 665-693.

Benfield, A. C. and Wright, E. P. 1978. Post-Eocene sedimentation in the eastern Sirte Basin, Libya. In: 2nd symp. Geol. Libya (Ed. by M. J. Salem and M. T. Busrewil). Fac. Sci., Univ. Libya, Tripoli, v. II, 464-499.

Bonnefous, J. 1972. Geology of the quartzitic "Gargaf Formation" in the Sirte Basin, Libya. *Bulletin du Centre de Recherches de Pau.* **6**, 225-261.

Conant, L.C. and Goudarzi, G.H. 1967. Stratigraphic and tectonic framework of Libya. *American Association of Petroleum Geologists Bulletin* **51**, 719-730.

Dix, C.H. 1955. Seismic velocities from surface measurements. *Geophysics* **20**, 68-86.

Dobrin, M.B. and Savit, C.H. 1988. Introduction to geophysical prospecting (fourth edition). Mc Graw-Hill Book Company.

El-Hawat, Ahmed S. 1978. Carbonate-terrigenous cyclic sedimentation and palaeogeography of the Marada formation (Middle Miocene), Sirte Basin. In: 2nd symp. Geol. Libya (Ed. by M. J. Salem and M. T. Busrewil). Fac. Sci., Univ. Libya, Tripoli, v. II, p 426-448.

Espey, H.R. 1983. Effective seismic data processing. Unpublished seminar, Crest hotel, Maidenhead, England.

Faust, L.Y. 1951. Seismic velocity as a function of depth and geological time. *Geophysics* **16**, 192-206.

Gumati, Y. D. and Kanes, W. H. 1985. Early Tertiary subsidence and sedimentary facies-northern Sirte Basin, Libya. *American Association of Petroleum Geologists Bulletin* **69**, 39-52.

Hatton, L., Worthington, M.H., and Makin, J. 1986. Seismic data processing (Theory and practice). Blackwell Scientific Publications.

Isaaks, E.H. and Srirastava, R.M. 1989. An introduction to applied Geostatistics. Oxford University Press, Inc.

Kearey, P. and Brooks, M. 1991. An introduction to geophysical exploration (second edition). Blackwell Scientific Publications.

Klemme, H.D. 1980. Petroleum Basins - classifications and characteristics. *Jour. Pet. Geol.* **3**, 187-207.

Levin, F.K. 1971. Apparent velocity from dipping interface reflections. *Geophysics* **36**, 510-516.

McQuillin, R., Bacon, M., and Barclay, W. 1979. An introduction to seismic interpretation. Graham & Trotman Limited.

Montalbetti, J.F. 1971. Computer determination of seismic velocities - a review. *Journal of the Canadian Society of Exploration Geophysics* **7**, 32-45.

Pickett, G.R. 1969. Principles for application of borehole measurements in Petroleum engineering. *Log Anal.* May-June, 22-33.

Selley, R.C. 1968. Facies profile and other new methods of graphic data presentation: application in a quantitative study of Libyan Tertiary shoreline deposits. *J. Sediment. Petrology* **38**, 363-372.

Shah, P.M. 1973. Use of wave front curvature to relate seismic data with subsurface parameters. *Geophysics* **38**, 812-825.

Sheriff, R.E. 1978. A first course in Geophysical exploration and interpretation. International Human Resources Development Corporation.

Sheriff, R.E. 1980. Seismic stratigraphy. International Human Resources Development Corporation.

Sheriff, R.E. and Geldart, L.P. 1983. Exploration Seismology. Volume (1), history, theory & data acquisition. Cambridge University Press.

Stulken, E.J. 1941. Seismic velocities in the southeastern San Joaquin valley of California. p. 327-355.

Suringa, R. 1988. Concession 6 north Nasser ("Mashinsky") time anomalies. Unpublished report (Sirte Oil Company).

Van Houten, F. B. 1980. Latest Jurassic-Early Cretaceous regressive facies, northeast Africa craton. *American Association of Petroleum Geologists Bulletin* **64**, 857-867.

Waters, K.H. 1978. Reflection seismology (a tool for energy resource exploration). John Wiley & Sons, Inc.

Wyllie, M.R., Gregory, A.R., and Gardner, G.H.F. 1958. An experimental investigation of factors affecting elastic wave velocities in porous media. *Geophysics* **23**, 459-493.

Yilmaz, O. 1988. Seismic data processing. (Investigation in Geophysics, Volume 2). Society of Exploration Geophysicists.

APPENDICES

Appendix 2.1

FORTRAN - 77 PROGRAM 3 CVL

```
c     ********************************************************************************
c     This program is design for the data from wells which have the continuous velocity log.
c     VAX/UNIX: CVL
c     Written by
c     Ben Ayad N.M.
c     at the department of Geology&Applied Geology.
c     University of Glasgow, Glasgow G12 8QQ (in June 1991)
c     This program calculates the average, interval, and rms velocities for those wells.
c     ********************************************************************************
c     PROGRAM CVL.F
      DIMENSION  ALAT(20), ALONG(20), AKB(20), STATIC(20), GL(20)
     *          , DD(20,20), ST(0:20,20),SD(0:20,20), SEAD(20,20)
     *          , SEAT(20,20), DELTAD(20,20), DELTAT(20,20), ICC(20)
     *          , VINT(20,20), VBAR(20,20), VRMS(20,20), WELL(20)
      CHARACTER *11 INDATA1, INDATA2*11, OUT1*11
      PRINT*," PRINT THE INPUT FILE NAME AS ( CVL.DATA ) "
      PRINT*," WHICH CONTAINING THE COMPUTER COMPANY CODE, "
      PRINT*," DRILLING DEPTH, AND TIME CORRESPONDING TO THE DEPTH "
      READ *, INDATA1
      PRINT*," PRINT THE INPUT FILE NAME AS ( CVL.DATA2 ) "
      PRINT*," WHICH CONTAINING THE WELL NAME, LATITUDE, LONGITUDE, "
      PRINT*," KELLY BUSHING ELEVATION, STATIC, AND GROUND LEVEL ELEVATION '
      READ *, INDATA2
      PRINT*," PRINT THE OUTPUT FILE NAME AS ( OUT.CVL ) "
      PRINT*," WHICH WILL CONTAINING THE RESULTS "
      READ *, OUT1
            OPEN ( 1, FILE = INDATA1 )
            OPEN ( 2, FILE = INDATA2 )
            OPEN ( 3, FILE = OUT1 )
c     I       - Counter for well data.
      DO 100 I = 1, 5
c     WELL    - Well name.
c     ALAT    - Latitude of the well.
c     ALONG   - Longitude of the well.
```

```
c       AKB     - Elevation of the kelly bushing.
c       STATIC  - Static correction.
c       GL      - Ground level elevation.
        READ (2,120) WELL(I), ALAT(I), ALONG(I), AKB(I), STATIC(I), GL(I)
100     CONTINUE
c       I       - Counter for the formations.
        DO 200 I = 1, 12
c       ICC     - Company computer code.
c       DD      - Drilling depth.
c       ST      - Time corresponding to the DD.
        READ (1,110) ICC(I), ( DD(I,J), ST(I,J), J = 1, 5 )
200     CONTINUE
c       J       - Counter for well data.
        DO 300 J = 1, 5
c       I       - Counter for formation.
        DO 400 I = 1, 12
              IF ( DD(I,J) .EQ. 0 ) THEN
c       SD      - Subsurface depth.
c       SEAD    - Subsea depth.
c       SEAT    - Subsea time.
                        SD(I,J)   = 0.0
                        SEAD(I,J) = 0.0
                        SEAT(I,J) = 0.0
              GO TO 111
        ELSE
                        SD(I,J)   = DD(I,J) - ( AKB(J) - GL(J) )
                        SEAD(I,J) = AKB(J) - DD(I,J)
                        SEAT(I,J) = ST(I,J) - ( STATIC(J)*2 )
111     PRINT*,"
        END IF
400     CONTINUE
300     CONTINUE
c       J       - Counter for the well data.
        DO 500 J = 1, 5
             ST(0,J) = 0.0
             SD(0,J) = 0.0
                N = 0
```

```
c       I         - Counter for the formation.
        DO 600 I = 1, 12
              IF ( ST(I,J) .EQ. 0 ) THEN
c       DELTAD          - Difference in depth.
c       DELTAT          - Difference in time.
c       VINT    - Interval velocity.
c       VBAR    - Average velocity.
                                    N  = N + 1
                          DELTAD(I,J)  = 0.0
                          DELTAT(I,J)  = 0.0
                          VINT(I,J)    = 0.0
                          VBAR(I,J)    = 0.0
              GO TO 222
        ELSE
                             II  = I - 1 - N
                   DELTAD(I,J)  = SD(I,J) - SD(II,J)
                   DELTAT(I,J)  = ST(I,J) - ST(II,J)
                   VINT(I,J)    = ( DELTAD(I,J) / DELTAT(I,J) )*2*1000.0
                   VBAR(I,J)    = ( SD(I,J) / ST(I,J) )*2*1000.0
                         N      = 0
222     PRINT*,"
        END IF
600     CONTINUE
c       SUMT    - Summation of the interval time.
c       SUMVT   - Summation of the product of the velocity and time.
                    SUMT   = 0.0
                    SUMVT  = 0.0
c       I         - Counter for formation code.
        DO 700 I = 1, 12
              IF ( DELTAT(I,J) .EQ. 0 ) THEN
c       VRMS    - Root mean square velocity.
                          VRMS(I,J)  = 0.0
              GO TO 333
        ELSE
c       SQRT    - Square root function.
              SUMT      = SUMT + DELTAT(I,J)
              SUMVT     = SUMVT + (DELTAT(I,J)*VINT(I,J)**2 )
```

```
            VRMS(I,J)  = SQRT ( SUMVT / SUMT )
333     PRINT*,"
        END IF
        WRITE (3,130) ICC(I), DD(I,J), SD(I,J), ST(I,J), SEAD(I,J), SEAT(I,J), DELTAD(I,J)
     *              , DELTAT(I,J), VINT(I,J), VBAR(I,J), VRMS(I,J)
700     CONTINUE
500     CONTINUE
110     FORMAT ( I2 , 10F5.0 )
120     FORMAT( A7 , 2F7.0 , F4.0 , F6.1 , F4.0 )
130     FORMAT ( I2 , 2X , F6.0 , 3X , F6.0 , 3X , F5.0 , 3X , F7.0 , 3X , F5.0 , 3X ,
     *          F5.0 , 3X , F4.0 , 3X , F7.0 , 3X , F6.0 , 3X , F6.0 )
        STOP
        END


        FORTRAN - 77  PROGRAM  4  CVL3
c       ********************************************************************************
c       This program is design for the data from wells which have the continuous velocity log.
c       VAX/UNIX: CVL3
c       Written by
c       Ben Ayad N.M.
c       at the department of Geology&Applied Geology.
c       University of Glasgow, Glasgow G12 8QQ (in June 1991)
c       This program calculates the average, interval, and rms velocities for those wells.
c       ********************************************************************************
c       PROGRAM  CVL3.F
        DIMENSION  D(50,10), T(50,10), VA(50,10), VI(50,10)
     *           , DD(50,10), DT(50,10), NS(10)
        CHARACTER *11  INDATA1, OUT1*11
        PRINT*," PRINT THE FILE NAME AS ( CVL3.DATA )"
        READ *, INDATA1
        PRINT*," PRINT THE FILE NAME AS ( OUT3.CVL )"
        READ *, OUT1
                OPEN ( 1, FILE = INDATA1 )
                OPEN ( 3, FILE = OUT1 )
c       J       - Counter for the well data.
        DO  100  J = 1, 6
```

```
c       NS      - Number of picked levels.
        READ (1,*)  NS(j)
c       I       - Counter for the levels.
        DO  200  I = 1, NS(j)
c       D       - Depth of the corresponding level.
c       T       - Time of the corresponding depth.
c       VA      - Average velocity.
                READ (1,110)  D(I,J),  T(I,J)
                VA(I,J) = D(I,J) / T(I,J)
200     CONTINUE
100     CONTINUE
c       I       - Counter for the well data.
        DO  400  I = 1, 6
c       J       - Counter for the picked levels.
        DO  300  J = 1, NS(I) - 1
c       DD      - Difference in depth.
c       DT      - Difference in time.
c       VI      - Interval velocity.
                        DD(J,I)  = D(J+1,I) - D(J,I)
                        DT(J,I)  = T(J+1,I) - T(J,I)
                        VI(J,I)  = DD(J,I) / DT(J,I)
                WRITE (3,120)  D(J,I),  T(J,I),  VA(J,I),  VI(J,I)
                WRITE (3,120)  D(J+1,I),  T(J+1,I),  VA(J+1,I),  VI(J,I)
300     CONTINUE
400     CONTINUE
110     FORMAT ( F5.0 , F7.4 )
120     FORMAT ( F8.1 , 2X , F6.4 , 2X , 2F8.1 )
        STOP
        END
```

Appendix 2.2

Table 2.1. Geological and Geophysical tops report.

Well name : C114-6

K.B.elevation : 187.5 m. G.L.elevation : 182.9 m.
Location on line : 6V261-85 Shot point : 150
One-way receiver static : 142.5 ms.

C.C.	Drill. depth	Subsur. depth	Subsur. time	Subsea depth	Subsea time	Iso-pach	Iso-chron	Interval velocity	Average velocity	R.M.S. velocity
1	398.	394.	458.	-211.	173.	394.	458.	1721.	1721.	1721.
2	655.	651.	670.	-468.	385.	257.	212.	2421.	1943.	1970.
3	699.	694.	704.	-511.	419.	44.	34.	2564.	1973.	2003.
4	1197.	1193.	970.	-1010.	685.	498.	266.	3747.	2459.	2600.
5	1641.	1637.	1176.	-1454.	891.	444.	206.	4312.	2784.	2972.
6	1748.	1743.	1226.	-1561.	941.	107.	50.	4267.	2844.	3036.
7	2129.	2125.	1412.	-1942.	1127.	382.	186.	4103.	3010.	3197.
8	2314.	2310.	1524.	-2127.	1239.	185.	112.	3298.	3031.	3204.
9	0.	0.	0.	0.	0.	0.	0.	0.	0.	0.
10	2324.	2319.	1530.	-2136.	1245.	9.	6.	3150.	3032.	3204.
11	2429.	2425.	1596.	-2242.	1311.	106.	66.	3205.	3039.	3204.
12	0.	0.	0.	0.	0.	0.	0.	0.	0.	0.

Table 2.2. Geological and Geophysical tops report.

Well name : C59-6

K.B.elevation : 189.3 m. G.L.elevation : 185 m.
Location on line : 6V264-85 Shot point : 385
One-way receiver static : 132 ms.

C.C.	Drill. depth	Subsur. depth	Subsur. time	Subsea depth	Subsea time	Iso-pach	Iso-chron	Interval velocity	Average velocity	R.M.S. velocity
1	419.	415.	476.	-230.	212.	415.	476.	1743.	1743.	1743.
2	640.	636.	636.	-451.	372.	221.	160.	2762.	2000.	2048.
3	680.	676.	674.	-491.	410.	40.	38.	2117.	2006.	2052.
4	1195.	1191.	966.	-1006.	702.	515.	292.	3524.	2465.	2587.
5	1683.	1679.	1222.	-1494.	958.	489.	256.	3817.	2748.	2888.
6	1788.	1783.	1278.	-1598.	1014.	104.	56.	3723.	2791.	2930.
7	2103.	2098.	1396.	-1913.	1132.	315.	118.	5337.	3006.	3204.
8	2345.	2340.	1488.	-2155.	1224.	242.	92.	5261.	3146.	3368.
9	0.	0.	0.	0.	0.	0.	0.	0.	0.	0.
10	2361.	2356.	1494.	-2171.	1230.	16.	6.	5385.	3154.	3378.
11	2430.	2425.	1520.	-2240.	1256.	69.	26.	5299.	3191.	3420.
12	0.	0.	0.	0.	0.	0.	0.	0.	0.	0.

C.C. = Computer code. 1 = Muailah formation. 2 = Etel formation. 3 = Sheghega formation.
4 = Domran formation. 5 = Ruaga formation. 6 = Zelten member.
7 = Heira formation. 8 = Zmam formation. 9 = Socna formation.
10 = Waha formation. 11 = Bahi formation. 12 = Gargaf formation.

Table 2.3. Geological and Geophysical tops report.

Well name : C85-6

K.B.elevation : 190.2 m. G.L.elevation : 185.9 m.
Location on line : 6V261-85 Shot point : 180
One-way receiver static : 140 ms.

C.C.	Drill. depth	Subsur. depth	Subsur. time	Subsea depth	Subsea time	Iso-pach	Iso-chron	Interval velocity	Average velocity	R.M.S. velocity
1	389.	385.	430.	-199.	150.	385.	430.	1790.	1790.	1790.
2	639.	635.	630.	-449.	350.	250.	200.	2502.	2017.	2044.
3	681.	677.	666.	-491.	386.	41.	36.	2303.	2032.	2058.
4	1189.	1184.	954.	-999.	674.	508.	288.	3526.	2483.	2591.
5	1661.	1656.	1192.	-1470.	912.	472.	238.	3965.	2779.	2917.
6	1762.	1757.	1242.	-1572.	962.	101.	50.	4048.	2830.	2971.
7	2120.	2116.	1400.	-1930.	1120.	358.	158.	4533.	3022.	3186.
8	2331.	2327.	1516.	-2141.	1236.	211.	116.	3642.	3070.	3223.
9	0.	0.	0.	0.	0.	0.	0.	0.	0.	0.
10	2338.	2334.	1520.	-2148.	1240.	7.	4.	3353.	3071.	3224.
11	0.	0.	0.	0.	0.	0.	0.	0.	0.	0.
12	2459.	2454.	1582.	-2268.	1302.	121.	62.	3894.	3103.	3253.

Table 2.4. Geological and Geophysical tops report.

Well name : VV1-6

K.B.elevation : 162.5 m. G.L.elevation : 158.2 m.
Location on line : 6V271-85 Shot point : 420
One-way receiver static : 120 ms.

C.C.	Drill. depth	Subsur. depth	Subsur. time	Subsea depth	Subsea time	Iso-pach	Iso-chron	Interval velocity	Average velocity	R.M.S. velocity
1	453.	449.	512.	-290.	272.	449.	512.	1753.	1753.	1753.
2	684.	680.	682.	-522.	442.	231.	170.	2722.	1994.	2038.
3	727.	722.	712.	-564.	472.	42.	30.	2825.	2029.	2077.
4	1240.	1235.	1016.	-1077.	776.	513.	304.	3375.	2432.	2536.
5	1722.	1718.	1274.	-1560.	1034.	483.	258.	3743.	2697.	2822.
6	1818.	1813.	1314.	-1655.	1074.	95.	40.	4755.	2760.	2900.
7	2049.	2045.	1412.	-1887.	1172.	232.	98.	4728.	2897.	3062.
8	2354.	2350.	1642.	-2192.	1402.	305.	230.	2651.	2862.	3008.
9	0.	0.	0.	0.	0.	0.	0.	0.	0.	0.
10	2362.	2358.	1648.	-2200.	1408.	8.	6.	2743.	2861.	3007.
11	0.	0.	0.	0.	0.	0.	0.	0.	0.	0.
12	0.	0.	0.	0.	0.	0.	0.	0.	0.	0.

C.C. = Computer code. 1 = Muailah formation. 2 = Etel formation. 3 = Sheghega formation.
4 = Domran formation. 5 = Ruaga formation. 6 = Zelten member.
7 = Heira formation. 8 = Zmam formation. 9 = Socna formation.
10 = Waha formation. 11 = Bahi formation. 12 = Gargaf formation.

Table 2.5. Geological and Geophysical tops report.

Well name : YYY1-6

K.B.elevation : 191.7 m. G.L.elevation : 187.1 m.
Location on line : 6V263-85 Shot point : 136
One-way receiver static : 135 ms.

C.C.	Drill. depth	Subsur. depth	Subsur. time	Subsea depth	Subsea time	Iso-pach	Iso-chron	Interval velocity	Average velocity	R.M.S. velocity
1	0.	0.	0.	0.	0.	0.	0.	0.	0.	0.
2	669.	664.	642.	-477.	372.	664.	642.	2070.	2070.	2070.
3	729.	725.	690.	-538.	420.	60.	48.	2515.	2101.	2104.
4	1268.	1263.	1004.	-1076.	734.	539.	314.	3431.	2517.	2593.
5	1825.	1820.	1288.	-1633.	1018.	557.	284.	3922.	2826.	2938.
6	1956.	1952.	1346.	-1765.	1076.	131.	58.	4530.	2900.	3024.
7	2353.	2349.	1516.	-2161.	1246.	397.	170.	4669.	3098.	3250.
8	2651.	2647.	1690.	-2459.	1420.	298.	174.	3426.	3132.	3269.
9	0.	0.	0.	0.	0.	0.	0.	0.	0.	0.
10	2832.	9275.	1772.	-2640.	1502.	180.	82.	4401.	3191.	3330.
11	3773.	3769.	2212.	-3581.	1942.	942.	440.	4280.	3407.	3539..
12	0.	0.	0.	0.	0.	0.	0.	0.	0.	0.

Table 2.6. Geological and Geophysical tops report based on velocity survey log analysis.

Well name : C114-6

K.B.elevation : 187.5 m. G.L.elevation : 182.9 m.
Location on line : 6V261-85 Shot point : 150
One-way receiver static : 142.5 ms.

C.C.	Drill. depth	Subsur. depth	Subsur. time	Subsea depth	Subsea time	Iso-pach	Iso-chron	Interval velocity	Average velocity	R.M.S. velocity
1	398.	394.	513.	-211.	228.	394.	513.	1537.	1537.	1537.
2	655.	651.	705.	-468.	420.	257.	192.	2673.	1846.	1914.
3	699.	694.	745.	-511.	460.	44.	40.	2179.	1864.	1929.
4	1197.	1193.	1012.	-1010.	727.	498.	267.	3733.	2357.	2533.
5	1641.	1637.	1213.	-1454.	928.	444.	201.	4419.	2699.	2931.
6	1748.	1743.	1275.	-1561.	990.	107.	62.	3441.	2735.	2958.
7	2129.	2125.	1450.	-1942.	1165.	382.	175.	4361.	2931.	3160.
8	2314.	2310.	1563.	-2127.	1278.	185.	113.	3269.	2956.	3168.
9	0.	0.	0.	0.	0.	0.	0.	0.	0.	0.
10	2319.	2315.	1565.	-2132.	1280.	5.	2.	5182.	2958.	3172.
11	2425.	2421.	1596.	-2238.	1311.	106.	31.	6824.	3033.	3282.
12	0.	0.	0.	0.	0.	0.	0.	0.	0.	0.

C.C. = Computer code. 1 = Muailah formation. 2 = Etel formation. 3 = Sheghega formation.
4 = Domran formation. 5 = Ruaga formation. 6 = Zelten member.
7 = Heira formation. 8 = Zmam formation. 9 = Socna formation.
10 = Waha formation. 11 = Bahi formation. 12 = Gargaf formation.

Table 2.7. Geological and Geophysical tops report based on velocity survey log analysis.

Well name : C85-6

K.B.elevation : 190.2 m. G.L.elevation : 185.9 m.
Location on line : 6V261-85 Shot point : 180
One-way receiver static : 140 ms.

C.C.	Drill. depth	Subsur. depth	Subsur. time	Subsea depth	Subsea time	Iso-pach	Iso-chron	Interval velocity	Average velocity	R.M.S. velocity
1	389.	385.	449.	-199.	169.	385.	449.	1715.	1715.	1715.
2	639.	635.	642.	-449.	362.	250.	193.	2593.	1979.	2019.
3	681.	677.	680.	-491.	400.	41.	38.	2182.	1990.	2029.
4	1189.	1184.	954.	-999.	674.	508.	274.	3707.	2483.	2623.
5	1661.	1656.	1222.	-1470.	942.	472.	268.	3521.	2711.	2844.
6	1762.	1757.	1276.	-1572.	996.	101.	54.	3748.	2755.	2888.
7	2120.	2116.	1442.	-1930.	1162.	358.	166.	4315.	2934.	3086.
8	2331.	2327.	1560.	-2141.	1280.	211.	118.	3580.	2983.	3126.
9	0.	0.	0.	0.	0.	0.	0.	0.	0.	0.
10	2338.	2334.	1563.	-2148.	1283.	7.	3.	4471.	2986.	3129.
11	2448.	2444.	1609.	-2258.	1329.	111.	46.	4811.	3038.	3190.
12	2459.	2454.	1614.	-2268.	1334.	10.	5.	4023.	3041.	3193.

Table 2.8. Geological and Geophysical tops report based on velocity survey log analysis.

Well name : C59-6

K.B.elevation : 189.3 m. G.L.elevation : 185 m.
Location on line : 6V264-85 Shot point : 385
One-way receiver static : 132 ms.

C.C.	Drill. depth	Subsur. depth	Subsur. time	Subsea depth	Subsea time	Iso-pach	Iso-chron	Interval velocity	Average velocity	R.M.S. velocity
1	419.	415.	484.	-230.	220.	415.	484.	1714.	1714.	1714.
2	640.	636.	648.	-451.	384.	221.	164.	2695.	1962.	2008.
3	680.	676.	684.	-491.	420.	40.	36.	2235.	1977.	2021.
4	1195.	1191.	965.	-1006.	701.	515.	281.	3662.	2467.	2608.
5	1683.	1679.	1228.	-1494.	964.	489.	263.	3716.	2735.	2881.
6	1788.	1783.	1282.	-1598.	1018.	104.	54.	3861.	2782.	2929.
7	2103.	2098.	1406.	-1913.	1142.	315.	124.	5078.	2985.	3178.
8	2345.	2340.	1488.	-2155.	1224.	242.	82.	5903.	3146.	3385.
9	0.	0.	0.	0.	0.	0.	0.	0.	0.	0.
10	2361.	2356.	1494.	-2171.	1230.	16.	6.	5385.	3154.	3396.
11	2430.	2425.	1520.	-2240.	1256.	69.	26.	5299.	3191.	3437.
12	0.	0.	0.	0.	0.	0.	0.	0.	0.	0.

C.C. = Computer code. 1 = Muailah formation. 2 = Etel formation. 3 = Sheghega formation.
4 = Domran formation. 5 = Ruaga formation. 6 = Zelten member.
7 = Heira formation. 8 = Zmam formation. 9 = Socna formation.
10 = Waha formation. 11 = Bahi formation. 12 = Gargaf formation.

Table 2.9. Geological and Geophysical tops report based on velocity survey log analysis.

Well name : C10-6

K.B.elevation : 155.4 m. G.L.elevation : 151.2 m.
Location on line : 6V250-85 Shot point : 313and on line : 6V259-85 S.P. : 412
One-way receiver static : 74 ms.

C.C.	Drill. depth	Subsur. depth	Subsur. time	Subsea depth	Subsea time	Iso-pach	Iso-chron	Interval velocity	Average velocity	R.M.S. velocity
1	0.	0.	0.	0.	0.	0.	0.	0.	0.	0.
2	0.	0.	0.	0.	0.	0.	0.	0.	0.	0.
3	736.	732.	671.	-581.	523.	732.	671.	2181.	2181.	2181.
4	1218.	1214.	932.	-1063.	784.	482.	261.	3695.	2605.	2692.
5	1678.	1674.	1177.	-1522.	1029.	460.	245.	3752.	2844.	2945.
6	1733.	1729.	1209.	-1577.	1061.	55.	32.	3429.	2859.	2958.
7	2254.	2250.	1432.	-2099.	1284.	522.	223.	4677.	3143.	3286.
8	2376.	2372.	1502.	-2220.	1354.	122.	70.	3475.	3158.	3295.
9	0.	0.	0.	0.	0.	0.	0.	0.	0.	0.
10	2382.	2378.	1515.	-2227.	1367.	6.	13.	938.	3139.	3282.
11	0.	0.	0.	0.	0.	0.	0.	0.	0.	0.
12	2405.	2401.	1525.	-2249.	1377.	23.	10.	4572.	3148.	3292.

Table 2.10. Geological and Geophysical tops report based on velocity survey log analysis.

Well name : YYY1-6

K.B.elevation : 191.7 m. G.L.elevation : 187.1 m.
Location on line : 6V263-85 Shot point : 136
One-way receiver static : 135 ms.

C.C.	Drill. depth	Subsur. depth	Subsur. time	Subsea depth	Subsea time	Iso-pach	Iso-chron	Interval velocity	Average velocity	R.M.S. velocity
1	0.	0.	0.	0.	0.	0.	0.	0.	0.	0.
2	669.	664.	0.	-477.	0.	0.	0.	0.	0.	0.
3	729.	725.	725.	-538.	455.	725.	725.	2000.	2000.	2000.
4	1268.	1263.	1014.	-1076.	744.	539.	289.	3727.	2492.	2611.
5	1825.	1820.	1300.	-1633.	1030.	557.	286.	3894.	2801.	2942.
6	1956.	1952.	1381.	-1765.	1111.	131.	81.	3244.	2826.	2960.
7	2353.	2349.	1522.	-2161.	1252.	397.	141.	5629.	3086.	3300.
8	2651.	2647.	1708.	-2459.	1438.	298.	186.	3205.	3099.	3289.
9	0.	0.	0.	0.	0.	0.	0.	0.	0.	0.
10	2832.	2827.	1780.	-2640.	1510.	180.	72.	5012.	3176.	3376.
11	3773.	3769.	2238.	-3581.	1968.	942.	458.	4111.	3368.	3539.
12	0.	0.	0.	0.	0.	0.	0.	0.	0.	0.

C.C. = Computer code. 1 = Muailah formation. 2 = Etel formation. 3 = Sheghega formation.
4 = Domran formation. 5 = Ruaga formation. 6 = Zelten member.
7 = Heira formation. 8 = Zmam formation. 9 = Socna formation.
10 = Waha formation. 11 = Bahi formation. 12 = Gargaf formation.

Appendix 3.1

FORTRAN - 77 PROGRAM 1 COORDINATE

```
c     ********************************************************************************
c     This program is design for the straight seismic lines in the program area.
c     VAX/UNIX: COORDINATE
c     Written by
c     Ben Ayad N.M.
c     at the department of Geology&Applied Geology.
c     University of Glasgow, Glasgow G12 8QQ (in June 1991)
c     This program calculates the coordinate for each 10 shots of the seismic lines, given the
c     first and the last shots coordinate for a straight seismic line, assuming that the area of
c     study is flat and does not take in our consideration the effect of the curvature of the earth.
c     ********************************************************************************
c     PROGRAM COORDINATE.F
      PARAMETER ( K = 600 )
      DIMENSION SP(K), HORIZ1(K), HORIZ2(K), HORIZ3(K), XCOOR(K), YCOOR(K)
      CHARACTER *10 INPUT, OUTPUT*11
      PRINT*," PRINT THE FILE NAME CONT. THE INPUT DATA AS [ COOR.INPUT ] "
      READ*, INPUT
      PRINT*," PRINT THE FILE NAME CONT. THE OUTPUT AS [ COOR.OUTPUT ] "
      READ*, OUTPUT
            OPEN ( 1, FILE = INPUT )
            OPEN ( 2, FILE = OUTPUT )
      PRINT*," NUMBER OF STRAIGHT LINES "
      READ*, NT
c     J       - Counter for straight lines number.
      DO 20 J = 1, NT
c     N       - Number of the picked shot points.
c     FIRSTCOORE   - Latitude of the first shot point in the line.
c     FIRSTCOORN   - Longitude of the first shot point in the line.
c     SECONDCOORE        - Latitude of the last shot point in the line.
c     SECONDCOORN        - Longitude of the last shot point in the line.
            READ (1,*) N
            READ (1,*) FIRSTCOORE, FIRSTCOORN
            READ (1,*) SECONDCOORE, SECONDCOORN
c     I       - Counter for picked shot points.
```

```
      DO 10 I = 1, N
c     SP      - Shot point number.
c     HORIZ1        - Time for horizon (1).
c     HORIZ2        - Time for horizon (2).
c     HORIZ3        - Time for horizon (3).
            READ (1,*) SP(I), HORIZ1(I), HORIZ2(I), HORIZ3(I)
10    CONTINUE
c     DIFFX - Difference in latitude.
c     DIFFY - Difference in longitude.
c     DALTAX        - Latitude increment.
c     DALTAY        - Longitude increment.
c     SUMX - Summation of latitude.
c     SUMY - Summation of longitude.
            DIFFX     = SECONDCOORE - FIRSTCOORE
            DIFFY     = SECONDCOORN - FIRSTCOORN
            DALTAX    = DIFFX / ( N - 1 )
            DALTAY    = DIFFY / ( N - 1 )
            SUMX      = 0.0
            SUMY      = 0.0
c     I       - Counter for picked shot points.
      DO 15 I = 1, N
c     XCOOR         - Required latitude of the shot point.
c     YCOOR         - Required longitude of the shot point.
            XCOOR(I) = FIRSTCOORE + SUMX
            YCOOR(I) = FIRSTCOORN + SUMY
            SUMX     = SUMX + DALTAX
            SUMY     = SUMY + DALTAY
      WRITE (2,100) SP(I), YCOOR(I), XCOOR(I), HORIZ1(I), HORIZ2(I), HORIZ3(I)
15    CONTINUE
20    CONTINUE
100   FORMAT ( F5.0 , 2F10.5 , 3F8.0 )
      STOP
      END
```

Appendix 3.2

FORTRAN - 77 PROGRAM 2 ALL2

```
c     ************************************************************************
c     This program is design for the velocity analysis data.
c     VAX/UNIX: ALL2
c     Written by
c     Ben Ayad N.M.
c     at the department of Geology&Applied Geology.
c     University of Glasgow, Glasgow G12 8QQ (in June 1991)
c     This program calculates the Dix average velocity, interval velocity, and rms velocity
c     for the seismic lines by interpolating between the levels reading.
c     ************************************************************************
c     PROGRAM ALL2.F
      DIMENSION  T(20,20), VEL(20,20), TC(200,20), VC(200,20), VI(200,20)
     *          , SP(20), VID(20,20), VAD(20,20), VADL(200,20), VIDL(200,20)
     *          , TCD(200,20), DEPR(200,20), DEPD(200,20), DIFFD(200,20)
     *          , DIFFT(200,20), DTC(200,20),DTCD(200,20), DDEPR(200,20)
     *          , DDEPD(200,20), VINTERR(200,20), VINTERD(200,20)
     *          , DIFDIX(200,20), DIFRMS(200,20), S(10,20), E(10,20)
      INTEGER S(10,20), E(10,20)
      CHARACTER *2 NA, VTDATA*9, VTR*7, VTI*7, VTS*7, DIXR*8
      CHARACTER *7 DIF, DDIF*8, SAE*7
      DATA NA / " NA " /
      PRINT*," PRINT THE FILE NAME CON. THE INPUT DATA AS [ DATA.*** ] "
      READ *, VTDATA
      PRINT*," PRINT THE FILE NAME CON. THE OUTPUT DATA AS [ VTR.*** ] "
      READ *, VTR
      PRINT*," PRINT THE FILE NAME CON. THE OUTPUT DATA AS [ VTI.*** ] "
      READ *, VTI
      PRINT*," PRINT THE FILE NAME CON. THE OUTPUT DATA AS [ VTS.*** ] "
      READ *, VTS
      PRINT*," PRINT THE FILE NAME CON. THE OUTPUT DATA AS [ DIXR.*** ] "
      READ *, DIXR
      PRINT*," PRINT THE FILE NAME CON. THE OUTPUT DATA AS [ DIF.*** ] "
      READ *, DIF
      PRINT*," PRINT THE FILE NAME CON. THE OUTPUT DATA AS [ DDIF.*** ] "
```

```
      READ *, DDIF
      PRINT*," PRINT THE FILE NAME CON. THE OUTPUT DATA AS [ SAE.*** ] "
      READ *, SAE
      PRINT*," PRINT 1 IF YOU WANT VELOCITY INCREMENT "
      PRINT*," PRINT 2 IF YOU WANT TIME INCREMENT "
      READ *, INC
            OPEN ( 1, FILE = VTDATA )
            OPEN ( 2, FILE = VTR )
            OPEN ( 3, FILE = VTI
            OPEN ( 4, FILE = VTS )
            OPEN ( 7, FILE = DIF )
            OPEN ( 9, FILE = DDIF )
            OPEN ( 11, FILE = DIXR )
            OPEN ( 13, FILE = SAE )
            IF ( INC .EQ. 2 ) THEN
      PRINT*," YOUR ANSWER 2 "
      PRINT*," PRINT THE INCREMENT VALUE OF THE T.W.TIME IN S "
      READ *, ALA
      PRINT*," PRINT THE STARTING VALUE OF THE T.W.TIME IN S "
      READ *, AMA
            GO TO 919
      ELSE
      PRINT*," YOUR ANSWER 1 "
      PRINT*," PRINT THE INC. VALUE OF THE VELOCITY IN M/S "
      READ *, ALA
      PRINT*," PRINT THE STARTING VALUE OF THE VELOCITY "
      READ *, AMA
919   END IF
      PRINT*," PRINT THE NUMBER OF VELOCITY ANALYSIS BOXES "
      READ (1,100) NN
c     LL      - Counter for boxes.
      DO 10 LL = 1, NN
c     AL      - Increment value (time or velocity).
c     AM      - Starting value (time or velocity).
c     NU1     - Counter of data which time values less than 4 s.
c     NU2     - Counter of data which time values less than 4 s.
c     NU3     - Counter of data which time values less than 2 s.
```

```
c       S       - Starting counting number.
c       K       - Counter.
                  AL      = ALA
                  AM      = AMA
                  NU1     = 0
                  NU2     = 0
                  NU3     = 0
                  S(1,1)  = 1
                  S(2,1)  = 1
                  S(3,1)  = 1
                  K       = 1
c       N       - Number of picked levels.
c       SP      - Shot point number.
        READ (1,200) N, SP(ll)
c       N       - Counter for levels.
        DO 20 I = 1, N
c       T       - Two-way time.
c       VEL     - Root mean square velocity.
c       VID     - Dix interval velocity.
        READ (1,300) T(I,LL), VEL(I,LL), VID(I,ll)
20      CONTINUE
                  T(1,LL) = 0.0005
c       VAD     - Dix average velocity calculated from DIX subroutine.
c-------------------------------------------------------
        CALL DIX ( INC, N, LL, T, VID, VAD )
c-------------------------------------------------------
c       I       - Counter for levels.
        DO 30 I = 1, N
        WRITE (11,500) SP(LL), T(I,LL), VAD(I,ll)
30      CONTINUE
                  IF ( INC .EQ. 2 ) THEN
c       TC      - Interpolated time calculated from SHORT2 subroutine corresponding
c                 to the rms velocity.
c       VI      - Interval velocity calculated from SHORT2 subroutine.
c       VC      - Interpolated rms velocity calculated from SHORT2 subroutine.
c-------------------------------------------------------------------------------
        CALL SHORT2 ( N, LL, K, T, VEL, AM, AL, KK, TC, VI,VC )
c-------------------------------------------------------------------------------
                  K = 1
```

```
                GO TO 123
        ELSE
c       TC      - Interpolated time calculated from SHORT subroutine corresponding
c               to the rms velocity.
c       VI      - Interval velocity calculated from SHORT subroutine.
c       VC      - Interpolated rms velocity calculated from SHORT subroutine.
c-------------------------------------------------------------------------------
        CALL  SHORT  ( N, LL, K, T, VEL, AM, AL, KK, TC, VI, VC )
c-------------------------------------------------------------------------------
                K = 1
                GO TO 918
123     AMM = AMA
c       TCD     - Interpolated time calculated from SHORT2 subroutine corresponding
c               to the Dix velocity.
c       VIDL    - Dix interval velocity calculated from SHORT subroutine.
c       VADL    - Interpolated Dix average velocity calculated from SHORT2 subroutine.
c-------------------------------------------------------------------------------
        CALL   SHORT2  ( N, LL, K, T, VAD, AMM, AL, KN, TCD, VIDL, VADL )
c-------------------------------------------------------------------------------
                GO TO 124
918             AMM = VAD(1,ll)
c       TCD     - Interpolated time calculated from SHORT subroutine.
c       VIDL    - Interval velocity calculated from SHORT subroutine.
c       VADL    - Interpolated velocity calculated from SHORT subroutine.
c-------------------------------------------------------------------------------
        CALL   SHORT  ( N, LL, K, T, VAD, AMM, AL, KN, TCD, VIDL, VADL )
c-------------------------------------------------------------------------------
124     END IF
                IF ( KK .GE. KN ) KN = KN
                IF ( KK .LT. KN ) KN = KK
c       DTC     - Difference in time calculated from DIFFER subroutine corresponding to
c               the rms velocity.
c       DTCD    - Difference in time calculated from DIFFER subroutine corresponding to
c               the Dix average velocity.
c       DEPR    - Depth calculated from DIFFER subroutine using rms velocity.
c       DEPD    - Depth calculated from DIFFER subroutine using Dix average velocity.
c       DIFFD   - Difference in depth calculated from DIFFER subroutine (DEPR-DEPD).
c       DIFFT   - Difference in time calculated from DIFFER subroutine (TC-TCD).
c       DDEPR           - Difference in depth calculated from DIFFER subroutine.
c       DDEPD           - Difference in depth calculated from DIFFER subroutine.
```

```
c       VINTERR       - Interval velocity (rms) calculated from DIFFER subroutine.
c       VINTERD       - Dix interval velocity calculated from DIFFER subroutine.
c-------------------------------------------------------------------------------------------------
        CALL   DIFFER  ( TCD, TC, KN, LL, VC, VADL, DEPR, DEPD, DIFFD, DIFFT
     *                 , DTC, DTCD, DDEPR, DDEPD, VINTERR, VINTERD )
c-------------------------------------------------------------------------------------------------
c       I       - Counter for shot number.
        DO 40 I = 1, KN - 1
        WRITE (7,400) TCD(I,LL), TC(I,LL), DIFFT(I,LL), DEPR(I,LL)
     *              , DEPD(I,LL), DIFFD(I,ll), VC(I,LL), VADL(I,LL)
40      CONTINUE
c       I       - Counter for shot number.
        DO 50 I = 1, KN - 1
              NU1 = NU1 + 1
        WRITE (2,900) SP(LL), TC(I,LL), VC(I,LL), TCD(I,ll)
     *              , VADL(I,LL), DEPR(I,LL), DEPD(I,ll)
50      CONTINUE
100     FORMAT ( I3 )
110     FORMAT ( 6I6 )
200     FORMAT ( I4 , F6.1 )
300     FORMAT ( F4.2 , 2F4.0 )
400     FORMAT ( 3F10.5 , 5F8.1 )
500     FORMAT ( F6.1 , F8.4 , 4F8.1 , F8.4 )
600     FORMAT ( 10A6 )
900     FORMAT ( F6.1 , F8.4 , F8.1 , F8.4 , F8.1 , 2F8.1 )
800     FORMAT ( F6.0 , F7.0 , F6.0 , 3F7.0 , 2F6.3 , 2F5.0 )
c       L       - Counter for shot number.
        DO 60 L = 1, KN - 2
              NU2 = NU2 + 1
        WRITE (3,500) SP(LL), TC(L,LL), VI(L,LL), VIDL(L,LL)
     *              , DEPR(L,LL), DEPD(L,LL), TCD(L,LL)
        WRITE (3,500) SP(LL), TC(L+1,LL), VI(L,LL), VIDL(L,LL)
     *              , DEPR(L+1,LL), DEPD(L+1,LL), TCD(L+1,LL)
              IF ( TC(L+1,LL) .LE. 2.0 ) THEN
                    NU3 = NU3 + 1
        WRITE (4,500) SP(LL), TC(L,LL), VI(L,LL), VIDL(L,LL)
     *              , DEPR(L,LL), DEPD(L,LL), TCD(L,LL)
        WRITE (4,500) SP(LL), TC(L+1,LL), VI(L,LL), VIDL(L,LL)
```

```
     *              , DEPR(L+1,LL), DEPD(L+1,LL), TCD(L+1,LL)
           ELSE
           END IF
60         CONTINUE
c          I       - Counter for shot number.
           DO 70 I = 1, KN - 2
c          DIFDIX          - Difference in Dix interval velocity.
c          DIFRMS          -Difference in interval velocity (rms).
                           DIFDIX(I,LL)    = VINTERD(I,LL) - VIDL(I,LL)
                           DIFRMS(I,LL)    = VINTERR(I,LL) - VI(I,LL)
           WRITE (9,800) VI(I,LL), VIDL(I,LL), DIFRMS(I,LL), DIFDIX(I,LL), VINTERR(I,LL)
     *              , VINTERD(I,LL), TC(I,LL), TCD(I,LL), DDEPR(I,LL), DDEPD(I,LL)
           WRITE (9,800) VI(I,LL), VIDL(I,LL), DIFRMS(I,LL), DIFDIX(I,LL), VINTERR(I,LL)
     *              , VINTERD(I,LL), TC(I+1,LL), TCD(I+1,LL), DDEPR(I,LL), DDEPD(I,LL)
70         CONTINUE
           WRITE (2,600) NA, NA, NA, NA, NA, NA, NA
           WRITE (3,600) NA, NA, NA, NA, NA, NA, NA
           WRITE (4,600) NA, NA, NA, NA, NA, NA, NA
           WRITE (7,600) NA, NA, NA, NA, NA, NA, NA, NA
           WRITE (9,600) NA, NA, NA, NA, NA, NA, NA, NA, NA, NA
           WRITE (11,600) NA, NA, NA
c          E       - Ending counter number.
                   E(1,LL) = NU1
                   E(2,LL) = NU2*2
                   E(3,LL) = NU3*2
10         CONTINUE
c          L       - Counter for shot point number.
           DO 80 I = 1, NN - 1
c          S       - Starting counter number.
c          E       - Ending counter number.
                   S(1,I+1) = E(1,I) + 2
                   S(2,I+1) = E(2,I) + 2
                   S(3,I+1) = E(3,I) + 2
                   E(1,I+1) = E(1,I+1) + S(1,I+1) - 1
                   E(2,I+1) = E(2,I+1) + S(2,I+1) - 1
                   E(3,I+1) = E(3,I+1) + S(3,I+1) - 1
80         CONTINUE
```

```
c       I       - Counter for number of boxes.
        DO 90 I = 1, NN
        WRITE (13,110) ( S(J,I), E(J,I), J = 1, 3 )
90      CONTINUE
        CLOSE(1)
        STOP
        END

c-------------------------------------------------------------------------------
        SUBROUTINE DIX ( INC, N, M, T, VID, VAD )
        DIMENSION T(20,20), VID(20,20), VAD(20,20)
c       SUMT  - Summation of the time.
c       SUMVT         - Summation of the product velocity and time.
c       VID   - Dix interval velocity.
c       VAD   - Dix average velocity.
              SUMT    = 0.0
              SUMVT   = 0.0
              VAD(1,M) =VID(1,M)
c       I     - Counter for calculated loops.
        DO 10 I = 1, N - 1
c       T     - Time.
c       DT    - Difference in time.
              DT          = T(I+1,M) - T(I,M)
              SUMT        = SUMT + DT
              SUMVT       = SUMVT + ( VID(I+1,M)*DT )
              VAD(I+1,M) = SUMVT / SUMT
10      CONTINUE
        RETURN
        END

c-------------------------------------------------------------------------------
        SUBROUTINE SHORT ( N, LL, K, T, VEL, AM, AL, KK, TC, VI, VC )
        DIMENSION T(20,20), VEL(20,20), TC(200,20), VI(200,20), VC(200,20)
c       I     - Counter for calculated loops.
        DO 10 I=1,N-1
c       T     - Time.
c       VEL   - Velocity.
c       DIFT  - Difference in time.
```

```
c       DIFV    - Difference in velocity.
                        DIFT   = T(I+1,LL) - T(I,LI)
                        DIFV   = VEL(I+1,LL) - VEL(I,LL)
                IF ( ( DIFV .LT. AL ) .AND. ( ( AM - VEL(I+1,LL) ) .GT. 0.0 ) ) GO TO 10
c       TC      - Interpolated time.
c       VC      - Corresponding velocity.
30                      VICOR   = DIFT / DIFV
50                      TC(K,LL)  = VICOR* ( AM - VEL(I,LL) ) + T(I,LL)
                        VC(K,LL)  = AM
                            AM    = AM + AL
                            K     = K + 1
                IF ( VEL(I+1,LL) .LE. AM ) GO TO 10
                GO TO 50
10      CONTINUE
c       L       - Counter for (K-2) number.
        DO 20 L = 1, K - 2
c       SQRT    - Square root function.
c       VI      - Interval velocity.
                TOP     = ( VC(L+1,LL)**2*TC(L+1,LL) ) - ( VC(L,LL)**2*TC(L,LL) )
                VI(L,LL)  = SQRT ( TOP / ( TC(L+1,LL) - TC(L,LL) ) )
20      CONTINUE
                    KK  = K
        RETURN
        END

c-----------------------------------------------------------------------------
        SUBROUTINE  SHORT2  ( N, LL, K, T, VEL, AM, AL, KK, TC, VI, VC )
        DIMENSION T(20,20), VEL(20,20), TC(200,20), VI(200,20), VC(200,20)
c       I       - Counter for calculated loops.
        DO 10 I = 1, N - 1
c       T       - Time.
c       VEL     - Velocity.
c       DIFT    - Difference in time.
c       DIFV    - Difference in velocity.
                        DIFT   = T(I+1,LL) - T(I,LL)
                        DIFV   = VEL(I+1,LL) - VEL(I,LL)
                IF ( ( DIFT .LT. AL ) .AND. ( ( AM - T(I+1,LL) ) .GT. 0.0 ) ) GO TO 10
c       VC      - Interpolated velocity.
```

```
c       TC      - Corresponding time.
30                      TICOR     = DIFV / DIFT
50                      VC(K,LL)  = TICOR* ( AM - T(I,LL) ) + VEL(I,LL)
                        TC(K,LL)  = AM
                            AM    = AM + AL
                            K     = K+1
                IF ( T(I+1,LL) .LE. AM ) GO TO 10
                GO TO 50
10      CONTINUE
c       L       - Counter for (K-2) number.
        DO 20 L = 1, K - 2
c       SQRT    - Square root function.
c       VI      - Interval velocity.
                TOP       = ( VC(L+1,LL)**2*TC(L+1,LL) ) - ( VC(L,LL)**2*TC(L,LL) )
                VI(L,LL)  = SQRT ( TOP / ( TC(L+1,LL) - TC(L,LL) ) )
20      CONTINUE
                    KK    = K
        RETURN
        END

c-------------------------------------------------------------------------------------------------
        SUBROUTINE    DIFFER   ( TCD, TC, KN, LL, VC, VADL, DEPR, DEPD, DIFFD, DIFFT
     *                                 , DTC, DTCD, DDEPR, DDEPD, VINTERR, VINTERD )
        DIMENSION TCD(200,20), TC(200,20), VC(200,20), VADL(200,20), DEPR(200,20)
     *          , DEPD(200,20), DIFFD(200,20), DIFFT(200,20), DTC(200,20)
     *          , DTCD(200,20), DDEPR(200,20), DDEPD(200,20)
     *          , VINTERR(200,20), VINTERD(200,20)
c       I       - Counter for shot point number.
        DO 10 I = 1, KN - 1
c       DEPR    - Depth calculated using rms velocity.
c       DEPD    - Depth calculated using Dix average velocity.
c       DIFFD   - Difference in depth.
c       DIFFT   - Difference in time.
                  DEPR(I,LL)  = VC(I,LL)*TC(I,LL) / 2
                  DEPD(I,LL)  = VADL(I,LL)*TCD(I,LL) / 2
                  DIFFD(I,LL) = DEPR(I,LL) - DEPD(I,LL)
                  DIFFT(I,LL) = ( TC(I,LL) - TCD(I,LL) ) / 2
10      CONTINUE
```

```
c       I       - Counter for shot point number.
        DO 20 I = 1, KN - 2
c       DTC     - Difference in time corresponding to rms velocity.
c       DTCD    - Difference in time corresponding to Dix average velocity.
c       DDEPR           - Difference in depth corresponding to rms velocity.
c       DDEPD           - Difference in depth corresponding to Dix average velocity.
c       VINTERR         - Interval velocity (rms).
c       VINTERD         - Dix interval velocity.
                DTC(I,LL)       = ( TC(I+1,LL) - TC(I,LL) ) / 2
                DTCD(I,LL)      = ( TCD(I+1,LL) - TCD(I,LL) ) / 2
                DDEPR(I,LL)     = DEPR(I+1,LL) - DEPR(I,LL)
                DDEPD(I,LL)     = DEPD(I+1,LL) - DEPD(I,LL)
                VINTERR(I,LL)   = DDEPR(I,LL) / DTC(I,LL)
                VINTERD(I,LL)   = DDEPD(I,LL) / DTCD(I,LL)
20      CONTINUE
        RETURN
        END
```

Appendix 3.3

FORTRAN - 77 PROGRAM 3 BOXMATCH

```
c     ************************************************************************
c     This program is design for the picked two-way time for the chosen horizons.
c     VAX/UNIX: BOXMATCH
c     Written by
c     Ben Ayad N.M.
c     at the department of Geology&Applied Geology.
c     University of Glasgow, Glasgow G12 8QQ (in June 1991)
c     This program calculates the velocity and the depth corresponding to the two-way time
c     picked from the seismic section for the chosen horizons.
c     ************************************************************************
c     PROGRAM BOXMATCH.F
      DIMENSION H(3,1000), TC(1000), VEL(1000), TH(3,25), SP(1000), SPB(1000), ST(1000)
     *        , VMATCH(3,1000), IS(20,10), IE(20,10), XX(1000), YY(1000), AVDL(1000)
     *        , CLAT(1000), CLONG(1000), DTIME(3,1000), TCD(1000), VH(3,25), T(3,1000)
     *        , DEPTH(3,1000), DDEPTH(3,1000), BLAT(25), BLONG(25), DH(3,25)
      CHARACTER *8 INDATA1, INDATA2*9, INDATA3*9
      CHARACTER *11 OUT1, OUT2*11, OUT3*11, NA*2
      PRINT*," PRINT THE FILE NAME CONT. THE INPUT DATA AS [ COOR.*** ] "
      READ(5,*) INDATA1
      PRINT*," PRINT THE FILE NAME CONT. THE INPUT DATA AS [ SAE.*** ] "
      READ(5,*) INDATA2
      PRINT*," PRINT THE FILE NAME CONT. THE INPUT DATA AS [ VTR.*** ] "
      READ(5,*) INDATA3
      PRINT*," PRINT THE FILE NAME CONT. THE OUTPUT AS [ OUTA.*** ] "
      READ(5,*) OUT1
      PRINT*," PRINT THE FILE NAME CONT. THE OUTPUT AS [ OUTB.*** ] "
      READ(5,*) OUT2
      PRINT*," PRINT THE FILE NAME CONT. THE OUTPUT AS [ OUTC.*** ] "
      READ(5,*) OUT3
            OPEN ( 1, FILE = INDATA1 )
            OPEN ( 2, FILE = INDATA2 )
            OPEN ( 3, FILE = INDATA3 )
            OPEN ( 4, FILE = OUT1 )
            OPEN ( 7, FILE = OUT3 )
```

```
      OPEN ( 8,  FILE = OUT2 )
900   FORMAT ( F6.1 , F8.4 , F8.1 , F8.4 , 3F8.1 )
990   FORMAT ( F5.0 , 2F10.5 , 4F8.5 )
      PRINT*," NUMBER OF VELOCITY ANALYSIS BOXES "
      READ(5,*) NN
c     J       - Counter for number of boxes.
      DO 54 J = 1, NN
c     IS      - Started counter of data.
c     IE      - Ended counter of data.
      READ (2,*) ( IS(J,I), IE(J,I+1), I = 1, 5, 2 )
54    CONTINUE
c     J       - Counter for number of boxes.
      DO 191 J = 1, NN
c     I       - Counter for data number.
      DO 292 I = IS(J,1), IE(J,2)
c     SPB     - Shot point number at the location of the velocity analysis.
c     VEL     - RMS velocity.
c     TC      - Time corresponding to the rms velocity.
c     TCD     - Time corresponding to the Dix average velocity.
c     XX      - Depth corresponding to the rms velocity.
c     YY      - Depth corresponding to the Dix average velocity.
      READ (3,900) SPB(I), TC(I), VEL(I), TCD(I), AVDL(I), XX(I), YY(I)
292   CONTINUE
      READ (3,*) NA, NA, NA, NA, NA, NA, NA
191   CONTINUE
c     M       - Counter for picked shot point.
999   M = 1
c     SP      - Shot point number.
c     CLAT    - Latitude for SP.
c     CLONG         - Longitude for SP.
c     T       - Picked two-way time for the horizons.
c     ST      - One-way static correction for SP.
1     READ (1,990,END=888) SP(M), CLAT(M), CLONG(M), T(1,M), T(2,M), T(3,M), ST(3,M)
c     H       - Subsurface two-way time for the horizons.
            H(1,M)  = (( T(1,M) + ( ST(M) * 2.0 )) / 1000.0 )
            H(2,M)  = (( T(2,M) + ( ST(M) * 2.0 )) / 1000.0 )
            H(3,M)  = (( T(3,M) + ( ST(M) * 2.0 )) / 1000.0 )
```

```
                    M       = M + 1
                GO TO 1
888     LL = 2
c       J       - Counter for number of boxes.
        DO 66 J = 1, NN
c       I       - Counter for picked shot point.
        DO 55 L = LL, M - 1
                IF ( ( ( SP(L) .LE. SPB( IS(J,1) ) ) .AND. ( SP(L-1) .LE. SPB( IS(J,1) ) ) ) GO TO 400
                ISS = IS(J,1)
c       BLAT    - Latitude for SPB calculated from SHORT3 subroutine.
c-------------------------------------------------------------------------
        CALL  SHORT3  ( SPB, SP, CLAT, L-1, ISS, J, BLAT )
c-------------------------------------------------------------------------
c
c       BLONG           - Longitude for SPB calculated from SHORT3 subroutine.
c-------------------------------------------------------------------------
        CALL  SHORT3  ( SPB, SP, CLONG, L-1, ISS, J, BLONG )
c-------------------------------------------------------------------------
15      PRINT*," "
c       K       - Counter for the horizons.
        DO 666 K = 1, 3
c       ISS     - Started counter.
c       IEE     - Ended counter.
c       DIFH    - Difference in time.
c       DIFSP   - Difference in shot point.
c       TH      - Two-way time to the horizons at SPB location.
                    ISS     = IS(J,1)
                    IEE     =IE(J,2)
                    DIFH    = H(K,L) - H(K,L-1)
                    DIFSP   = SP(L) - SP(L-1)
                    TH(K,J) = ( DIFH / DIFSP* ( SPB(ISS) - SP(L-1) ) ) + H(K,L-1)
c       I       - Counter for levels.
        DO 6 I = ISS, IEE - 1
                IF ( ( TH(K,J) .GE. TCD(I) ) .AND. ( TH(K,J) .LE. TCD(I+1) ) ) THEN
c       VH      - Velocity corresponding to TH for SPB calculated from SHORT1 subroutine.
c-------------------------------------------------------------------------
        CALL  SHORT1  ( TH, TCD, AVDL, I, K, L, J, VH )
c-------------------------------------------------------------------------
                GO TO 16
        ELSE
```

```
      END IF
6     CONTINUE
16    PRINT*," "
c     DH      - Depth corresponding to TH and VH at SPB location.
            DH(K,J) = VH(K,J)*TH(K,J) / 2.0
666   CONTINUE
      WRITE (7,123) SPB(ISS), VH(1,J), VH(2,J), VH(3,J), DH(1,J), DH(2,J)
     *              , DH(3,J), BLAT(J), BLONG(J)
            GO TO 200
400   PRINT*," "
55    CONTINUE
200         LL = L + 1
66    CONTINUE
            LL = 1
c     J       - Counter for loops.
      DO 122 J = 1, NN - 1
c     L       - Counter for picked shot point.
      DO 222 L = LL, M - 1
            IF ( ( ( SP(L) .LT. SPB( IS(1,1) ) ) .OR. ( SP(L) .GT. SPB( IS(NN,1) ) ) ) GO TO 333
      DO 322 K = 1, 3
c     VMATCH      - Required velocity corresponding to SP calculated from SHORT2 subroutine.
c-----------------------------------------------------------------------------------------
      CALL SHORT2 ( SP, SPB, VH, IS, J, K, L, LL, M, NN, VMATCH )
c-----------------------------------------------------------------------------------------
322   CONTINUE
            GO TO 422
333   PRINT*," "
222   CONTINUE
422   PRINT*," "
122   CONTINUE
c     I       - Counter for picked shot point.
      DO 522 I = 1, M - 1
c     K       - Counter for horizons.
      DO 722 K=1, 3
c     DEPTH       - Required depth to the horizon at SP location.
            DEPTH(K,I)  = VMATCH(K,I) * ( T(K,I) / 1000.0 ) / 2.0
722   CONTINUE
c     L       - Counter for layers.
```

```
      DO 922 L = 2, 3
c     DTIME - Difference in time.
c     DDEPTH        - Difference in depth.
            DTIME(L,I)   = T(L,I) - T(L-1,I)
            DDEPTH(L,I) = DEPTH(L,I) - DEPTH(L-1,I)
922   CONTINUE
      WRITE (8,822) SP(I), DTIME(2,I), DTIME(3,I), DDEPTH(2,I), DDEPTH(3,I)
     *            , CLAT(I), CLONG(I)
      WRITE (4,622) SP(I), VMATCH(1,I), VMATCH(2,I), VMATCH(3,I), DEPTH(1,I)
     *            , DEPTH(2,I), DEPTH(3,I), CLAT(I), CLONG(I)
522   CONTINUE
622   FORMAT ( F5.0 , 6F7.0 , 2F10.5 )
822   FORMAT ( 3F5.0 , 2F6.1 , 2F10.5 )
123   FORMAT ( F6.1 , 6F7.0 , 2F10.5 )
      STOP
      END

c-----------------------------------------------------------------------------
      SUBROUTINE SHORT1 ( TH, TCD, VEL, I, K, L, J, VH )
      DIMENSION TCD(1000), VEL(1000), VH(3,25), TH(3,25)
c     DIFV  - Difference in velocity.
c     DIFT  - Difference in depth.
c     VH    - Velocity.
            DIFV   = VEL(I+1) - VEL(I)
            DIFT   = TCD(I+1) - TCD(I)
            TCOR   = DIFV / DIFT
            VH(K,J) = TCOR* ( TH(K,J) - TCD(I) ) + VEL(I)
      RETURN
      END
c-----------------------------------------------------------------------------
      SUBROUTINE SHORT3 ( SPB, SP, CLAT, I, J, L, BLAT )
      DIMENSION SP(1000), CLAT(1000), BLAT(25), SPB(1000)
c     DIFV  - Difference in latitude or longitude.
c     DIFT  - Difference in shot point.
c     BLAT  - Latitude or longitude.
            DIFV   = CLAT(I+1) - CLAT(I)
            DIFT   = SP(I+1) - SP(I)
            TCOR   = DIFV / DIFT
```

```
            BLAT(L)  = TCOR* ( SPB(J) - SP(I) ) + CLAT(I)
        RETURN
        END

c-------------------------------------------------------------------------------
        SUBROUTINE SHORT2  ( SP, SPB, VH, IS, J, K, L, LL, M, NN, VMATCH )
        DIMENSION SP(1000), SPB(1000), VMATCH(3,1000), IS(20,10), VH(3,25)
c       DIFV    - Difference in velocity.
c       DIFT    - Difference in shot point.
c       VMATCH      - Velocity.
            DIFV    = VH(K,J+1) - VH(K,J)
            DIFT    = SPB( IS(J+1,1) ) - SPB( IS(J,1) )
            TCOR    = DIFV / DIFT
            IF ( ( J .EQ. 1 ) .AND. ( K .EQ. 1 ) ) L = 1
c       I       - Counter for (M-1) number.
        DO 100 I = L, M - 1
            IF ( J .EQ. ( NN - 1 ) ) GO TO 40
            IF ( SP(I) .GE. SPB( IS(J+1,1) ) ) GO TO 50
40                  VMATCH(K,I) = TCOR* ( SP(I) - SPB( IS(J,1) ) ) + VH(K,J)
100     CONTINUE
50          LL = I
        RETURN
        END
```

Appendix 3.4

```
# The macro GATEST use to generate two time-velocity (average) plots corresponding the required
# seismic line.This Macro need three files from the output ALL2 program.
# The velocity scale of the two plots will be not the exact values, only for the first velocity
# analyses, for the other its a kind of multiplying values as mention later.

MACRO  GATEST
# Type the file name started with VTR. following by the line number, eg. 248 for seismic line V248.
PRINT ( " TYPE THE FILE CONTAINING THE DATA AS ( VTR.*** ) ", QUOTE = F )
# Read the name of the file as ?T(FILNM2).
        ?T(FILNM2)      <- READ ( , LENGTH = 1, PRINT = F )
# Type the file name started with DIF. following by the line number, eg. 248 for seismic line V248.
PRINT ( " TYPE THE FILE CONTAINING THE DATA AS ( DIF.*** ) ", QUOTE = F )
# Read the name of the file as ?T(FILNM).
        ?T(FILNM)       <- READ ( , LENGTH = 1, PRINT = F )
# Type the file name started with SAE. following by the line number, eg. 248 for seismic line V248.
PRINT ( " TYPE THE FILE CONT. START & END OF EACH BOX AS ( SAE.*** ) ", QUOTE = F )
# Read the name of the file as ?T(FILNM1).
        ?T(FILNM1)      <- READ ( , LENGTH = 1, PRINT = F )
# Read the ?T(FILNM1) file from Suilven system into a matrix of 6 columns ?T(SAE) file in S system.
        ?T(SAE)                 <- MATRIX ( READ ( ?T(FILNM1) ), NCOL = 6, BYROW = T )
# Read the ?T(FILNM) file from Suilven system into a matrix of 7 columns ?T(DATA) file in S system.
        ?T(DATA)        <- MATRIX ( READ ( ?T(FILNM) ), NCOL = 7, BYROW = T )
# Read the ?T(FILNM2) file from Suilven system into a matrix of 6 columns ?T(DATA2) file in S system.
        ?T(DATA2)       <- MATRIX ( READ ( ?T(FILNM2) ), NCOL = 6, BYROW = T )
# Change the sign of all time values (from DIX) in the first column from the ?T(DATA) matrix by
# multiplying all column values by (-1) and put the results into ?T(TCD1) file.
        ?T(TCD1)        <- ?T(DATA)[ , 1 ] * ( - 1 )
# Put all shot point numbers in the first column from the ?T(DATA2) matrix into ?T(SP).
        ?T(SP)          <- ?T(DATA2)[ , 1 ]
# Change the sign of all time values (from RMS) in the second column from the ?T(DATA) matrix by
# multiplying all column values by (-1) and put the results into ?T(TC1) file.
        ?T(TC1)                 <- ?T(DATA)[ , 2 ] * ( - 1 )
# Put all time differences values in the third column from the ?T(DATA) matrix into ?T(DIFFT).
        ?T(DIFFT)       <- ?T(DATA)[ , 3 ]
# Change the sign of all depth values (from RMS) in the forth column from the ?T(DATA) matrix by
```

```
# multiplying all column values by (-1) and put the results into ?T(DEPR1) file.
        ?T(DEPR1)       <-  ?T(DATA)[ , 4 ] * ( - 1 )
# Change the sign of all depth values (from DIX) in the fifth column from the ?T(DATA) matrix by
# multiplying all column values by (-1) and put the results into ?T(DEPD1) file.
        ?T(DEPD1)       <-  ?T(DATA)[ , 5 ] * ( - 1 )
# Put all depth differences values in the sixth column from the ?T(DATA) matrix into ?T(DIFFD).
        ?T(DIFFD)       <-  ?T(DATA)[ , 6 ]
# Put all velocity values in the seventh column from the ?T(DATA) matrix into ?T(VC).
        ?T(VC)          <-  ?T(DATA)[ , 7 ]
# Use the LEN function to find the length of the first column from the ?T(SAE) matrix and put the
# value into ?T(LEN) file, which will be the same number of velocity analysis boxes used in the line.
        ?T(LEN)         <-  LEN (? T(SAE)[ , 1 ] )
# Do the next two operations ?T(LEN) times.
        FOR  ( I  IN  1 : ?T(LEN) )  {
# Subtract the second shot point from the first shot point then multiply the result by 15 and put the
# output value in ?T(N) file.
?T(N)                   <- ( ?T(SP)[ ?T(SAE)[I,1] ] - ?T(SP)[ ?T(SAE) [1,1] ] ) * 15
# Add the previous value to all velocity values corresponding to the same shot point number.
?T(VC)[ ?T(SAE)[I,1] : ?T(SAE)[I,2] ]       <- ( ?T(VC)[ ?T(SAE)[I,1] : ?T(SAE)[I,2] ] + ?T(N) )
        }
# Plot the time-velocity curve equivalent to the RMS velocity.
PLOT ( ?T(VC),  ?T(TC1),  TYPE = " L ",  XLIM = C(0,10000),  YLIM = C(-3,0),
        XLAB = " VELOCITY_IN ( M / S ) ---> ",  YLAB = " T.W.T. IN ( S ) ",  AXES = F )
        AXIS ( 3 ) ; AXIS ( 2 )
        TITLE ( MAIN = " " )
# Plot the time-velocity curve equivalent to the Dix average velocity.
PLOT ( ?T(VC),  ?T(TCD1),  TYPE = " L ",  XLIM = C(0,10000),  YLIM = C(-3,0),
        XLAB = " VELOCITY_IN ( M / SEC ) ---> ",  YLAB = " T.W.T. IN ( SEC ) ",  AXES = F )
        AXIS ( 3 ) ; AXIS ( 2 )
        TITLE ( MAIN = " " )
# Apply ZAP Macro to remove all previous files which started with T.
        ?ZAP(T*)
END
```

```
# The macro GATEST2 use to generate four time-velocity (interval) plots corresponding the required
# seismic line.This Macro need three files from the output ALL2 program.
# The velocity scale of the four plots will be not the exact values, only for the first velocity
# analyses, for the other its a kind of multiplying values as mention later.
```

MACRO GATEST2

```
# Type the file name started with VTR. following by the line number, eg. 248 for seismic line V248.
PRINT ( " TYPE THE FILE CONTAINING THE DATA AS ( VTR.*** ) ", QUOTE = F )
# Read the name of the file as ?T(FILNM2).
        ?T(FILNM2)      <- READ ( , LENGTH = 1, PRINT = F )
# Type the file name started with DDIF. following by the line number, eg. 248 for seismic line V248.
PRINT ( " TYPE THE FILE CONTAINING THE DATA AS ( DDIF.*** ) ", QUOTE = F )
# Read the name of the file as ?T(FILNM).
        ?T(FILNM)       <- READ ( , LENGTH = 1, PRINT = F )
# Type the file name started with SAE. following by the line number, eg. 248 for seismic line V248.
PRINT ( " TYPE THE FILE CONT. START & END OF EACH BOX AS ( SAE.*** ) ", QUOTE = F )
# Read the name of the file as ?T(FILNM1).
        ?T(FILNM1)      <- READ ( , LENGTH = 1, PRINT = F )
# Read the ?T(FILNM1) file from Suilven system into a matrix of 6 columns ?T(SAE) file in S system.
        ?T(SAE)         <- MATRIX ( READ ( ?T(FILNM1) ), NCOL = 6, BYROW = T )
# Read the ?T(FILNM) file from Suilven system into a matrix of 10 columns ?T(DATA) file in S system.
        ?T(DATA)        <- MATRIX ( READ ( ?T(FILNM) ), NCOL = 10, BYROW = T )
# Read the ?T(FILNM2) file from Suilven system into a matrix of 6 columns ?T(DATA2) file in S system.
        ?T(DATA2)       <- MATRIX ( READ ( ?T(FILNM2) ), NCOL = 6, BYROW = T )
# Put all shot point numbers in the first column from the ?T(DATA2) matrix into ?T(SP).
        ?T(SP)          <- ?T(DATA2)[ , 1 ]
# Put all interval velocity values in the first column from the ?T(DATA) matrix into ?T(VI).
        ?T(VI)          <- ?T(DATA)[ , 1 ]
# Put all Dix interval velocity values in the second column from the ?T(DATA) matrix into ?T(VIDL).
        ?T(VIDL)        <- ?T(DATA)[ , 2 ]
# Put all RMS velocity differences values in the third column from the ?T(DATA) matrix into ?T(DIFRMS).
        ?T(DIFRMS)      <- ?T(DATA)[ , 3 ]
# Put all Dix velocity differences values in the forth column from the ?T(DATA) matrix into ?T(DIFDIX).
        ?T(DIFDIX)      <- ?T(DATA)[ , 4 ]
# Put all interval velocity (rms) differences values in the fifth column from the ?T(DATA) matrix into ?T(VINTERR)
        ?T(VINTERR)     <- ?T(DATA)[ , 5 ]
# Put all Dix interval velocity differences values in the sixth column from the ?T(DATA) matrix into ?T(VINTERD)
```

```
        ?T(VINTERD)    <-  ?T(DATA)[ , 6 ]
# Change the sign of all time values (from RMS) in the seventh column from the ?T(DATA) matrix by
# multiplying all column values by (-1) and put the results into ?T(TC2) file.
        ?T(TC2)        <-  ?T(DATA)[ , 7 ] * ( - 1 )
# Change the sign of all time values (from DIX) in the eight column from the ?T(DATA) matrix by
# multiplying all column values by (-1) and put the results into ?T(TCD2) file.
        ?T(TCD2)       <-  ?T(DATA)[ , 8 ] * ( - 1 )
# Put all depth differences values (from RMS) in the ninth column from the ?T(DATA) matrix into ?T(DDEPR).
        ?T(DDEPR)      <-  ?T(DATA)[ , 9 ]
# Put all depth differences values (from DIX) in the tenth column from the ?T(DATA) matrix into ?T(DDEPD).
        ?T(DDEPD)      <-  ?T(DATA)[ , 10 ]
# Use the LEN function to find the length of the first column from the ?T(SAE) matrix and put the
# value into ?T(LEN) file, which will be the same number of velocity analysis boxes used in the line.
        ?T(LEN)        <-  LEN (? T(SAE)[ , 1 ] )
# Do the next five operations ?T(LEN) times.
        FOR  ( I IN 1 : ?T(LEN) ) {
# Subtract the second shot point from the first shot point then multiply the result by 100 and put the
# output value in ?T(N) file.
?T(N)                                          <- ( ?T(SP)[ ?T(SAE)[I,1] ] - ?T(SP)[ ?T(SAE) [1,1] ] ) * 100
# Add the previous value to all interval velocity values corresponding to the same shot point number.
?T(VI)[ ?T(SAE)[I,3] : ?T(SAE)[I,4] ]          <- ( ?T(VI)[ ?T(SAE)[I,3] : ?T(SAE)[I,4] ] + ?T(N) )
?T(VIDL)[ ?T(SAE)[I,3] : ?T(SAE)[I,4] ]        <- ( ?T(VIDL)[ ?T(SAE)[I,3] : ?T(SAE)[I,4] ] + ?T(N) )
?T(VINTERR)[ ?T(SAE)[I,3] : ?T(SAE)[I,4] ]     <- ( ?T(VINTERR)[ ?T(SAE)[I,3] : ?T(SAE)[I,4] ] + ?T(N) )
?T(VINTERD)[ ?T(SAE)[I,3] : ?T(SAE)[I,4] ]     <- ( ?T(VINTERD)[ ?T(SAE)[I,3] : ?T(SAE)[I,4] ] + ?T(N) )
        }
# Plot the time-velocity curve.
PLOT ( ?T(VINTERR), ?T(TC2), TYPE = " L ", XLIM = C(0,50000), YLIM = C(-3,0),
        XLAB = " INT.VELOCITY_IN ( M / S ) ---> ", YLAB = " T.W.T. IN ( S ) ", AXES = F )
        AXIS ( 3 ) ; AXIS ( 2 )
        TITLE ( MAIN = " " )
# Plot the time-velocity curve.
PLOT ( ?T(VINTERD), ?T(TCD2), TYPE = " L ", XLIM = C(0,50000), YLIM = C(-3,0),
        XLAB = " INT.VELOCITY_IN ( M / S ) ---> ", YLAB = " T.W.T. IN ( S ) ", AXES = F )
        AXIS ( 3 ) ; AXIS ( 2 )
        TITLE ( MAIN = " " )
# Plot the time-velocity curve.
PLOT ( ?T(VI), ?T(TC2), TYPE = " L ", XLIM = C(0,50000), YLIM = C(-3,0),
```

```
        XLAB = " INT.VELOCITY_IN ( M / S ) ---> ",  YLAB = " T.W.T. IN ( S ) ",  AXES = F )
        AXIS ( 3 ) ; AXIS ( 2 )
        TITLE ( MAIN = " " )
# Plot the time-velocity curve.
PLOT ( ?T(VIDL),  ?T(TCD2),  TYPE = " L ",  XLIM = C(0,50000),  YLIM = C(-3,0),
        XLAB = " INT.VELOCITY_IN ( M / S ) ---> ",  YLAB = " T.W.T. IN ( S ) ",  AXES = F )
        AXIS ( 3 ) ; AXIS ( 2 )
        TITLE ( MAIN = " " )
# Apply ZAP Macro to remove all previous files which started with T.
        ?ZAP(T*)
END
```

Appendix 3.5

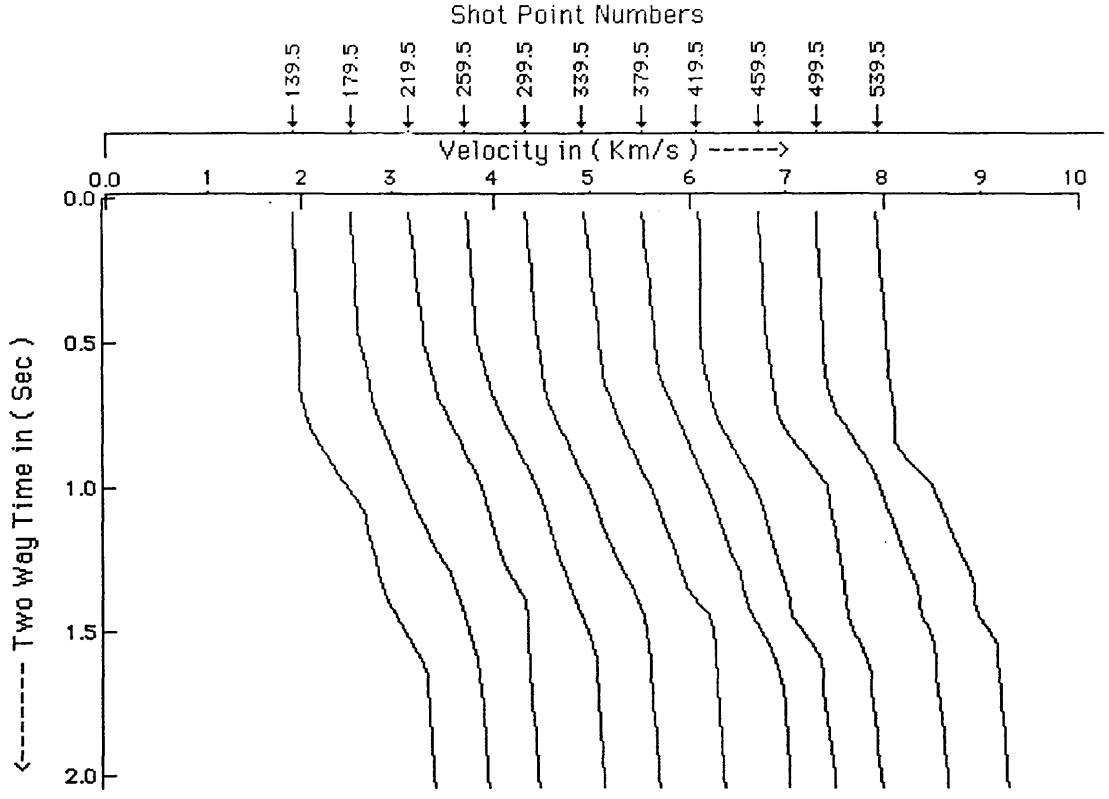

Fig.3.11a Stacking velocity - two-way time relationships along seismic line 6V250.

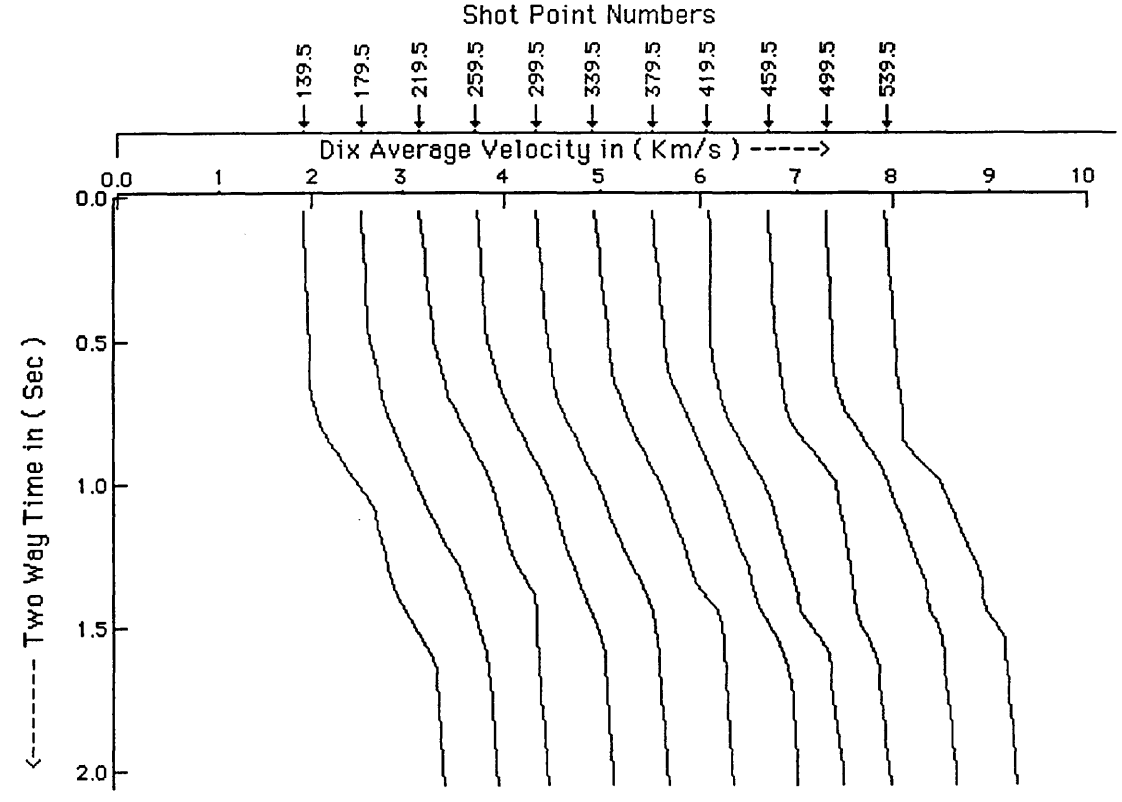

Fig.3.11b Dix average velocity - two-way time relationships along seismic line 6V250.

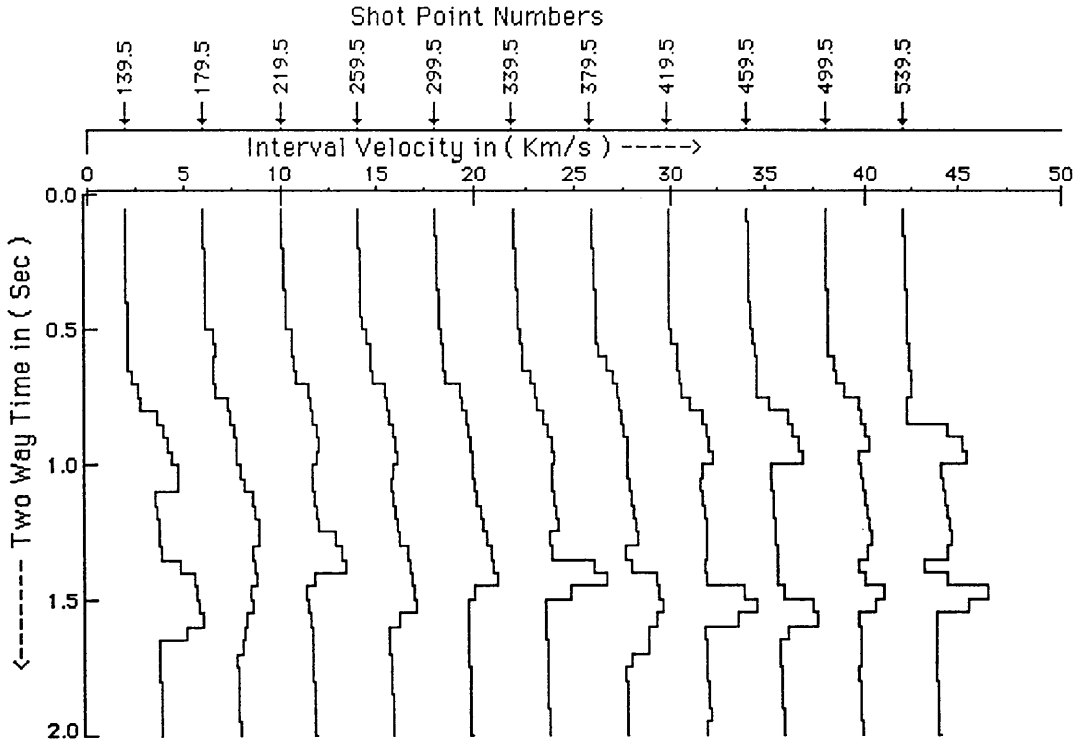

Fig.3.11c Interval velocity - two-way time two-way along seismic line 6V250, using the depth (D1) applied on equation (3.4).

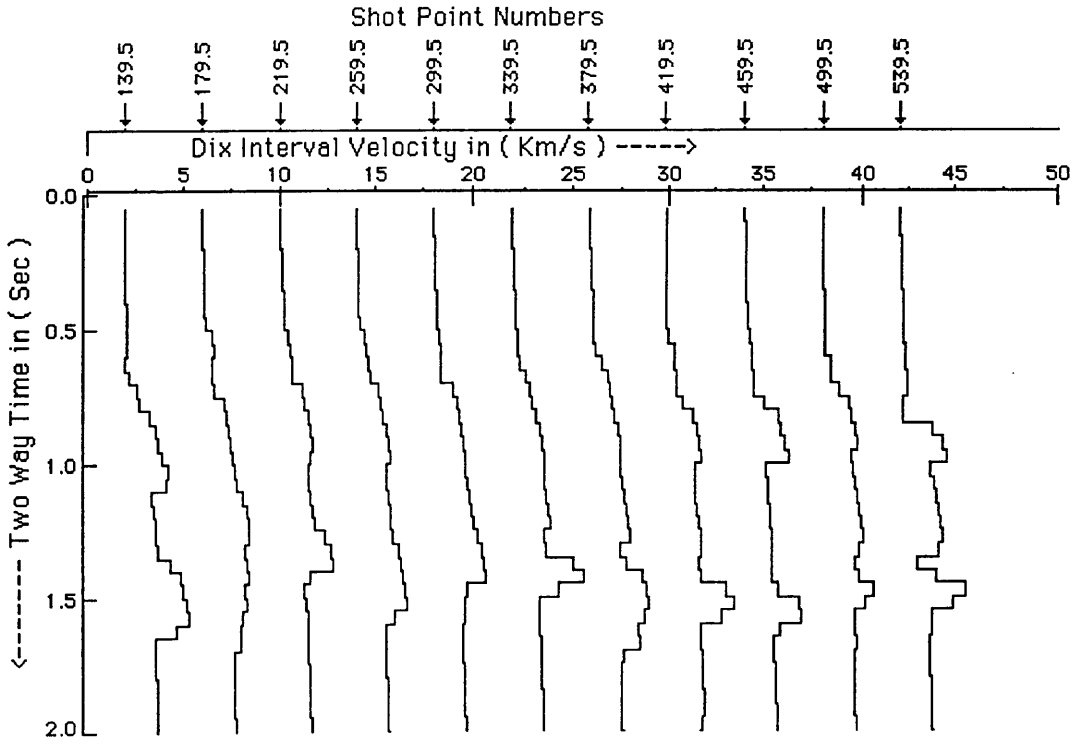

Fig.3.11d Interval velocity - two-way time two-way along seismic line 6V250, using the depth (D2) applied on equation (3.4).

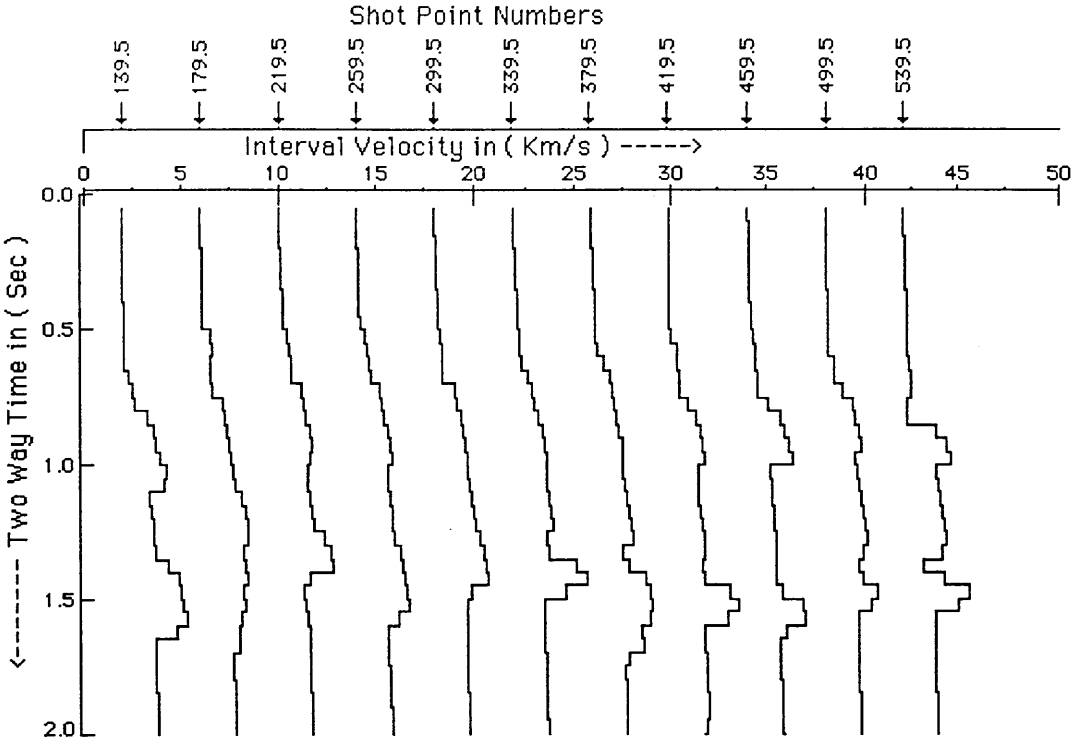

Fig.3.11e Interval velocity - two-way time two-way along seismic line 6V250, using stacking velocity applied on equation (3.13).

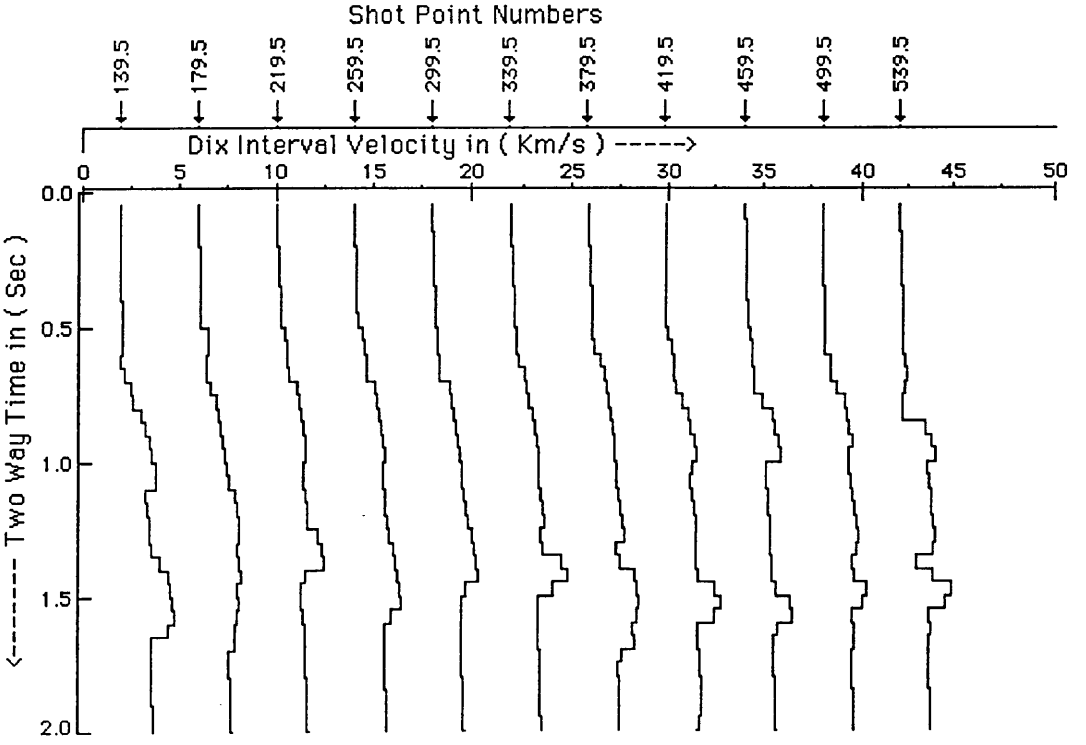

Fig.3.11f Interval velocity - two-way time two-way along seismic line 6V250, using Dix average velocity applied on equation (3.13).

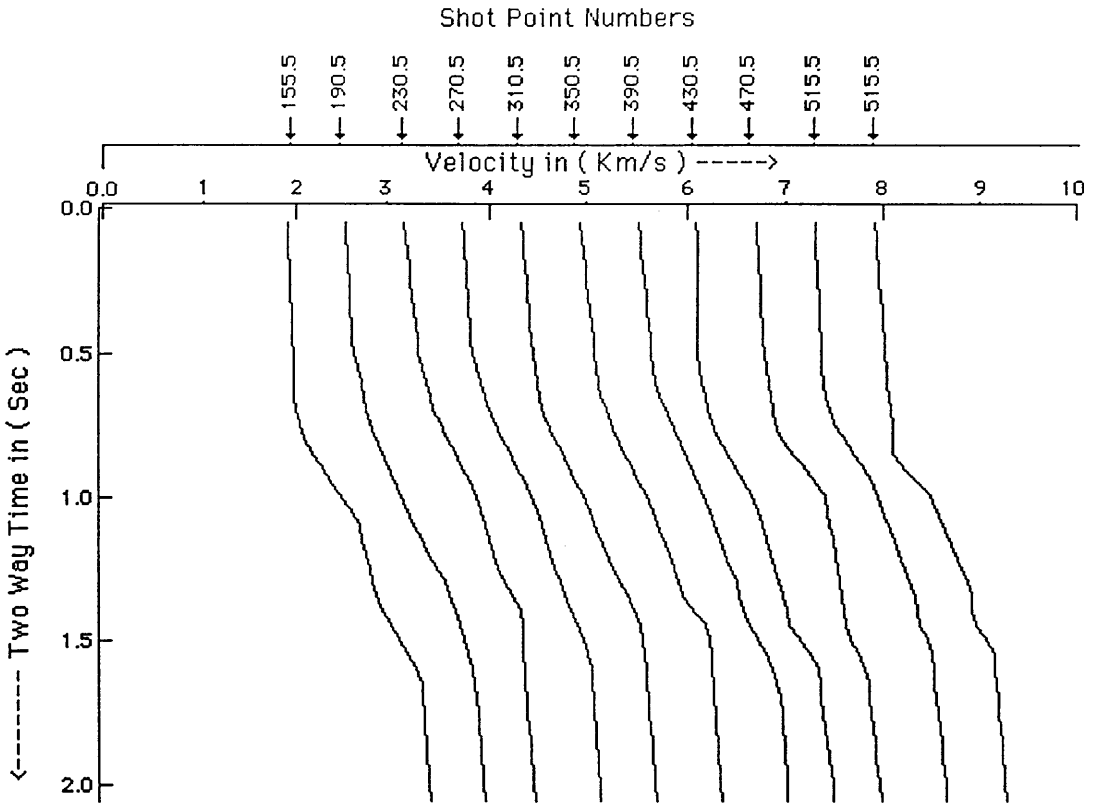

Fig.3.12a Stacking velocity - two-way time relationships along seismic line 6V252.

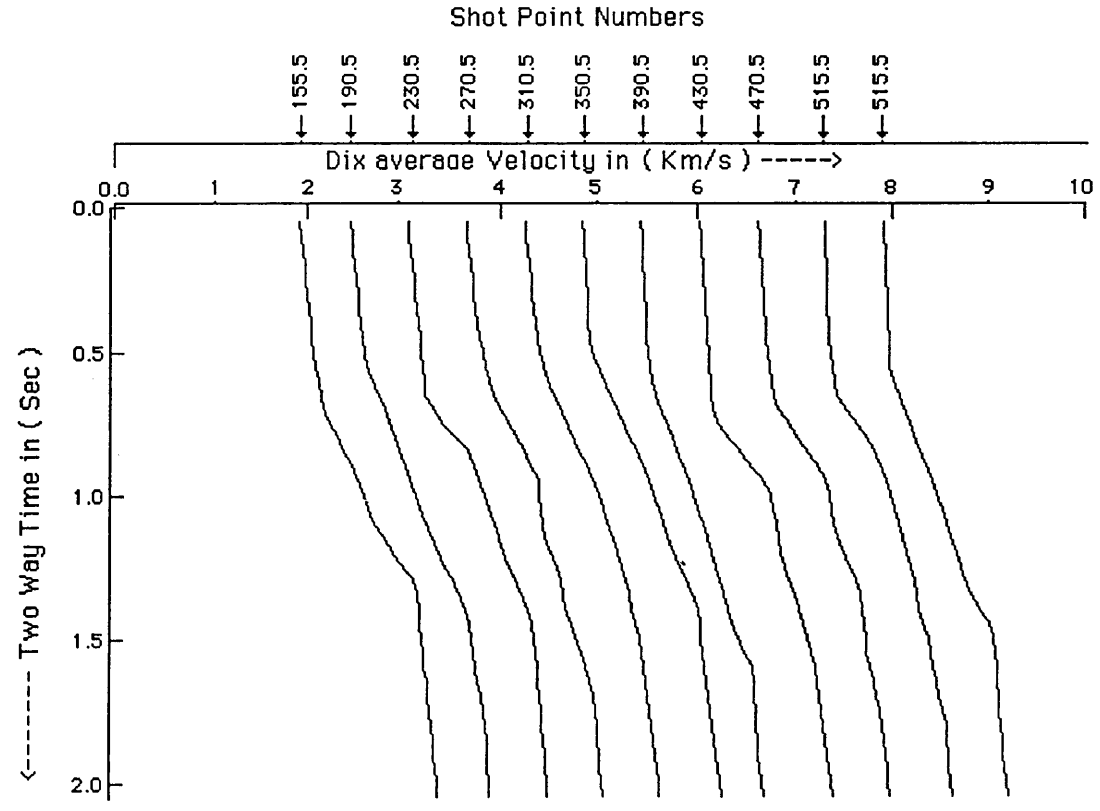

Fig.3.12b Dix average velocity - two-way time relationships along seismic line 6V252.

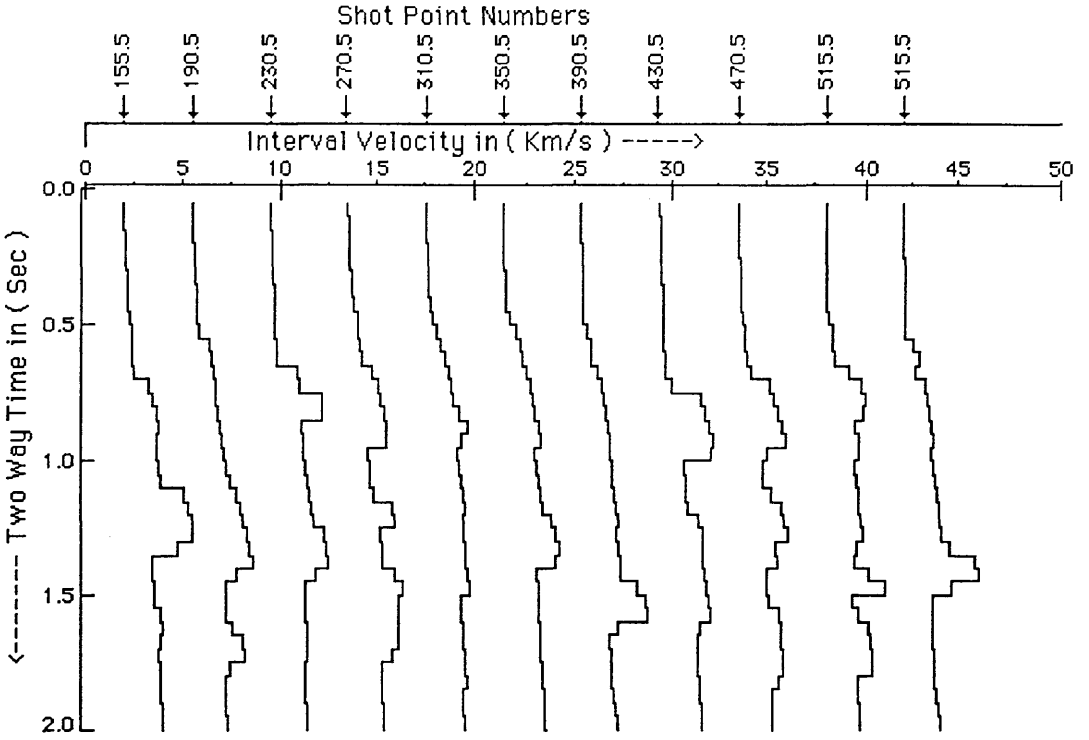

Fig.3.12c Interval velocity - two-way time two-way along seismic line 6V252, using the depth (D1) applied on equation (3.4).

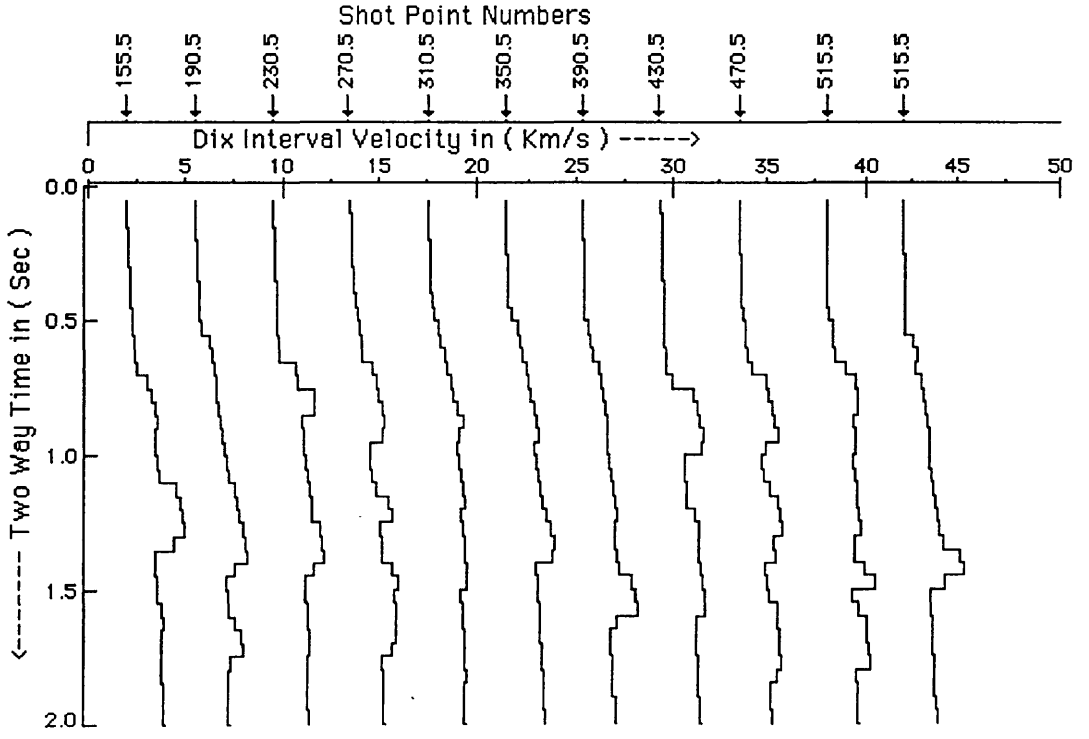

Fig.3.12d Interval velocity - two-way time two-way along seismic line 6V252, using the depth (D2) applied on equation (3.4).

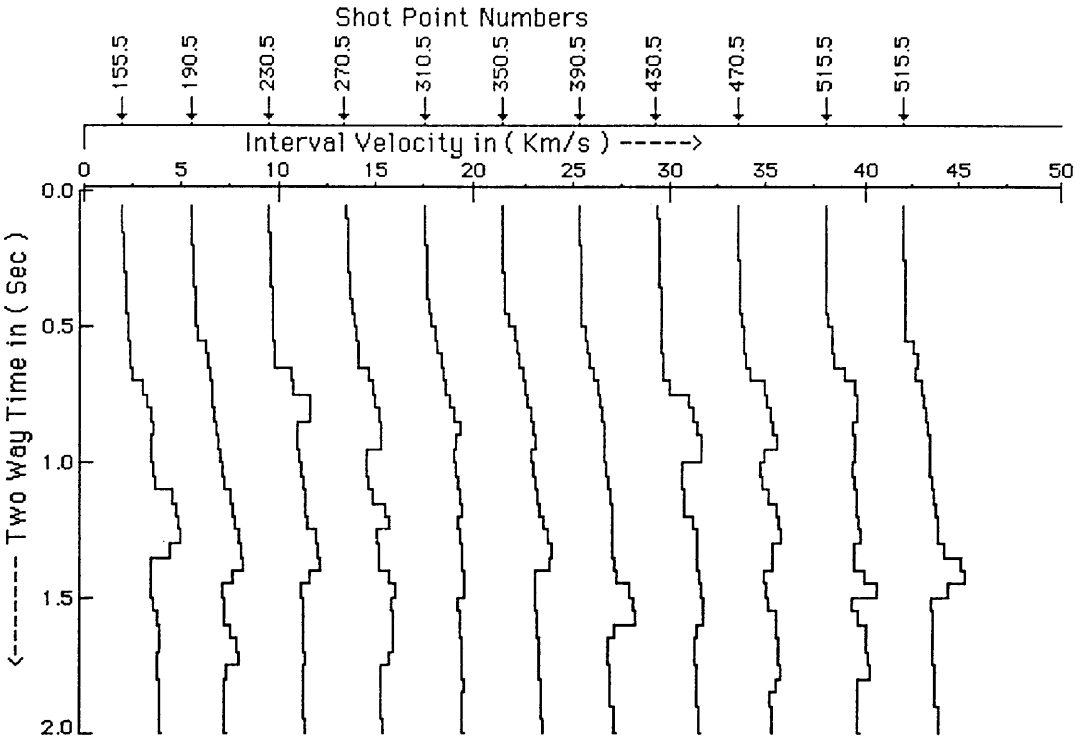

Fig.3.12e Interval velocity - two-way time two-way along seismic line 6V252, using stacking velocity applied on equation (3.13).

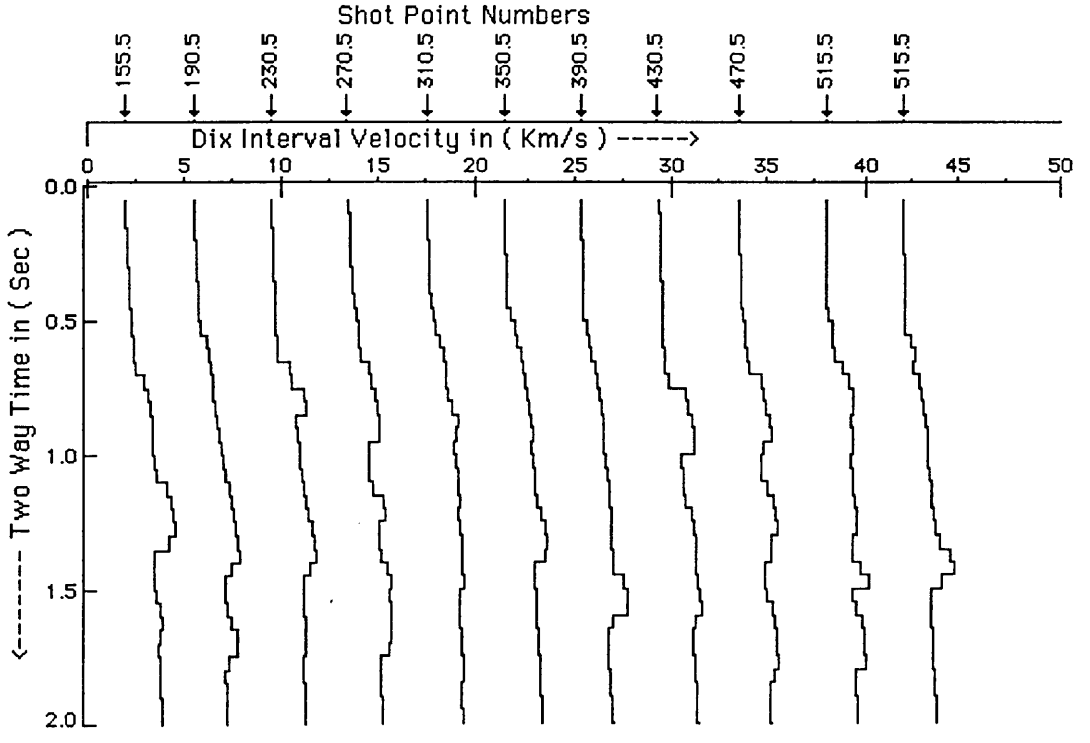

Fig.3.12f Interval velocity - two-way time two-way along seismic line 6V252, using Dix average velocity applied on equation (3.13).

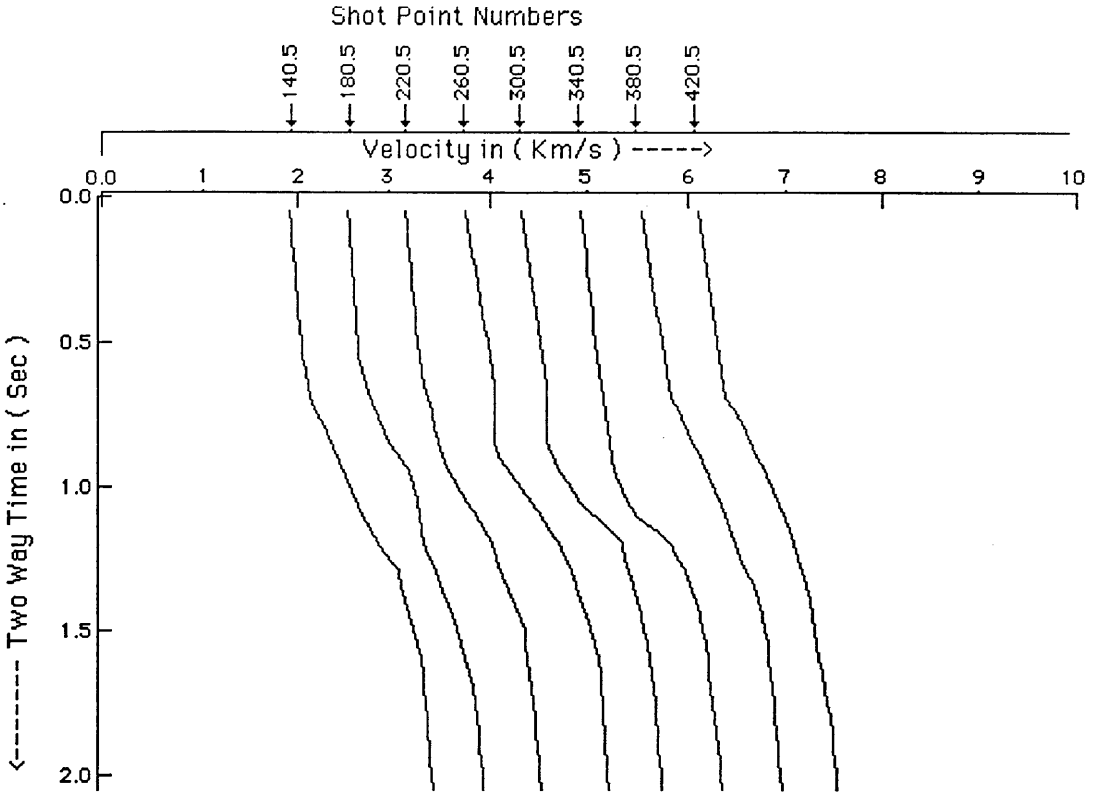

Fig.3.13a Stacking velocity - two-way time relationships along seismic line 6V253.

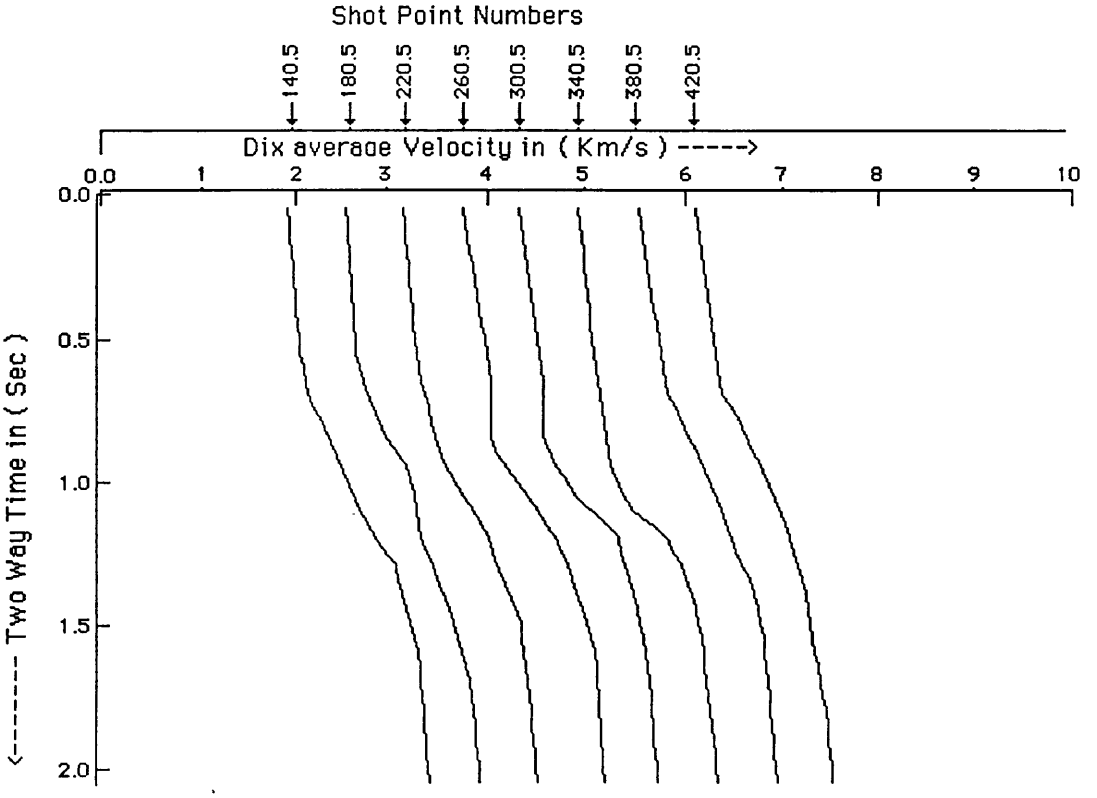

Fig.3.13b Dix average velocity - two-way time relationships along seismic line 6V253.

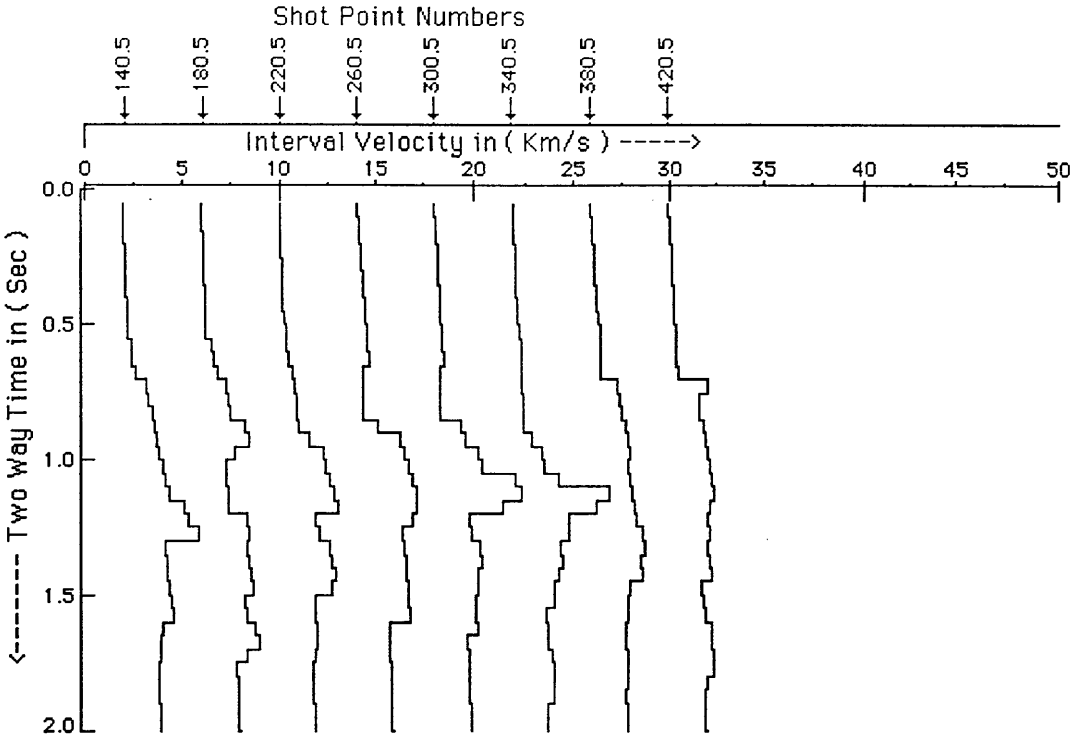

Fig.3.13c Interval velocity - two-way time two-way along seismic line 6V253, using the depth (D1) applied on equation (3.4).

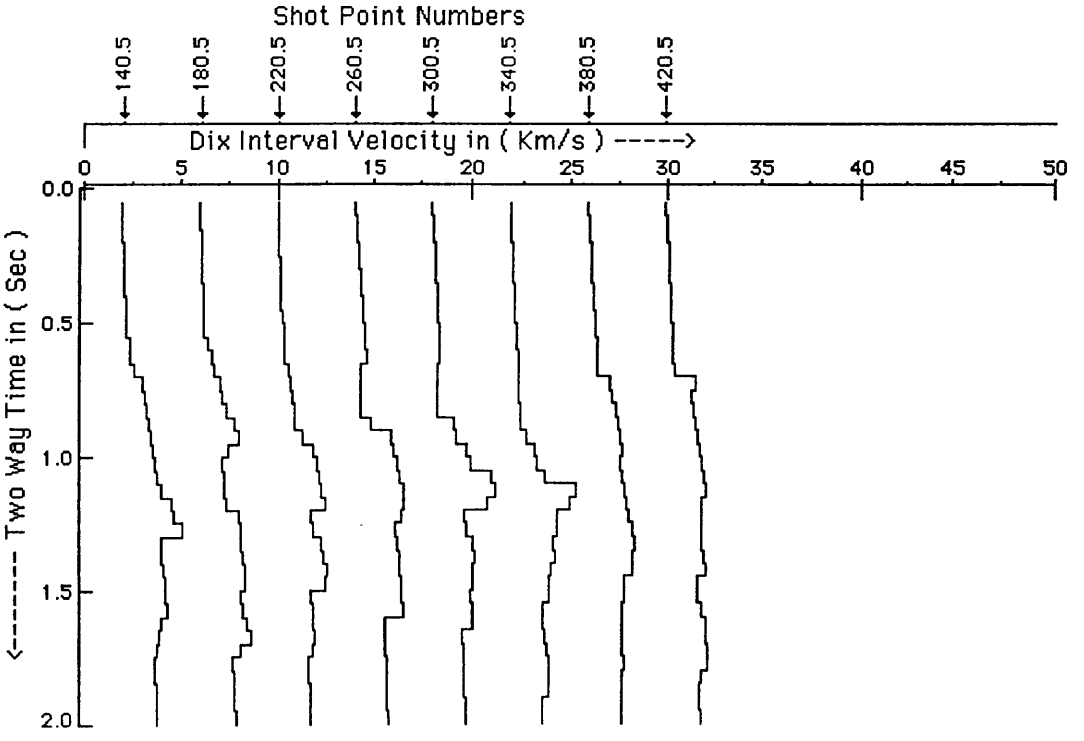

Fig.3.13d Interval velocity - two-way time two-way along seismic line 6V253, using the depth (D2) applied on equation (3.4).

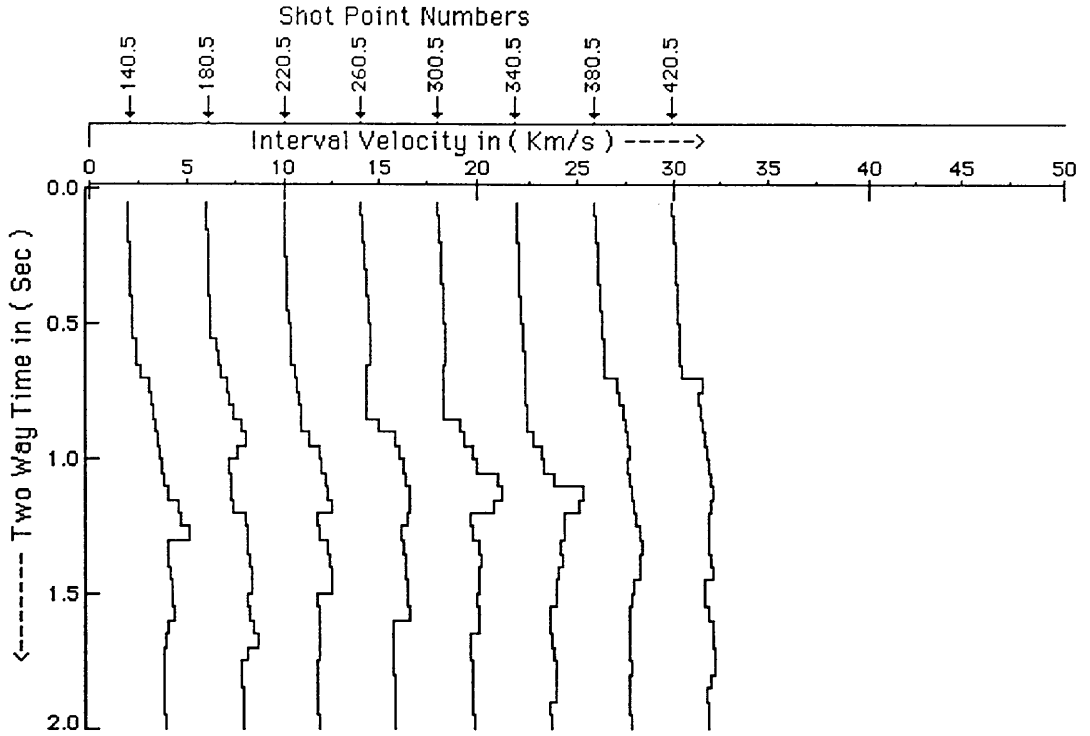

Fig.3.13e Interval velocity - two-way time two-way along seismic line 6V253, using stacking velocity applied on equation (3.13).

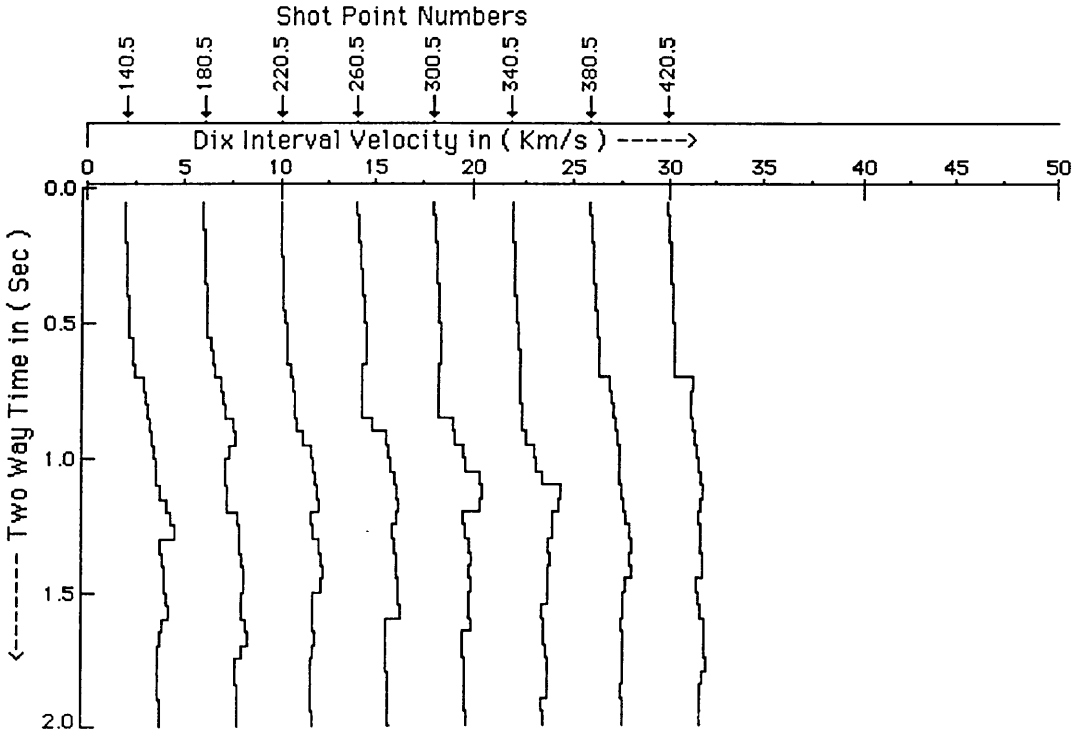

Fig.3.13f Interval velocity - two-way time two-way along seismic line 6V253, using Dix average velocity applied on equation (3.13).

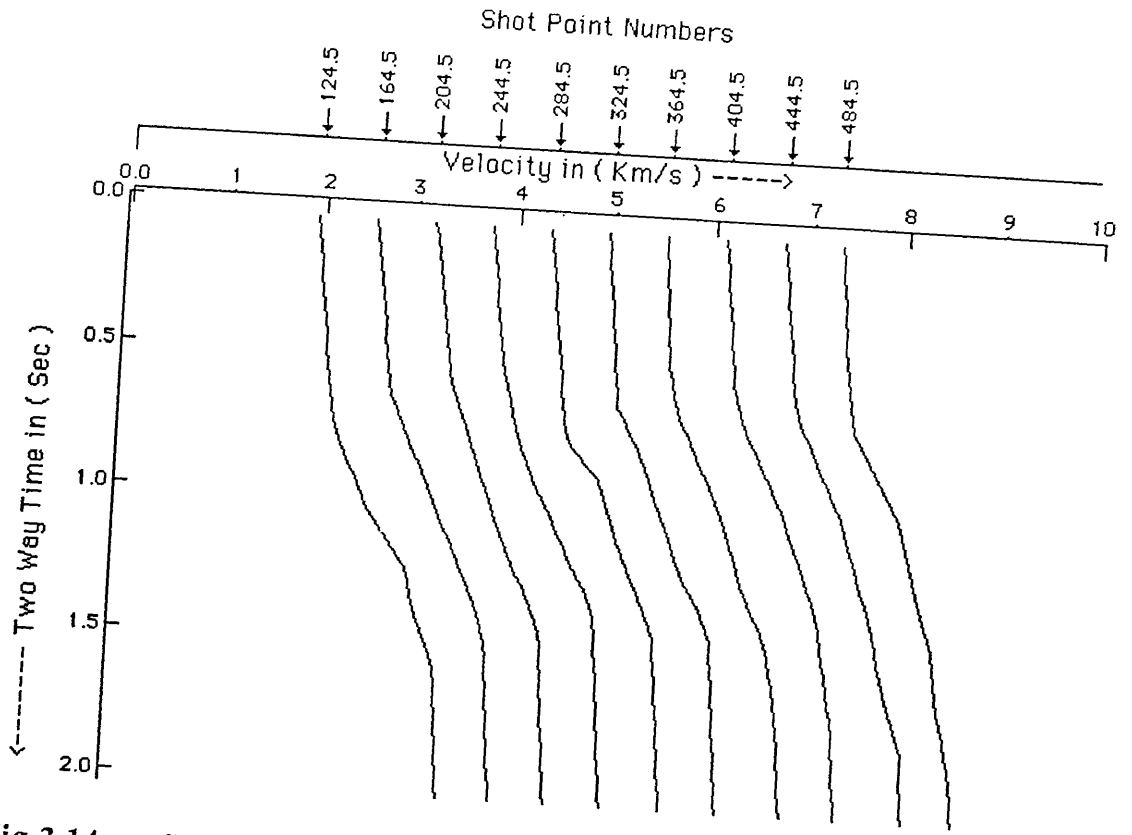

Fig.3.14a Stacking velocity - two-way time relationships along seismic line 6V254.

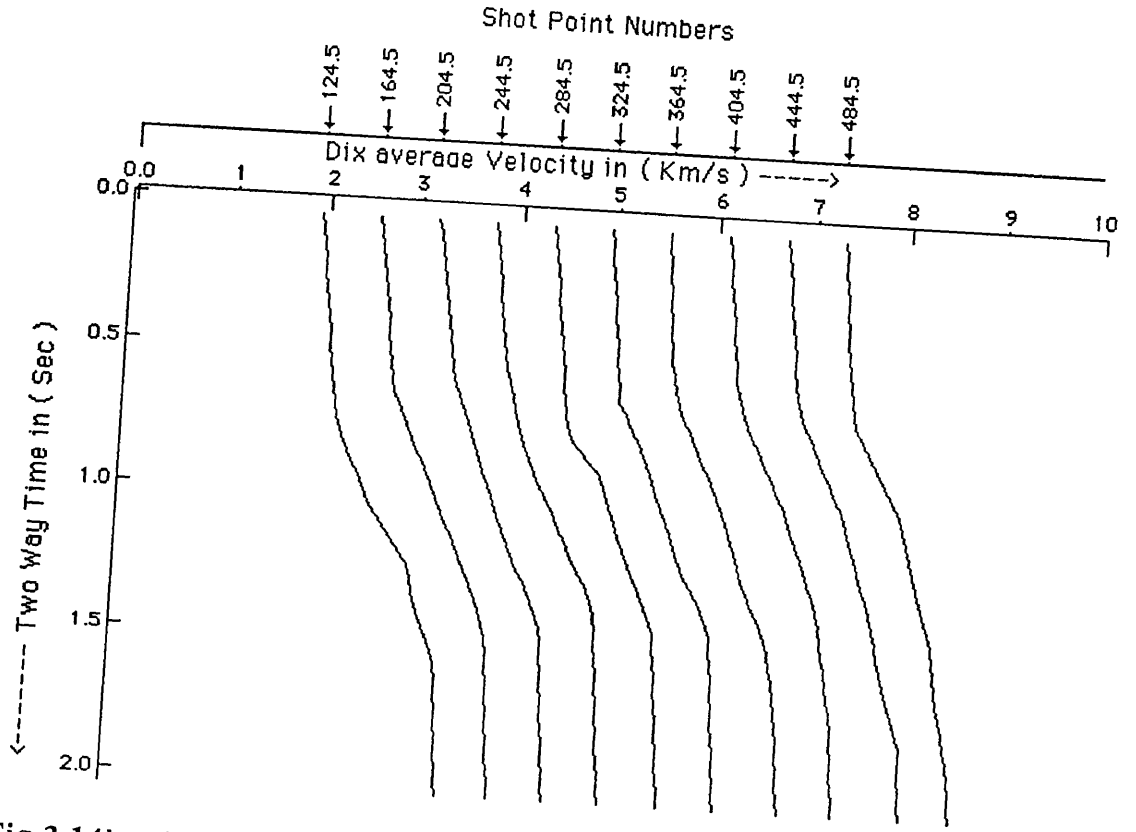

Fig.3.14b Dix average velocity - two-way time relationships along seismic line 6V254.

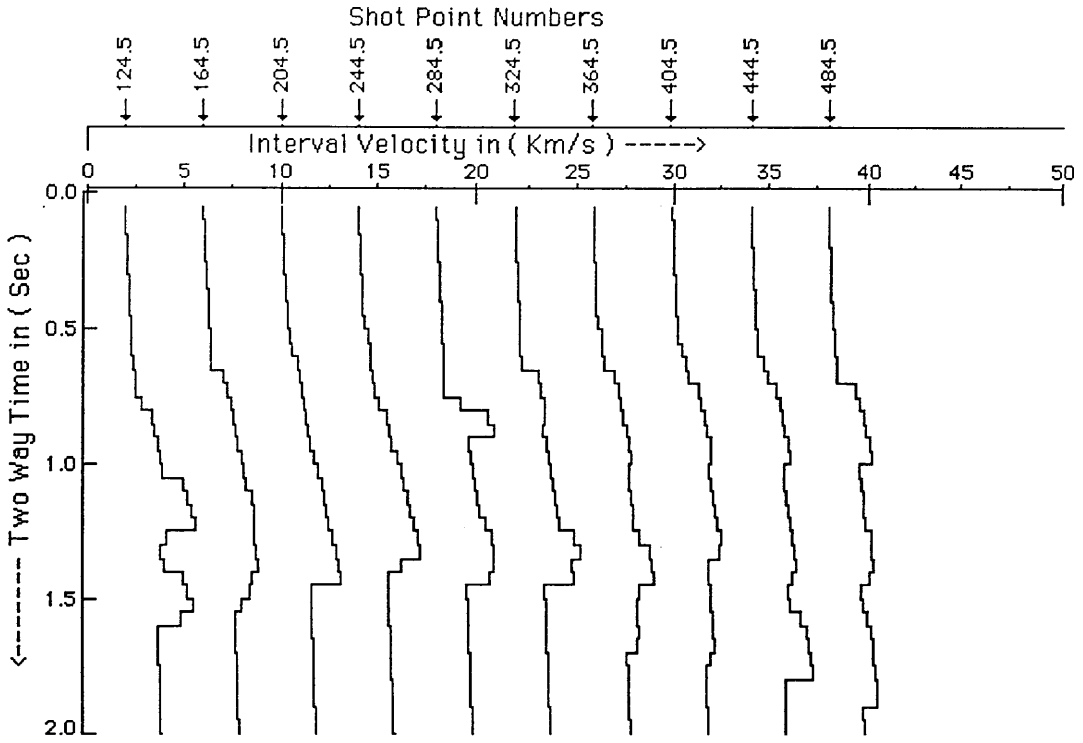

Fig.3.14c Interval velocity - two-way time two-way along seismic line 6V254, using the depth (D1) applied on equation (3.4).

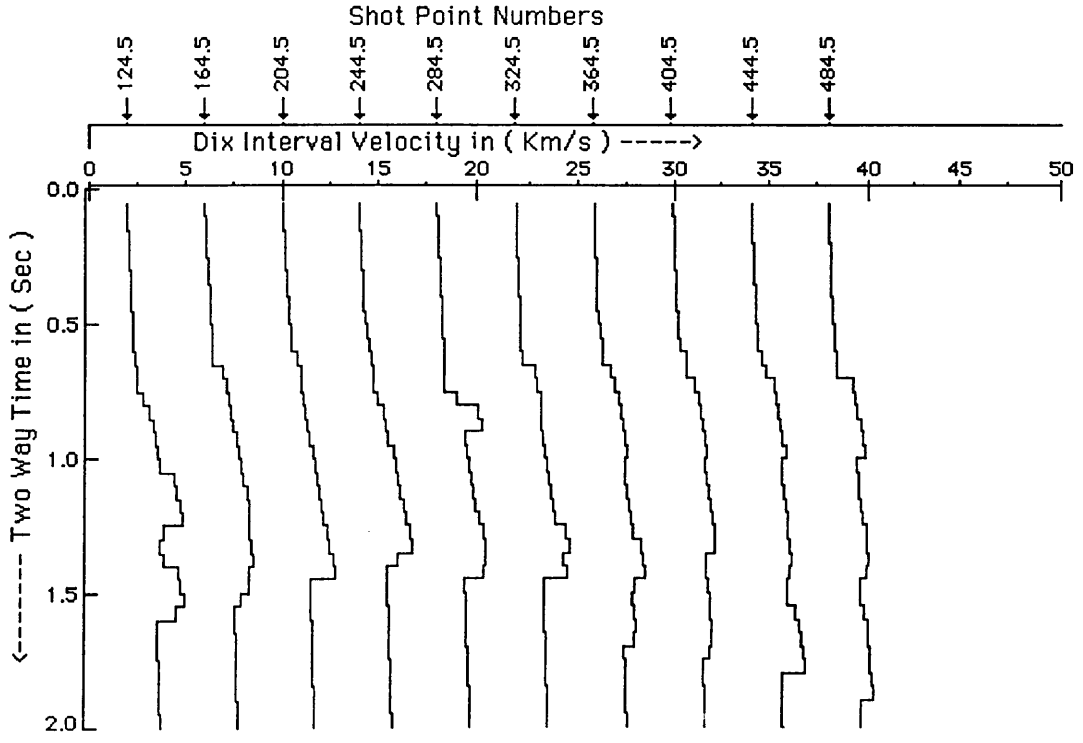

Fig.3.14d Interval velocity - two-way time two-way along seismic line 6V254, using the depth (D2) applied on equation (3.4).

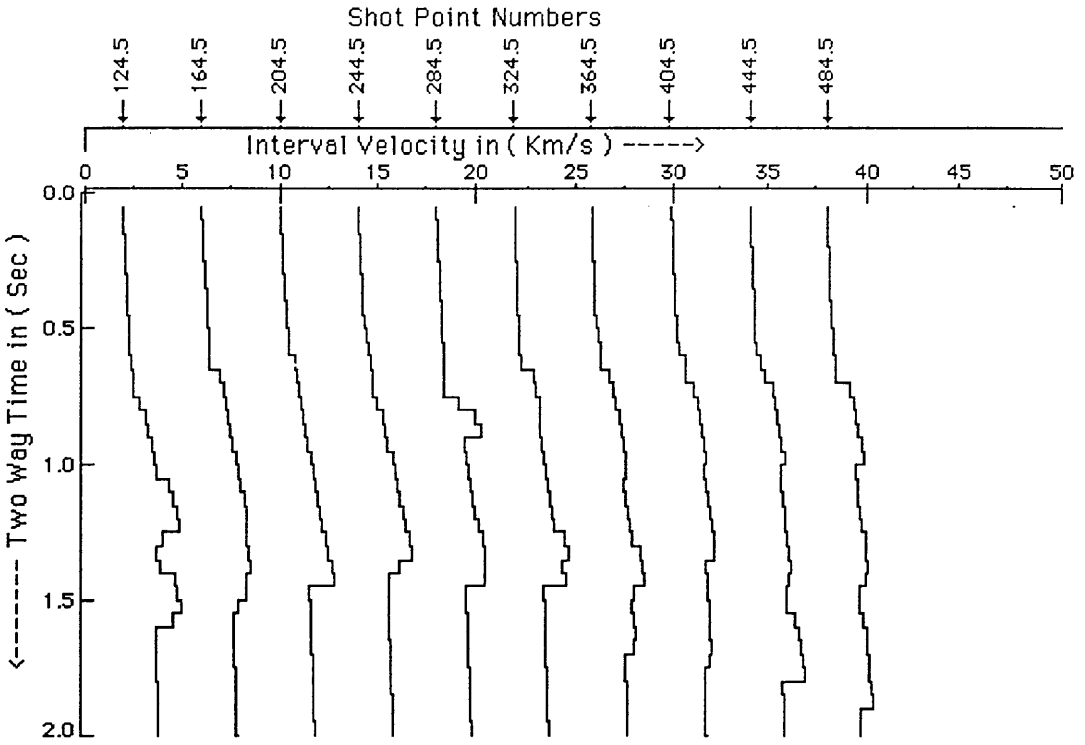

Fig.3.14e Interval velocity - two-way time two-way along seismic line 6V254, using stacking velocity applied on equation (3.13).

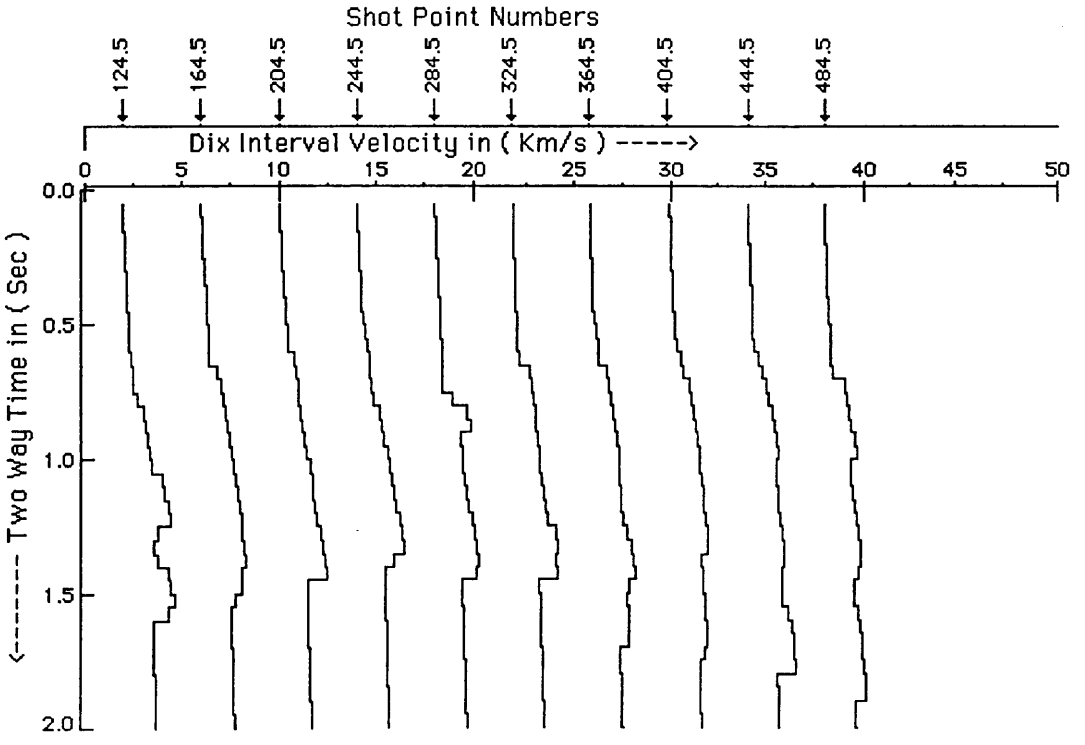

Fig.3.14f Interval velocity - two-way time two-way along seismic line 6V254, using Dix average velocity applied on equation (3.13).

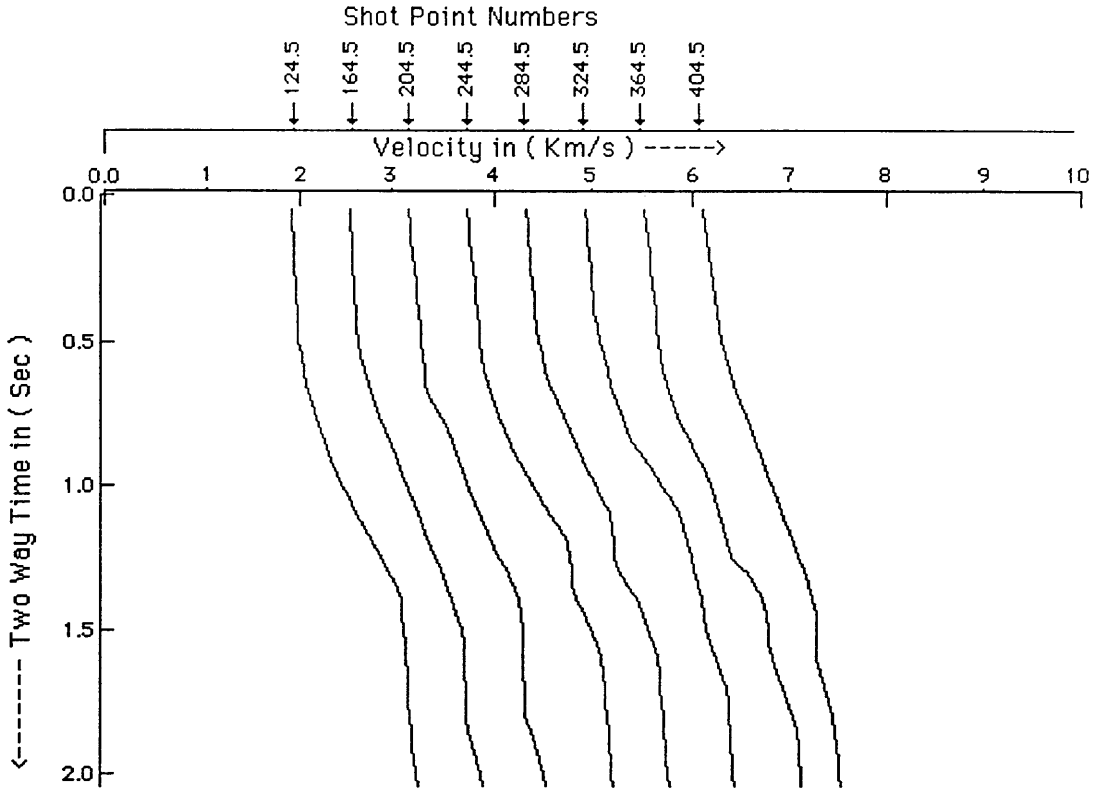

Fig.3.15a Stacking velocity - two-way time relationships along seismic line 6V255.

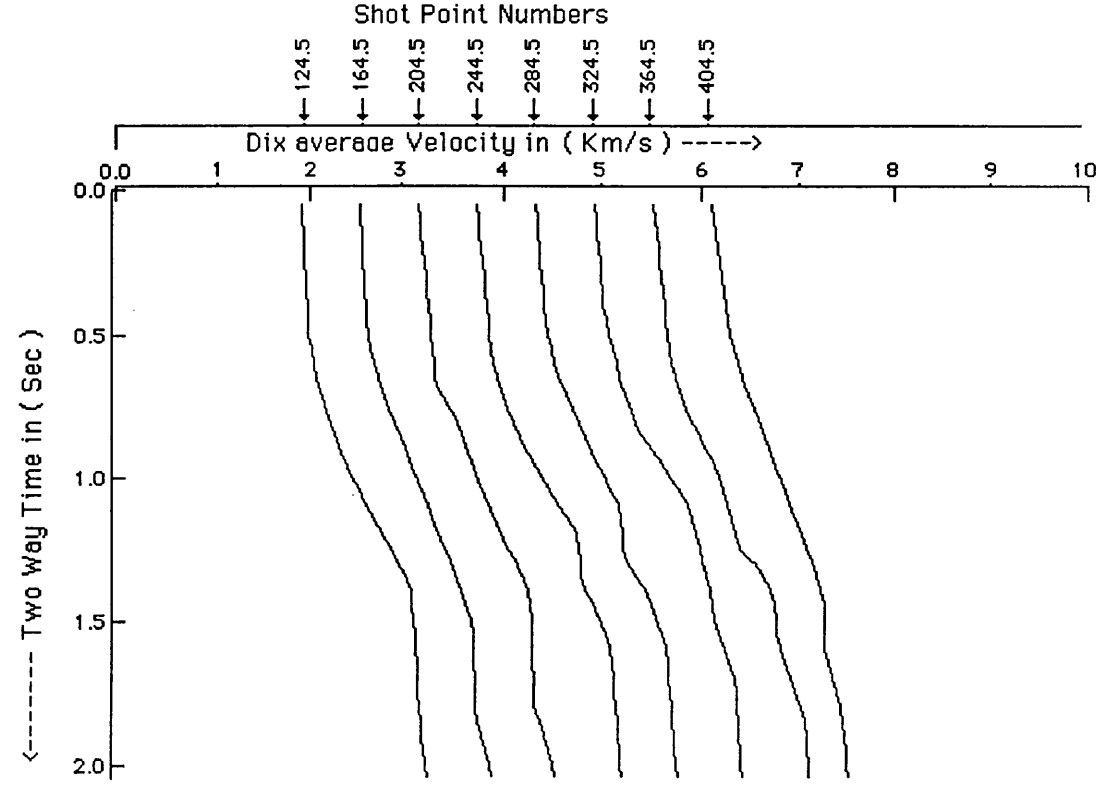

Fig.3.15b Dix average velocity - two-way time relationships along seismic line 6V255.

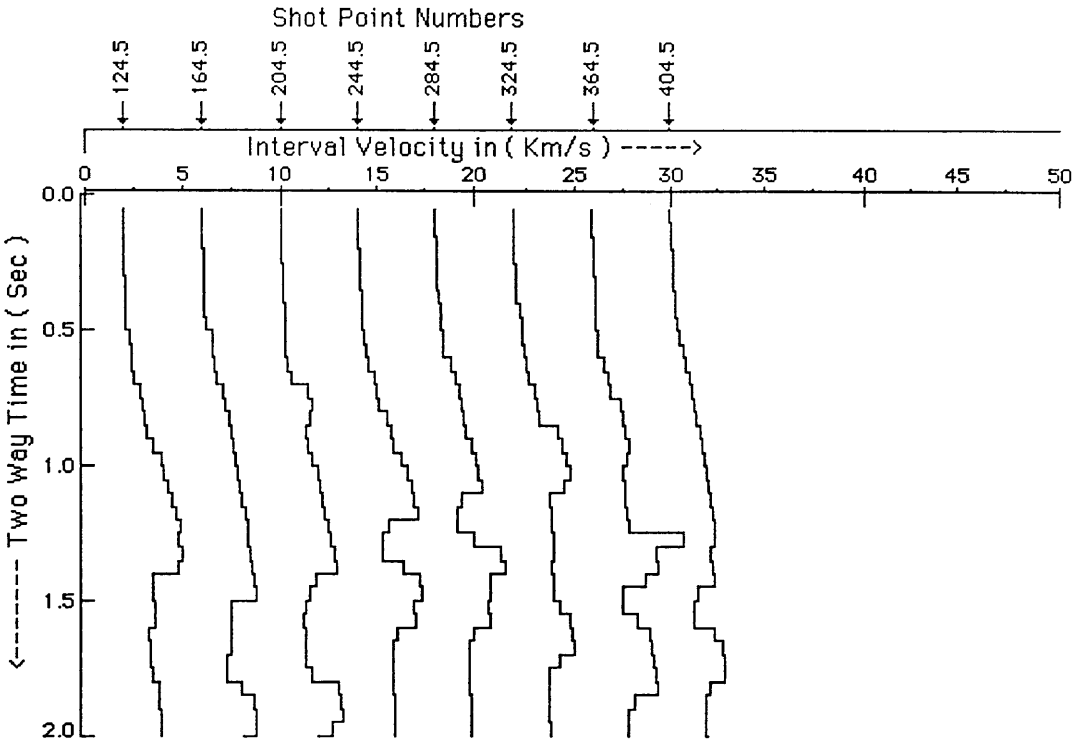

Fig.3.15c Interval velocity - two-way time two-way along seismic line 6V255, using the depth (D1) applied on equation (3.4).

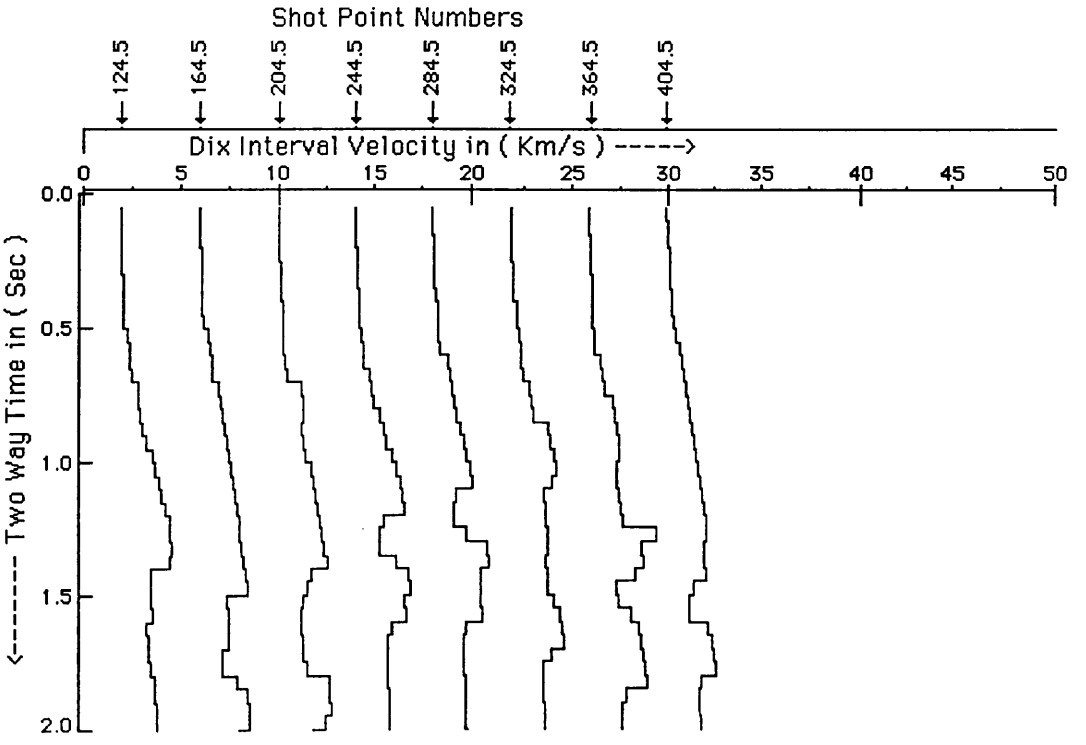

Fig.3.15d Interval velocity - two-way time two-way along seismic line 6V255, using the depth (D2) applied on equation (3.4).

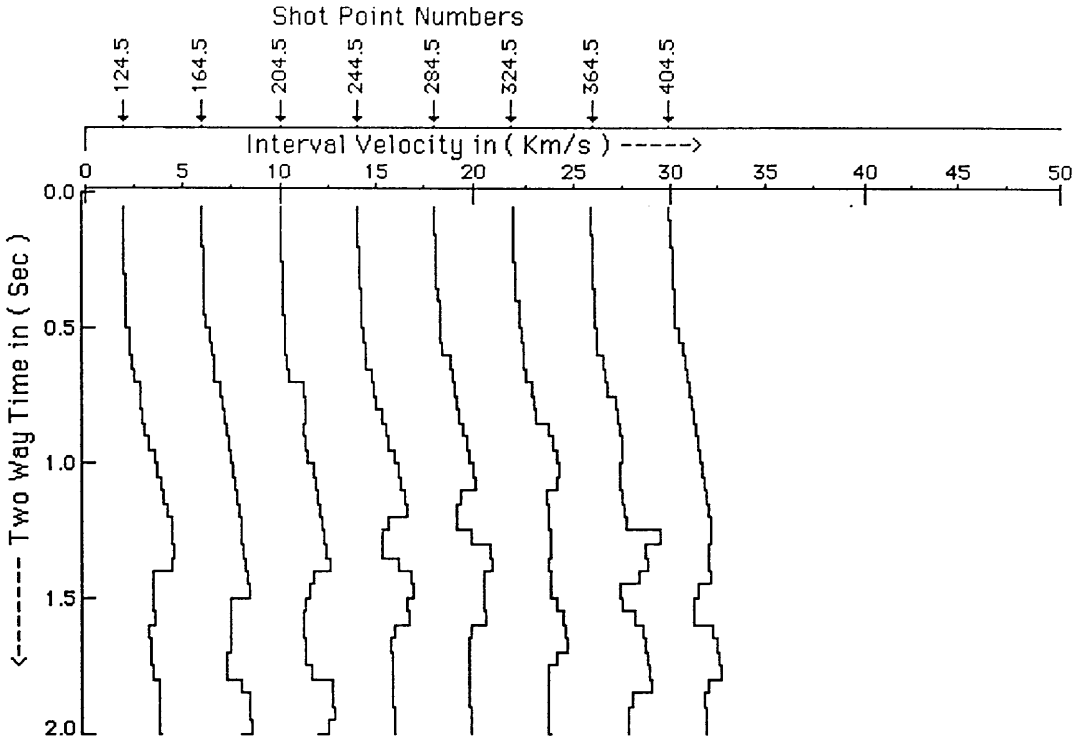

Fig.3.15e Interval velocity - two-way time two-way along seismic line 6V255, using stacking velocity applied on equation (3.13).

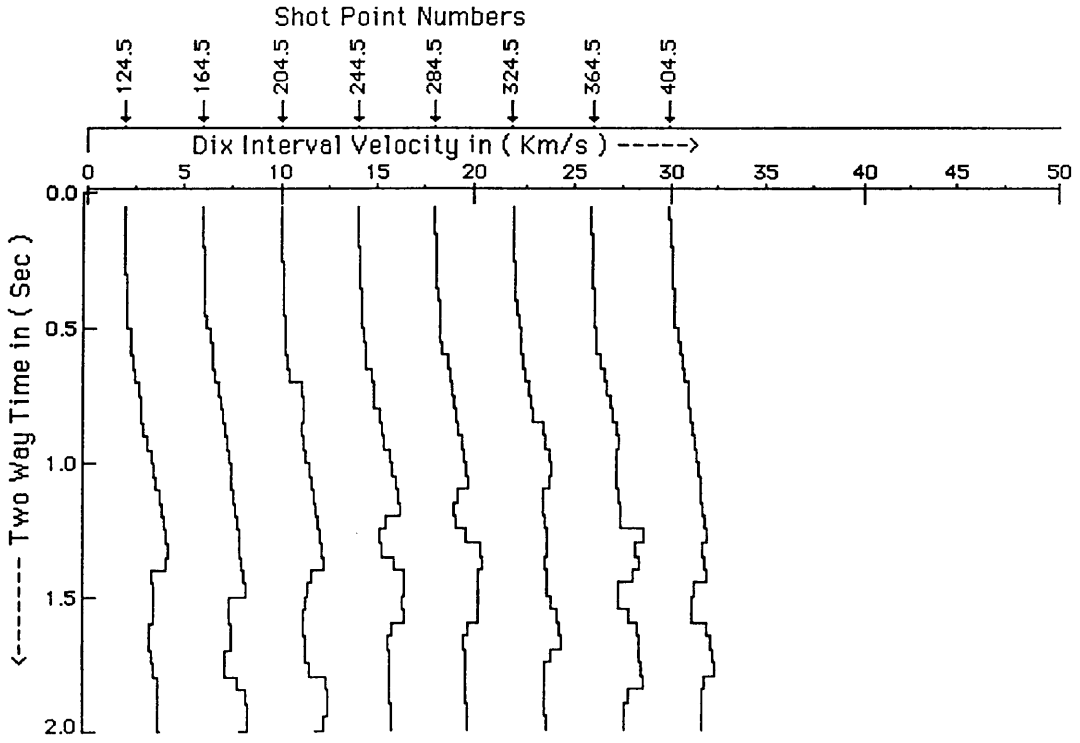

Fig.3.15f Interval velocity - two-way time two-way along seismic line 6V255, using Dix average velocity applied on equation (3.13).

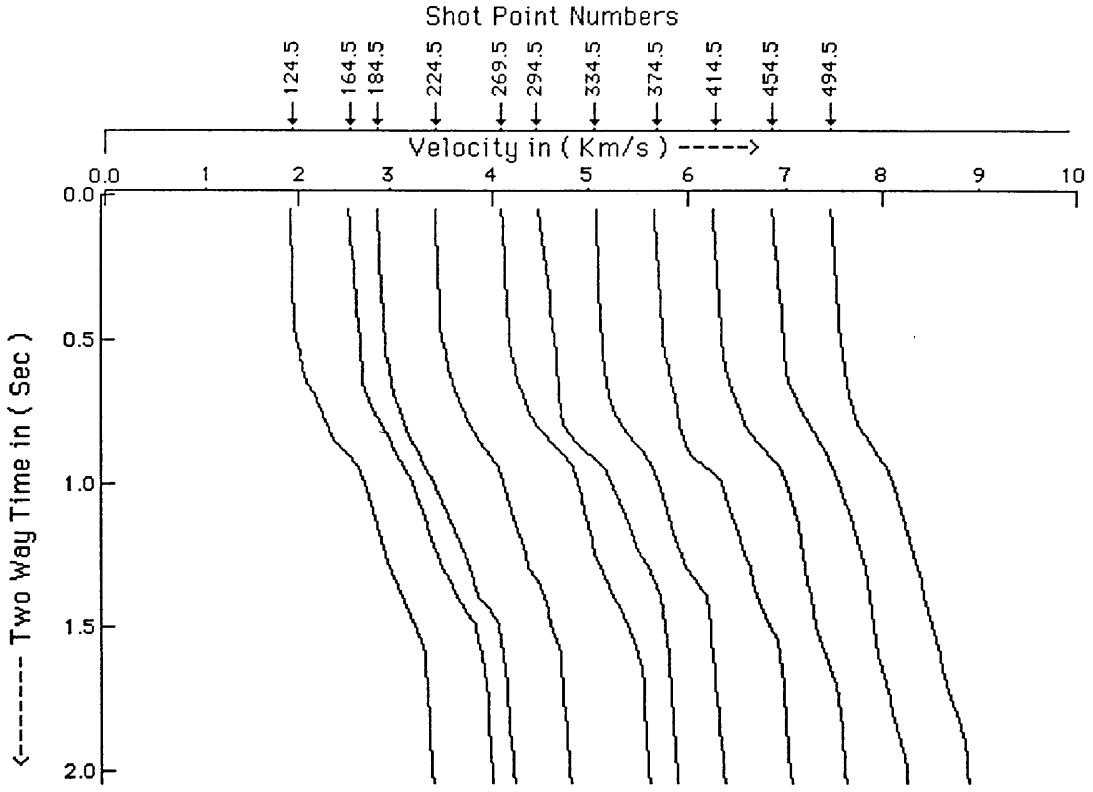

Fig.3.16a Stacking velocity - two-way time relationships along seismic line 6V256.

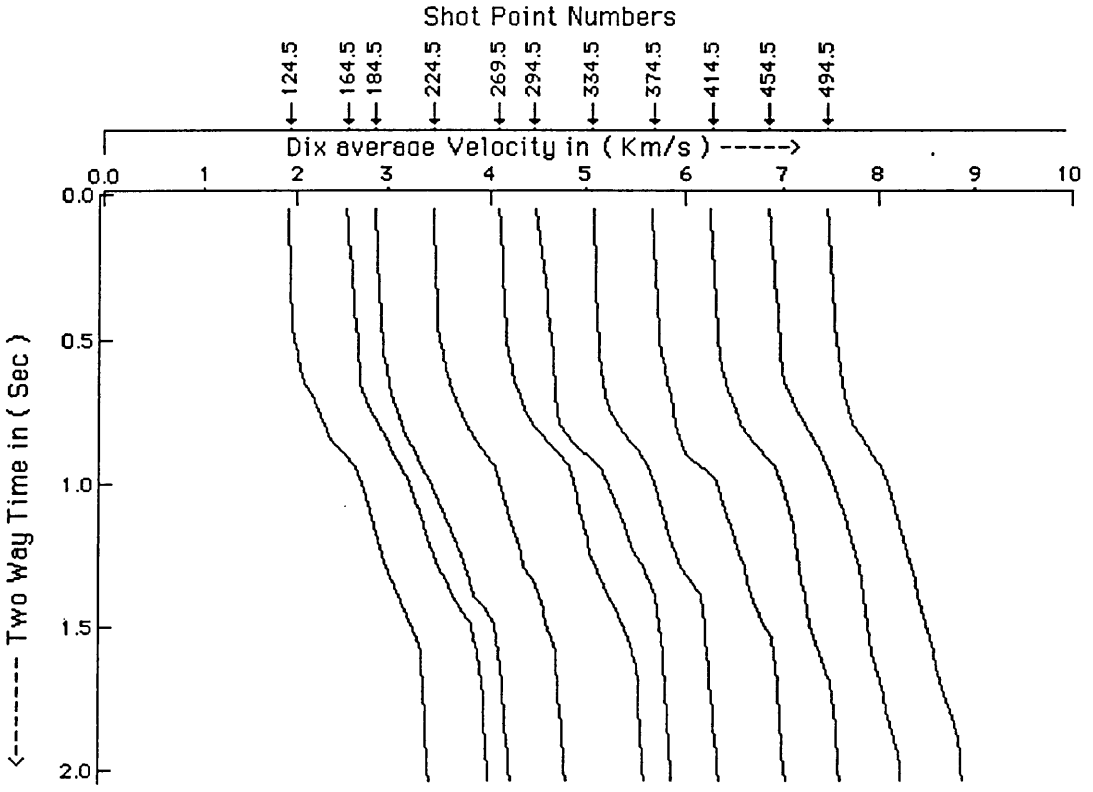

Fig.3.16b Dix average velocity - two-way time relationships along seismic line 6V256.

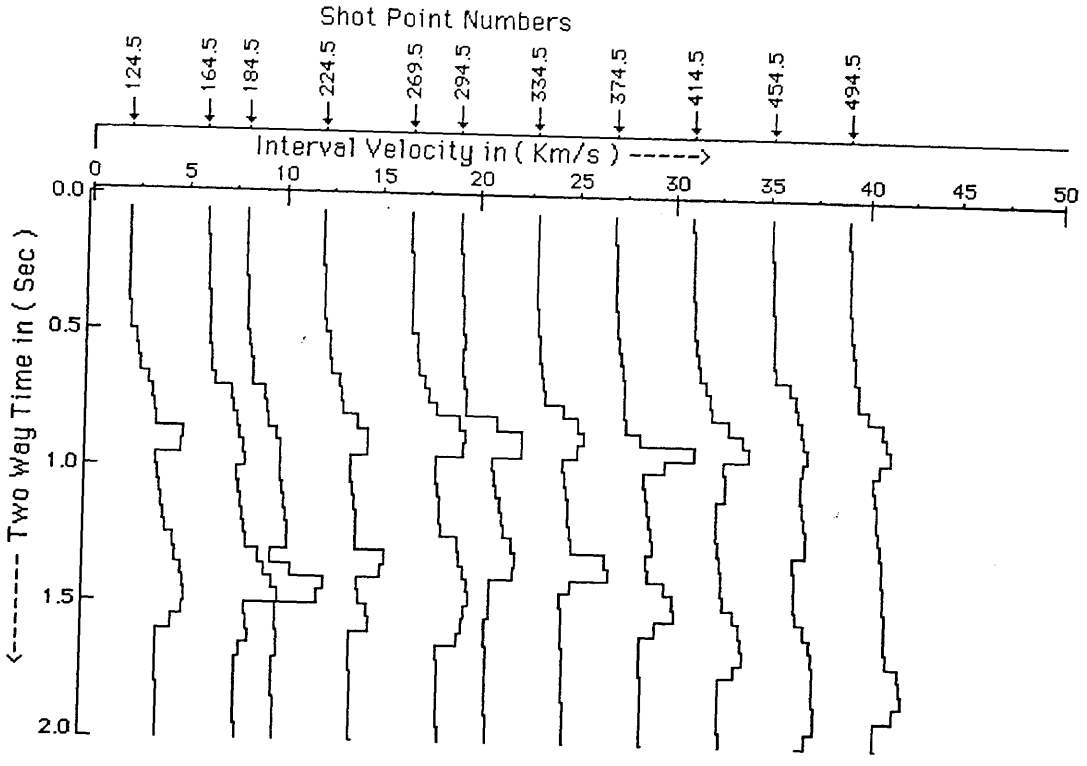

Fig.3.16c Interval velocity - two-way time two-way along seismic line 6V256, using the depth (D1) applied on equation (3.4).

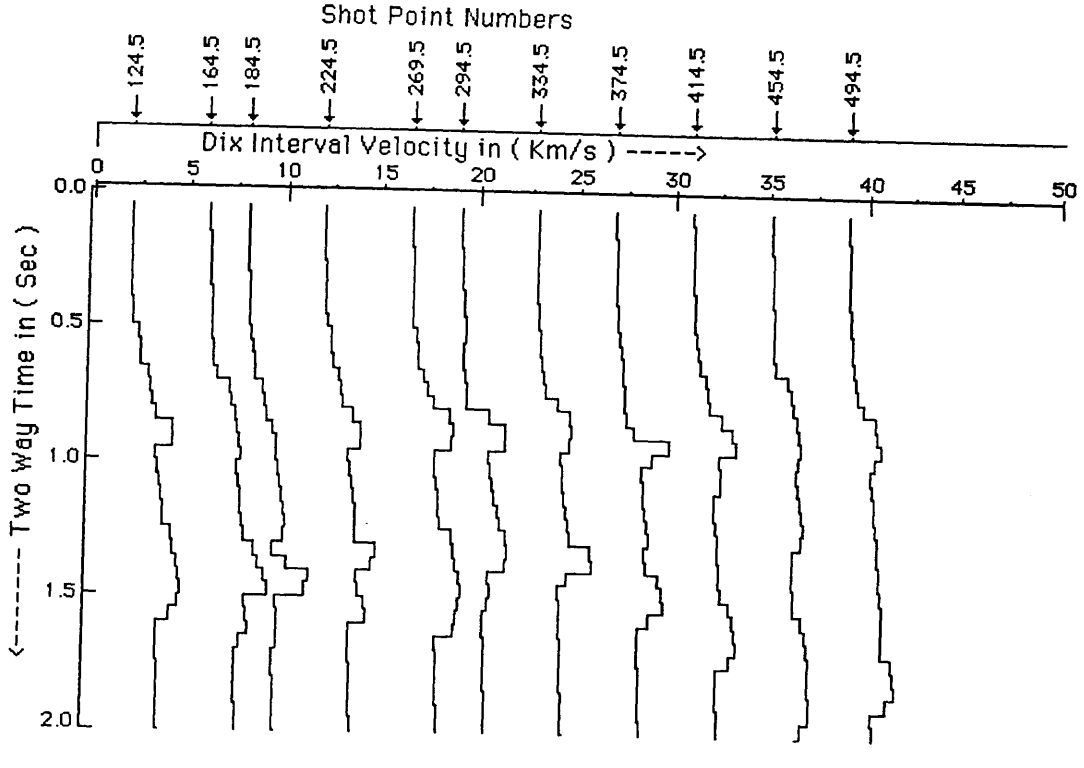

Fig.3.16d Interval velocity - two-way time two-way along seismic line 6V256, using the depth (D2) applied on equation (3.4).

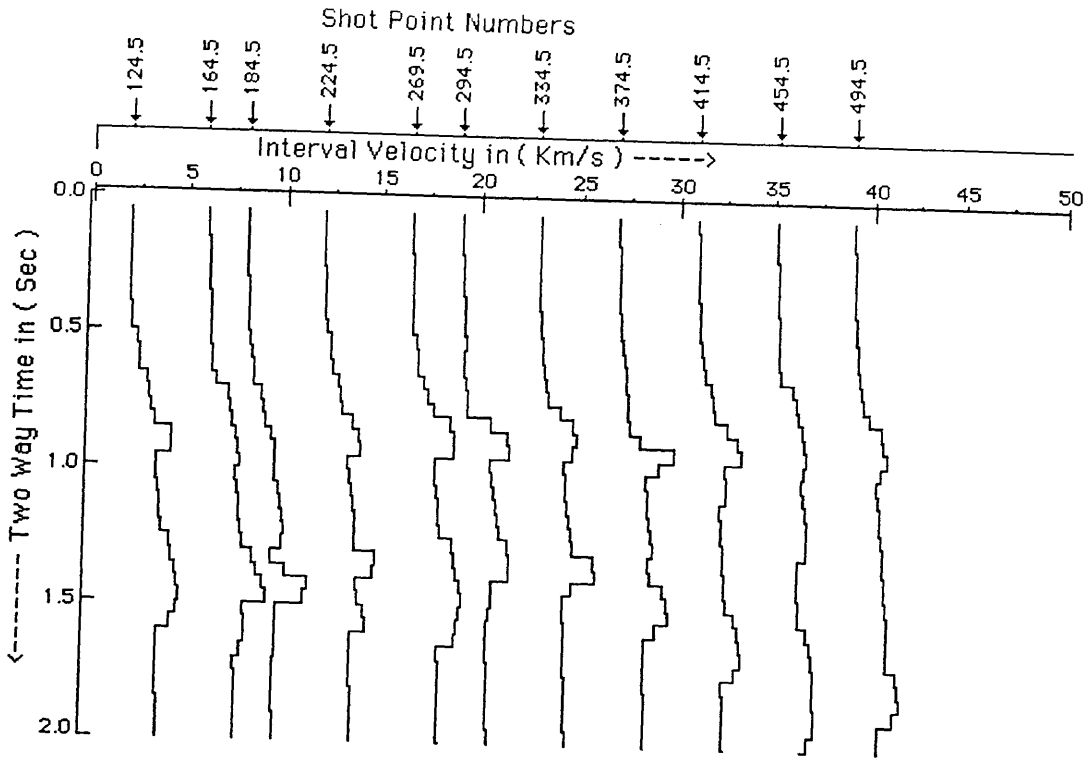

Fig.3.16e Interval velocity - two-way time two-way along seismic line 6V256, using stacking velocity applied on equation (3.13).

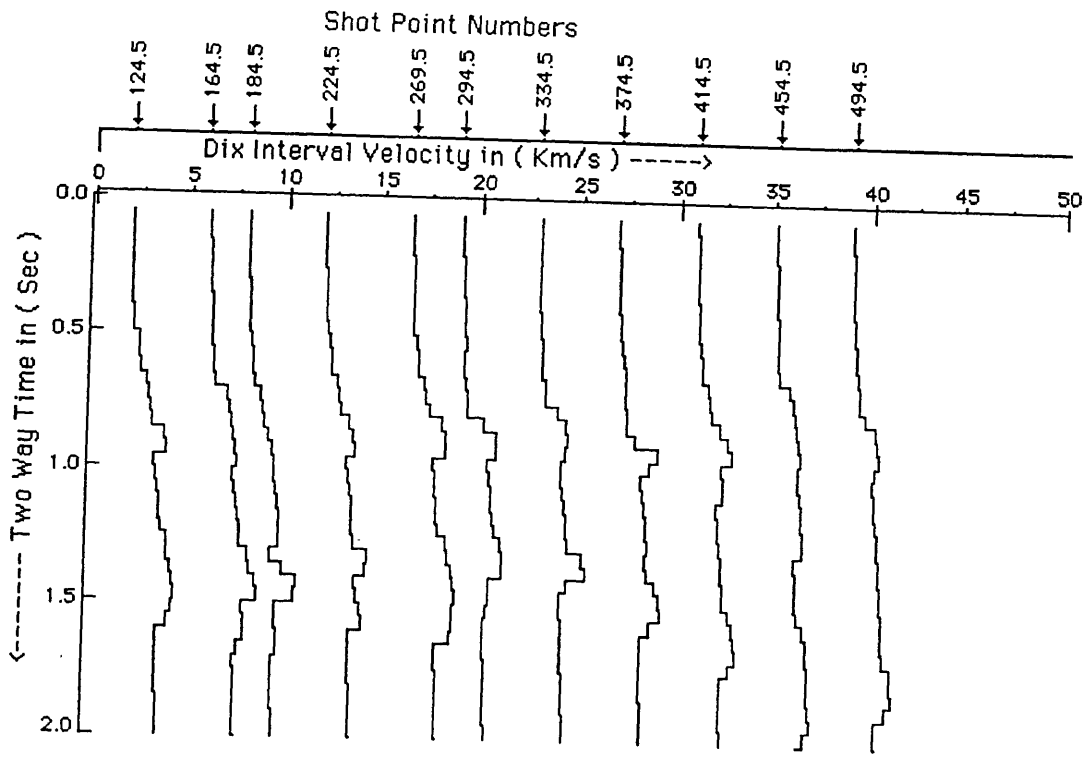

Fig.3.16f Interval velocity - two-way time two-way along seismic line 6V256, using Dix average velocity applied on equation (3.13).

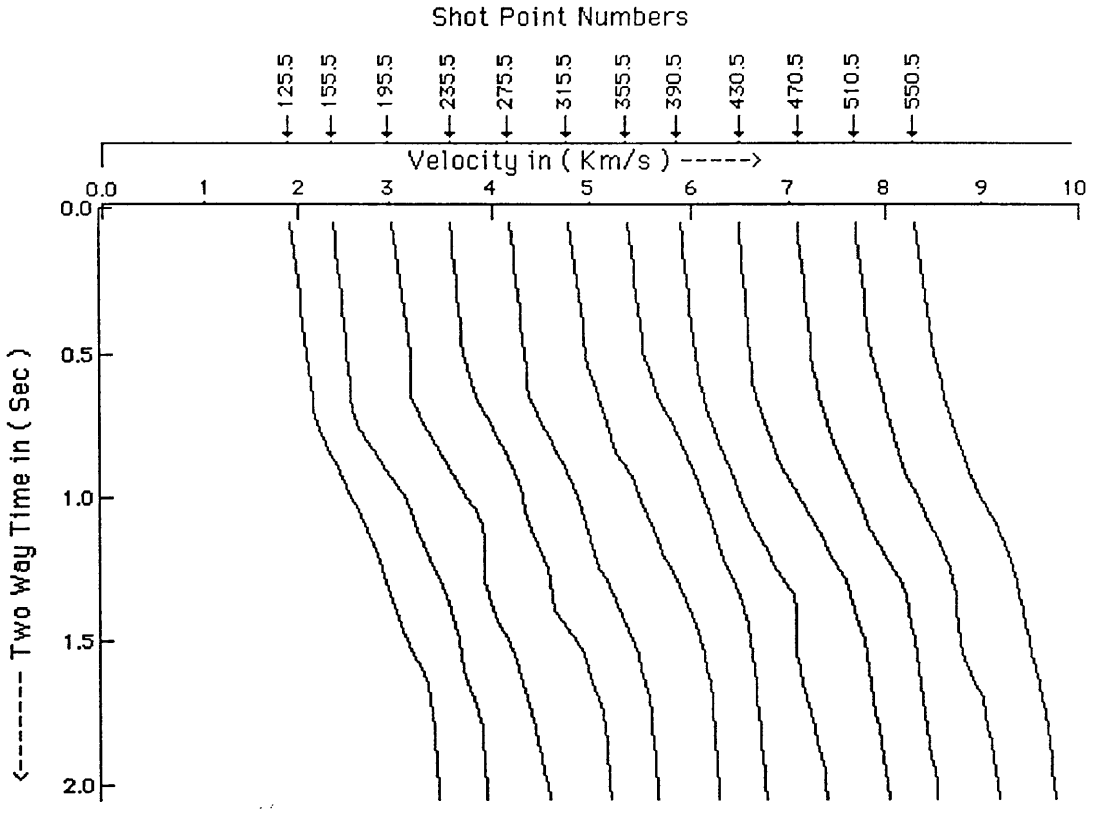

Fig.3.17a Stacking velocity - two-way time relationships along seismic line 6V257.

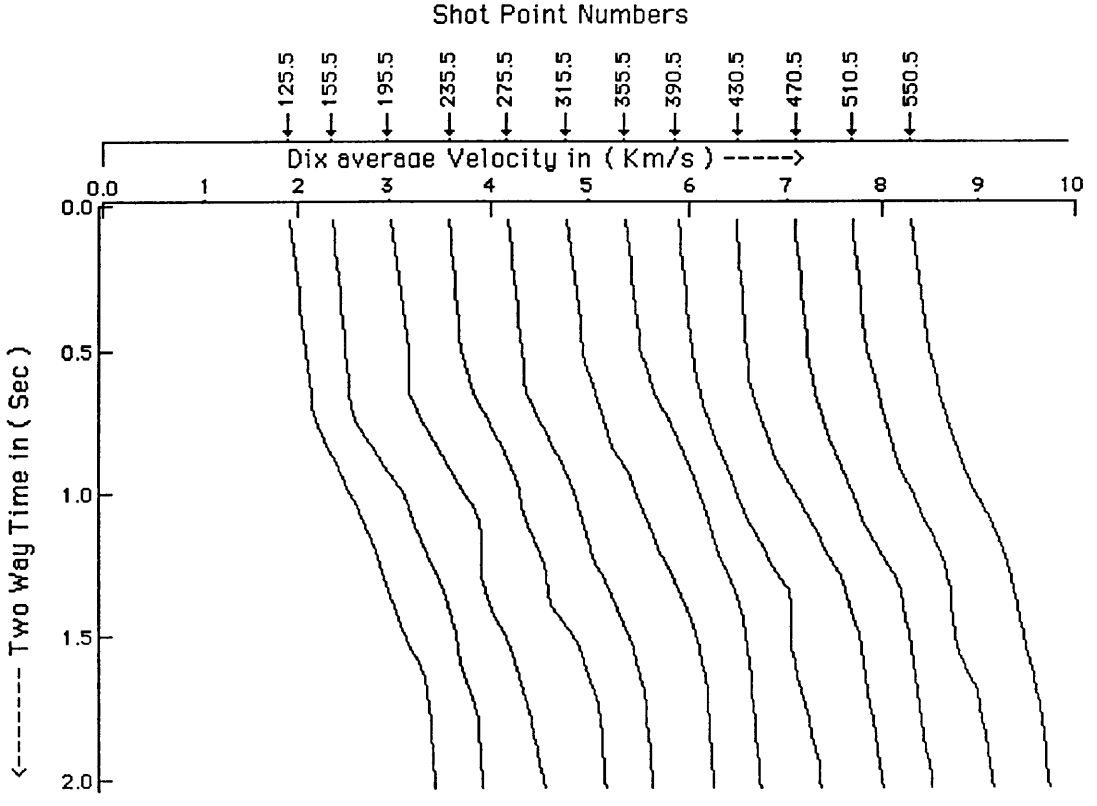

Fig.3.17b Dix average velocity - two-way time relationships along seismic line 6V257.

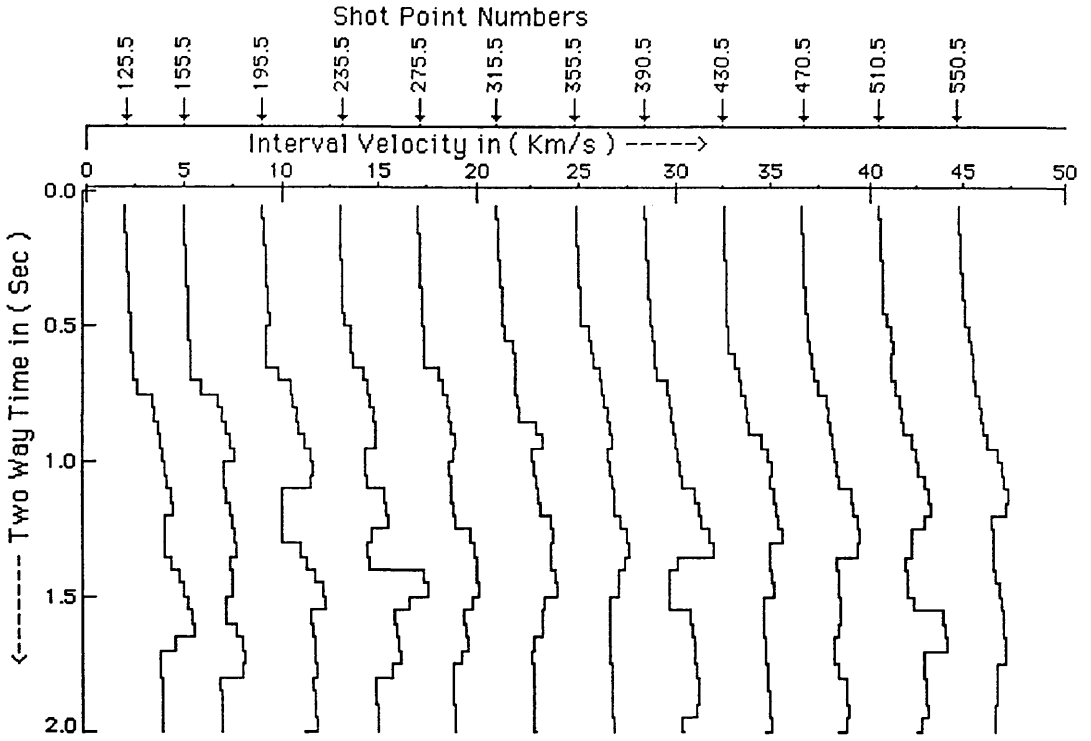

Fig.3.17c Interval velocity - two-way time two-way along seismic line 6V257, using the depth (D1) applied on equation (3.4).

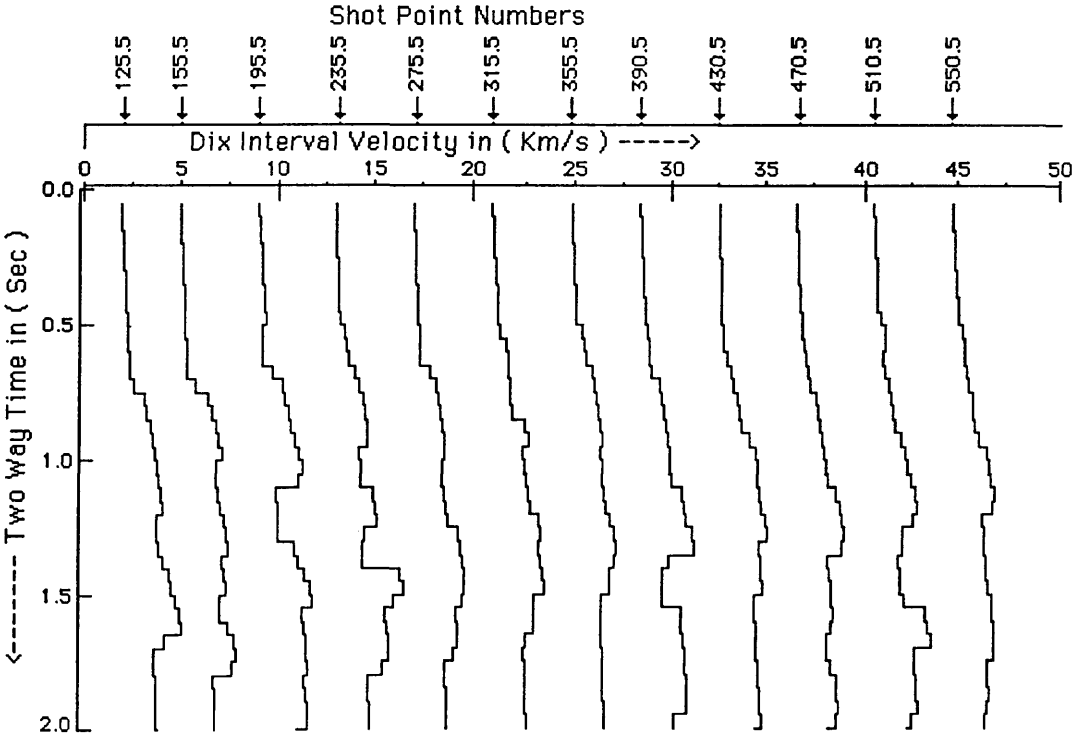

Fig.3.17d Interval velocity - two-way time two-way along seismic line 6V257, using the depth (D2) applied on equation (3.4).

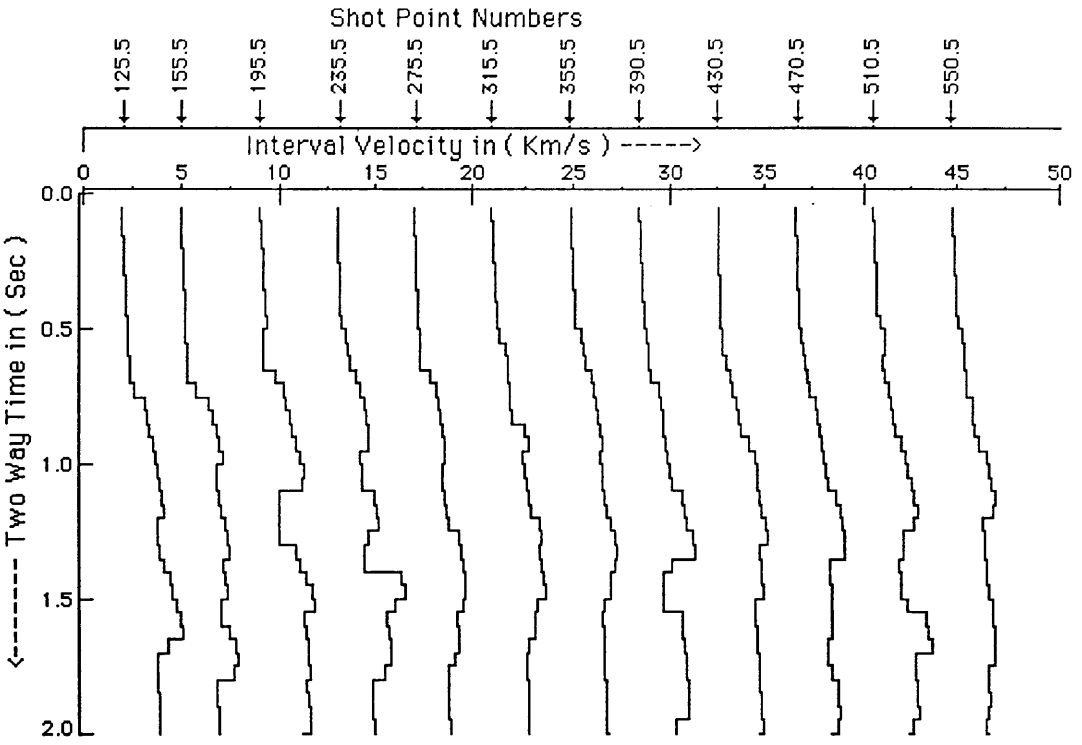

Fig.3.17e Interval velocity - two-way time two-way along seismic line 6V257, using stacking velocity applied on equation (3.13).

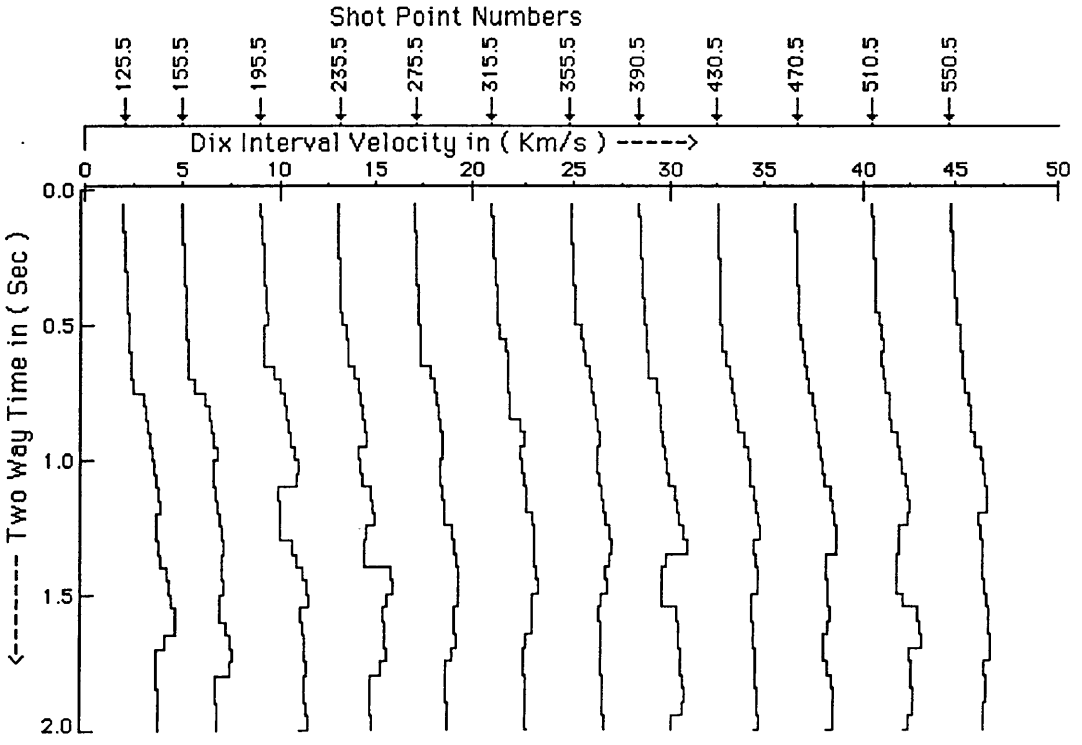

Fig.3.17f Interval velocity - two-way time two-way along seismic line 6V257, using Dix average velocity applied on equation (3.13).

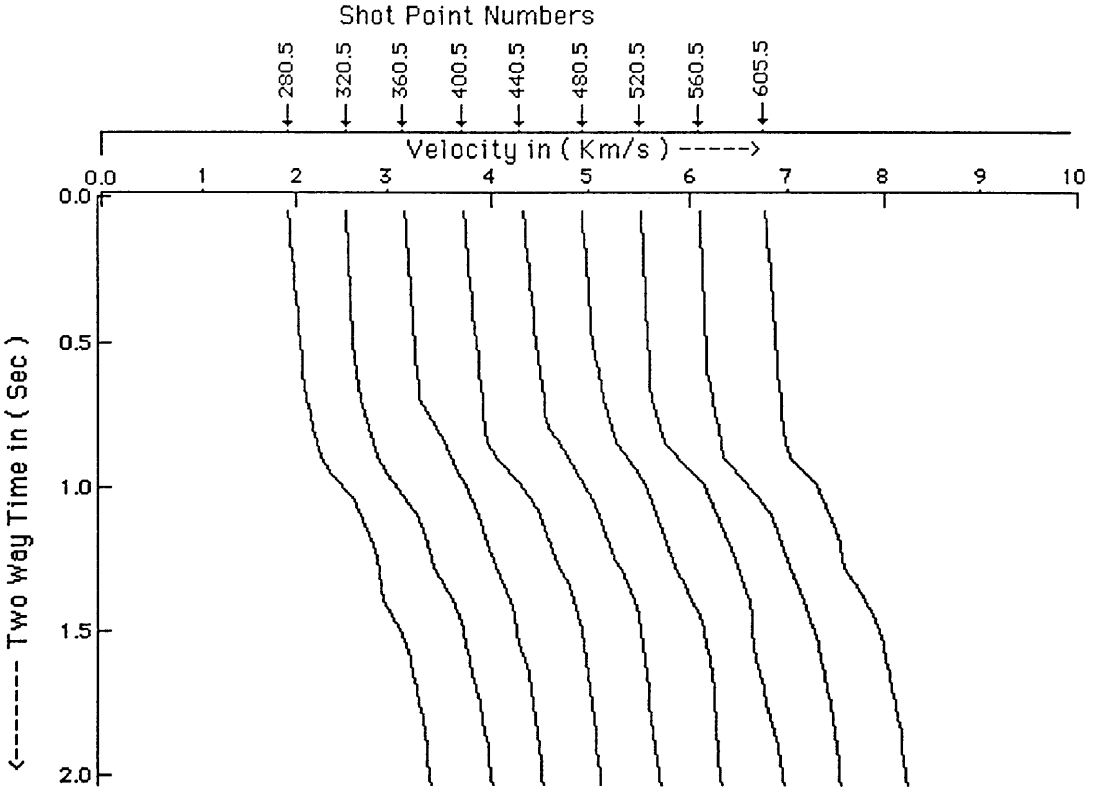

Fig.3.18a Stacking velocity - two-way time relationships along seismic line 6V258.

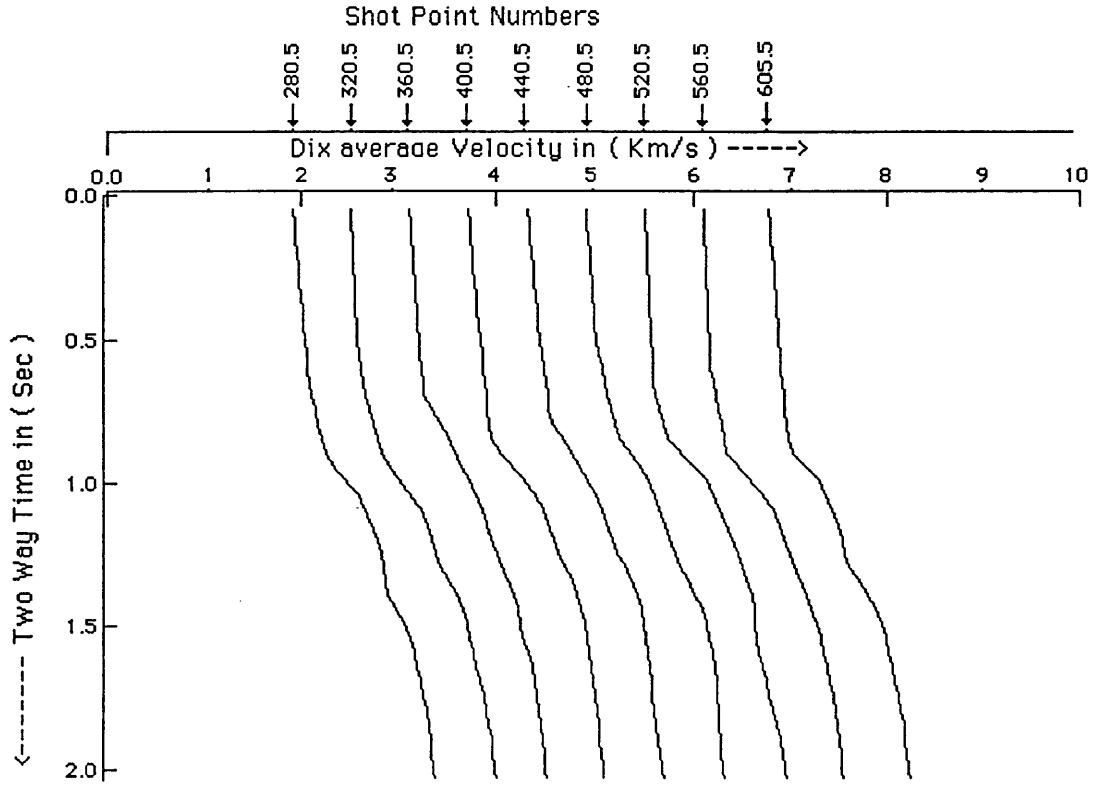

Fig.3.18b Dix average velocity - two-way time relationships along seismic line 6V258.

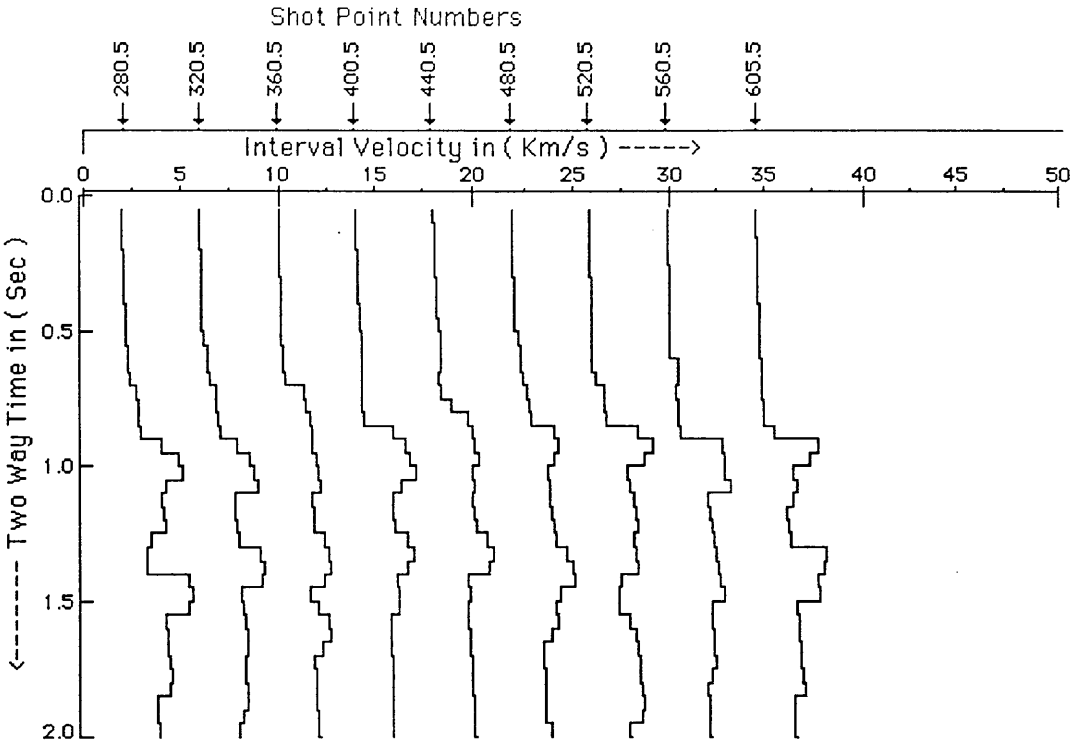

Fig.3.18c Interval velocity - two-way time relationships along seismic line 6V258, using the depth (D1) applied on equation (3.4).

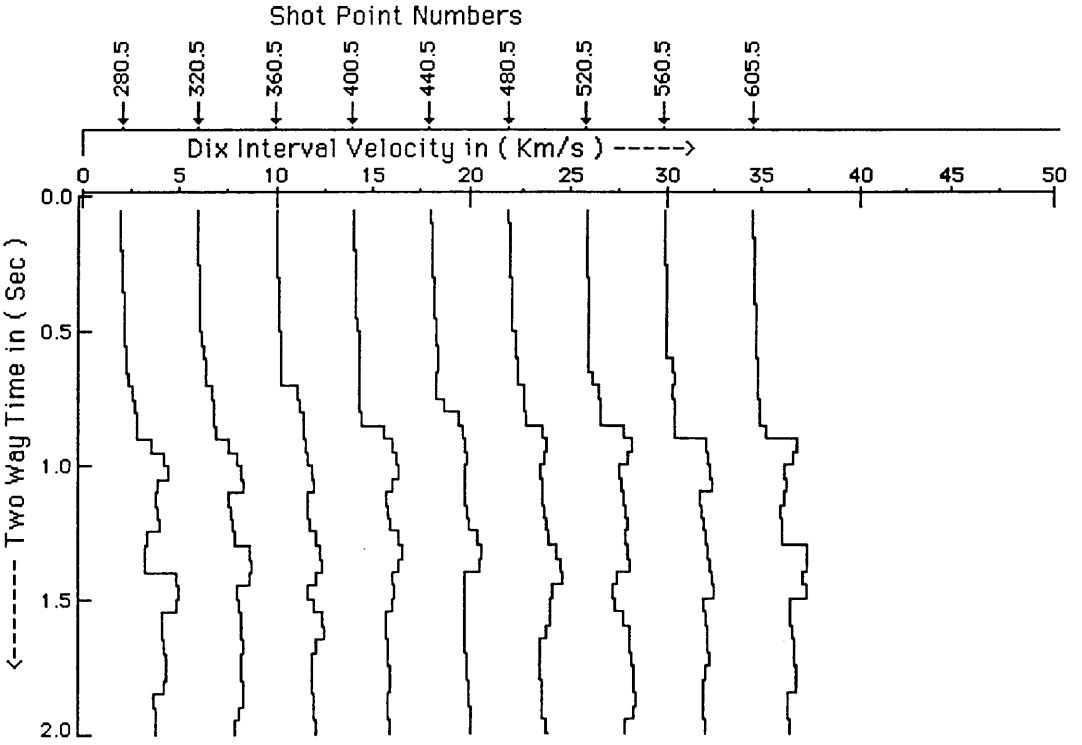

Fig.3.18d Interval velocity - two-way time relationships along seismic line 6V258, using the depth (D2) applied on equation (3.4).

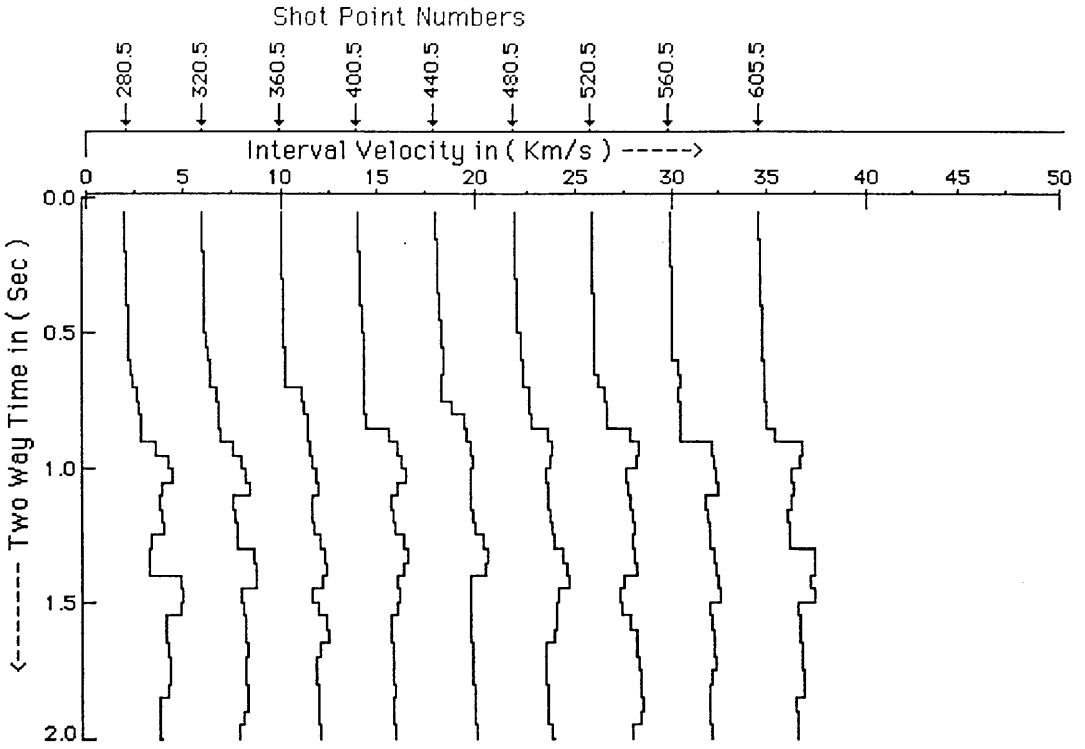

Fig.3.18e Interval velocity - two-way time relationships along seismic line 6V258, using stacking velocity applied on equation (3.13).

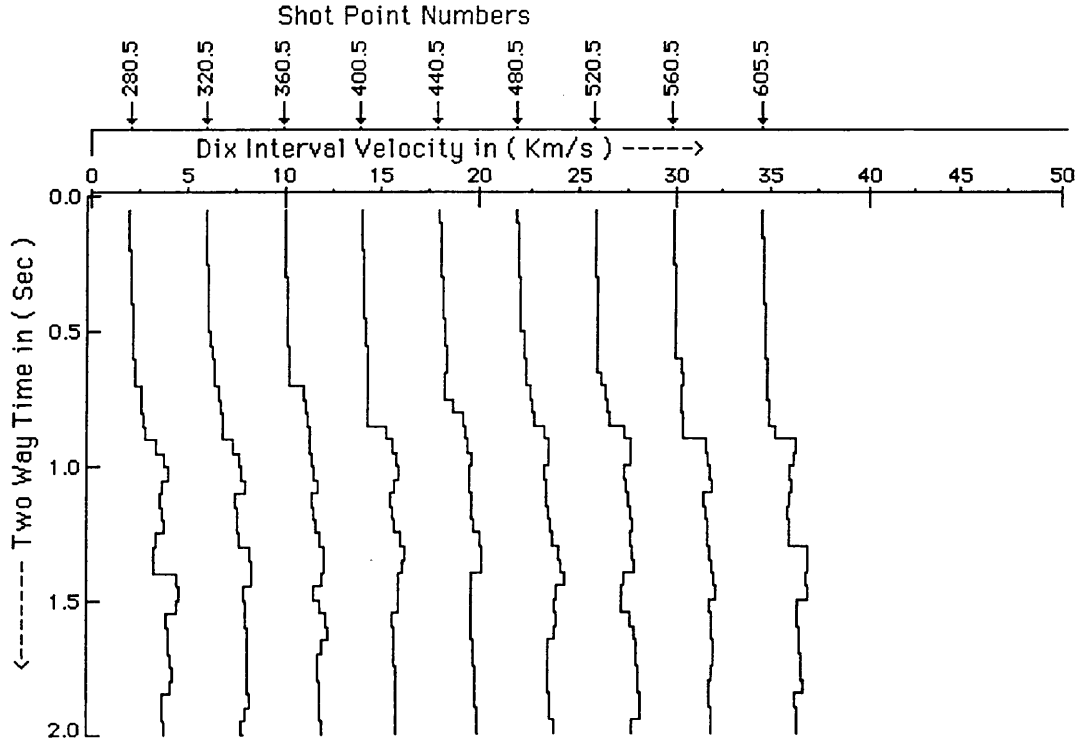

Fig.3.18f Interval velocity - two-way time relationships along seismic line 6V258, using Dix average velocity applied on equation (3.13).

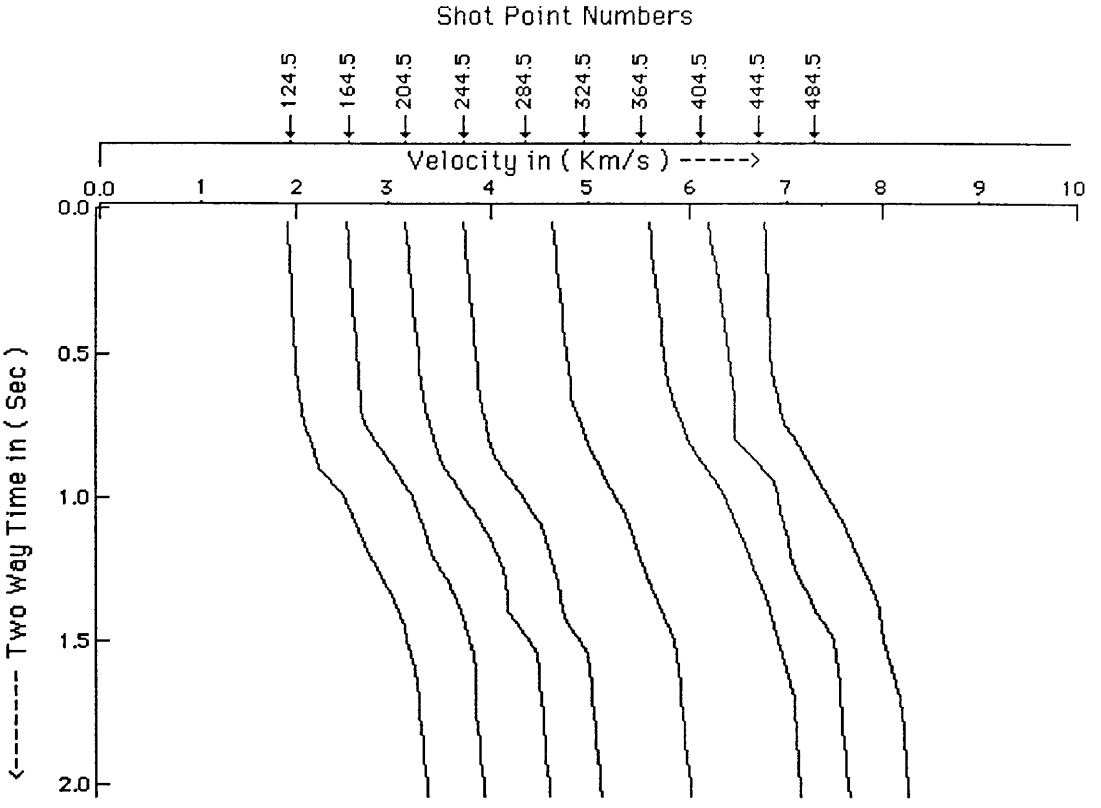

Fig.3.19a Stacking velocity - two-way time relationships along seismic line 6V259.

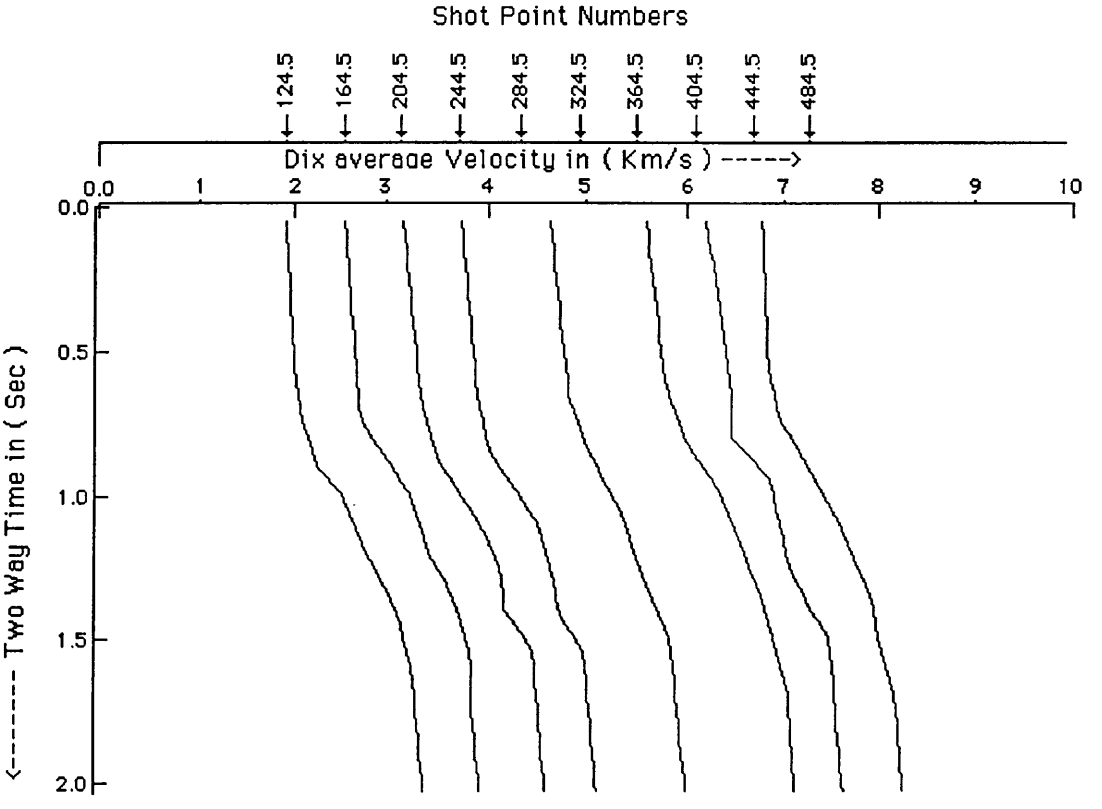

Fig.3.19b Dix average velocity - two-way time relationships along seismic line 6V259.

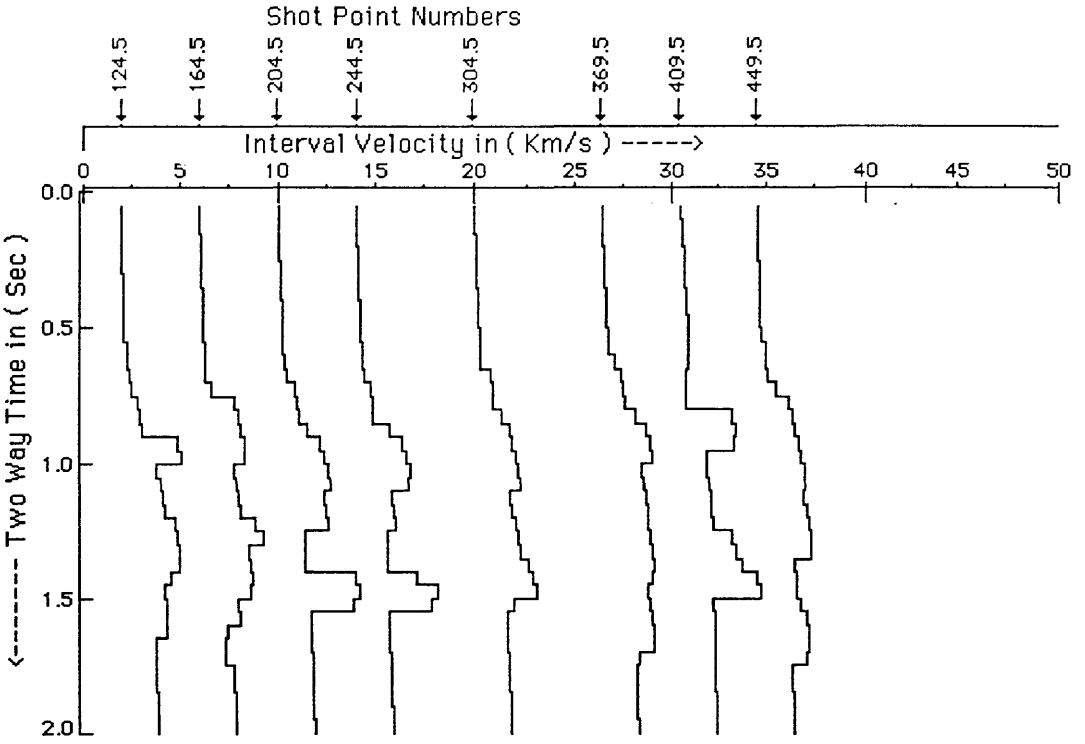

Fig.3.19c Interval velocity - two-way time relationships along seismic line 6V259, using the depth (D1) applied on equation (3.4).

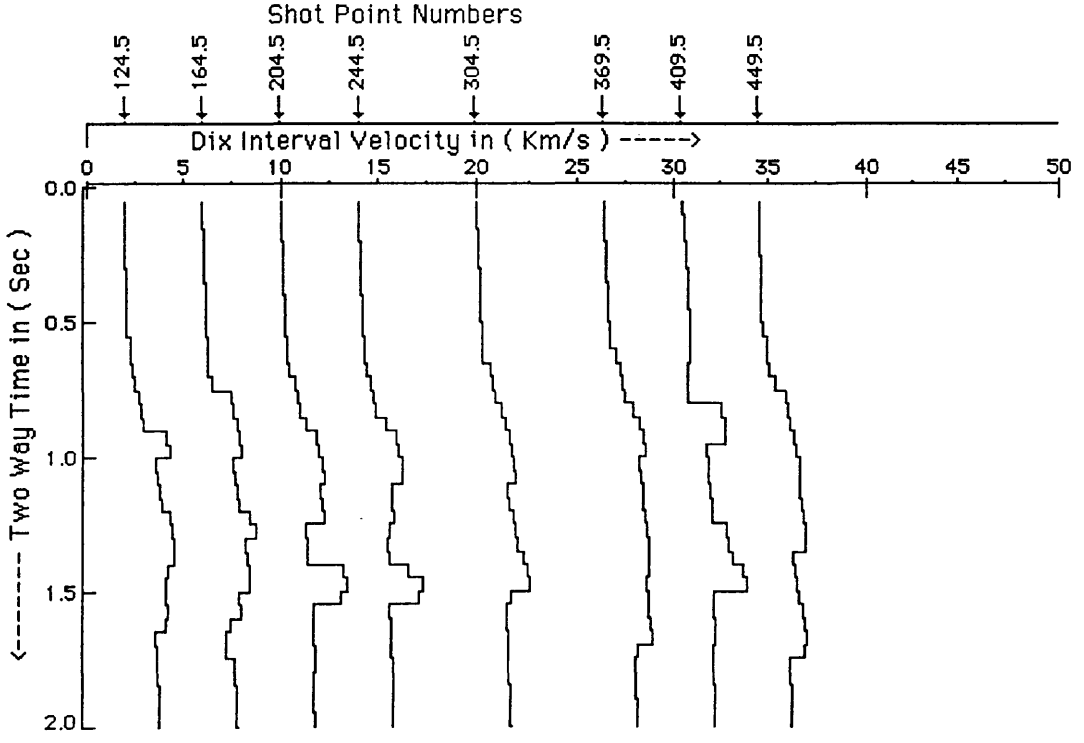

Fig.3.19d Interval velocity - two-way time relationships along seismic line 6V259, using the depth (D2) applied on equation (3.4).

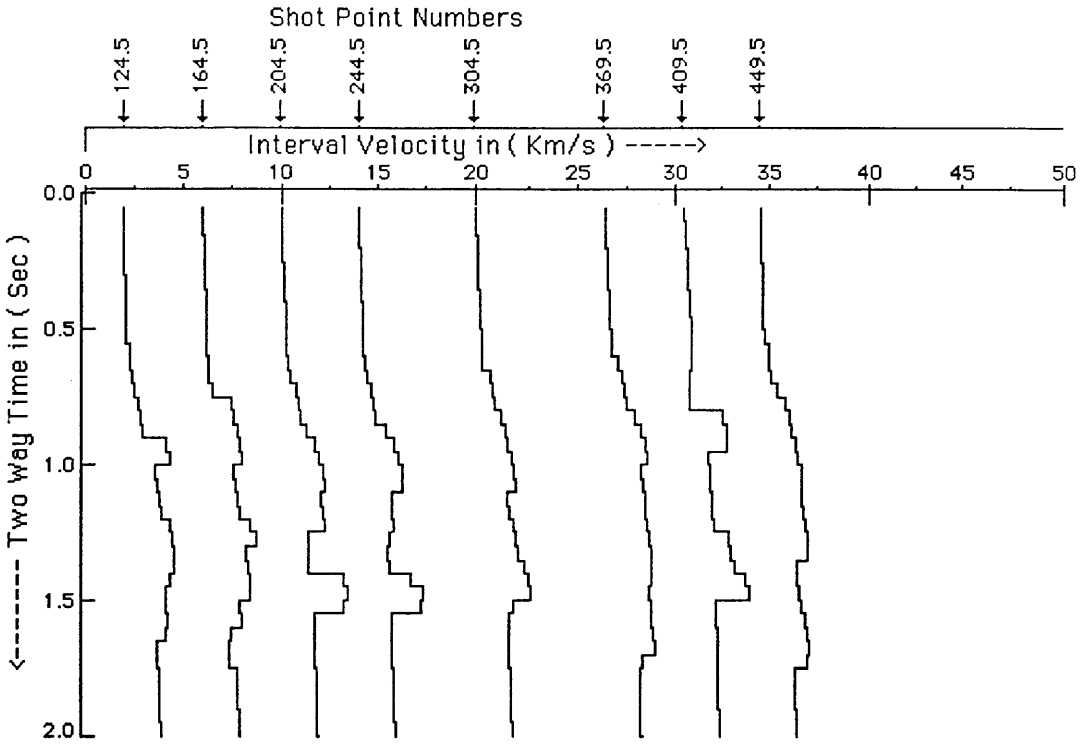

Fig.3.19e Interval velocity - two-way time relationships along seismic line 6V259, using stacking velocity applied on equation (3.13).

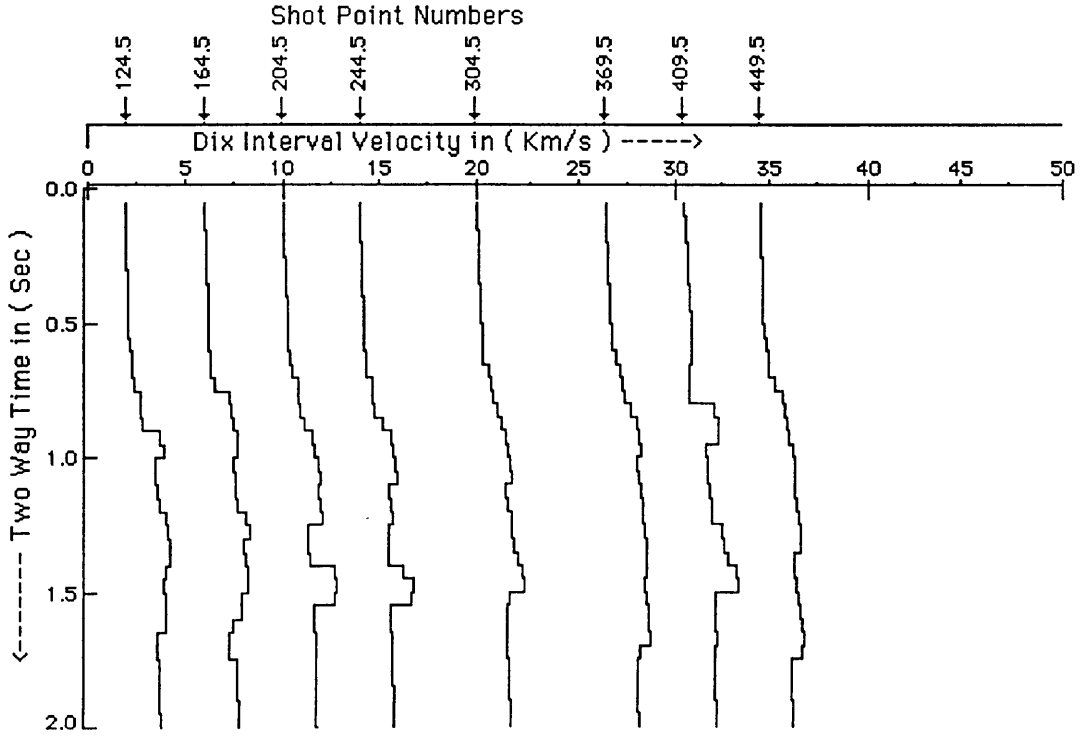

Fig.3.19f Interval velocity - two-way time relationships along seismic line 6V259, using Dix average velocity applied on equation (3.13).

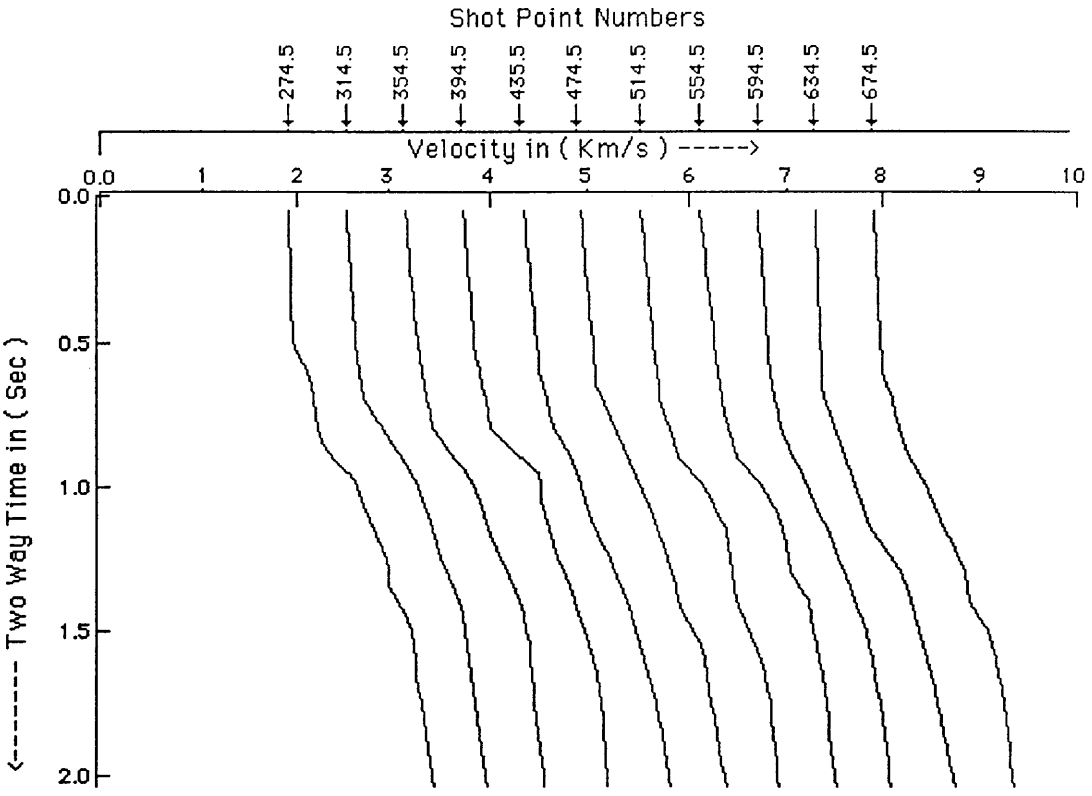

Fig.3.20a Stacking velocity - two-way time relationships along seismic line 6V260.

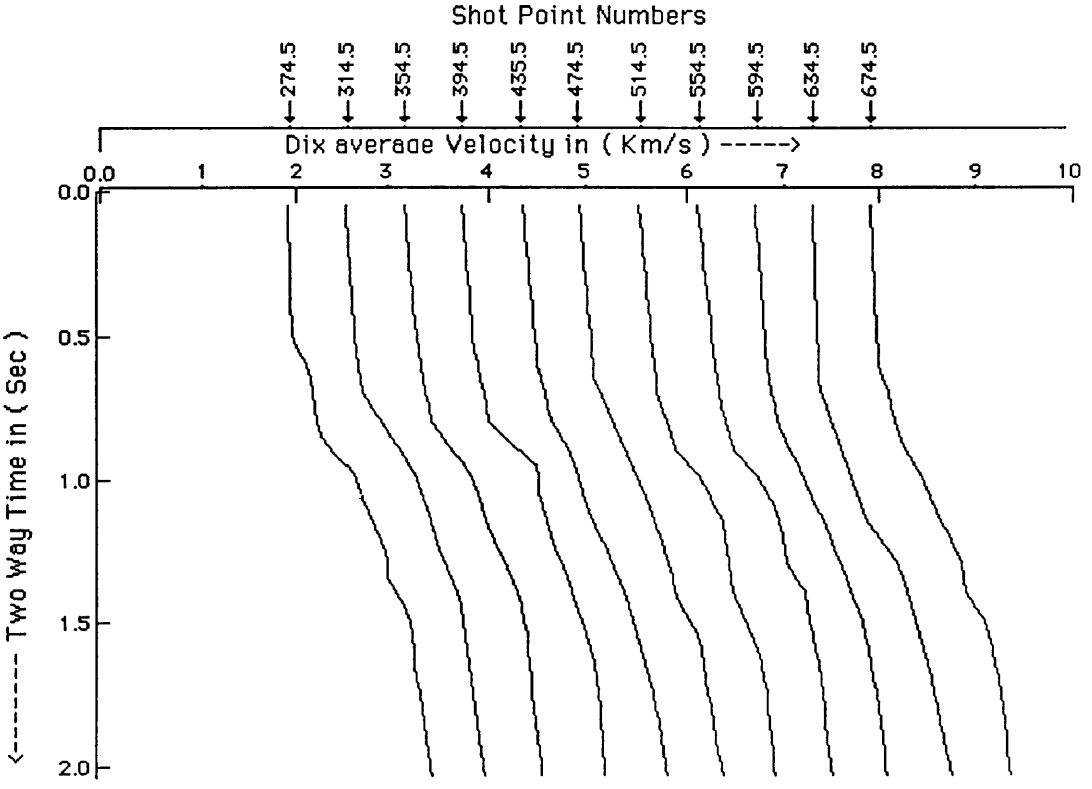

Fig.3.20b Dix average velocity - two-way time relationships along seismic line 6V260.

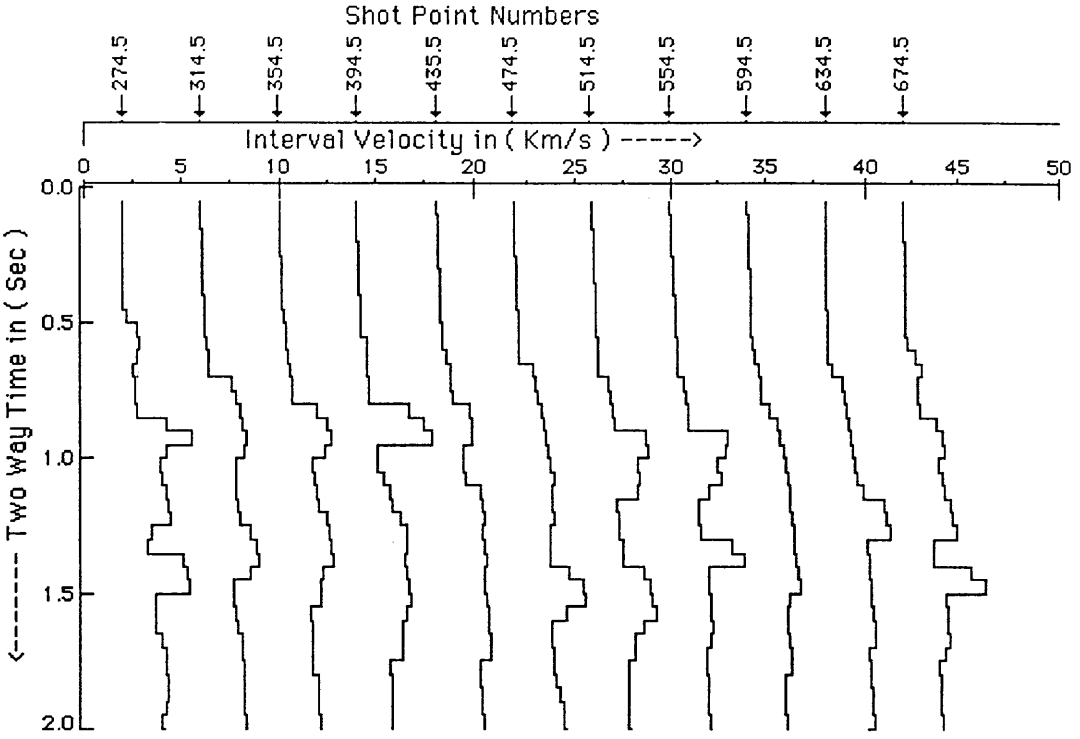

Fig.3.20c Interval velocity - two-way time relationships along seismic line 6V260, using the depth (D1) applied on equation (3.4).

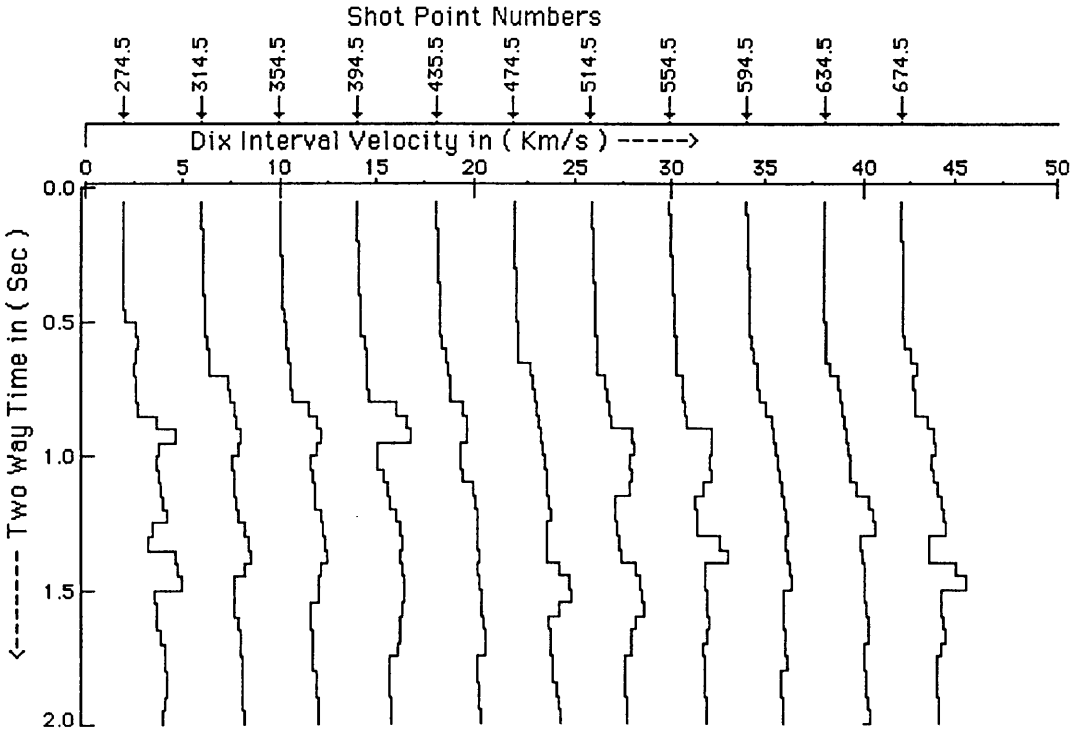

Fig.3.20d Interval velocity - two-way time relationships along seismic line 6V260, using the depth (D2) applied on equation (3.4).

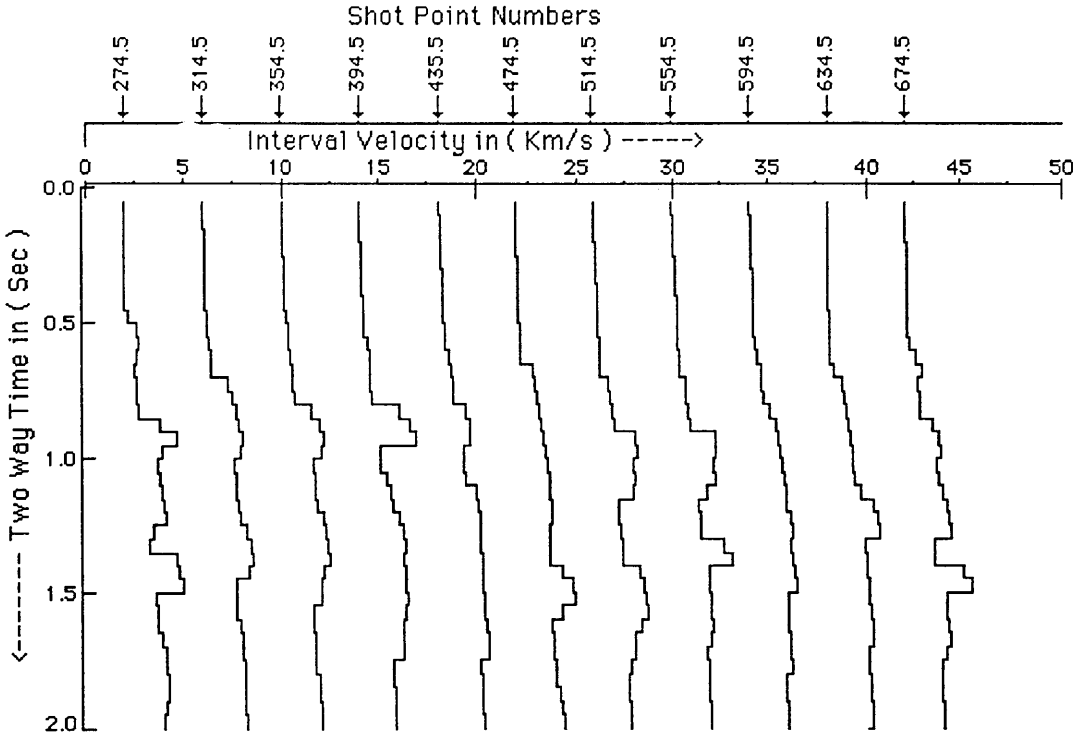

Fig.3.20e Interval velocity - two-way time relationships along seismic line 6V260, using stacking velocity applied on equation (3.13).

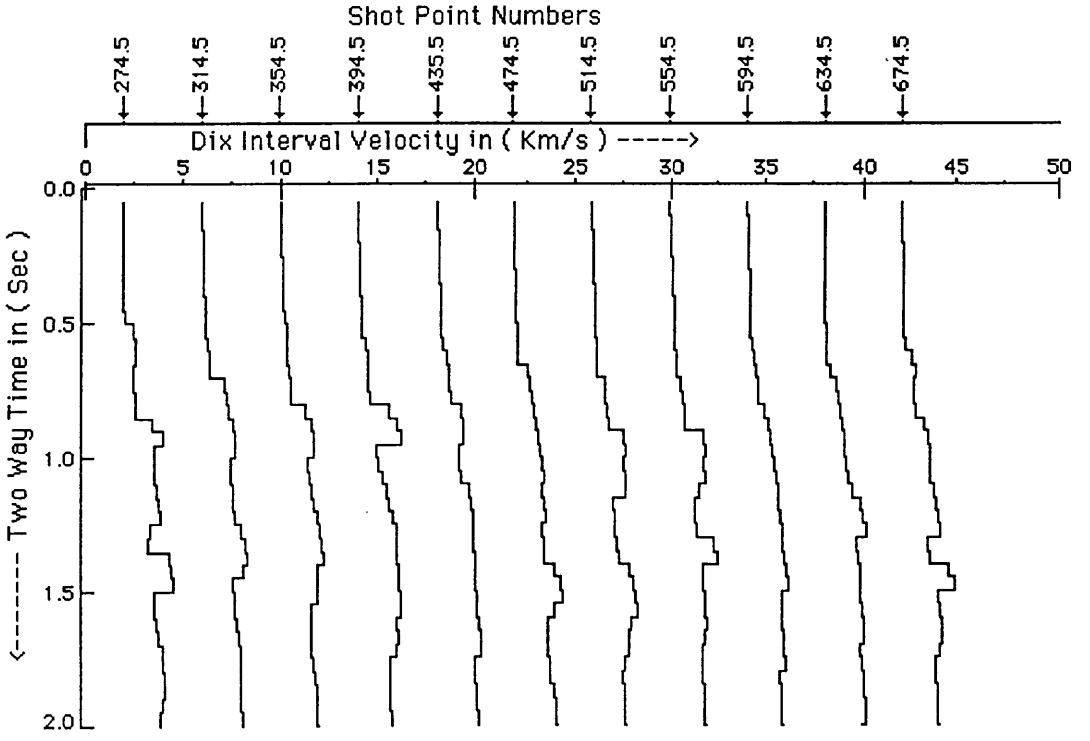

Fig.3.20f Interval velocity - two-way time relationships along seismic line 6V260, using Dix average velocity applied on equation (3.13).

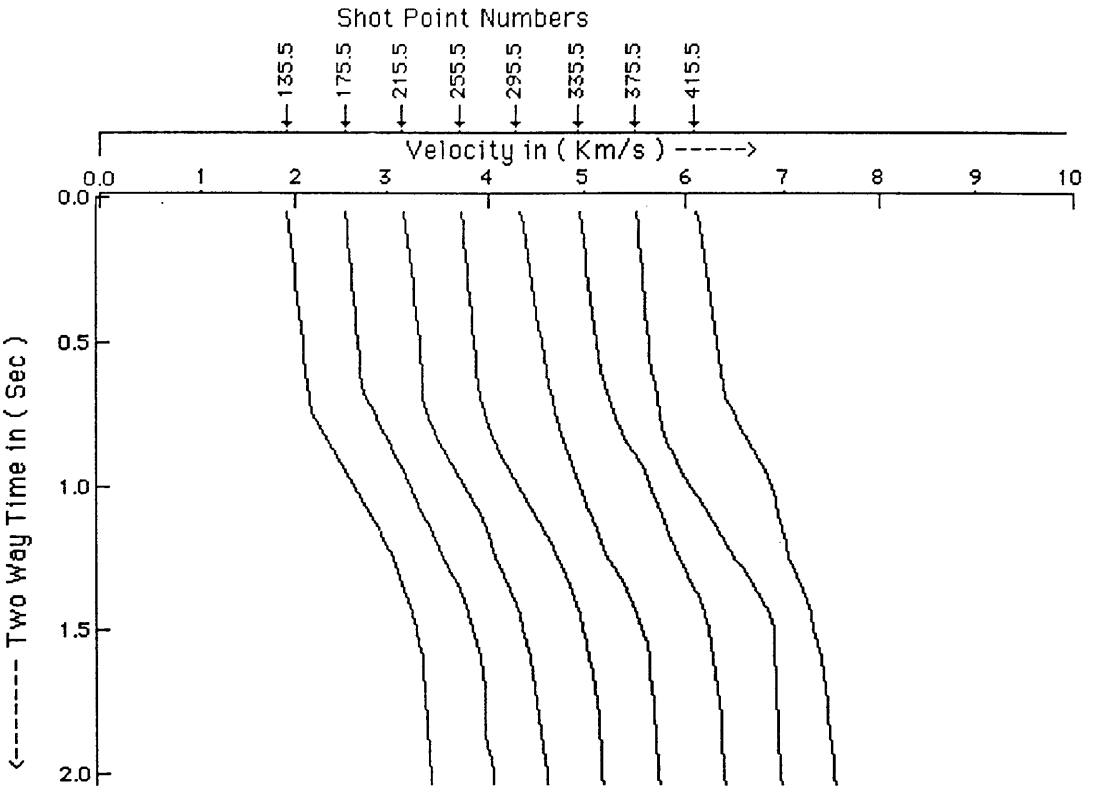

Fig.3.21a Stacking velocity - two-way time relationships along seismic line 6V261.

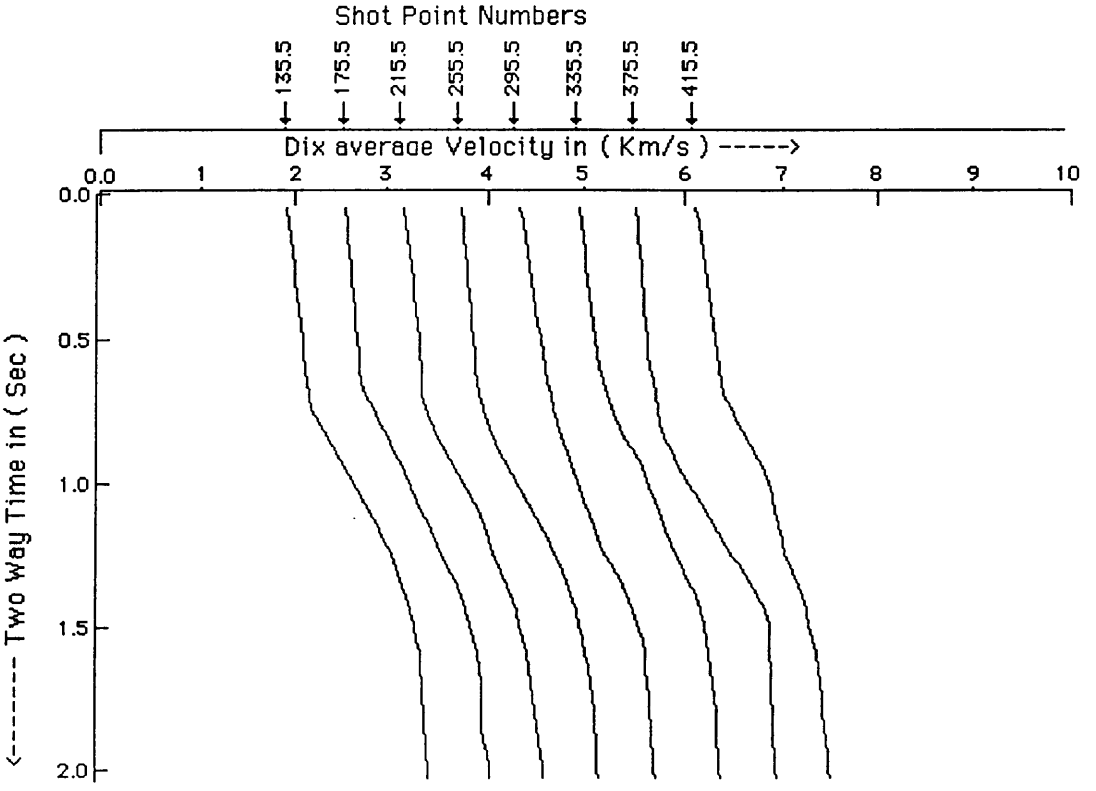

Fig.3.21b Dix average velocity - two-way time relationships along seismic line 6V261.

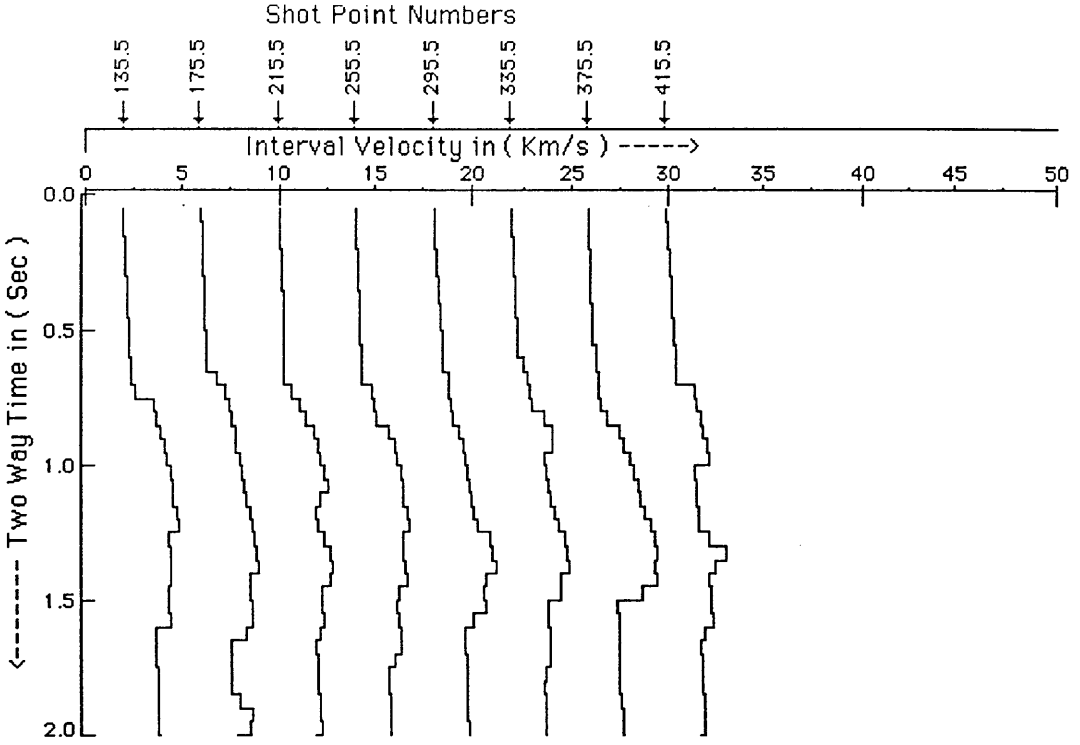

Fig.3.21c Interval velocity - two-way time relationships along seismic line 6V261, using the depth (D1) applied on equation (3.4).

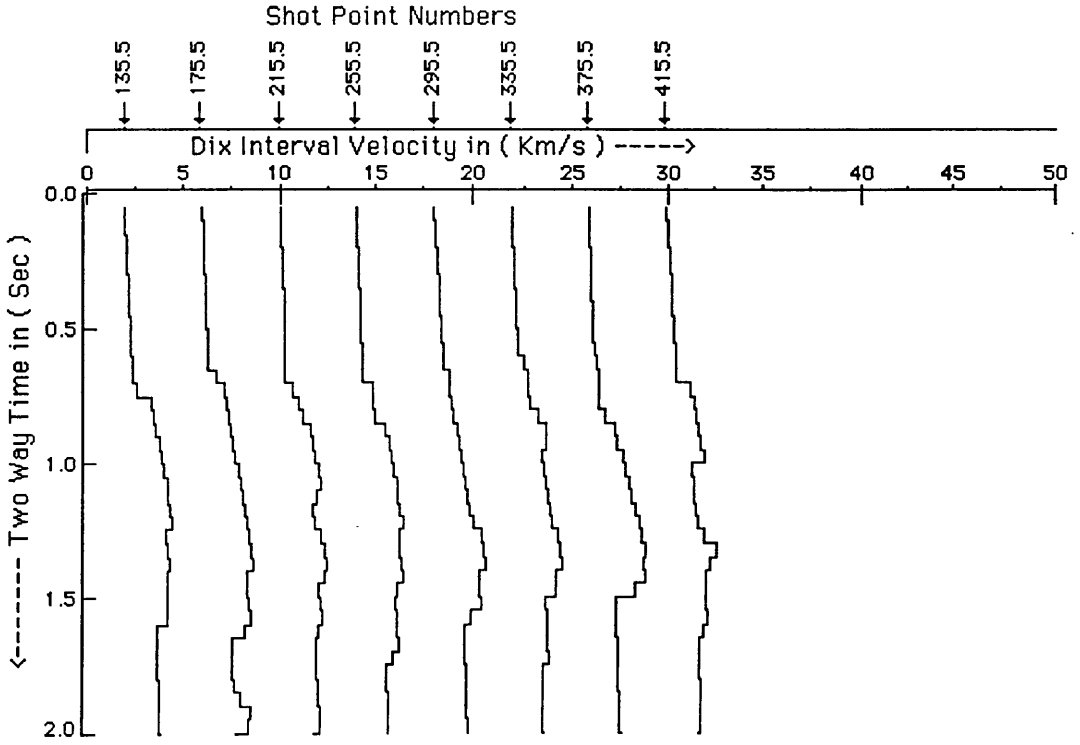

Fig.3.21d Interval velocity - two-way time relationships along seismic line 6V261, using the depth (D2) applied on equation (3.4).

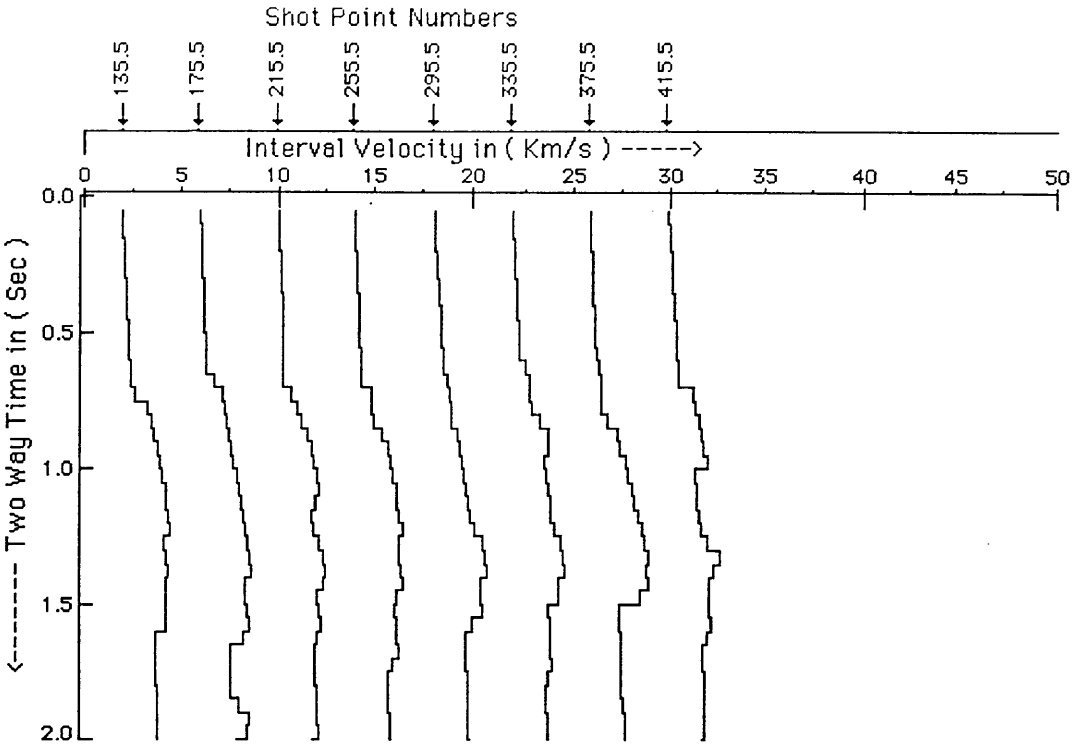

Fig.3.21e Interval velocity - two-way time relationships along seismic line 6V261, using stacking velocity applied on equation (3.13).

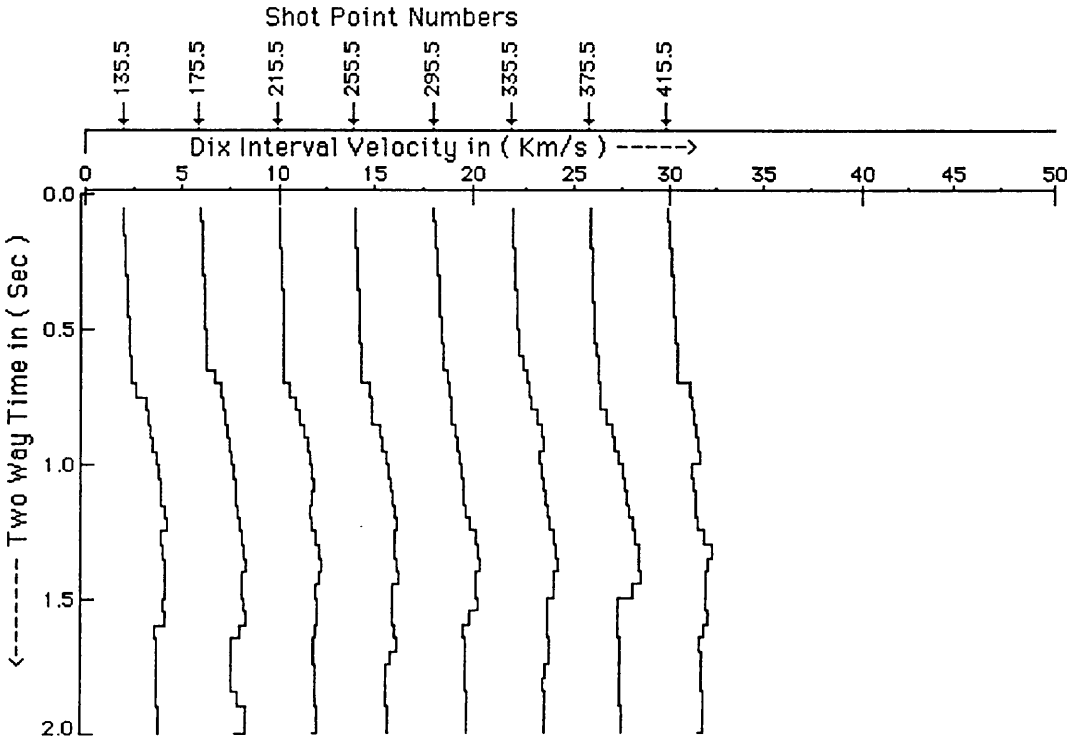

Fig.3.21f Interval velocity - two-way time relationships along seismic line 6V261, using Dix average velocity applied on equation (3.13).

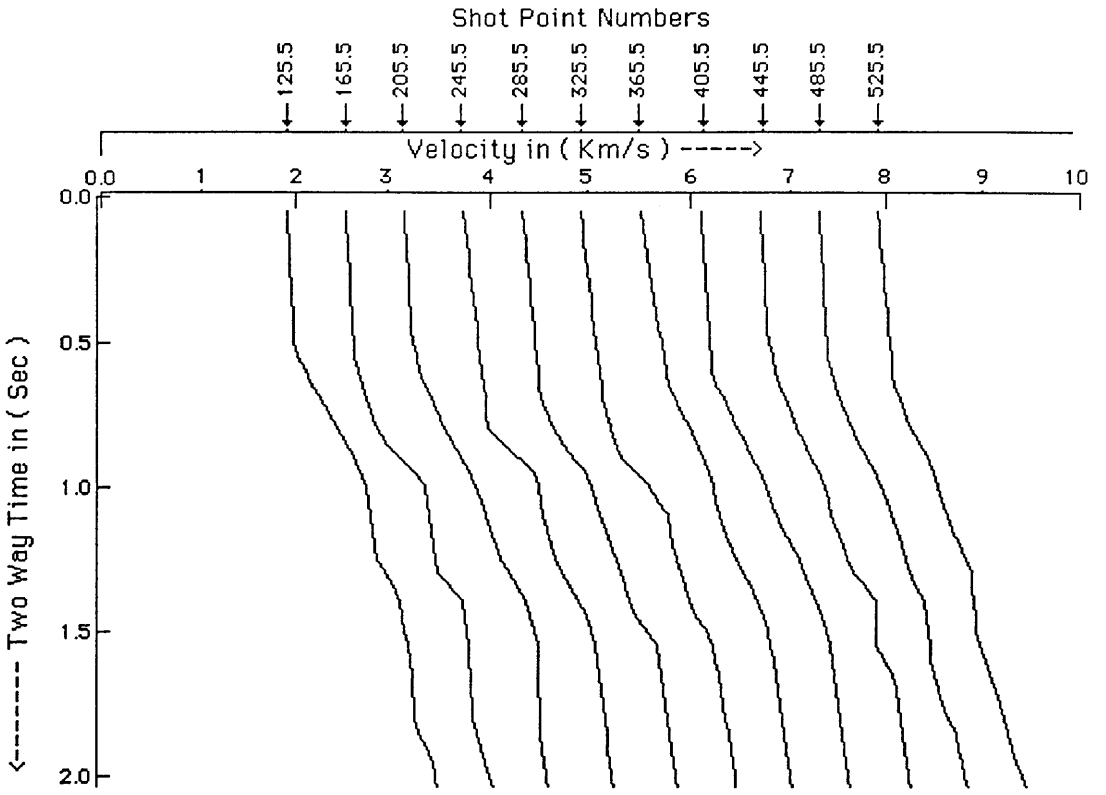

Fig.3.22a Stacking velocity - two-way time relationships along seismic line 6V262.

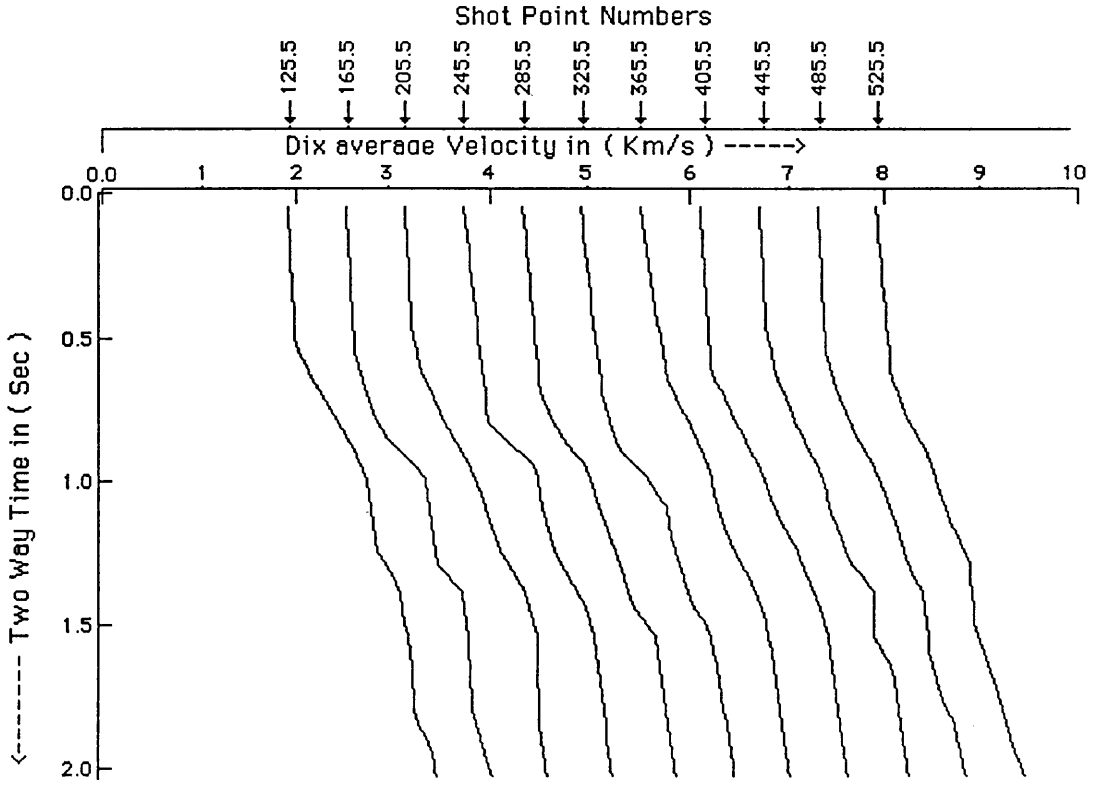

Fig.3.22b Dix average velocity - two-way time relationships along seismic line 6V262.

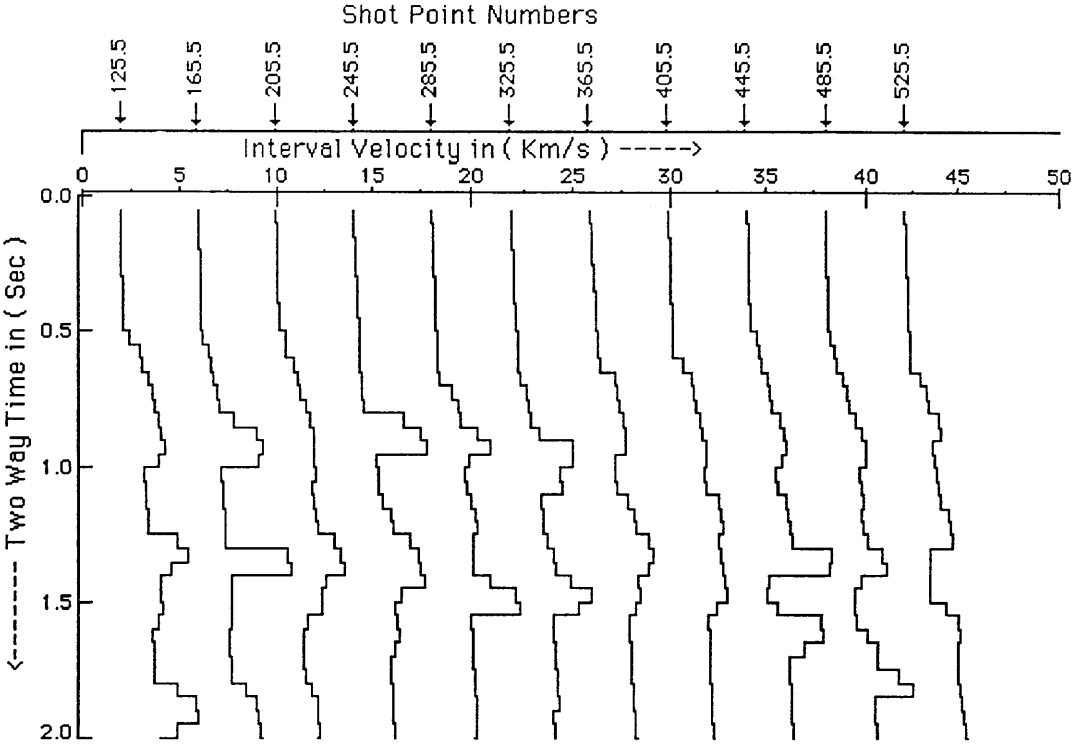

Fig.3.22c Interval velocity - two-way time relationships along seismic line 6V262, using the depth (D1) applied on equation (3.4).

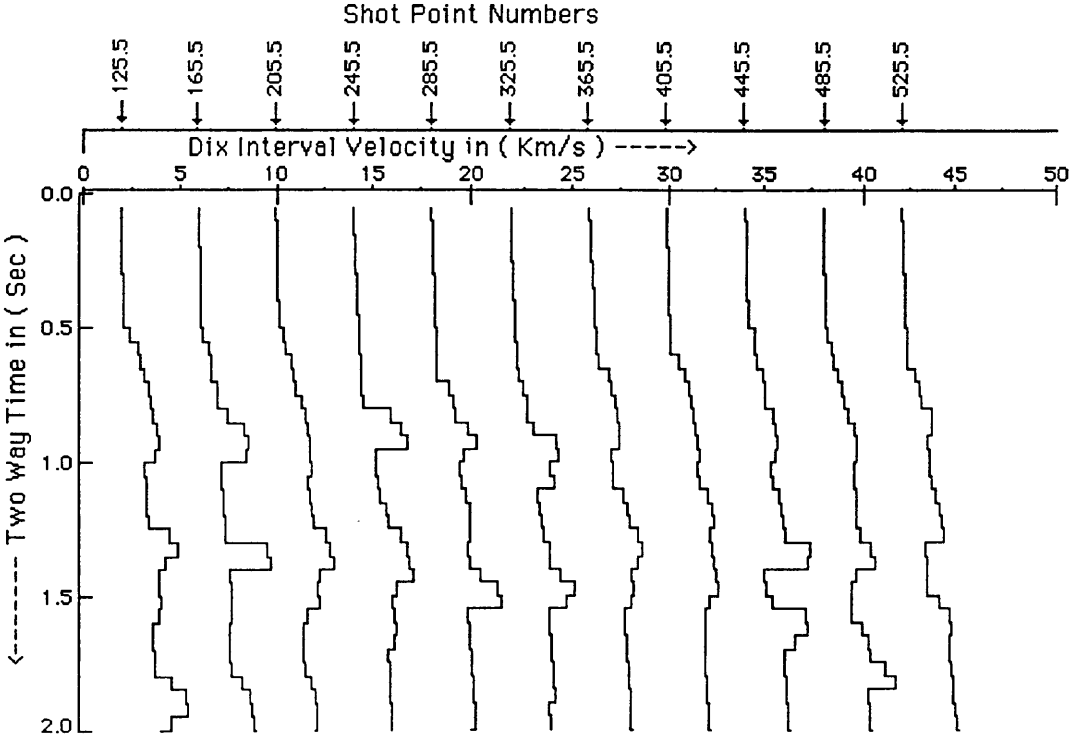

Fig.3.22d Interval velocity - two-way time relationships along seismic line 6V262, using the depth (D2) applied on equation (3.4).

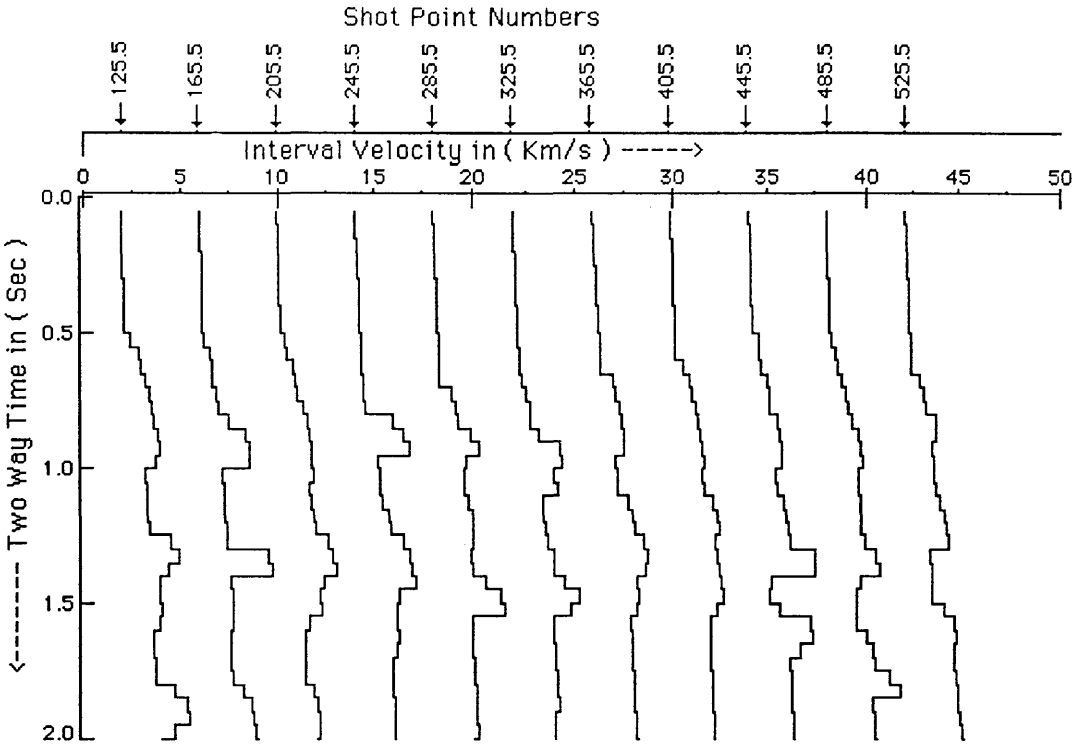

Fig.3.22e Interval velocity - two-way time relationships along seismic line 6V262, using stacking velocity applied on equation (3.13).

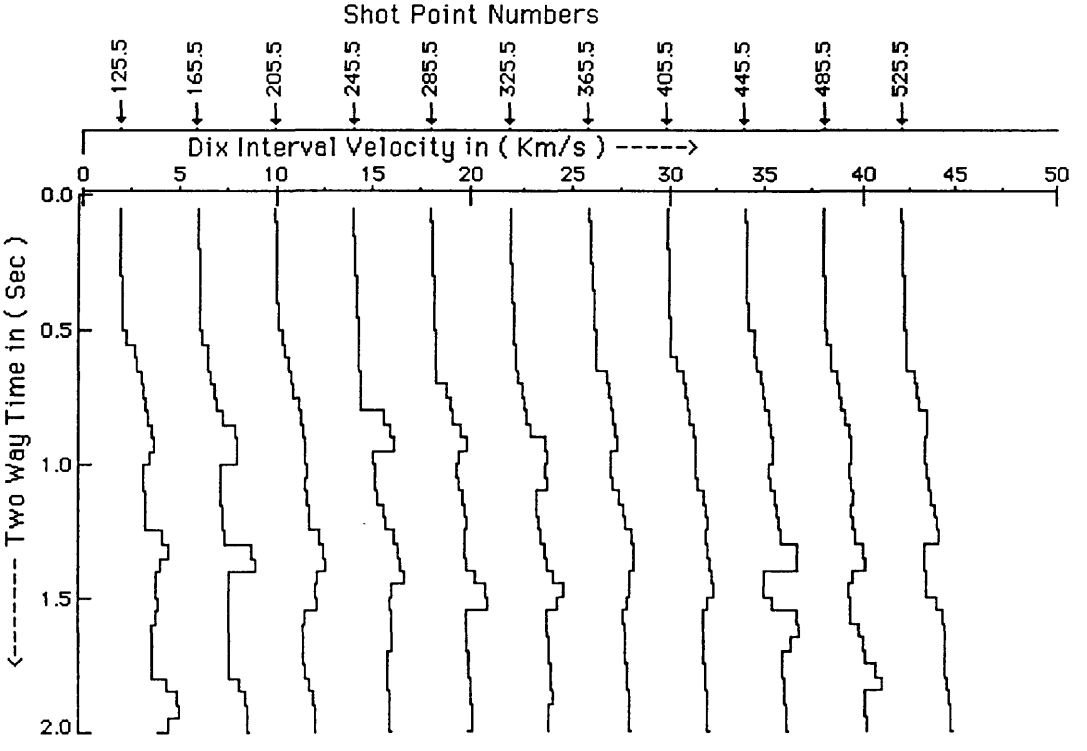

Fig.3.22f Interval velocity - two-way time relationships along seismic line 6V262, using Dix average velocity applied on equation (3.13).

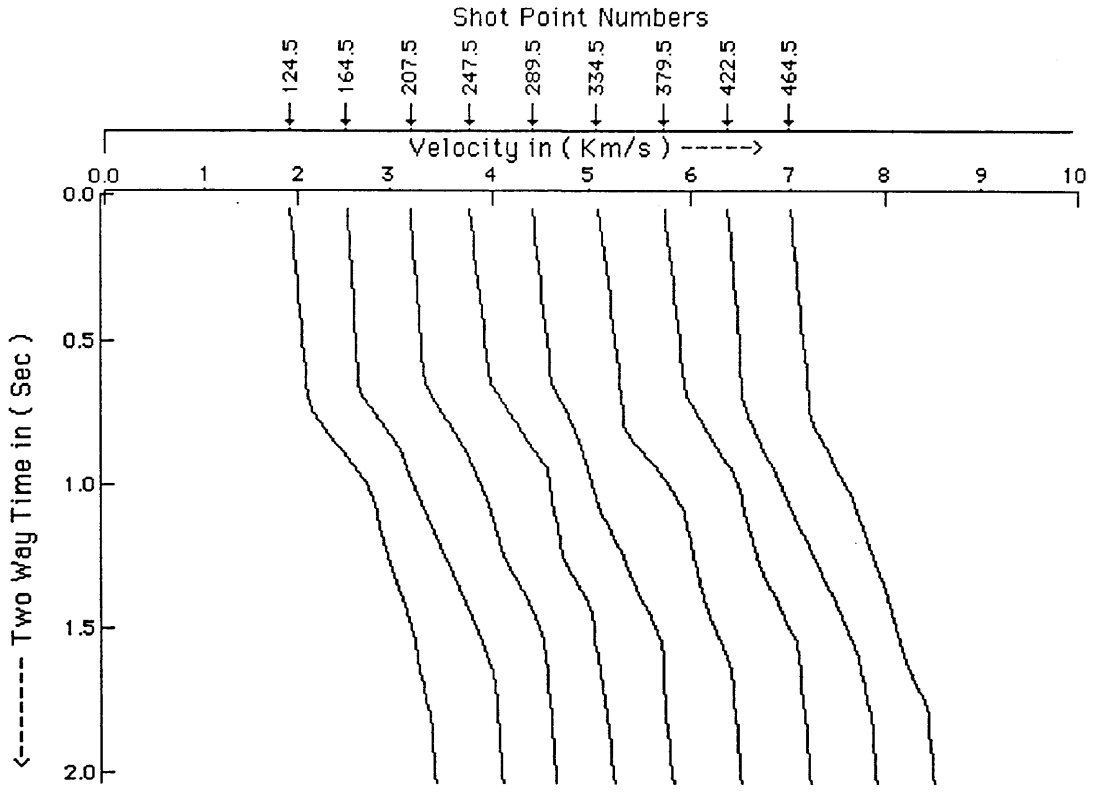

Fig.3.23a Stacking velocity - two-way time relationships along seismic line 6V263.

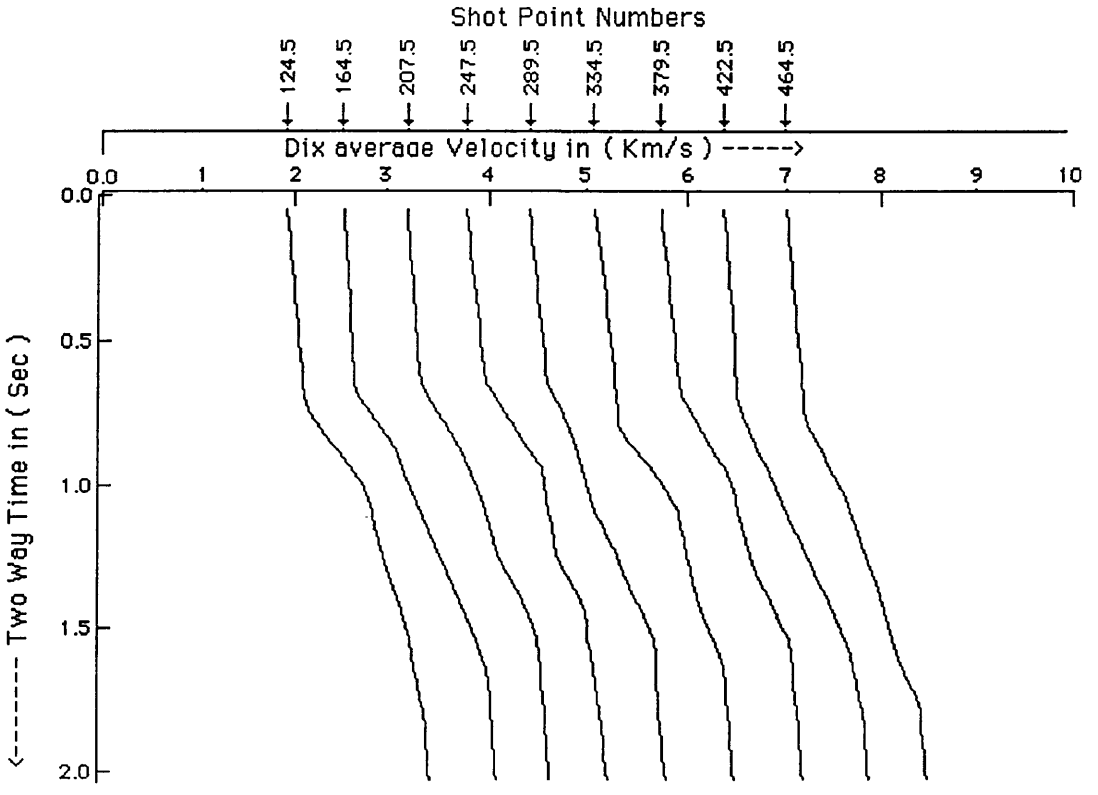

Fig.3.23b Dix average velocity - two-way time relationships along seismic line 6V263.

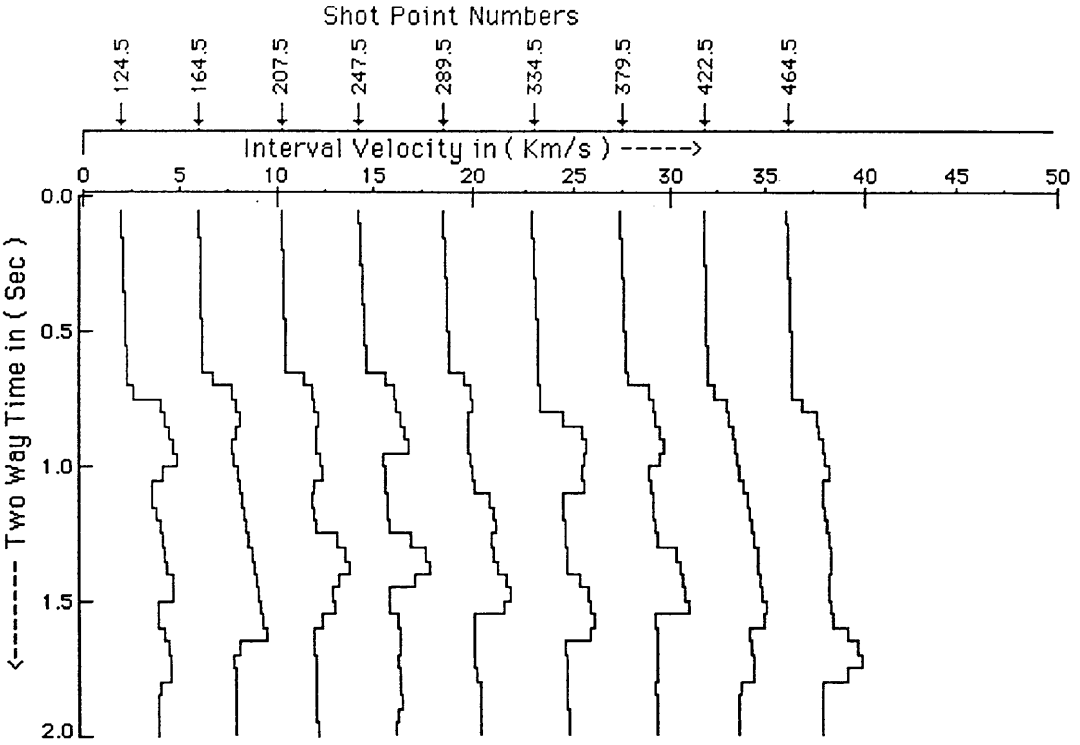

Fig.3.23c Interval velocity - two-way time relationships along seismic line 6V263, using the depth (D1) applied on equation (3.4).

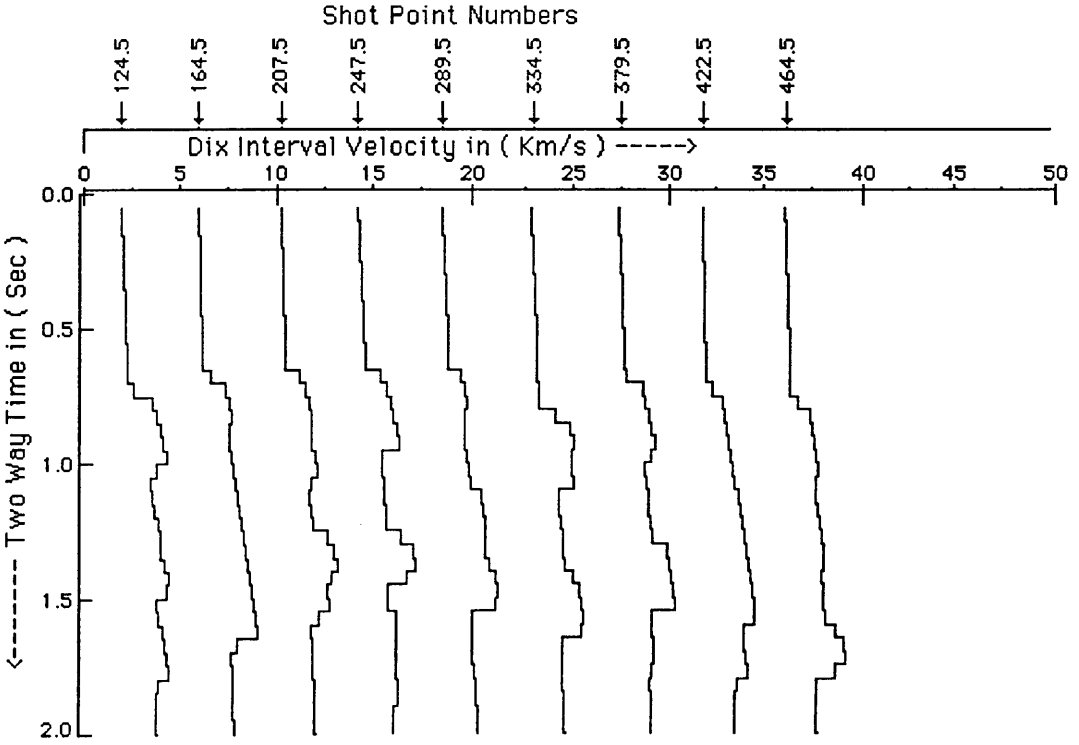

Fig.3.23d Interval velocity - two-way time relationships along seismic line 6V263, using the depth (D2) applied on equation (3.4).

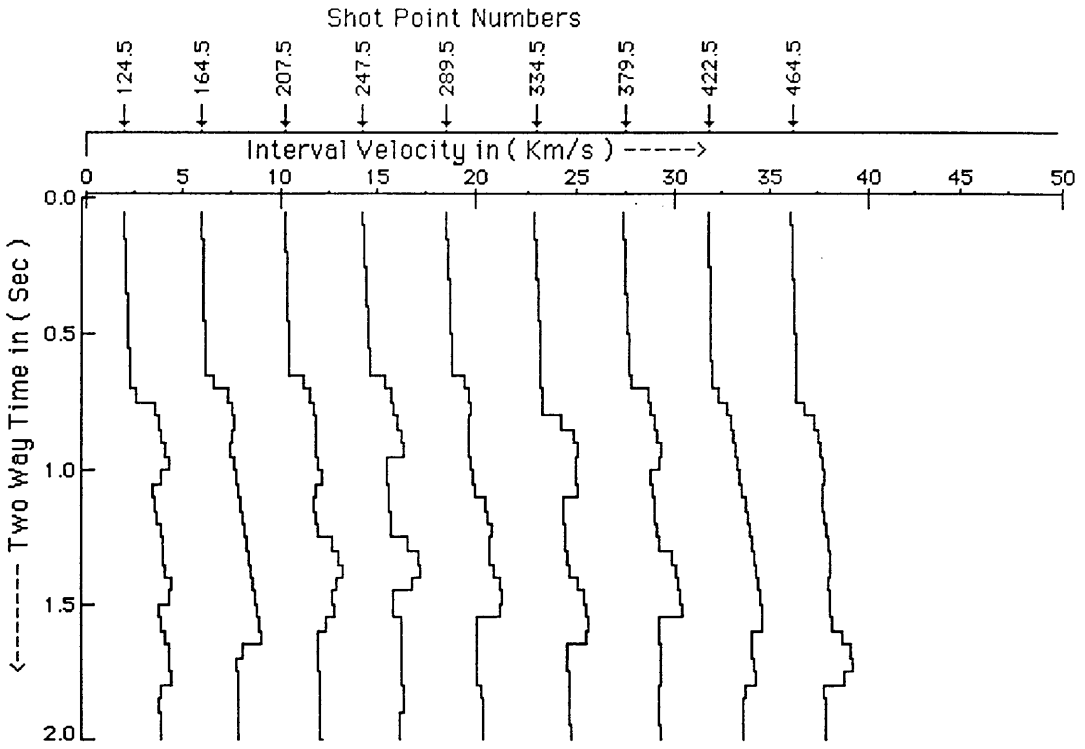

Fig.3.23e Interval velocity - two-way time relationships along seismic line 6V263, using stacking velocity applied on equation (3.13).

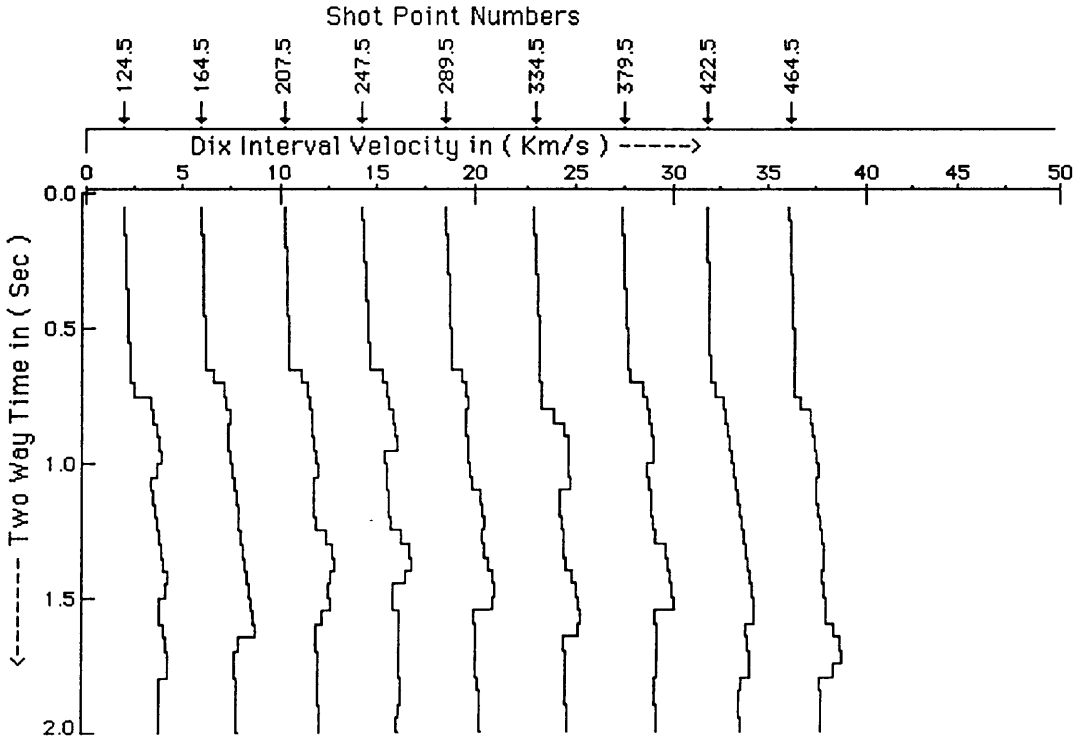

Fig.3.23f Interval velocity - two-way time relationships along seismic line 6V263, using Dix average velocity applied on equation (3.13).

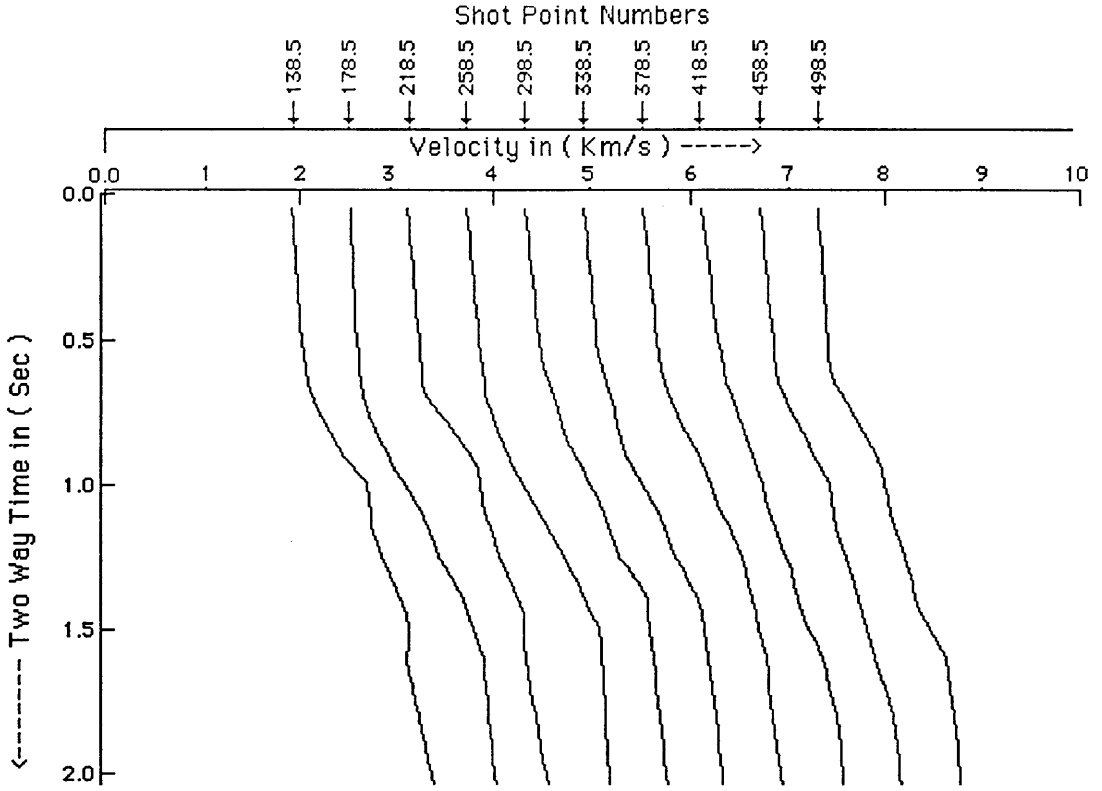

Fig.3.24a Stacking velocity - two-way time relationships along seismic line 6V264.

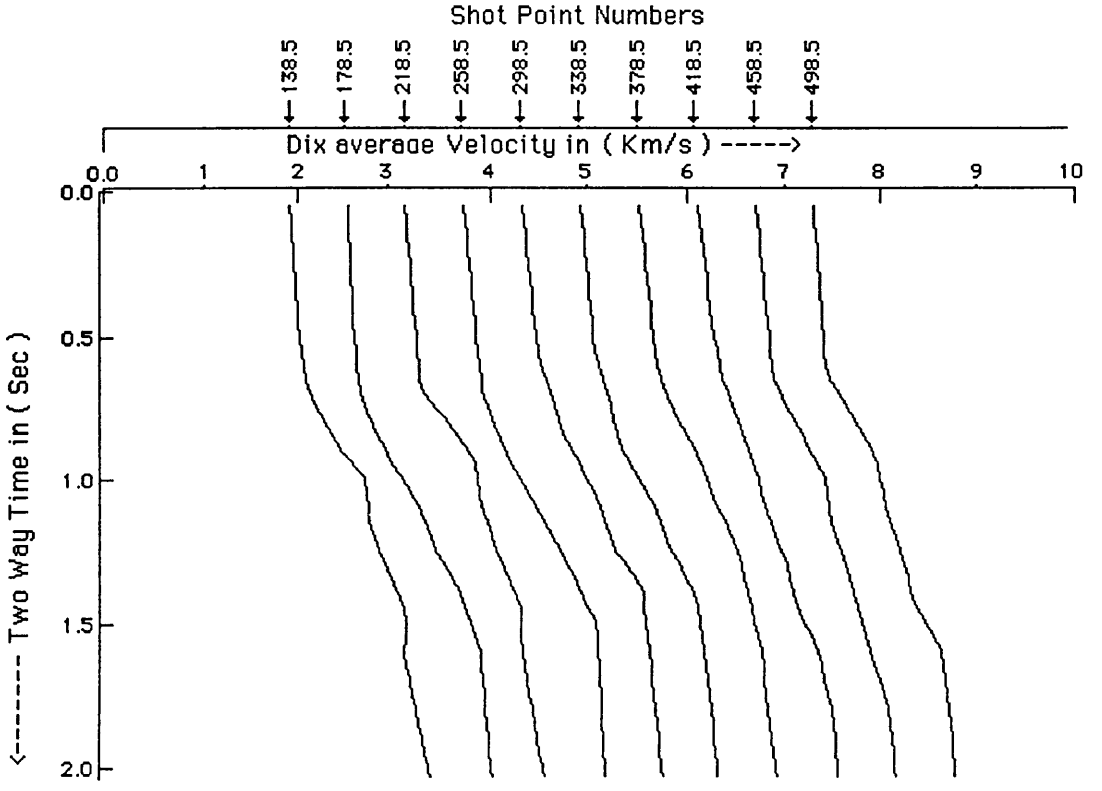

Fig.3.24b Dix average velocity - two-way time relationships along seismic line 6V264.

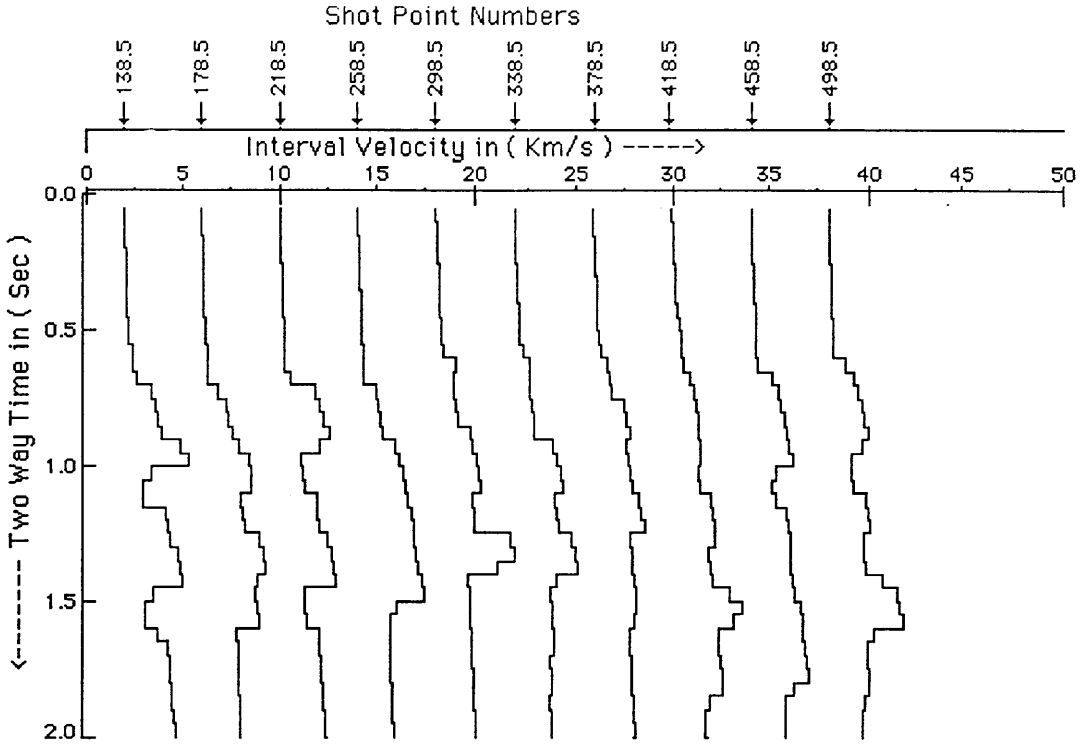

Fig.3.24c Interval velocity - two-way time relationships along seismic line 6V264, using the depth (D1) applied on equation (3.4).

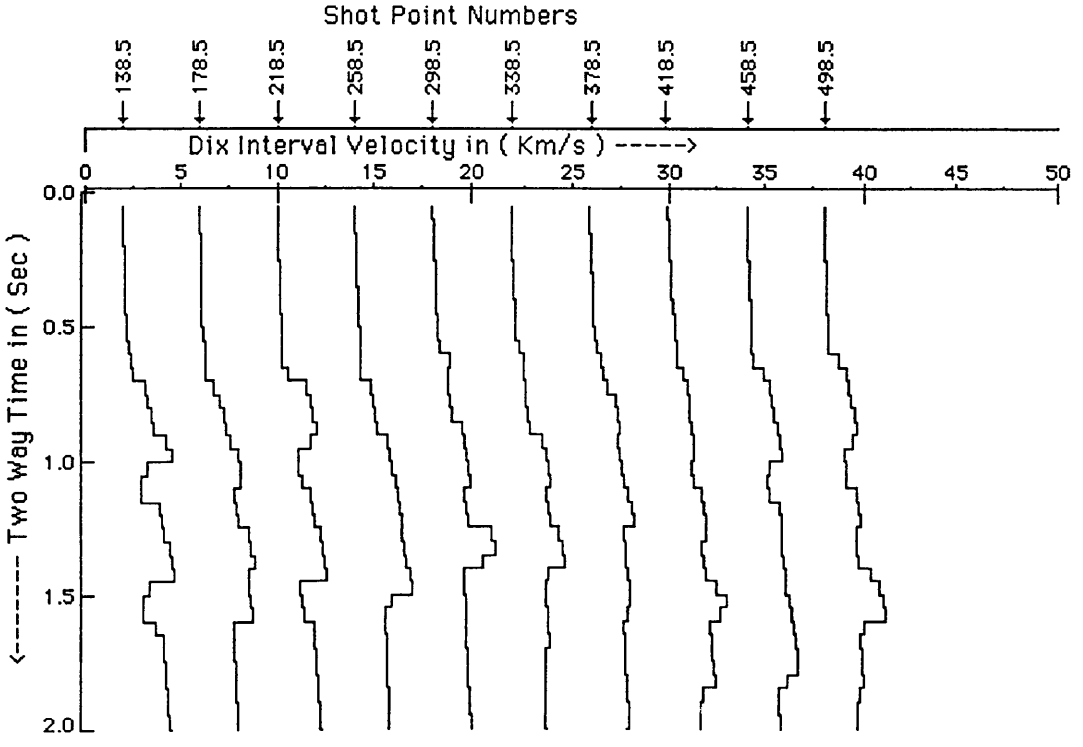

Fig.3.24d Interval velocity - two-way time relationships along seismic line 6V264, using the depth (D2) applied on equation (3.4).

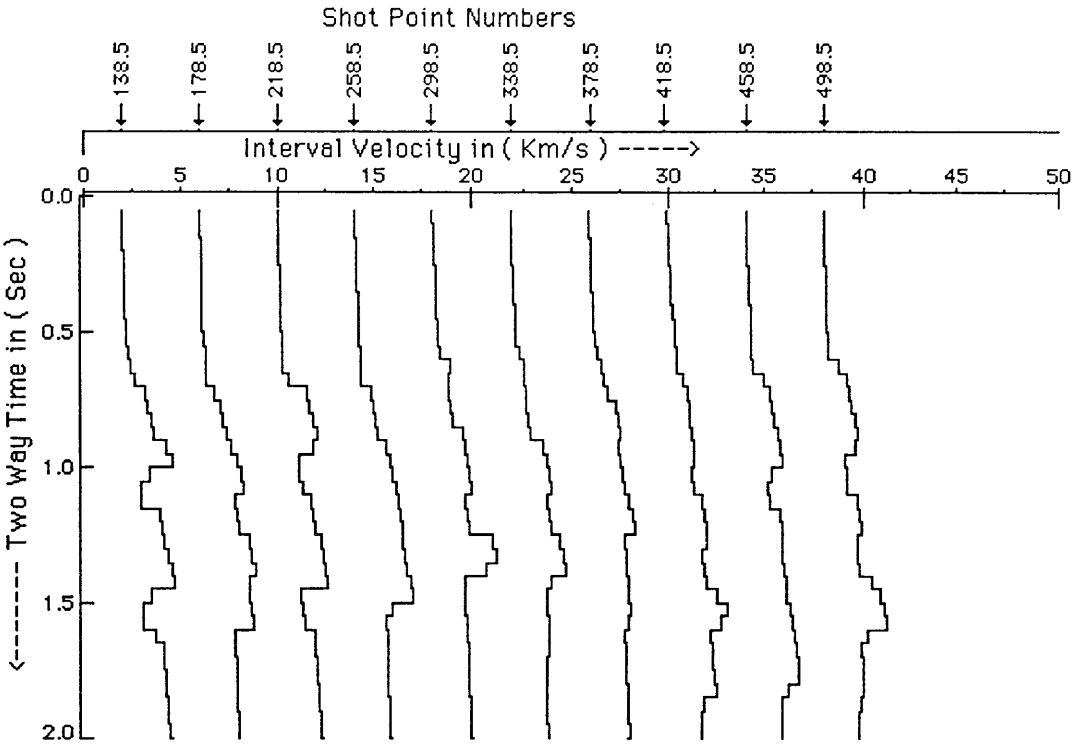

Fig.3.24e Interval velocity - two-way time relationships along seismic line 6V264, using stacking velocity applied on equation (3.13).

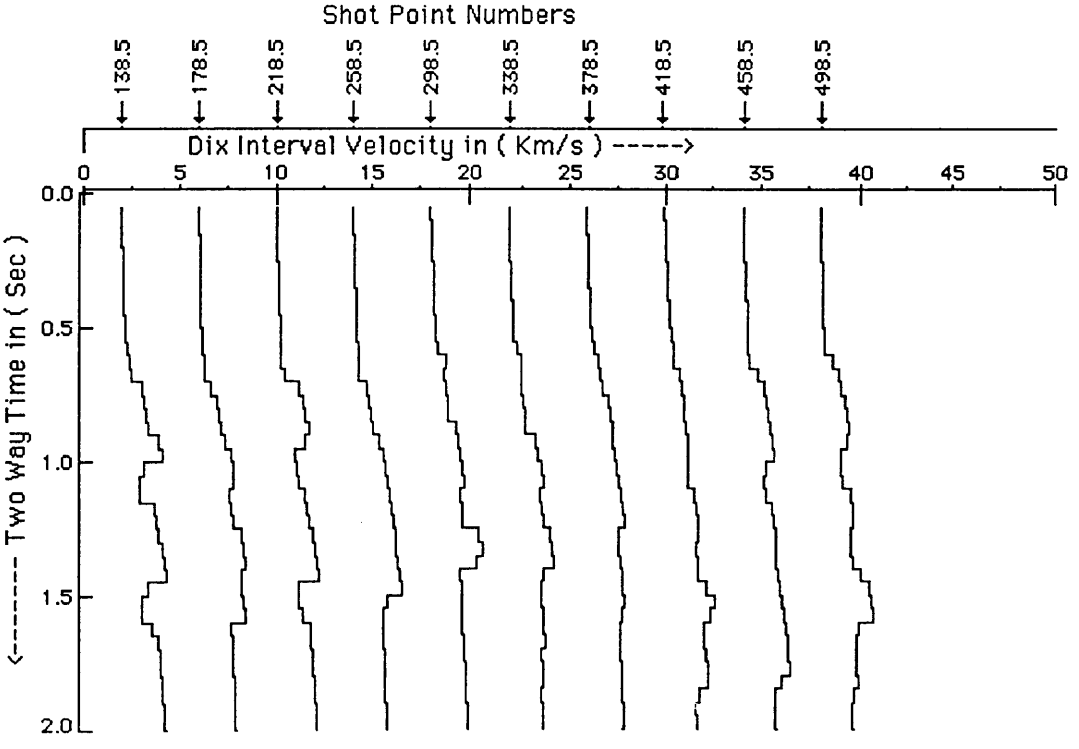

Fig.3.24f Interval velocity - two-way time relationships along seismic line 6V264, using Dix average velocity applied on equation (3.13).

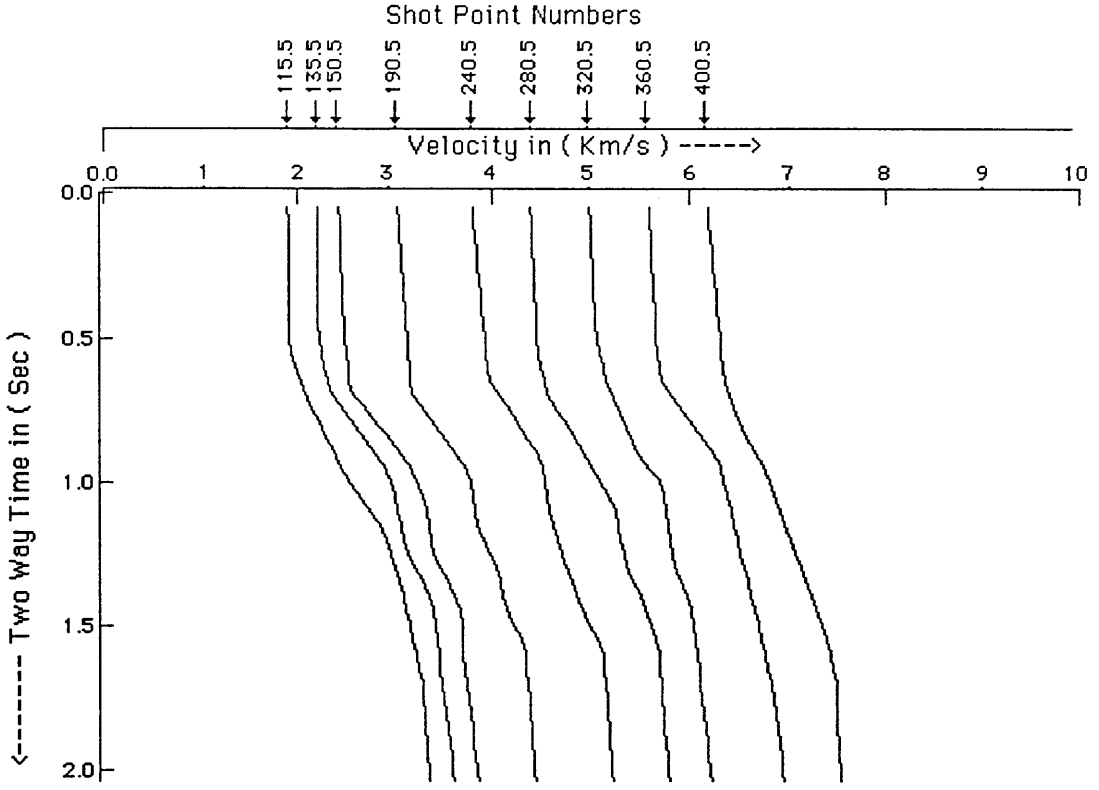

Fig.3.25a Stacking velocity - two-way time relationships along seismic line 6V265.

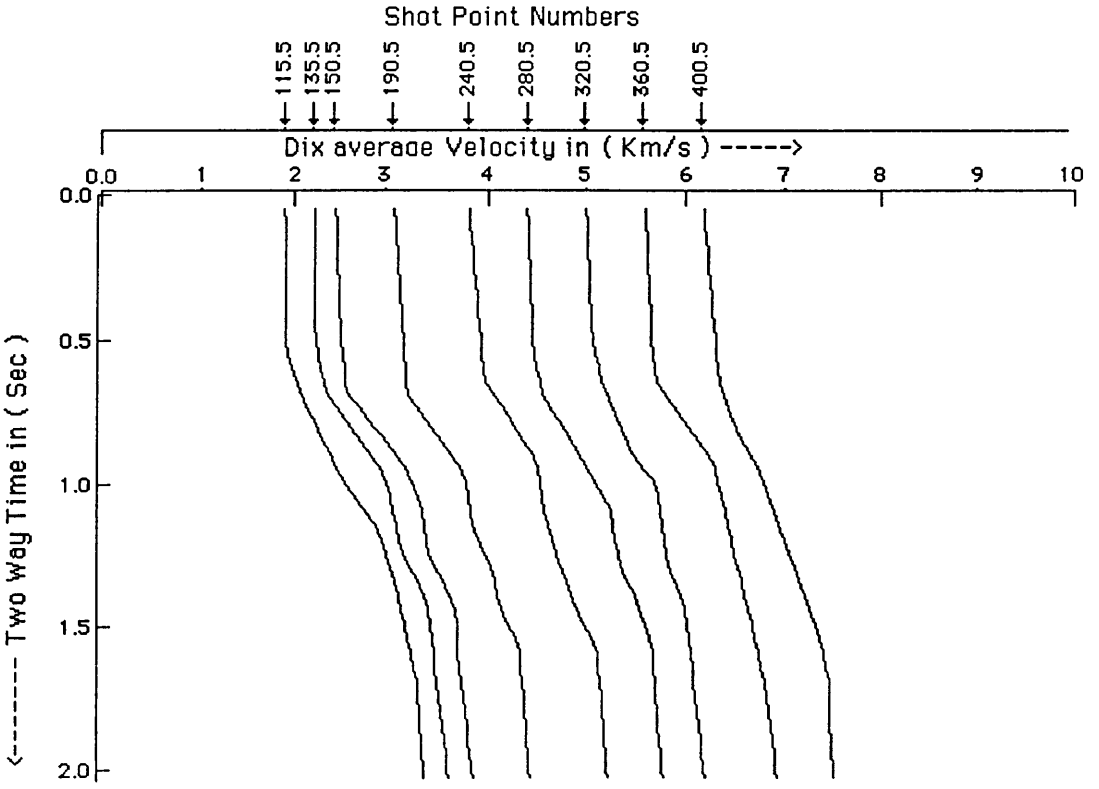

Fig.3.25b Dix average velocity - two-way time relationships along seismic line 6V265.

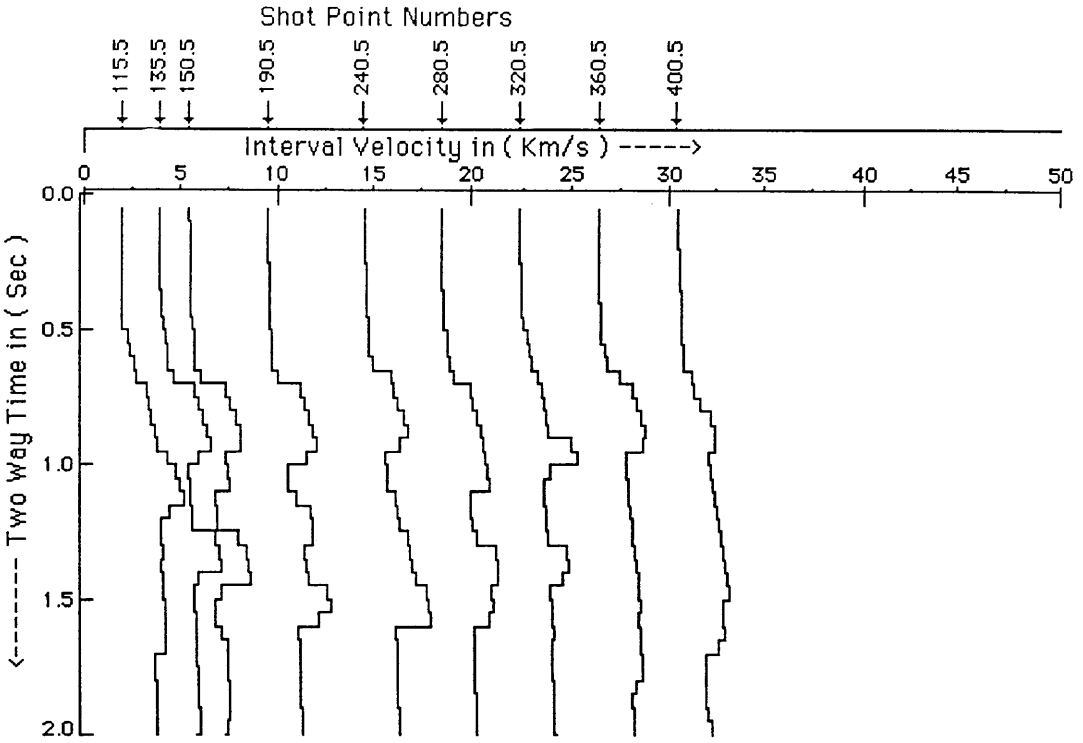

Fig.3.25c Interval velocity - two-way time relationships along seismic line 6V265, using the depth (D1) applied on equation (3.4).

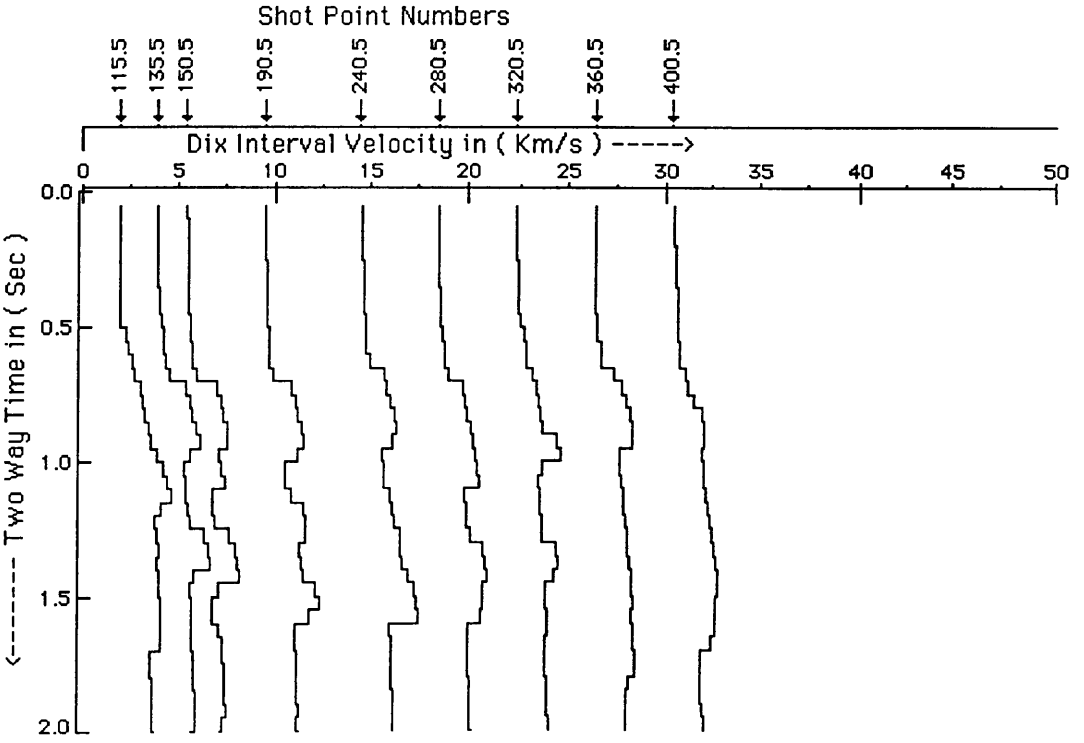

Fig.3.25d Interval velocity - two-way time relationships along seismic line 6V265, using the depth (D2) applied on equation (3.4).

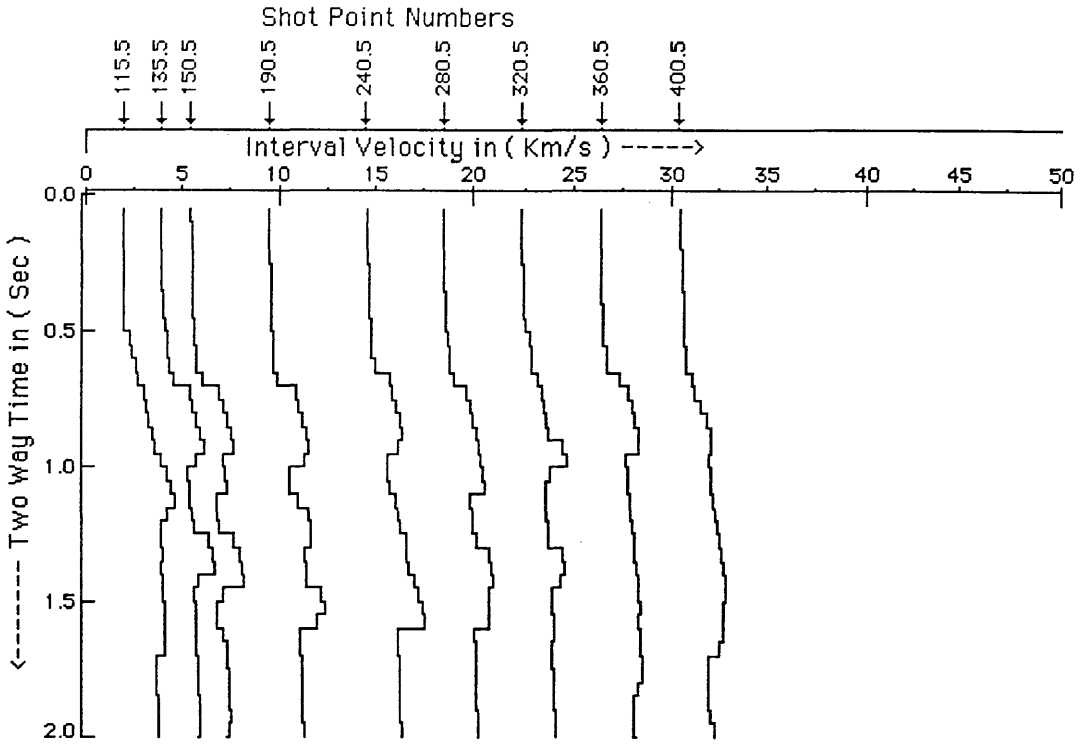

Fig.3.25e Interval velocity - two-way time relationships along seismic line 6V265, using stacking velocity applied on equation (3.13).

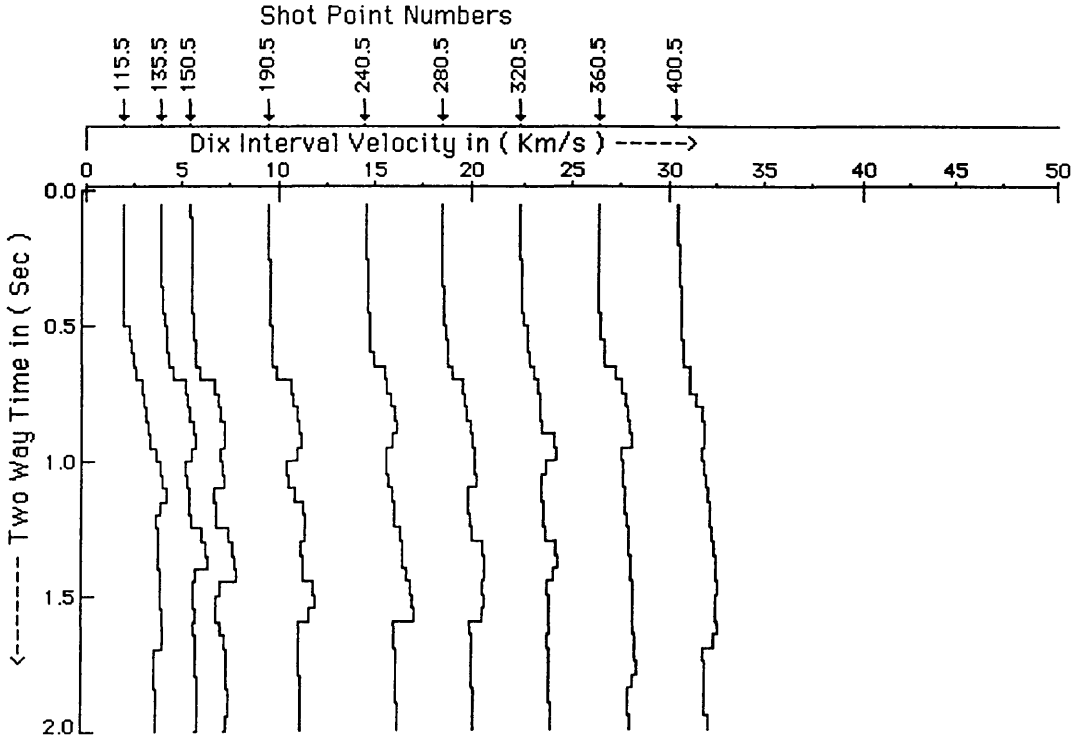

Fig.3.25f Interval velocity - two-way time relationships along seismic line 6V265, using Dix average velocity applied on equation (3.13).

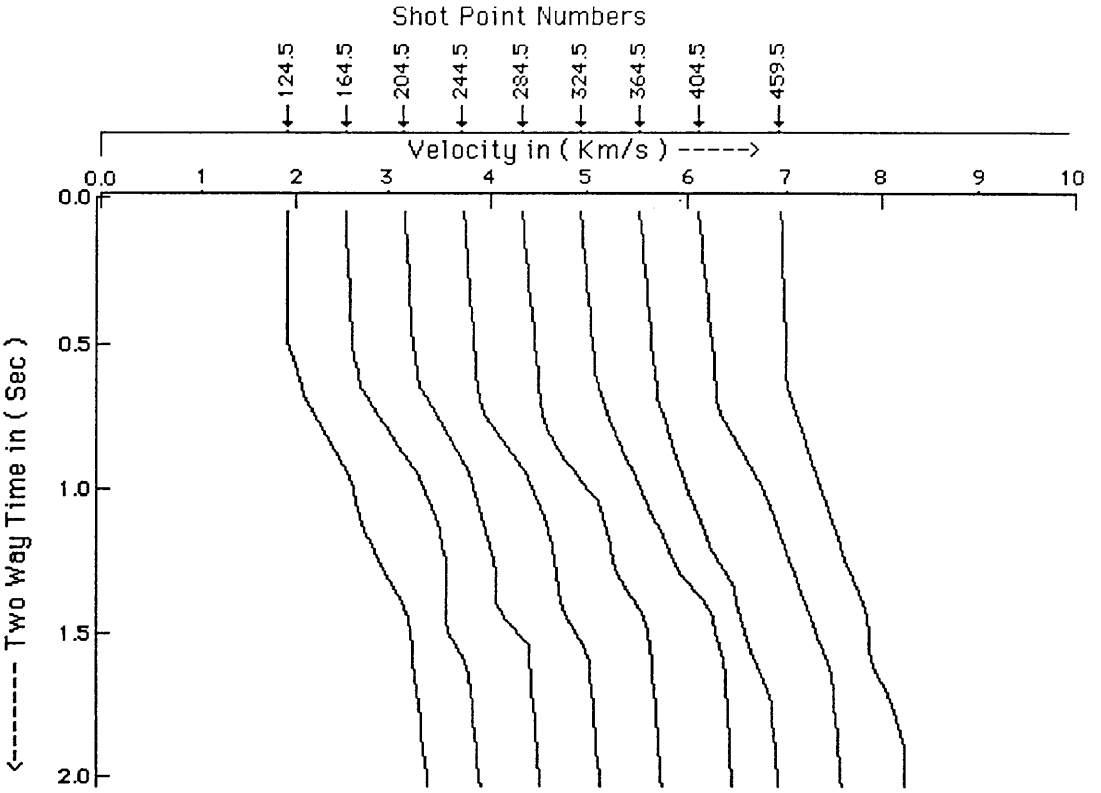

Fig.3.26a Stacking velocity - two-way time relationships along seismic line 6V301.

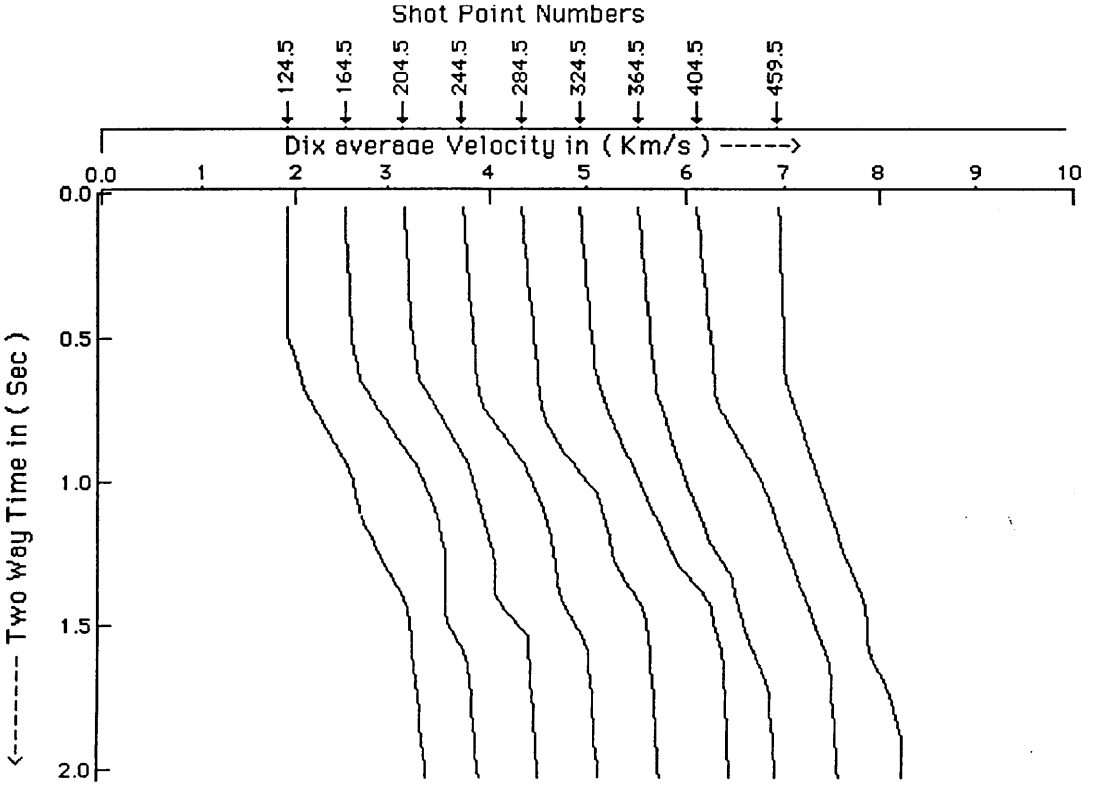

Fig.3.26b Dix average velocity - two-way time relationships along seismic line 6V301.

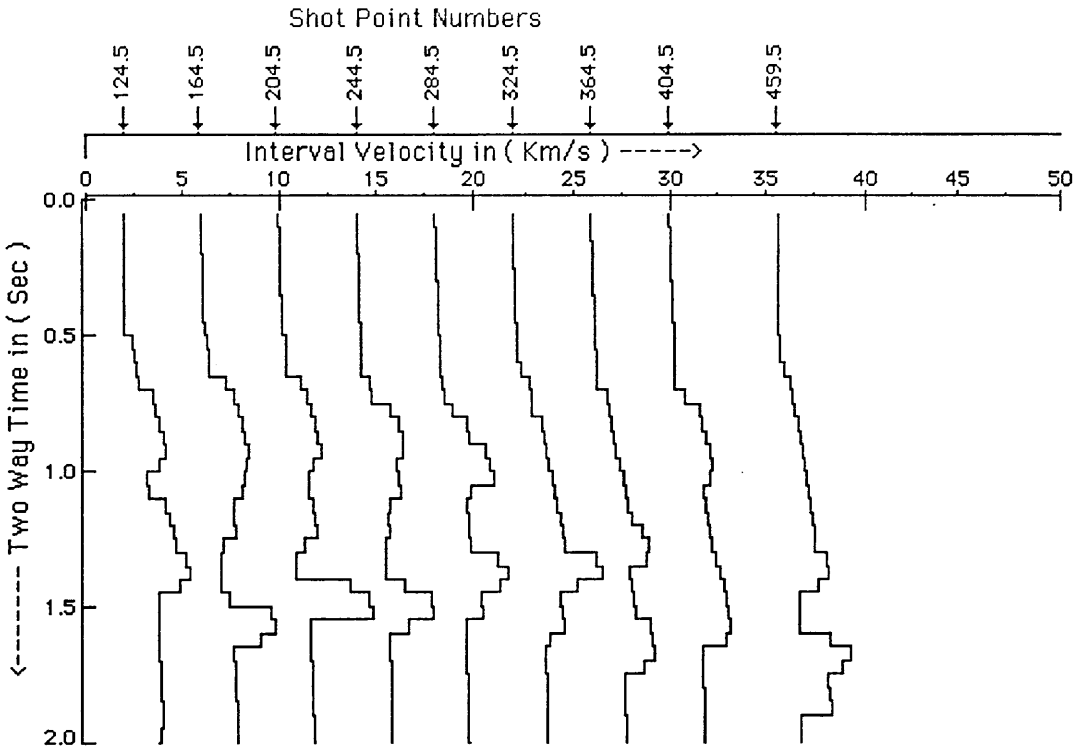

Fig.3.26c Interval velocity - two-way time relationships along seismic line 6V301, using the depth (D1) applied on equation (3.4).

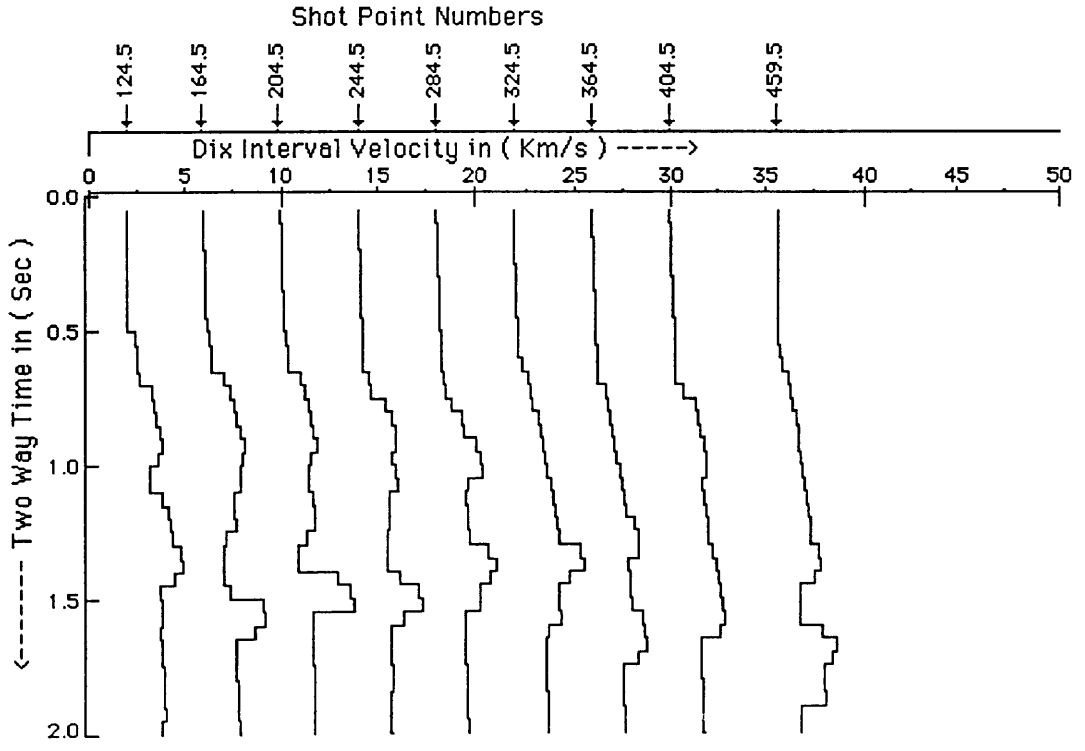

Fig.3.26d Interval velocity - two-way time relationships along seismic line 6V301, using the depth (D2) applied on equation (3.4).

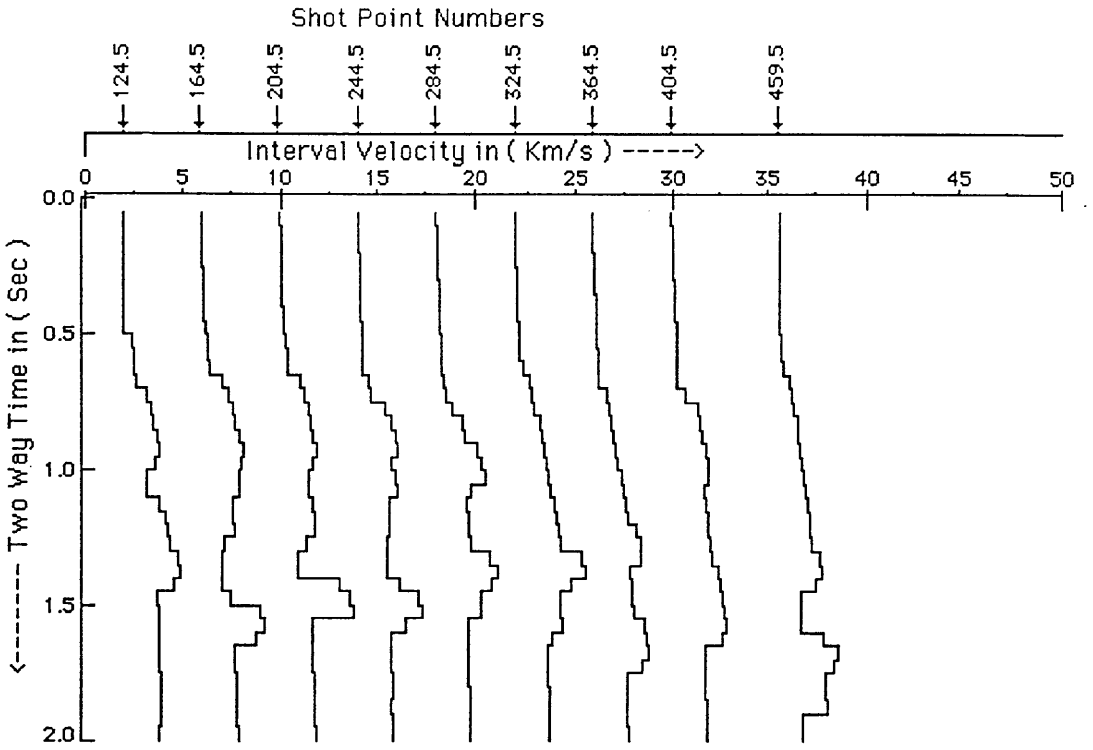

Fig.3.26e Interval velocity - two-way time relationships along seismic line 6V301, using stacking velocity applied on equation (3.13).

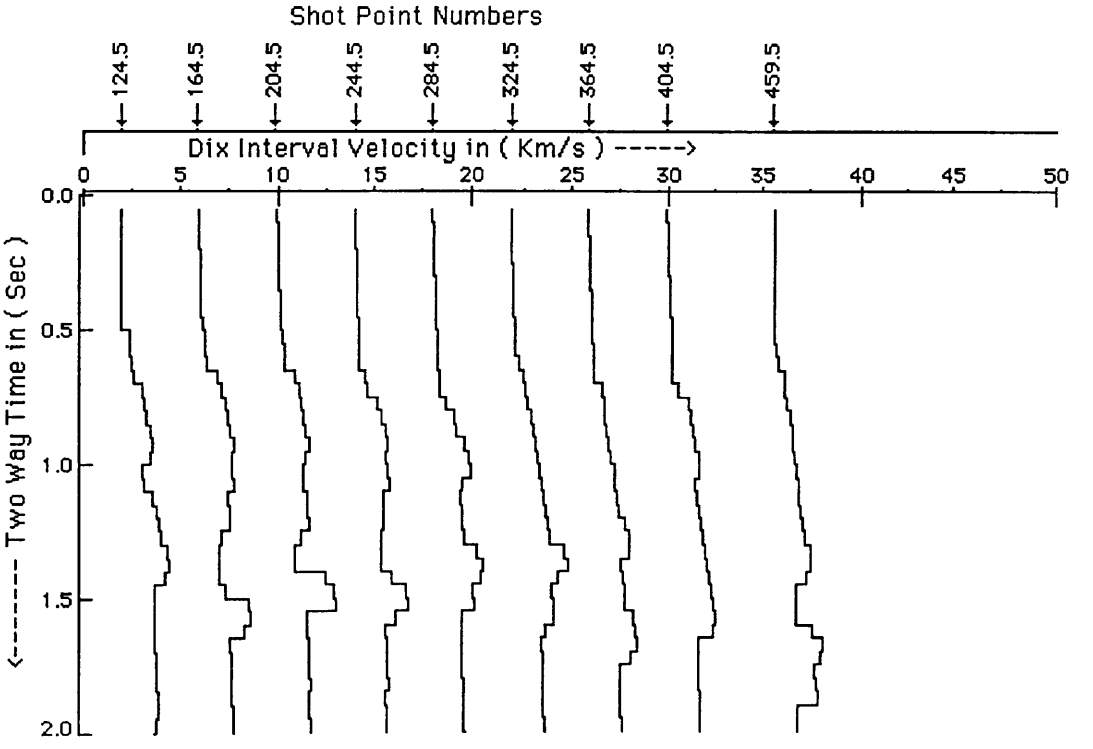

Fig.3.26f Interval velocity - two-way time relationships along seismic line 6V301, using Dix average velocity applied on equation (3.13).

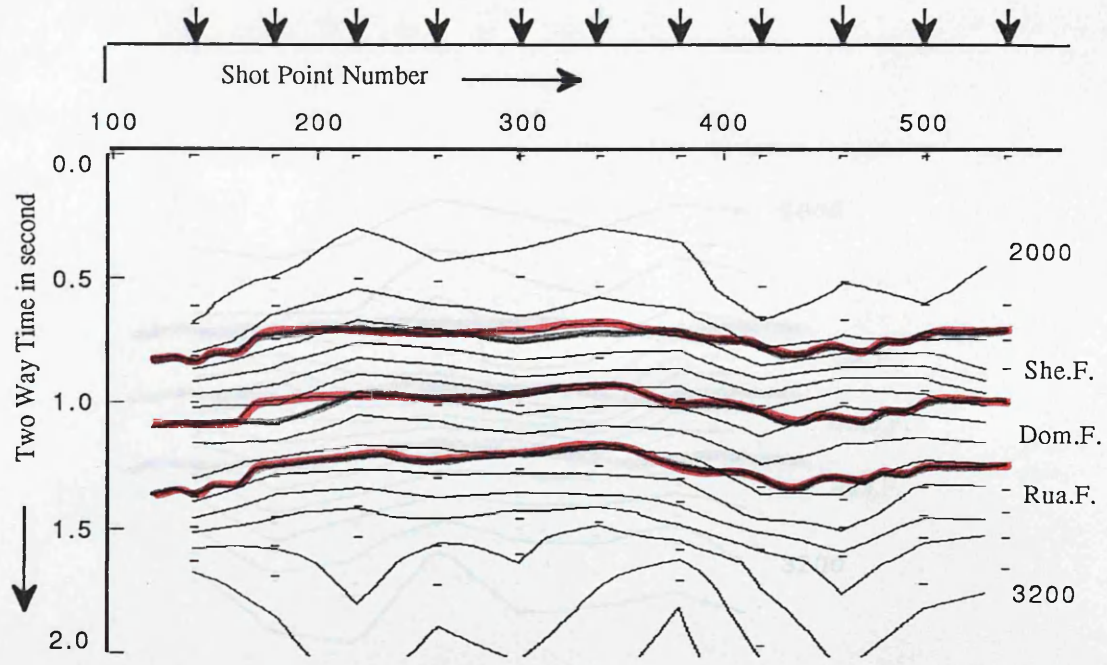

Fig. 3.28 Interpolated stacking velocities on line 6V250-85. Velocity analyses are made at locations indicated by ↓ at top. Times individual picks are shown by small dashes. Computer interpolates in time and then in space to get complete stacking velocity field indicated by the 100 m/s contours. Times picks from seismic section for different horizons are shown in red.

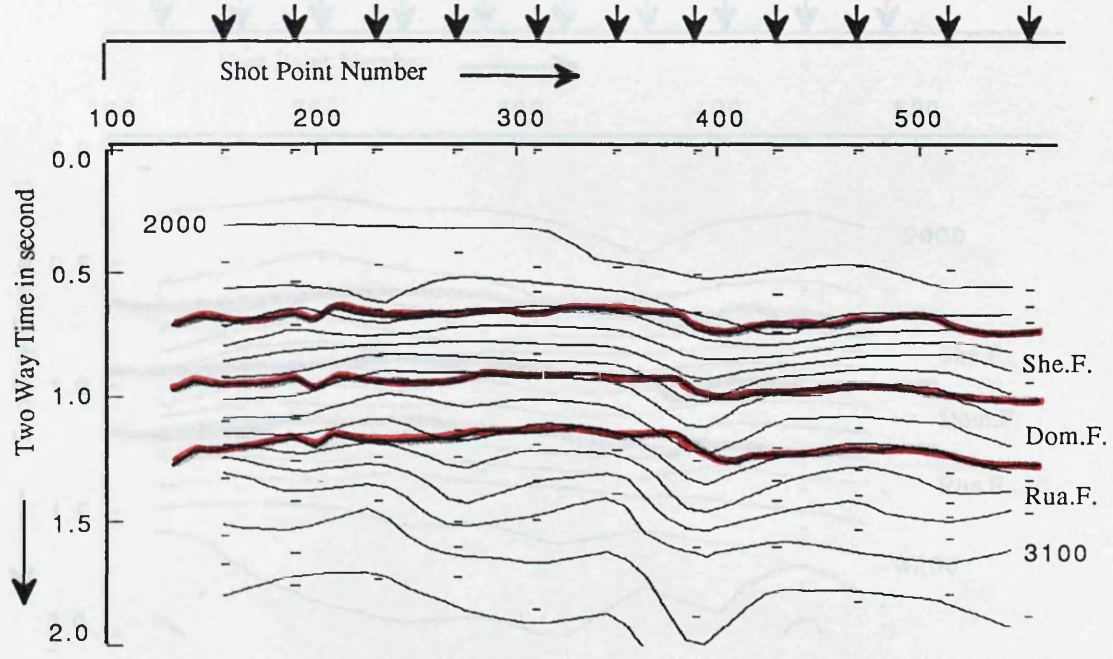

Fig. 3.29 Interpolated stacking velocities on line 6V252-85. Velocity analyses are made at locations indicated by ↓ at top. Times individual picks are shown by small dashes. Computer interpolates in time and then in space to get complete stacking velocity field indicated by the 100 m/s contours. Times picks from seismic section for different horizons are shown in red.

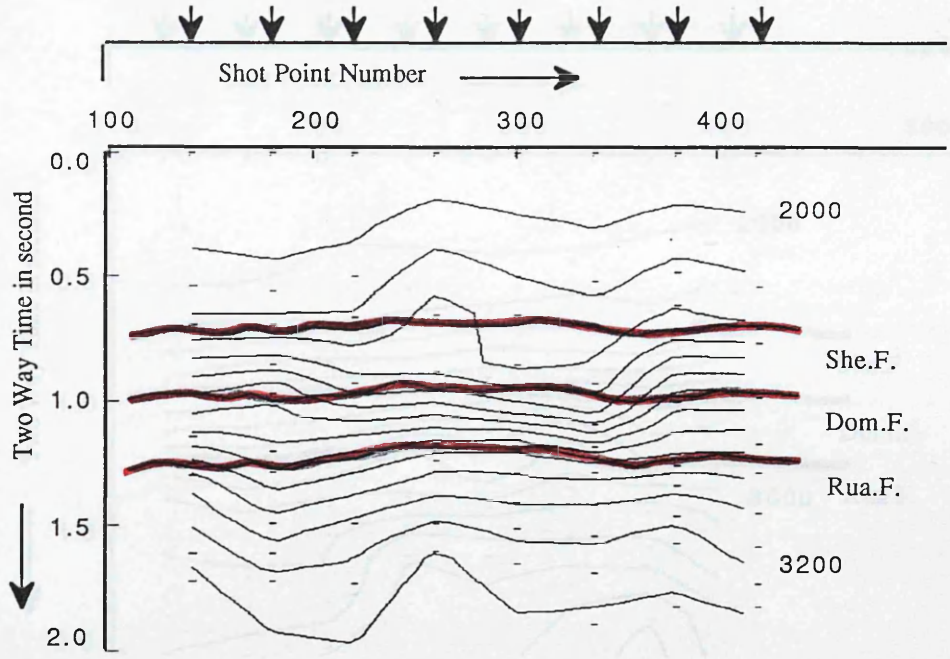

Fig. 3.30 Interpolated stacking velocities on line 6V253-85. Velocity analyses are made at locations indicated by ↓ at top. Times individual picks are shown by small dashes. Computer interpolates in time and then in space to get complete stacking velocity field indicated by the 100 m/s contours. Times picks from seismic section for different horizons are shown in red.

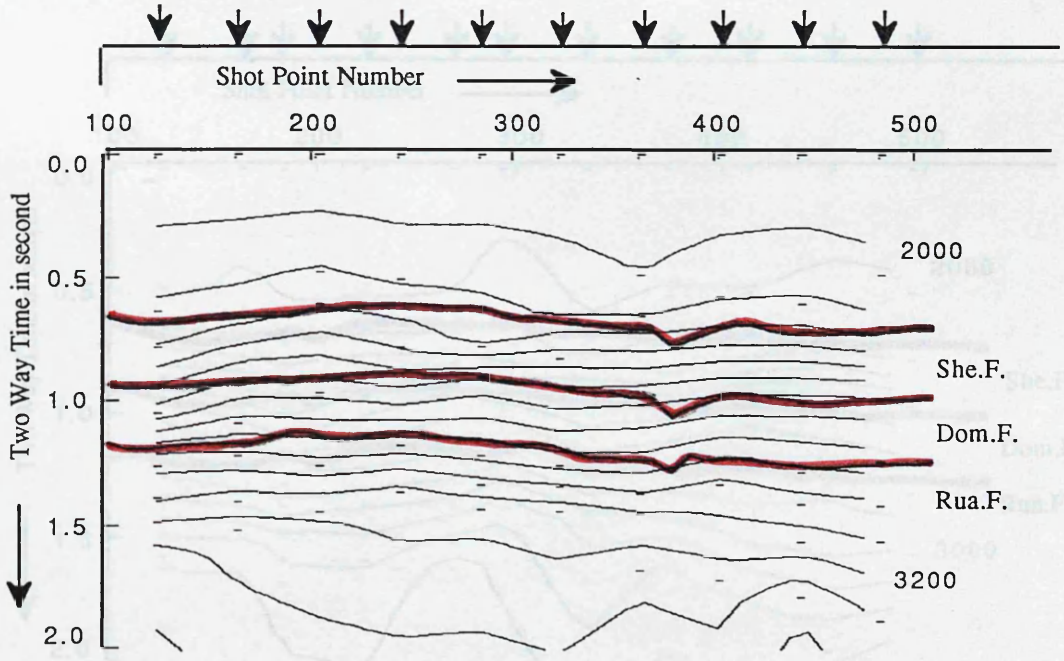

Fig. 3.31 Interpolated stacking velocities on line 6V254-85. Velocity analyses are made at locations indicated by ↓ at top. Times individual picks are shown by small dashes. Computer interpolates in time and then in space to get complete stacking velocity field indicated by the 100 m/s contours. Times picks from seismic section for different horizons are shown in red.

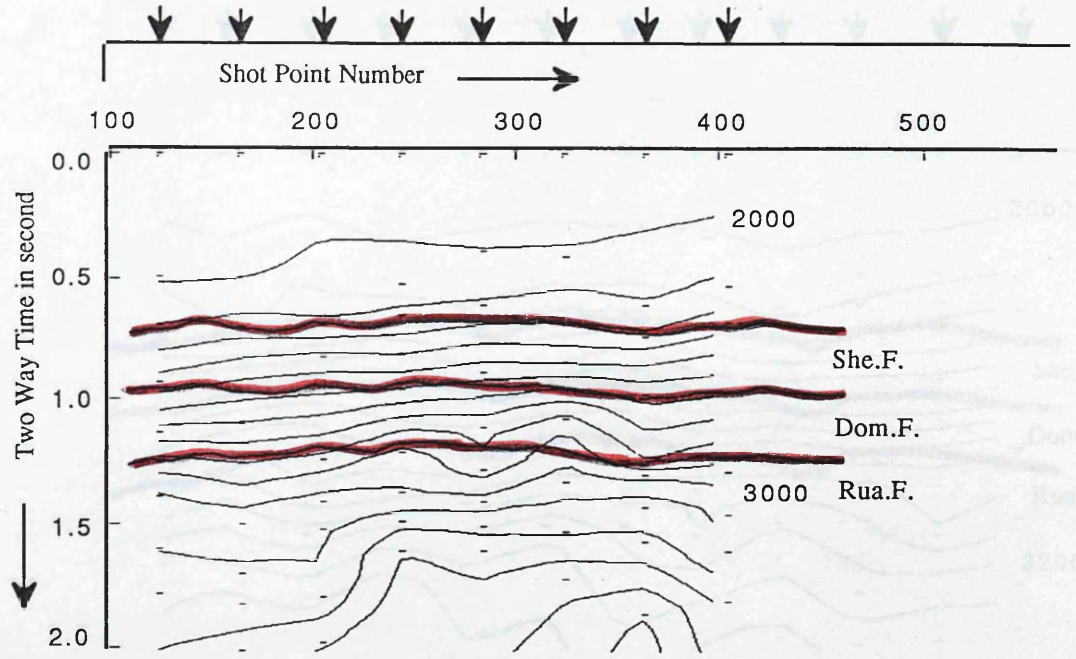

Fig. 3.32 Interpolated stacking velocities on line 6V255-85. Velocity analyses are made at locations indicated by ↓ at top. Times individual picks are shown by small dashes. Computer interpolates in time and then in space to get complete stacking velocity field indicated by the 100 m/s contours. Times picks from seismic section for different horizons are shown in red.

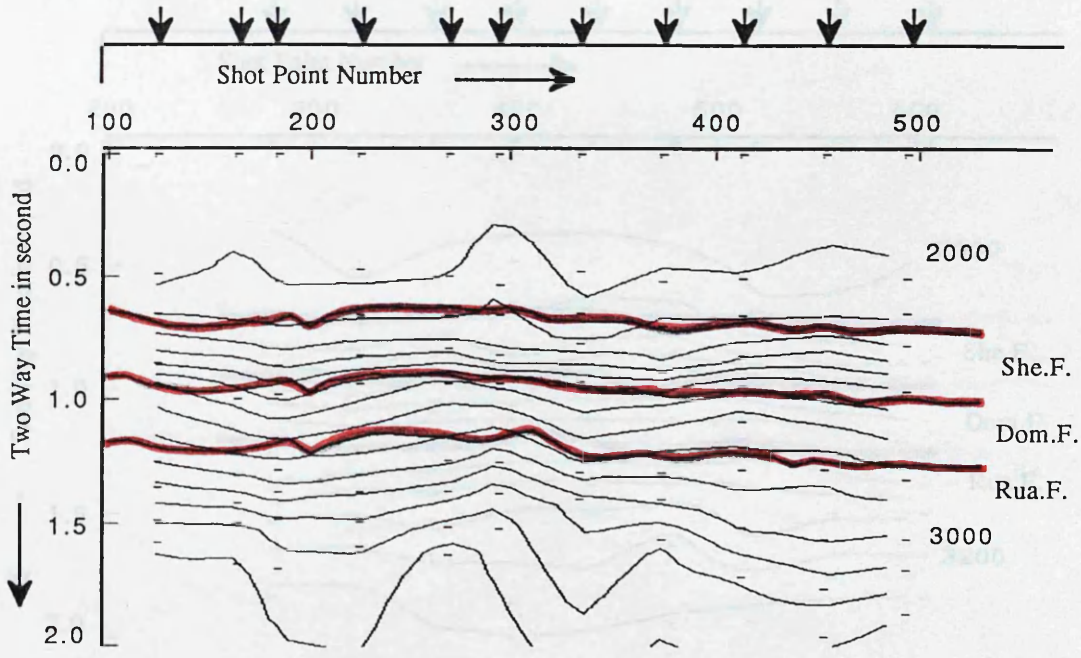

Fig. 3.33 Interpolated stacking velocities on line 6V256-85. Velocity analyses are made at locations indicated by ↓ at top. Times individual picks are shown by small dashes. Computer interpolates in time and then in space to get complete stacking velocity field indicated by the 100 m/s contours. Times picks from seismic section for different horizons are shown in red.

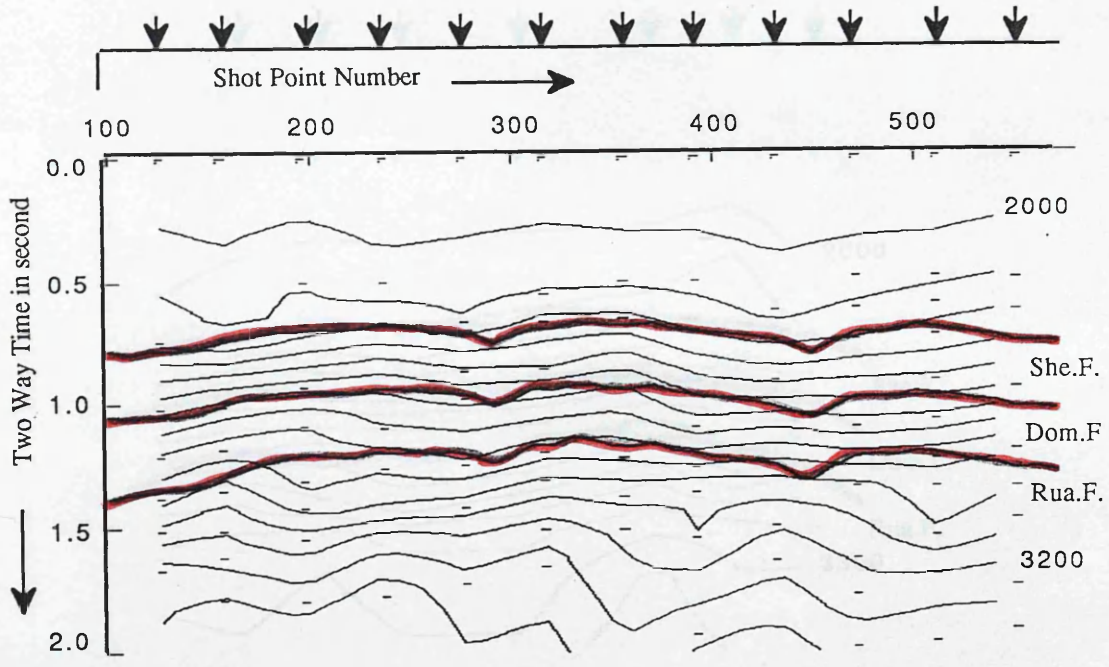

Fig. 3.34 Interpolated stacking velocities on line 6V257-85. Velocity analyses are made at locations indicated by ↓ at top. Times individual picks are shown by small dashes. Computer interpolates in time and then in space to get complete stacking velocity field indicated by the 100 m/s contours. Times picks from seismic section for different horizons are shown in red.

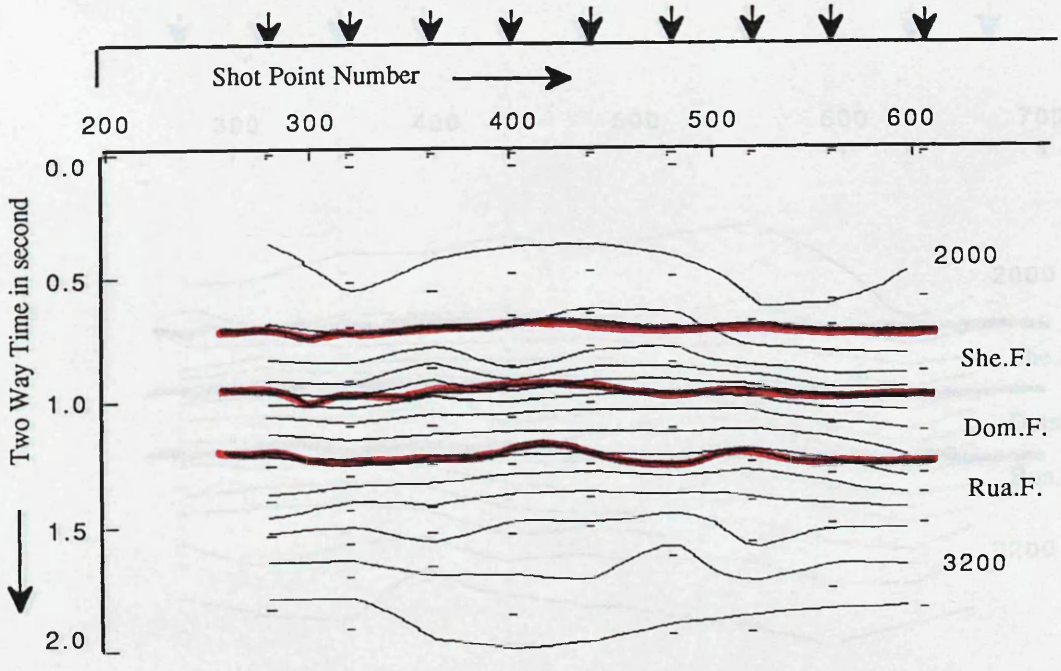

Fig. 3.35 Interpolated stacking velocities on line 6V258-85. Velocity analyses are made at locations indicated by ↓ at top. Times individual picks are shown by small dashes. Computer interpolates in time and then in space to get complete stacking velocity field indicated by the 100 m/s contours. Times picks from seismic section for different horizons are shown in red.

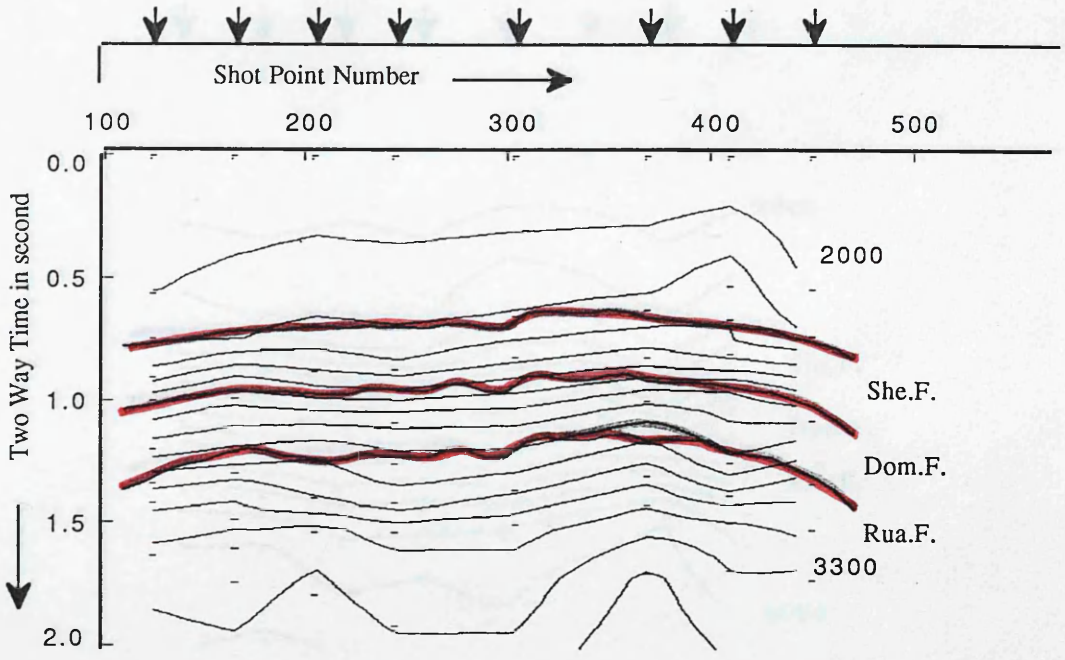

Fig. 3.36 Interpolated stacking velocities on line 6V259-85. Velocity analyses are made at locations indicated by ↓ at top. Times individual picks are shown by small dashes. Computer interpolates in time and then in space to get complete stacking velocity field indicated by the 100 m/s contours. Times picks from seismic section for different horizons are shown in red.

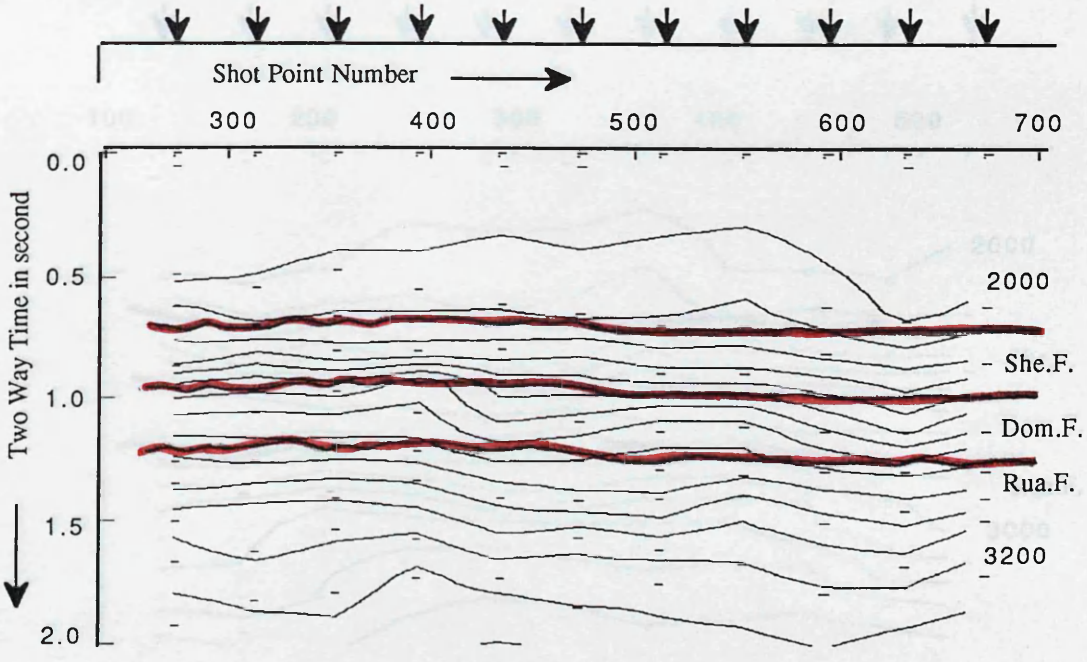

Fig. 3.37 Interpolated stacking velocities on line 6V260-85. Velocity analyses are made at locations indicated by ↓ at top. Times individual picks are shown by small dashes. Computer interpolates in time and then in space to get complete stacking velocity field indicated by the 100 m/s contours. Times picks from seismic section for different horizons are shown in red.

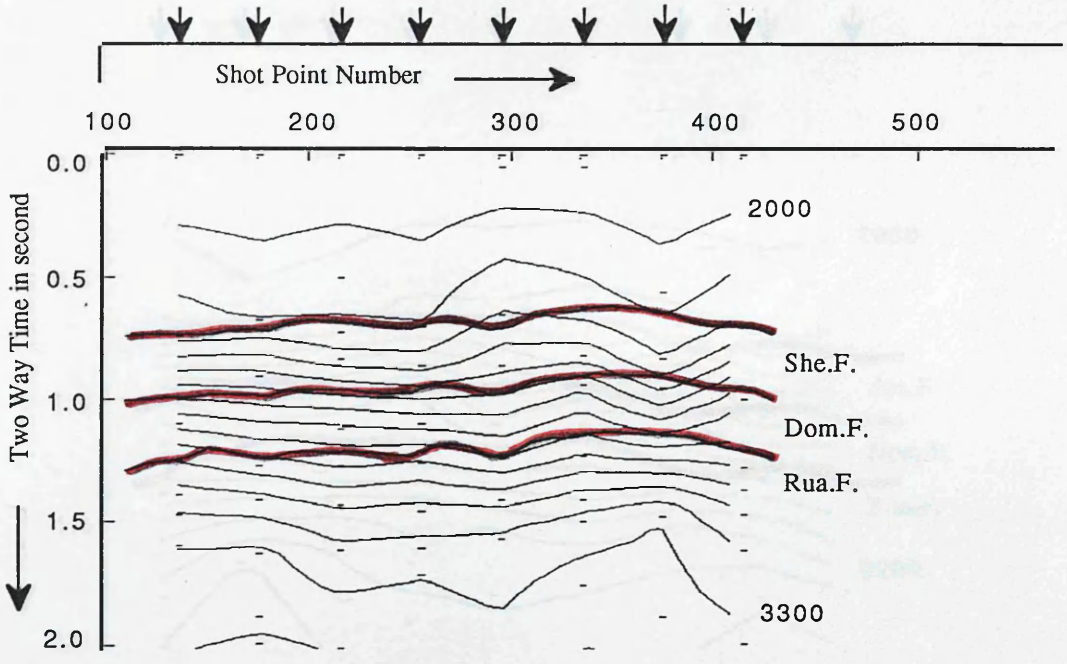

Fig. 3.38 Interpolated stacking velocities on line 6V261-85. Velocity analyses are made at locations indicated by ↓ at top. Times individual picks are shown by small dashes. Computer interpolates in time and then in space to get complete stacking velocity field indicated by the 100 m/s contours. Times picks from seismic section for different horizons are shown in red.

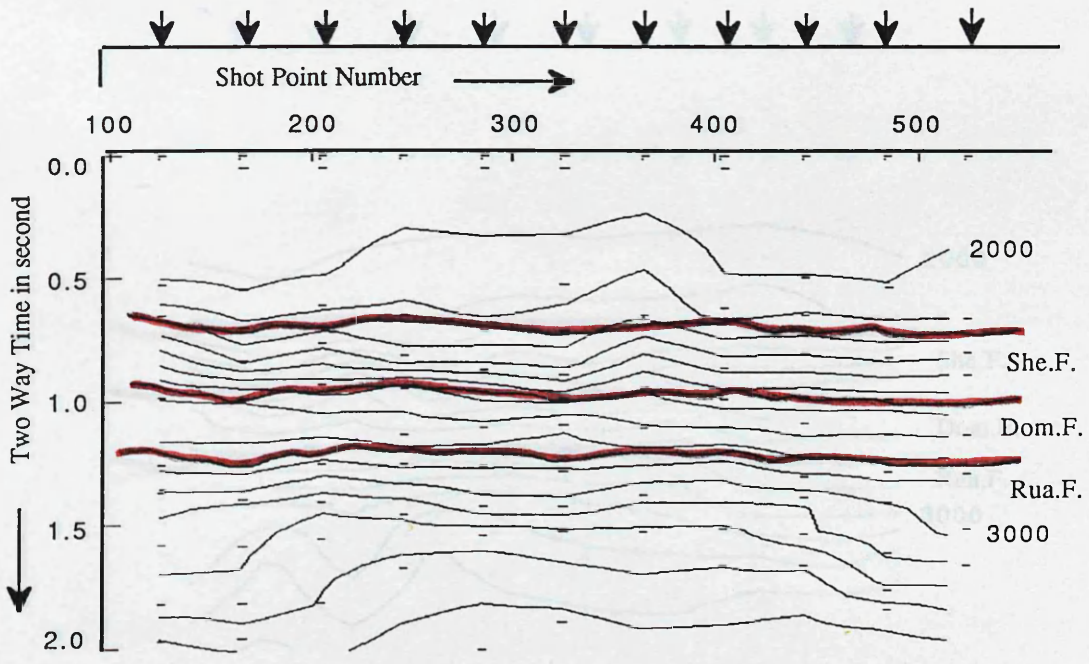

Fig. 3.39 Interpolated stacking velocities on line 6V262-85. Velocity analyses are made at locations indicated by ↓ at top. Times individual picks are shown by small dashes. Computer interpolates in time and then in space to get complete stacking velocity field indicated by the 100 m/s contours. Times picks from seismic section for different horizons are shown in red.

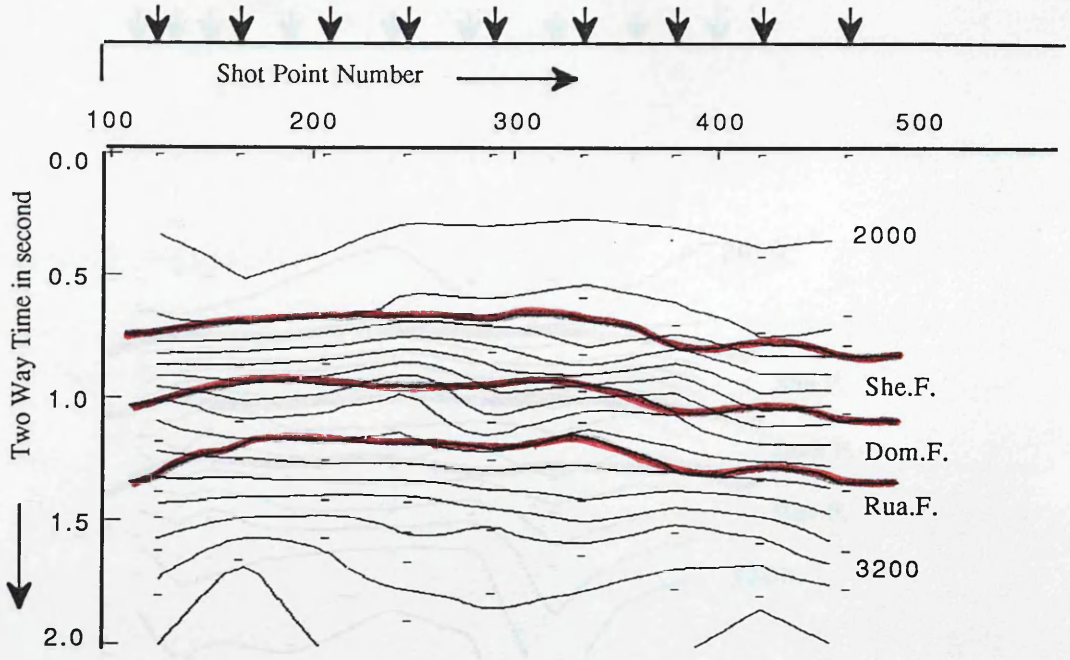

Fig. 3.40 Interpolated stacking velocities on line 6V263-85. Velocity analyses are made at locations indicated by ↓ at top. Times individual picks are shown by small dashes. Computer interpolates in time and then in space to get complete stacking velocity field indicated by the 100 m/s contours. Times picks from seismic section for different horizons are shown in red.

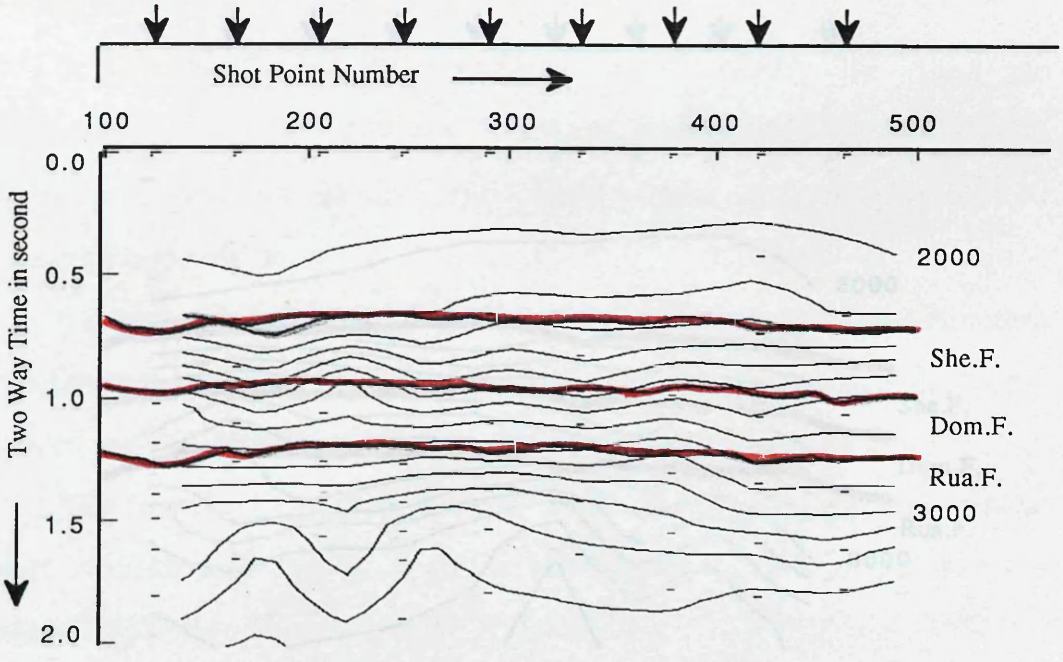

Fig. 3.41 Interpolated stacking velocities on line 6V264-85. Velocity analyses are made at locations indicated by ↓ at top. Times individual picks are shown by small dashes. Computer interpolates in time and then in space to get complete stacking velocity field indicated by the 100 m/s contours. Times picks from seismic section for different horizons are shown in red.

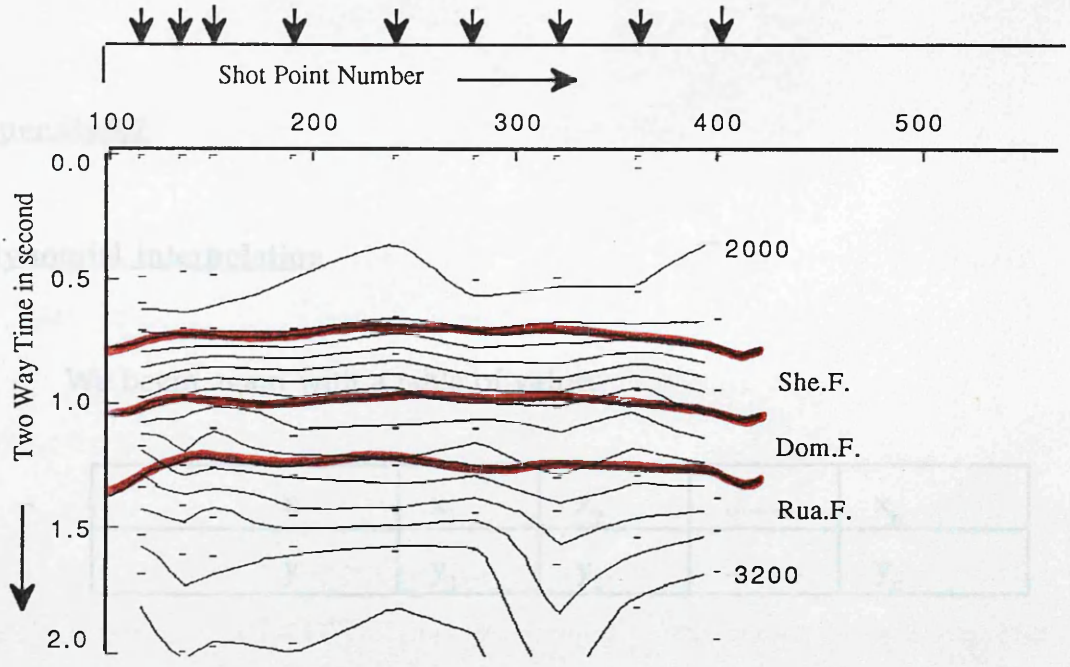

Fig. 3.42 Interpolated stacking velocities on line 6V265-85. Velocity analyses are made at locations indicated by ↓ at top. Times individual picks are shown by small dashes. Computer interpolates in time and then in space to get complete stacking velocity field indicated by the 100 m/s contours. Times picks from seismic section for different horizons are shown in red.

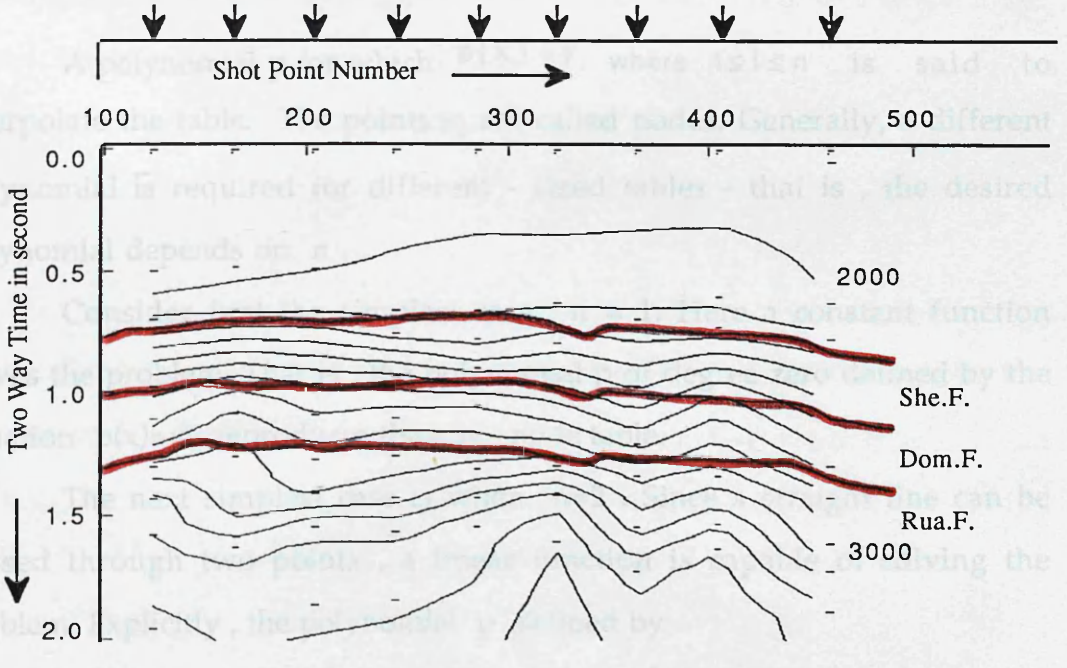

Fig. 3.43 Interpolated stacking velocities on line 6V301-85. Velocity analyses are made at locations indicated by ↓ at top. Times individual picks are shown by small dashes. Computer interpolates in time and then in space to get complete stacking velocity field indicated by the 100 m/s contours. Times picks from seismic section for different horizons are shown in red.

Appendix 3.7

Polynomial interpolation

We begin again with a table of values

x	x_1	x_2	.....	x_n
y	y_1	y_2	.....	y_n

and assume that the x_i's form a set of n distinct points. The table represents n points in the Cartesian plane , and we want to find a polynomial curve that passes through the points. Thus we seek to determine a polynomial , which is defined for all x , that takes on the corresponding values yi for each of the n distinct x_i's in this table.

A polynomial p for which $p(x_i) = y_i$ where $1 \le i \le n$ is said to interpolate the table. The points x_i are called nodes. Generally, a different polynomial is required for different - sized tables - that is , the desired polynomial depends on n .

Consider first the simplest case , n = 1. Here a constant function solves the problem. That is , the polynomial p of degree zero defined by the equation p(x)=yi reproduces the one - node table.

The next simplest case is when n=2 . Since a straight line can be passed through two points , a linear function is capable of solving the problem. Explicitly , the polynomial p defined by

$$p(x) = y_1 + \left(\frac{y_2 - y_1}{x_2 - x_1}\right)(x - x_1)$$

is of fist degree (at most) and reproduces the table.

That means (in the case) that p(x1)=y1 and p(x2)=y2 as in easily verified.

LAGRANGE interpolating polynomial :

Interpolating polynomials can be written in a variety of forms , and among these the NEWTON form is probably the most convenient and efficient.

Conceptually , however , the form known by the name of LAGRANGE has several advantages.

Suppose that we wish to interpolate arbitrary functions at a set of fixed nodes x1 x2 ..... xn . We first define a system of n special polynomials of degree n-1 known as cardinal functions in interpolation theory. These are denoted by

L1,L2,.....,Ln and have the property.

$$L_i(x_j) = \delta_{ij} = \begin{cases} 0 & \text{if } i \neq j \\ 1 & \text{if } i = j \end{cases}$$

Once these are available , we can interpolate any function f by the formula of LAGRANGE

$$P_{n-1}(x) = \sum_{i=1}^{n} f(x_i)\, L_i(x)$$

This function pn-1 being a linear combination of the polynomials Li , is itself a polynomial of degree < n-1 .

Furthermore , when we evaluate pn-1 at xi , we get f(xj) :

$$P_{n-1}(x_j) = \sum_{i=1}^{n} f(x_i) L_i(x_j) = f(x_j) L_j(x_j) = f(x_j)$$

Thus pn-1 is the interpolating polynomial for the function f at nodes x1 x2 ..... xn .

It only remains now to write the formula for Li which is

$$L_i(x) = \prod_{\substack{j=1 \\ j \neq i}}^{n} \left(\frac{x - x_j}{x_i - x_j} \right) \qquad \text{where } 1 \leq i \leq n$$

This formula indicates that Li(x) is the product of n-1 linear factors :

$$L_i(x) = \left(\frac{x - x_1}{x_i - x_1} \right) \left(\frac{x - x_2}{x_i - x_2} \right) \cdots\cdots \left(\frac{x - x_n}{x_i - x_n} \right)$$

(The denominators are just numbers , the variable x occur only in the numerator .)

Thus Li is a polynomial of degree n-1 . Notice that when Li(x) is evaluated at x=xi , each factor in the preceding equation becomes 1 . But when Li(x) is evaluated at any other nods , say xk one of the factors in the above equation will be 0 , and Li(xk)=0 .

Appendix 4.1

Table 4.2 Mis-tie values at the seismic line intersections.

INTERSECTION			HORIZON 1			HORIZON 2			HORIZON 3			COORDINATE	
SL1	SP1	SL2	MT1	MV1	MD1	MT2	MV2	MD2	MT3	MV3	MD3	LAT.	LONG.
248	115.	255	0.	132.	37.	10.	199.	96.	15.	106.	81.	28.97484	19.77836
	150.	257	-3.	46.	10.	2.	121.	54.	-5.	0.	7.	28.96539	19.79346
	200.	259	-2.	-14.	-7.	-5.	-69.	-34.	-20.	-134.	-102.	28.95151	19.81250
	230.	261	20.	-92.	-4.	5.	-234.	-90.	10.	-86.	-32.	28.94123	19.82430
	290.	263	10.	39.	0.	0.	-50.	-21.	0.	-37.	-20.	28.92541	19.84885
	295.	301	3.	-22.	-4.	-5.	-21.	-15.	5.	6.	9.	28.92340	19.85086
250	190.	253	5.	5.	7.	5.	183.	79.	0.	42.	22.	28.97623	19.75420
	230.	255	5.	21.	10.	10.	33.	26.	0.	-62.	-32.	28.96405	19.76881
	265.	257	8.	7.	10.	5.	58.	29.	8.	6.	13.	28.95365	19.78312
	310.	259	5.	-64.	-12.	0.	-49.	-19.	-15.	15.	-12.	28.94043	19.80109
	350.	261	-7.	-8.	-10.	-10.	-29.	-24.	-10.	-2.	-14.	28.93052	19.81632
	405.	263	-5.	-6.	-7.	-8.	19.	-1.	-2.	-43.	-27.	28.91370	19.83806
	410.	301	-10.	-54.	-26.	-5.	-67.	-33.	0.	-88.	-47.	28.91254	19.84088
	430.	265	2.	-94.	-23.	2.	-39.	-12.	5.	-95.	-45.	28.90691	19.84811
252	190.	253	0.	61.	16.	0.	206.	79.	0.	3.	1.	28.96122	19.74197
	225.	255	-3.	-21.	-8.	-3.	76.	25.	-1.	65.	32.	28.95040	19.75575
	265.	257	-2.	-26.	-9.	1.	37.	16.	-4.	-45.	-29.	28.93930	19.77121
	310.	259	3.	55.	18.	8.	72.	37.	-7.	-18.	-18.	28.92699	19.79010
	345.	261	4.	69.	22.	5.	190.	78.	-6.	94.	40.	28.91699	19.80366
	400.	263	-5.	-108.	-34.	0.	-134.	-54.	5.	-162.	-93.	28.90139	19.82597
	410.	301	0.	-44.	-12.	0.	65.	26.	0.	-52.	-28.	28.89848	19.82920
	425.	265	-10.	-91.	-34.	-10.	-56.	-34.	20.	-84.	-72.	28.89445	19.83632
254	115.	253	-2.	-85.	-25.	5.	16.	12.	5.	-18.	-3.	28.95057	19.73279
	150.	255	-5.	11.	-3.	5.	15.	12.	0.	-15.	-7.	28.93984	19.74622
	190.	257	-5.	-52.	-18.	0.	-56.	-21.	-10.	-15.	-21.	28.92865	19.76163
	240.	259	-1.	15.	2.	-1.	-46.	-19.	-6.	-64.	-40.	28.91551	19.78141
	270.	261	-5.	-24.	-11.	0.	-31.	-12.	0.	-30.	-15.	28.90528	19.79311
	325.	263	-4.	-66.	-23.	-5.	-51.	-26.	-4.	-44.	-30.	28.89021	19.81452
	335.	301	-2.	-19.	-8.	0.	2.	1.	-18.	-74.	-62.	28.88762	19.81916
	355.	265	-2.	21.	2.	0.	-23.	-8.	-13.	30.	-1.	28.88196	19.82645
256	110.	253	-5.	-68.	-23.	5.	188.	75.	5.	17.	15.	28.94145	19.72520
	145.	255	0.	-22.	-5.	5.	69.	33.	-2.	-29.	-18.	28.93177	19.73923
	185.	257	-5.	-164.	-46.	3.	-148.	-52.	12.	-109.	-35.	28.92058	19.75468
	235.	259	0.	-77.	-18.	7.	-9.	5.	-10.	-76.	-50.	28.90654	19.77373
	265.	261	-2.	-143.	-36.	0.	-12.	-5.	5.	-37.	-13.	28.89725	19.78621
	315.	263	-7.	-69.	-23.	-2.	0.	-3.	-5.	-13.	-13.	28.88247	19.80533
	330.	301	-6.	-87.	-24.	-3.	-35.	-16.	-11.	-102.	-65.	28.87880	19.81142
	350.	265	-15.	-40.	-25.	-15.	-55.	-38.	-20.	-19.	-36.	28.87313	19.81875
258	270.	255	5.	-4.	4.	-10.	-85.	-44.	3.	-18.	-5.	28.92322	19.73249
	310.	257	-10.	-100.	-33.	-10.	-151.	-66.	-5.	-49.	-30.	28.91196	19.74796
	355.	259	5.	-45.	-5.	8.	14.	13.	-8.	-31.	-26.	28.89857	19.76601
	390.	261	5.	-116.	-21.	-5.	-122.	-50.	5.	-69.	-27.	28.88853	19.77943
	435.	263	0.	-37.	-8.	-5.	-45.	-21.	-13.	-5.	-20.	28.87566	19.79787
	450.	301	0.	16.	3.	-5.	-25.	-15.	0.	-25.	-13.	28.87077	19.80352
	470.	265	0.	38.	9.	0.	-51.	-19.	-5.	-6.	-10.	28.86596	19.81165

Table 4.2 (continued) Mis-tie values at the seismic line intersections.

INTERSECTION			HORIZON 1			HORIZON 2			HORIZON 3			COORDINATE	
SL1	SP1	SL2	MT1	MV1	MD1	MT2	MV2	MD2	MT3	MV3	MD3	LAT.	LONG.
260	280.	255	-5.	17.	-2.	-5.	49.	11.	-10.	49.	11.	28.91623	19.72583
	320.	257	2.	-75.	-14.	5.	-9.	2.	-3.	8.	1.	28.90496	19.74137
	365.	259	0.	10.	2.	10.	86.	42.	-8.	11.	-6.	28.89157	19.75945
	400.	261	0.	-11.	-2.	3.	108.	41.	-5.	-46.	-28.	28.88156	19.77288
	450.	263	0.	-33.	-7.	0.	-25.	-9.	-10.	-29.	-27.	28.86803	19.79226
	460.	301	16.	19.	21.	-6.	-48.	-24.	-14.	-58.	-47.	28.86475	19.79772
	480.	265	10.	21.	15.	-5.	-87.	-38.	-5.	-46.	-29.	28.85906	19.80508
262	160.	253	-5.	-32.	-12.	0.	55.	20.	-5.	6.	-4.	28.91717	19.70660
	190.	255	5.	10.	7.	10.	129.	59.	5.	59.	36.	28.90764	19.71830
	230.	257	0.	-35.	-8.	0.	-20.	-7.	0.	-18.	-9.	28.89635	19.73385
	275.	259	2.	2.	1.	11.	114.	53.	-2.	10.	2.	28.88383	19.75270
	310.	261	8.	22.	14.	3.	109.	43.	2.	13.	9.	28.87384	19.76612
	360.	263	-5.	67.	9.	-5.	21.	1.	-10.	29.	0.	28.85946	19.78461
	375.	301	-8.	106.	14.	-8.	38.	4.	0.	13.	6.	28.85548	19.79104
	390.	265	-10.	19.	-6.	0.	-49.	-17.	-8.	31.	4.	28.85051	19.79743
264	130.	253	8.	15.	11.	-5.	146.	46.	10.	-84.	-28.	28.90134	19.69307
	160.	255	-5.	-9.	-7.	0.	95.	33.	-5.	14.	0.	28.89296	19.70517
	250.	259	5.	-14.	2.	5.	16.	12.	-20.	-48.	-50.	28.86749	19.73992
	280.	261	0.	32.	6.	-10.	5.	-11.	-10.	-4.	-16.	28.85827	19.75233
	330.	263	-1.	57.	10.	-9.	-112.	-50.	6.	0.	8.	28.84489	19.77146
	345.	301	-7.	26.	-2.	-10.	-118.	-54.	0.	-17.	-8.	28.84006	19.77711
	360.	265	-10.	62.	3.	-10.	-95.	-46.	-5.	19.	3.	28.83507	19.78354

Abbreviation:

SL1 = First seismic line number
SL2 = Second seismic line number
SP1 = Shot point number at the intersection for the SL1
MT1 = Mis-tie in two-way time at the intersection in ms. for horizon 1
MT2 = Mis-tie in two-way time at the intersection in ms. for horizon 2
MT3 = Mis-tie in two-way time at the intersection in ms. for horizon 3
MV1 = Mis-tie in velocity at the intersection in m/s. for horizon 1
MV2 = Mis-tie in velocity at the intersection in m/s. for horizon 2
MV3 = Mis-tie in velocity at the intersection in m/s. for horizon 3
MD1 = Mis-tie in depth at the intersection in m. for horizon 1
MD2 = Mis-tie in depth at the intersection in m. for horizon 2
MD3 = Mis-tie in depth at the intersection in m. for horizon 3

Appendix 4.2

```
#   The steps to digitising the contour maps into files used by DIGITAL #
    or DIGITAL2 programs, starting by:
#   Doing an interpolating file (i) by using the (interp) function. The
#   output structure contains three components i$x, i$y, and i$z. The
#   first two are vectors defining the i$x-i$y grid, and the last is the
#   matrix of interpolated values.

    i     <- interp ( long , lat , z )

#   long  = Longitude of the values to be contouring.
#   lat   = Latitude of the values to be contouring.
#   z     = Values to be contouring.
#   i     = Interpolating file.
#   Read the first component into a  5 column matrix file (i.x).

    i.x   <- matrix ( i $ x , ncol = 5 , byrow = T )

#   Transfer the i.x file to the suilven system into a 8 column matrix file
#   (file1).

    write ( i.x , " file1 " , ncol = 8 )

#   Read the second component into a  5 column matrix file (i.x).

    i.y   <- matrix ( i $ y , ncol = 5 , byrow = T )

#   Transfer the i.y file to the suilven system into a 8 column matrix file
#   (file2).

    write ( i.y , " file2 " , ncol = 8 )

#   Read the third component into an array file (i.z).

    i.z   <- i $ z

#   Since (interp) function produces NAs rather than extrapolating, so
#   next step is to replace NAs by zeros value.

    i.z   <- ifelse ( NA ( i.z ) , 0 , i.z )

#   Transfer the i.z file to the suilven system into a 1 column
#   matrix(vector) file (file3).

    write ( i.z , " file3 " , ncol = 1 )
```

Appendix 4.3

FORTRAN - 77 PROGRAM 5 DIGITAL

```
c     ************************************************************************
c     This program is design for the data files after digitising the depth contour map based on the
c     well data.
c     VAX/UNIX: DIGITAL
c     Written by
c     Ben Ayad N.M.
c     at the department of Geology&Applied Geology.
c     University of Glasgow, Glasgow G12 8QQ (in June 1991)
c     This program calculates the velocity for the shot points for the seismic lines after digitising
c     the depth contour map based on the well data.
c     ************************************************************************
c     PROGRAM DIGITAL.F
      DIMENSION AL(2000), ALONG(50), ALAT(50), Z(50,50), SP(1000)
     *        , ALT(1000), ALG(1000), T1(1000), T2(1000)
     *        , T3(1000), ZF(1000), AT(5,8), AG(5,8), V(1000)
      CHARACTER *10 INDATA1,INDATA2*10
      CHARACTER *10 INDATA3, OUT1*10, INDATA4*10
      PRINT*," PRINT THE FILE NAME AS AN INPUT ( I***.X ) "
      READ *, INDATA1
      PRINT*," PRINT THE FILE NAME AS AN INPUT ( I***.Y ) "
      READ *, INDATA2
      PRINT*," PRINT THE FILE NAME AS INPUT ( I***.Z ) "
      READ *, INDATA3
      PRINT*," PRINT THE FILE NAME AS INPUT AS ( COOR.ALL ) "
      READ *, INDATA4
      PRINT*," PRINT THE FILE NAME AS AN OUTPUT ( OUT.*** ) "
      READ *, OUT1
      PRINT*," TYPE 1 IF YOU ARE DOING HORIZON(1) "
      PRINT*," TYPE 2 IF YOU ARE DOING HORIZON(2) "
      PRINT*," TYPE 3 IF YOU ARE DOING HORIZON(3) "
c     NUH    - Horizon number.
      READ *, NUH
              OPEN ( 1, FILE = INDATA1 )
              OPEN ( 2, FILE = INDATA2 )
```

```
                OPEN ( 3,  FILE = INDATA3 )
                OPEN ( 4,  FILE = OUT1 )
                OPEN ( 7,  FILE = INDATA4 )
c       J       - Counter for depth values.
        DO  100  J = 1, 1600
c       AL      - Depth value.
        READ (3,*)  AL(J)
100     CONTINUE
c       I       - Counter for matrix rows.
        DO  500  I = 1, 5
c       AT      - Latitude value of the corresponding depth.
        READ (2,*)  ( AT(I,J),  J = 1, 8 )
500     CONTINUE
c       J       - Counter for matrix rows.
        DO  600  I = 1, 5
c       AG      - Longitude value of the corresponding depth.
        READ (1,*)  ( AG(I,J),  J = 1, 8 )
600     CONTINUE
                        K  = 1
c       J       - Counter for matrix columns.
        DO  555  J = 1, 8
c       I       - Counter for matrix rows.
        DO  666  I = 1, 5
c       ALONG           - Longitude value.
c       ALAT    - Latitude value.
                ALONG(K)  = AG(I,J)
                ALAT(K)   = AT(I,J)
                K         = K + 1
666     CONTINUE
555     CONTINUE
                    MM  = 1
c       J       - Counter for matrix rows.
        DO  200  J = 1, 40
c       I       - Counter for matrix rows.
        DO  300  I = 1, 40
c       Z       - Depth value..
                    Z(J,I)  = AL(MM)
```

```
                MM  = MM + 1
300     CONTINUE
200     CONTINUE
c       I       - Counter for Shot point data.
        DO 700 I = 1, 630
c       SP      - Shot point number.
c       ALT     - Latitude value of the corresponding SP.
c       ALG     - Longitude value of the corresponding SP.
c       T1      - Picked time for horizon 1.
c       T2      - Picked time for horizon 2.
c       T3      - Picked time for horizon 3.
        READ (7,120) SP(I), ALT(I), ALG(I), T1(I), T2(I), T3(I)
c       I       - Counter for loops of calculation.
        DO 800 J = 1, 39
                IF ( ALT(I) .GE. ALAT(J) .AND. ALT(I) .LT. ALAT(J+1) ) N = J
                IF ( ALG(I) .GE. ALONG(J) .AND. ALG(I) .LT. ALONG(J+1) ) M = J
800     CONTINUE
c       ZF      - Output depth value from subroutine INT calculation.
c-------------------------------------------------------------------------
        CALL  INT  ( Z, M, N, I, ALT, ALAT, ALG, ALONG, ZF )
c-------------------------------------------------------------------------
                IF ( ZF(I) .EQ. 0.0 ) GO TO 700
c       V       - Average velocity.
                IF ( NUH .EQ. 1 ) V(I) = ZF(I) / (T1(I) / 1000.0)
                IF ( NUH .EQ. 2 ) V(I) = ZF(I) / (T2(I) / 1000.0)
                IF ( NUH .EQ. 3 ) V(I) = ZF(I) / (T3(I) / 1000.0)
        WRITE (4,130) ALG(I), ALT(I), ZF(I), V(I)
700     CONTINUE
120     FORMAT ( F5.0 , 2F10.5 , 3F8.0 )
130     FORMAT ( 4F13.5 )
        STOP
        END
```

```
      FORTRAN - 77  PROGRAM  6  DIGITAL2
c     ********************************************************************************
c     This program is design for the data files after digitising the two-way time contour map
c     based on the seismic data.
c     VAX/UNIX: DIGITAL
c     Written by
c     Ben Ayad N.M.
c     at the department of Geology&Applied Geology.
c     University of Glasgow, Glasgow G12 8QQ (in June 1991)
c     This program calculates the velocity for the shot points for the wells after digitising
c     the two-way time contour map based on the seismic data.
c     ********************************************************************************
c     PROGRAM DIGITAL2.F
      DIMENSION AL(2000), ALONG(50), ALAT(50), Z(50,50), SP(1000), ALT(1000)
     *          , ALG(1000), T1(1000), T2(1000), T3(1000), ZF(1000), AT(5,8)
     *          , AG(5,8), V(1000), D21(1000), D32(1000)
      CHARACTER *10 INDATA1,INDATA2*10
      CHARACTER *10 INDATA3, OUT1*10, INDATA4*10
      PRINT*," PRINT THE FILE NAME AS AN INPUT ( I***2.X ) "
      READ *, INDATA1
      PRINT*," PRINT THE FILE NAME AS AN INPUT ( I***2.Y ) "
      READ *, INDATA2
      PRINT*," PRINT THE FILE NAME AS INPUT ( I***2.Z ) "
      READ *, INDATA3
      PRINT*," PRINT THE FILE NAME AS INPUT AS ( WELL.OUT ) "
      READ *, INDATA4
      PRINT*," PRINT THE FILE NAME AS AN OUTPUT ( OUT2.*** ) "
      READ *, OUT1
      PRINT*," TYPE 1 IF YOU ARE DOING HORIZON ( 1 ). "
      PRINT*," TYPE 2 IF YOU ARE DOING HORIZON ( 2 ). "
      PRINT*," TYPE 3 IF YOU ARE DOING HORIZON ( 3 ). "
c     NUH    - Horizon number.
      READ *, NUH
      PRINT*," NUMBER OF AN INPUT DATA AS  ( NVAL ). "
      READ *, NVAL
            OPEN ( 1, FILE = INDATA1 )
            OPEN ( 2, FILE = INDATA2 )
```

```
                OPEN ( 3,  FILE = INDATA3 )
                OPEN ( 4,  FILE = OUT1 )
                OPEN ( 7,  FILE = INDATA4 )
c       J       - Counter for two-way time values.
        DO  100  J = 1, 1600
c       AL      - Two way time value.
        READ (3,*)  AL(J)
100     CONTINUE
c       I       - Counter for matrix rows.
        DO  500  I = 1, 5
c       AT      - Latitude value of the corresponding two-way time.
        READ (2,*)  ( AT(I,J),  J = 1, 8 )
500     CONTINUE
c       I       - Counter for matrix rows.
        DO  600  I = 1, 5
c       AG      - Longitude value of the corresponding two-way time.
        READ (1,*)  ( AG(I,J),  J = 1, 8 )
600     CONTINUE
                        K  = 1
c       J       - Counter for matrix columns.
c       I       - Counter for matrix rows.
c       ALONG           - Longitude value.
c       ALAT    - Latitude value.
        DO  555  J = 1, 8
        DO  666  I = 1, 5
                ALONG(K)  = AG(I,J)
                ALAT(K)   = AT(I,J)
                K         = K + 1
666     CONTINUE
555     CONTINUE
                    MM  = 1
c       J       - Counter for matrix rows.
        DO  200  J = 1, 40
c       I       - Counter for matrix columns.
        DO  300  I = 1, 40
c       Z       - Two way time value.
                    Z(J,I)  = AL(MM)
```

```
                MM  = MM + 1
300     CONTINUE
200     CONTINUE
c       I       - Counter for input data.
        DO 700 I = 1, NVAL
c       ALT     - Latitude value.
c       ALG     - Longitude value.
c       T1      - Picked time for horizon 1 corresponding to the coordinate.
c       T2      - Picked time for horizon 2 corresponding to the coordinate.
c       T3      - Picked time for horizon 3 corresponding to the coordinate.
c       D21     - Difference in depth between horizons 2 and 1.
c       D32     - Difference in depth between horizons 3 and 2.
        READ (7,120) ALT(I), ALG(I), T1(I), T2(I), T3(I), D21(I), D32(I)
c       I       - Counter for loops of calculation.
        DO 800 J = 1, 39
                IF ( ALT(I) .GE. ALAT(J) .AND. ALT(I) .LT. ALAT(J+1) ) N = J
                IF ( ALG(I) .GE. ALONG(J) .AND. ALG(I) .LT. ALONG(J+1) ) M = J
800     CONTINUE
c       ZF      - Output two-way time value from subroutine INT calculation.
c-------------------------------------------------------------------------------
        CALL  INT  ( Z, M, N, I, ALT, ALAT, ALG, ALONG, ZF )
c-------------------------------------------------------------------------------
                IF ( ZF(I) .EQ. 0.0 ) GO TO 700
        IF ( NUH .EQ. 1 ) THEN
c       V       - Average velocity.
                V(I) = 2*T1(I) / (ZF(I) / 1000.0)
                WRITE (4,130) ALG(I), ALT(I), ZF(I), V(I), T1(I)
        GO TO 699
        IF ( NUH .EQ. 2 ) THEN
                V(I) = 2*T2(I) / (ZF(I) / 1000.0)
                WRITE (4,130) ALG(I), ALT(I), ZF(I), V(I), T2(I)
        GO TO 699
        IF ( NUH .EQ. 3 ) THEN
                V(I) = 2*T3(I) / (ZF(I) / 1000.0)
                WRITE (4,130) ALG(I), ALT(I), ZF(I), V(I), T3(I)
699     END IF
700     CONTINUE
120     FORMAT ( 2F9.4 , 3F8.1 , 2F7.1 )
```

```
130     FORMAT ( 5F13.5 )
        STOP
        END

c-------------------------------------------------------------------------------
        SUBROUTINE  INT  ( Z, M, N, I, ALT, ALAT, ALG, ALONG, ZF )
        DIMENSION Z(50,50), ALT(1000), ALG(1000), ZF(1000), ALAT(50), ALONG(50)
c       DY      - Difference in latitude.
c       DX      - Difference in longitude.
                  DY    = ALAT(N+1) - ALAT(N)
                  DX    = ALONG(M+1) - ALONG(M)
              IF ( ( ALT(I) .LT. ALAT(1) ) .OR. ( ALT(I) .GT. ALAT(40) ) ) GO TO 999
              IF ( ( ALG(I) .LT. ALONG(1) ) .OR. ( ALG(I) .GT. ALONG(40) ) ) GO TO 999
c-------------------------------------------------------------------------------
        IF ( ( Z(N,M) .EQ. 0.0 ) .AND. ( Z(N,M+1) .EQ. 0.0 )
     *      .AND. ( Z(N+1,M) .EQ. 0.0 ) .AND. ( Z(N+1,M+1) .EQ. 0.0 ) ) THEN
        ZF(I) = 0.0
        GO TO 999
c-------------------------------------------------------------------------------
        ELSE IF ( ( Z(N,M) .EQ. 0.0 ) .AND. ( Z(N,M+1) .EQ. 0.0 )
     *      .AND. ( Z(N+1,M) .EQ. 0.0 ) .AND. ( Z(N+1,M+1) .NE. 0.0 ) ) THEN
        ZF(I) = Z(N+1,M+1)
        GO TO 999
c-------------------------------------------------------------------------------
        ELSE IF ( ( Z(N,M) .EQ. 0.0 ) .AND. ( Z(N,M+1) .EQ. 0.0 )
     *      .AND. ( Z(N+1,M+1) .EQ. 0.0 ) .AND. ( Z(N+1,M) .NE. 0.0 ) ) THEN
        ZF(I) = Z(N+1,M)
        GO TO 999
c-------------------------------------------------------------------------------
        ELSE IF ( ( Z(N,M) .EQ. 0.0 ) .AND. ( Z(N+1,M+1) .EQ. 0.0 )
     *      .AND. ( Z(N+1,M) .EQ. 0.0 ) .AND. ( Z(N,M+1) .NE. 0.0 ) ) THEN
        ZF(I) = Z(N,M+1)
        GO TO 999
c-------------------------------------------------------------------------------
        ELSE IF ( ( Z(N+1,M) .EQ. 0.0 ) .AND. ( Z(N,M+1) .EQ. 0.0 )
     *      .AND. ( Z(N+1,M+1) .EQ. 0.0 ) .AND. ( Z(N,M) .NE. 0.0 ) ) THEN
        ZF(I) = Z(N,M)
        GO TO 999
c-------------------------------------------------------------------------------
        ELSE IF ( ( Z(N,M) .EQ. 0.0 ) .AND. ( Z(N,M+1) .EQ. 0.0 )
     *      .AND. ( Z(N+1,M) .NE. 0.0 ) .AND. ( Z(N+1,M+1) .NE. 0.0 ) ) THEN
        Z(N,M)    = Z(N+1,M)
```

```
            Z(N,M+1)  = Z(N+1,M+1)
            GO TO 888
c-----------------------------------------------------------------------------------------------
            ELSE IF ( ( Z(N,M)  .EQ. 0.0 ) .AND. ( Z(N+1,M)  .EQ. 0.0 )
           *     .AND. ( Z(N,M+1) .NE. 0.0 ) .AND. ( Z(N+1,M+1) .NE. 0.0 ) ) THEN
            Z(N,M)    = Z(N,M+1)
            Z(N+1,M)  = Z(N+1,M+1)
            GO TO 888
c-----------------------------------------------------------------------------------------------
            ELSE IF ( ( Z(N,M+1) .EQ. 0.0 ) .AND. ( Z(N+1,M+1) .EQ. 0.0 )
           *     .AND. ( Z(N,M)  .NE. 0.0 ) .AND. ( Z(N+1,M)  .NE. 0.0 ) ) THEN
            Z(N,M+1)    = Z(N,M)
            Z(N+1,M+1)  = Z(N+1,M)
            GO TO 888
c-----------------------------------------------------------------------------------------------
            ELSE IF ( ( Z(N+1,M) .EQ. 0.0 ) .AND. ( Z(N+1,M+1) .EQ. 0.0 )
           *     .AND. ( Z(N,M)  .NE. 0.0 ) .AND. ( Z(N,M+1)  .NE. 0.0 ) ) THEN
            Z(N+1,M)    = Z(N,M)
            Z(N+1,M+1)  = Z(N,M+1)
            GO TO 888
c-----------------------------------------------------------------------------------------------
            ELSE IF ( ( Z(N,M)  .EQ. 0.0 ) .AND. ( Z(N,M+1)  .NE. 0.0 )
           *     .AND. ( Z(N+1,M) .NE. 0.0 ) .AND. ( Z(N+1,M+1) .NE. 0.0 ) ) THEN
            Z(N,M)  = Z(N,M+1)
            GO TO 888
c-----------------------------------------------------------------------------------------------
            ELSE IF ( ( Z(N,M+1) .EQ. 0.0 ) .AND. ( Z(N+1,M)  .NE. 0.0 )
           *     .AND. ( Z(N,M)  .NE. 0.0 ) .AND. ( Z(N+1,M+1) .NE. 0.0 ) ) THEN
            Z(N,M+1)  = Z(N,M)
            GO TO 888
c-----------------------------------------------------------------------------------------------
            ELSE IF ( ( Z(N+1,M) .EQ. 0.0 ) .AND. ( Z(N+1,M+1) .NE. 0.0 )
           *     .AND. ( Z(N,M)  .NE. 0.0 ) .AND. ( Z(N,M+1)  .NE. 0.0 ) ) THEN
            Z(N+1,M)  = Z(N+1,M+1)
            GO TO 888
c-----------------------------------------------------------------------------------------------
            ELSE IF ( ( Z(N+1,M+1) .EQ. 0.0 ) .AND. ( Z(N+1,M)  .NE. 0.0 )
           *     .AND. ( Z(N,M)  .NE. 0.0 ) .AND. ( Z(N,M+1)  .NE. 0.0 ) ) THEN
            Z(N+1,M+1)  = Z(N+1,M)
            GO TO 888
c-----------------------------------------------------------------------------------------------
            ELSE
c           CORD  - Increment of the lower values in longitude direction.
```

```
c       CORU  - Increment of the upper values in latitude direction.
c       ZD    - Lower value.
c       ZU    - Upper value.
c       CORR  - Increment of the values in latitude direction.
c       ZF    - Required value.
888             CORD  = ( Z(N,M+1) - Z(N,M) ) / DX
                CORU  = ( Z(N+1,M+1) - Z(N+1,M) ) / DX
                ZD    = ( ALG(I) - ALONG(M))*CORD + Z(N,M)
                ZU    = ( ALG(I) - ALONG(M))*CORU + Z(N+1,M)
                CORR  = ( ZU - ZD ) / DY
                ZF(I) = ( ALT(I)-ALAT(N))*CORR+ZD
        END IF
999     RETURN
        END
```

Appendix 4.4

Table 4.3a Results of calculation for seismic line 6V248-85

S.P.	T(1)	V(1)	D(1)	T(2)	V(2)	D(2)	T(3)	V(3)	D(3)	dT1	dD1	dT2	dD2	IV21	IV32	LAT.	LONG.
100.	550.	2378.	654.	830.	2772.	1150.	1100.	2909.	1600.	280.	496.	270.	450.	3543.	3333.	28.979	19.773
110.	555.	2345.	651.	830.	2738.	1136.	1100.	2887.	1588.	275.	486.	270.	452.	3527.	3348.	28.976	19.777
120.	565.	2312.	653.	840.	2704.	1136.	1130.	2865.	1619.	275.	482.	290.	483.	3513.	3331.	28.974	19.781
130.	585.	2279.	666.	855.	2669.	1141.	1090.	2843.	1549.	270.	475.	235.	408.	3519.	3472.	28.971	19.785
140.	570.	2246.	640.	850.	2635.	1120.	1090.	2821.	1537.	280.	480.	240.	418.	3429.	3475.	28.968	19.789
150.	565.	2213.	625.	840.	2601.	1092.	1080.	2799.	1511.	275.	467.	240.	419.	3396.	3492.	28.965	19.793
160.	560.	2180.	610.	830.	2567.	1065.	1075.	2777.	1493.	270.	455.	245.	427.	3370.	3494.	28.962	19.797
170.	555.	2147.	596.	825.	2533.	1045.	1080.	2755.	1488.	270.	449.	255.	443.	3326.	3475.	28.959	19.801
180.	560.	2133.	597.	825.	2500.	1031.	1090.	2743.	1495.	265.	434.	265.	464.	3275.	3502.	28.957	19.805
190.	560.	2121.	594.	820.	2467.	1011.	1090.	2731.	1488.	260.	418.	270.	477.	3208.	3533.	28.954	19.809
200.	560.	2108.	590.	820.	2434.	998.	1090.	2719.	1482.	260.	408.	270.	484.	3138.	3585.	28.951	19.813
210.	560.	2096.	587.	825.	2401.	990.	1075.	2707.	1455.	265.	404.	250.	465.	3042.	3720.	28.948	19.817
220.	560.	2128.	596.	825.	2415.	996.	1070.	2715.	1453.	265.	401.	245.	456.	3019.	3731.	28.945	19.821
230.	570.	2162.	616.	825.	2432.	1003.	1070.	2724.	1457.	255.	387.	245.	454.	3035.	3706.	28.942	19.825
240.	570.	2196.	626.	825.	2449.	1010.	1070.	2733.	1462.	255.	384.	245.	452.	3012.	3690.	28.939	19.829
250.	570.	2177.	620.	825.	2452.	1011.	1080.	2732.	1475.	255.	391.	255.	464.	3067.	3639.	28.937	19.833
260.	565.	2155.	609.	830.	2454.	1018.	1080.	2731.	1475.	265.	409.	250.	456.	3087.	3656.	28.934	19.837
270.	565.	2134.	603.	830.	2456.	1019.	1090.	2729.	1487.	265.	416.	260.	468.	3140.	3600.	28.931	19.841
280.	570.	2112.	602.	835.	2458.	1026.	1095.	2727.	1493.	265.	424.	260.	467.	3200.	3592.	28.928	19.845
290.	570.	2130.	607.	835.	2458.	1026.	1090.	2725.	1485.	265.	419.	255.	459.	3162.	3600.	28.925	19.849
300.	565.	2150.	607.	835.	2458.	1026.	1090.	2722.	1483.	270.	419.	255.	457.	3104.	3584.	28.922	19.853
310.	560.	2170.	608.	830.	2458.	1020.	1090.	2719.	1482.	270.	413.	260.	462.	3052.	3554.	28.920	19.857
320.	560.	2190.	613.	830.	2459.	1020.	1090.	2716.	1480.	270.	407.	260.	460.	3015.	3538.	28.917	19.861
330.	560.	2200.	616.	830.	2470.	1025.	1090.	2733.	1489.	270.	409.	260.	464.	3030.	3569.	28.914	19.864
340.	570.	2209.	630.	830.	2482.	1030.	1090.	2750.	1499.	260.	400.	260.	469.	3077.	3608.	28.911	19.868
350.	570.	2218.	632.	830.	2493.	1035.	1090.	2767.	1508.	260.	402.	260.	473.	3100.	3638.	28.908	19.872
360.	570.	2229.	635.	830.	2496.	1036.	1090.	2774.	1512.	260.	401.	260.	476.	3085.	3662.	28.905	19.875
370.	560.	2242.	628.	820.	2489.	1020.	1090.	2770.	1510.	260.	392.	270.	489.	3015.	3630.	28.902	19.879
380.	560.	2255.	631.	820.	2481.	1017.	1075.	2765.	1486.	260.	386.	255.	469.	2969.	3678.	28.899	19.883
390.	560.	2268.	635.	820.	2473.	1014.	1075.	2760.	1484.	260.	379.	255.	470.	2915.	3686.	28.896	19.886
400.	550.	2281.	627.	820.	2465.	1011.	1070.	2756.	1474.	270.	384.	250.	464.	2844.	3704.	28.893	19.890

Abbreviations:

S.P. = Shot point number.
T(1) = Two-way time in ms. to the top of horizon 1.
V(1) = Dix average velocity for horizon 1 in m/s.
D(1) = Depth for horizon 1 in meter .
T(2) = Two-way time in ms. to the top of horizon 2.
V(2) = Dix average velocity for horizon 2 in m/s.
D(2) = Depth for horizon 2 in meter .
T(3) = Two-way time in ms. to the top of horizon 3.
V(3) = Dix average velocity for horizon 3 in m/s.
D(3) = Depth for horizon 3 in meter.
dT1 = Difference in time between horizon 2 and horizon 1.
dD1 = Difference in depth between horizon 2 and horizon 1.
dT2 = Difference in time between horizon 3 and horizon 2.
dD2 = Difference in depth between horizon 3 and horizon 2.
LAT. = Latitude of corresponding shot point.
LONG. = Longitude of corresponding shot point.

Horizon 1 = Sheghega Formation.
Horizon 2 = Domran Formation.
Horizon 3 = Ruaga Formation.

IV21 = Interval velocity for She. Formation.
IV32 = Interval velocity for Dom. Formation.

Table 4.3b Results of calculation for seismic line 6V250-85

S.P.	T(1)	V(1)	D(1)	T(2)	V(2)	D(2)	T(3)	V(3)	D(3)	dT1	dD1	dT2	dD2	IV21	IV32	LAT.	LONG.
120.	560.	2097.	587.	840.	2575.	1081.	1100.	2715.	1493.	280.	494.	260.	412.	3529.	3169.	28.998	19.729
130.	570.	2103.	599.	840.	2549.	1071.	1100.	2720.	1496.	270.	471.	260.	426.	3496.	3269.	28.995	19.733
140.	570.	2110.	601.	835.	2523.	1053.	1100.	2725.	1499.	265.	452.	265.	446.	3411.	3366.	28.992	19.736
150.	565.	2116.	598.	840.	2497.	1049.	1090.	2730.	1488.	275.	451.	250.	439.	3280.	3512.	28.989	19.740
160.	560.	2122.	594.	835.	2471.	1032.	1090.	2736.	1491.	275.	438.	255.	459.	3185.	3600.	28.986	19.743
170.	550.	2128.	585.	820.	2446.	1003.	1080.	2741.	1480.	270.	418.	260.	477.	3096.	3669.	28.983	19.747
180.	540.	2135.	576.	810.	2423.	981.	1070.	2746.	1469.	270.	405.	260.	488.	3000.	3754.	28.979	19.751
190.	530.	2154.	571.	805.	2459.	990.	1060.	2750.	1457.	275.	419.	255.	468.	3047.	3663.	28.976	19.754
200.	520.	2173.	565.	800.	2495.	998.	1050.	2754.	1446.	280.	433.	250.	448.	3093.	3584.	28.973	19.758
210.	520.	2192.	570.	800.	2531.	1013.	1040.	2759.	1435.	280.	443.	240.	422.	3164.	3517.	28.970	19.762
220.	520.	2210.	575.	800.	2565.	1026.	1035.	2763.	1430.	280.	452.	235.	404.	3221.	3438.	28.967	19.765
230.	520.	2206.	573.	800.	2557.	1023.	1030.	2761.	1422.	280.	449.	230.	399.	3214.	3470.	28.964	19.769
240.	525.	2201.	578.	800.	2549.	1019.	1050.	2760.	1449.	275.	442.	250.	430.	3207.	3440.	28.961	19.773
250.	535.	2197.	588.	800.	2540.	1016.	1050.	2758.	1448.	265.	428.	250.	432.	3230.	3456.	28.958	19.777
260.	540.	2192.	592.	805.	2531.	1019.	1050.	2756.	1447.	265.	427.	245.	428.	3223.	3494.	28.956	19.781
270.	535.	2176.	582.	805.	2510.	1010.	1045.	2746.	1435.	270.	428.	240.	424.	3170.	3542.	28.953	19.785
280.	530.	2160.	572.	800.	2488.	995.	1040.	2735.	1422.	270.	423.	240.	427.	3133.	3558.	28.950	19.789
290.	530.	2144.	568.	790.	2466.	974.	1035.	2725.	1410.	260.	406.	245.	436.	3123.	3559.	28.947	19.793
300.	530.	2129.	564.	790.	2446.	966.	1030.	2714.	1398.	260.	402.	240.	432.	3092.	3600.	28.944	19.797
310.	530.	2136.	566.	780.	2443.	953.	1030.	2710.	1396.	250.	387.	250.	443.	3096.	3544.	28.941	19.801
320.	525.	2143.	562.	775.	2441.	946.	1020.	2707.	1380.	250.	384.	245.	435.	3072.	3543.	28.938	19.805
330.	520.	2149.	559.	770.	2439.	939.	1010.	2703.	1365.	250.	380.	240.	426.	3040.	3550.	28.936	19.809
340.	515.	2156.	555.	770.	2438.	938.	1005.	2700.	1357.	255.	383.	235.	418.	3004.	3566.	28.933	19.813
350.	515.	2170.	559.	770.	2458.	946.	1010.	2716.	1372.	255.	388.	240.	425.	3035.	3550.	28.930	19.817
360.	515.	2183.	562.	780.	2479.	967.	1020.	2732.	1393.	265.	405.	240.	426.	3057.	3550.	28.927	19.820
370.	520.	2196.	571.	790.	2500.	988.	1030.	2747.	1415.	270.	417.	240.	427.	3089.	3558.	28.924	19.824
380.	530.	2207.	585.	800.	2519.	1008.	1045.	2761.	1442.	270.	423.	245.	435.	3133.	3543.	28.921	19.828
390.	540.	2172.	587.	800.	2495.	998.	1060.	2733.	1448.	260.	412.	260.	450.	3162.	3462.	28.918	19.832
400.	550.	2138.	588.	810.	2472.	1001.	1065.	2705.	1440.	260.	413.	255.	439.	3177.	3443.	28.916	19.836
410.	550.	2104.	578.	815.	2449.	998.	1070.	2677.	1432.	265.	419.	255.	434.	3170.	3404.	28.913	19.840
420.	555.	2072.	575.	820.	2428.	995.	1080.	2651.	1431.	265.	421.	260.	436.	3170.	3354.	28.910	19.844
430.	560.	2088.	585.	830.	2457.	1020.	1090.	2656.	1447.	270.	435.	260.	428.	3222.	3285.	28.907	19.848
440.	560.	2105.	589.	830.	2486.	1032.	1090.	2661.	1450.	270.	442.	260.	418.	3281.	3215.	28.904	19.852
450.	555.	2122.	589.	830.	2516.	1044.	1075.	2666.	1433.	275.	455.	245.	389.	3309.	3176.	28.901	19.856
460.	560.	2137.	598.	840.	2542.	1068.	1075.	2671.	1436.	280.	469.	235.	368.	3357.	3132.	28.898	19.860
470.	560.	2117.	593.	840.	2519.	1058.	1080.	2684.	1449.	280.	465.	240.	391.	3321.	3258.	28.896	19.864
480.	555.	2098.	582.	835.	2496.	1042.	1080.	2696.	1456.	280.	460.	245.	414.	3286.	3380.	28.893	19.868
490.	555.	2078.	577.	830.	2473.	1026.	1090.	2709.	1476.	275.	450.	260.	450.	3265.	3462.	28.890	19.872
500.	550.	2060.	566.	830.	2450.	1017.	1090.	2720.	1482.	280.	450.	260.	466.	3221.	3577.	28.887	19.875
510.	555.	2067.	573.	830.	2431.	1009.	1090.	2706.	1475.	275.	435.	260.	466.	3171.	3585.	28.884	19.879
520.	555.	2073.	575.	830.	2412.	1001.	1090.	2693.	1468.	275.	426.	260.	466.	3098.	3592.	28.881	19.883
530.	550.	2080.	572.	830.	2393.	993.	1090.	2679.	1460.	280.	421.	260.	467.	3007.	3592.	28.878	19.887
540.	545.	2087.	569.	830.	2374.	985.	1080.	2665.	1439.	285.	417.	250.	454.	2919.	3632.	28.875	19.891

Abbreviations:

S.P. = Shot point number.
T(1) = Two-way time in ms. to the top of horizon 1.
V(1) = Dix average velocity for horizon 1 in m/s.
D(1) = Depth for horizon 1 in meter .
T(2) = Two-way time in ms. to the top of horizon 2.
V(2) = Dix average velocity for horizon 2 in m/s.
D(2) = Depth for horizon 2 in meter .
T(3) = Two-way time in ms. to the top of horizon 3.
V(3) = Dix average velocity for horizon 3 in m/s.
D(3) = Depth for horizon 3 in meter.
dT1 = Difference in time between horizon 2 and horizon 1.
dD1 = Difference in depth between horizon 2 and horizon 1.
dT2 = Difference in time between horizon 3 and horizon 2.
dD2 = Difference in depth between horizon 3 and horizon 2.
LAT. = Latitude of corresponding shot point.
LONG. = Longitude of corresponding shot point.

Horizon 1 = Sheghega Formation.
Horizon 2 = Domran Formation.
Horizon 3 = Ruaga Formation.

IV21 = Interval velocity for She. Formation.
IV32 = Interval velocity for Dom. Formation.

Table 4.3c Results of calculation for seismic line 6V252-85

S.P.	T(1)	V(1)	D(1)	T(2)	V(2)	D(2)	T(3)	V(3)	D(3)	dT1	dD1	dT2	dD2	IV21	IV32	LAT.	LONG.
130.	510.	2107.	537.	775.	2470.	957.	1080.	2865.	1547.	265.	420.	305.	590.	3170.	3869.	28.978	19.718
140.	515.	2126.	547.	780.	2473.	964.	1060.	2843.	1507.	265.	417.	280.	543.	3147.	3879.	28.975	19.722
150.	525.	2146.	563.	795.	2475.	984.	1060.	2822.	1496.	270.	421.	265.	512.	3119.	3864.	28.972	19.726
160.	535.	2165.	579.	790.	2477.	978.	1045.	2800.	1463.	255.	399.	255.	485.	3129.	3804.	28.969	19.730
170.	525.	2185.	573.	790.	2479.	979.	1040.	2779.	1445.	265.	406.	250.	466.	3064.	3728.	28.967	19.734
180.	515.	2204.	568.	780.	2482.	968.	1025.	2757.	1413.	265.	400.	245.	445.	3019.	3633.	28.964	19.738
190.	510.	2223.	567.	770.	2484.	956.	1010.	2736.	1381.	260.	389.	240.	425.	2992.	3542.	28.961	19.742
200.	496.	2203.	546.	770.	2500.	963.	1007.	2748.	1384.	274.	416.	237.	421.	3044.	3553.	28.958	19.746
210.	477.	2181.	520.	766.	2517.	964.	995.	2763.	1374.	289.	444.	229.	410.	3073.	3581.	28.955	19.750
220.	489.	2158.	528.	754.	2533.	955.	1003.	2777.	1393.	265.	427.	249.	438.	3223.	3518.	28.952	19.754
230.	495.	2136.	529.	760.	2550.	969.	1005.	2791.	1403.	265.	440.	245.	434.	3321.	3543.	28.950	19.758
240.	498.	2155.	537.	763.	2558.	976.	1008.	2771.	1396.	265.	439.	245.	420.	3313.	3429.	28.947	19.762
250.	505.	2176.	550.	765.	2566.	981.	1005.	2748.	1381.	260.	432.	240.	399.	3315.	3333.	28.944	19.766
260.	497.	2198.	546.	767.	2573.	987.	997.	2725.	1358.	270.	441.	230.	372.	3267.	3226.	28.941	19.770
270.	500.	2219.	555.	765.	2581.	987.	995.	2702.	1344.	265.	432.	230.	357.	3260.	3104.	28.938	19.774
280.	500.	2219.	555.	760.	2572.	977.	985.	2714.	1337.	260.	422.	225.	360.	3246.	3200.	28.935	19.778
290.	500.	2218.	554.	760.	2562.	973.	985.	2728.	1344.	260.	419.	225.	370.	3223.	3298.	28.933	19.782
300.	505.	2216.	560.	770.	2552.	982.	990.	2742.	1357.	265.	423.	220.	375.	3185.	3409.	28.930	19.786
310.	500.	2215.	554.	765.	2542.	972.	990.	2756.	1364.	265.	418.	225.	392.	3155.	3484.	28.927	19.790
320.	490.	2203.	540.	760.	2533.	962.	980.	2750.	1347.	270.	423.	220.	385.	3126.	3500.	28.924	19.794
330.	480.	2191.	526.	750.	2523.	946.	970.	2743.	1330.	270.	420.	220.	384.	3111.	3491.	28.921	19.798
340.	480.	2179.	523.	750.	2514.	943.	975.	2735.	1334.	270.	420.	225.	391.	3111.	3476.	28.919	19.802
350.	485.	2167.	525.	760.	2505.	952.	990.	2728.	1350.	275.	426.	230.	399.	3105.	3461.	28.916	19.806
360.	490.	2161.	529.	760.	2480.	942.	1000.	2697.	1348.	270.	413.	240.	406.	3059.	3383.	28.913	19.810
370.	485.	2156.	523.	750.	2454.	920.	975.	2664.	1299.	265.	398.	225.	378.	2996.	3369.	28.910	19.814
380.	490.	2151.	527.	750.	2428.	911.	970.	2631.	1276.	260.	384.	220.	365.	2954.	3318.	28.907	19.818
390.	530.	2145.	568.	790.	2403.	949.	1010.	2598.	1312.	260.	381.	220.	363.	2931.	3300.	28.904	19.822
400.	540.	2124.	574.	810.	2429.	984.	1060.	2616.	1386.	270.	410.	250.	403.	3037.	3216.	28.902	19.825
410.	540.	2103.	568.	810.	2457.	995.	1070.	2636.	1410.	270.	428.	260.	415.	3163.	3192.	28.899	19.829
420.	515.	2081.	536.	790.	2486.	982.	1040.	2657.	1382.	275.	446.	250.	400.	3244.	3200.	28.896	19.833
430.	515.	2059.	530.	790.	2515.	993.	1040.	2678.	1392.	275.	463.	250.	399.	3367.	3192.	28.893	19.837
440.	525.	2070.	543.	800.	2521.	1008.	1040.	2690.	1399.	275.	465.	240.	390.	3382.	3258.	28.890	19.841
450.	525.	2083.	547.	800.	2526.	1010.	1040.	2701.	1405.	275.	464.	240.	394.	3367.	3292.	28.887	19.845
460.	525.	2095.	550.	800.	2531.	1012.	1040.	2712.	1410.	275.	462.	240.	398.	3360.	3317.	28.885	19.849
470.	515.	2108.	543.	795.	2536.	1008.	1035.	2724.	1410.	280.	465.	240.	402.	3321.	3350.	28.882	19.853
480.	520.	2113.	549.	790.	2530.	999.	1045.	2722.	1422.	270.	450.	255.	423.	3333.	3318.	28.879	19.857
490.	520.	2117.	550.	795.	2523.	1003.	1050.	2718.	1427.	275.	452.	255.	424.	3295.	3325.	28.876	19.861
500.	525.	2121.	557.	805.	2516.	1013.	1055.	2715.	1432.	280.	456.	250.	420.	3257.	3352.	28.873	19.865
510.	530.	2126.	563.	810.	2509.	1016.	1060.	2712.	1437.	280.	453.	250.	421.	3236.	3368.	28.870	19.869
520.	530.	2131.	565.	800.	2498.	999.	1060.	2706.	1434.	270.	434.	260.	435.	3215.	3346.	28.868	19.873
530.	520.	2137.	556.	800.	2482.	993.	1050.	2696.	1416.	280.	437.	250.	423.	3121.	3384.	28.865	19.877
540.	515.	2143.	552.	780.	2465.	961.	1045.	2687.	1404.	265.	410.	265.	442.	3087.	3343.	28.862	19.881
550.	505.	2149.	543.	780.	2449.	955.	1040.	2677.	1392.	275.	413.	260.	437.	2996.	3362.	28.859	19.885
560.	500.	2154.	539.	780.	2433.	949.	1040.	2667.	1387.	280.	410.	260.	438.	2929.	3369.	28.856	19.889

S.P. = Shot point number.

T(1) = Two-way time in ms. to the top of horizon 1.

V(1) = Dix average velocity for horizon 1 in m/s.

D(1) = Depth for horizon 1 in meter .

T(2) = Two-way time in ms. to the top of horizon 2.

V(2) = Dix average velocity for horizon 2 in m/s.

D(2) = Depth for horizon 2 in meter .

T(3) = Two-way time in ms. to the top of horizon 3.

V(3) = Dix average velocity for horizon 3 in m/s.

D(3) = Depth for horizon 3 in meter.

dT1 = Difference in time between horizon 2 and horizon 1.

dD1 = Difference in depth between horizon 2 and horizon 1.

dT2 = Difference in time between horizon 3 and horizon 2.

dD2 = Difference in depth between horizon 3 and horizon 2.

LAT. = Latitude of corresponding shot point.

LONG. = Longitude of corresponding shot point.

Horizon 1 = Sheghega Formation.

Horizon 2 = Domran Formation.

Horizon 3 = Ruaga Formation.

IV21 = Interval velocity for She. Formation.

IV32 = Interval velocity for Dom. Formation.

Table 4.3d Results of calculation for seismic line 6V253-85

S.P.	T(1)	V(1)	D(1)	T(2)	V(2)	D(2)	T(3)	V(3)	D(3)	dT1	dD1	dT2	dD2	IV21	IV32	LAT.	LONG.
110.	470.	2136.	502.	730.	2382.	869.	1020.	2945.	1502.	260.	367.	290.	632.	2823.	4366.	28.892	19.686
120.	460.	2140.	492.	720.	2402.	865.	1000.	2912.	1456.	260.	372.	280.	591.	2869.	4221.	28.895	19.689
130.	460.	2143.	493.	720.	2422.	872.	1000.	2879.	1439.	260.	379.	280.	568.	2915.	4050.	28.899	19.692
140.	465.	2146.	499.	720.	2442.	879.	1020.	2846.	1451.	255.	380.	300.	572.	2980.	3813.	28.903	19.695
150.	465.	2149.	500.	720.	2462.	886.	1005.	2813.	1414.	255.	387.	285.	527.	3027.	3705.	28.906	19.698
160.	465.	2152.	500.	730.	2482.	906.	1010.	2780.	1404.	265.	406.	280.	498.	3064.	3557.	28.910	19.701
170.	460.	2155.	496.	730.	2502.	913.	1010.	2747.	1387.	270.	418.	280.	474.	3089.	3386.	28.914	19.704
180.	460.	2158.	496.	740.	2522.	933.	1015.	2714.	1377.	280.	437.	275.	444.	3121.	3229.	28.917	19.707
190.	460.	2154.	495.	735.	2485.	913.	1015.	2716.	1378.	275.	418.	280.	465.	3040.	3321.	28.921	19.710
200.	460.	2150.	495.	740.	2446.	905.	1010.	2719.	1373.	280.	410.	270.	468.	2929.	3467.	28.925	19.712
210.	465.	2147.	499.	740.	2406.	890.	1000.	2723.	1361.	275.	391.	260.	471.	2844.	3623.	28.928	19.715
220.	470.	2143.	504.	735.	2367.	870.	990.	2726.	1349.	265.	366.	255.	480.	2762.	3757.	28.932	19.718
230.	475.	2166.	514.	735.	2363.	868.	985.	2728.	1343.	260.	354.	250.	475.	2723.	3800.	28.936	19.721
240.	490.	2191.	537.	740.	2361.	874.	995.	2729.	1358.	250.	337.	255.	484.	2696.	3796.	28.939	19.724
250.	500.	2216.	554.	750.	2359.	885.	995.	2730.	1358.	250.	331.	245.	474.	2648.	3861.	28.943	19.727
260.	505.	2241.	566.	770.	2357.	907.	1000.	2731.	1366.	265.	342.	230.	458.	2574.	3991.	28.947	19.730
270.	510.	2223.	567.	765.	2338.	894.	1005.	2732.	1373.	255.	327.	240.	479.	2565.	3992.	28.950	19.733
280.	510.	2203.	562.	780.	2318.	904.	1000.	2732.	1366.	270.	342.	220.	462.	2533.	4200.	28.954	19.736
290.	510.	2182.	556.	775.	2298.	890.	1005.	2733.	1373.	265.	334.	230.	483.	2521.	4200.	28.958	19.739
300.	510.	2162.	551.	770.	2278.	877.	1010.	2733.	1380.	260.	326.	240.	503.	2508.	4192.	28.961	19.742
310.	505.	2158.	545.	780.	2277.	888.	1015.	2727.	1384.	275.	343.	235.	496.	2495.	4221.	28.965	19.745
320.	510.	2155.	550.	780.	2277.	888.	1040.	2721.	1415.	270.	338.	260.	527.	2504.	4054.	28.969	19.748
330.	515.	2152.	554.	785.	2276.	894.	1050.	2714.	1425.	270.	339.	265.	532.	2519.	4008.	28.972	19.751
340.	525.	2149.	564.	800.	2276.	911.	1060.	2708.	1435.	275.	346.	260.	525.	2524.	4031.	28.976	19.754
350.	535.	2172.	581.	815.	2349.	957.	1070.	2739.	1465.	280.	376.	255.	508.	2686.	3984.	28.980	19.757
360.	550.	2197.	604.	820.	2425.	994.	1085.	2772.	1504.	270.	390.	265.	509.	2889.	3849.	28.983	19.760
370.	550.	2222.	611.	825.	2502.	1032.	1080.	2804.	1514.	275.	421.	255.	482.	3062.	3780.	28.987	19.763
380.	550.	2247.	618.	820.	2578.	1057.	1070.	2837.	1518.	270.	439.	250.	461.	3252.	3688.	28.991	19.766
390.	545.	2231.	608.	820.	2572.	1055.	1065.	2837.	1511.	275.	447.	245.	456.	3251.	3722.	28.994	19.769
400.	545.	2213.	603.	815.	2562.	1044.	1070.	2834.	1516.	270.	441.	255.	472.	3267.	3702.	28.998	19.772
410.	550.	2195.	603.	820.	2552.	1046.	1080.	2832.	1529.	270.	443.	260.	483.	3281.	3715.	29.002	19.775
420.	550.	2176.	598.	825.	2541.	1048.	1090.	2830.	1542.	275.	450.	265.	494.	3273.	3728.	29.005	19.778
430.	550.	2158.	594.	825.	2531.	1044.	1090.	2827.	1541.	275.	450.	265.	497.	3273.	3751.	29.009	19.781
440.	565.	2140.	605.	835.	2521.	1052.	1100.	2825.	1554.	270.	448.	265.	502.	3311.	3789.	29.013	19.784

Abbreviations:

S.P. = Shot point number.
T(1) = Two-way time in ms. to the top of horizon 1.
V(1) = Dix average velocity for horizon 1 in m/s.
D(1) = Depth for horizon 1 in meter .
T(2) = Two-way time in ms. to the top of horizon 2.
V(2) = Dix average velocity for horizon 2 in m/s.
D(2) = Depth for horizon 2 in meter .
T(3) = Two-way time in ms. to the top of horizon 3.
V(3) = Dix average velocity for horizon 3 in m/s.
D(3) = Depth for horizon 3 in meter.
dT1 = Difference in time between horizon 2 and horizon 1.
dD1 = Difference in depth between horizon 2 and horizon 1.
dT2 = Difference in time between horizon 3 and horizon 2.
dD2 = Difference in depth between horizon 3 and horizon 2.
LAT. = Latitude of corresponding shot point.
LONG. = Longitude of corresponding shot point.

Horizon 1 = Sheghega Formation.
Horizon 2 = Domran Formation.
Horizon 3 = Ruaga Formation.

IV21 = Interval velocity for She. Formation.
IV32 = Interval velocity for Dom. Formation.

Table 4.3e Results of calculation for seismic line 6V254-85

S.P.	T(1)	V(1)	D(1)	T(2)	V(2)	D(2)	T(3)	V(3)	D(3)	dT1	dD1	dT2	dD2	IV21	IV32	LAT.	LONG.
100.	500.	2131.	533.	775.	2318.	898.	1005.	2698.	1356.	275.	366.	230.	458.	2655.	3983.	28.955	19.726
110.	505.	2136.	539.	770.	2342.	902.	1010.	2709.	1368.	265.	362.	240.	466.	2740.	3883.	28.952	19.730
120.	510.	2141.	546.	770.	2366.	911.	1010.	2719.	1373.	260.	365.	240.	462.	2808.	3850.	28.949	19.734
130.	505.	2146.	542.	765.	2391.	914.	1000.	2730.	1365.	260.	373.	235.	450.	2862.	3838.	28.946	19.738
140.	495.	2151.	532.	760.	2415.	918.	995.	2740.	1363.	265.	385.	235.	446.	2913.	3787.	28.944	19.742
150.	490.	2156.	528.	755.	2439.	921.	990.	2751.	1362.	265.	392.	235.	441.	2966.	3753.	28.941	19.746
160.	490.	2161.	529.	750.	2463.	924.	990.	2761.	1367.	260.	394.	240.	443.	3038.	3692.	28.938	19.750
170.	480.	2169.	521.	750.	2473.	927.	990.	2759.	1366.	270.	407.	240.	438.	3007.	3658.	28.935	19.754
180.	480.	2180.	523.	740.	2472.	914.	970.	2747.	1332.	260.	391.	230.	418.	3008.	3635.	28.932	19.758
190.	480.	2190.	526.	750.	2470.	926.	945.	2735.	1292.	270.	400.	195.	366.	2963.	3754.	28.929	19.762
200.	475.	2201.	523.	745.	2468.	919.	970.	2722.	1320.	270.	397.	225.	401.	2933.	3564.	28.926	19.766
210.	480.	2198.	528.	750.	2456.	921.	990.	2713.	1343.	270.	394.	240.	422.	2911.	3517.	28.923	19.770
220.	475.	2185.	519.	750.	2436.	914.	1000.	2706.	1353.	275.	395.	250.	440.	2873.	3512.	28.921	19.774
230.	480.	2171.	521.	750.	2416.	906.	995.	2700.	1343.	270.	385.	245.	437.	2852.	3567.	28.918	19.778
240.	475.	2158.	512.	750.	2396.	898.	995.	2693.	1340.	275.	386.	245.	441.	2807.	3608.	28.915	19.782
250.	470.	2148.	505.	745.	2392.	891.	985.	2690.	1325.	275.	386.	240.	433.	2807.	3617.	28.912	19.785
260.	470.	2141.	503.	750.	2403.	901.	990.	2689.	1331.	280.	398.	240.	430.	2843.	3583.	28.909	19.789
270.	475.	2134.	507.	750.	2413.	905.	995.	2688.	1337.	275.	398.	245.	433.	2895.	3527.	28.906	19.793
280.	475.	2127.	505.	745.	2423.	903.	1000.	2688.	1344.	270.	398.	255.	441.	2948.	3459.	28.903	19.797
290.	480.	2125.	510.	755.	2430.	917.	995.	2689.	1338.	275.	407.	240.	420.	2960.	3508.	28.900	19.801
300.	485.	2127.	516.	755.	2434.	919.	995.	2692.	1339.	270.	403.	240.	420.	2985.	3500.	28.898	19.805
310.	485.	2129.	516.	755.	2439.	921.	995.	2694.	1340.	270.	404.	240.	420.	3000.	3492.	28.895	19.809
320.	495.	2131.	527.	760.	2443.	928.	1000.	2697.	1348.	265.	401.	240.	420.	3026.	3500.	28.892	19.813
330.	500.	2136.	534.	770.	2452.	944.	1015.	2704.	1372.	270.	410.	245.	428.	3037.	3494.	28.889	19.817
340.	495.	2143.	531.	770.	2466.	950.	1030.	2714.	1398.	275.	419.	260.	448.	3047.	3446.	28.886	19.821
350.	500.	2151.	538.	770.	2480.	955.	1030.	2725.	1403.	270.	417.	260.	448.	3089.	3446.	28.883	19.825
360.	495.	2159.	534.	770.	2494.	960.	1020.	2736.	1395.	275.	426.	250.	435.	3098.	3480.	28.880	19.829
370.	475.	2166.	515.	750.	2507.	940.	1000.	2751.	1375.	275.	426.	250.	435.	3091.	3480.	28.878	19.833
380.	460.	2174.	500.	750.	2519.	945.	970.	2769.	1343.	290.	445.	220.	398.	3069.	3618.	28.875	19.837
390.	470.	2181.	512.	750.	2531.	949.	940.	2787.	1310.	280.	437.	190.	361.	3121.	3800.	28.872	19.840
400.	480.	2188.	525.	760.	2543.	966.	1005.	2805.	1410.	280.	441.	245.	443.	3150.	3624.	28.869	19.844
410.	475.	2195.	521.	755.	2552.	963.	1010.	2812.	1420.	280.	442.	255.	457.	3157.	3584.	28.866	19.848
420.	475.	2203.	523.	750.	2557.	959.	1010.	2811.	1420.	275.	436.	260.	460.	3171.	3546.	28.863	19.852
430.	480.	2211.	531.	750.	2563.	961.	1015.	2809.	1426.	270.	430.	265.	465.	3185.	3509.	28.860	19.856
440.	490.	2218.	544.	760.	2568.	976.	1020.	2808.	1432.	270.	432.	260.	456.	3200.	3508.	28.857	19.860
450.	485.	2212.	536.	770.	2568.	989.	1030.	2802.	1443.	285.	452.	260.	454.	3179.	3492.	28.855	19.864
460.	490.	2195.	538.	770.	2562.	986.	1030.	2792.	1438.	280.	448.	260.	452.	3200.	3477.	28.852	19.868
470.	485.	2178.	528.	765.	2556.	978.	1025.	2782.	1426.	280.	450.	260.	448.	3214.	3446.	28.849	19.872
480.	490.	2161.	529.	765.	2550.	975.	1025.	2772.	1421.	275.	446.	260.	445.	3244.	3431.	28.846	19.876
490.	480.	2144.	514.	760.	2544.	967.	1020.	2762.	1409.	280.	452.	260.	442.	3236.	3400.	28.843	19.880
500.	470.	2126.	500.	760.	2539.	965.	1020.	2752.	1404.	290.	465.	260.	439.	3207.	3377.	28.840	19.884
510.	465.	2109.	490.	750.	2533.	950.	1010.	2742.	1385.	285.	459.	260.	435.	3228.	3346.	28.837	19.888

Abbreviations:

S.P. = Shot point number.
T(1) = Two-way time in ms. to the top of horizon 1.
V(1) = Dix average velocity for horizon 1 in m/s.
D(1) = Depth for horizon 1 in meter .
T(2) = Two-way time in ms. to the top of horizon 2.
V(2) = Dix average velocity for horizon 2 in m/s.
D(2) = Depth for horizon 2 in meter .
T(3) = Two-way time in ms. to the top of horizon 3.
V(3) = Dix average velocity for horizon 3 in m/s.
D(3) = Depth for horizon 3 in meter.
dT1 = Difference in time between horizon 2 and horizon 1.
dD1 = Difference in depth between horizon 2 and horizon 1.
dT2 = Difference in time between horizon 3 and horizon 2.
dD2 = Difference in depth between horizon 3 and horizon 2.
LAT. = Latitude of corresponding shot point.
LONG. = Longitude of corresponding shot point.

Horizon 1 = Sheghega Formation.
Horizon 2 = Domran Formation.
Horizon 3 = Ruaga Formation.

IV21 = Interval velocity for She. Formation.
IV32 = Interval velocity for Dom. Formation.

Table 4.3f Results of calculation for seismic line 6V255-85

S.P.	T(1)	V(1)	D(1)	T(2)	V(2)	D(2)	T(3)	V(3)	D(3)	dT1	dD1	dT2	dD2	IV21	IV32	LAT.	LONG.
110.	465.	2093.	487.	705.	2308.	814.	1000.	2717.	1358.	240.	327.	295.	545.	2725.	3688.	28.889	19.702
120.	455.	2101.	478.	700.	2327.	815.	980.	2711.	1328.	245.	336.	280.	514.	2751.	3664.	28.893	19.706
130.	450.	2109.	475.	700.	2346.	821.	990.	2705.	1339.	250.	347.	290.	518.	2768.	3572.	28.896	19.709
140.	440.	2117.	466.	700.	2366.	828.	985.	2699.	1329.	260.	362.	285.	502.	2785.	3516.	28.900	19.712
150.	440.	2125.	467.	710.	2385.	847.	980.	2694.	1320.	270.	379.	270.	473.	2815.	3504.	28.903	19.715
160.	445.	2133.	475.	710.	2404.	853.	975.	2688.	1310.	265.	379.	265.	457.	2853.	3449.	28.907	19.718
170.	450.	2132.	480.	715.	2412.	862.	970.	2684.	1302.	265.	382.	255.	440.	2883.	3451.	28.911	19.721
180.	460.	2125.	489.	720.	2411.	868.	965.	2683.	1294.	260.	379.	245.	426.	2915.	3478.	28.914	19.724
190.	470.	2118.	498.	730.	2410.	880.	975.	2681.	1307.	260.	382.	245.	427.	2938.	3486.	28.918	19.728
200.	480.	2110.	507.	745.	2409.	897.	990.	2679.	1326.	265.	391.	245.	429.	2943.	3502.	28.921	19.731
210.	490.	2112.	517.	755.	2409.	910.	995.	2692.	1339.	265.	392.	240.	430.	2966.	3575.	28.925	19.734
220.	500.	2120.	530.	760.	2411.	916.	1000.	2716.	1358.	260.	386.	240.	442.	2969.	3683.	28.928	19.737
230.	500.	2129.	532.	765.	2413.	923.	1010.	2740.	1384.	265.	391.	245.	461.	2951.	3763.	28.932	19.740
240.	500.	2138.	534.	760.	2415.	918.	1000.	2764.	1382.	260.	383.	240.	464.	2954.	3867.	28.935	19.743
250.	495.	2145.	531.	750.	2424.	909.	990.	2766.	1369.	255.	378.	240.	460.	2965.	3833.	28.939	19.746
260.	490.	2153.	527.	760.	2438.	926.	990.	2750.	1361.	270.	399.	230.	435.	2956.	3783.	28.943	19.749
270.	490.	2160.	529.	755.	2452.	926.	1000.	2735.	1367.	265.	396.	245.	442.	2996.	3600.	28.946	19.753
280.	495.	2168.	536.	760.	2466.	937.	1005.	2719.	1366.	265.	401.	245.	429.	3026.	3502.	28.950	19.756
290.	500.	2173.	543.	765.	2481.	949.	1010.	2729.	1378.	265.	406.	245.	429.	3064.	3502.	28.953	19.759
300.	500.	2177.	544.	770.	2495.	961.	1020.	2760.	1408.	270.	416.	250.	447.	3089.	3576.	28.957	19.762
310.	505.	2181.	551.	780.	2510.	979.	1025.	2791.	1431.	275.	428.	245.	452.	3113.	3690.	28.960	19.765
320.	515.	2185.	563.	790.	2524.	997.	1030.	2823.	1454.	275.	434.	240.	457.	3156.	3808.	28.964	19.768
330.	530.	2189.	580.	805.	2529.	1018.	1055.	2822.	1489.	275.	438.	250.	471.	3185.	3768.	28.968	19.771
340.	545.	2192.	597.	820.	2525.	1035.	1075.	2796.	1503.	275.	438.	255.	468.	3185.	3671.	28.971	19.774
350.	560.	2196.	615.	825.	2522.	1040.	1100.	2770.	1523.	265.	426.	275.	483.	3208.	3513.	28.975	19.778
360.	565.	2199.	621.	835.	2518.	1051.	1095.	2744.	1502.	270.	430.	260.	451.	3185.	3469.	28.978	19.781
370.	570.	2209.	630.	830.	2521.	1046.	1080.	2743.	1481.	260.	416.	250.	435.	3200.	3480.	28.982	19.784
380.	560.	2226.	623.	830.	2528.	1049.	1080.	2762.	1492.	270.	426.	250.	443.	3156.	3544.	28.985	19.787
390.	555.	2243.	622.	830.	2535.	1052.	1085.	2782.	1509.	275.	430.	255.	457.	3127.	3584.	28.989	19.790
400.	555.	2259.	627.	830.	2542.	1055.	1090.	2801.	1527.	275.	428.	260.	472.	3113.	3631.	28.992	19.793
410.	560.	2276.	637.	830.	2549.	1058.	1090.	2821.	1537.	270.	420.	260.	480.	3119.	3685.	28.996	19.796
420.	555.	2293.	636.	830.	2556.	1061.	1100.	2841.	1562.	275.	424.	270.	502.	3091.	3711.	29.000	19.799
430.	570.	2309.	658.	845.	2563.	1083.	1105.	2860.	1580.	275.	425.	260.	498.	3091.	3823.	29.003	19.803
440.	580.	2326.	674.	855.	2570.	1099.	1120.	2880.	1613.	275.	424.	265.	514.	3091.	3879.	29.007	19.806
450.	585.	2342.	685.	865.	2577.	1114.	1125.	2899.	1631.	280.	429.	260.	516.	3064.	3977.	29.010	19.809
460.	590.	2359.	696.	865.	2584.	1117.	1120.	2919.	1635.	275.	422.	255.	517.	3062.	4063.	29.014	19.812

Abbreviations:

S.P. = Shot point number.
T(1) = Two-way time in ms. to the top of horizon 1.
V(1) = Dix average velocity for horizon 1 in m/s.
D(1) = Depth for horizon 1 in meter .
T(2) = Two-way time in ms. to the top of horizon 2.
V(2) = Dix average velocity for horizon 2 in m/s.
D(2) = Depth for horizon 2 in meter .
T(3) = Two-way time in ms. to the top of horizon 3.
V(3) = Dix average velocity for horizon 3 in m/s.
D(3) = Depth for horizon 3 in meter.
dT1 = Difference in time between horizon 2 and horizon 1.
dD1 = Difference in depth between horizon 2 and horizon 1.
dT2 = Difference in time between horizon 3 and horizon 2.
dD2 = Difference in depth between horizon 3 and horizon 2.
LAT. = Latitude of corresponding shot point.
LONG. = Longitude of corresponding shot point.

Horizon 1 = Sheghega Formation.
Horizon 2 = Domran Formation.
Horizon 3 = Ruaga Formation.

IV21 = Interval velocity for She. Formation.
IV32 = Interval velocity for Dom. Formation.

Table 4.3g Results of calculation for seismic line 6V256-85

S.P.	T(1)	V(1)	D(1)	T(2)	V(2)	D(2)	T(3)	V(3)	D(3)	dT1	dD1	dT2	dD2	IV21	IV32	LAT.	LONG.
100.	480.	2144.	515.	750.	2566.	962.	1010.	2757.	1392.	270.	448.	260.	430.	3311.	3308.	28.944	19.721
110.	490.	2136.	523.	750.	2548.	955.	1000.	2747.	1373.	260.	432.	250.	418.	3323.	3344.	28.942	19.725
120.	495.	2127.	527.	760.	2529.	961.	1005.	2736.	1375.	265.	434.	245.	414.	3275.	3380.	28.939	19.729
130.	500.	2119.	530.	760.	2510.	954.	1005.	2726.	1370.	260.	424.	245.	416.	3262.	3396.	28.936	19.733
140.	500.	2111.	528.	770.	2491.	959.	1005.	2716.	1365.	270.	431.	235.	406.	3193.	3455.	28.933	19.736
150.	500.	2103.	526.	770.	2473.	952.	1010.	2706.	1366.	270.	426.	240.	414.	3156.	3450.	28.930	19.740
160.	495.	2095.	518.	765.	2454.	939.	1010.	2695.	1361.	270.	420.	245.	422.	3119.	3445.	28.927	19.744
170.	490.	2084.	511.	760.	2418.	919.	1000.	2671.	1335.	270.	408.	240.	417.	3022.	3467.	28.924	19.748
180.	490.	2071.	507.	750.	2367.	888.	985.	2635.	1298.	260.	380.	235.	410.	2931.	3489.	28.922	19.752
190.	480.	2064.	495.	745.	2352.	876.	980.	2622.	1285.	265.	381.	235.	409.	2875.	3481.	28.919	19.756
200.	470.	2062.	485.	740.	2364.	875.	985.	2627.	1294.	270.	390.	245.	419.	2889.	3420.	28.916	19.760
210.	460.	2060.	474.	730.	2377.	868.	985.	2633.	1297.	270.	394.	255.	429.	2919.	3365.	28.913	19.764
220.	460.	2058.	473.	735.	2390.	878.	980.	2639.	1293.	275.	405.	245.	415.	2945.	3388.	28.910	19.768
230.	465.	2057.	478.	740.	2403.	889.	980.	2647.	1297.	275.	411.	240.	408.	2989.	3400.	28.907	19.772
240.	465.	2057.	478.	745.	2415.	900.	980.	2657.	1302.	280.	421.	235.	402.	3014.	3421.	28.904	19.776
250.	470.	2057.	483.	750.	2428.	910.	990.	2667.	1320.	280.	427.	240.	410.	3050.	3417.	28.902	19.780
260.	470.	2057.	483.	745.	2440.	909.	995.	2678.	1332.	275.	426.	250.	423.	3098.	3384.	28.899	19.784
270.	465.	2058.	479.	745.	2451.	913.	995.	2688.	1337.	280.	434.	250.	424.	3100.	3392.	28.896	19.788
280.	460.	2082.	479.	745.	2435.	907.	995.	2701.	1344.	285.	428.	250.	437.	3004.	3496.	28.893	19.792
290.	455.	2105.	479.	740.	2419.	895.	990.	2715.	1344.	285.	416.	250.	449.	2919.	3592.	28.890	19.796
300.	450.	2105.	474.	735.	2412.	886.	965.	2712.	1309.	285.	413.	230.	422.	2891.	3678.	28.887	19.800
310.	435.	2085.	453.	705.	2411.	850.	920.	2696.	1240.	270.	396.	215.	390.	2941.	3628.	28.884	19.803
320.	440.	2065.	454.	710.	2411.	856.	930.	2680.	1246.	270.	402.	220.	390.	2978.	3545.	28.882	19.807
330.	440.	2045.	450.	715.	2410.	862.	985.	2664.	1312.	275.	412.	270.	450.	2996.	3333.	28.879	19.811
340.	445.	2048.	456.	720.	2414.	869.	995.	2662.	1324.	275.	414.	275.	455.	3004.	3309.	28.876	19.815
350.	445.	2069.	460.	725.	2422.	878.	995.	2671.	1329.	280.	418.	270.	451.	2986.	3341.	28.873	19.819
360.	445.	2090.	465.	720.	2430.	875.	985.	2681.	1320.	275.	410.	265.	445.	2982.	3358.	28.870	19.823
370.	445.	2111.	470.	720.	2438.	878.	970.	2690.	1305.	275.	408.	250.	427.	2967.	3416.	28.867	19.827
380.	450.	2118.	477.	720.	2452.	883.	970.	2696.	1308.	270.	406.	250.	425.	3007.	3400.	28.864	19.831
390.	455.	2114.	481.	725.	2472.	896.	980.	2701.	1323.	270.	415.	255.	427.	3074.	3349.	28.862	19.835
400.	460.	2110.	485.	730.	2491.	909.	980.	2705.	1325.	270.	424.	250.	416.	3141.	3328.	28.859	19.839
410.	450.	2107.	474.	730.	2510.	916.	975.	2709.	1321.	280.	442.	245.	404.	3157.	3306.	28.856	19.843
420.	445.	2110.	469.	735.	2517.	925.	990.	2717.	1345.	290.	456.	255.	420.	3145.	3294.	28.853	19.847
430.	455.	2119.	482.	730.	2515.	918.	995.	2728.	1357.	275.	436.	265.	439.	3171.	3313.	28.850	19.851
440.	460.	2128.	489.	735.	2512.	923.	1010.	2739.	1383.	275.	434.	275.	460.	3156.	3345.	28.847	19.855
450.	460.	2137.	491.	740.	2510.	929.	1010.	2750.	1389.	280.	437.	270.	460.	3129.	3407.	28.844	19.859
460.	460.	2138.	492.	740.	2504.	926.	1010.	2746.	1387.	280.	435.	270.	460.	3100.	3415.	28.842	19.863
470.	465.	2132.	496.	750.	2495.	936.	1015.	2730.	1385.	285.	440.	265.	450.	3088.	3389.	28.839	19.867
480.	465.	2126.	494.	750.	2487.	933.	1010.	2714.	1370.	285.	438.	260.	438.	3081.	3362.	28.836	19.870
490.	460.	2120.	488.	740.	2479.	917.	1010.	2698.	1362.	280.	429.	270.	445.	3064.	3296.	28.833	19.874
500.	460.	2115.	486.	740.	2470.	914.	1010.	2682.	1354.	280.	428.	270.	440.	3057.	3259.	28.830	19.878
510.	460.	2109.	485.	750.	2462.	923.	1015.	2666.	1353.	290.	438.	265.	430.	3021.	3245.	28.827	19.882
520.	470.	2103.	494.	750.	2454.	920.	1020.	2650.	1351.	280.	426.	270.	431.	3043.	3193.	28.824	19.886
530.	470.	2097.	493.	750.	2445.	917.	1020.	2634.	1343.	280.	424.	270.	426.	3029.	3156.	28.822	19.890

S.P. = Shot point number.

T(1) = Two-way time in ms. to the top of horizon 1.

V(1) = Dix average velocity for horizon 1 in m/s.

D(1) = Depth for horizon 1 in meter .

T(2) = Two-way time in ms. to the top of horizon 2.

V(2) = Dix average velocity for horizon 2 in m/s.

D(2) = Depth for horizon 2 in meter .

T(3) = Two-way time in ms. to the top of horizon 3.

V(3) = Dix average velocity for horizon 3 in m/s.

D(3) = Depth for horizon 3 in meter.

dT1 = Difference in time between horizon 2 and horizon 1.

dD1 = Difference in depth between horizon 2 and horizon 1.

dT2 = Difference in time between horizon 3 and horizon 2.

dD2 = Difference in depth between horizon 3 and horizon 2.

LAT. = Latitude of corresponding shot point.

LONG. = Longitude of corresponding shot point.

Horizon 1 = Sheghega Formation.

Horizon 2 = Domran Formation.

Horizon 3 = Ruaga Formation.

IV21 = Interval velocity for She. Formation.

IV32 = Interval velocity for Dom. Formation.

Table 4.3h Results of calculation for seismic line 6V257-85

S.P.	T(1)	V(1)	D(1)	T(2)	V(2)	D(2)	T(3)	V(3)	D(3)	dT1	dD1	dT2	dD2	IV21	IV32	LAT.	LONG.
100.	500.	2292.	573.	770.	2553.	983.	1100.	2824.	1553.	270.	410.	330.	570.	3037.	3455.	28.846	19.690
110.	510.	2263.	577.	775.	2550.	988.	1080.	2831.	1529.	265.	411.	305.	541.	3102.	3548.	28.849	19.693
120.	500.	2235.	559.	770.	2548.	981.	1075.	2839.	1526.	270.	422.	305.	545.	3126.	3574.	28.853	19.696
130.	500.	2207.	552.	770.	2545.	980.	1060.	2847.	1509.	270.	428.	290.	529.	3170.	3648.	28.857	19.699
140.	495.	2178.	539.	760.	2543.	966.	1055.	2855.	1506.	265.	427.	295.	540.	3223.	3661.	28.860	19.703
150.	475.	2150.	511.	740.	2540.	940.	1040.	2862.	1488.	265.	429.	300.	548.	3238.	3653.	28.864	19.706
160.	470.	2136.	502.	730.	2535.	925.	1020.	2853.	1455.	260.	423.	290.	530.	3254.	3655.	28.867	19.709
170.	455.	2140.	487.	710.	2527.	897.	990.	2822.	1397.	255.	410.	280.	500.	3216.	3571.	28.871	19.712
180.	440.	2143.	472.	700.	2518.	881.	975.	2792.	1361.	260.	410.	275.	480.	3146.	3491.	28.874	19.715
190.	440.	2147.	472.	690.	2510.	866.	950.	2761.	1312.	250.	394.	260.	446.	3152.	3431.	28.878	19.718
200.	430.	2152.	463.	690.	2507.	865.	945.	2745.	1297.	260.	402.	255.	432.	3092.	3388.	28.882	19.721
210.	430.	2159.	464.	690.	2513.	867.	950.	2744.	1304.	260.	403.	260.	437.	3100.	3362.	28.885	19.724
220.	430.	2166.	466.	700.	2518.	881.	955.	2744.	1310.	270.	416.	255.	429.	3074.	3365.	28.889	19.727
230.	430.	2173.	467.	700.	2523.	883.	955.	2744.	1310.	270.	416.	255.	427.	3081.	3349.	28.892	19.730
240.	430.	2177.	468.	700.	2522.	883.	960.	2739.	1315.	270.	415.	260.	432.	3074.	3323.	28.896	19.734
250.	440.	2175.	479.	705.	2514.	886.	955.	2728.	1303.	265.	408.	250.	416.	3072.	3336.	28.899	19.737
260.	450.	2173.	489.	700.	2505.	877.	940.	2717.	1277.	250.	388.	240.	400.	3104.	3333.	28.903	19.740
270.	445.	2172.	483.	700.	2497.	874.	935.	2706.	1265.	255.	391.	235.	391.	3067.	3328.	28.907	19.743
280.	450.	2179.	490.	710.	2494.	886.	950.	2705.	1285.	260.	395.	240.	399.	3046.	3325.	28.910	19.746
290.	470.	2197.	516.	730.	2499.	912.	960.	2715.	1303.	260.	396.	230.	391.	3046.	3400.	28.914	19.749
300.	480.	2215.	531.	745.	2504.	933.	970.	2726.	1322.	265.	401.	225.	390.	3034.	3458.	28.917	19.752
310.	490.	2232.	547.	745.	2508.	934.	970.	2737.	1327.	255.	387.	225.	393.	3035.	3493.	28.921	19.755
320.	490.	2242.	549.	750.	2515.	943.	970.	2745.	1331.	260.	394.	220.	388.	3031.	3527.	28.925	19.758
330.	485.	2242.	544.	750.	2526.	947.	955.	2750.	1313.	265.	403.	205.	366.	3042.	3571.	28.928	19.761
340.	490.	2242.	549.	750.	2536.	951.	970.	2756.	1337.	260.	402.	220.	386.	3092.	3509.	28.932	19.764
350.	500.	2242.	561.	760.	2546.	968.	995.	2761.	1374.	260.	407.	235.	406.	3131.	3455.	28.935	19.768
360.	500.	2234.	559.	765.	2540.	971.	1000.	2759.	1380.	265.	413.	235.	408.	3109.	3481.	28.939	19.771
370.	510.	2217.	565.	770.	2512.	967.	1000.	2748.	1374.	260.	402.	230.	407.	3092.	3539.	28.942	19.774
380.	515.	2199.	566.	780.	2484.	969.	1015.	2738.	1389.	265.	403.	235.	420.	3042.	3574.	28.946	19.777
390.	525.	2181.	572.	790.	2457.	970.	1020.	2727.	1391.	265.	398.	230.	420.	3004.	3661.	28.950	19.780
400.	530.	2177.	577.	800.	2462.	985.	1040.	2745.	1428.	270.	408.	240.	443.	3022.	3692.	28.953	19.783
410.	540.	2173.	587.	810.	2470.	1000.	1050.	2766.	1452.	270.	414.	240.	452.	3059.	3767.	28.957	19.786
420.	550.	2170.	597.	820.	2477.	1016.	1060.	2786.	1477.	270.	419.	240.	461.	3104.	3842.	28.960	19.789
430.	565.	2166.	612.	835.	2485.	1037.	1070.	2807.	1502.	270.	425.	235.	464.	3148.	3957.	28.964	19.792
440.	570.	2168.	618.	840.	2476.	1040.	1100.	2791.	1535.	270.	422.	260.	495.	3126.	3808.	28.967	19.795
450.	580.	2169.	629.	840.	2467.	1036.	1095.	2774.	1519.	260.	407.	255.	483.	3131.	3788.	28.971	19.799
460.	570.	2171.	619.	840.	2458.	1032.	1080.	2757.	1489.	270.	414.	240.	456.	3059.	3808.	28.975	19.802
470.	570.	2173.	619.	840.	2449.	1028.	1080.	2740.	1480.	270.	409.	240.	451.	3030.	3767.	28.978	19.805
480.	570.	2180.	621.	840.	2448.	1028.	1070.	2741.	1466.	270.	407.	230.	438.	3015.	3809.	28.982	19.808
490.	570.	2188.	624.	840.	2447.	1028.	1075.	2742.	1474.	270.	404.	235.	446.	2993.	3796.	28.985	19.811
500.	565.	2196.	620.	840.	2447.	1028.	1080.	2744.	1482.	275.	407.	240.	454.	2967.	3783.	28.989	19.814
510.	570.	2204.	628.	845.	2447.	1034.	1085.	2746.	1490.	275.	406.	240.	456.	2953.	3800.	28.993	19.817
520.	585.	2226.	651.	855.	2477.	1059.	1100.	2770.	1524.	270.	408.	245.	465.	3022.	3796.	28.996	19.820
530.	595.	2249.	669.	870.	2508.	1091.	1120.	2796.	1566.	275.	422.	250.	475.	3069.	3800.	29.000	19.823
540.	605.	2272.	687.	875.	2539.	1111.	1125.	2822.	1587.	270.	424.	250.	476.	3141.	3808.	29.003	19.826
550.	610.	2296.	700.	880.	2571.	1131.	1130.	2848.	1609.	270.	431.	250.	478.	3193.	3824.	29.007	19.830
560.	610.	2319.	707.	880.	2602.	1145.	1125.	2874.	1617.	270.	438.	245.	472.	3244.	3853.	29.010	19.833
570.	610.	2342.	714.	890.	2634.	1172.	1140.	2900.	1653.	280.	458.	250.	481.	3271.	3848.	29.014	19.836

S.P. = Shot point number.

T(1) = Two-way time in ms. to the top of horizon 1.

V(1) = Dix average velocity for horizon 1 in m/s.

D(1) = Depth for horizon 1 in meter .

T(2) = Two-way time in ms. to the top of horizon 2.

V(2) = Dix average velocity for horizon 2 in m/s.

D(2) = Depth for horizon 2 in meter .

T(3) = Two-way time in ms. to the top of horizon 3.

V(3) = Dix average velocity for horizon 3 in m/s.

D(3) = Depth for horizon 3 in meter.

dT1 = Difference in time between horizon 2 and horizon 1.

dD1 = Difference in depth between horizon 2 and horizon 1.

dT2 = Difference in time between horizon 3 and horizon 2.

dD2 = Difference in depth between horizon 3 and horizon 2.

Horizon 1 = Sheghega Formation.

Horizon 2 = Domran Formation.

Horizon 3 = Ruaga Formation.

IV21 = Interval velocity for She. Formation.

IV32 = Interval velocity for Dom. Formation.

Table 4.3i Results of calculation for seismic line 6V258-85

S.P.	T(1)	V(1)	D(1)	T(2)	V(2)	D(2)	T(3)	V(3)	D(3)	dT1	dD1	dT2	dD2	IV21	IV32	LAT.	LONG.
260.	505.	2112.	533.	755.	2319.	876.	1000.	2670.	1335.	250.	342.	245.	459.	2744.	3747.	28.926	19.729
270.	490.	2107.	516.	740.	2324.	860.	995.	2668.	1327.	250.	344.	255.	467.	2752.	3663.	28.923	19.733
280.	485.	2102.	510.	740.	2330.	862.	980.	2666.	1306.	255.	352.	240.	444.	2761.	3700.	28.921	19.737
290.	480.	2098.	503.	730.	2335.	852.	970.	2665.	1292.	250.	349.	240.	440.	2792.	3667.	28.918	19.741
300.	465.	2093.	487.	730.	2340.	854.	960.	2663.	1278.	265.	368.	230.	424.	2770.	3687.	28.915	19.745
310.	450.	2088.	470.	710.	2345.	833.	950.	2661.	1264.	260.	363.	240.	432.	2792.	3592.	28.912	19.748
320.	450.	2084.	469.	710.	2350.	834.	960.	2660.	1277.	260.	366.	250.	442.	2808.	3544.	28.909	19.752
330.	445.	2082.	463.	705.	2367.	834.	965.	2664.	1286.	260.	371.	260.	451.	2854.	3477.	28.906	19.756
340.	450.	2080.	468.	705.	2384.	840.	965.	2669.	1288.	255.	372.	260.	448.	2918.	3446.	28.903	19.760
350.	445.	2078.	462.	710.	2401.	852.	965.	2675.	1290.	265.	390.	255.	438.	2943.	3435.	28.900	19.764
360.	445.	2076.	462.	710.	2418.	858.	960.	2680.	1286.	265.	396.	250.	428.	2989.	3424.	28.897	19.768
370.	445.	2078.	462.	710.	2388.	848.	960.	2672.	1283.	265.	385.	250.	435.	2913.	3480.	28.895	19.772
380.	450.	2080.	468.	710.	2355.	836.	960.	2664.	1279.	260.	368.	250.	442.	2831.	3544.	28.892	19.776
390.	450.	2082.	468.	710.	2322.	824.	965.	2655.	1281.	260.	356.	255.	457.	2738.	3584.	28.889	19.780
400.	440.	2084.	458.	705.	2290.	807.	960.	2647.	1271.	265.	349.	255.	463.	2634.	3639.	28.886	19.784
410.	440.	2091.	460.	700.	2312.	809.	950.	2659.	1263.	260.	349.	250.	454.	2685.	3632.	28.883	19.788
420.	435.	2099.	456.	700.	2338.	818.	940.	2672.	1256.	265.	362.	240.	438.	2732.	3650.	28.880	19.792
430.	440.	2106.	463.	700.	2364.	827.	950.	2685.	1275.	260.	364.	250.	448.	2800.	3584.	28.877	19.796
440.	440.	2113.	465.	710.	2389.	848.	975.	2698.	1315.	270.	383.	265.	467.	2837.	3525.	28.874	19.800
450.	450.	2116.	476.	720.	2403.	865.	1000.	2706.	1353.	270.	389.	280.	488.	2881.	3486.	28.872	19.803
460.	460.	2119.	487.	730.	2416.	882.	1010.	2715.	1371.	270.	394.	280.	489.	2926.	3493.	28.869	19.807
470.	470.	2122.	499.	740.	2429.	899.	1015.	2723.	1382.	270.	400.	275.	483.	2963.	3513.	28.866	19.811
480.	470.	2124.	499.	740.	2442.	903.	1020.	2731.	1393.	270.	404.	280.	490.	2993.	3500.	28.863	19.815
490.	465.	2101.	488.	735.	2425.	891.	1020.	2721.	1388.	270.	403.	285.	496.	2985.	3488.	28.860	19.819
500.	465.	2076.	483.	730.	2407.	879.	990.	2710.	1341.	265.	396.	260.	463.	2989.	3554.	28.857	19.823
510.	460.	2052.	472.	720.	2389.	860.	975.	2698.	1315.	260.	388.	255.	455.	2985.	3569.	28.854	19.827
520.	460.	2027.	466.	725.	2370.	859.	975.	2687.	1310.	265.	393.	250.	450.	2966.	3608.	28.851	19.831
530.	460.	2033.	468.	730.	2355.	859.	985.	2683.	1322.	270.	392.	255.	462.	2896.	3631.	28.848	19.835
540.	460.	2041.	470.	730.	2339.	854.	990.	2680.	1327.	270.	384.	260.	473.	2844.	3638.	28.846	19.839
550.	460.	2049.	471.	725.	2324.	842.	990.	2677.	1325.	265.	371.	265.	483.	2800.	3645.	28.843	19.843
560.	470.	2057.	483.	730.	2308.	842.	1000.	2674.	1337.	260.	359.	270.	495.	2762.	3667.	28.840	19.847
570.	470.	2061.	484.	730.	2310.	843.	1005.	2659.	1336.	260.	359.	275.	493.	2762.	3585.	28.837	19.851
580.	470.	2064.	485.	730.	2314.	844.	1005.	2643.	1328.	260.	360.	275.	484.	2762.	3520.	28.834	19.855
590.	470.	2067.	486.	730.	2317.	846.	1005.	2627.	1320.	260.	360.	275.	474.	2769.	3447.	28.831	19.858
600.	470.	2070.	486.	730.	2320.	847.	1005.	2610.	1312.	260.	360.	275.	465.	2777.	3382.	28.828	19.862
610.	470.	2073.	487.	730.	2323.	848.	1005.	2594.	1304.	260.	361.	275.	456.	2777.	3316.	28.825	19.866

Abbreviations:

S.P. = Shot point number.
T(1) = Two-way time in ms. to the top of horizon 1.
V(1) = Dix average velocity for horizon 1 in m/s.
D(1) = Depth for horizon 1 in meter .
T(2) = Two-way time in ms. to the top of horizon 2.
V(2) = Dix average velocity for horizon 2 in m/s.
D(2) = Depth for horizon 2 in meter .
T(3) = Two-way time in ms. to the top of horizon 3.
V(3) = Dix average velocity for horizon 3 in m/s.
D(3) = Depth for horizon 3 in meter.
dT1 = Difference in time between horizon 2 and horizon 1.
dD1 = Difference in depth between horizon 2 and horizon 1.
dT2 = Difference in time between horizon 3 and horizon 2.
dD2 = Difference in depth between horizon 3 and horizon 2.
LAT. = Latitude of corresponding shot point.
LONG. = Longitude of corresponding shot point.

Horizon 1 = Sheghega Formation.
Horizon 2 = Domran Formation.
Horizon 3 = Ruaga Formation.

IV21 = Interval velocity for She. Formation.
IV32 = Interval velocity for Dom. Formation.

Table 4.3j Results of calculation for seismic line 6V259-85

S.P.	T(1)	V(1)	D(1)	T(2)	V(2)	D(2)	T(3)	V(3)	D(3)	dT1	dD1	dT2	dD2	IV21	IV32	LAT.	LONG.
110.	495.	2099.	520.	755.	2422.	914.	1085.	2820.	1530.	260.	395.	330.	615.	3031.	3733.	28.832	19.709
120.	485.	2095.	508.	745.	2426.	904.	1055.	2798.	1476.	260.	396.	310.	572.	3046.	3690.	28.835	19.712
130.	475.	2091.	497.	725.	2430.	881.	1010.	2775.	1402.	250.	384.	285.	521.	3072.	3656.	28.839	19.715
140.	465.	2087.	485.	705.	2433.	858.	985.	2753.	1356.	240.	372.	280.	498.	3108.	3557.	28.842	19.718
150.	450.	2083.	469.	695.	2437.	847.	965.	2731.	1318.	245.	378.	270.	471.	3086.	3489.	28.846	19.721
160.	435.	2080.	452.	685.	2441.	836.	935.	2709.	1267.	250.	384.	250.	430.	3072.	3448.	28.850	19.724
170.	430.	2083.	448.	685.	2439.	835.	915.	2711.	1240.	255.	387.	230.	405.	3035.	3522.	28.853	19.727
180.	425.	2093.	445.	685.	2431.	833.	925.	2732.	1264.	260.	388.	240.	431.	2985.	3592.	28.857	19.730
190.	425.	2103.	447.	685.	2424.	830.	950.	2754.	1308.	260.	383.	265.	478.	2946.	3608.	28.860	19.733
200.	415.	2113.	438.	690.	2416.	834.	955.	2775.	1325.	275.	395.	265.	491.	2880.	3706.	28.864	19.737
210.	415.	2114.	439.	695.	2406.	836.	970.	2774.	1345.	280.	397.	275.	509.	2836.	3702.	28.868	19.740
220.	420.	2109.	443.	695.	2393.	832.	960.	2755.	1322.	275.	389.	265.	491.	2829.	3698.	28.871	19.743
230.	430.	2104.	452.	695.	2380.	827.	955.	2736.	1306.	265.	375.	260.	479.	2830.	3685.	28.875	19.746
240.	435.	2099.	456.	695.	2367.	823.	970.	2716.	1317.	260.	366.	275.	495.	2823.	3593.	28.878	19.749
250.	435.	2099.	457.	700.	2365.	828.	970.	2708.	1313.	265.	371.	270.	485.	2800.	3593.	28.882	19.752
260.	438.	2104.	461.	698.	2372.	828.	973.	2708.	1318.	260.	367.	275.	490.	2823.	3564.	28.886	19.755
270.	441.	2110.	465.	691.	2379.	822.	966.	2709.	1308.	250.	357.	275.	486.	2856.	3535.	28.889	19.758
280.	440.	2115.	465.	690.	2386.	823.	965.	2709.	1307.	250.	358.	275.	484.	2864.	3520.	28.893	19.761
290.	440.	2120.	466.	700.	2393.	838.	970.	2709.	1314.	260.	371.	270.	476.	2862.	3526.	28.896	19.764
300.	440.	2125.	468.	705.	2400.	846.	970.	2709.	1314.	265.	378.	265.	468.	2853.	3532.	28.900	19.767
310.	453.	2130.	482.	713.	2408.	859.	983.	2716.	1335.	260.	376.	270.	476.	2900.	3526.	28.904	19.771
320.	465.	2134.	496.	735.	2418.	889.	990.	2728.	1350.	270.	393.	255.	462.	2911.	3616.	28.907	19.774
330.	475.	2138.	508.	750.	2428.	910.	1000.	2740.	1370.	275.	403.	250.	459.	2924.	3680.	28.911	19.777
340.	475.	2141.	509.	750.	2438.	914.	1000.	2751.	1376.	275.	406.	250.	462.	2945.	3696.	28.914	19.780
350.	477.	2145.	512.	752.	2447.	920.	1002.	2763.	1384.	275.	409.	250.	464.	2967.	3712.	28.918	19.783
360.	488.	2149.	524.	748.	2457.	919.	998.	2775.	1385.	260.	395.	250.	466.	3038.	3728.	28.922	19.786
370.	494.	2153.	532.	754.	2467.	930.	999.	2785.	1391.	260.	398.	245.	461.	3062.	3763.	28.925	19.789
380.	500.	2166.	541.	760.	2473.	940.	995.	2762.	1374.	260.	398.	235.	434.	3069.	3694.	28.929	19.792
390.	510.	2178.	555.	760.	2479.	942.	1000.	2738.	1369.	250.	387.	240.	427.	3096.	3558.	28.932	19.795
400.	520.	2190.	569.	765.	2486.	951.	1000.	2715.	1357.	245.	381.	235.	407.	3118.	3455.	28.936	19.798
410.	525.	2200.	578.	780.	2492.	972.	1045.	2695.	1408.	255.	394.	265.	436.	3090.	3291.	28.940	19.801
420.	540.	2178.	588.	795.	2495.	992.	1060.	2740.	1452.	255.	404.	265.	460.	3169.	3472.	28.943	19.804
430.	540.	2156.	582.	800.	2498.	999.	1070.	2785.	1490.	260.	417.	270.	491.	3208.	3637.	28.947	19.808
440.	555.	2133.	592.	810.	2501.	1013.	1090.	2830.	1543.	255.	421.	280.	530.	3302.	3786.	28.950	19.811
450.	570.	2111.	602.	840.	2505.	1052.	1130.	2876.	1625.	270.	450.	290.	573.	3333.	3952.	28.954	19.814
460.	575.	2089.	601.	870.	2508.	1091.	1160.	2921.	1694.	295.	490.	290.	603.	3322.	4159.	28.958	19.817
470.	580.	2066.	599.	895.	2511.	1124.	1200.	2966.	1780.	315.	524.	305.	656.	3333.	4302.	28.961	19.820

Abbreviations:

S.P. = Shot point number.

T(1) = Two-way time in ms. to the top of horizon 1.

V(1) = Dix average velocity for horizon 1 in m/s.

D(1) = Depth for horizon 1 in meter.

T(2) = Two-way time in ms. to the top of horizon 2.

V(2) = Dix average velocity for horizon 2 in m/s.

D(2) = Depth for horizon 2 in meter.

T(3) = Two-way time in ms. to the top of horizon 3.

V(3) = Dix average velocity for horizon 3 in m/s.

D(3) = Depth for horizon 3 in meter.

dT1 = Difference in time between horizon 2 and horizon 1.

dD1 = Difference in depth between horizon 2 and horizon 1.

dT2 = Difference in time between horizon 3 and horizon 2.

dD2 = Difference in depth between horizon 3 and horizon 2.

LAT. = Latitude of corresponding shot point.

LONG. = Longitude of corresponding shot point.

Horizon 1 = Sheghega Formation.

Horizon 2 = Domran Formation.

Horizon 3 = Ruaga Formation.

IV21 = Interval velocity for She. Formation.

IV32 = Interval velocity for Dom. Formation.

Table 4.3k Results of calculation for seismic line 6V260-85

S.P.	T(1)	V(1)	D(1)	T(2)	V(2)	D(2)	T(3)	V(3)	D(3)	dT1	dD1	dT2	dD2	IV21	IV32	LAT.	LONG.
260.	455.	2165.	492.	720.	2435.	877.	980.	2739.	1342.	265.	384.	260.	465.	2906.	3577.	28.922	19.718
270.	460.	2152.	495.	720.	2447.	881.	960.	2735.	1313.	260.	386.	240.	432.	2969.	3600.	28.919	19.722
280.	460.	2139.	492.	720.	2459.	885.	960.	2731.	1311.	260.	393.	240.	426.	3023.	3550.	28.917	19.726
290.	450.	2125.	478.	715.	2470.	883.	960.	2728.	1309.	265.	405.	245.	426.	3057.	3478.	28.914	19.730
300.	450.	2112.	475.	710.	2482.	881.	950.	2724.	1294.	260.	406.	240.	413.	3123.	3442.	28.911	19.734
310.	450.	2099.	472.	710.	2493.	885.	940.	2720.	1278.	260.	413.	230.	393.	3177.	3417.	28.908	19.738
320.	450.	2097.	472.	705.	2492.	878.	935.	2720.	1272.	255.	406.	230.	394.	3184.	3426.	28.905	19.741
330.	445.	2105.	468.	705.	2479.	874.	940.	2724.	1280.	260.	406.	235.	406.	3123.	3455.	28.902	19.745
340.	440.	2113.	465.	705.	2467.	870.	950.	2727.	1295.	265.	405.	245.	426.	3057.	3469.	28.899	19.749
350.	440.	2121.	467.	700.	2455.	859.	960.	2730.	1311.	260.	393.	260.	451.	3015.	3477.	28.896	19.753
360.	440.	2123.	467.	700.	2459.	861.	960.	2726.	1308.	260.	393.	260.	448.	3031.	3438.	28.894	19.757
370.	440.	2122.	467.	700.	2476.	867.	955.	2715.	1296.	260.	400.	255.	430.	3077.	3365.	28.891	19.761
380.	435.	2120.	461.	700.	2494.	873.	950.	2704.	1284.	265.	412.	250.	412.	3109.	3288.	28.888	19.765
390.	435.	2119.	461.	700.	2511.	879.	950.	2693.	1279.	265.	418.	250.	400.	3155.	3200.	28.885	19.769
400.	440.	2119.	466.	705.	2504.	883.	945.	2683.	1268.	265.	416.	240.	385.	3147.	3208.	28.882	19.773
410.	430.	2121.	456.	700.	2476.	867.	950.	2674.	1270.	270.	411.	250.	404.	3044.	3224.	28.879	19.777
420.	440.	2122.	467.	705.	2449.	863.	965.	2666.	1286.	265.	396.	260.	423.	2989.	3254.	28.876	19.781
430.	430.	2124.	457.	700.	2421.	847.	960.	2657.	1275.	270.	391.	260.	428.	2889.	3292.	28.873	19.785
440.	435.	2123.	462.	700.	2406.	842.	955.	2656.	1268.	265.	380.	255.	426.	2868.	3341.	28.871	19.789
450.	440.	2118.	466.	710.	2406.	854.	960.	2665.	1279.	270.	388.	250.	425.	2874.	3400.	28.868	19.793
460.	450.	2113.	475.	710.	2406.	854.	970.	2674.	1297.	260.	379.	260.	443.	2915.	3408.	28.865	19.797
470.	445.	2108.	469.	715.	2406.	860.	985.	2683.	1321.	270.	391.	270.	461.	2896.	3415.	28.862	19.801
480.	460.	2109.	485.	725.	2411.	874.	990.	2691.	1332.	265.	389.	265.	458.	2936.	3457.	28.859	19.805
490.	460.	2115.	486.	730.	2420.	883.	995.	2699.	1343.	270.	397.	265.	460.	2941.	3472.	28.856	19.808
500.	465.	2121.	493.	735.	2428.	892.	1000.	2707.	1354.	270.	399.	265.	461.	2956.	3487.	28.853	19.812
510.	465.	2127.	495.	730.	2436.	889.	1005.	2715.	1364.	265.	395.	275.	475.	2974.	3455.	28.850	19.816
520.	460.	2134.	491.	720.	2440.	879.	990.	2719.	1346.	260.	388.	270.	467.	2985.	3459.	28.847	19.820
530.	455.	2140.	487.	725.	2440.	885.	975.	2719.	1326.	270.	398.	250.	441.	2948.	3528.	28.845	19.824
540.	455.	2146.	488.	720.	2440.	879.	980.	2719.	1332.	265.	390.	260.	454.	2951.	3485.	28.842	19.828
550.	460.	2152.	495.	720.	2441.	879.	985.	2719.	1339.	260.	384.	265.	461.	2954.	3472.	28.839	19.832
560.	460.	2147.	494.	730.	2432.	888.	990.	2713.	1343.	270.	394.	260.	456.	2919.	3500.	28.836	19.836
570.	455.	2134.	485.	730.	2415.	882.	990.	2703.	1338.	275.	396.	260.	456.	2887.	3508.	28.833	19.840
580.	440.	2120.	466.	720.	2399.	863.	990.	2692.	1332.	280.	397.	270.	469.	2836.	3474.	28.830	19.844
590.	450.	2107.	474.	725.	2382.	864.	990.	2681.	1327.	275.	390.	265.	464.	2836.	3494.	28.827	19.848
600.	440.	2088.	459.	725.	2362.	856.	985.	2667.	1313.	285.	397.	260.	457.	2786.	3515.	28.824	19.852
610.	440.	2065.	454.	725.	2338.	847.	980.	2650.	1298.	285.	393.	255.	451.	2758.	3537.	28.822	19.856
620.	440.	2042.	449.	725.	2314.	839.	980.	2633.	1290.	285.	390.	255.	451.	2737.	3537.	28.819	19.860
630.	440.	2019.	444.	720.	2290.	824.	990.	2616.	1295.	280.	380.	270.	471.	2714.	3489.	28.816	19.864
640.	450.	2021.	455.	730.	2294.	837.	990.	2620.	1297.	280.	382.	260.	460.	2729.	3538.	28.813	19.868
650.	455.	2044.	465.	730.	2320.	847.	995.	2641.	1314.	275.	382.	265.	467.	2778.	3525.	28.810	19.871
660.	455.	2066.	470.	735.	2346.	862.	1010.	2661.	1344.	280.	392.	275.	482.	2800.	3505.	28.807	19.875
670.	455.	2088.	475.	735.	2372.	872.	1005.	2682.	1348.	280.	397.	270.	476.	2836.	3526.	28.804	19.879
680.	460.	2111.	485.	740.	2398.	887.	995.	2703.	1345.	280.	402.	255.	457.	2871.	3592.	28.801	19.883
690.	455.	2133.	485.	730.	2424.	885.	995.	2724.	1355.	275.	400.	265.	470.	2909.	3547.	28.799	19.887
700.	455.	2155.	490.	735.	2450.	900.	1005.	2744.	1379.	280.	410.	270.	479.	2929.	3548.	28.796	19.891

S.P. = Shot point number.

T(1) = Two-way time in ms. to the top of horizon 1.

V(1) = Dix average velocity for horizon 1 in m/s.

D(1) = Depth for horizon 1 in meter .

T(2) = Two-way time in ms. to the top of horizon 2.

V(2) = Dix average velocity for horizon 2 in m/s.

D(2) = Depth for horizon 2 in meter .

T(3) = Two-way time in ms. to the top of horizon 3.

V(3) = Dix average velocity for horizon 3 in m/s.

D(3) = Depth for horizon 3 in meter.

dT1 = Difference in time between horizon 2 and horizon 1.

dD1 = Difference in depth between horizon 2 and horizon 1.

dT2 = Difference in time between horizon 3 and horizon 2.

dD2 = Difference in depth between horizon 3 and horizon 2.

LAT. = Latitude of corresponding shot point.

LONG. = Longitude of corresponding shot point.

Horizon 1 = Sheghega Formation.

Horizon 2 = Domran Formation.

Horizon 3 = Ruaga Formation.

IV21 = Interval velocity for She. Formation.

IV32 = Interval velocity for Dom. Formation.

Table 4.31 Results of calculation for seismic line 6V261-85

S.P.	T(1)	V(1)	D(1)	T(2)	V(2)	D(2)	T(3)	V(3)	D(3)	dT1	dD1	dT2	dD2	IV21	IV32	LAT.	LONG.
110.	460.	2176.	500.	725.	2537.	920.	1010.	2904.	1467.	265.	419.	285.	547.	3170.	3839.	28.826	19.725
120.	450.	2171.	489.	720.	2529.	910.	980.	2887.	1415.	270.	422.	260.	504.	3119.	3885.	28.829	19.728
130.	450.	2167.	487.	710.	2521.	895.	970.	2869.	1392.	260.	407.	260.	497.	3138.	3823.	28.833	19.731
140.	450.	2162.	486.	710.	2512.	892.	955.	2852.	1362.	260.	405.	245.	470.	3123.	3837.	28.836	19.734
150.	450.	2157.	485.	700.	2504.	876.	915.	2835.	1297.	250.	391.	215.	421.	3128.	3916.	28.840	19.737
160.	435.	2152.	468.	700.	2495.	873.	930.	2818.	1310.	265.	405.	230.	437.	3057.	3800.	28.843	19.740
170.	430.	2147.	462.	700.	2487.	870.	950.	2800.	1330.	270.	409.	250.	460.	3022.	3680.	28.847	19.743
180.	435.	2140.	466.	705.	2474.	872.	960.	2783.	1336.	270.	406.	255.	464.	3007.	3639.	28.851	19.746
190.	425.	2130.	453.	700.	2455.	859.	955.	2765.	1320.	275.	407.	255.	461.	2953.	3616.	28.854	19.750
200.	410.	2120.	435.	700.	2437.	853.	950.	2747.	1305.	290.	418.	250.	452.	2883.	3616.	28.858	19.753
210.	415.	2111.	438.	700.	2418.	846.	955.	2729.	1303.	285.	408.	255.	457.	2863.	3584.	28.861	19.756
220.	425.	2104.	447.	700.	2404.	842.	950.	2721.	1292.	275.	394.	250.	451.	2873.	3600.	28.865	19.759
230.	430.	2103.	452.	710.	2396.	850.	955.	2724.	1300.	280.	398.	245.	450.	2843.	3673.	28.869	19.762
240.	440.	2101.	462.	715.	2387.	853.	965.	2726.	1316.	275.	391.	250.	462.	2844.	3704.	28.872	19.765
250.	445.	2099.	467.	710.	2378.	844.	970.	2729.	1324.	265.	377.	260.	480.	2845.	3692.	28.876	19.768
260.	440.	2114.	465.	700.	2384.	834.	960.	2730.	1310.	260.	370.	260.	476.	2838.	3662.	28.879	19.771
270.	440.	2147.	472.	705.	2408.	849.	940.	2728.	1282.	265.	376.	235.	433.	2845.	3685.	28.883	19.774
280.	440.	2181.	480.	710.	2432.	863.	950.	2725.	1295.	270.	384.	240.	431.	2837.	3600.	28.886	19.777
290.	450.	2214.	498.	720.	2455.	884.	970.	2723.	1321.	270.	386.	250.	437.	2859.	3496.	28.890	19.781
300.	460.	2223.	511.	730.	2465.	900.	985.	2721.	1340.	270.	389.	255.	440.	2881.	3451.	28.894	19.784
310.	470.	2201.	517.	745.	2458.	916.	990.	2720.	1347.	275.	398.	245.	431.	2902.	3518.	28.897	19.787
320.	480.	2180.	523.	750.	2451.	919.	995.	2719.	1353.	270.	396.	245.	434.	2933.	3543.	28.901	19.790
330.	480.	2158.	518.	750.	2444.	917.	995.	2718.	1352.	270.	399.	245.	436.	2956.	3551.	28.904	19.793
340.	480.	2140.	514.	750.	2422.	908.	995.	2706.	1346.	270.	395.	245.	438.	2919.	3576.	28.908	19.796
350.	475.	2126.	505.	755.	2381.	899.	990.	2678.	1326.	280.	394.	235.	427.	2814.	3634.	28.912	19.799
360.	475.	2111.	501.	750.	2340.	877.	985.	2651.	1306.	275.	376.	235.	428.	2735.	3651.	28.915	19.802
370.	480.	2097.	503.	750.	2299.	862.	990.	2624.	1299.	270.	359.	240.	437.	2659.	3642.	28.919	19.805
380.	485.	2103.	510.	750.	2308.	866.	985.	2626.	1293.	265.	356.	235.	428.	2687.	3634.	28.922	19.808
390.	495.	2133.	528.	755.	2380.	898.	970.	2662.	1291.	260.	370.	215.	393.	2846.	3656.	28.926	19.811
400.	515.	2163.	557.	770.	2451.	944.	1000.	2699.	1350.	255.	387.	230.	406.	3035.	3530.	28.929	19.815
410.	530.	2193.	581.	790.	2523.	996.	1040.	2736.	1423.	260.	415.	250.	426.	3192.	3416.	28.933	19.818
420.	540.	2224.	600.	805.	2594.	1044.	1050.	2773.	1456.	265.	444.	245.	412.	3351.	3363.	28.937	19.821
430.	550.	2254.	620.	820.	2666.	1093.	1060.	2810.	1489.	270.	473.	240.	396.	3504.	3300.	28.940	19.824

Abbreviations:

S.P. = Shot point number.
T(1) = Two-way time in ms. to the top of horizon 1.
V(1) = Dix average velocity for horizon 1 in m/s.
D(1) = Depth for horizon 1 in meter.
T(2) = Two-way time in ms. to the top of horizon 2.
V(2) = Dix average velocity for horizon 2 in m/s.
D(2) = Depth for horizon 2 in meter.
T(3) = Two-way time in ms. to the top of horizon 3.
V(3) = Dix average velocity for horizon 3 in m/s.
D(3) = Depth for horizon 3 in meter.
dT1 = Difference in time between horizon 2 and horizon 1.
dD1 = Difference in depth between horizon 2 and horizon 1.
dT2 = Difference in time between horizon 3 and horizon 2.
dD2 = Difference in depth between horizon 3 and horizon 2.
LAT. = Latitude of corresponding shot point.
LONG. = Longitude of corresponding shot point.

Horizon 1 = Sheghega Formation.
Horizon 2 = Domran Formation.
Horizon 3 = Ruaga Formation.

IV21 = Interval velocity for She. Formation.
IV32 = Interval velocity for Dom. Formation.

Table 4.3m Results of calculation for seismic line 6V262-85

S.P.	T(1)	V(1)	D(1)	T(2)	V(2)	D(2)	T(3)	V(3)	D(3)	dT1	dD1	dT2	dD2	IV21	IV32	LAT.	LONG.
110.	445.	2194.	488.	720.	2558.	921.	1005.	2739.	1376.	275.	433.	285.	455.	3149.	3193.	28.931	19.687
120.	460.	2180.	501.	725.	2562.	929.	995.	2735.	1361.	265.	427.	270.	432.	3230.	3200.	28.928	19.691
130.	455.	2166.	493.	730.	2566.	936.	1000.	2731.	1366.	275.	444.	270.	429.	3222.	3185.	28.926	19.695
140.	460.	2153.	495.	730.	2569.	938.	1000.	2727.	1364.	270.	443.	270.	426.	3281.	3156.	28.923	19.699
150.	460.	2139.	492.	730.	2573.	939.	1005.	2724.	1369.	270.	447.	275.	429.	3311.	3127.	28.920	19.703
160.	455.	2126.	484.	740.	2577.	953.	1010.	2720.	1373.	285.	470.	270.	420.	3291.	3111.	28.917	19.707
170.	455.	2123.	483.	730.	2570.	938.	1010.	2723.	1375.	275.	455.	280.	437.	3309.	3121.	28.914	19.711
180.	450.	2133.	480.	725.	2551.	925.	1000.	2735.	1368.	275.	445.	275.	443.	3236.	3222.	28.911	19.715
190.	450.	2143.	482.	720.	2533.	912.	980.	2747.	1346.	270.	429.	260.	434.	3185.	3338.	28.908	19.718
200.	440.	2154.	474.	705.	2514.	886.	970.	2759.	1338.	265.	412.	265.	452.	3109.	3411.	28.905	19.722
210.	440.	2156.	474.	700.	2503.	876.	950.	2758.	1310.	260.	402.	250.	434.	3092.	3472.	28.903	19.726
220.	435.	2149.	467.	700.	2502.	876.	945.	2739.	1294.	265.	408.	245.	418.	3087.	3412.	28.900	19.730
230.	430.	2142.	460.	700.	2502.	876.	960.	2721.	1306.	270.	415.	260.	430.	3081.	3308.	28.897	19.734
240.	435.	2135.	464.	700.	2501.	875.	970.	2703.	1311.	265.	411.	270.	435.	3102.	3230.	28.894	19.738
250.	440.	2127.	468.	705.	2498.	881.	965.	2696.	1301.	265.	413.	260.	420.	3117.	3231.	28.891	19.742
260.	440.	2117.	466.	710.	2492.	884.	980.	2705.	1326.	270.	419.	270.	441.	3096.	3274.	28.888	19.746
270.	435.	2108.	459.	710.	2485.	882.	970.	2714.	1316.	275.	424.	260.	434.	3076.	3338.	28.885	19.750
280.	440.	2099.	462.	710.	2478.	880.	970.	2723.	1321.	270.	418.	260.	441.	3096.	3392.	28.882	19.754
290.	440.	2099.	462.	710.	2478.	880.	960.	2730.	1310.	270.	418.	250.	431.	3096.	3440.	28.880	19.758
300.	445.	2111.	470.	710.	2484.	882.	965.	2736.	1320.	265.	412.	255.	438.	3109.	3435.	28.877	19.762
310.	450.	2122.	478.	715.	2491.	891.	970.	2741.	1329.	265.	413.	255.	439.	3117.	3435.	28.874	19.766
320.	450.	2134.	480.	720.	2498.	899.	975.	2747.	1339.	270.	419.	255.	440.	3104.	3451.	28.871	19.770
330.	440.	2151.	473.	720.	2508.	903.	965.	2750.	1327.	280.	430.	245.	424.	3071.	3461.	28.868	19.774
340.	440.	2173.	478.	710.	2522.	895.	955.	2749.	1313.	270.	417.	245.	418.	3089.	3412.	28.865	19.777
350.	425.	2196.	467.	705.	2537.	894.	940.	2749.	1292.	280.	428.	235.	398.	3050.	3387.	28.862	19.781
360.	425.	2219.	472.	700.	2551.	893.	940.	2749.	1292.	275.	421.	240.	399.	3062.	3325.	28.859	19.785
370.	425.	2216.	471.	700.	2546.	891.	950.	2748.	1305.	275.	420.	250.	414.	3055.	3312.	28.856	19.789
380.	420.	2181.	458.	705.	2517.	887.	950.	2745.	1304.	285.	430.	245.	417.	3011.	3404.	28.854	19.793
390.	420.	2145.	451.	710.	2489.	884.	960.	2743.	1316.	290.	433.	250.	433.	2986.	3456.	28.851	19.797
400.	425.	2110.	448.	715.	2460.	880.	960.	2740.	1315.	290.	431.	245.	436.	2979.	3551.	28.848	19.801
410.	430.	2099.	451.	710.	2450.	870.	965.	2735.	1320.	280.	418.	255.	450.	2993.	3529.	28.845	19.805
420.	450.	2118.	477.	730.	2461.	898.	980.	2728.	1337.	280.	422.	250.	438.	3007.	3512.	28.842	19.809
430.	455.	2136.	486.	730.	2473.	903.	990.	2722.	1347.	275.	417.	260.	444.	3033.	3415.	28.839	19.813
440.	455.	2155.	490.	730.	2485.	907.	980.	2715.	1330.	275.	417.	250.	423.	3033.	3384.	28.836	19.817
450.	450.	2161.	486.	725.	2491.	903.	970.	2712.	1315.	275.	417.	245.	412.	3033.	3363.	28.833	19.821
460.	450.	2153.	485.	730.	2490.	909.	975.	2714.	1323.	280.	424.	245.	415.	3029.	3380.	28.831	19.825
470.	450.	2146.	483.	730.	2488.	908.	980.	2717.	1331.	280.	426.	250.	423.	3036.	3384.	28.828	19.829
480.	440.	2138.	470.	730.	2487.	908.	990.	2719.	1346.	290.	438.	260.	438.	3021.	3369.	28.825	19.832
490.	450.	2137.	481.	730.	2486.	907.	985.	2724.	1342.	280.	427.	255.	434.	3043.	3412.	28.822	19.836
500.	450.	2143.	482.	730.	2486.	907.	980.	2732.	1339.	280.	425.	250.	431.	3036.	3456.	28.819	19.840
510.	445.	2150.	478.	730.	2485.	907.	985.	2740.	1349.	285.	429.	255.	442.	3011.	3467.	28.816	19.844
520.	440.	2157.	475.	730.	2484.	907.	985.	2748.	1353.	290.	432.	255.	447.	2979.	3498.	28.813	19.848
530.	450.	2164.	487.	730.	2484.	907.	990.	2756.	1364.	280.	420.	260.	458.	3000.	3515.	28.810	19.852
540.	450.	2171.	488.	730.	2483.	906.	990.	2764.	1368.	280.	418.	260.	462.	2986.	3554.	28.808	19.856
550.	450.	2178.	490.	730.	2483.	906.	990.	2772.	1372.	280.	416.	260.	466.	2971.	3585.	28.805	19.860

S.P. = Shot point number.

T(1) = Two-way time in ms. to the top of horizon 1.

V(1) = Dix average velocity for horizon 1 in m/s.

D(1) = Depth for horizon 1 in meter .

T(2) = Two-way time in ms. to the top of horizon 2.

V(2) = Dix average velocity for horizon 2 in m/s.

D(2) = Depth for horizon 2 in meter .

T(3) = Two-way time in ms. to the top of horizon 3.

V(3) = Dix average velocity for horizon 3 in m/s.

D(3) = Depth for horizon 3 in meter.

dT1 = Difference in time between horizon 2 and horizon 1.

dD1 = Difference in depth between horizon 2 and horizon 1.

dT2 = Difference in time between horizon 3 and horizon 2.

dD2 = Difference in depth between horizon 3 and horizon 2.

LAT. = Latitude of corresponding shot point.

LONG. = Longitude of corresponding shot point.

Horizon 1 = Sheghega Formation.

Horizon 2 = Domran Formation.

Horizon 3 = Ruaga Formation.

IV21 = Interval velocity for She. Formation.

IV32 = Interval velocity for Dom. Formation.

Table 4.3n Results of calculation for seismic line 6V263-85

S.P.	T(1)	V(1)	D(1)	T(2)	V(2)	D(2)	T(3)	V(3)	D(3)	dT1	dD1	dT2	dD2	IV21	IV32	LAT.	LONG.
110.	500.	2153.	538.	790.	2664.	1052.	1110.	2912.	1616.	290.	514.	320.	564.	3545.	3525.	28.805	19.735
120.	490.	2136.	523.	770.	2622.	1009.	1090.	2877.	1568.	280.	486.	320.	559.	3471.	3494.	28.808	19.738
130.	470.	2118.	498.	750.	2579.	967.	1040.	2842.	1478.	280.	470.	290.	511.	3350.	3524.	28.812	19.741
140.	460.	2100.	483.	730.	2537.	926.	1005.	2807.	1410.	270.	443.	275.	485.	3281.	3520.	28.815	19.744
150.	450.	2082.	468.	710.	2494.	885.	980.	2772.	1358.	260.	417.	270.	473.	3208.	3504.	28.819	19.747
160.	440.	2064.	454.	700.	2452.	858.	970.	2737.	1327.	260.	404.	270.	469.	3108.	3474.	28.822	19.751
170.	440.	2059.	453.	690.	2437.	841.	925.	2718.	1257.	250.	388.	235.	416.	3104.	3540.	28.826	19.754
180.	430.	2065.	444.	685.	2446.	838.	920.	2714.	1248.	255.	394.	235.	410.	3090.	3489.	28.829	19.757
190.	420.	2070.	435.	680.	2455.	835.	920.	2709.	1246.	260.	400.	240.	412.	3077.	3425.	28.833	19.760
200.	420.	2076.	436.	690.	2464.	850.	920.	2705.	1244.	270.	414.	230.	394.	3067.	3426.	28.837	19.763
210.	415.	2085.	433.	695.	2480.	862.	930.	2704.	1257.	280.	429.	235.	396.	3064.	3362.	28.840	19.766
220.	415.	2104.	436.	695.	2513.	873.	930.	2714.	1262.	280.	437.	235.	389.	3121.	3311.	28.844	19.770
230.	418.	2122.	443.	703.	2546.	895.	938.	2724.	1277.	285.	452.	235.	382.	3172.	3251.	28.847	19.773
240.	426.	2140.	456.	706.	2580.	911.	946.	2733.	1293.	280.	455.	240.	382.	3250.	3183.	28.851	19.776
250.	430.	2153.	463.	710.	2591.	920.	950.	2737.	1300.	280.	457.	240.	380.	3264.	3167.	28.854	19.779
260.	430.	2153.	463.	705.	2550.	899.	950.	2726.	1295.	275.	436.	245.	396.	3171.	3233.	28.858	19.782
270.	430.	2152.	463.	705.	2510.	885.	950.	2715.	1290.	275.	422.	245.	405.	3069.	3306.	28.861	19.785
280.	440.	2151.	473.	710.	2470.	877.	960.	2704.	1298.	270.	404.	250.	421.	2993.	3368.	28.865	19.789
290.	440.	2151.	473.	710.	2431.	863.	970.	2694.	1306.	270.	390.	260.	443.	2889.	3408.	28.868	19.792
300.	440.	2149.	473.	710.	2426.	861.	980.	2695.	1321.	270.	388.	270.	460.	2874.	3407.	28.872	19.795
310.	440.	2147.	472.	710.	2421.	859.	975.	2697.	1315.	270.	387.	265.	456.	2867.	3442.	28.875	19.798
320.	440.	2145.	472.	700.	2416.	846.	945.	2699.	1275.	260.	374.	245.	430.	2877.	3502.	28.879	19.802
330.	445.	2144.	477.	710.	2411.	856.	930.	2701.	1256.	265.	379.	220.	400.	2860.	3636.	28.882	19.805
340.	480.	2158.	518.	740.	2433.	900.	960.	2713.	1302.	260.	382.	220.	402.	2938.	3655.	28.885	19.809
350.	495.	2186.	541.	760.	2477.	941.	1000.	2734.	1367.	265.	400.	240.	426.	3019.	3550.	28.888	19.812
360.	510.	2214.	565.	780.	2521.	983.	1025.	2754.	1412.	270.	418.	245.	428.	3096.	3502.	28.892	19.816
370.	530.	2242.	594.	800.	2565.	1026.	1035.	2775.	1436.	270.	432.	235.	410.	3200.	3489.	28.895	19.819
380.	535.	2267.	606.	800.	2605.	1042.	1045.	2793.	1459.	265.	435.	245.	418.	3291.	3404.	28.898	19.823
390.	545.	2232.	608.	810.	2563.	1038.	1065.	2778.	1479.	265.	430.	255.	441.	3245.	3459.	28.901	19.826
400.	550.	2196.	604.	820.	2521.	1034.	1080.	2763.	1492.	270.	430.	260.	458.	3185.	3523.	28.904	19.830
410.	550.	2161.	594.	820.	2479.	1016.	1075.	2748.	1477.	270.	422.	255.	460.	3126.	3616.	28.908	19.833
420.	550.	2125.	584.	820.	2437.	999.	1070.	2732.	1462.	270.	415.	250.	463.	3074.	3704.	28.912	19.836
430.	560.	2129.	596.	820.	2445.	1003.	1070.	2736.	1464.	260.	406.	250.	461.	3131.	3688.	28.915	19.840
440.	561.	2142.	601.	826.	2466.	1019.	1076.	2745.	1477.	265.	418.	250.	458.	3155.	3664.	28.919	19.843
450.	568.	2156.	612.	833.	2487.	1036.	1083.	2753.	1491.	265.	424.	250.	455.	3200.	3640.	28.922	19.846
460.	560.	2169.	607.	835.	2508.	1047.	1090.	2762.	1505.	275.	440.	255.	458.	3200.	3592.	28.926	19.849
470.	565.	2182.	617.	830.	2529.	1049.	1090.	2770.	1510.	265.	433.	260.	460.	3260.	3546.	28.929	19.852
480.	560.	2196.	615.	830.	2550.	1058.	1090.	2779.	1515.	270.	443.	260.	456.	3281.	3515.	28.933	19.855
490.	560.	2209.	619.	830.	2570.	1067.	1090.	2788.	1519.	270.	448.	260.	452.	3319.	3477.	28.936	19.859

Abbreviations:

S.P. = Shot point number.
T(1) = Two-way time in ms. to the top of horizon 1.
V(1) = Dix average velocity for horizon 1 in m/s.
D(1) = Depth for horizon 1 in meter.
T(2) = Two-way time in ms. to the top of horizon 2.
V(2) = Dix average velocity for horizon 2 in m/s.
D(2) = Depth for horizon 2 in meter.
T(3) = Two-way time in ms. to the top of horizon 3.
V(3) = Dix average velocity for horizon 3 in m/s.
D(3) = Depth for horizon 3 in meter.
dT1 = Difference in time between horizon 2 and horizon 1.
dD1 = Difference in depth between horizon 2 and horizon 1.
dT2 = Difference in time between horizon 3 and horizon 2.
dD2 = Difference in depth between horizon 3 and horizon 2.
LAT. = Latitude of corresponding shot point.
LONG. = Longitude of corresponding shot point.

Horizon 1 = Sheghega Formation.
Horizon 2 = Domran Formation.
Horizon 3 = Ruaga Formation.

IV21 = Interval velocity for She. Formation.
IV32 = Interval velocity for Dom. Formation.

Table 4.3o Results of calculation for seismic line 6V264-85

S.P.	T(1)	V(1)	D(1)	T(2)	V(2)	D(2)	T(3)	V(3)	D(3)	dT1	dD1	dT2	dD2	IV21	IV32	LAT.	LONG.
100.	450.	2226.	501.	730.	2734.	998.	1000.	2831.	1416.	280.	497.	270.	418.	3550.	3096.	28.910	19.681
110.	475.	2203.	523.	725.	2682.	972.	1000.	2813.	1407.	250.	449.	275.	434.	3592.	3164.	28.908	19.685
120.	475.	2181.	518.	730.	2630.	960.	1010.	2796.	1412.	255.	442.	280.	452.	3467.	3229.	28.905	19.689
130.	470.	2159.	507.	715.	2578.	922.	1020.	2778.	1417.	245.	414.	305.	495.	3388.	3246.	28.902	19.693
140.	460.	2136.	491.	715.	2526.	903.	1005.	2760.	1387.	255.	412.	290.	484.	3231.	3338.	28.899	19.697
150.	455.	2114.	481.	710.	2474.	878.	1000.	2742.	1371.	255.	397.	290.	493.	3114.	3400.	28.896	19.701
160.	450.	2092.	471.	700.	2422.	848.	975.	2725.	1328.	250.	377.	275.	480.	3016.	3491.	28.893	19.705
170.	445.	2070.	460.	700.	2370.	830.	975.	2707.	1320.	255.	369.	275.	490.	2902.	3564.	28.890	19.709
180.	435.	2052.	446.	680.	2333.	793.	960.	2692.	1292.	245.	347.	280.	499.	2833.	3564.	28.887	19.713
190.	430.	2060.	443.	690.	2381.	822.	950.	2696.	1280.	260.	379.	260.	459.	2915.	3523.	28.885	19.717
200.	430.	2067.	445.	690.	2429.	838.	940.	2699.	1268.	260.	394.	250.	430.	3023.	3440.	28.882	19.720
210.	430.	2075.	446.	695.	2477.	861.	950.	2702.	1284.	265.	415.	255.	423.	3132.	3318.	28.879	19.724
220.	430.	2083.	448.	700.	2514.	880.	960.	2706.	1299.	270.	432.	260.	419.	3200.	3223.	28.876	19.728
230.	420.	2089.	439.	700.	2483.	869.	955.	2713.	1295.	280.	430.	255.	426.	3071.	3341.	28.873	19.732
240.	420.	2094.	440.	710.	2453.	871.	955.	2719.	1298.	290.	431.	245.	428.	2972.	3486.	28.870	19.736
250.	420.	2100.	441.	700.	2422.	848.	950.	2726.	1295.	280.	407.	250.	447.	2907.	3576.	28.867	19.740
260.	420.	2108.	443.	710.	2399.	852.	950.	2732.	1298.	290.	409.	240.	446.	2821.	3717.	28.864	19.744
270.	420.	2130.	447.	695.	2421.	841.	945.	2737.	1293.	275.	394.	250.	452.	2865.	3616.	28.862	19.748
280.	410.	2152.	441.	690.	2442.	842.	940.	2743.	1289.	280.	401.	250.	447.	2864.	3576.	28.859	19.752
290.	405.	2174.	440.	690.	2463.	850.	945.	2748.	1298.	285.	410.	255.	449.	2877.	3514.	28.856	19.756
300.	410.	2191.	449.	690.	2478.	855.	940.	2751.	1293.	280.	406.	250.	438.	2900.	3504.	28.853	19.760
310.	415.	2184.	453.	690.	2458.	848.	940.	2740.	1288.	275.	395.	250.	440.	2873.	3520.	28.850	19.764
320.	410.	2177.	446.	690.	2438.	841.	935.	2729.	1276.	280.	395.	245.	435.	2821.	3551.	28.847	19.768
330.	415.	2170.	450.	690.	2418.	834.	940.	2719.	1278.	275.	384.	250.	443.	2793.	3552.	28.844	19.772
340.	425.	2164.	460.	700.	2405.	842.	945.	2713.	1282.	275.	382.	245.	440.	2778.	3592.	28.842	19.776
350.	425.	2163.	460.	700.	2428.	850.	960.	2733.	1312.	275.	390.	260.	462.	2836.	3554.	28.839	19.780
360.	435.	2162.	470.	710.	2451.	870.	970.	2752.	1335.	275.	400.	260.	465.	2909.	3577.	28.836	19.784
370.	430.	2162.	465.	710.	2474.	878.	970.	2772.	1345.	280.	414.	260.	466.	2950.	3592.	28.833	19.787
380.	425.	2164.	460.	710.	2493.	885.	970.	2787.	1352.	285.	425.	260.	467.	2982.	3592.	28.830	19.791
390.	425.	2178.	463.	700.	2490.	871.	965.	2771.	1337.	275.	408.	265.	466.	2967.	3517.	28.827	19.795
400.	430.	2193.	472.	700.	2486.	870.	965.	2756.	1330.	270.	398.	265.	460.	2948.	3472.	28.824	19.799
410.	435.	2208.	480.	700.	2482.	869.	970.	2740.	1329.	265.	389.	270.	460.	2936.	3407.	28.821	19.803
420.	440.	2219.	488.	710.	2482.	881.	990.	2727.	1350.	270.	393.	280.	468.	2911.	3350.	28.819	19.807
430.	445.	2209.	491.	730.	2503.	913.	990.	2727.	1350.	285.	422.	260.	436.	2961.	3362.	28.816	19.811
440.	455.	2198.	500.	730.	2523.	921.	975.	2727.	1329.	275.	421.	245.	408.	3062.	3331.	28.813	19.815
450.	450.	2188.	492.	710.	2543.	903.	970.	2727.	1323.	260.	410.	260.	420.	3162.	3231.	28.810	19.819
460.	440.	2180.	480.	730.	2559.	934.	980.	2727.	1336.	290.	454.	250.	402.	3131.	3216.	28.807	19.823
470.	450.	2181.	491.	720.	2550.	918.	970.	2725.	1322.	270.	427.	250.	404.	3163.	3232.	28.804	19.827
480.	450.	2183.	491.	715.	2541.	908.	970.	2724.	1321.	265.	417.	255.	413.	3147.	3239.	28.801	19.831
490.	440.	2185.	481.	710.	2532.	899.	960.	2722.	1307.	270.	418.	250.	408.	3096.	3264.	28.798	19.835
500.	440.	2186.	481.	710.	2523.	896.	960.	2721.	1306.	270.	415.	250.	410.	3074.	3280.	28.796	19.839

Abbreviations:

S.P. = Shot point number.
T(1) = Two-way time in ms. to the top of horizon 1.
V(1) = Dix average velocity for horizon 1 in m/s.
D(1) = Depth for horizon 1 in meter.
T(2) = Two-way time in ms. to the top of horizon 2.
V(2) = Dix average velocity for horizon 2 in m/s.
D(2) = Depth for horizon 2 in meter.
T(3) = Two-way time in ms. to the top of horizon 3.
V(3) = Dix average velocity for horizon 3 in m/s.
D(3) = Depth for horizon 3 in meter.
dT1 = Difference in time between horizon 2 and horizon 1.
dD1 = Difference in depth between horizon 2 and horizon 1.
dT2 = Difference in time between horizon 3 and horizon 2.
dD2 = Difference in depth between horizon 3 and horizon 2.
LAT. = Latitude of corresponding shot point.
LONG. = Longitude of corresponding shot point.

Horizon 1 = Sheghega Formation.
Horizon 2 = Domran Formation.
Horizon 3 = Ruaga Formation.

IV21 = Interval velocity for She. Formation.
IV32 = Interval velocity for Dom. Formation.

Table 4.3p Results of calculation for seismic line 6V265-85

S.P.	T(1)	V(1)	D(1)	T(2)	V(2)	D(2)	T(3)	V(3)	D(3)	dT1	dD1	dT2	dD2	IV21	IV32	LAT.	LONG.
100.	485.	2153.	522.	765.	2453.	938.	1095.	2970.	1626.	280.	416.	330.	688.	2971.	4170.	28.799	19.752
110.	480.	2132.	512.	760.	2471.	939.	1050.	2896.	1520.	280.	427.	290.	581.	3050.	4007.	28.803	19.755
120.	460.	2111.	485.	720.	2489.	896.	1000.	2822.	1411.	260.	410.	280.	515.	3162.	3679.	28.806	19.758
130.	450.	2089.	470.	705.	2506.	883.	980.	2748.	1346.	255.	413.	275.	463.	3239.	3367.	28.810	19.761
140.	450.	2080.	468.	710.	2523.	896.	950.	2718.	1291.	260.	428.	240.	395.	3292.	3292.	28.813	19.765
150.	450.	2084.	469.	705.	2538.	895.	955.	2742.	1309.	255.	426.	250.	415.	3341.	3312.	28.817	19.768
160.	445.	2086.	464.	705.	2541.	896.	960.	2742.	1316.	260.	431.	255.	421.	3323.	3294.	28.820	19.771
170.	445.	2088.	465.	715.	2542.	909.	960.	2741.	1316.	270.	444.	245.	407.	3289.	3322.	28.824	19.774
180.	445.	2090.	465.	725.	2544.	922.	975.	2740.	1336.	280.	457.	250.	414.	3264.	3312.	28.827	19.777
190.	440.	2092.	460.	720.	2545.	916.	975.	2739.	1335.	280.	456.	255.	419.	3257.	3286.	28.831	19.780
200.	445.	2100.	467.	720.	2546.	916.	975.	2733.	1332.	275.	449.	255.	416.	3265.	3263.	28.834	19.784
210.	430.	2108.	453.	720.	2546.	916.	975.	2726.	1329.	290.	463.	255.	413.	3193.	3239.	28.838	19.787
220.	425.	2117.	450.	720.	2546.	916.	970.	2720.	1319.	295.	467.	250.	403.	3159.	3224.	28.841	19.790
230.	420.	2125.	446.	710.	2546.	904.	965.	2714.	1309.	290.	457.	255.	406.	3159.	3176.	28.845	19.793
240.	425.	2134.	453.	710.	2546.	904.	965.	2707.	1306.	285.	450.	255.	402.	3165.	3153.	28.849	19.796
250.	435.	2119.	461.	710.	2531.	898.	970.	2717.	1318.	275.	437.	260.	419.	3178.	3231.	28.852	19.799
260.	440.	2104.	463.	720.	2514.	905.	980.	2727.	1336.	280.	442.	260.	431.	3157.	3315.	28.856	19.802
270.	450.	2088.	470.	730.	2498.	912.	995.	2737.	1361.	280.	442.	265.	450.	3157.	3389.	28.859	19.806
280.	460.	2073.	477.	735.	2482.	912.	1010.	2747.	1387.	275.	436.	275.	475.	3164.	3455.	28.863	19.809
290.	470.	2084.	490.	740.	2480.	918.	1020.	2729.	1392.	270.	428.	280.	474.	3170.	3386.	28.866	19.812
300.	465.	2096.	487.	740.	2479.	917.	1020.	2709.	1382.	275.	430.	280.	465.	3127.	3321.	28.870	19.815
310.	460.	2109.	485.	740.	2477.	916.	1015.	2690.	1365.	280.	432.	275.	449.	3079.	3265.	28.873	19.818
320.	475.	2121.	504.	750.	2476.	928.	1020.	2670.	1362.	275.	424.	270.	434.	3084.	3215.	28.877	19.821
330.	490.	2130.	522.	760.	2498.	949.	1025.	2689.	1378.	270.	428.	265.	429.	3163.	3238.	28.880	19.825
340.	510.	2138.	545.	780.	2522.	984.	1050.	2710.	1423.	270.	438.	270.	439.	3252.	3252.	28.884	19.828
350.	515.	2147.	553.	790.	2547.	1006.	1050.	2731.	1434.	275.	453.	260.	428.	3295.	3292.	28.887	19.831
360.	525.	2156.	566.	800.	2571.	1028.	1055.	2752.	1452.	275.	462.	255.	423.	3360.	3325.	28.891	19.834
370.	525.	2161.	567.	800.	2556.	1022.	1060.	2752.	1459.	275.	455.	260.	436.	3309.	3362.	28.894	19.837
380.	540.	2167.	585.	805.	2539.	1022.	1060.	2752.	1459.	265.	437.	255.	437.	3298.	3427.	28.898	19.840
390.	550.	2173.	598.	815.	2521.	1028.	1070.	2752.	1472.	265.	430.	255.	445.	3245.	3482.	28.902	19.844
400.	560.	2179.	610.	830.	2504.	1039.	1080.	2751.	1486.	270.	429.	250.	446.	3178.	3576.	28.905	19.847
410.	555.	2184.	606.	825.	2487.	1026.	1090.	2751.	1499.	270.	420.	265.	473.	3111.	3570.	28.909	19.850
420.	555.	2190.	608.	825.	2470.	1019.	1090.	2751.	1499.	270.	411.	265.	480.	3044.	3623.	28.912	19.853

Abbreviations:

S.P. = Shot point number.
T(1) = Two-way time in ms. to the top of horizon 1.
V(1) = Dix average velocity for horizon 1 in m/s.
D(1) = Depth for horizon 1 in meter .
T(2) = Two-way time in ms. to the top of horizon 2.
V(2) = Dix average velocity for horizon 2 in m/s.
D(2) = Depth for horizon 2 in meter .
T(3) = Two-way time in ms. to the top of horizon 3.
V(3) = Dix average velocity for horizon 3 in m/s.
D(3) = Depth for horizon 3 in meter.
dT1 = Difference in time between horizon 2 and horizon 1.
dD1 = Difference in depth between horizon 2 and horizon 1.
dT2 = Difference in time between horizon 3 and horizon 2.
dD2 = Difference in depth between horizon 3 and horizon 2.
LAT. = Latitude of corresponding shot point.
LONG. = Longitude of corresponding shot point.

Horizon 1 = Sheghega Formation.
Horizon 2 = Domran Formation.
Horizon 3 = Ruaga Formation.

IV21 = Interval velocity for She. Formation.
IV32 = Interval velocity for Dom. Formation.

Table 4.3q Results of calculation for seismic line 6V301-85

S.P.	T(1)	V(1)	D(1)	T(2)	V(2)	D(2)	T(3)	V(3)	D(3)	dT1	dD1	dT2	dD2	IV21	IV32	LAT.	LONG.
100.	490.	2144.	525.	735.	2466.	906.	1025.	2726.	1397.	245.	381.	290.	491.	3110.	3386.	28.806	19.747
110.	470.	2142.	503.	730.	2482.	906.	1010.	2738.	1383.	260.	402.	280.	477.	3100.	3407.	28.810	19.750
120.	460.	2141.	492.	720.	2497.	899.	985.	2749.	1354.	260.	406.	265.	455.	3131.	3434.	28.814	19.753
130.	455.	2139.	487.	710.	2512.	892.	980.	2761.	1353.	255.	405.	270.	461.	3176.	3415.	28.817	19.756
140.	445.	2137.	476.	700.	2527.	885.	940.	2773.	1303.	255.	409.	240.	418.	3208.	3483.	28.821	19.759
150.	435.	2136.	465.	690.	2543.	877.	930.	2784.	1295.	255.	413.	240.	417.	3231.	3483.	28.824	19.762
160.	425.	2134.	454.	690.	2558.	882.	940.	2796.	1314.	265.	429.	250.	432.	3230.	3456.	28.828	19.766
170.	430.	2134.	459.	700.	2559.	896.	950.	2790.	1325.	270.	437.	250.	430.	3237.	3432.	28.831	19.769
180.	430.	2135.	459.	705.	2549.	898.	950.	2770.	1316.	275.	439.	245.	417.	3193.	3412.	28.835	19.772
190.	430.	2137.	459.	710.	2539.	901.	955.	2750.	1313.	280.	442.	245.	412.	3157.	3363.	28.838	19.775
200.	435.	2138.	465.	710.	2529.	898.	950.	2731.	1297.	275.	433.	240.	399.	3149.	3325.	28.842	19.778
210.	435.	2131.	464.	715.	2519.	901.	960.	2724.	1307.	280.	437.	245.	407.	3121.	3314.	28.845	19.781
220.	435.	2118.	461.	715.	2511.	898.	955.	2727.	1302.	280.	437.	240.	404.	3121.	3367.	28.849	19.785
230.	435.	2105.	458.	715.	2502.	895.	955.	2730.	1304.	280.	437.	240.	409.	3121.	3408.	28.852	19.788
240.	430.	2092.	450.	710.	2494.	885.	950.	2733.	1298.	280.	435.	240.	413.	3107.	3442.	28.856	19.791
250.	428.	2089.	447.	713.	2480.	884.	968.	2734.	1323.	285.	437.	255.	439.	3067.	3443.	28.859	19.794
260.	435.	2093.	455.	715.	2463.	880.	980.	2733.	1339.	280.	425.	265.	459.	3036.	3464.	28.863	19.797
270.	432.	2096.	453.	717.	2445.	877.	987.	2732.	1348.	285.	424.	270.	472.	2975.	3489.	28.867	19.800
280.	450.	2100.	473.	725.	2428.	880.	1000.	2731.	1366.	275.	408.	275.	486.	2960.	3535.	28.870	19.804
290.	445.	2110.	470.	725.	2427.	880.	995.	2741.	1363.	280.	410.	270.	484.	2929.	3578.	28.874	19.807
300.	440.	2125.	467.	715.	2439.	872.	990.	2758.	1365.	275.	404.	275.	493.	2945.	3585.	28.877	19.810
310.	451.	2139.	482.	721.	2451.	884.	1001.	2775.	1389.	270.	401.	280.	505.	2978.	3607.	28.881	19.813
320.	463.	2154.	499.	743.	2464.	915.	1018.	2793.	1421.	280.	416.	275.	506.	2971.	3680.	28.884	19.816
330.	500.	2159.	540.	770.	2457.	946.	1040.	2783.	1447.	270.	406.	270.	501.	3007.	3711.	28.888	19.819
340.	525.	2155.	566.	790.	2435.	962.	1045.	2751.	1438.	265.	396.	255.	476.	2989.	3733.	28.891	19.823
350.	530.	2151.	570.	800.	2414.	965.	1060.	2720.	1442.	270.	396.	260.	476.	2926.	3669.	28.895	19.826
360.	540.	2147.	580.	810.	2392.	969.	1070.	2688.	1438.	270.	389.	260.	470.	2881.	3608.	28.898	19.829
370.	540.	2147.	580.	810.	2403.	973.	1070.	2688.	1438.	270.	393.	260.	465.	2911.	3577.	28.902	19.832
380.	550.	2151.	591.	820.	2440.	1001.	1075.	2714.	1459.	270.	409.	255.	458.	3037.	3592.	28.905	19.835
390.	550.	2154.	592.	820.	2478.	1016.	1070.	2739.	1466.	270.	424.	250.	450.	3141.	3600.	28.909	19.838
400.	560.	2158.	604.	820.	2516.	1031.	1070.	2765.	1479.	260.	427.	250.	448.	3285.	3584.	28.912	19.842
410.	555.	2160.	599.	830.	2521.	1046.	1075.	2764.	1486.	275.	447.	245.	439.	3251.	3592.	28.916	19.845
420.	560.	2161.	605.	840.	2500.	1050.	1080.	2741.	1480.	280.	445.	240.	430.	3179.	3583.	28.919	19.848
430.	565.	2162.	611.	840.	2479.	1041.	1085.	2718.	1475.	275.	430.	245.	434.	3127.	3543.	28.923	19.851
440.	570.	2163.	617.	845.	2458.	1038.	1085.	2695.	1462.	275.	422.	240.	424.	3062.	3533.	28.927	19.854
450.	575.	2165.	622.	845.	2437.	1029.	1090.	2672.	1456.	270.	407.	245.	427.	3015.	3486.	28.930	19.857
460.	580.	2166.	628.	850.	2415.	1027.	1090.	2650.	1444.	270.	398.	240.	417.	2956.	3475.	28.934	19.861
470.	590.	2167.	639.	860.	2394.	1030.	1110.	2627.	1458.	270.	390.	250.	428.	2896.	3424.	28.937	19.864
480.	600.	2168.	650.	880.	2373.	1044.	1125.	2604.	1465.	280.	394.	245.	420.	2814.	3437.	28.940	19.867
490.	615.	2169.	667.	890.	2352.	1047.	1140.	2581.	1471.	275.	380.	250.	424.	2764.	3392.	28.944	19.871

Abbreviations:

S.P. = Shot point number.

T(1) = Two-way time in ms. to the top of horizon 1.

V(1) = Dix average velocity for horizon 1 in m/s.

D(1) = Depth for horizon 1 in meter.

T(2) = Two-way time in ms. to the top of horizon 2.

V(2) = Dix average velocity for horizon 2 in m/s.

D(2) = Depth for horizon 2 in meter.

T(3) = Two-way time in ms. to the top of horizon 3.

V(3) = Dix average velocity for horizon 3 in m/s.

D(3) = Depth for horizon 3 in meter.

dT1 = Difference in time between horizon 2 and horizon 1.

dD1 = Difference in depth between horizon 2 and horizon 1.

dT2 = Difference in time between horizon 3 and horizon 2.

dD2 = Difference in depth between horizon 3 and horizon 2.

LAT. = Latitude of corresponding shot point.

LONG. = Longitude of corresponding shot point.

Horizon 1 = Sheghega Formation.

Horizon 2 = Domran Formation.

Horizon 3 = Ruaga Formation.

IV21 = Interval velocity for She. Formation.

IV32 = Interval velocity for Dom. Formation.

Table 4.4 Results of calculation from well data.

WN.	T(1)	V(1)	D(1)	T(2)	V(2)	D(2)	T(3)	V(3)	D(3)	dT1	dD1	dT2	dD2	IV21	IV32	LAT.	LONG.
C001	478.	2215.	530.	755.	2680.	1012.	992.	2914.	1445.	277.	482.	237.	433.	3485.	3661.	28.911	19.801
C003	480.	2335.	560.	758.	2779.	1054.	1007.	3058.	1540.	279.	494.	249.	486.	3545.	3907.	28.868	19.847
C004	448.	2180.	488.	733.	2745.	1006.	991.	3013.	1493.	285.	518.	257.	486.	3631.	3778.	28.807	19.811
C006	459.	2421.	555.	732.	2867.	1049.	1013.	3064.	1553.	273.	494.	282.	504.	3618.	3577.	28.939	19.697
C008	435.	2353.	512.	702.	2865.	1005.	958.	3085.	1479.	266.	493.	257.	473.	3703.	3688.	28.876	19.784
C009	522.	2110.	551.	787.	2654.	1044.	1025.	2909.	1491.	265.	493.	239.	447.	3726.	3748.	28.916	19.825
C011	487.	2224.	541.	750.	2714.	1018.	997.	2925.	1458.	263.	477.	247.	440.	3620.	3564.	28.922	19.784
C013	471.	2269.	534.	725.	2793.	1012.	965.	2987.	1441.	254.	478.	240.	429.	3765.	3574.	28.916	19.738
C015	434.	2435.	529.	701.	2896.	1015.	959.	3113.	1493.	267.	486.	258.	478.	3648.	3703.	28.896	19.735
C017	439.	2371.	521.	706.	2869.	1013.	967.	3080.	1490.	267.	493.	261.	476.	3688.	3650.	28.882	19.755
C019	495.	2204.	545.	755.	2720.	1027.	1001.	2942.	1472.	260.	481.	246.	446.	3702.	3624.	28.935	19.728
C021	488.	2167.	529.	758.	2671.	1013.	997.	2902.	1446.	270.	484.	239.	434.	3579.	3637.	28.894	19.810
C023	431.	2316.	499.	710.	2840.	1009.	951.	3110.	1479.	279.	509.	241.	470.	3650.	3905.	28.853	19.782
C025	430.	2326.	500.	709.	2859.	1013.	966.	3091.	1493.	279.	513.	257.	480.	3681.	3730.	28.840	19.802
C027	491.	2247.	552.	753.	2731.	1028.	986.	2992.	1476.	261.	476.	234.	448.	3640.	3832.	28.936	19.762
C029	473.	2282.	540.	746.	2742.	1023.	992.	2968.	1472.	273.	483.	247.	450.	3542.	3650.	28.919	19.771
C033	476.	2256.	537.	742.	2744.	1018.	979.	2966.	1452.	266.	482.	237.	433.	3617.	3659.	28.918	19.759
C034	467.	2269.	529.	743.	2717.	1010.	993.	2947.	1463.	277.	480.	250.	454.	3473.	3628.	28.896	19.788
C036	451.	2344.	528.	711.	2835.	1008.	951.	3043.	1447.	260.	480.	240.	439.	3687.	3660.	28.910	19.746
C038	491.	2190.	537.	746.	2732.	1019.	992.	2941.	1459.	255.	482.	246.	440.	3774.	3574.	28.925	19.727
C040	506.	2305.	583.	774.	2782.	1077.	1012.	2986.	1510.	268.	494.	237.	433.	3681.	3650.	28.961	19.743
C042	534.	2214.	591.	796.	2717.	1081.	1050.	2910.	1527.	262.	491.	254.	446.	3743.	3514.	28.971	19.733
C044	499.	2196.	548.	760.	2698.	1026.	990.	2942.	1456.	261.	478.	229.	430.	3657.	3753.	28.928	19.793
C046	509.	2196.	558.	769.	2708.	1041.	999.	2956.	1476.	260.	483.	230.	435.	3710.	3784.	28.928	19.815
C049	469.	2341.	549.	737.	2815.	1037.	993.	3058.	1518.	267.	488.	256.	482.	3649.	3756.	28.932	19.718
C051	498.	2189.	545.	764.	2681.	1024.	1000.	2942.	1470.	266.	478.	236.	447.	3602.	3787.	28.939	19.740
C053	449.	2278.	511.	706.	2886.	1018.	956.	3108.	1485.	257.	507.	250.	467.	3949.	3735.	28.816	19.767
C055	431.	2324.	501.	687.	2914.	1001.	922.	3163.	1458.	256.	500.	235.	457.	3908.	3889.	28.853	19.729
C057	433.	2395.	518.	692.	2926.	1013.	951.	3154.	1499.	260.	495.	258.	486.	3812.	3763.	28.880	19.722
C059	434.	2261.	491.	704.	2857.	1006.	965.	3096.	1494.	270.	515.	261.	488.	3814.	3743.	28.824	19.790
C061	428.	2303.	494.	696.	2876.	1001.	954.	3072.	1465.	268.	508.	258.	464.	3794.	3603.	28.856	19.740
C063	424.	2374.	504.	701.	2868.	1006.	957.	3119.	1492.	277.	502.	255.	486.	3622.	3809.	28.875	19.733
C066	491.	2315.	569.	759.	2784.	1057.	1042.	2950.	1538.	268.	488.	283.	481.	3644.	3398.	28.959	19.717
C069	458.	2403.	550.	729.	2855.	1040.	981.	3108.	1524.	270.	490.	252.	484.	3619.	3843.	28.853	19.836
C073	467.	2235.	522.	741.	2781.	1031.	1010.	3026.	1528.	274.	509.	268.	497.	3709.	3704.	28.833	19.866
C074	465.	2230.	518.	734.	2796.	1025.	1007.	3029.	1525.	269.	507.	273.	500.	3775.	3655.	28.855	19.815
C076	431.	2318.	500.	709.	2828.	1002.	953.	3107.	1481.	278.	503.	244.	479.	3619.	3918.	28.859	19.773
C078	485.	2191.	531.	757.	2689.	1017.	995.	2906.	1446.	272.	486.	238.	429.	3580.	3595.	28.913	19.807
C080	483.	2258.	545.	749.	2731.	1023.	986.	2978.	1468.	266.	477.	237.	445.	3590.	3760.	28.934	19.756
C082	461.	2301.	531.	721.	2797.	1008.	956.	3007.	1437.	259.	477.	235.	429.	3678.	3654.	28.913	19.742
C085	429.	2289.	491.	700.	2852.	998.	952.	3090.	1470.	271.	508.	252.	472.	3742.	3750.	28.849	19.750
C088	418.	2360.	494.	692.	2891.	1000.	932.	3144.	1466.	274.	507.	240.	465.	3704.	3873.	28.844	19.760
C090	475.	2198.	522.	747.	2684.	1002.	989.	2919.	1444.	272.	480.	243.	442.	3533.	3645.	28.914	19.785
C096	501.	2166.	542.	763.	2673.	1019.	1003.	2926.	1467.	262.	477.	240.	448.	3644.	3729.	28.931	19.733
C105	476.	2224.	530.	751.	2637.	990.	984.	2937.	1444.	274.	460.	233.	454.	3353.	3905.	28.915	19.802
C107	499.	2222.	555.	766.	2691.	1030.	999.	2959.	1479.	266.	476.	234.	448.	3571.	3835.	28.949	19.741
C109	443.	2321.	514.	709.	2809.	995.	960.	3048.	1463.	266.	482.	252.	468.	3622.	3720.	28.885	19.787
C111	427.	2312.	494.	690.	2890.	997.	937.	3093.	1449.	262.	503.	247.	453.	3833.	3657.	28.855	19.735
C116	444.	2250.	499.	696.	2847.	991.	919.	3142.	1444.	252.	492.	223.	453.	3896.	4063.	28.844	19.734
C118	446.	2300.	513.	700.	2935.	1028.	938.	3233.	1516.	254.	515.	237.	488.	4050.	4113.	28.832	19.743
C120	476.	2233.	531.	752.	2685.	1009.	983.	2945.	1448.	276.	478.	232.	439.	3465.	3790.	28.914	19.796
C122	483.	2170.	525.	756.	2671.	1009.	993.	2905.	1442.	272.	485.	237.	433.	3558.	3655.	28.908	19.806
C124	490.	2205.	540.	753.	2695.	1015.	981.	2929.	1437.	263.	475.	228.	422.	3606.	3704.	28.925	19.797
C127	458.	2366.	542.	716.	2815.	1008.	953.	3014.	1436.	258.	466.	237.	428.	3609.	3618.	28.912	19.737
C129	506.	2197.	556.	767.	2706.	1038.	1004.	2945.	1478.	261.	482.	236.	440.	3691.	3721.	28.947	19.736
C131	455.	2288.	520.	719.	2780.	1000.	979.	2970.	1454.	265.	480.	260.	455.	3625.	3497.	28.903	19.771
C133	472.	2240.	529.	749.	2687.	1006.	986.	2939.	1449.	277.	477.	237.	443.	3447.	3738.	28.912	19.790

Table 4.4 (Continued) Results of calculation from well data.

WN.	T(1)	V(1)	D(1)	T(2)	V(2)	D(2)	T(3)	V(3)	D(3)	dT1	dD1	dT2	dD2	IV21	IV32	LAT.	LONG.
C135	471.	2278.	536.	740.	2740.	1014.	984.	2968.	1460.	269.	478.	243.	446.	3547.	3660.	28.918	19.763
C142	431.	2293.	494.	692.	2862.	990.	926.	3129.	1449.	261.	496.	234.	459.	3800.	3921.	28.850	19.734
C144	427.	2337.	499.	707.	2834.	1002.	947.	3096.	1466.	280.	504.	240.	463.	3591.	3867.	28.850	19.777
C145	477.	2233.	533.	745.	2695.	1004.	980.	2964.	1452.	268.	472.	235.	448.	3518.	3818.	28.921	19.763
C147	430.	2271.	489.	709.	2801.	993.	954.	3066.	1462.	278.	504.	245.	469.	3621.	3831.	28.839	19.776
C150	429.	2295.	492.	709.	2834.	1005.	949.	3091.	1466.	280.	512.	240.	462.	3660.	3849.	28.845	19.777
C152	415.	2389.	496.	692.	2889.	1000.	935.	3124.	1460.	277.	504.	243.	461.	3636.	3795.	28.845	19.766
C154	478.	2215.	530.	750.	2680.	1005.	997.	2905.	1448.	272.	475.	247.	444.	3498.	3590.	28.917	19.781
C156	452.	2340.	529.	710.	2830.	1006.	945.	3053.	1443.	259.	477.	235.	438.	3687.	3728.	28.909	19.742
C158	417.	2374.	494.	693.	2883.	999.	929.	3153.	1464.	276.	504.	236.	465.	3652.	3945.	28.841	19.765
C161	415.	2410.	500.	691.	2884.	997.	937.	3119.	1461.	277.	497.	246.	464.	3594.	3779.	28.849	19.761
C163	430.	2315.	498.	709.	2828.	1002.	961.	3067.	1474.	279.	505.	252.	472.	3619.	3741.	28.841	19.781
C165	442.	2281.	504.	701.	2905.	1018.	949.	3130.	1485.	259.	514.	248.	468.	3968.	3764.	28.821	19.768
C166	429.	2298.	494.	700.	2886.	1010.	946.	3116.	1474.	271.	517.	246.	463.	3819.	3773.	28.832	19.769
C167	462.	2321.	536.	732.	2766.	1013.	983.	2975.	1462.	270.	476.	251.	450.	3527.	3586.	28.913	19.765
C171	431.	2361.	508.	709.	2839.	1006.	950.	3107.	1476.	278.	498.	241.	470.	3578.	3895.	28.857	19.778
C168	432.	2325.	502.	711.	2817.	1002.	953.	3092.	1473.	280.	500.	242.	471.	3578.	3899.	28.847	19.780
C174	429.	2323.	498.	708.	2830.	1001.	955.	3096.	1478.	279.	503.	247.	476.	3610.	3857.	28.862	19.768
C178	419.	2397.	502.	697.	2872.	1001.	946.	3103.	1468.	278.	499.	249.	467.	3586.	3749.	28.857	19.763
C177	482.	2200.	530.	753.	2699.	1016.	989.	2926.	1447.	271.	486.	236.	430.	3588.	3652.	28.917	19.805
C181	417.	2412.	503.	696.	2877.	1001.	946.	3107.	1470.	278.	497.	250.	469.	3574.	3746.	28.859	19.759
C002	413.	2373.	490.	692.	2904.	1005.	943.	3106.	1464.	279.	515.	250.	459.	3689.	3667.	28.855	19.759
C005	488.	2254.	550.	755.	2740.	1034.	996.	2965.	1476.	267.	485.	241.	442.	3630.	3670.	28.942	19.753
C010	529.	2194.	580.	781.	2721.	1062.	1029.	2958.	1522.	252.	482.	248.	460.	3827.	3702.	28.940	19.802
C012	466.	2245.	523.	743.	2723.	1012.	984.	2947.	1451.	277.	489.	241.	439.	3525.	3636.	28.902	19.779
C014	506.	2238.	566.	768.	2733.	1049.	1000.	3007.	1503.	262.	483.	232.	454.	3689.	3912.	28.941	19.773
C016	476.	2194.	522.	751.	2695.	1012.	996.	2913.	1451.	275.	490.	245.	438.	3564.	3581.	28.900	19.799
C018	485.	2211.	536.	749.	2713.	1016.	964.	2981.	1437.	264.	480.	215.	421.	3638.	3915.	28.926	19.760
C020	445.	2367.	527.	705.	2875.	1013.	963.	3053.	1471.	259.	486.	259.	458.	3749.	3536.	28.903	19.757
C022	484.	2232.	540.	751.	2715.	1019.	984.	2957.	1455.	267.	480.	233.	436.	3589.	3736.	28.921	19.749
C024	488.	2210.	539.	755.	2718.	1027.	997.	2955.	1473.	268.	488.	242.	446.	3643.	3697.	28.933	19.750
C026	496.	2180.	541.	759.	2697.	1024.	1001.	2937.	1470.	263.	483.	242.	446.	3671.	3692.	28.927	19.739
C028	493.	2248.	554.	756.	2725.	1030.	990.	2975.	1473.	264.	477.	234.	443.	3616.	3785.	28.931	19.771
C030	474.	2233.	529.	749.	2710.	1015.	995.	2917.	1451.	275.	485.	246.	436.	3532.	3545.	28.913	19.779
C032	487.	2190.	533.	752.	2705.	1017.	980.	2966.	1453.	265.	484.	228.	436.	3652.	3824.	28.905	19.812
C031	482.	2228.	537.	750.	2709.	1016.	977.	2944.	1438.	268.	479.	226.	422.	3574.	3722.	28.921	19.802
C035	489.	2237.	547.	753.	2706.	1019.	977.	2962.	1447.	264.	472.	224.	428.	3574.	3822.	28.916	19.812
C037	462.	2389.	551.	735.	2839.	1043.	975.	3127.	1525.	273.	492.	240.	482.	3600.	4007.	28.864	19.838
C039	477.	2239.	534.	748.	2719.	1017.	981.	2958.	1450.	271.	483.	232.	433.	3564.	3727.	28.917	19.792
C041	459.	2305.	529.	728.	2789.	1015.	982.	2968.	1458.	269.	486.	254.	442.	3614.	3482.	28.908	19.769
C043	568.	2156.	612.	831.	2662.	1106.	1090.	2886.	1573.	263.	494.	260.	468.	3753.	3603.	28.938	19.840
C045	473.	2218.	525.	749.	2697.	1011.	991.	2915.	1444.	276.	486.	242.	434.	3520.	3591.	28.907	19.789
C047	424.	2303.	489.	702.	2854.	1001.	943.	3114.	1468.	277.	513.	242.	467.	3699.	3870.	28.837	19.770
C050	455.	2258.	514.	737.	2716.	1001.	975.	2967.	1447.	282.	487.	238.	446.	3457.	3744.	28.889	19.799
C052	431.	2335.	503.	694.	2900.	1006.	937.	3143.	1472.	264.	504.	242.	465.	3821.	3841.	28.840	19.749
C054	420.	2351.	494.	700.	2873.	1005.	957.	3067.	1467.	280.	512.	257.	462.	3655.	3594.	28.868	19.742
C056	456.	2319.	529.	718.	2946.	1058.	988.	3194.	1577.	262.	528.	270.	520.	4038.	3857.	28.832	19.725
C058	467.	2284.	534.	727.	2894.	1052.	1016.	3150.	1600.	260.	519.	288.	547.	3990.	3795.	28.866	19.709
C060	448.	2379.	532.	719.	2847.	1023.	990.	3076.	1522.	271.	491.	271.	499.	3620.	3683.	28.909	19.715
C062	433.	2256.	488.	697.	2862.	997.	932.	3119.	1453.	264.	509.	235.	456.	3856.	3881.	28.847	19.738
C064	426.	2351.	500.	690.	2904.	1001.	944.	3122.	1473.	264.	501.	254.	472.	3796.	3711.	28.863	19.730
C067	449.	2302.	516.	724.	2812.	1018.	996.	3034.	1512.	275.	502.	272.	494.	3643.	3624.	28.872	19.806
C068	482.	2263.	545.	757.	2761.	1046.	1008.	3014.	1519.	275.	500.	251.	474.	3632.	3780.	28.879	19.831
C071	460.	2255.	518.	727.	2841.	1033.	996.	3047.	1518.	268.	515.	269.	485.	3846.	3604.	28.836	19.846
C077	465.	2147.	499.	737.	2747.	1013.	1022.	2918.	1492.	272.	514.	285.	479.	3772.	3361.	28.797	19.797
C079	479.	2197.	526.	753.	2685.	1011.	995.	2907.	1447.	274.	485.	243.	436.	3536.	3597.	28.905	19.800
C081	461.	2334.	538.	724.	2805.	1015.	965.	3013.	1453.	263.	477.	241.	438.	3630.	3638.	28.913	19.752
C084	450.	2105.	473.	716.	2784.	997.	972.	3038.	1477.	266.	524.	257.	481.	3931.	3748.	28.799	19.829

Table 4.4 (Continued) Results of calculation from well data.

WN.	T(1)	V(1)	D(1)	T(2)	V(2)	D(2)	T(3)	V(3)	D(3)	dT1	dD1	dT2	dD2	IV21	IV32	LAT.	LONG.
C089	418.	2341.	490.	696.	2870.	1000.	940.	3098.	1457.	278.	510.	244.	457.	3666.	3747.	28.848	19.771
C095	449.	2182.	490.	724.	2789.	1009.	975.	3059.	1492.	274.	519.	252.	483.	3783.	3836.	28.811	19.835
C097	493.	2200.	543.	755.	2723.	1028.	988.	2945.	1455.	261.	485.	233.	427.	3710.	3662.	28.925	19.808
C106	488.	2238.	546.	752.	2664.	1001.	983.	2982.	1466.	264.	456.	232.	465.	3452.	4011.	28.926	19.753
C108	454.	2296.	522.	723.	2773.	1002.	974.	2994.	1458.	268.	481.	251.	456.	3581.	3628.	28.900	19.773
C110	418.	2374.	496.	696.	2874.	1000.	948.	3095.	1467.	278.	504.	252.	467.	3623.	3706.	28.862	19.751
C112	431.	2302.	496.	701.	2864.	1004.	954.	3083.	1470.	270.	508.	252.	466.	3758.	3690.	28.849	19.748
C114	445.	2300.	511.	700.	2886.	1010.	926.	3138.	1454.	255.	498.	227.	444.	3909.	3915.	28.838	19.740
C117	484.	2207.	534.	741.	2721.	1008.	982.	2942.	1445.	257.	474.	242.	437.	3687.	3622.	28.921	19.737
C119	467.	2292.	535.	729.	2769.	1010.	961.	3019.	1451.	263.	475.	232.	442.	3615.	3805.	28.914	19.747
C121	480.	2257.	542.	742.	2729.	1013.	973.	2977.	1449.	262.	471.	231.	436.	3593.	3772.	28.918	19.754
C123	476.	2258.	538.	746.	2714.	1013.	979.	2972.	1455.	270.	475.	233.	442.	3521.	3796.	28.924	19.766
C125	484.	2219.	537.	745.	2692.	1003.	970.	2974.	1442.	261.	465.	225.	439.	3571.	3907.	28.931	19.760
C126	469.	2224.	522.	747.	2690.	1005.	991.	2936.	1455.	278.	484.	244.	450.	3475.	3692.	28.895	19.799
C128	469.	2235.	524.	744.	2701.	1005.	991.	3014.	1493.	275.	481.	246.	488.	3498.	3958.	28.899	19.783
C130	459.	2277.	523.	731.	2755.	1007.	977.	3001.	1466.	272.	484.	246.	459.	3562.	3733.	28.897	19.778
C132	476.	2195.	522.	748.	2694.	1007.	997.	2900.	1445.	272.	485.	249.	438.	3563.	3522.	28.903	19.795
C134	475.	2220.	528.	751.	2686.	1008.	993.	2918.	1449.	275.	480.	242.	441.	3489.	3636.	28.908	19.796
C136	458.	2149.	492.	727.	2767.	1006.	999.	2976.	1486.	269.	514.	272.	480.	3820.	3534.	28.798	19.812
C141	443.	2252.	499.	699.	2840.	993.	925.	3118.	1441.	256.	494.	226.	449.	3858.	3977.	28.842	19.737
C143	424.	2352.	498.	702.	2842.	998.	946.	3106.	1469.	279.	500.	244.	471.	3589.	3865.	28.852	19.772
C146	418.	2347.	491.	695.	2857.	993.	943.	3084.	1454.	277.	502.	248.	461.	3629.	3721.	28.851	19.767
C148	488.	2222.	542.	753.	2704.	1019.	985.	2943.	1449.	265.	476.	231.	430.	3591.	3720.	28.923	19.792
C149	481.	2216.	533.	744.	2708.	1007.	975.	2964.	1445.	262.	473.	232.	439.	3612.	3784.	28.919	19.757
C151	485.	2216.	538.	748.	2719.	1017.	996.	2919.	1454.	263.	479.	248.	437.	3650.	3520.	28.920	19.785
C153	461.	2323.	536.	722.	2777.	1002.	965.	2996.	1445.	261.	467.	243.	442.	3581.	3646.	28.915	19.732
C155	417.	2379.	496.	695.	2862.	994.	938.	3111.	1459.	278.	499.	243.	465.	3586.	3821.	28.844	19.771
C160	449.	2349.	527.	710.	2833.	1006.	959.	3029.	1452.	261.	478.	249.	446.	3665.	3588.	28.908	19.752
C159	483.	2162.	522.	754.	2672.	1007.	991.	2912.	1442.	271.	486.	237.	435.	3579.	3675.	28.902	19.805
C162	470.	2255.	530.	747.	2668.	997.	988.	2909.	1437.	277.	466.	241.	440.	3370.	3657.	28.910	19.785
C164	481.	2237.	538.	748.	2704.	1012.	972.	2988.	1452.	267.	474.	224.	440.	3548.	3937.	28.928	19.766
C170	424.	2314.	490.	702.	2839.	996.	949.	3090.	1467.	278.	506.	248.	471.	3638.	3803.	28.857	19.767
C169	444.	2352.	522.	707.	2833.	1001.	967.	3040.	1470.	263.	480.	260.	468.	3643.	3602.	28.898	19.767
C172	488.	2134.	520.	746.	2687.	1002.	987.	2922.	1441.	258.	481.	241.	440.	3732.	3648.	28.922	19.739
C173	493.	2154.	531.	754.	2699.	1017.	989.	2919.	1443.	261.	486.	235.	426.	3731.	3626.	28.926	19.804
C175	483.	2227.	538.	750.	2722.	1021.	984.	2948.	1450.	267.	483.	234.	429.	3617.	3674.	28.921	19.806
C180	423.	2341.	496.	702.	2836.	996.	950.	3086.	1466.	279.	500.	248.	471.	3587.	3793.	28.860	19.764
C176	430.	2323.	499.	708.	2837.	1004.	963.	3077.	1481.	278.	505.	255.	478.	3633.	3741.	28.838	19.780
C179	481.	2177.	523.	754.	2668.	1005.	993.	2915.	1448.	273.	482.	239.	442.	3532.	3694.	28.899	19.803

Abbreviations:

WN = Well name.
T(1) = Two-way time in ms. to the top of horizon 1.
V(1) = Dix average velocity for horizon 1 in m/s.
D(1) = Depth for horizon 1 in meter .
T(2) = Two-way time in ms. to the top of horizon 2.
V(2) = Dix average velocity for horizon 2 in m/s.
D(2) = Depth for horizon 2 in meter .
T(3) = Two-way time in ms. to the top of horizon 3.
V(3) = Dix average velocity for horizon 3 in m/s.
D(3) = Depth for horizon 3 in meter.
dT1 = Difference in time between horizon 2 and horizon 1.
dD1 = Difference in depth between horizon 2 and horizon 1.
dT2 = Difference in time between horizon 3 and horizon 2.
dD2 = Difference in depth between horizon 3 and horizon 2.
LAT. = Latitude of corresponding well location.
LONG. = Longitude of corresponding well location.

Horizon 1 = Sheghega Formation.
Horizon 2 = Domran Formation.
Horizon 3 = Ruaga Formation.

IV21 = Interval velocity for She. Formation.
IV32 = Interval velocity for Dom. Formation.

Appendix 4.5

```
# The macro VDCONT use to contour the require data from the input file
# using X1, X2, Y1, and Y2 are the input coordinates for the size of the contour
# map and M as the instruction to the contour function to write or not the countour
# values on the graph(0 or 1).

MACRO  VDCONT( X1, X2, Y1, Y2, M )
# Type the file name OUT.ALL.
PRINT ( " PRINT THE FILE CONTAINING ALL THE DATA AS ( OUT.ALL ) ", QUOTE = F )
# Read the name of the file as ?T(FILNM).
        ?T(FILNM)       <- READ ( , LENGTH = 1, PRINT = F )
# Type the file name COOR.NA.
PRINT ( " PRINT THE FILE CONTAINING THE DATA AS ( COOR.NA ) ", QUOTE = F )
# Read the name of the file as ?T(FILNM2).
        ?T(FILNM2)      <- READ ( , LENGTH = 1, PRINT = F )
# Read the ?T(FILNM) file from Suilven system into a matrix of 18 columns ?T(DATA) file in S system.
        ?T(DATA)        <- MATRIX ( READ ( ?T(FILNM) ), NCOL = 18, BYROW = T )
# Read the ?T(FILNM2) file from Suilven system into a matrix of 6 columns ?T(COOR) file in S system.
        ?T(COOR)        <- MATRIX ( READ ( ?T(FILNM2) ), NCOL = 6, BYROW = T )
PRINT ( "      SP   T(1)   V(1)   D(1)   T(2)   V(2)   D(2)   T(3)   V(3)   ", QUOTE = F )
PRINT ( "COL.  1    2      3      4      5      6      7      8      9      ", QUOTE = F )
PRINT ( "      D(3) dT1    dD1    dT2    dD2    IV21   IV32   LAT.   LONG.  ", QUOTE = F )
PRINT ( "COL.  10   11     12     13     14     15     16     17     18     ", QUOTE = F )
# Type the required number of column.
PRINT ( " WHICH COLUMN. NUMBER DO YOU WISH TO CONTOUR ? ", QUOTE = F )
# Read the column number as ?T(M1).
        ?T(M1)          <- READ ( , LENGTH = 1, PRINT = F )
# Put all data values in the previous column from the ?T(DATA) matrix into ?T(MZ).
        ?T(MZ)          <- ?T(DATA)[ , ?T(M1) ]
# Put all longitude values in the 18 th column from the ?T(DATA) matrix into ?T(MX).
        ?T(MX)          <- ?T(DATA)[ , 18 ]
# Put all latitude values in the 17 th column from the ?T(DATA) matrix into ?T(MY).
        ?T(MY)          <- ?T(DATA)[ , 17 ]
# Put all longitude values in the third column from the ?T(COOR) matrix into ?T(LONG).
        ?T(LONG)        <- ?T(COOR)[ , 3 ]
# Put all latitude values in the second column from the ?T(COOR) matrix into ?T(LAT).
```

```
        ?T(LAT)          <- ?T(COOR)[ , 2 ]
# Do an interpolating file ?T(X) by using the (inter) function. The output structure contains three components
# ?T(X)$x, ?T(X)$y, and ?T(X)$z. The first two are vectors defining the ?T(X)$x - ?T(X)$y grid, and the last is
# the matrix of interpolated values.
        ?T(X)            <- INTERP ( ?T(MX), ?T(MY), ?T(MZ) )
# Find the minimum value using MIN function.
        ?T(MI )          <- MIN ( ?T(X)$z )
# Find the maximum value using MAX function.
        ?T(MA)           <- MAX ( ?T(X)$z )
# Print the minimum value.
PRINT ( ENCODE ( " MINIMUM READING MIN = ", ?T(MI) ) )
# Print the maximum value.
PRINT ( ENCODE ( " MAXIMUM READING MAX = ", ?T(MA) ) )
# Print number of colours do you want to use it in the contouring.
PRINT ( " HOW MANY COLOUR DO YOU WISH TO USE ? ", QUOTE = F )
# Read the above number as ?T(N).
        ?T(N)            <- READ ( , LENGTH = 1, PRINT = F )
# Do eight times the second Macro (PRE) to find the suitable contour numbers.
        FOR (I IN 1 : 8 ) {
                         ?PRE( ?T(X), ( I + ( I*4 ) ) )
        }
PRINT ( " ENTER APPROXIMATE CONTOUR NUMBERS ", QUOTE = F )
# Read the contour numbers as ?T(CNU).
        ?T(CNU)          <- READ ( , LENGTH = 1, PRINT = F )
# Use the PRETTY and ROUND functions.
        ?T(CVALES)       <- PRETTY ( ?T(X)$Z, NINT = ?T(CNU) )
        ?T(CVALES)       <- ROUND ( ?T(CVALES), ?T(N) )
        ?T(CINT2)        <- ( ?T(CVALES)[2] - ?T(CVALES)[1] )
PRINT ( " ENTER THE FIRST SEPARATED VALUE ", QUOTE = F )
# Read the first separated values as ?T(VAL1).
        ?T(VAL1)         <- READ ( , LENGTH = 1, PRINT = F )
        ?T(VAL2)         <- 0
        ?T(J)            <- 2
# Do number of colours times contouring as a separate parts with different colours.
        FOR ( I IN 1 : ?T(N) ) {
        ?T(II)           <- C ( ?T(CVALES) > = ?T(VAL1) | ?T(CVALES) < ( ?T(VAL1) - 100 ) )
        ?T(SET)          <- ?T(CVALES)[ ! ?T(II)]
```

```
                    PAR ( COL = ?T(J))
                    PAR ( PIN = C(5.22,6) )
# Use contour function to contour the required column using the X1, X2, Y1, Y2 values for map size.
CONTOUR ( ?T(X), V = ?T(SET), XLIM = C (X1,X2), YLIM = C (Y1,Y2), LABEX = M )
# Plot on the same graph.
                    PAR ( NEW = T )
      ?T(VAL1)      <- ?T(VAL1) + 100
      ?T(VAL2)      <- ?T(VAL1)
      ?T(J)         <- ?T(J) + 1
      }
# Plot on the same graph.
                    PAR ( NEW = T )
# Plot the seismic lines on the contour map.
PLOT ( ?T(LONG), ?T(LAT), TYPE = " L ", XLIM = C (X1,X2), YLIM = C (Y1,Y2), COL = 1 )
# Apply ZAP Macro to remove all previous files which started with T.
      ?ZAP(T*)
END

# Macro PRE to find and to print the Pretty value and contour interval equivalent
# using X as an input and N as an output.

MACRO  PRE ( X, N )
# Use PRETTY function to find the Pretty value.
      ?T(NINT)      <- PRETTY ( X$Z, N )
# Find the contour interval.
      ?T(CINT)      <- ( ?T(NINT)[2] - ?T(NINT)[1] )
# Print the Pretty value NINT and contour interval equivalent ?T(CINT)>
PRINT ( ENCODE ( " NINT = ", N, " CONTOUR INTERVAL = ", ?T(CINT) ) )
END
```

Appendix 5.1

FORTRAN - 77 PROGRAM 2 STATIC

```
c     ********************************************************************************
c     This program is design for the  static corrections calculation.
c     VAX/UNIX: STATIC
c     Written by
c     Ben Ayad N.M.
c     at the department of Geology&Applied Geology.
c     University of Glasgow, Glasgow G12 8QQ (in June 1991)
c     This program calculates the static corrections for the shots and receivers at there location
c     using:
c           A) Uphole data.
c           B) Formulae applied in the previous seismic processing.
c     ********************************************************************************
c     PROGRAM     STATIC.F
      DIMENSION STN(10), ELU(10), WV(10), UHD(10), DIFST(500)
     *          , UHT(10), ST(10), EL(500), STATIC(500), STXD(500)
     *          , STX(500), WVX(500), ELX(500),DELX(500), SINTER(500)
     *          , STNX(500), SLEHIB(500), SSABKHA(500)
      CHARACTER *10 INDATA1, INDATA2*10, OUT1*10, OUT2*10
      PRINT*," PRINT THE INPUT FILE NAME AS ( UPH.DATA ) "
      PRINT*," WHICH CONTAINING THE "
      PRINT*,""
      PRINT*," STATION NUMBER, ELEVATION
     *       , WEATHERING VELOCITY, UPHOLE DEPTH, UPHOLE TIME"
      PRINT*,""
      READ *, INDATA1
      PRINT*,""
      PRINT*," PRINT THE INPUT FILE NAME AS ( ELES.DATA ) "
      PRINT*," WHICH CONTAINING THE SHOT ELEVATIONS "
      PRINT*,""
      PRINT*," OR "
      PRINT*,""
      PRINT*," PRINT THE INPUT FILE NAME AS ( ELEG.DATA ) "
      PRINT*,"WHICH CONTAINING THE RECEIVER ELEVATIONS"
      PRINT*,""
```

```
      READ *, INDATA2
      PRINT*,""
      PRINT*," PRINT THE OUTPUT FILE NAME AS ( STS.DATA )"
      PRINT*," WHICH WILL CONTAIN
     *          THE STATIC RESULTS FOR THE SHOTS "
      PRINT*,""
      PRINT*," OR "
      PRINT*,""
      PRINT*," PRINT THE OUTPUT FILE NAME AS ( STG.DATA )"
      PRINT*," WHICH WILL CONTAIN
     *          THE STATIC RESULTS FOR THE RECEIVERS "
      PRINT*,""
      READ *, OUT1
      PRINT*,""
      PRINT*," PRINT THE OUTPUT FILE NAME AS ( STS2.DATA )"
      PRINT*," WHICH WILL CONTAIN
     *          THE STATIC RESULTS FOR THE SHOTS
     *          AND THE DIFFERENCES IN STATICS "
      PRINT*,""
      PRINT*," OR "
      PRINT*,""
      PRINT*," PRINT THE OUTPUT FILE NAME AS ( STG2.DATA )"
      PRINT*," WHICH WILL CONTAIN
     *          THE STATIC RESULTS FOR THE RECEIVERS
     *          AND THE DIFFERENCES IN STATICS"
      PRINT*,""
      READ *, OUT2
            OPEN ( 1, FILE = INDATA1 )
            OPEN ( 2, FILE = INDATA2 )
            OPEN ( 3, FILE = OUT1 )
            OPEN ( 4, FILE = OUT2 )
c     M       - Number of upholes.
c     SM1     - Last station number in Lehib part.
c     SM2     - First station number in Sabkha part.
c     SM3     - First station number in Lehib part.
c     SM4     - Last station number in Sabkha part.
c     DATUM         - Datum plane (sea level).
```

```
                M     = 6
                SM1   = 298.0
                SM2   = 314.0
                SM3   = 100.0
                SM4   = 835.0
                DATUM = 0.0
c       I       - Counter for uphole data.
        DO  100 I = 1, M
c       STN     - Station number.
c       ELU     - Uphole elevation.
c       WV      - Weathering velocity.
c       UHD     - Uphole depth.
c       UHT     - Uphole time.
c       ST      - Static correction at the uphole location.
                READ (1,111) STN(I), ELU(I), WV(I), UHD(I), UHT(I)
                ST(I) = ( ( ( DATUM - ELU(I) + UHD(I) ) / WV(I))*1000.0 ) - UHT(I)
100     CONTINUE
c       N       - Number of station.
c       N1      - Number of station in Lahib part.
c       N2      - Number of the first station in Sabkha.
                    N   = STN(M) - STN(1) + 1.0
                    N1  = SM1 - STN(1) + 1.0
                    N2  = SM2 - STN(1) + 1.0
c       EL      - Elevation of the stations.
        READ (2,*) ( EL(J), J = 1, N )
c       NS      - Counter.
                    NS  = 1
c       I       - Counter of loops of the calculation.
        DO  200 I = 1, M - 1
c       NE      - Number of stations to be calculated..
c       DSTN    - Number of station intervals to be calculated.
c       DEL1    - Difference in elevation.
c       DST     - Difference in static correction.
c       DWV     - Difference in weathering velocity.
                    NE    = STN(I+1) - STN(1) + 1
                    DSTN  = STN(I+1) - STN(I)
                    DEL1  = ELU(I+1) - ELU(I)
```

```
                DST   = ST(I+1) - ST(I)
                DWV   = WV(I+1) - WV(I)
c       J       - Counter for station number.
        DO 300 J = NS, NE
c       STNX    - Station number to be calculated.
c       DSTNX   - Difference in stations.
c       STX     - Static correction at that particular station.
c       WVX     - Weathering velocity at that particular station.
c       ELX     - Elevation at that particular station.
c       DELX    - Difference in elevation.
c       STXD    - Static correction for the DELX.
c       STATIC  - Total static correction.
c       SLEHIB  - Lehib formula.
c       SSABKHA - Sabkha formula.
c       DIFST   - Difference in static correction.
                STNX(J)    = STN(I) + J - NS
                DSTNX      = STNX(J) - STN(I)
                STX(J)     = ( ( DST / DSTN )*DSTNX ) + ST(I)
                WVX(J)     = ( ( DWV / DSTN )*DSTNX ) + WV(I)
                ELX(J)     = ( ( DEL1 / DSTN )*DSTNX ) + ELU(I)
                DELX(J)    = EL(J) - ELX(J)
                STXD(J)    = ( ( ( DATUM - DELX(J) ) / WVX(J) )*1000.0 )
                STATIC(J)  = STXD(J) + STX(J)
            IF ( STNX(J) .GE. SM3 .AND. STNX(J) .LE. SM1 ) THEN
                SLEHIB(J)  = ( - ( EL(J) / 1880.0 ) + 0.007 )*1000.0
                DIFST(J)   = ( STATIC(J) - SLEHIB(J) )
            ELSE IF ( STNX(J) .GE. SM2 .AND. STNX(J) .LE. SM4 ) THEN
                SSABKHA(J) = ( - ( EL(J) / 1500.0 ) + 0.012 )*1000.0
                DIFST(J)   = ( STATIC(J) - SSABKHA(J) )
        ELSE
        END IF
            IF ( STNX(J) .EQ. SM1 ) THEN
c       JJ      - Counter.
                        JJ  = J + 1
        END IF
            IF ( STNX(J) .EQ. SM2 ) THEN
                        KK = J + 1
```

```
c       DSSSL  - Difference in static between Sabkha and Lehib.
                                  DSSSL = SSABKHA(KK+1) - SLEHIB(JJ-1)
c       K      - Counter for the station between the two areas.
        D0 400 K = JJ, KK
c       SINTER - Interpolated static correction in the area between Sabkha and Lehib parts.
                 SINTER(K) = ( ( DSSSL / ( KK - JJ + 2 ) )*( K - JJ + 1 ) + SLEHIB(JJ-1)
                 DIFST(K)  = ( STATIC(K) - SINTER(K) )
400     CONTINUE
        END IF
300     CONTINUE
                    NS = J - 1
200     CONTINUE
                    WRITE (3,333)   ( STATIC(I)   , I = 1, N )
                    WRITE (4,333)   ( SLEHIB(I)   , I = 1, N1 )
      *                           , ( SINTER (I)  , I = N1 + 1, N2 - 1 )
      *                           , ( SSABKHA(I)  , I = N2, N )
                    WRITE (4,333)   DIFST(I)      , I = 1, N )
      *                           , ( DELX(I)     , I = 1, N )
333     FORMAT ( F12.1 , 8F8.1 )
111     FORMAT ( 5F8.1 )
        STOP
        END
```

Appendix 5.2

Table 5.2. Selected static correction calculation from line 6V256-85.

	Static correction for the shots			Static correction for the receivers			Total static correction		
STN	STS.EQ	STS.FOR	DSTS	STG.EQ	STG.FOR	DSTG	TST.EQ	TST.FOR	DTST
150	-103.2	-97.4	-5.7	-103.2	-97.4	-5.7	-206.4	-194.8	-11.4
155	-101.9	-96.4	-5.5	-101.9	-96.4	-5.5	-203.8	-192.8	-11
160	-101.9	-96.9	- 5	-101.9	-96.9	- 5	-203.8	-193.8	-10
165	-102.4	-98	-4.5	-102.4	-98	-4.5	-204.8	-196	- 9
170	-103	-99	-3.9	-103	-99	-3.9	-206	-198	-7.8
175	-100.3	-96.4	- 4	-100.3	-96.4	- 4	-200.6	-192.8	- 8
180	-101.3	-98	-3.4	-101.3	-98	-3.4	-202.6	-196	-6.8
185	-101	-98	-3.1	-101	-98	-3.1	-202	-196	-6.2
190	-98.4	-95.3	-3.1	-98.4	-95.3	-3.1	-196.8	-190.6	-6.2
195	-99.5	-96.9	-2.6	-99.5	-96.9	-2.6	-199	-193.8	-5.2
200	-100.6	-98.5	-2.1	-112.4	-111.8	-0.6	-213	-210.3	-2.7
205	-123.6	-124.6	+1	-137.8	-140.5	+2.7	-261.4	-265.1	+3.7
210	-102.9	-101.7	-1.2	-102.9	-101.7	-1.2	-205.8	-203.4	-2.4
215	-92.1	-90	-2.1	-92.1	-90	-2.1	-184.2	-180	-4.2
220	-90.4	-88.4	- 2	-90.4	-88.4	- 2	-180.8	-176.8	- 4
225	-88.1	-86.3	-1.9	-88.1	-86.3	-1.9	-176.2	-172.6	-3.8
230	-84.4	-82.5	-1.9	-84.4	-82.5	-1.9	-168.8	-165	-3.8
235	-80.9	-78.8	-2.1	-80.9	-78.8	-2.1	-161.8	-157.6	-4.2
240	-80.9	-77.7	-3.1	-80.9	-77.7	-3.1	-161.8	-155.4	-6.2
245	-82.3	-78.3	- 4	-82.3	-78.3	- 4	-164.6	-156.6	- 8
250	-86.3	-81.5	-4.8	-86.3	-81.5	-4.8	-172.6	-163	-9.6
255	-87.7	-82	-5.7	-87.7	-82	-5.7	-175.4	-164	-11.4
260	-90.2	-83.6	-6.6	-90.2	-83.6	-6.6	-180.4	-167.2	-13.2
265	-92.7	-85.2	-7.5	-92.7	-85.2	-7.5	-185.4	-170.4	-15
270	-93.1	-84.7	-8.5	-93.1	-84.7	-8.5	-186.2	-169.4	-17
275	-94.6	-85.2	-9.4	-94.6	-85.2	-9.4	-189.2	-170.4	-18.8
280	-96.1	-85.7	-10.3	-96.1	-85.7	-10.3	-192.2	-171.4	-20.6
285	-99.5	-88.4	-11.1	-99.5	-88.4	-11.1	-199	-176.8	-22.2
290	-101.5	-89.4	-12	-101.5	-89.4	-12	-203	-178.8	-24
295	-101.4	-88.4	-13.1	-101.4	-88.4	-13.1	-202.8	-176.8	-26.2
300	-103.8	-92.4	-11.5	-103.8	-92.4	-11.5	-207.6	-184.8	-23
305	-104.7	-101.1	-3.6	-104.7	-101.1	-3.6	-209.4	-202.2	-7.2
310	-104.9	-109.7	+4.8	-104.9	-109.7	+4.8	-209.8	-219.4	+9.6
315	-108.3	-118.7	+10.4	-108.3	-118.7	+10.4	-216.6	-237.4	+20.8
320	-108.7	-118.7	+10	-108.7	-118.7	+10	-217.4	-237.4	+20
325	-109.3	-119.3	+10	-109.3	-119.3	+10	-218.6	-238.6	+20
330	-109.4	-119.3	+9.9	-109.4	-119.3	+9.9	-218.8	-238.6	+19.8
335	-110.6	-120.7	+10.1	-110.6	-120.7	+10.1	-221.2	-241.4	+20.2

Abbreviations:

STN = Station number.
STS.EQ = Shot static correction using uphole data.
STS.FOR = Shot static correction using formula.
DSTS = Differences in shot static.
STG.EQ = Receiver static correction using uphole data.
STG.FOR = Receiver static correction using formula.
DSTG = Differences in receiver static.
TST.EQ = Total static correction using uphole data.
TST.FOR = Total static correction using formula.
DTST = Differences in total static.

Table 5.2. (Continued) Selected static correction calculation from line 6V256-85.

	Static correction for the shots			Static correction for the receivers			Total static correction		
STN	STS.EQ	STS.FOR	DSTS	STG.EQ	STG.FOR	DSTG	TST.EQ	TST.FOR	DTST
340	-111.7	-122	+10.3	-111.7	-122	+10.3	-223.4	-244	+20.6
345	-111.3	-121.3	+10	-111.3	-121.3	+10	-222.6	-242.6	+20
350	-112.5	-122.7	+10.2	-112.5	-122.7	+10.2	-225	-245.4	+20.4
355	-112.6	-122.7	+10.1	-112.6	-122.7	+10.1	-225.2	-245.4	+20.2
360	-114.2	-124.7	+10.4	-114.2	-124.7	+10.4	-228.4	-249.4	+20.8
365	-116.4	-127.3	+10.9	-116.4	-127.3	+10.9	-232.8	-254.6	+21.8
370	-118.6	-130	+11.4	-118.6	-130	+11.4	-237.2	-260	+22.8
375	-120.2	-132	+11.8	-120.2	-132	+11.8	-240.4	-264	+23.6
380	-121.9	-134	+12.1	-121.9	-134	+12.1	-243.8	-268	+24.2
385	-120	-131.3	+11.4	-120	-131.3	+11.4	-240	-262.6	+22.8
390	-117	-127.3	+10.3	-117	-127.3	+10.3	-234	-254.6	+20.6
395	-115.7	-125.3	+9.6	-115.7	-125.3	+9.6	-231.4	-250.6	+19.2
400	-114.4	-123.3	+8.9	-114.4	-123.3	+8.9	-228.8	-246.6	+17.8
405	-112.6	-120.7	+8.1	-112.6	-120.7	+8.1	-225.2	-241.4	+16.2
410	-112.8	-120.7	+7.9	-112.8	-120.7	+7.9	-225.6	-241.4	+15.8
415	-111.4	-118.7	+7.2	-111.4	-118.7	+7.2	-222.8	-237.4	+14.4
420	-113.2	-120.7	+7.5	-113.2	-120.7	+7.5	-226.4	-241.4	+15
425	-112.9	-120	+7.1	-112.9	-120	+7.1	-225.8	-240	+14.2
430	-115.1	-122.7	+7.5	-115.1	-122.7	+7.5	-230.2	-245.4	+15
435	-117.4	-125.3	+8	-117.4	-125.3	+8	-234.8	-250.6	+16
440	-119.6	-128	+8.4	-119.6	-128	+8.4	-239.2	-256	+16.8
445	-117.8	-125.3	+7.6	-117.8	-125.3	+7.6	-235.6	-250.6	+15.2
450	-117.5	-124.7	+7.2	-117.5	-124.7	+7.2	-235	-249.4	+14.4
455	-120.7	-128.7	+8	-120.7	-128.7	+8	-241.4	-257.4	+16
460	-118.9	-126	+7.1	-118.9	-126	+7.1	-237.8	-252	+14.2
465	-119.6	-126.7	+7.1	-119.6	-126.7	+7.1	-239.2	-253.4	+14.2
470	-121.3	-128.7	+7.4	-121.3	-128.7	+7.4	-242.6	-257.4	+14.8
475	-118.5	-124.7	+6.2	-118.5	-124.7	+6.2	-237	-249.4	+12.4
480	-118.2	-124	+5.8	-118.2	-124	+5.8	-236.4	-248	+11.6
485	-120.4	-126.7	+6.3	-120.4	-126.7	+6.3	-240.8	-253.4	+12.6
490	-121.6	-128	+6.4	-121.6	-128	+6.4	-243.2	-256	+12.8
495	-121.3	-127.3	+6	-121.3	-127.3	+6	-242.6	-254.6	+12
500	-123	-129.3	+6.3	-123	-129.3	+6.3	-246	-258.6	+12.6
505	-122.2	-128	+5.8	-122.2	-128	+5.8	-244.4	-256	+11.6

Abbreviations:

STN = Station number.
STS.EQ = Shot static correction using uphole data.
STS.FOR = Shot static correction using formula.
DSTS = Differences in shot static.
STG.EQ = Receiver static correction using uphole data.
STG.FOR = Receiver static correction using formula.
DSTG = Differences in receiver static.
TST.EQ = Total static correction using uphole data.
TST.FOR = Total static correction using formula.
DTST = Differences in total static.

Appendix 6.1

```
( Procedur before gathering the data into common depth point (CDP) gather.
/JOB  ACCT  'READ.t3'
( DIN processor to read the data from disc file.
/DIN  FILENAME  'S180.test'  BI 1 EI 180
( GEOMETRY processor to define the geometry information needed to process the data.
/GEOMETRY  GEOMFILE  'GEO.999E'
( ZERO processor to sets all the samples of each input trace to zero.
/ZERO
( AGC processor to apply balancing scalar that equalize amplitude within the trace.
/AGC  WINDOW 400
( MUTE processor to selects zeros data samples at either end of the input trace.
/MUTE  FMUTE 1,1 1460,38 600,45 420,48 250,49 250,52 420,59 600,96 1460  BYTRACE
( DECONV processor to generate the single channel, time and space-varying requested
(                    type of the deconvolution
/DECONV  PULSDCON
ZONE 1  OPERATOR 1 1500 250 36
DESIGN 1 1 1500 25 1100 31 850 39 750 46 400 51 400 58 750 66 850 72 1100 96 1500
DESIGN 180 1 1500 25 1100 31 850 39 750 46 400 51 400 58 750 66 850 72 1100 96 1500
ZONE 2  OPERATOR 1 2000 250 36
DESIGN 1 1 2000 48 1500 49 1500 96 2000
DESIGN 180 1 2000 48 1500 49 1500 96 2000
PREWHITE 1  BYFILE  BYTRACE
( STVF processor to compute and apply space and time-varing filter.
/STVF  NORMAL  BANDPASS  MIN  FILT 1 12 24 50 24
APPLY 1 2 1 4000 180 4000  BYFILE
( STATAPLY processor to apply a static shift to traces.
/STATAPLY
( GATHER processor to sort the data from one data order to another data order.
/GATHER  OUTSORT 2
( DOUT processor to store the data into disc file for further need.
/DOUT  FILENAME  'GATH.260E'
(-------------------------------------------------------------------------------
( Procedur after gathering the data in to common depth point (CDP) gather.
/JOB  ACCT  'MIG.1'
/DIN  FILENAME  'GATH.260E'  BI 152 EI 410
```

(VELOCITY processor to specify the RMS velocity values distribution as a function of time.
/VELOCITY UNITS M MSEC '
CMP 157, 4 1900, 480 2500,1040 2920,1110 3000,1200 3150,1340 3280,1780 3570,
3000 4300,4000 5000
CMP 180, 4 1900, 480 2520, 820 2980,1020 3100,1100 3180,1300 3300,2080 4000,
4000 5000
CMP 198, 4 1900, 560 2550, 860 3050,1050 3320,1130 3360,1280 3590,1900 4250,
4000 5000
CMP 225, 4 1900, 500 2500, 830 3000,1080 3100,1230 3200,1280 3550,1660 3950,
2280 4300,4000 5000
CMP 250, 4 1900, 750 2750,1010 3000,1050 3300,1200 3500,1650 4000,2730 4400,
4000 5000
CMP 280, 4 1900, 420 2750, 770 3250,1080 3370,1180 3700,1550 4150,4000 5000
CMP 290, 4 1900, 480 2750, 640 3150, 750 3380, 900 3500,1200 3600,2100 4500,
4000 5500
CMP 300, 4 1900, 600 2700, 900 3000,1100 3400,1500 3750,1940 4500,4000 5500
CMP 310, 4 1900, 470 2800, 740 3150,1000 3750,1180 4200,2880 4900,4000 5500
CMP 320, 4 1900, 470 2800, 740 3150,1000 3750,1200 4220,2880 4900,4000 5500
CMP 330, 4 1900, 470 2800, 740 3150,1000 3750,1230 3950,2880 4900,4000 5500
CMP 340, 4 1900, 470 2800, 740 3150,1000 3750,1230 3950,2880 4900,4000 5500
CMP 350, 4 1900, 413 2500, 990 3200,1150 3650,2120 4750,4000 5500
CMP 367, 4 1900, 700 2900,1020 3150,1200 3450,1550 3800,1970 4600,4000 5500
CMP 400, 4 1900, 350 2700, 700 3000,1040 3200,1180 3400,1870 4000,4000 5500
(NMO processor to apply a normal moveout correction to seismic traces.
/NMO
(RSESTIM processor to compute nonsurface-consistent residual statics.
/RSESTIM FILENAME 'REF.EQ'
WINDOW 152 400 1400 410 400 1400 MAXPEAK NOAMPADJ LNCOR 200 NOAPLY
(RSSAVE processor to store static shifts and peak-to-peak separation times for each
(trace into residual statics disk file.
/RSSAVE STATFILE 'RS.EQ' DELETE
(RSCALCSC processor to perform a surface-consistent analysis of the statics
(determined by the RSESTIM processor.
/RSCALCSC STATFILE 'RS.EQ' SEPARATE CKSM 24 ITER 10 25
/STATAPLY RSFILE 'RS.EQ' NOGEOM RSTYPE 3
/RSESTIM FILENAME 'REF.EQ'
WINDOW 152 400 1400 410 400 1400 MAXPEAK NOAMPADJ LNCOR 200 NOAPLY

```
/RSSAVE  STATFILE  'RS.EQ'  DELETE
/RSCALCSC  STATFILE  'RS.EQ'  SEPARATE  CKSM 24  ITER 10 25
/STATAPLY  RSFILE  'RS.EQ'  NOGEOM  RSTYPE 3
/RSESTIM FILENAME 'REF.EQ'
WINDOW 152 400 1400 410 400 1400  MAXPEAK  NOAMPADJ  LNCOR 200  NOAPLY
/RSSAVE  STATFILE  'RS.EQ'  DELETE
/RSCALCSC  STATFILE  'RS.EQ'  SEPARATE  CKSM 24  ITER 10 25
/STATAPLY  RSFILE  'RS.EQ'  NOGEOM  RSTYPE 3
/MUTE  FMUTE 152,250 50,450 300,1050 500,1750 800,2550 1000
( MEDSTK processor to perform median trace stacking of NMO corrected CDP gathers.
/MEDSTK  PERC 80  USEMUTE
/DECONV
ZONE 1  OPERATOR 152 2000 250 36
DESIGN 152 0 800  DESIGN 410 0 800
ZONE 2  OPERATOR 152 1500 250 36
DESIGN 152 750 2000  DESIGN 410 750 2000
PREWHITE 1
/STVF  NORMAL  BANDPASS MIN
FILT 1 15 24 30 24  FILT 2 10 24 48 24  FILT 3 10 24 48 24
APPLY 1 2 152 500 410 500  APPLY 2 2 152 900 410 900  APPLY 3 2 152 2500 410 2500
( PGAIN processor to apply balancing scalar that equalize amplitudes within a trace.
/PGAIN  WINDOW 200 300 200 500  CDPTIMES 152 400 750 1100 1700
( TREQ processor to balances the average amplitude of a window of a seismic trace to that
(                    of the same window of surrounding traces.
/TREQ  NAJ 3  WINDOW 1000  PCT 80
( WTAVG processor to sum shot sequential or stacked traces using a weighted average sum.
/WTAVG  WEIGHT 0.2 0.3 1.0 0.3 0.2
( RPOL processor to reverses the polarity of seismic traces.
/RPOL
( FDMIG processor to migrate the data, using the finite-difference migration method.
/FDMIG  TRSP 25  BOTDEP 9000  NSMOTH 3  TSMOTH 500
LOWFRQ 10  HIGFRQ 48  TIMSEC
( DISPLAY processor to create a disc file for display purpose.
/DISPLAY
```